Immobilization of Photocatalysts on Solid Support and Photochemical Decarboxylations

Dissertation

Zur Erlangung des Doktorgrades der Naturwissenschaften

Dr. rer. nat.

der Fakultät für Chemie und Pharmazie

der Universität Regensburg

vorgelegt von

Christian Eichinger

aus Neukirchen-Balbini

2020

Die Arbeit wurde angeleitet von: Prof. Dr. Oliver Reiser

Promotionsgesuch eingereicht am: 09.06.2020

Promotionskolloquium am: 29.07.2020

Prüfungsausschuss:
Vorsitz: Apl. Prof. Dr. Rainer Müller
1. Gutachter: Prof. Dr. Oliver Reiser
2. Gutachter: Prof. Dr. Julia Rehbein
3. Prüfer: Prof. Dr. Frank-Michael Matysik

Der experimentelle Teil der vorliegenden Arbeit wurde in der Zeit von November 2016 bis April 2020 unter der Leitung von Herrn Prof. Dr. Oliver Reiser am Institut für Organische Chemie der Universität Regensburg angefertigt.

Herrn Prof. Dr. Oliver Reiser möchte ich herzlich für die Themenstellung, die anregenden Diskussionen und seine stete Unterstützung während der Durchführung dieser Arbeit danken.

Meiner Familie

“The most exciting phrase to hear in science,
the one that heralds the most discoveries,
is not ‘Eureka!’ but ‘that’s funny…’”

Isaac Asimov

Table of contents

A. Introduction 1

1. Photocatalysis – photophysical aspects 1

2. Recent advancements in photocatalytic flow chemistry 6

3. Literature 12

B. Recyclable Photocatalysts 15

1. Introduction 15

   1.1. Homogeneously operating recyclable transition metal-based photocatalysts 16

   1.2. Heterogeneously operating recyclable transition metal-based photocatalysts 23

2. Immobilization of transition metal-based photocatalysts on Nafion 31

   2.1. Introduction 31

   2.2. Immobilization strategy 32

   2.3. Application of immobilized catalyst in photochemical reactions 34

   2.4. Development of a two-phase flow process 40

   2.5. Immobilization of an iridium-based catalyst 44

   2.6. Conclusion 45

3. Magnetic nanoparticles as solid support for transition metal-based photocatalysts 46

   3.1. Introduction 46

   3.2. Magnetic nanoparticles as non-covalent solid support 48

      3.2.1. Synthesis of particles 48

      3.2.2. Application of the immobilized catalyst in photochemical reactions 51

   3.3. Magnetic nanoparticles as covalent solid support 54

      3.3.1. Synthesis of particles 54

      3.3.2. Application of the immobilized catalyst in photochemical reactions 59

   3.4. Conclusion 62

4. Graphitic carbon nitrides as novel photoredox catalysts 63

4.1. Introduction 63
4.2. Application of graphitic carbon nitrides in photochemical reactions 69
4.3. Conclusion 77
6. Literature 78
C. Photochemical Decarboxylations 85
1. Introduction 85
2. Synthesis of starting materials 90
3. Photochemical reactions 92
3.1. Intermolecular reactions exploiting the reductive quenching cycle of catalyst 92
3.2. Intermolecular reactions exploiting the oxidative quenching cycle of catalyst 96
3.3. Reaction upscaling 101
3.4. Intramolecular reactions 103
4. Synthesis of pipecolic acid derivatives 105
5. Conclusion 106
6. Literature 107
D. Summary / Zusammenfassung 109
1. Summary 109
2. Zusammenfassung 111
E. Experimental Part 113
1. General information 113
2. Chapter B: Recyclable Photocatalysts 116
2.1. Immobilization of photocatalysts on Nafion 116
2.2. Photochemical reactions employing photocatalyst on Nafion 117
2.3. Reaction upscaling employing photocatalyst on Nafion 123
2.4. Non-covalent immobilization of photocatalysts on magnetic nanoparticles 126
2.5. Photochemical reactions employing electrostatically bound catalyst 128
2.6. Covalent immobilization of photocatalysts on magnetic nanoparticles 131

2.7. Photochemical reactions employing covalently bound catalyst 140

2.8. Photochemical reactions employing graphitic carbon nitrides as catalyst 143

3. Chapter C: Photochemical Decarboxylations 148

3.1. Synthesis of *N*-(acyloxy)phthalimides for intermolecular reactions 148

3.2. Synthesis of trapping reagents 151

3.3. Photochemical reactions exploiting the reductive quenching cycle 152

3.4. Photochemical reactions exploiting the oxidative quenching cycle 155

3.5. Upscaling of photoreaction 162

3.6. Intramolecular reactions 165

3.7. Synthesis of pipecolic acid derivatives 166

4. Literature 170

F. Appendix 173

1. GC-FID analysis 173

2. NMR spectra 174

3. X-Ray 224

4. List of abbreviation 225

5. Curriculum vitae 228

G. Acknowledgement 231

H. Declaration 233

A. Introduction

1. Photocatalysis – photophysical aspects

With the commencement of industrialization at the end of the 18th century, greenhouse gas emissions have increased drastically worldwide.[1] This is mainly caused by the combustion of fossil fuels such as coal or oil, to generate electricity or to power any class of engines, and the accompanying release of carbon dioxide. In this context, a name often mentioned is that of the Italian chemist Giacomo Ciamician (1857 – 1922). He was a real visionary of his time and aware of the finiteness of these sources and the associated environmental pollution. Therefore, he suggested the sunlight as the sole, infinite energy source.[2] A closer look into the actual energy from the sun that strikes the surface of the earth, underpins his statement. Given the fact that the world energy consumption in 2018 was estimated to be 161 PWh,[3] this could be covered within only a single hour by solar energy, as continuously 173 PW reach earth.[4] Until now, however, this is unquestionably utopian, even though mankind developed highly capable solar cells to transform sunlight directly into electrical energy, as well as options, to exploit energy from secondary sources, such as wind or waves. Since particularly the former is increasingly to be found in private households, this is nevertheless driving the prospective getaway from fossil fuels.[5]

Exemplary for chemical transformations mediated by visible light is the nature herself. Since the beginning of time, plants use photosynthesis to generate carbohydrates and oxygen from carbon dioxide and water, solely driven through solar energy. Transferring this process to a laboratory scale, however, proved to be challenging. This begins with the fact that most organic molecules do not absorb in the visible, but rather in the ultraviolet (UV) light range. The excitation spectrum of the sun reveals only roughly 3% in this region, and is, consequently, inefficient.[6] Moreover, UV irradiation is very high in energy, which often causes unselective chemical transformations and leads to numerous inadvertent side products. Realizing that complexes, applied for the conversion of solar energy into an electrochemical potential, may also function as photocatalysts for chemical transformations, coined the last century as photochemistry experienced a remarkable upswing.[6b] With these, it was feasible to conduct photoreactions with solely visible light in conventional lab glassware.[7] Therefore, common transformations which are making use of harsh reaction conditions or stoichiometric amounts of toxic reagents are replaced progressively.[8] This process was further improved by the development of energy-saving light-emitting diodes (LEDs) and became particularly interesting for industry through implementation of micro-reactors, as flow conditions entail numerous advantages, such as improved mass transfer or cooling process.[9] Therefore, visible light photoredox chemistry has emerged as one of the most powerful tools for a variety of chemical transformations.[10]

There are different types of photocatalysts and photosensitizers, i.e. organic and inorganic semiconductors being the most durable,[11] organic dyes which are comparatively cheap and increasingly used,[12] and transition metal-based complexes.[13] The latter are, due to their versatility and high chemical stability, very prominent. They consist of copper,[14] cobalt,[15] and other non-noble metals,[16] but also expensive noble metals like ruthenium and iridium,[17] which are the most frequently used. One of the first discovered, very well studied pyridyl complex, based on ruthenium, is $[Ru(bpy)_3]^{2+}$ (bpy = 2,2'-bipyridine).[18] To understand the function of this photocatalyst, a brief overview of the mechanisms of catalytic processes and the underlying photophysical principals is provided in the following.

The task of a photocatalyst, in general, is to absorb in the visible light range and make the solar energy accessible to molecules, thus initiating a variety of reactions. This can be accomplished in several different manners, of which an outline is given in Scheme 1. After getting excited through visible light irradiation, the easiest way to interact with molecules is *via* sensitization (Scheme 1, middle), which means that an energy-transfer (ET) towards a substrate takes place. Whereas this molecule is now in an excited electronic state, therefore high in energy, and may undergo various reactions, such as [2+2] cycloaddition or isomerization,[19] the catalyst reaches its ground-state again.

Other pathways imply single-electron transfers (SET), also known as photoinduced electron transfers (PET). Here, a distinction has to be made between oxidative and reductive quenching of the catalyst. Whereas for the oxidative cycle at first an electron is donated from the catalyst to an acceptor molecule (Scheme 1, left side, $E_{1/2}^{III/II*} = -0.81$ V),[20] at the reductive cycle a donor gets oxidized by the catalyst (right side, $E_{1/2}^{II*/I} = 0.77$ V). Since the phrase *catalyst* implies, that only sub-stoichiometric amounts are necessary, and it is not consumed during the reaction,[21] the ground-state has to be reached again. The Ru^{III} species has a comparable high oxidation potential ($E_{1/2}^{III/II} = 1.29$ V) and is, therefore, reduced by a donor to its ground-state. Ru^{I}, on the other hand, has a very high reduction potential ($E_{1/2}^{II/I} = -1.33$ V) and falls back to Ru^{II} through oxidation by an acceptor molecule. Due to the outstanding properties of Ru^{I} a sacrificial electron donor, such as NEt_3 or other higher molecular substrates, is often used. While this is certainly adverse given the atom economy, one aims for photoredox-neutral transformations. It implies that an oxidation/reduction through the catalyst leads to an intermediate, which itself is subsequently reduced/oxidized to give back the catalyst in its ground-state.[22]

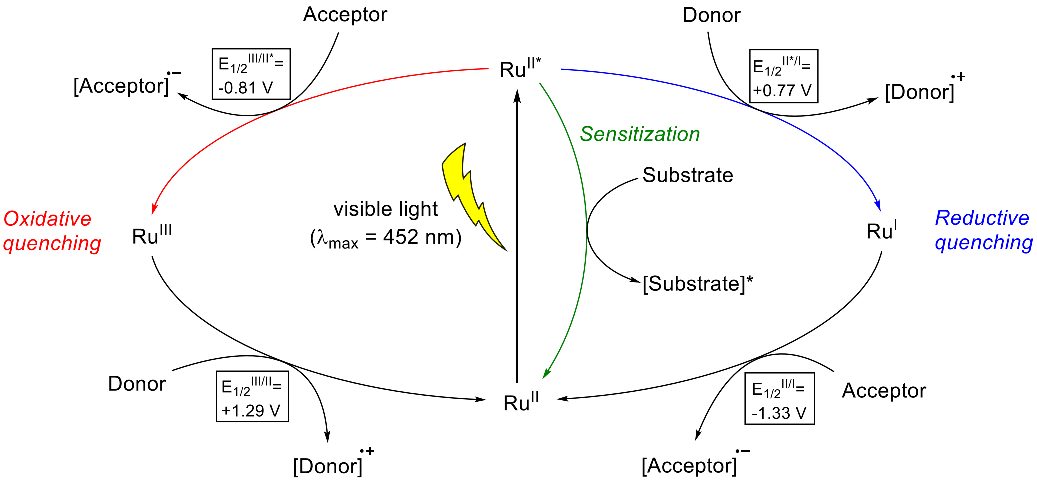
Acceptor
$[\text{Acceptor}]^{\bullet-}$
$E_{1/2}^{\text{III/II*}}$= -0.81 V
$\text{Ru}^{\text{II*}}$
Donor
$E_{1/2}^{\text{II*/I}}$= +0.77 V
$[\text{Donor}]^{\bullet+}$
Sensitization
Substrate
Oxidative quenching
Ru^{III}
visible light
(λ_{max} = 452 nm)
[Substrate]*
Ru^{I}
Reductive quenching
Donor
$E_{1/2}^{\text{III/II}}$= +1.29 V
Ru^{II}
$E_{1/2}^{\text{II/I}}$= -1.33 V
Acceptor
$[\text{Donor}]^{\bullet+}$
$[\text{Acceptor}]^{\bullet-}$

Scheme 1: Reaction pathways of $[\text{Ru(bpy)}_3]^{2+}$. Oxidative quenching cycle on the left-hand side, reductive quenching cycle on the right-hand side and sensitization pathway in the middle.

After this brief overview of possible reaction pathways of an excited transition-metal based pyridyl complex, the underlying photophysical aspects are discussed in the following exemplary on $[\text{Ru(bpy)}_3]^{2+}$ (**1**, Scheme 2). Since this catalyst has an absorption-maxima at 452 nm, through visible light irradiation an electron is excited *via* metal to ligand charge-transfer (MLCT) from the fully occupied t_{2g} orbital into the ligand-centered singlet π* (S_1) orbital. This directly undergoes inter-system crossing (ISC) to obtain the lower-energy triplet π* (T_1) state and, therefore, the excited catalyst $[\text{Ru(bpy)}_3]^{*2+}$ (**2**). A decisive characteristic of a photocatalyst is the *excited-state lifetime*, which must be sufficient for the catalyst to interact with molecules. Otherwise, it would directly fall back to its ground state *via* photoluminescence or vibrational relaxation. Since the direct decay to its ground-state, however, is spin-forbidden, the excited state lifetime for **2** is in a comparable high range of 1100 ns.[20] Therefore, **2** is long-lived enough, to interact with other substrates. Whereas for the oxidative quenching cycle the electron from π* (T_1) is shifted to the lowest unoccupied molecule orbital (LUMO) of the substrate, for the reductive quenching cycle an electron from the highest occupied molecule orbital (HOMO) of the substrate is donated to the metal-centered t_{2g} orbital of the catalyst. As already discussed, $[\text{Ru(bpy)}_3]^{3+}$ (**3**) and $[\text{Ru(bpy)}_2]^{+}$ (**4**) exhibit a very high oxidation or reduction potential, respectively. Therefore, the ground state **1** is straightforwardly obtained *via* a second single electron transfer.[10a,23]

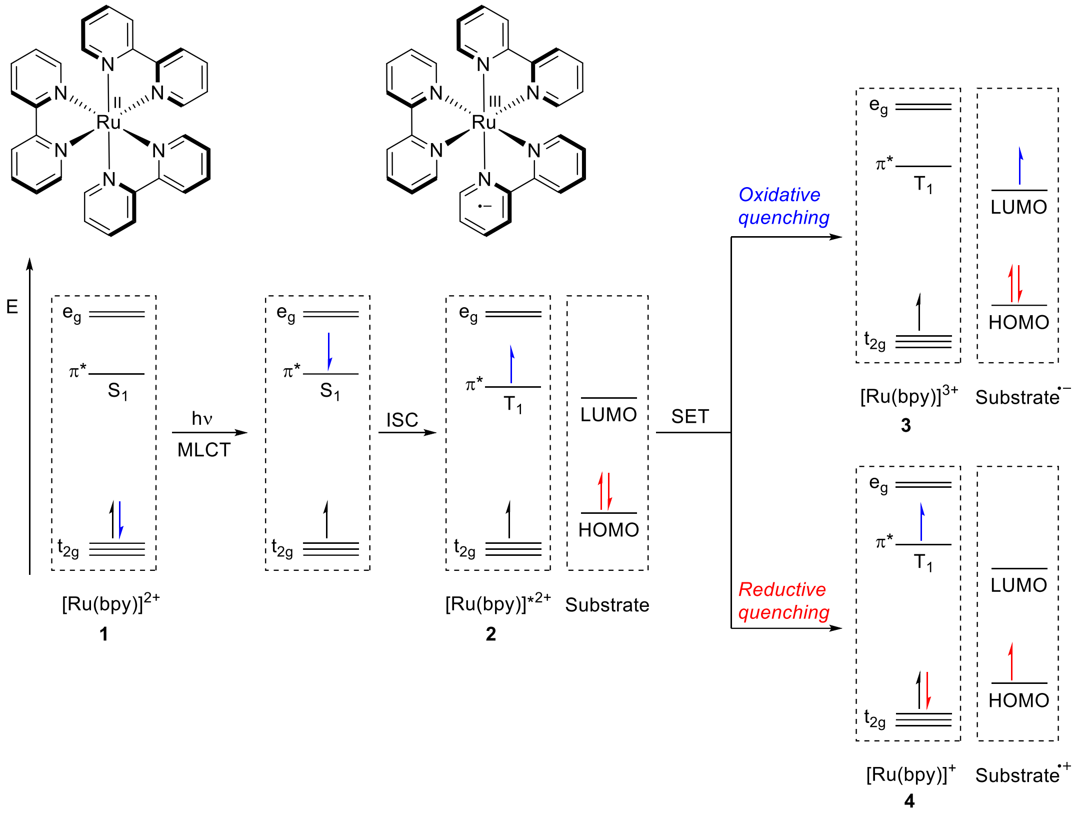
E
e_g
π^*
S_1
t_{2g}
hν
MLCT
ISC
T_1
LUMO
HOMO
SET
Oxidative quenching
Reductive quenching
$[Ru(bpy)]^{2+}$
1
$[Ru(bpy)]^{*2+}$
2
Substrate
$[Ru(bpy)]^{3+}$
3
$Substrate^{\bullet-}$
$[Ru(bpy)]^{+}$
4
$Substrate^{\bullet+}$
Ru
II
III
N

Scheme 2: Jablonski diagram of a visible light-excitation of $[Ru(bpy)_3]^{2+}$ (**1**) and subsequent quenching *via* SET.

Apart from photoredox pathways, there is the possibility of a sensitization mechanism, of which Dexter energy transfer and Förster resonance energy transfer (FRET) are the most common. The underlying photophysical processes are depicted in Scheme 3. In case of physical contact between photocatalyst and substrate, i.e. if the orbitals are overlapping, a Dexter electron-transfer can occur (left side). This implies a two-electron transfer, i.e. the electron from π* (T_1) is shifted to the LUMO of the substrate, whereas an electron from its HOMO is transferred to the t_{2g} orbital of the catalyst, giving back its ground state **1**. The Förster resonance energy-transfer can occur, if on the one hand a suitable substrate and photocatalyst are closer than 10 nm to each other, and on the other hand, the emission spectrum of the catalyst overlaps with the absorption spectrum of the substrate (right side). If this is the case, an electron is shifted from the HOMO to the LUMO through the relaxation energy of π* (T_1) which funnels a vibrational mode of the substrate.[24]

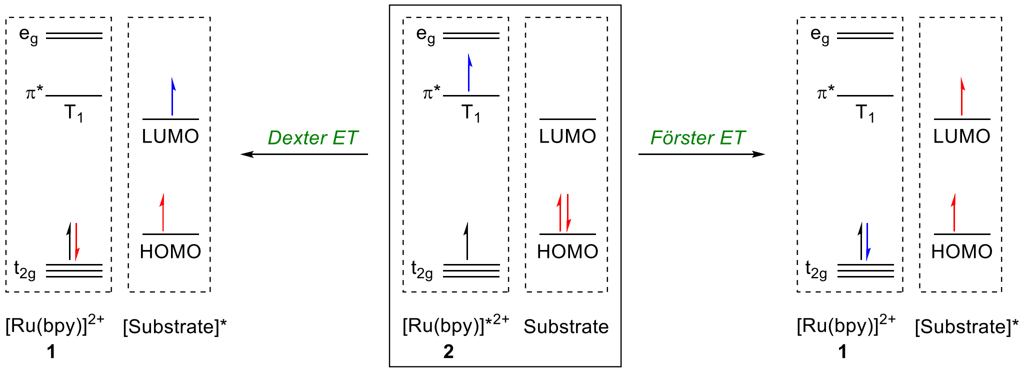

Scheme 3: Jablonski diagram of catalyst-quenching *via* Dexter energy-transfer (left) and Förster energy-transfer (right).

Besides $[Ru(bpy)_3]^{2+}$ (**1**) there are numerous other transition metal-based photocatalysts, bearing different characteristics. Therefore, depending on the substrates and striven chemical transformations, the catalyst must be chosen accordingly. Table 1 shows further metal complexes used in this work, along with their decisive properties, i.e. excited state lifetimes, reduction potentials and excitation as well as emission wavelengths.

Table 1: Transition metal-based *fac*-$Ir(ppy)_3$ (**5**), $[Ir(ppy)(dtb\text{-}bpy)]^+$ (**6**) and $[Cu(dap)_2]^+$ (**7**) and their corresponding relevant photoredox properties. [a]

	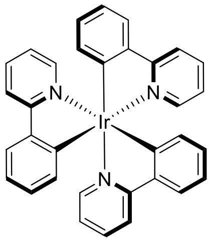 *fac*-$Ir(ppy)_3$ (**5**)	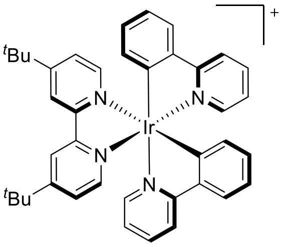 $[Ir(ppy)_2(dtb\text{-}bpy)]^+$ (**6**)	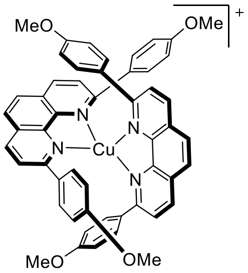 $[Cu(dap)_2]^+$ (**7**)
$E_{1/2}$ (C^+/C^*) [V]	-1.73	-0.96	-1.43
$E_{1/2}$ (C^*/C^-) [V]	+0.31	+0.66	
$E_{1/2}$ (C^+/C) [V]	+0.77	+1.21	+0.62
$E_{1/2}$ (C/C^-) [V]	-2.19	-1.51	
excited-state lifetime τ [ns]	1900	557	260
excitation λ_{max} [nm]	375	-	
emission λ_{max} [nm]	494 [b]	581	670 [c]
references	[25]	[26]	[27]

[a]Unless otherwise noted, potentials were measured in acetonitrile at room temperature and are relative to the saturated calomel electrode. [b]Determined in ethanol/methanol (1:1) glass at 77 K. [c]Determined in DCM.

2. Recent advancements in photocatalytic flow chemistry

As already stated, the development of flow reactors has contributed significantly to increasing the scope of photochemical applications in the industry. While there has lately been tremendous progress, only a small part will be reflected in this chapter. To gain a deeper insight, it is redirected to more detailed reviews covering this topic.[9,28]

The implementation of flow reactions requires special equipment, which ranges from inexpensive self-made reactors of perfluorinated polymer tubes wrapped around a light source to pricy glass plates with etched channels.[28e] However, they all have one in common: the reagent mixtures are flushed through tubes of very small diameters. This unique construction opens up new possibilities for performing reactions in a two-phase fashion, i.e. using two immiscible solvents,[29] a liquid/gas[30] or liquid/solid system, or even triphasic systems.[28d] Heterogeneous catalysts have also permanently been installed within tubes, allowing for flow systems with continuous catalyst recycling.[28b]

Compared to batch setups, the undisputed advantages are inter alia temporal and safety aspects as well as enhanced scalability. The small diameters of the tubes lead to an improved mixing and mass transfer. Therefore, reactions proceed many times faster, while simultaneously the total amount of hazardous or explosive compounds within the reaction unit is diminished. Besides, the resulting large surface-to-volume ratios allow for a superior heat transfer, which is especially important for exothermal reactions and those that need to be heated. Moreover, translating small scale reactions to a big scale is facilitated, since the same setup can be utilized and several flow reactors can be connected in series.[28b] The arguably most important aspect for successfully scaling up visible light-driven reactions, however, is the enhanced irradiation of the reaction mixture. A closer look into the Bouguer-Lambert-Beer law (Eq. 1) reveals why this is so important:

$$A = log_{10} \frac{I_0}{I} = \varepsilon \cdot c \cdot l \qquad \textit{(Eq. 1)}$$

The absorbance (A) is the product of the molar extinction coefficient (ε) as well as concentration (c) of the light-absorbing molecules and the optical path length (l).[28c] Due to these correlations, an upscaling in batch setup by enlarging the reaction vessel is hampered, as the transmittance of light attenuates when distancing from the light source, i.e. when the liquid medium becomes thicker. A graphical illustration is given in Figure 1, with various concentrations of $[Ru(bpy)_3]^{2+}$ (**1**) representing the light-absorbing species. Due to its exceptional high extinction coefficient of $\varepsilon = 14{,}600\ M^{-1} \cdot cm^{-1}$,[20a] at common concentrations of 0.25 mM and 0.10 mM, the transmittance is halved already at path lengths of 1 mm or 2 mm, respectively. Hence, there are two possibilities to circumvent the attenuation of light intensity: decreasing either the concentration of the light-absorbing species which may be disadvantageous for some reactions, or the path length, being the most convenient option. Flow reactors follow the last principle, as they usually exhibit tubes with very thin inner diameters. This promises a largely homogeneous light transmittance.

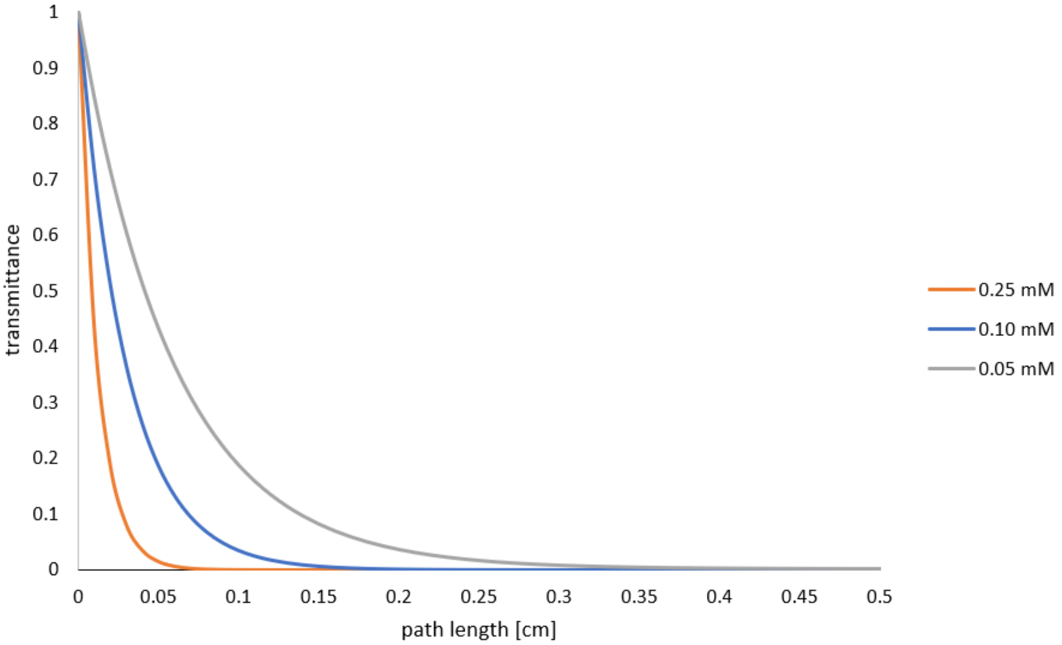

Figure 1: Light transmittance as a function of the optical path length. $[Ru(bpy)_3]^{2+}$ was used as light-absorbing species ($\varepsilon = 14{,}600\ M^{-1} * cm^{-1}$). Transmission = $10^{(-\varepsilon * c * l)}$.[28e]

Not only the assembly of micro reactors has been improved over time, inasmuch as the tubes are getting, on the one hand, smaller and may even be found on microchips and, on the other hand, bigger for large scale purposes, but also the light sources have changed. From conventional compact fluorescence light bulbs (CFL) to LEDs, recently an operational simple 24 W laser-driven flow process in a continuous stirred 100 mL tank reactor was presented by Wittenberger *et al*.[31] Thorough optimization of catalyst concentration, liquid depth, and laser configuration allowed them to decrease the catalyst loading while having simultaneously a tremendous reaction time acceleration for a visible light-mediated C-N coupling towards **10** (Scheme 4). Moreover, this setup allowed the authors to perform the reaction on a kilogram scale at throughput rates of 48 g/h, therefore, furnishing 1.54 kg product **10** (85% yield, 99.5% purity) within 32 h.

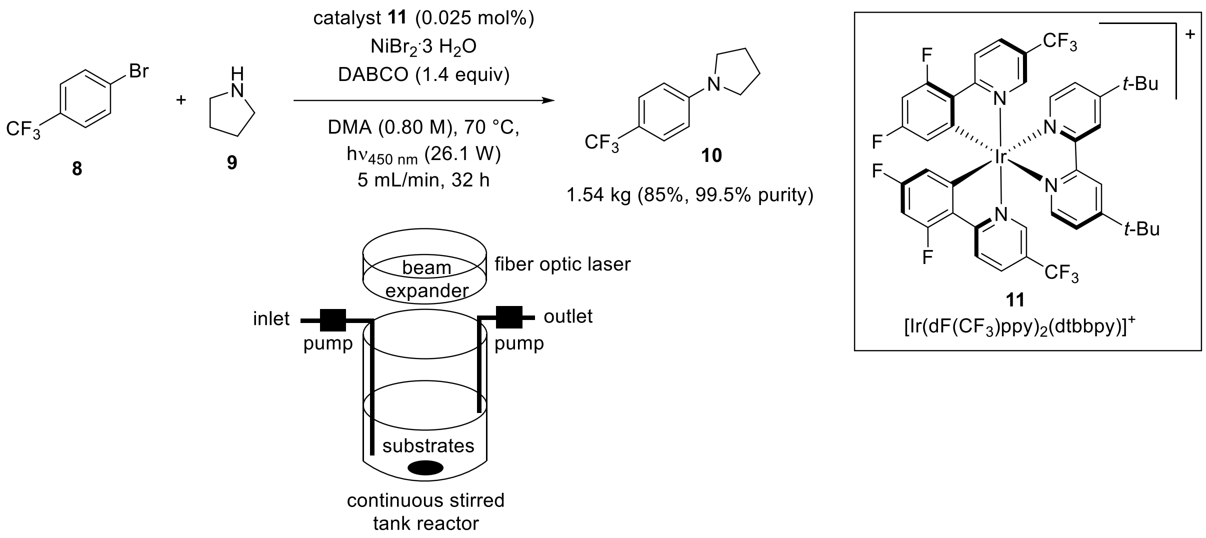
catalyst 11 (0.025 mol%)
NiBr2·3 H2O
DABCO (1.4 equiv)
DMA (0.80 M), 70 °C,
hν450 nm (26.1 W)
5 mL/min, 32 h
8
9
10
1.54 kg (85%, 99.5% purity)
beam expander
fiber optic laser
inlet
pump
outlet
pump
substrates
continuous stirred tank reactor
11
[Ir(dF(CF3)ppy)2(dtbbpy)]+

Scheme 4: Visible light-mediated C-N coupling towards **10** in a 100 mL continuous stirred tank reactor employing an optic laser as light source.

That performing reactions in a flow setup not only have time-related advantages but may also entail positive impacts in yield was demonstrated amongst others by Reiser *et al.* on a deoxygenative cyclization of **12** (Table 2).[32] Although this reaction provides in a 0.1 mmol batch setup full conversion and 70% product **13** within 20 h (entry 1), upscaling to 1.0 mmol proved to be disadvantageous as the reaction time increased to 7 d to achieve full conversion. Moreover, also a deterioration of yield to 54% was obtained (entry 2). Only when a micro reactor system was employed, the reaction time could be reduced to 28 h while furnishing 73% product **13** (entry 3).

Table 2: Photocatalyzed deoxygenative cyclization of **12** under batch and flow conditions.

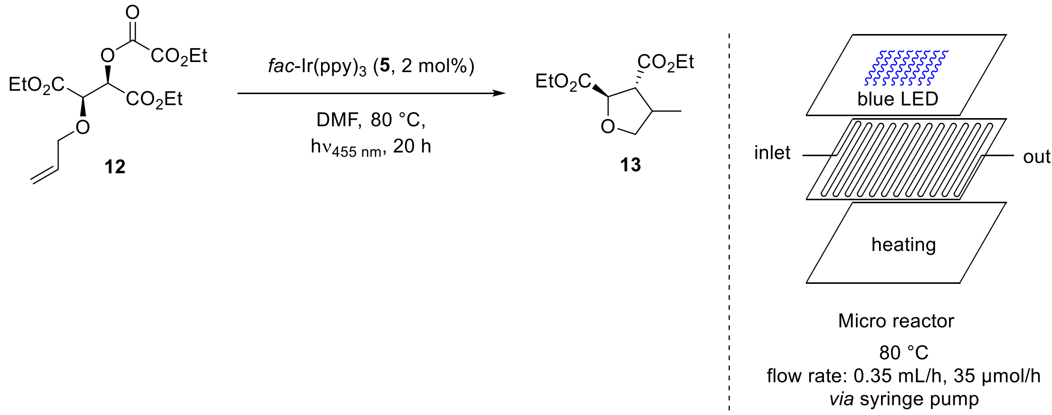
12
fac-Ir(ppy)3 (5, 2 mol%)
DMF, 80 °C,
hν455 nm, 20 h
13
blue LED
inlet
outlet
heating
Micro reactor
80 °C
flow rate: 0.35 mL/h, 35 μmol/h
via syringe pump

Entry	Setup	Scale [mmol]	Time	Conversion [%]	Yield [%]
1	batch	0.1	20 h	100	70
2	batch	1.0	7 d	100	54
3	flow	1.0	28 h	100	73

Another example worth mentioning is the pioneering work from Stephenson *et al*. Since fluorination is especially important for medicinal applications, the production of those, however, limited and expensive, a cost-efficient upscaling is highly desirable.[33] This was achieved by employing $[Ru(bpy)_3]^+$ (**1**, 0.1 mol%) as catalyst and the in-situ generated trifluoromethyl source **17**, obtained from readily available trifluoroacetic anhydride (TFAA, **15**) and pyridine *N*-oxide **16** (Scheme 5).[34] Whereas in previous studies a 100 g scale in batch was due to severely increased reaction times and deterioration of yield inconvenient,[34a] a transfer to flow setup allowed them to even run this reaction on a kilogram scale.[34b] This was demonstrated on the trifluoromethylation of 1.2 kg pyrrole **14** furnishing 0.98 kg (50% yield, 81% purity) of product **18** within 48 h (Scheme 5). The customized flow reactor employed consists of a PFA tubing with a total volume of 150 mL, which was wrapped around a cylinder hosting three blue LEDs in the middle. Despite the energy efficiency of LEDs, they present a considerable heat source, wherefore the reactor was immersed into water. Noteworthy, another major benefit is the ability to mix the reactive reagents only shortly before entering the reactor. In this case, TFAA (**15**) was blended with the other substrates *via* a T-mixer, accordingly.

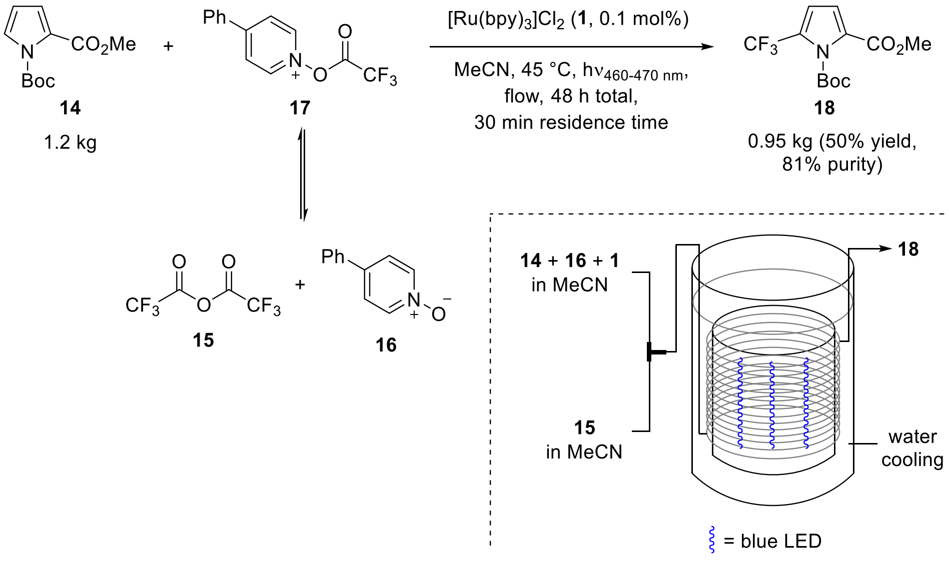

Scheme 5: Trifluoromethylation of pyrrole **14** in a flow reactor.

Pursuing this principle enables elegantly the safe operation with chlorine, which is otherwise frequently shunned in laboratories. Kappe *et al.*[35] and Ryu *et al.*[36] presented a flow-process for the photochlorination of alkenes through on-demand generated Cl_2. Exemplary for such a reaction is the chlorination of cyclohexane (**19**), depicted in Scheme 6. Aqueous solutions of HCl and NaOCl are firstly combined generating chlorine gas which is further mixed *via* a T-piece with the alkene **19**. These gas/liquid phases are subsequently transferred to a glass-made flow reactor and irradiated with UV-light. After exiting the reactor, the solution is quenched by aqueous Na_2SO_3 furnishing the product **20** in 94% yield after a residence time of only 1 min. Both the *in situ* generation of chlorine and the closed flow system as well as the subsequent quenching contribute to secure handling and minimizing of safety hazards.

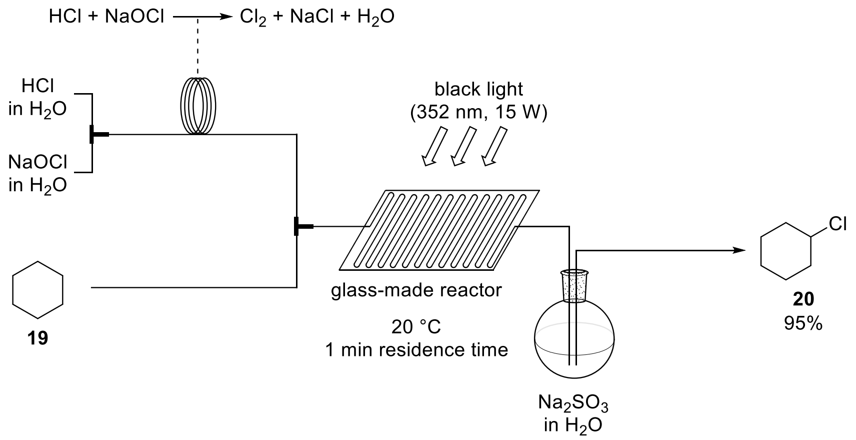
HCl + NaOCl → Cl2 + NaCl + H2O
HCl in H2O
NaOCl in H2O
black light (352 nm, 15 W)
glass-made reactor
20 °C
1 min residence time
19
Na2SO3 in H2O
Cl
20
95%

Scheme 6: Photochlorination of **19** in flow through *in situ* generated chlorine.

Gilmore *et al*. established another very valuable liquid/gas flow reaction, i.e. the synthesis of the antimalarial drug artemisinin (**23**, Scheme 7) from crude extracts of *Artemisia annua* leaves.[37] The advantage of this procedure is that not only a previous, arduous purification of the starting materials is circumvented, but the plant extract also contains both the artemisinin precursor dihydroartemisinic acid (DHAA, **21**) and chlorophyll, which is exploited as photocatalyst for the generation of singlet oxygen. A solution of DHAA (**21**), chlorophyll and trifluoroacetic acid in toluene is blended *via* a T-mixer with pure oxygen before being flushed through a cooled microreactor (Scheme 7). Upon visible light irradiation, $^1O_2$ is generated, which undergoes reaction with **21** towards allylic hydroperoxide **22**. This intermediate is further converted in the presence of the strong acid TFA to the target molecule **23** *via* a Hock cleavage.

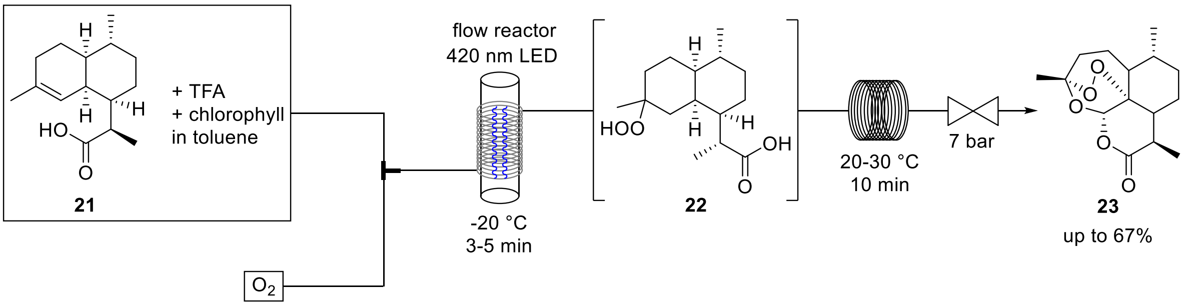
H
H
H
HO
O
21
+ TFA
+ chlorophyll
in toluene
O2
flow reactor
420 nm LED
-20 °C
3-5 min
H
HOO
H
H
OH
O
22
20-30 °C
10 min
7 bar
O
O
O
O
O
23
up to 67%

Scheme 7: Photochemical synthesis of artemisinin **23** from crude plant extract.

One more interesting feature flow systems offer is automatization.[28b] In very small scale reactions, numerous conditions in view of residence time, temperature, etc., as well as various substrates can be screened in a short time while being directly analyzed on-line. The advantages are obvious: it saves a lot of time and chemicals, which is for instance especially valuable if scarcely available precursors for pharmaceutical applications are employed.[38] This, however, has so far found only little use in photoredox chemistry, yet has very high potential and could become even more important in the future.[28b]

Despite all the advantages mentioned, flow reactors also have some apparent drawbacks and limitations. These are partially high prices of the reactors themselves as well as the pump system. Due to the small diameters of the tubes, clogging through precipitation may occur during the reaction. Besides, a translation from batch setup to flow is not as trivial and requires somewhat more effort. All things considered, however, one can say that the advantages outweigh these drawbacks.

The flow reactor system used in the present work consists of a glass-made plate which is irradiated from above with 8 high-power blue LEDs (λ = 455 nm). Temperature control is ensured by a water-cooled aluminum block, the glass cartridge is inserted in (Figure 2). The flow rates can be adjusted *via* a syringe pump.

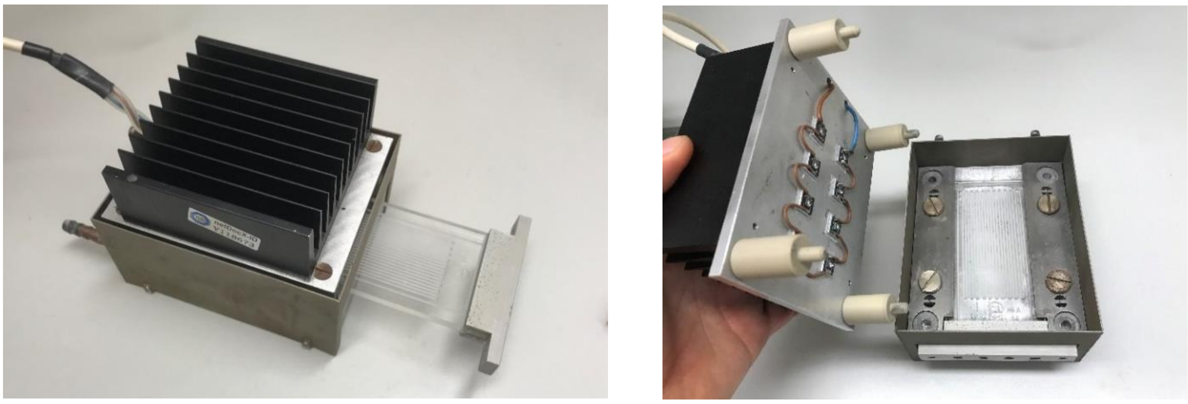

Figure 2: Micro reactor system employed in this work.

3. Literature

[1] T. Boden, G. Marland, R. J. Andres, *Global, Regional, and National Fossil-Fuel CO2 Emissions (1751 - 2014) (V. 2017)*, Carbon Dioxide Information Analysis Center (CDIAC), Oak Ridge National Laboratory (ORNL), Oak Ridge, TN (United States), **2017**.

[2] G. Ciamician, *Science* **1912**, *36*, 385–394.

[3] BP Statistical Review of World Energy, to be found under https://www.bp.com/content/dam/bp/business-sites/en/global/corporate/pdfs/energy-economics/statistical-review/bp-stats-review-2019-full-report.pdf, **2019**.

[4] D. L. Chandler, "Shining brightly", to be found under http://news.mit.edu/2011/energy-scale-part3-1026, **2011**.

[5] Bundesverband Solarwirtschaft e.V. (BSW-Solar), "Statistische Zahlen der deutschen Solarstrombranche (Photovoltaik)", to be found under https://www.solarwirtschaft.de/fileadmin/user_upload/bsw_faktenblatt_pv_2019_3.pdf, **2019**.

[6] a) M. P. Thekaekara, *Solar Energy* **1976**, *18*, 309–325; b) D. M. Schultz, T. P. Yoon, *Science* **2014**, *343*, 1239176.

[7] E. Speckmeier, K. Zeitler in *Science of Synthesis: Photocatalysis in Organic Synthesis*; (Ed. B. König), Thieme, **2019**, pp. 101–131.

[8] L. Marzo, S. K. Pagire, O. Reiser, B. König, *Agew. Chem. Int. Ed.* **2018**, *57*, 10034–10072.

[9] D. Cambié, C. Bottecchia, N. J. W. Straathof, V. Hessel, T. Noël, *Chem. Rev.* **2016**, *116*, 10276–10341.

[10] a) J. W. Tucker, C. R. J. Stephenson, *J. Org. Chem.* **2012**, *77*, 1617–1622; b) K. Zeitler, *Angew. Chem. Int. Ed.* **2009**, *48*, 9785–9789; c) C. K. Prier, D. A. Rankic, D. W. C. MacMillan, *Chem. Rev.* **2013**, *113*, 5322–5363; d) M. H. Shaw, J. Twilton, D. W. C. MacMillan, *J. Org. Chem.* **2016**, *81*, 6898–6926; e) B. König, *Eur. J. Org. Chem.* **2017**, *2017*, 1979–1981; f) N. A. Romero, D. A. Nicewicz, *Chem. Rev.* **2016**, *116*, 10075–10166; g) C. R. J. Stephenson, D. W. C. MacMillan, T. P. Yoon, Eds, *Visible Light Photocatalysis in Organic Chemistry;* Wiley-VCH, **2018**; h) R. C. McAtee, E. J. McClain, C. R.J. Stephenson, *Trends Chem.* **2019**, *1*, 111–125; i) G. E. M. Crisenza, P. Melchiorre, *Nat. Commun.* **2020**, *11*, 803.

[11] a) D. Friedmann, A. Hakki, H. Kim, W. Choi, D. Bahnemann, *Green Chem.* **2016**, *18*, 5391–5411; b) X. Lang, X. Chen, J. Zhao, *Chem. Soc. Rev.* **2014**, *43*, 473–486; c) J. Chen, J. Cen, X. Xu, X. Li, *Catal. Sci. Technol.* **2016**, *6*, 349–362; d) D. W. Manley, J. C. Walton, *Beilstein J. Org. Chem* **2015**, *11*, 1570–1582.

[12] a) S. Fukuzumi, K. Ohkubo, *Org. Biomol. Chem.* **2014**, *12*, 6059–6071; b) D. A. Nicewicz, T. M. Nguyen, *ACS Catal.* **2014**, *4*, 355–360; c) B. König, S. Kümmel, E. Svobodová, R. Cibulka, *Phys. Sci. Rev.* **2018**, *3*, 15; d) D. P. Hari, B. König, *Chem. Commun.* **2014**, *50*, 6688–6699.

[13] a) F. Glaser, O. S. Wenger, *Coord. Chem. Rev.* **2020**, *405*, 213129; b) Hockin, Bryony, M, C. Li, N. Robertson, E. Zysman-Colman, *Catal. Sci. Technol.* **2019**, *9*, 889–915; c) J.-H. Shon, T. S. Teets, *Comment. Inorg. Chem.* **2019**, *40*, 53–85.

[14] a) A. Hossain, A. Bhattacharyya, O. Reiser, *Science* **2019**, *364*, 450–461; b) O. Reiser, *Acc. Chem. Res.* **2016**, *49*, 1990–1996.

[15] A. K. Pal, C. Li, G. S. Hanan, E. Zysman-Colman, *Angew. Chem. Int. Ed.* **2018**, *57*, 8027–8031.

[16] L. Traub, O. Reiser, *Phys. Sci. Rev.* **2019**, *4*, 20170172.

[17] a) K. Teegardin, J. I. Day, J. Chan, J. Weaver, *Org. Process Res. Dev.* **2016**, *20*, 1156–1163; b) T. Koike, M. Akita, *Inorg. Chem. Front.* **2014**, *1*, 562–576.

[18] F. Teplý, *Collect. Czech. Chem. Commun.* **2011**, *76*, 859–917.

[19] Q.-Q. Zhou, Y.-Q. Zou, L.-Q. Lu, W.-J. Xiao, *Angew. Chem. Int. Ed.* **2018**, *58*, 1586–1604.

[20] a) K. Kalyanasundaram, *Coord. Chem. Rev.* **1982**, *46*, 159–244; b) A. Juris, V. Balzani, P. Belser, A. von Zelewsky, *Helv. Chim. Acta* **1981**, *64*, 2175–2182.

[21] A. D. MacNaught, A. Wilkinson, *Compendium of chemical terminology*: IUPAC recommendations; Blackwell Science, Oxford, **1997**.

[22] R. J. Wiles, G. A. Molander, *Isr. J. Chem.* **2020**, *60*, 281–293.

[23] a) N. H. Damrauer, G. Cerullo, A. Yeh, T. R. Boussie, C. V. Shank, J. K. McCusker, *Science* **1997**, *275*, 54–57; b) V. Balzani, G. Bergamini, S. Campagna, F. Puntoriero in *Photochemistry and Photophysics of Coordination Compounds, Topics in current chemistry, Vol. 280*; (Eds. V. Balzani, S. Campagna), Springer, Berlin, Heidelberg, **2007**, pp. 1–36.

[24] a) F. Scandola, M. T. Indelli, C. Chiorboli, C. A. Bignozzi in *Photoinduced Electron Transfer II*; (Ed. J. Mattay), Springer, Berlin, Heidelberg, **1990**; b) G. D. Scholes, *Annu. Rev. Phys. Chem.* **2003**, *54*, 57–87.

[25] L. Flamigni, A. Barbieri, C. Sabatini, B. Ventura, F. Barigelletti, *Top. Curr. Chem.* **2007**, *281*, 143–203.

[26] a) J. D. Slinker, A. A. Gorodetsky, M. S. Lowry, J. Wang, S. Parker, R. Rohl, S. Bernhard, G. G. Malliaras, *J. Am. Chem. Soc.* **2004**, *126*, 2763–2767; b) M. S. Lowry, J. I. Goldsmith, J. D. Slinker, R. Rohl, R. Pascal, *Chem. Mater.* **2005**, *17*, 5712–5719.

[27] J.-M. Kern, J.-P. Sauvage, *J. Chem. Soc, Chem. Commun.* **1987**, 546–548.

[28] a) Z. J. Garlets, J. D. Nguyen, C. R. J. Stephenson, *Isr. J. Chem.* **2014**, *54*, 351–360; b) C. Sambiagio, T. Noël, *Trends Chem.* **2020**, *2*, 92–106; c) Y. Su, N. J. W. Straathof, V. Hessel, T. Noël, *Chem. Eur. J.* **2014**, *20*, 10562–10589; d) B. Pieber, M. Shalom, M. Antonietti, P. H. Seeberger, K. Gilmore, *Angew. Chem. Int. Ed.* **2018**, *57*, 9976–9979; e) M. B. Plutschack, B. Pieber, K. Gilmore, P. H. Seeberger, *Chem. Rev.* **2017**, *117*, 11796–11893; f) M. Neumann, K. Zeitler, *Org. Lett.* **2012**, *14*, 2658–2661; g) O. Reiser, *Chem* **2016**, *1*, 344–345.

[29] D. Rackl, P. Kreitmeier, O. Reiser, *Green Chem.* **2016**, *18*, 214–219.

[30] C. J. Mallia, I. R. Baxendale, *Org. Process Res. Dev.* **2016**, *20*, 327–360.

[31] K. C. Harper, E. G. Moschetta, S. V. Bordawekar, S. J. Wittenberger, *ACS Cent. Sci.* **2019**, *5*, 109–115.

[32] D. Rackl, V. Kais, E. Lutsker, O. Reiser, *Eur. J. Org. Chem.* **2017**, 2130–2138.

[33] C. Alonso, E. Martínez de Marigorta, G. Rubiales, F. Palacios, *Chem. Rev.* **2015**, *115*, 1847–1935.

[34] a) J. W. Beatty, J. J. Douglas, K. P. Cole, C. R. J. Stephenson, *Nat. Commun.* **2015**, *6*, 1–6; b) J. W. Beatty, J. J. Douglas, R. Miller, R. C. McAtee, K. P. Cole, C. R.J. Stephenson, *Chem* **2016**, *1*, 456–472.

[35] F. J. Strauss, D. Cantillo, J. Guerra, C. O. Kappe, *React. Chem. Eng.* **2016**, *1*, 472–476.

[36] T. Fukuyama, M. Tokizane, A. Matsui, I. Ryu, *React. Chem. Eng.* **2016**, *1*, 613–615.

[37] S. Triemer, K. Gilmore, G. T. Vu, P. H. Seeberger, A. Seidel-Morgenstern, *Angew. Chem. Int. Ed.* **2018**, *57*, 5525–5528.

[38] a) M. Baumann, T. S. Moody, M. Smyth, S. Wharry, *Org. Process Res. Dev.* **2020**, doi: 10.1021/acs.oprd.9b00524; b) D. Perera, J. W. Tucker, S. Brahmbhatt, C. J. Helal, A. Chong, W. Farrell, P. Richardson, N. W. Sach, *Science* **2018**, *359*, 429–434.

B. Recyclable Photocatalysts

1. Introduction

In the year 1835, Berzelius coined the term ‘catalysis’, derived from the Greek words *kata* and *lyein*, which means ‘down’ and ‘loosen’, respectively.[1] With this, he concluded that there is something beyond chemical affinity, i.e. the property of a substance to take part in a reaction whereby remaining unchanged itself. Catalysis only emerged as a tool for complex chemical reactions in the 20th century,[2] even though it has been applied for a long time.[3]

In view of photochemistry, transition metal-based catalysts are still very popular due to their versatility and chemical stability. Their scarcity and, therefore, high price, however, severely impedes the applicability on large-scale for the industry as the typical catalyst loading is 1 mol%. For this, it is highly desirable to invent recyclable versions of those. This would not only reduce the arising expenses but also prevent contamination of the products with potentially toxic complexes, which is particularly important concerning drug synthesis.

A distinction is to be made between heterogeneous and homogenous catalysis.[4] Homogeneous catalysts are usually located in the same phase as the reagents, which typically results in high reaction rates. However, a recovery of these is sometimes not feasible or involves a great deal of time and effort and is, therefore, too expensive to be considered for industrial applications. Contrary to that, heterogeneous catalysts are found in a different phase than the reagents. Typically, the catalytic species is present in its solid state to promote reactions in a gaseous or liquid phase, which has the advantage of an easy recovery. This is reflected in the fact, that more than 90% of the chemical transformations in the industry are heterogeneously catalyzed.[5] Despite all these advantages, heterogeneity is considered critical in photochemistry due to its limitations in mass transfer and photon propagation.

Nonetheless, there are numerous successful examples of both homogeneously and heterogeneously operating recyclable transition metal-based photocatalysts. Using iridium and ruthenium as the basis, in this chapter, a brief overview is given over various synthesis and recycling strategies and reactions performed. Since a crucial criterion to function as a recyclable catalyst is that the reactivity is still given after several successive reaction runs, this will also be considered.

1.1. Homogeneously operating recyclable transition metal-based photocatalysts

Due to their high catalytic activity and simultaneous high cost, a lot of effort was invested in the development of recyclable versions of homogeneously operating iridium- and ruthenium-based photocatalysts and to date, various strategies have been established. As this usually means to properly functionalize an existing catalyst, it is associated with a time-consuming synthetical effort.

An easy to implement and therefore very appealing recycling approach, however, was presented by Rueping *et al.*[6] Taking advantage of the solubility of the positively charged complex $[Ir(ppy)_2(bpy)]^+$ (**6**) in ionic liquids, they conceived a process to perform visible light-mediated *E/Z*-isomerizations of *trans*-stilbene (**24**) and derivatives in a two-phase system (Scheme 8). Without the need of pre-functionalization, $[Ir(ppy)_2(bpy)]PF_6$ was dissolved in bmim/BF_4, whereas *trans*-stilbene (**24**) was accordingly dissolved in toluene. Owing to the two-phase nature, the catalyst-containing layer could easily be separated after a reaction and thus, reused for eight consecutive runs without any loss in reactivity. This system was improved even further by transferring it to a two-phase flow system with continuous recycling. For this, the substrates were dissolved in *n*-pentane and the catalyst in bmim/BF_4 and both phases were passed through a microreactor by two individual pumps. The layers were continuously separated, and, whereas the catalyst was directly reused, the product was collected separately. With this, quantitative conversions on a 1.8 g scale could be achieved at flowrates up to 10-20 mL/h. However, as attractive as this system is, it is only suitable for substrates soluble, and reactions proceeding in non-polar solvents such as pentane or toluene which drastically limits its applicability.

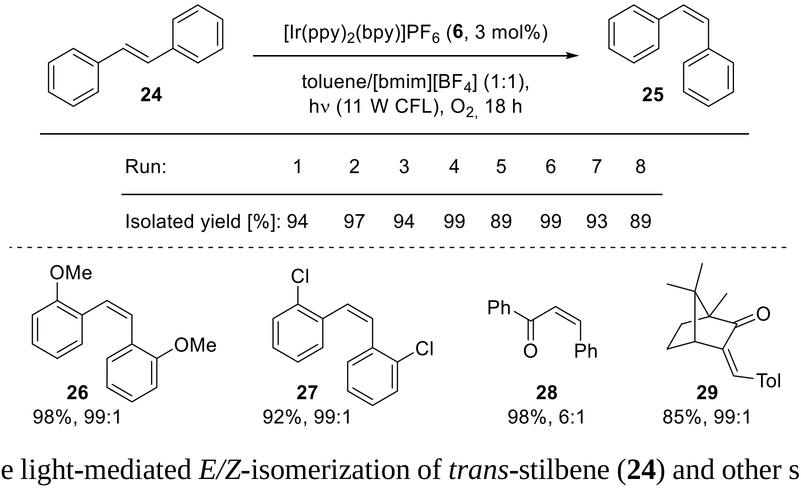

Run:	1	2	3	4	5	6	7	8
Isolated yield [%]:	94	97	94	99	89	99	93	89

Scheme 8: Visible light-mediated *E/Z*-isomerization of *trans*-stilbene (**24**) and other selected examples with their respective recovery rate in [%] and *Z/E* ratios after chromatographic purification.

Another method that has emerged as a very common and appealing strategy is to tag a photosensitizer to soluble polymers.[7] Catalysts modified in this way provide homogeneity, wherefore the light penetration is not disturbed, and, since the polarity is altered, they simultaneously allow for exclusive recycling methods which are presented in the following.

The first soluble polymer-tagged photocatalyst was established by Bergbreiter *et al*.[8] A $[Ru(bpy)_3]^{2+}$ complex was equipped with up to six polyisobutylene (PIB) chains and, although the attachment of PIB onto the bpy-ligands was unselective and led therefore also to unevenly substituted complexes, the behavior in solutions was similarly for all of them. For clarity, no differentiation is made between the derivatives and they are referred to as $[Ru(PIB\text{-}bpy)_3]Cl_2$ (**30**). Thanks to its high lipophilicity and the resulting solubility in non-polar solvents, the catalyst could be employed to promote free radical polymerizations of acrylates **32** in heptane (Scheme 9). The products **33** precipitate and can easily be separated by filtration while the catalyst remains in the heptane phase. This allows for a reusage by simply adding fresh starting material. The effectiveness of this method was reflected in the low Ru contamination of the products of 1.9 ppm, which corresponds to less than 1% Ru leaching. In contrast, performing the reaction with $[Ru(bpy)_3]^{2+}$ in heptane/DMF and subsequent precipitation of product by adding excess MeOH led to a contamination of 48.4 ppm, corresponding to 30% Ru leaching. However, already in the third consecutive run, the yield dropped from 82 to 70%, which was addressed to the degradation of the complex.

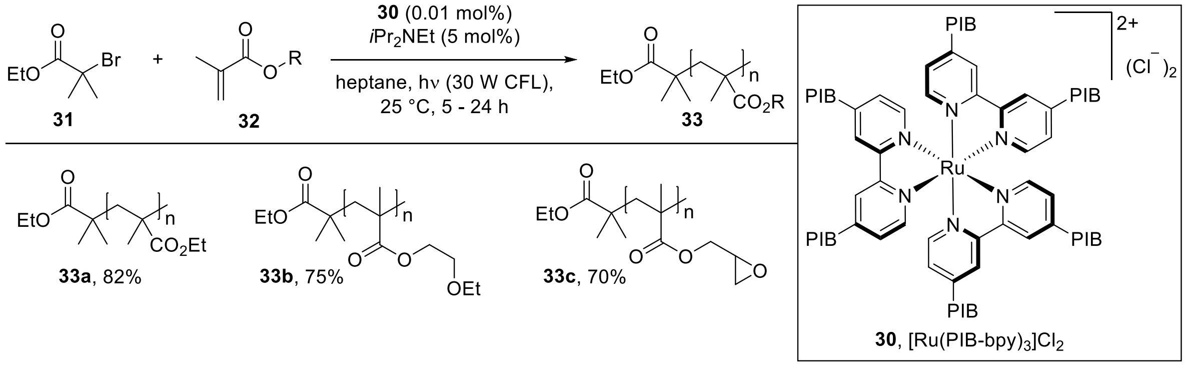

Scheme 9: Free radical polymerizations catalyzed by $[Ru(PIB\text{-}bpy)_3]Cl_2$ (**30**).

However, the catalyst **30** with only one PIB chain per ligand, which proved to be sufficient for it to be soluble in heptane and ensure phase-selectivity, was later used for more challenging reactions in the same group (Scheme 10).[9] Contrary to the free radical polymerizations, precipitation of products and therefore a solid/liquid separation was no longer conceivable. Instead, they made use of a DCM/MeCN solvent mixture to ensure the solubility of both the catalyst and substrates in a single phase. After the reaction, the solvents were evaporated, and the catalyst was recovered *via* a liquid/liquid extraction from heptane and acetonitrile. This procedure was applied to the reactions depicted in Scheme 10. Although the oxidative C-C bond cleavage of **34** was originally run in pure acetonitrile,[10] this method functioned very well and showed as excellent catalytic activity as pristine [Ru(bpy)$_3$]Cl$_2$ (Scheme 10, a). Moreover, outstanding recyclability was evident, and the catalyst could be reused for at least five runs without any loss in activity. To avoid the extraction step, a heptane/THF/MeCN (1:4:1, v/v/v) solvent mixture was successfully employed, which has the advantage that after adding water the phases separate and the catalyst containing heptane-phase could be simply separated and directly reused in a following run. Furthermore, a [2 + 2] cycloaddition of **36** established by Yoon *et al.*[11] was performed (b). Even though high conversions were obtained, due to the change in solvent polarity by using DCM/MeCN (9:1) instead of pure MeCN, the product **37a** was afforded in an average of 42% yield within 5 runs, but also the undesired reductive cyclization product **37b** was obtained in an average of 39% per cycle. However, the recyclability was satisfactory showing no loss in activity within five consecutive runs. Attempts towards a third reaction, i.e. a conversion of alcohol **38** to bromide **39** remained unsuccessful, as the transformation suffered from the change in polarity, thus exhibiting the limitations of this system (c). It should be further noted that the leaching of Ru of the well-performing reactions was determined to be roughly 1% in the third runs, respectively.

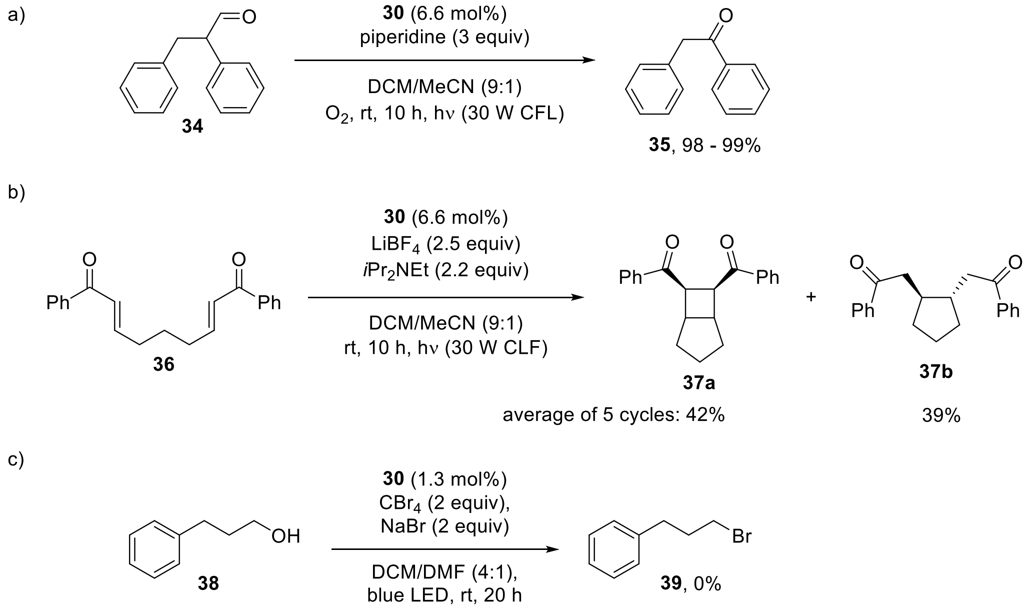
a)
O
34
30 (6.6 mol%)
piperidine (3 equiv)
DCM/MeCN (9:1)
O2, rt, 10 h, hν (30 W CFL)
O
35, 98 - 99%
b)
O
Ph
O
Ph
36
30 (6.6 mol%)
LiBF4 (2.5 equiv)
iPr2NEt (2.2 equiv)
DCM/MeCN (9:1)
rt, 10 h, hν (30 W CLF)
O
O
Ph
Ph
37a
+
O
O
Ph
Ph
37b
average of 5 cycles: 42%
39%
c)
OH
38
30 (1.3 mol%)
CBr4 (2 equiv),
NaBr (2 equiv)
DCM/DMF (4:1),
blue LED, rt, 20 h
Br
39, 0%

Scheme 10: Application of [Ru(PIB-bpy)$_3$]Cl$_2$ (**30**) in various visible light-mediated reactions.

Reiser *et al*. followed this concept of using soluble polymers and established the first recyclable version of a homogeneously operating *fac*-Ir(ppy)$_3$ by tagging one of its ligands with a PIB chain, forming *fac*-Ir(PIB-ppy)(ppy)$_2$ (**40**, Scheme 11).[12] Instead of precipitating reaction products or using homogeneous reaction mixtures and a subsequent liquid/liquid extraction to recover the catalyst as in the aforementioned examples, the hydrophobic catalyst was dissolved in heptane, whereas the reactants were placed in acetonitrile. Since these two solvents form a thermomorphic system, they show full miscibility at elevated temperatures (85 – 90 °C), however, they separate again after cooling down. This strategy allows conducting reactions in only one phase while simultaneously ensure easy separation of the catalyst after a reaction. With this, deiodation of **41** and deiodation/cyclization reactions of **43** were performed, while the catalyst was recycled for at least ten times without any greater loss in reactivity (Scheme 11, a and b). Moreover, a flow system with continuous catalyst recycling was invented to perform an *E/Z*-isomerization of **45** (c). Once again, the catalyst performed remarkably well allowing for effective reuse for at least 30 times without any loss in reactivity and hardly any leaching of Ir into the reaction mixture. Not only is this reaction feasible in a one-phase system at elevated temperatures, but also without heating and, therefore, in a two-phase fashion. This is especially valuable for reactions suffering from high temperatures. In the first cycle, though, the iridium leaching was determined to be 2.6%, however, it declined in course of further runs to below 0.1%. This comparable high value in the beginning was addressed to a small amount of shorter PIB chains present in their PIB source Glissopal® and the accompanying lower lipophilicity of the resulting complexes.

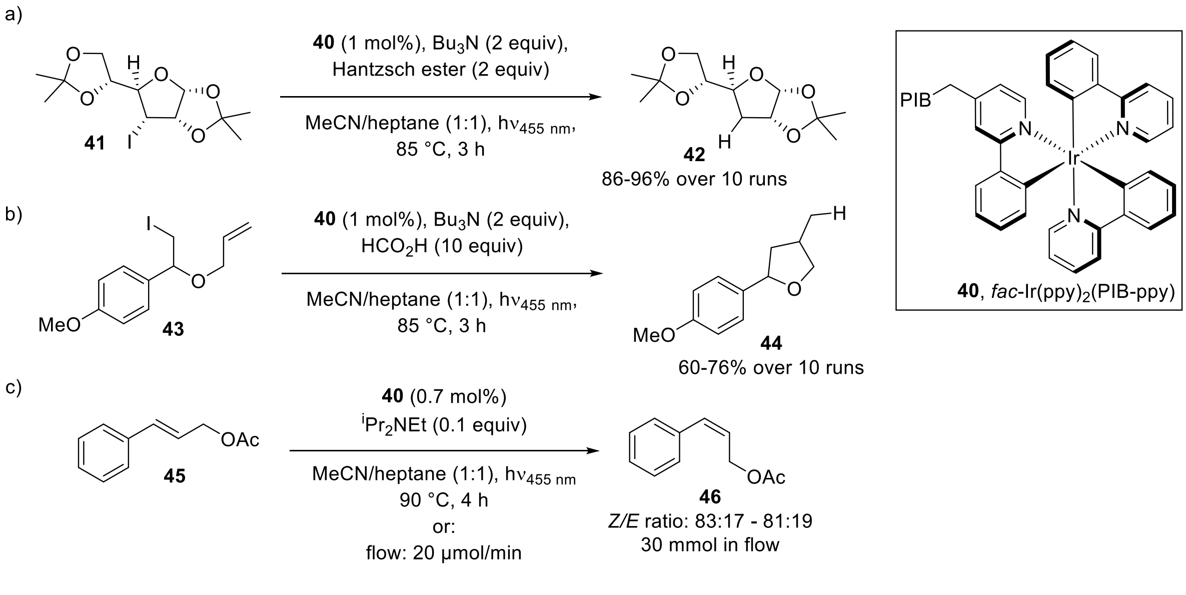
a)
41
40 (1 mol%), Bu3N (2 equiv),
Hantzsch ester (2 equiv)
MeCN/heptane (1:1), hν455 nm,
85 °C, 3 h
42
86-96% over 10 runs
b)
43
40 (1 mol%), Bu3N (2 equiv),
HCO2H (10 equiv)
MeCN/heptane (1:1), hν455 nm,
85 °C, 3 h
44
60-76% over 10 runs
c)
45
40 (0.7 mol%)
iPr2NEt (0.1 equiv)
MeCN/heptane (1:1), hν455 nm
90 °C, 4 h
or:
flow: 20 µmol/min
46
Z/E ratio: 83:17 - 81:19
30 mmol in flow
PIB
Ir
40, fac-Ir(ppy)2(PIB-ppy)

Scheme 11: Application of PIB tagged iridium catalyst **40** in various visible light-mediated reactions.

Considering previous examples of photocatalysts tagged with a soluble polymer as a basis, the group of Duan presented both a recyclable polyalkylated $[Ru(bpy)_3]^{2+}$ [13] as well as a recyclable polyalkylated *fac*-$Ir(ppy)_3$ complex.[14] They aimed to circumvent the issues arising from PIB, such as the unevenly distributed chain length and the accompanied catalyst leaching, or the partially unselective substitution. Therefore, catalysts with a well-defined and consistent structure were established. The dinonylmethyl-substituted catalyst $[Ru((DNM)_2bpy)_3]^{2+}$ (**47**) was effectively employed for perfluoromethylations of various coumarins **48** using a 1:1 mixture of DCM/MeCN as solvent (Scheme 12). However, the reaction time had to be increased threefold to obtain the same yields as with non-immobilized $[Ru(bpy)_3]^{2+}$. Through recovery by liquid/liquid extraction from heptane/MeCN, the catalyst could be reused with evident recyclability as the yield for **50d** only dropped from 66% in the first to 51% in the sixth run. After the last cycle, however, only 57% of the catalyst could be recovered, as determined by ICP measurement.

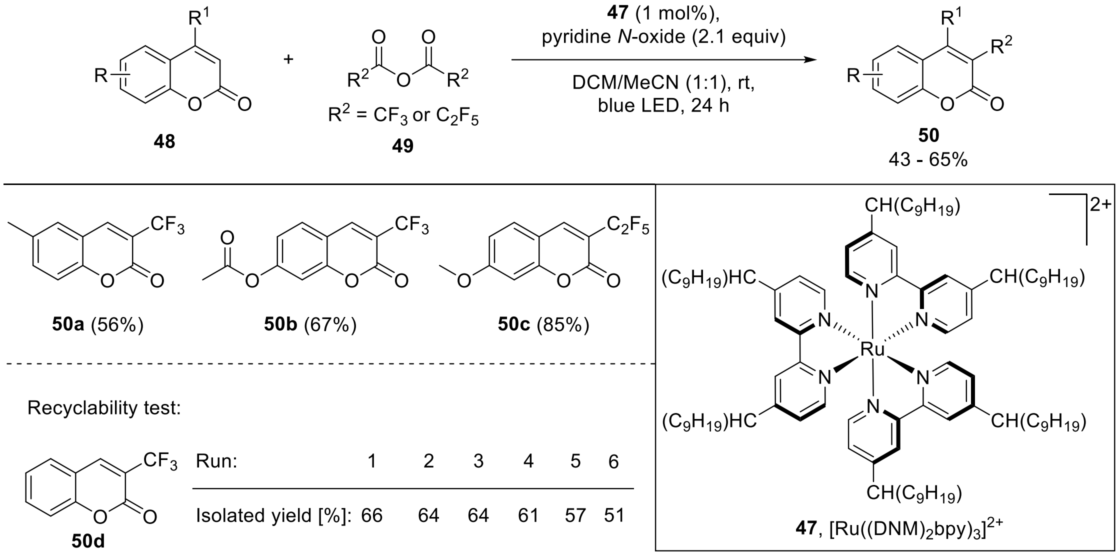
R¹
R
O
O
48
+
O O
R² O R²
R² = CF₃ or C₂F₅
49
47 (1 mol%),
pyridine N-oxide (2.1 equiv)
DCM/MeCN (1:1), rt,
blue LED, 24 h
R¹
R²
R
O
O
50
43 - 65%
CF₃
50a (56%)
CF₃
50b (67%)
C₂F₅
50c (85%)
Recyclability test:
CF₃
50d
CH(C₉H₁₉)
2+
(C₉H₁₉)HC
CH(C₉H₁₉)
N
Ru
(C₉H₁₉)HC
CH(C₉H₁₉)
CH(C₉H₁₉)
47, [Ru((DNM)₂bpy)₃]²⁺

Run:	1	2	3	4	5	6
Isolated yield [%]:	66	64	64	61	57	51

Scheme 12: Dinonylmethyl-substituted $[Ru((DNM)_2bpy)_3]^{2+}$ (**47**) and its application for visible light-mediated perfluoroalkylations of various coumarins **48** and recyclability test.

The heptadecanyl-alkylated *fac*-$Ir(hdppy)_3$ (**51**) on the other hand was employed for the synthesis of 3-trifluoromethyl-4-phenyl coumarins **55** and 3-difluoroacetyl-4-phenyl coumarins **56** (Scheme 13).[14] Taking advantage of the fact that DMF and heptane form a thermomorphic solvent system, they followed the same recycling strategy as conceived from Reiser *et al.*[12] which was presented before. Again, excellent recyclability was achieved and no decrease in activity was observed within five consecutive runs for both trifluoromethyl- and difluoroacetyl-substituted coumarins **55a** and **56a**. The recovered catalyst in the last cycles was determined to be 79% and 83%, respectively.

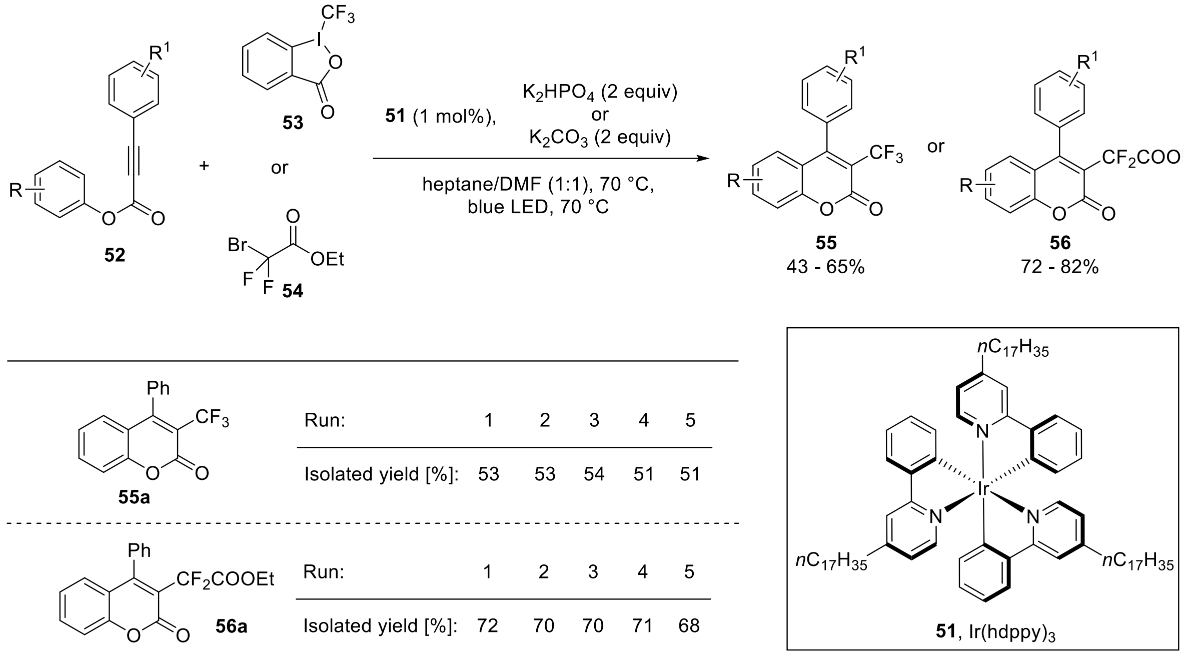

Run:	1	2	3	4	5
Isolated yield [%]:	53	53	54	51	51

Run:	1	2	3	4	5
Isolated yield [%]:	72	70	70	71	68

Scheme 13: Application of polyalkylated *fac*-Ir(hdppy)$_3$ (**51**) for visible light-mediated coumarin-derivative synthesis and its recyclability performance.

In contrast to all previously presented recycling strategies, a different approach was followed by Kappe *et al.*[15] whose group merged photoredox chemistry with organic solvent nanofiltration. More precisely, several [Ru(bpy)$_3$]$^{2+}$ complexes (**1**) were anchored to a 2nd generation PAMAM dendrimer (**64**). Therefore, one ligand of **1** was equipped with an aldehyde functionalization and thus linked to one of the dendrimers 16 terminal amino groups (Scheme 14). This led to dendrimer units with an average of 14.7 ruthenium atoms (determined by ICP). Thanks to this macromolecular photosensitizer **57**, a continuous catalyst recycling in a flow-setup through a size-exclusion membrane - as these are only permeable for the products formed - could be realized. The catalytic performance of G2-PAMAM(Ru)$_{16}$ with chloride or hexafluorophosphate as counter anion, respectively, was tested utilizing an Appel reaction (Scheme 14, a), a reductive opening of chalcone epoxide **60** (b) and a reduction of azide **62** (c). Thanks to its solubility in acetonitrile and acetone/DMF, it showed activities as excellent as the non-immobilized parent complex **1**. However, the recycling proved to be challenging as several problems occurred. These were for the continuous-flow Appel reaction that pressures beyond the limits of the membrane should have been applied. This was most likely caused by the too low solubility of the catalyst in the solvent mixture and therefore, it partially stuck to the membrane which decreased the catalytic activity. The reductive opening of the chalcone epoxide **60** as well as the azide reduction towards **61**, on the other hand, make use of an excess of formic acid, which degraded the dendrimeric structure and a drop of 70% in yield was observed already after the second run. Only when they switched to hydrazine hydrate as a reducing agent for the azide reduction this issue could be circumvented (c, lower pathway). Although the yield decreased from 99% to about 50% when changing the conditions, excellent recyclability is given and after five runs no decrease in catalytic activity was observed.

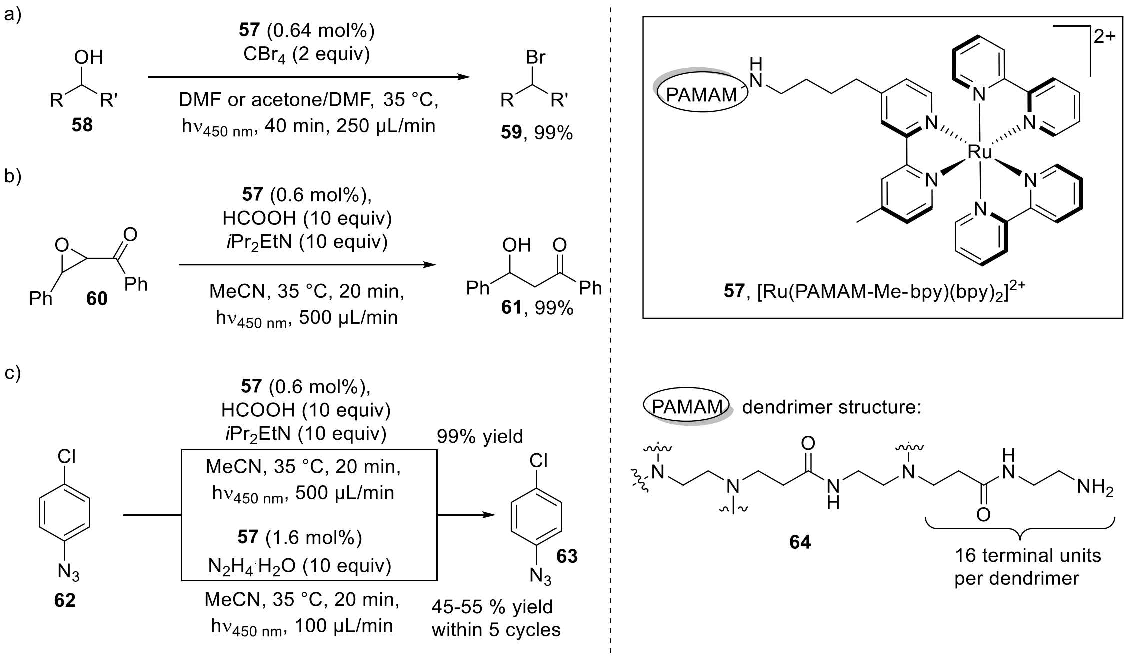
a)
OH
R R'
58
57 (0.64 mol%)
CBr4 (2 equiv)
DMF or acetone/DMF, 35 °C,
hν450 nm, 40 min, 250 µL/min
Br
R R'
59, 99%
b)
O
O
Ph
Ph
60
57 (0.6 mol%),
HCOOH (10 equiv)
iPr2EtN (10 equiv)
MeCN, 35 °C, 20 min,
hν450 nm, 500 µL/min
OH O
Ph Ph
61, 99%
c)
Cl
N3
62
57 (0.6 mol%),
HCOOH (10 equiv)
iPr2EtN (10 equiv)
MeCN, 35 °C, 20 min,
hν450 nm, 500 µL/min
57 (1.6 mol%)
N2H4·H2O (10 equiv)
MeCN, 35 °C, 20 min,
hν450 nm, 100 µL/min
99% yield
Cl
N3
63
45-55 % yield
within 5 cycles
PAMAM
H
N
N
N
N
N
N
N
Ru
2+
57, [Ru(PAMAM-Me-bpy)(bpy)2]2+
PAMAM dendrimer structure:
N
N
O
N
H
N
H
N
O
NH2
64
16 terminal units
per dendrimer

Scheme 14: $[Ru(bpy)_3]^{2+}$ attached on PAMAM and its application as recyclable photocatalyst *via* size exclusion.

1.2. Heterogeneously operating recyclable transition metal-based photocatalysts

Although homogeneously operating catalysts have the advantage of higher activity, a lot of effort has to be put into the development of proper recycling strategies. Heterogeneous photocatalysts, on the other hand, fight against mass transfer resistance and photon propagation hindrance. Nonetheless, they offer a more convincing recovery technique through simple filtration or centrifugation. This makes them particularly valuable for industrial applications and more and more examples are currently sprouting, some of which are presented hereafter.

Next to the incorporation of iridium and ruthenium-based photocatalysts into metal-organic frameworks (MOFs), which has experienced huge upsurge recently,[16] the most predominant technique is to link the photosensitizer to solid supports or insoluble polymeric resins. This idea already arose in the year 1980 when Spiro *et al.* were able to coat an n-type SnO_2 grafted glass with roughly 1000 layers of a -$SiCl_3$ functionalized $[Ru(bpy)_3]^{2+}$ complex.[17] As photoredox chemistry was not yet established at that time, only photoelectrochemical experiments were performed. Thenceforth, other examples followed, however, were only considered lately to be employed as recyclable photoredox catalyst. One of the first exemplars was presented by Huang *et al.*[18] In the course of their studies, one ligand of $[Ru(bpy)_3]^{2+}$ (**1**) was equipped with an aldehyde to be attached to amine-functionalized mesoporous silica nanoparticles affording a ruthenium loading of 0.11 mmol/g. With this, an easy oxidation of thioanisole was conducted, resulting in 89% conversion compared to 98% with the non-immobilized parent complex **1**. A recovery through filtration and reusage of the catalyst revealed only a slight decline in activity over five consecutive runs, inasmuch as the conversion dropped to 82%. Unfortunately, the only information about the leaching given is that ‘it can be ignored’.

Similar to that, a $[Ru(bpy)_3]^{2+}$ photocatalyst with terminal -$Si(OH)_3$ groups was covalently attached to mesoporous organosilica to be used for water oxidation in presence of IrO_x and $S_2O_8^{2-}$.[19] However, no further experiments were performed.

Yet another silica-bound ruthenium complex was introduced by Francis *et al.*[20] Likewise, commercially available amine-functionalized silica beads were used as solid support for $[Ru(bpy)_3]^{2+}$ complexes decorated with carboxylic acids. With this easy to prepare catalyst **65**, intramolecular visible light-mediated cyclizations of **66** were performed (Scheme 15). Noteworthy, the heterogeneous catalyst afforded thanks to a loading of 0.033 mmol/g ruthenium the same yield as the non-immobilized version. Being easily recovered by vacuum filtration, it could be reused for at least eight consecutive reaction runs towards **67a** without any loss in activity. Moreover, this way the purification of products was facilitated, as precipitation from water/ethanol proved to be sufficient and no subsequent column chromatography was needed.

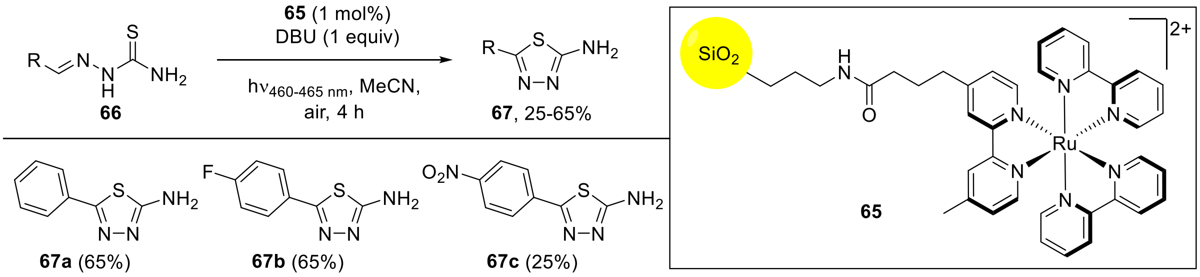

Scheme 15: Application of silica-bound photocatalyst **65** for intramolecular cyclizations.

Following a slightly different approach, Bhaumik and Zhao *et al*. presented in the same year another Ru^{II} complex incorporated into silica.[21] This was achieved by equipping $[Ru(bpy)_3]^{2+}$ with six terminal -$Si(OEt)_3$ groups and reacting them with TEOS and CTAB. Having a somewhat higher loading of 0.0495 mmol/g, this catalyst performed well for various transformations, such as dehalogenations of alkyl halides, or Appel reactions.

Following up on this idea, in the course of his Ph.D. thesis, P. Kohls conceived a silica-bound iridium catalyst.[22] This was realized through click reactions between azide-functionalized silica and $[Ir(ppy)_2(dtbbpy)]PF_6$ equipped with a terminal alkyne. Although substitution of the non-immobilized catalyst with the silica-bound version **68** proved to be very promising for the deoxygenation reaction performed, the recyclability was poor and the yield dropped from 92 to 29% already in the second run (Scheme 16). This might be addressed to a catalyst decomposition, as through filtration only 72% of the employed particles could be recovered after the first cycle.

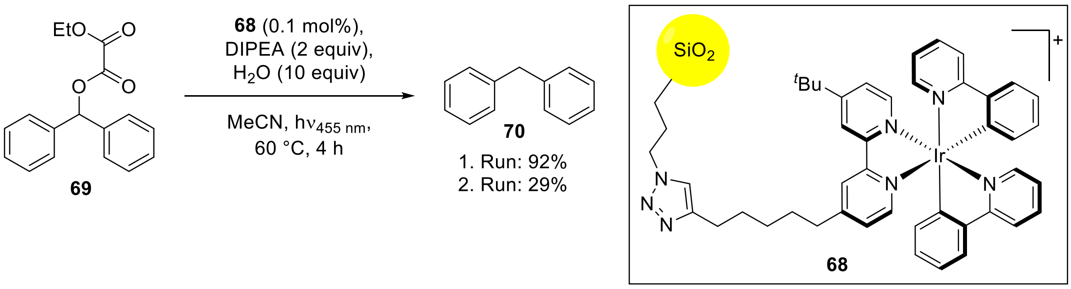

Scheme 16: Silica-bound Ir^{III} catalyst **68** and its application for a deoxygenation reaction.

The same Ir^{III} complex tagged with a vinyl group was only lately anchored to another silica support, i.e. thiol-functionalized mesocellular silica foams (MCFs), *via* a thiol-ene reaction.[23] Thanks to the 3D pore structure and the high transparency, the resulting $[Ir(ppy)_2(bpy)$-

MCFs] with a loading of 0.14 mmol/g, performed as well as its homogeneous parent complex **6**, affording almost quantitative product formation for the reductive depolymerization of oxidized lignin compounds **71** (Scheme 17). Besides, after a reaction, the catalyst was allowed to settle down and the supernatant was decanted. By adding fresh starting materials, a consecutive run could directly be performed. This way, six consecutive cycles were conducted with scarcely any loss in activity and only less leaching (the loading of the particles dropped to 0.13 mmol/g after the recyclability test).

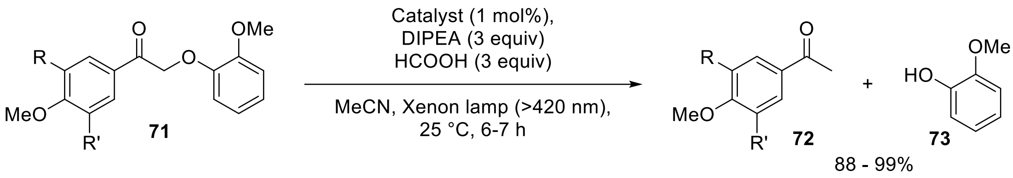

Scheme 17: Depolymerization of oxidized lignin β-O-4 model compounds **71** with silica-bound iridium catalyst.

A special kind of solid support offers TiO_2 which was targeted as such by Jain *et al.*[24] Nanocrystalline TiO_2 grafted with hydroxy groups served as an anchor for a Ru^{II} polyazine complex to perform visible light-mediated oxidative cyanations of tertiary amines **75** (Scheme 18). It has not only been established that after filtration, the catalyst **74** can be reused for at least eight times without a significant loss in activity, but also that the TiO_2 proved to have a synergistic effect in this transformation. This could be demonstrated by control experiments towards **76a**, since solely TiO_2 as catalyst afforded no product at all and merely the non-immobilized Ru^{II} polyazine gave less yield (90%) than the combination of both (96%). Throughout moderate to excellent yields were obtained for various tertiary amines and ICP measurements revealed no detectable leaching of ruthenium evincing the robustness of the particles.

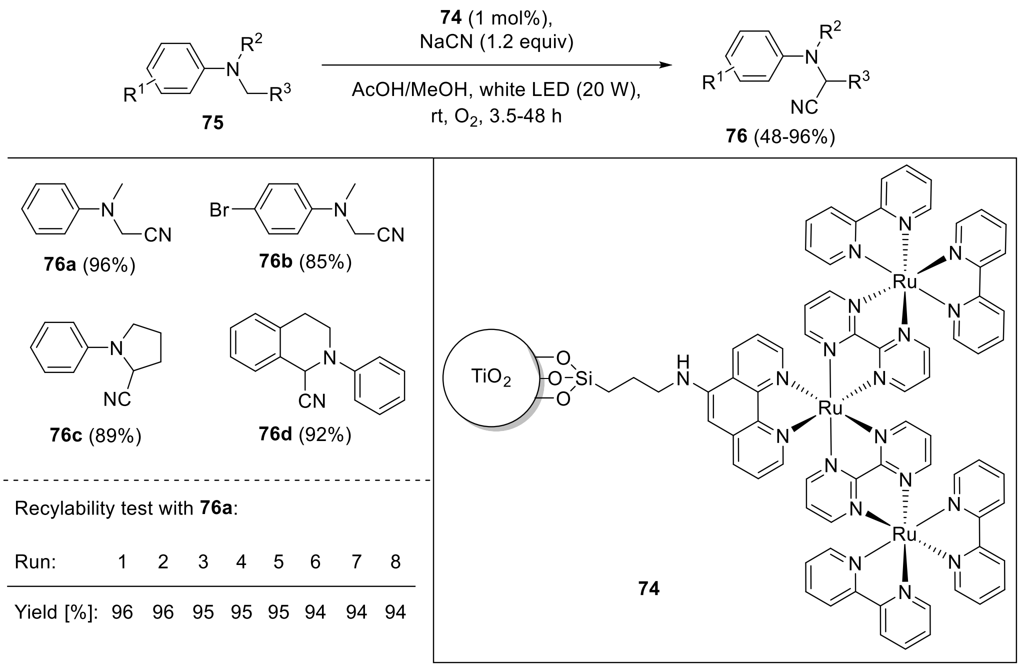

Recylability test with **76a**:

Run:	1	2	3	4	5	6	7	8
Yield [%]:	96	96	95	95	95	94	94	94

Scheme 18: Visible light-mediated cyanation catalyzed by TiO_2 immobilized ruthenium polyazine **74**.

An unusual procedure towards a solid support is the immobilization of an Ir^{III} complex on pyridine-modified nanoporous polydivinylbenzene (PDVB), established by Shen *et al.*[25] Therefore, PDVB, which was obtained from divinylbenzene and various amounts of 4-vinylpyridine, was chelated with $[Ir(ppy)_2Cl]_2$ to generate heterogeneous catalysts **77** with iridium contents up to 7.54 wt%. Its catalytic activity was tested on cyclization reactions between *N*,*N*-dimethylanilines **78** and maleimides **79** (Scheme 19, a). As the results were comparable to those with $[Ir(ppy)_2(dtbbpy)]PF_6$ (**6**),[26] and no leaching of iridium was detectable by ICP, the catalyst was recovered by centrifugation and submitted to various consecutive reaction runs. Only a slight decline in yield was obtained within four cycles. Recently, this catalyst was also successfully applied in the same group for other visible light-mediated reactions, such as Beckmann rearrangements of **81** (b), conversion of aldoximes **83** to nitriles (c) or the reaction of carboxylic acids towards their corresponding anhydrides.[27]

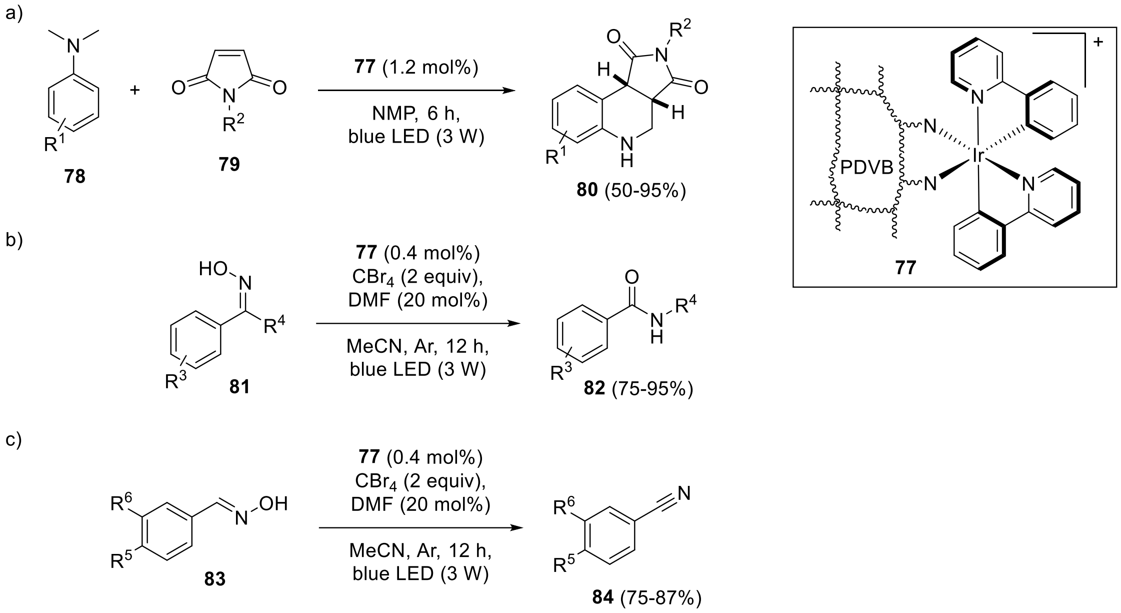

Scheme 19: Application of PDVB anchored iridium photocatalyst **77** in various visible light-mediated reactions.

Besides the immobilization strategies presented before, heterogeneous catalysts can not only be obtained *via* post-grafting of pre-functionalized transition-metal based complexes but also through polymerization and cross-linking. An effective method for heterogenization of active metal centers is directing to porous organic polymers,[28] and is still a great deal of interest for ruthenium and iridium based photocatalysts as new publications are emerging.[29] One of the first examples was established by Lin *et al*. in 2011.[30] *Via* alkyne trimerization reactions employing modified $[Ru(bpy)_3]^{2+}$ or $[Ir(ppy)_2(bpy)]^{+}$ as fundamental building blocks, porous cross-linked polymers (PCPs) **87** and **88** were obtained (Scheme 20). They show high thermal and chemical stability and exhibit great surface areas in the range of 1348 and 1547 m^2/g. Despite the low catalyst loadings of 4.5 and 2.2 wt% for Ir-PCP (**88**) and Ru-PCP (**87**), respectively, their catalytic activity is exceptional for photocatalytic aza-Henry reactions of *N*-aryltetrahydroisoquinolines **89** affording the same or even higher yields compared to their homogeneous versions. Through filtration, the catalyst was recovered and could be reused for at least five consecutive runs without loss in activity and any leaching of Ir or Ru. Moreover, Ru-PCP (**87**) was successfully employed for other reactions such as the α-arylation of bromomalonate and the oxyamination of 3-phenylpropanal.[30]

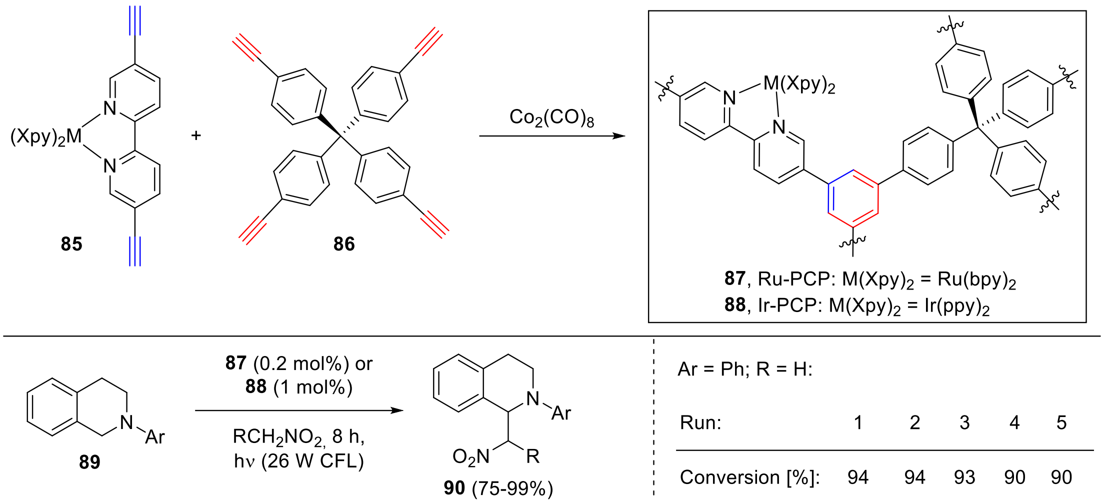

Scheme 20: Cross-linkage of ruthenium and iridium complexes and their application in photochemical aza-Henry reactions.

As the low catalyst loadings may be disadvantageous, the same group further improved this protocol and established a cross-linked polymer from a modified Ru^{II} complex to obtain loadings as high as 96 wt%.[31] This could be realized by omitting the crosslinker **86** and installing only two bpy ligands in the Ru^{II} complex instead, with respectively two alkynyl groups at 4 and 4'- or 5 and 5'- position. *Via* oxidative Eglinton coupling reactions, the resulting polymers exhibited surface areas of 15 or 198 m^2/g, respectively. Despite the almost non-porous nature, both polymers performed well in an aza-Henry reaction between various *N*-aryltetrahydroisoquinolines **89** and nitromethane as well as aerobic oxidative coupling reactions of amines and photocatalytic dehalogenation of benzyl bromoacetate. Since even non-porous cross-linked polymers with surface areas between 2.7 and 2.9 m^2/g were highly reactive for visible light-mediated reactions,[32] they proposed a light-harvesting mechanism. That means that Ru chromophores inside the polymer can collect the photon energy by excitation of the ^{3}MLCT state which subsequently migrates through Dexter triplet to triplet energy transfer to the surface, where the photochemical transformation takes place at.

Another strategy towards cross-linked polymers to heterogenize an Ir^{III} complex was conceived by Kobayashi *et al.*[33] An [Ir(ppy)$_2$(dtbbpy)]PF$_6$ photocatalyst, whose ppy-ligands were equipped with one vinyl group each (**91**), was brought to a polymerization reaction with acrylate **93** and cross-linker **92** (Scheme 21). As a first test reaction, i.e. a cross-dehydrogenative coupling (CDC) of *N*-phenyltetrahydroisoquinoline with diethyl phosphite, revealed an iridium leaching of 0.9%, the particles **94** were re-submitted to the same polymerization reaction. Although the additional polymer-layer slightly decreased the Ir loading and thus led to prolonged reaction times, the leaching could be diminished to 0.3%. Having the optimized catalyst in hand, the substrate scope was extended by submitting various phosphites or phosphine oxides **95** to the CDC reaction. The particles were found to be successfully recyclable for at least four times having only slight deterioration in product formation towards **96a**.

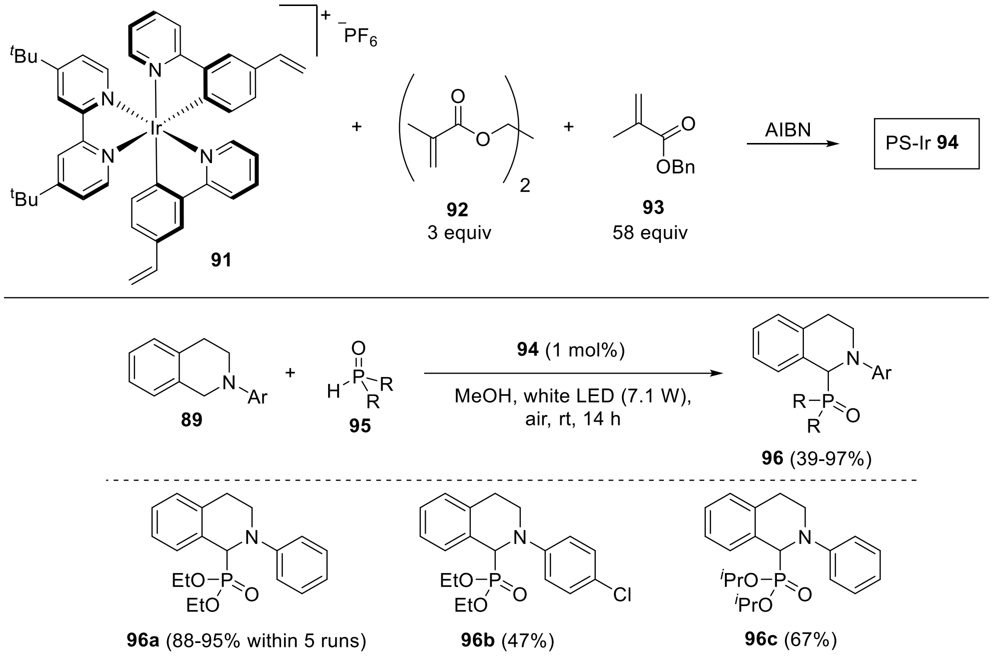

Scheme 21: Heterogenization of iridium complex **91** *via* polymerization and its application for visible light-mediated aza-Henry reactions.

Only recently, Han *et al.* developed cross-linked polymers bearing [Ir(ppy)$_2$(bpy)]$^+$ moieties *via* oxidative coupling reactions, comprising sizes of 100 – 200 nm, surface areas between 76 and 97 m^2/g, and iridium contents up to 17 wt%.[34] A comparison between the cationic polycarbazole networks with (**98**) and without CF$_3$ (**99**) substitution revealed that the fluorinated moiety is beneficial towards photochemical reactions and affords up to 28% higher yields (Scheme 22). This was tested for photocatalytic oxidation of sulfides **100** (a), hydroxylation of arylboronic acids **103** (b) and aza-Henry reactions between *N*-aryltetrahydroisoquinolines **89** and various nucleophiles. The catalyst **98** was easily recovered *via* centrifugation and reused in a fresh reaction solution with only a slight decrease in catalytic activity, as the conversion for reaction (a) dropped continuously from 99 to 90% within five runs.

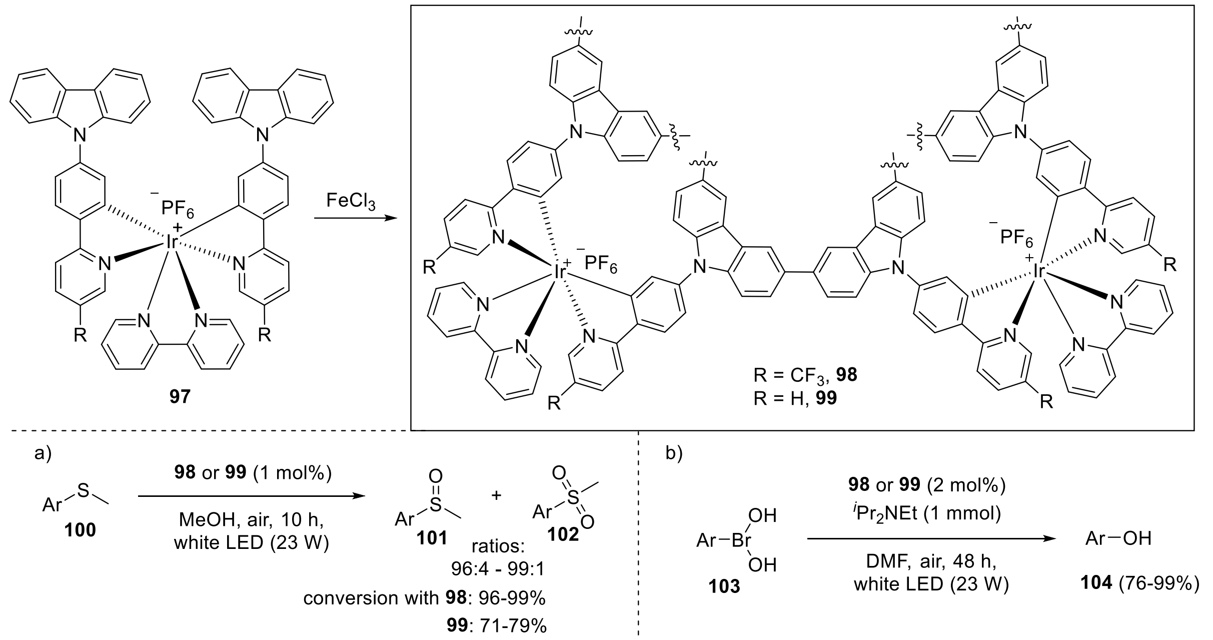
97
FeCl3
PF6
Ir
R = CF3, 98
R = H, 99
a)
98 or 99 (1 mol%)
MeOH, air, 10 h,
white LED (23 W)
100
101
102
ratios:
96:4 - 99:1
conversion with 98: 96-99%
99: 71-79%
b)
98 or 99 (2 mol%)
iPr2NEt (1 mmol)
DMF, air, 48 h,
white LED (23 W)
103
Ar−OH
104 (76-99%)

Scheme 22: Synthesis of heterogeneous iridium complexes **98** and **99** *via* cross-linking and application as catalyst in visible light-mediated reactions.

2. Immobilization of transition metal-based photocatalysts on Nafion

2.1. Introduction

As discussed in the previous chapter, transition metal catalysts based on iridium or ruthenium are usually very expensive and it is therefore highly desirable to develop recyclable versions of these. One fact, however, withheld before: due to its ionic nature, $[Ru(bpy)_3]Cl_2$ (**1**) offers a special kind of immobilization without the need of previous functionalization, i.e. the non-covalent attachment on solid supports *via* electrostatic interactions. Following this idea, in 2011 Choi *et al.* used Nafion-coated silica as solid support.[35] They have demonstrated that Nafion, a perfluoronic scaffold with terminal sulfonic acid groups, is a beneficial support compared to silica itself since the electrostatic attraction of sulfonate groups is superior. The immobilized catalyst is stable in most commonly used organic solvents, only in DMF minor leaching of ruthenium was observed. To prove the catalytic performance, visible light-driven free radical polymerizations of various acrylates were performed. Through recovery by centrifugation, the particles could be reused for at least five cycles without any greater loss in activity. Amara and coworkers found, that for photochemical oxidations *via* singlet oxygen, $[Ru(bpy)_3]Cl_2$ which is electrostatically immobilized on silica particles increases the reactivity almost ten times compared to its pristine parent complex **1**.[36] This was addressed to the so-caused localized higher concentrations of reactive species, i.e., in this case, singlet oxygen.

Based on this immobilization strategy, Li *et al.* used sulfonic acid-functionalized reduced graphene oxide as a solid support to perform visible light-mediated reductive dehalogenation reactions of 2-bromoacetophenone.[37] Again, the catalyst performed well and only a slight decrease in the activity was obtained within five consecutive runs.

In this chapter, the idea of immobilizing $[Ru(bpy)_3]Cl_2$ (**1**) on Nafion *via* electrostatic interactions to obtain an easily accessible recyclable photocatalyst was pursued further. The catalyst was tested for its stability in different solvents, followed by the conduction of various photochemically driven reactions to prove its reactivity and recyclability. Moreover, a flow-system was developed to scale reactions up, to improve the recyclability, and simultaneously decrease the reaction time.

2.2. Immobilization strategy

Already in the course of my master thesis, we started to investigate this concept using commercially available Nafion® SAC-13 (**105**) as solid support.[38] Elemental analysis and additional titration with 0.1 M NaOH of this resin revealed 0.15 mmol/g free accessible sulfonic acid groups, which therefore corresponds to the maximal possible loading of $[Ru(bpy)_3]^{2+}$ (**1**). The immobilization strategy is shown in Scheme 23. At first, Nafion (**105**) is deprotonated by treatment with 2 M NaCl to give the corresponding sodium salt **106**.[39] For the final ionic exchange, **106** is stirred with different amounts of $[Ru(bpy)_3]Cl_2$ (**1**) in various solvents to examine which combination gives both the highest loading and best incorporation.

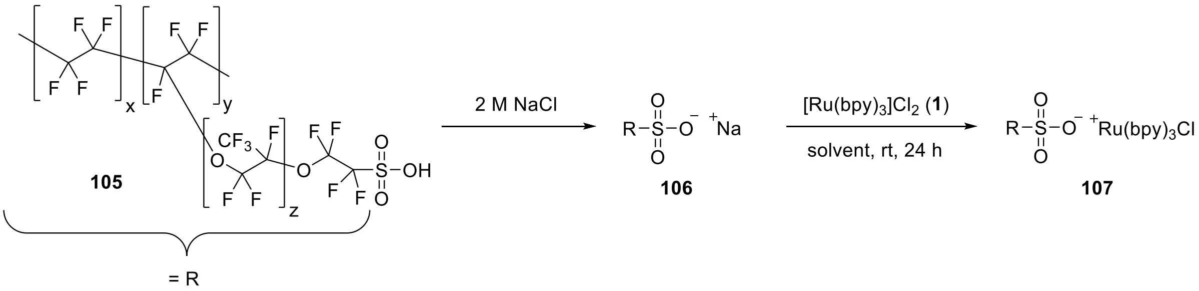

Scheme 23: Immobilization of $[Ru(bpy)_3]Cl_2$ (**1**) onto Nafion® SAC-13 (**105**).

Since in the aforementioned literature examples the immobilization was performed in aqueous media, the first approach was employing water as solvent and 2.0 equiv $[Ru(bpy)_3]Cl_2$ (**1**). With regard to the maximal possible loading, 24% of the free sulfonic acids were occupied and therefore an incorporation of 12% was achieved (Table 3, entry 1). Examination of other solvents revealed that MeCN gave the highest ruthenium loading. Although the incorporation could be increased to 85% using 0.68 equiv $[Ru(bpy)_3]Cl_2$ (**1**), the loading simultaneously decreased to 58% (entry 6). Therefore, we decided to proceed with employing 1.0 equiv of the catalyst to be immobilized, resulting in a loading of 67%, or rather 0.101 mmol/g, and an incorporation of 67% (entry 5).

Table 3: Different catalyst loadings and solvents tested for immobilization.

entry	solvent	equiv. [Ru(bpy)$_3$]Cl$_2$ [a]	loading Ru [mmol/g], (%) [b]	incorporation Ru [%] [b]
1	H_2O	2.0	0.036, (24)	12
2	MeOH	2.0	0.074, (49)	25
3[c]	DCM	2.0	0.096, (64)	32
4	MeCN	2.0	0.102, (68)	34
5		1.0	0.101, (67)	67
6		0.68	0.087, (58)	85

[a]Corresponding to 0.15 mmol/g sulfonic acid groups. [b]Determined by ICP-OES. [c] [Ru(bpy)$_3$](BF$_4$)$_2$ was used.

Having the immobilized catalyst **107** in hand, we further explored its stability in commonly used organic solvents by stirring 10 mg of the particles for 16 h at room temperature in the respective solvent. We found that the higher the dipole moment or the more polar the solvents are, the higher the leaching is into the supernatant solvent (Figure 3). Moreover, the electrostatically bound catalyst suffers when adding small amounts of strong acids such as trifluoroacetic acid yet remains unimpaired in the presence of bases like NEt_3. This is especially advantageous since the latter is often used as a sacrificial electron donor in reactions making use of the reductive quenching cycle of the catalyst.

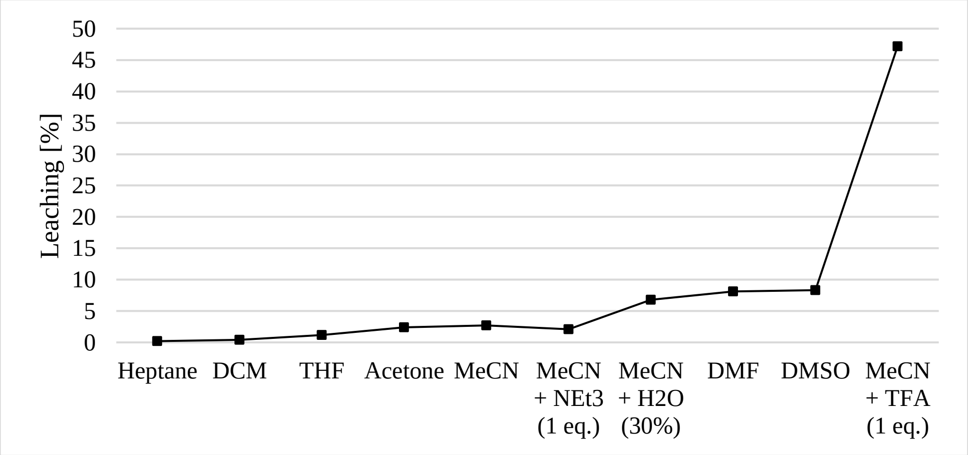

Figure 3: Leaching of ruthenium in [%] into various commonly used organic solvents.

2.3. Application of immobilized catalyst in photochemical reactions

To test the photocatalytic performance of **107**, an irreversible *E/Z*-isomerization of readily available *E*-stilbene (**24**), developed in the group of Rueping, was performed (Table 4).[6] Through an energy transfer of an excited photocatalyst, the double bond of **24** is broken, forming a biradical species **108** which is isomerized to product **25** *via* intersystem crossing. An advantage of this reaction is its feasibility in non-polar solvents like heptane or DCM. Since the particles proved to be insufficiently dispersible in heptane, we continued with DCM. To our delight employing Nafion-Ru(bpy)$_3$Cl (**107**) resulted in only a small deviation from the homogeneous catalyst **1** for the generated *Z/E*-ratio (93:7 compared to 84:16, entry 1 and 3) and only minimal leaching of ruthenium was observed (< 0.4%). Driven by these promising results the catalyst was recovered by centrifugation and reused in several consecutive runs. Within five cycles only a negligible loss in activity was obtained (entry 3 – 7).

Table 4: Photochemical *E/Z*-isomerization of stilbene **24**.

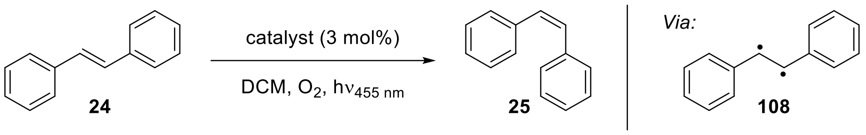

Entry	Run	Time [h]	Catalyst	Z/E ratio[a]	Leaching [%][b]
1[c]	-	8	[Ru(bpy)$_3$]Cl$_2$ (**1**)	93:7	-
2	-	16	-	15:85	-
3	1	8	Nafion-Ru(bpy)$_3$Cl (**107**)	84:16	0.33
4	2	8		88:12	0.35
5	3	8		86:14	0.31
6	4	8		89:11	0.27
7	5	8		80:20	0.30

The reactions were performed on a 0.2 mmol scale, using *E*-stilbene (**24**, 0.2 mmol, 1.0 equiv), catalyst (3.0 mol%) and DCM (2 mL). The reactions were irradiated with a blue LED (λ = 455 nm) under an oxygen atmosphere for the indicated time. [a]Ratio determined by GC-FID. [b]Leaching determined by ICP-OES. [c]Reaction was performed in MeCN.

To further explore the potential of the immobilized catalyst **107**, an ATRA reaction between hexenol **109** and diethyl bromomalonate **110** was conducted (Scheme 24).[40] Since no byproducts are formed, such transformations captivate through their excellent atom economy. Contrary to the photochemical isomerization of stilbene, this conversion is not triggered *via* an energy transfer but rather a single electron transfer (SET) of the photocatalyst promotes the reaction by exploiting its oxidative quenching cycle. Upon excitation with visible light, the photocatalyst can directly transfer a single electron to the bromomalonate **110** causing a mesolysis of the C-Br bond towards the carbon-centered radical **112** and bromide. The former subsequently undergoes addition to hexenol **109**. The so caused intermediate **113** is oxidized to the carbocation **114** which is nucleophilically attacked by the bromide forming the desired product **111**. Therefore, it is a redox-neutral transformation without the need for an external electron donor. In this case, however, the Lewis acid LiBr is required to facilitate the C-Br mesolysis by coordination to the diethyl bromomalonate **110**.

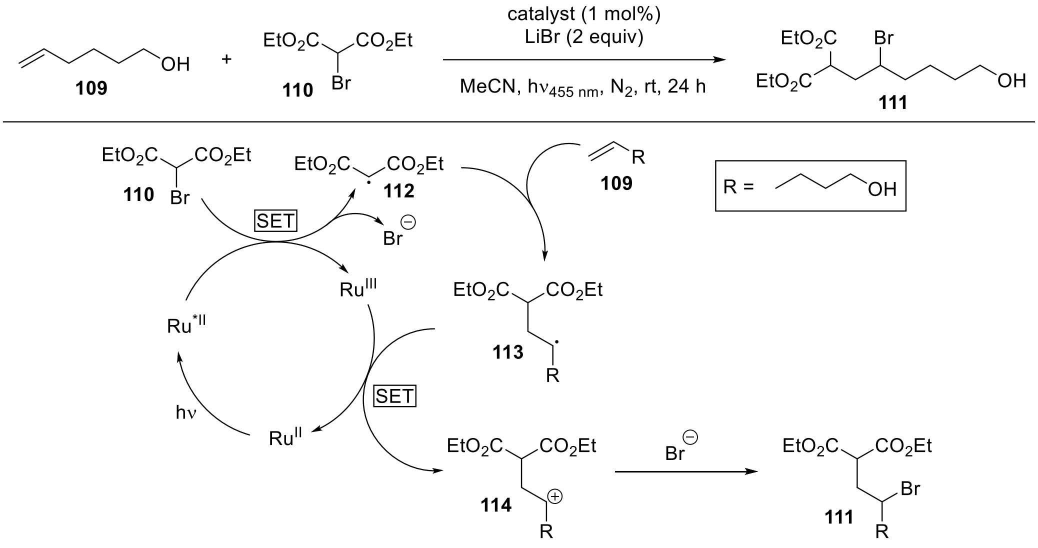

Scheme 24: Photochemical ATRA reaction between **109** and **110** and its corresponding reaction mechanism.

Following the literature conditions afforded 83% yield (Table 5, entry 1). We were pleased to see that once again a substitution of the homogeneously operating catalyst **1** with Nafion-Ru(bpy)$_3$Cl (**107**) gave only a slightly diminished reaction outcome of 68% (entry 2), which is most likely caused by its heterogeneity and the consequent disturbance of the light transmission. Interestingly, the reaction mixture became dark over time and, although the particles could be recovered and the leaching of ruthenium was very low (2.4%, entry 2), they kept the dark color, which may be an indication for the deactivation of the photocatalyst. This was confirmed when we attempted a consecutive run since no reaction could be observed.

Table 5: Visible light-mediated ATRA reaction between hexenol **109** and diethyl bromomalonate **110**.

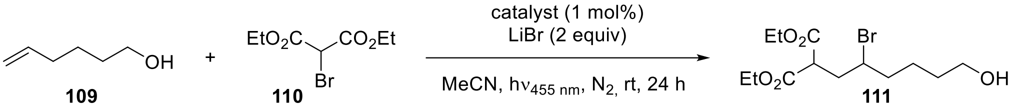
catalyst (1 mol%)
LiBr (2 equiv)
MeCN, hν455 nm, N2, rt, 24 h
EtO2C
CO2Et
Br
OH
109
110
111

Entry	Catalyst	Run	Yield [%] [a]	Leaching Ru [%] [b]
1	$[Ru(bpy)_3]Cl_2$ (**1**)	-	83 [c]	-
2	Nafion-$Ru(bpy)_3Cl$ (**107**)	1	68	2.4
3		2	n.r.	-

The reactions were performed on a 0.25 mmol scale using hex-5-en-1-ol (**109**, 0.25 mmol, 1.0 equiv), bromomalonate **110** (0.50 mmol, 2.0 equiv), catalyst (2.5 µmol, 1.0 mol%), LiBr (0.50 mmol, 2.0 equiv) and MeCN (1.0 mL). The reactions were irradiated by a blue LED (λ = 455 nm) for 24 h under a nitrogen atmosphere. [a]Yields determined by ^{1}H-NMR using 1,3,5-trimethoxybenzene as internal standard. [b]Leaching determined by ICP-OES. [c]Isolated yield.

Astonished by this result, as the inactivity could not be addressed to the ruthenium leaching, we searched for other possible explanations. To investigate if this catalyst degradation arises from exploiting its oxidative quenching cycle, another ATRA reaction between hexenol **109** and perfluoroiodooctane **115** was performed (Scheme 25).[40b] Due to the comparable high reduction potential of **115** (- 1.32 V vs SCE),[40b] the transformation can only be mediated through the reductive quenching cycle of $[Ru(bpy)_3]Cl_2$ (Ru^{II}/Ru^{I} = - 1.33 V vs SCE)[41]. Remarkably, substoichiometric amounts of sodium ascorbate as sacrificial electron donor are sufficient to complete the reaction. This can be explained by the fact that once the Ru^{I} species is formed, the C-I bond of **115** can be heterolytically cleaved forming the corresponding radical **117**. This adds to hexenol **109** and the formed intermediate **118** is oxidized by the excited catalyst Ru^{*II} to **119** and, therefore, initiates a propagation mechanism.

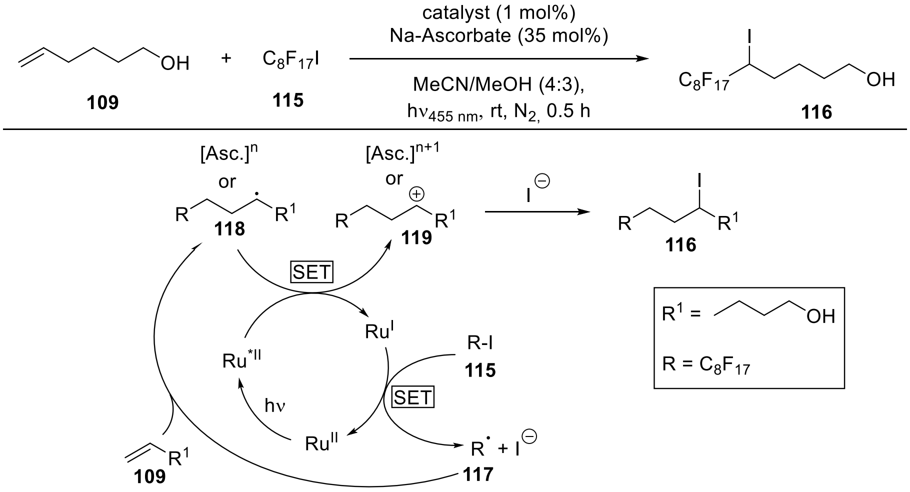
catalyst (1 mol%)
Na-Ascorbate (35 mol%)
MeCN/MeOH (4:3),
hν455 nm, rt, N2, 0.5 h
C8F17I
OH
109
115
116
[Asc.]n
or
[Asc.]n+1
118
119
R
R1
I⊖
SET
RuI
Ru*II
RuII
hν
R-I
115
R• + I⊖
117
R1 = OH
R = C8F17

Scheme 25: ATRA reaction between **109** and **115** and its corresponding reaction mechanism.

To our delight, the immobilized catalyst **107** performed as well as the homogeneous [Ru(bpy)$_3$]Cl$_2$ (**1**) and afforded almost quantitative yields (99% and 97%, entry 1 and 3). Moreover, this time the catalyst remained active after the first cycle and could be reused for several runs, however, the yield continuously decreased from 97% in the first run to even no reaction in the fifth run (entry 3 – 7). In terms of catalyst coloring, the opposite of the previous reaction was observed: instead of turning dark, the catalyst bleached and became almost completely white after the last run. Just like before, this observation is not because of the ruthenium leaching, which was only very little in the first run (1.3%, entry 3), but rather due to a potential catalyst degradation.

Table 6: Visible light-mediated ATRA reaction between hexenol **109** and perfluoroiodooctane **115**.

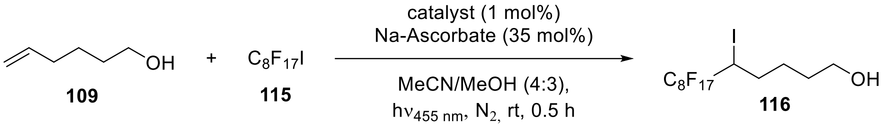

Entry	Catalyst	Run	Yield [%] [a]	Leaching Ru [%][b]
1	[Ru(bpy)$_3$]Cl$_2$ (**1**)	-	99 (95)[c]	-
2	-	-	n.r.	-
3	Nafion-Ru(bpy)$_3$Cl (**107**)	1	97	1.3
4		2	78	-
5		3	60	-
6		4	20	-
7		5	n.r.	-

The reactions were performed on a 0.25 mmol scale using 5-hexen-1-ol (**109**, 0.25 mmol, 1.0 equiv), perfluoroiodooctane **115** (0.33 mmol, 1.3 equiv), sodium ascorbate (88 µmol, 0.35 equiv), catalyst (2.5 µmol, 1.0 mol%), MeOH (1.5 mL) and MeCN (2.0 mL). The reactions were irradiated by a blue LED (λ = 455 nm) for 0.5 h under a nitrogen atmosphere. [a]Yield determined by ^{1}H-NMR using 1,3,5-trimethoxybenzene as internal standard. [b]Leaching determined by ICP-OES. [c]Isolated yield.

Combining these findings, it seems like electron transfers impair the photocatalyst more than energy transfers do. Whereas exploiting the oxidative quenching cycle colors the complex brownish, which suggests a catalyst degradation, and, therefore, no recyclability is given, the reductive quenching cycle brightens the catalyst and the reactivity decreases more slowly. To exclude that this coloring arises from the different irradiation times, 10 mg of the immobilized catalyst **107** were dispersed in MeCN and irradiated for 24 h, however without any visible impact.

Therefore, we decided to focus on reactions taking advantage of the reductive quenching cycle. A prominent example of this is the visible light driven aza-Henry reaction established by Stephenson *et al.* (Table 7).[42] Since *N*-phenyltetrahydroisoquinoline (**89a**) acts as the electron donor itself to initiate the reaction *via* a SET to the excited catalyst, and nitromethane (**120**) functions as both solvent and nucleophile, no other chemicals are needed for this transformation. Although the reaction would even proceed with only light,[43] the catalyst accelerates the product formation (83% with catalyst, 30% without catalyst after 4 h, entry 1 and 2). Also in this case, Nafion-Ru(bpy)$_3$Cl (**107**) performed well, however, a slight and continuous decrease in yield from 72% in the first run to 59% in the fifth run (entry 3 – 7) was observed. Most importantly, the leaching of ruthenium remained in a low range between 1.8 to 2.8% per run.

Table 7: Photocatalyzed Aza-Henry reaction between **89a** and **120**.

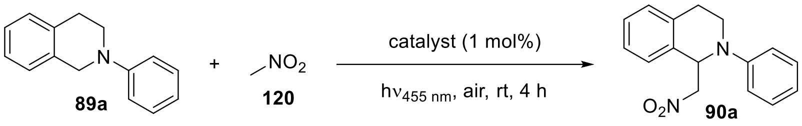

Entry	Catalyst	Run	Conversion [%][a]	Yield [%][a]	Leaching [%][b]
1	[Ru(bpy)$_3$]Cl$_2$ (**1**)	-	98	83[c]	-
2	-	-	34	30	-
3	Nafion-Ru(bpy)$_3$Cl (**107**)	1	86	72	1.8
4		2	79	66	2.2
5		3	76	64	2.8
6		4	74	62	2.4
7		5	71	59	2.3

The reactions were performed on a 0.25 mmol scale using *N*-phenyltetrahydroisoquinoline (**89a**, 0.25 mmol, 1.0 equiv), nitromethane (**120**, 1.0 mL, excess) and catalyst (1.0 mol%). The reaction was irradiated for 4 h at room temperature open to air. [a]Yield determined by ^{1}H-NMR using 1,3,5-trimethoxybenzene as internal standard. [b]Leaching determined by ICP-OES. [c]Isolated yield.

Next, we decided to perform a reaction established in our group, i.e. the decarboxylation of *N*-(acyloxy)phthalimide **121a**, which reacts with crotonate **122a** to the product **123aa** (Table 8).[44] This transformation is especially attractive, since the furnished substances may be further converted to potentially bioactive amino acids and pipecolic acid derivatives (for detailed reaction mechanism and further transformations see chapter C). Therefore, the reaction would benefit from low catalyst leaching to reduce its contamination with the ruthenium complex **1**. As expected, employing **107** as catalyst gave almost the same reaction outcome as its homogeneous version **1** (entry 1 and 3). Although a decline in yield from 48% in the first to 36% in the fifth run could be observed (entry 3 – 7), the leaching of ruthenium into the solvent mixture was reasonably low (2.9 to 3.8%).

Table 8: Photochemical decarboxylation towards **123aa**.

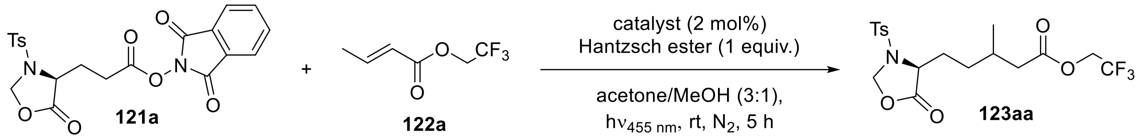
Ts
N
O
O
O
O
O
N
O
121a
+
O
CF3
O
122a
catalyst (2 mol%)
Hantzsch ester (1 equiv.)
acetone/MeOH (3:1),
hν455 nm, rt, N2, 5 h
Ts
N
O
O
O
O
CF3
123aa

Entry	Catalyst	Run	Yield [%][a]	Leaching Ru [%][b]
1	[Ru(bpy)$_3$]Cl$_2$ (**1**)	-	51	-
2	-	-	n.r.	-
3	Nafion-Ru(bpy)$_3$Cl (**107**)	1	48	3.8
4		2	46	3.5
5		3	47	2.9
6		4	43	3.2
7		5	36	3.0

The reactions were performed on a 0.2 mmol scale using *N*-(acyloxy)phthalimide **121a** (0.20 mmol, 1.0 equiv), crotonate **122a** (2.0 mmol, 10 equiv), Hantzsch ester (0.20 mmol, 1.0 equiv) and photocatalyst (2.0 mol%) in acetone/MeOH (3:1, 2 mL). The reaction was irradiated for 5 h with a blue LED (λ = 455 nm) at room temperature under a nitrogen atmosphere. [a]Yield determined by ^{19}F-NMR using 1,4-bis(trifluoromethyl)benzene as an internal standard. [b]Leaching determined by ICP-OES.

2.4. Development of a two-phase flow process

Prompted by the auspicious results obtained for the photochemical *E/Z*-isomerization of stilbene **24**, we envisioned to conduct this reaction in a flow system. As discussed in chapter A, this would bring along several advantages such as improved mixing, better mass transfer and easy control of the residence time to decrease the reaction time.[45] Therefore, we built a flow reactor similar to that of the Rueping group.[46] An actual representation is shown in Figure 4. A column (1) was equipped with a glass rod that was surrounded by a mixture of 60 mg Nafion-Ru(bpy)$_3$Cl (**107**) and 2.5 g silica (2). The irradiation was ensured by 2 x 8 high power blue LEDs (4) and cooling was provided by a stream of N_2 (5). The substrate **24** was dissolved in DCM, saturated with oxygen and transferred to a syringe. The flow rates could be adjusted using a syringe pump (6). As can be seen further, irradiation causes the characteristic pink photoluminescence (3).

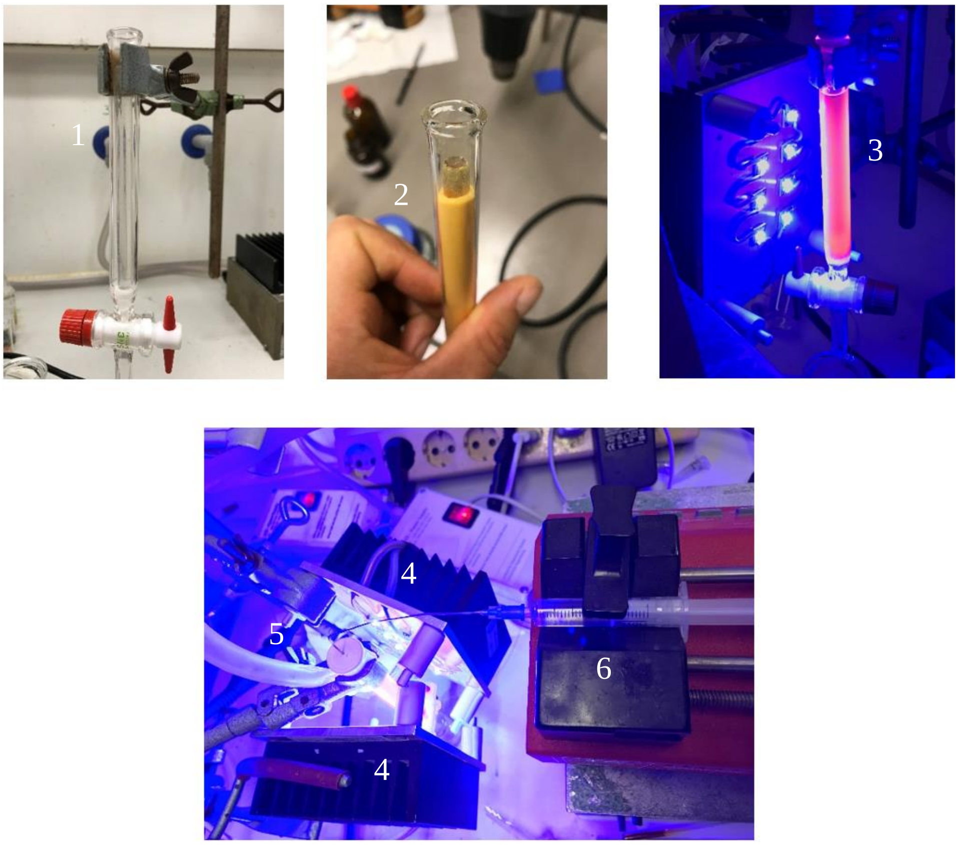

Figure 4: Setup of photochemical flow-reactor.

In the next step, the most suitable flow rates were evaluated. In Table 9, the residence time in the reactor, the *Z/E*-ratios of **25**, and how much faster the reaction proceeds compared to a similar batch setup, are given. Starting with a flow rate of 1 mL/h (equal to 0.1 mmol/h), the same *Z/E*-ratio as in batch was achieved (88:12, entry 1). However, due to the slow flow rate, the cooling was insufficient for the low boiling DCM causing a break inside the column. This was not the case at four times the speed and an even better *Z/E*-ratio of 93:7 was obtained (entry 2). This excellent outcome could be maintained up to 20 mL/h (2 mmol/h), which accelerates the conversion by 80 times compared to a similar batch reaction (entry 8). However, from 30 mL/h it started to drop (entry 9). Conducting the control experiment at 10 mL/h without catalyst, almost no product was formed (entry 6).

Table 9: Evaluation of the best reaction conditions for the *E/Z*-isomerization of *trans*-stilbene (**24**) in a flow process.

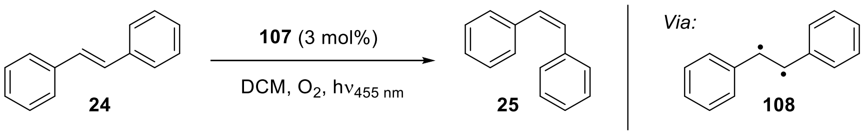

Entry	Flow rate [mL/h]	Residence time [min][a]	X times faster[b]	Z/E ratio[c]
1	1	120	4	88:12
2	4	30	16	93:7
3	6	20	24	93:7
4	8	15	32	92:8
5	10	12	40	92:8
6[d]	10	12	-	10:90
7	16	7.5	64	90:10
8	20	6	80	90:10
9	30	4	120	86:14
10	40	3	160	83:17
11	50	2.4	200	78:22

Reactions were performed on a 0.20 mmol scale using *trans*-stilbene (**24**, 0.20 mmol, 1.0 equiv), catalyst **107** (60 mg, 6.0 µmol, 3.0 mol%) and oxygen saturated DCM (2 mL, 0.1 M). [a]Based on a dead volume of 2 mL. [b]Compared to batch reactions with reaction times of 8 h. [c]Determined by ^{1}H-NMR. [d]Without catalyst.

Encouraged by the outstanding catalytic performance, we employed this set-up for an upscaling to 6.0 mmol (1.06 g *E*-stilbene (**24**)) at a flow rate of 20 mL/h. The substrate was collected in 1 mmol fractions to determine the respective *Z/E*-ratios *via* ^{1}H-NMR as well as the leaching of ruthenium *via* ICP-OES. The results are depicted in Figure 5. As can be seen, throughout the whole reaction process, the *Z/E*-ratio remains at constant high levels (88:12 to 91:9). Noteworthy, no ruthenium leaching at all could be detected. Since the catalyst loading in this reaction corresponds to the amount usually employed in a 0.2 mmol batch reaction, it was theoretically recycled 30 times, which leads to a turnover number of 900.

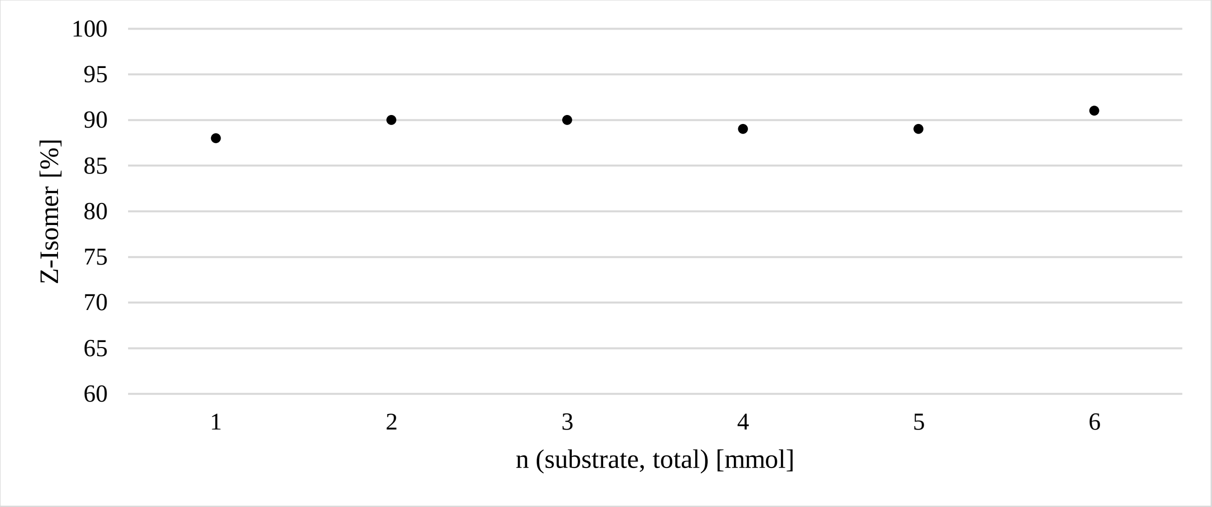

Figure 5: Photochemical *E/Z*-isomerization of *trans*-stilbene (**24**) in a flow process. The reaction parameters are as follows: 6 mmol *trans*-stilbene (**24**, 1.0 equiv), 6 µmol Nafion-Ru(bpy)$_3$Cl (**107**, 0.001 mol%) which was ground with 2.5 g silica, and 60 mL DCM, saturated with O_2. The flow rate was set to 20 mL/h (2 mmol/h).

Driven by this excellent outcome, we were faced with the question of whether we can also increase the activity of the catalyst in other reactions by applying this flow-process. Therefore, the ATRA reaction between hexenol **109** and perfluoroiodooctane **115** was chosen (Table 10). Once again, the amount of catalyst was adjusted to a 0.2 mmol scale to get a comparison to the batch system previously presented. With this, the reaction was performed twice, on a 1.0 mmol and 1.5 mmol scale, corresponding to a theoretical catalyst recycling of five or eight times, respectively. We were very pleased to see that yields of 87% or rather 78% could be achieved. Given the fact that in the batch setup the catalyst could only be recycled four times with a total yield of 64% (see above, Table 6), this is a remarkable improvement. It should also be noted that after the reaction the catalyst lost its characteristic red/orange color and, therefore, remained inactive. This may also be the explanation for the drop in yield when the reaction was upscaled from 1.0 mmol to 1.5 mmol.

Table 10: ATRA reaction between hexenol **109** and perfluoroiodooctane **115** in a flow process.

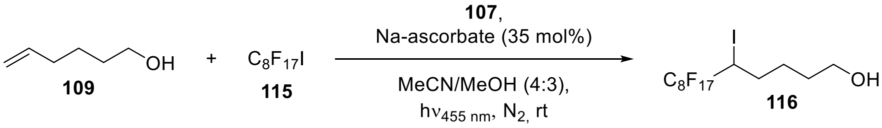

Entry	Flow rate [mL/h]	Scale [mmol]	Catalyst recycling[a]	Yield [%][b]
1	40	1.0	5.0 x	87
2	40	1.5	7.5 x	78

The reaction was performed using 5-hexen-1-ol (**109**, 1.0 equiv), perfluoroiodooctane **115** (1.3 equiv), sodium ascorbate (0.35 equiv), Nafion-Ru(bpy)$_3$Cl (**107**, 2.5 µmol) and MeOH/MeCN (4:3, 0.125 M) [a]Based on a 0.25 mmol scale. [b]Determined by ^{1}H-NMR using 1,3,5-trimethoxybenzene as internal standard.

At the same time, the group of Amara researched a similar topic and only recently published a continuous-flow system using [Ru(bpy)$_3$]Cl$_2$ (**1**) electrostatically bound to silica as catalyst.[47] Comparing batch and flow-process, 1,5-dihydroxynaphthalene was photo-oxidized to juglone. Just like in our studies, the flow-process accelerates the reaction, and no leaching at all was obtained. However, since SiO$_2$ was used as solid support, the catalyst loading was determined to be only 0.003 mmol/g. Using Nafion instead may further improve their results due to the higher catalyst density which proved to be an important aspect of this oxidation process.

2.5. Immobilization of an iridium-based catalyst

To circumvent the issues $[Ru(bpy)_3]^{2+}$ (**1**) brings along for reactions implying an electron transfer and thus, make the system of anchoring catalysts on a solid support *via* electrostatic interactions even more attractive, the Ir^{III} catalyst **6** depicted in Figure 6 should have been immobilized.

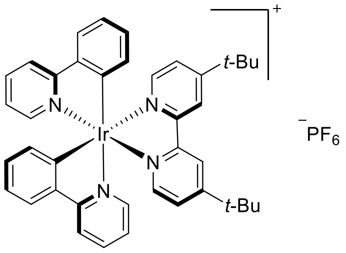

6

Figure 6: $[Ir(ppy)_2(dtb\text{-}bpy)]PF_6$ (**6**).

Although the immobilization itself worked quite well using DCM as solvent - the loading of iridium on Nafion has not been determined, however, the particles turned yellowish, gained in weight and were stable in DCM - the ionic bond between Nafion and the iridium catalyst proved to be considerable weak. In two different reactions performed, the yields of the first runs were comparable to the literature outcome using a homogeneous catalyst, respectively. Unfortunately, the solution turned yellow and it seemed that the complete iridium catalyst leached into the solution which is reflected in the drastically decreased yield in the second runs. Notably, this leaching was not observed, when only irradiating the catalyst in the solvent. Therefore, this idea was not pursued any further.

2.6. Conclusion

A very simple and therefore attractive method to immobilize $[Ru(bpy)_3]Cl_2$ (**1**) onto Nafion® SAC-13 (**105**) was further investigated. In addition to previously presented reactions, i.e. the polymerization of various acrylates or the photooxidation of 1,5-dihydroxynaphthalene (see above), the photochemical *E/Z*-isomerization of stilbene **24** in batch and flow-process was successfully conducted. Moreover, since non-polar solvents like DCM or heptane could be utilized the leaching of ruthenium was reduced to a minimum. However, the step towards more difficult reactions proved to be challenging, since in the case of exploiting the oxidative quenching cycle for an ATRA reaction the catalyst darkened and no recyclability was given. On the other hand, using its reductive quenching cycle bleached the catalyst, however, the particles could be recovered and reused for at least four consecutive cycles.

3. Magnetic nanoparticles as solid support for transition metal-based photocatalysts

3.1. Introduction

Despite the excellent results achieved by immobilizing [Ru(bpy)$_3$]Cl$_2$ (**1**) onto Nafion® SAC-13 (**105**), there was still some room for improvement. Although especially the flow process is very convincing and thus may also be applied for several other reactions, in batch set up the recovery of the particles *via* centrifugation is time-consuming and, therefore, unpersuasive. For this reason, we conceived a strategy to use magnetic nanoparticles as solid support as these already found application as such for various other catalysts.[48]

Magnetic nanoparticles consist of a metal or metal oxide core and are, depending on their size, ferromagnetic, or superparamagnetic.[49] Due to their easy synthesis, low toxicity and decent magnetic saturation, iron oxide particles, above all Magnetite (Fe_3O_4), are one of the most commonly used nanoparticles. To increase their stability in solvents, which is especially important in biomedical applications, a widely used method is to coat the particles with polymeric surfactants or inorganic materials such as gold or silica.[50] However, a coating increases the weight of the particles and is, therefore, accompanied by a decrease in their magnetization. For instance, Simard in his group reported the incorporation of [Ru(bpy)$_3$]Cl$_2$ (**1**) in magnetic nanoparticles as a dye for biomedical application. For this, they firstly coated superparamagnetic Fe_3O_4 with a 12 nm silica shell to prevent any luminescence quenching originating from the dark-colored magnetic core. In a second silica layer, the dye was enclosed *via* a reverse microemulsion method. Already the first silica shell, however, led to a drop of the magnetization from 53 to 10 emu/g.[51]

Since the recovery of the particles would benefit from higher magnetization, especially when it comes to building up large polymer scaffolds, for our studies we focused on ferromagnetic carbon-coated magnetic nanobeads (Co/C). They are synthesized *via* a large scale reducing flame-spray pyrolysis and not only have a superior magnetization of 158 emu/g but also show an exceptional thermal and chemical stability thanks to their carbon layer.[52] Moreover, the graphene-like outer shell allows for covalent functionalization *via* diazonium chemistry. With this, various recyclable catalysts have been synthesized, for instance for hydrogenations through encapsulated palladium,[53] or through an immobilized Noyori-type ruthenium catalyst.[54] S. Fernandes developed a procedure to coat amine-functionalized Co/C nanoparticles in the course of her Ph.D. thesis, showing excellent stability in solvents as well as a high magnetization of 140 emu/g (~ 50 nm silica shell).[55] This value not only exceeds the magnetization of the uncoated magnetite nanoparticles but is also at least twice as high as the silica-coated versions established by Simard *et al*. (12 mm silica shell, 10 emu/g)[51] and Kim *et al.* (1.5 mm silica shell, 64 emu/g)[56] and offers, therefore, an exceptional support for the photocatalyst to be installed.

Employing magnetic nanoparticles as solid support for photocatalysts was so far mainly focused on semiconductors such as TiO_2,[57] MoS_2,[58] or graphitic carbon nitride,[59] which were applied for water purification by photodegradation of dyes. Although semiconductors can already be easily recovered by nature through filtration or centrifugation, their magnetic support facilitates this process and thus paves the way for applications in large scale.

Only recently, Wang *et al*. came up with the idea of anchoring eosin Y on Fe_3O_4 *via* an ionic exchange.[60] Therefore, the nanoparticles were coated with silica and subsequently equipped with a terminal ammonium salt. A simple stirring of these particles in a solution of eosin Y in acetone/water afforded the heterogenized photocatalyst with a loading of 0.10 mmol/g. With this, oxidative CDC reactions between *N*-aryltetrahydroisoquinolines **89** and various nucleophiles were performed affording moderate to excellent yields. Moreover, a recyclability test on *N*-phenyltetrahydroisoquinoline (**89a**) and nitromethane (**120**) proved that it is re-usable for at least eight consecutive runs without a loss in catalytic activity, as the yield only dropped from 92% in the first to 89% in the last cycle.

This chapter encloses the immobilization of different transition metal-based photocatalysts on magnetic Co/C nanoparticles and their subsequent application in various visible light-mediated photoreactions.

3.2. Magnetic nanoparticles as non-covalent solid support

3.2.1. Synthesis of particles

Following the same concept as in the previous chapter, i.e. immobilizing positively charged $[Ru(bpy)_3]^{2+}$ (**1**) on Nafion® *via* electrostatic interactions, the aim was to employ carbon-coated ferromagnetic cobalt nanoparticles (Co/C) as solid support.[i] Therefore, we envisioned to establish a similar scaffold to Nafion®, more precisely to functionalize the magnetic nanoparticles with terminal sulfonic acid groups. The first impediment to be overcome, however, is the dark nature of the particles, which usually causes luminescence quenching. As demonstrated by the group of Simard, a previous coating of the particles with silica can effectively suppress this effect.[51a] Hence, a procedure established by S. Fernandes within our group was followed (Scheme 26).[55] To increase on the one hand the stability of the silica-coated nanoparticles **127** and, on the other hand, to improve the size control of the silica layer, at first amino-functionalized particles **126** were synthesized *via* diazonium chemistry. Subsequent treatment with TEOS in presence of catalytic amounts of ammonia gave the desired particles **127**. Notably, the nanobeads became four times as heavy as at the beginning, which suggests a considerable enlargement of the surface area.

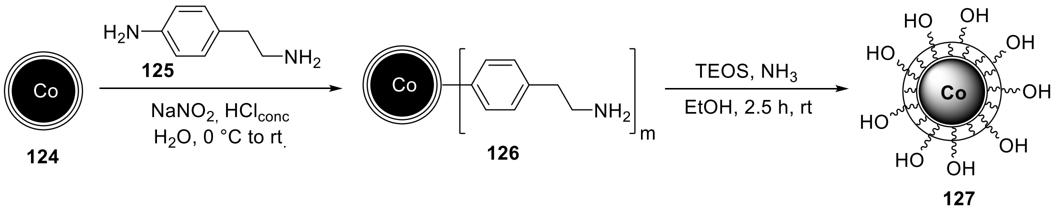

Scheme 26: Synthesis of silica-coated Co/C nanoparticles **127**.

The next step was to generate the sulfonic acid scaffold by adopting a literature-known procedure, where silica-coated cobalt spinel ferrite ($CoFe_2O_4$) nanoparticles have been used as solid support.[61] Therefore, the particles **127** were firstly polymerized with (3-mercaptopropyl)trimethoxysilane (**128**) furnishing thiol functionalized particles **129**. These were then further oxidized to the corresponding sulfonic acid **130** (Scheme 27). Elemental analysis revealed 3.8 mmol sulfur per gram MNPs, of which the amount of free accessible sulfonic acid groups was determined to be 1.8 mmol per gram MNPs *via* titration with 0.1 M NaOH. This value represents the maximal possible loading for $[Ru(bpy)_3]Cl_2$ (**1**) to be immobilized.

---

[i] This topic was investigated in the Bachelor thesis of Lisa Uhlstein.

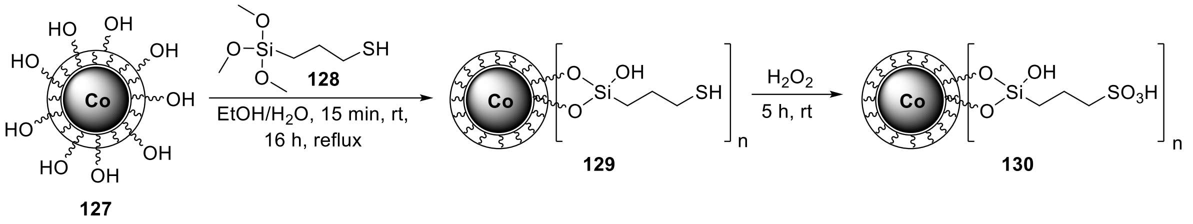

Scheme 27: Functionalization of silica-coated nanoparticles **127** with terminal sulfonic acid groups.

For the final steps, the sulfonic acid groups of **130** were firstly transferred to their corresponding sodium salt by treatment with a brine solution until the pH value of the supernatant remained neutral (Scheme 28). The subsequent immobilization was realized by simply stir the catalyst **1** along with the sodium form of the particles **130** under various conditions. Performing the reaction at room temperature in methanol gave only a poor loading of 0.076 mmol/g (determined by ICP-OES). Replacing the solvent with water, however, increased the loading to 0.463 mmol/g, corresponding to 25.7% of the maximal possible value. Elevated temperatures led to no improvement (80 °C, 0.406 mmol/g). It should be further noted that the particles **131** exhibit a light brown discoloration, which suggests that the catalyst is sufficiently shielded from the magnetic core.

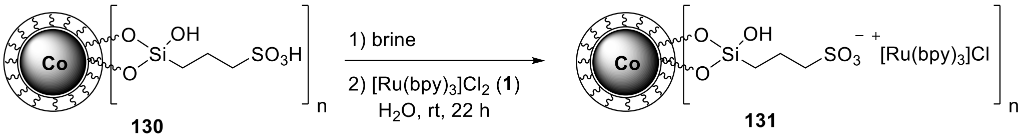

Scheme 28: Immobilization of [Ru(bpy)$_3$]Cl$_2$ (**1**) onto sulfonic acid functionalized Co/C-NP **130**.

To get a first insight into the behavior of MNP-Ru(bpy)$_3$Cl (**131**), i.e. the strength of the ionic bond in solvents commonly used in photoredox chemistry, 5.0 mg of **131** were stirred for 16 h at room temperature in 1 mL of the respective solvent. The particles were magnetically collected, and the supernatant was submitted to ICP-OES. In accordance with the previous chapter, the same trend could be observed, i.e. the more polar the solvent, the higher the leaching of ruthenium (Figure 7). Moreover, the dispersibility proved not to be satisfactory in both heptane and DCM. Unfortunately, compared to Nafion-Ru(bpy)$_3$Cl (**107**), the values are about twice as high and even reach up to 16% in DMF. This may be due to the remarkable higher loading (0.10 mmol/g compared to 0.46 mmol/g) and the accompanying steric repulsion. Another explanation could be that the catalyst is electrostatically attached to the silica scaffold, whose binding is less strong as to sulfonates.

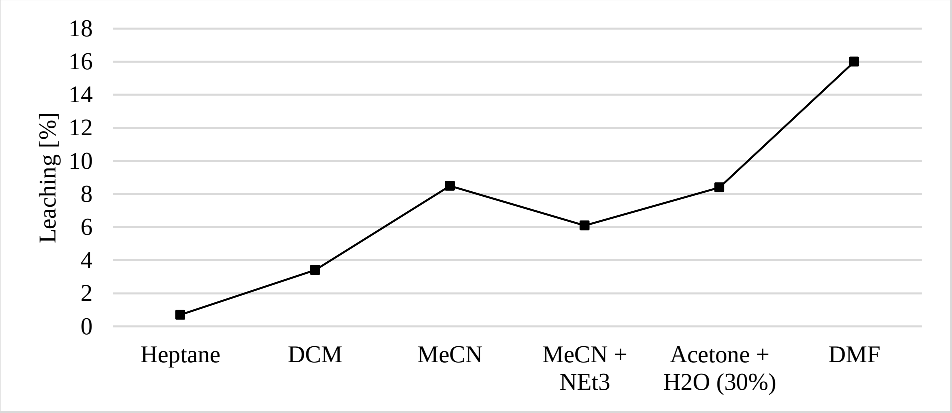

Figure 7: Leaching of ruthenium in [%] into various commonly used organic solvent/-mixtures.

3.2.2. Application of the immobilized catalyst in photochemical reactions

To test the catalytic performance of the recyclable catalyst **131**, the previously described photochemical *E/Z*-isomerization of *trans*-stilbene (**24**) was performed.[6] We were very pleased to see that the reaction worked just as decent as with the homogeneous catalyst **1** (Table 11, entry 2). To ensure that there is no disturbance arising from the nanoparticles themselves, silica-coated MNP **127** (5.0 mg) were added to a reaction mixture which was set up as described in the literature (entry 3). Although no impact in yield was observed in this case, increasing the amount of **127** to 13.5 mg turned out to be disadvantageous, inasmuch as the *Z/E*-ratio decreased to 70:30 (entry 4). To ensure that the graphene layer or the silica scaffold themselves are not photochemically active, the reaction was performed with only silica-coated MNP **127**. As expected, scarcely any product formation took place (entry 6).

Table 11: Photochemical isomerization of *trans*-stilbene **24** employing **131** as catalyst.

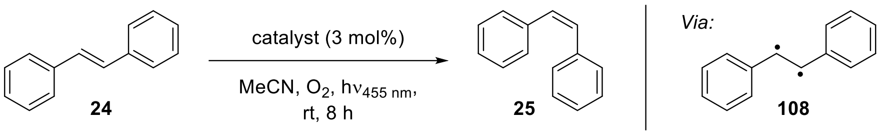

Entry	Catalyst	*Z/E*-ratio[a]	Leaching [%][b]
1	[Ru(bpy)$_3$]Cl$_2$ (**1**, 3.0 mol%)	93:7	-
2	MNP-Ru(bpy)$_3$Cl (**131**, 3.0 mol%)	89:11	8.0
3	MNP **127** (5.0 mg) + **1** (3.0 mol%)	92:8	-
4	MNP **127** (13.5 mg) + **1** (3.0 mol%)	70:30	-
5[c]	no photocatalyst	15:85	-
6	MNP **127** (5.0 mg) without photocatalyst	7:93	-

Unless otherwise noted, the reaction was performed on a 0.20 mmol scale using *trans*-stilbene (0.20 mmol, 1.0 equiv), catalyst (3.0 mol%) and MeCN (2 mL). The reactions were irradiated with a blue LED (λ = 455 nm) under an oxygen atmosphere for 8 h. [a]Ratio determined by GC-FID. [b]Leaching determined by ICP-OES. [c]Irradiation for 16 h.

In Figure 8 the immobilized catalyst MNP-Ru(bpy)$_3$Cl (**131**) is depicted while a) dispersed in MeCN, b) irradiated by blue light and c) magnetically collected. Notably, during irradiation, the catalyst exhibited the typical pink luminescence, which is once again an indication that the transition metal complex is sufficiently shielded from the magnetic core.

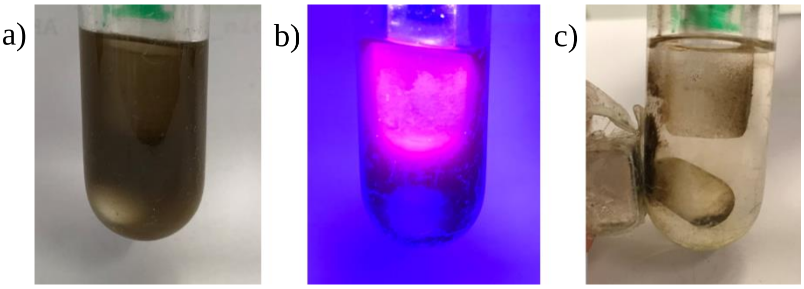

Figure 8: Immobilized catalyst **131** a) dispersed in MeCN, b) irradiated by blue light, c) magnetically collected.

To test the recyclability of the catalyst, 3.0 mol% **131**, corresponding to 13.5 mg, were employed in the *E/Z*-isomerization of **24**. Once the reaction was completed, the particles were magnetically collected, the supernatant decanted, and the catalyst was submitted to another run. The ratio was determined by GC-FID. Unfortunately, in the course of the recycling runs the conversion deteriorated and already in the third cycle only a ratio of 65:35 was obtained (Table 12, entry 3). This was attributed to the leaching of ruthenium, as this proved to be significantly high for the single runs (6 – 10%), and the accompanying worse catalyst-to-nanoparticle ratio.

In order to circumvent this issue, the isomerization was performed employing merely 1.0 mol% of the catalyst. Although the reaction time had to be increased to 16 h and the leaching was again very high (between 8% and 16%), much to our delight the particles could be recovered and reused for several consecutive reaction runs. Only from run five, the *Z/E*-ratio dropped from 87:13 to 68:32.

Table 12: Nafion-Ru(bpy)$_3$Cl (**131**) catalyzed photochemical isomerization of **24**.

Entry	Run	Time [h]	Amount of catalyst [mol%]	*Z/E*-ratio[a]	Leaching [%][b]
1	1	8	3.0 (13.5 mg)	89:11	8
2	2			79:21	6
3	3			65:35	10
4	1	16	1.0 (4.5 mg)	87:13	16
5	2			87:13	11
6	3			87:13	13
7	4			87:13	10
8	5			68:32	8

Unless otherwise stated, the reactions were performed on a 0.20 mmol scale using *trans*-stilbene (**24**, 0.20 mmol, 1.0 equiv), catalyst **131** (1.0 – 3.0 mol%) and MeCN (2 mL) under an oxygen atmosphere. Irradiation was ensured by a blue LED (λ = 455 nm). [a]Ratio determined by GC-FID. [b]Leaching determined by ICP-OES.

The potential of catalyst **131** was further explored by conducting a visible light-mediated aza-Henry reaction (Table 13).[42] *N*-phenyltetrahydroisoquinoline (**89a**) is oxidized through the excited photocatalyst, allowing a nucleophilic attack by nitroethane (**132**), which acts as both a reactant and solvent. After conducting the blank experiments, i.e. MNP **127** and homogeneous [Ru(bpy)$_3$]Cl$_2$ (**1**), solely MNP **127**, and without catalyst (entry 2 – 4), the particles **131** were submitted to the reaction. Although they performed well in the first run, a tremendous ruthenium leaching of 18% was observed (entry 5). This was most likely the reason for the decline in yield from 77% to 44% in the following run (entry 6). Even if the leaching of ruthenium decreased to 3.5%, the yield also continuously dropped to 12% in the fifth run (entry 9) which corresponds to the reaction outcome without catalyst (entry 4).

Table 13: Photochemical aza-Henry reaction between *N*-phenyltetrahydroisoquinoline (**89a**) and nitroethane (**132**).

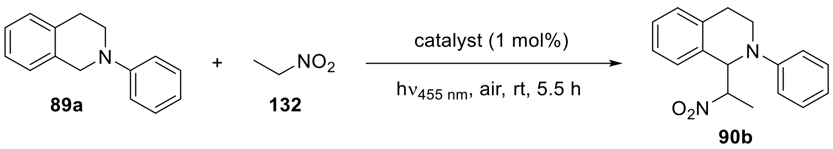

Entry	Run	Catalyst	Conversion [%][a]	Yield [%][a]	Leaching [%][b]
1	-	[Ru(bpy)$_3$]Cl$_2$ (**1**)	100	85 (72[c])	-
2	-	MNP **127** (5.0 mg) + **1**	80	77	-
3	-	no catalyst	21	16	-
4	-	MNP **127** (5 mg) w/o catalyst	12	12	-
5	1	MNP-Ru(bpy)$_3$Cl (**131**)	82	77	18
6	2		48	44	3.5
7	3		52	46	5.6
8	4		38	32	4.2
9	5		14	12	3.9

Unless otherwise noted, the reaction was performed under air using *N*-phenyltetrahydroisoquinoline (**89a**, 0.25 mmol, 1.0 equiv), nitroethane (**132**, 1 mL) and catalyst (1 mol%). Irradiation was ensured by a blue LED (λ = 455 nm) for 5.5 h. [a]Determined by ^{1}H-NMR using 1,3,5-trimethoxy benzene as an internal standard. [b]Determined by ICP-OES. [c]Isolated yield.

3.3. Magnetic nanoparticles as covalent solid support

3.3.1. Synthesis of particles

The next logical step for reducing the leaching was to attach the photocatalyst covalently to the magnetic nanoparticles. Since we already had the thiol functionalized particles **129** in hand, the idea was to immobilize a Ru^{II} complex, which is equipped with a terminal alkene (**134**) on them *via* a thiol-ene reaction (Scheme 29).

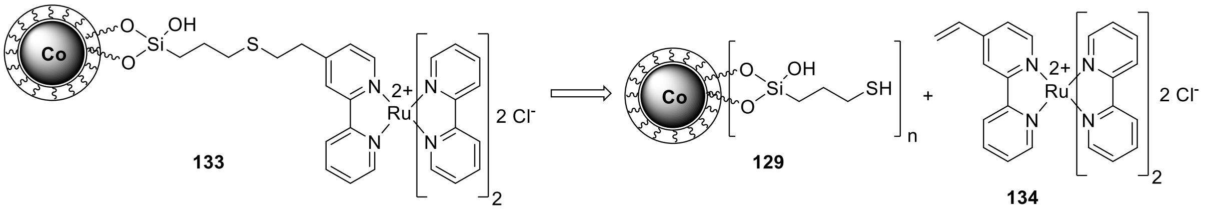

Scheme 29: Retrosynthesis of the recyclable photocatalyst **133** *via* thiol-ene reaction.

Since the complex **134** initially conceived may cause issues in the thiol-ene reaction we decided to synthesize the photocatalyst **137**, which ensures a sufficient distance of the terminal alkene from the aromatic system. To do so, Ru(bpy)$_2$Cl$_2$ (**135**)[62] was complexed with the ligand **136** to give the desired catalyst in excellent yields (95%, Scheme 30). The ligand **136** was prepared from 4,4'-dimethyl-2,2'-dipyridyl and allyl bromide within one step following a literature-known procedure.[63]

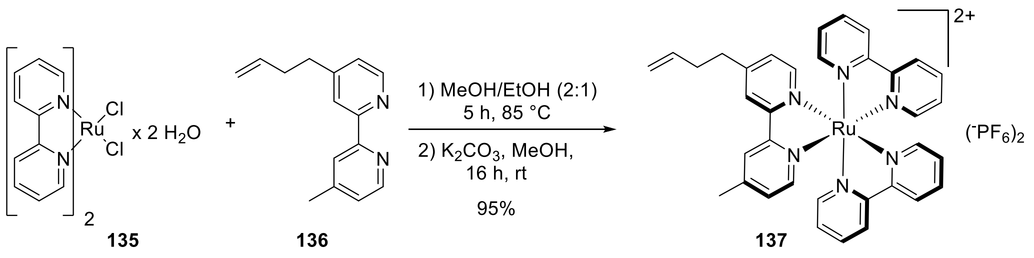

Scheme 30: Synthesis of allyl substituted ruthenium-based photocatalyst **137**.

With the starting materials **129** and **137** in hand, several immobilization attempts *via* a thiol-ene reaction have been made. More precisely, AIBN was employed as radical initiator using heat and ultrasonication to promote the transformation. Although the reaction between the free ligand **136** and mercaptosilane **128** is known to proceed,[63] we had no success in following this procedure and no reaction took place. This may be elucidated by the fact that there is a limitation in the solvent applied as the catalyst is not soluble in chloroform, which is the one of choice in the previously mentioned reaction. Instead, acetonitrile was used. Further efforts such as changing the solvent to DCM or acetone remained fruitless.

Therefore, we followed another literature procedure, synthesizing the complex **138** depicted in Figure 9.[19] This was realized by complexing Ru(bpy)$_2$Cl$_2$ (**135**) with the corresponding ligand, which was obtained through a thiol-ene reaction between the precursor **136** and (3-mercaptopropyl)trimethoxysilane (**128**). With this, the aim was to directly attach the catalyst on silica-coated nanoparticles **127**, however, without success.

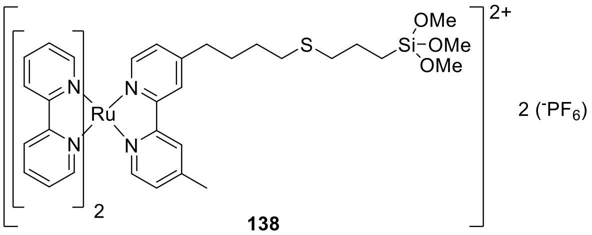

138

Figure 9: Ru^{II} complex attached to (3-mercaptopropyl)trimethoxysilane.

Since various attempts to immobilize a Ru^{II} complex *via* thiol-ene reaction on magnetic nanoparticles remained fruitless, we changed our strategy. As has already been demonstrated in literature examples, copper(I)-catalyzed azide-akyne cycloadditions (CuAAC) have great potential to even build up large polymer scaffolds and thus allow for the immobilization of complex structures.[64] This is why we aspired to apply this to our system. Therefore, we conceived to equip the magnetic nanoparticles with an azide functionalization and the catalyst accordingly with an alkyne moiety. The overall synthesis is shown in Scheme 31. To begin with, the silica-coated MNP **127** were reacted with (3-azidopropyl)trimethoxysilane (**139**) furnishing **140**. Elemental analysis revealed a loading of 14.7 mmol/g N, corresponding to approximately 4.9 mmol/g azide. Previous attempts towards employing (3-azidopropyl)triethoxysilane instead did not lead to satisfactory results regarding polymerization degree and azide loading. Due to the sterically demanding catalyst to be installed, however, only the external azide groups might be occupied, lowering the maximal possible catalyst loading, yet being easier accessible for substrates in subsequent photoreactions. The photosensitizer, on the other hand, was synthesized *via* complexation between Ru(bpy)$_2$Cl$_2$ (**135**) and hexyne tagged bipyridine ligand **141**. The latter was obtained by reacting lithiated 4,4'-dimethyl-2,2'-bipyridine with (6-iodohex-1-yn-yl)trimethylsilane.

Having both starting materials in hand, a CuAAC was conducted in DCM using Cu(I)I and DIPEA as a catalytic system. To our delight, after three days the mixture lost its characteristic reddish color caused by the ruthenium complex and turned almost colorless, which suggests an excellent immobilization degree. And indeed, ICP-OES revealed a loading of 0.45 mmol/g ruthenium for the final catalyst **143**.

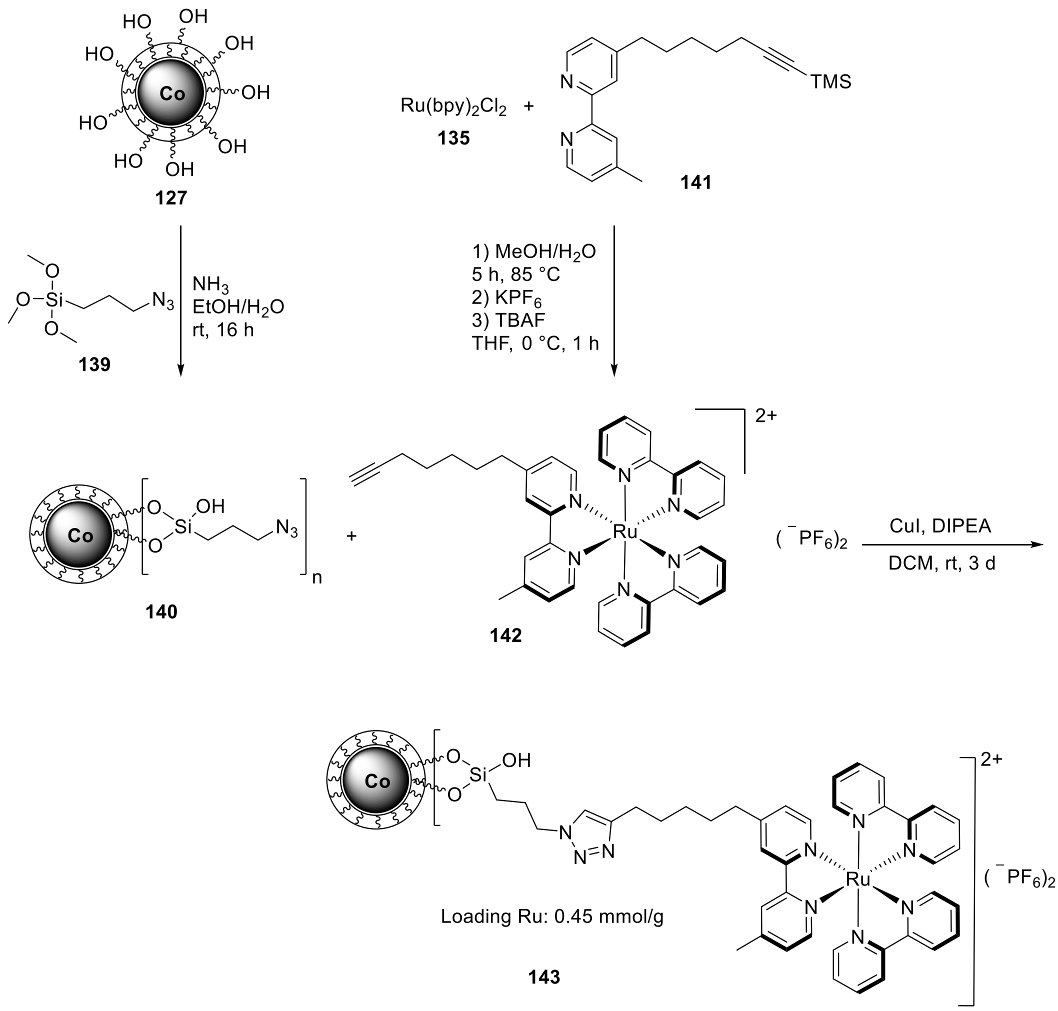
127
Ru(bpy)$_2$Cl$_2$ +
135
TMS
141
139
NH$_3$
EtOH/H$_2$O
rt, 16 h
1) MeOH/H$_2$O
5 h, 85 °C
2) KPF$_6$
3) TBAF
THF, 0 °C, 1 h
140
142
CuI, DIPEA
DCM, rt, 3 d
Loading Ru: 0.45 mmol/g
143

Scheme 31: Synthesis of covalently immobilized ruthenium catalyst **143** *via* CuAAC.

When the catalyst was employed for the photochemical driven *E/Z*-isomerization of stilbene **24**, however, no catalytic activity was obtained. Moreover, the typical bright pink photoluminescence caused by irradiation was not visible, as this was the case for the electrostatically immobilized catalyst **131** (see above). Astonished about this outcome, we searched for a possible rationalization. Since the bare catalyst **142**, as well as the bare catalyst **142** and additional silica-coated MNP **127**, proved to be active for this reaction, the explanation had to be found in the immobilization step. To exclude an exchange of the catalyst's counterion, the particles were treated with a saturated aqueous KPF$_6$ solution. Thereupon, the mixture turned bright red indicating the leaching of the ruthenium complex **142**. A reason for this might be the basic conditions the immobilization takes place at, consequently deprotonating the remaining hydroxy groups of the silica shell. These may act as counterions and therefore bind the catalyst electrostatically and capture it inside the polymer which makes it no longer available for photochemical reactions. A solution for this could have been a previous end-capping of the hydroxy groups by treatment with HMDS. If this was done, however, the click reaction did not work anymore, as this might have also affected the azide functionalization.

To overcome the aforementioned issues, we switched to a modified version of *fac*-Ir(ppy)$_3$, equipped with a terminal alkyne group. This complex is not only uncharged but also opens the way to further photoreactions which are not feasible with the ruthenium-based catalyst. In contrast to the synthesis of *fac*-Ir(ppy)$_2$(PIB-ppy) (**40**), which is the first recyclable version of this photosensitizer,[12] the route *via* an on-complex modification of *fac*-Ir(ppy)$_2$(Me-ppy) only led to non-, mono- and twofold-alkylated derivatives which could not be separated from each other. For this reason, we followed the inverted strategy, i.e. firstly tag the 4-Me-ppy ligand with hexyne by reacting lithiated 4-methyl-2-phenylpyridine with (6-iodohex-1-yn-1-yl)trimethylsilane to give **145** followed by the reaction with [Ir(ppy)$_2$(MeOH)$_2$]OTf (**144**). Subsequent cleavage of the TMS protection group with TBAF furnished the final hexyne-tagged catalyst **146** in moderate yield (50%, Scheme 32).

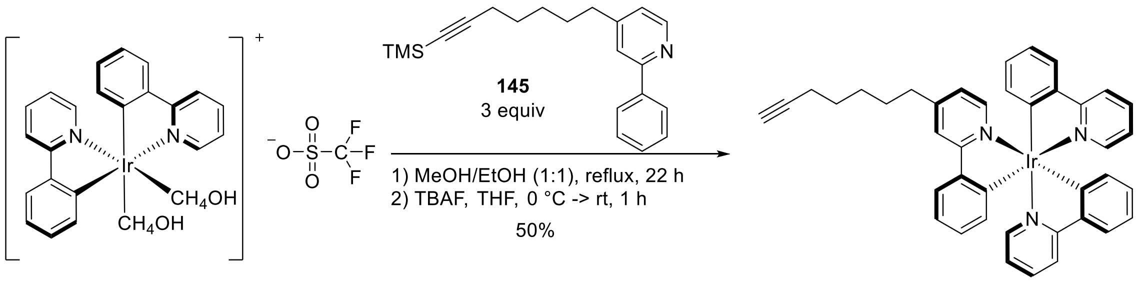
TMS
145
3 equiv
1) MeOH/EtOH (1:1), reflux, 22 h
2) TBAF, THF, 0 °C -> rt, 1 h
50%

Ir(ppy)$_2$(MeOH)$_2$(OTf) **144**

146

Scheme 32: Synthesis of alkyne tagged Ir^{III} complex **146**.

The click reaction towards the immobilized catalyst MNP-Ir(ppy)$_3$ (**147**) was performed straightforward employing Cu(I)I and DIPEA as a catalytic system (Scheme 33). Washing and drying gave slightly greenish particles. However, when these particles were to be used for a reaction performed in DMF, this proved to be disadvantageous as apparently the silica polymer entirely degraded. Since this may be caused by hydrolysis, the TMS end-capping of the free hydroxy groups using HMDS evidenced to be crucial. In fact, the particles obtained were even stable in concentrated hydrochloric acid or sulfuric acid. It should be further noted that the end-capping of the free hydroxy groups should only be performed after the CuAAC, as the immobilization did not work anymore if it was done beforehand. ICP-OES revealed a loading of 0.236 mmol/g iridium, corresponding to an overall incorporation of 86% of the utilized Ir^{III} complex **146**.

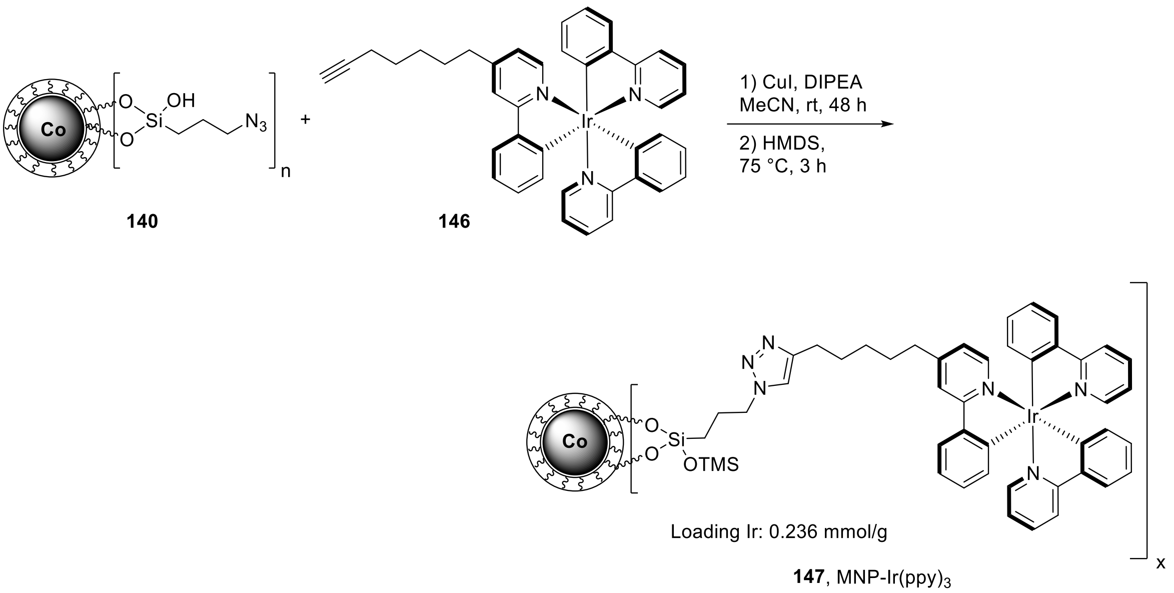
Co
O
OH
Si
N_3
n
+
N
Ir
1) CuI, DIPEA
MeCN, rt, 48 h
2) HMDS,
75 °C, 3 h
140
146
N
N
N
O
Si
OTMS
x
Loading Ir: 0.236 mmol/g
147, MNP-$Ir(ppy)_3$

Scheme 33: Immobilization of **146** onto magnetic nanoparticles **140** *via* click chemistry.

In Figure 10 the immobilized catalyst **147** is depicted dispersed in 1.5 mL MeCN (left-hand side) and magnetically collected (right-hand side). A noteworthy aspect is the color of the particles. Starting from black Co/C nanoparticles **124**, the color changed to greenish upon silica coating and immobilization of the yellow iridium complex. This suggests that the catalyst is sufficiently shielded from the magnetic core, which is an important aspect to be employed in photochemical reactions.

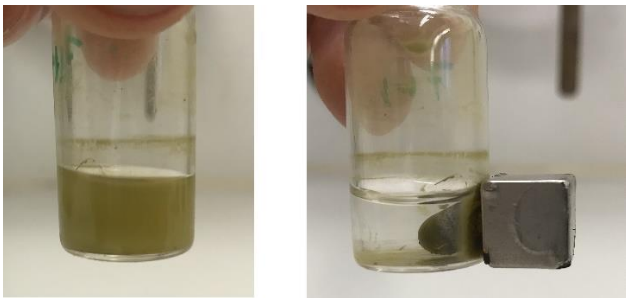

Figure 10: Catalyst **147** (4.5 mg) dispersed in 1.5 mL MeCN (left-hand side) and magnetically collected (right-hand side).

3.3.2. Application of the immobilized catalyst in photochemical reactions

To prove its photocatalytic performance as well as recyclability the immobilized catalyst **147** was applied for an *E/Z*-isomerization of the pinacol ester **148** which was originally developed by Gilmour *et al.* (Table 14).[65] Similar to the isomerization of stilbene (**24**, see above), the reaction is triggered *via* an energy transfer from the excited catalyst to break the double bond, forming the biradical intermediate **150**. This transformation would particularly benefit from its easy recovery and low iridium leaching into the reaction mixture, since apart from the removal of the catalyst no further workup is required. Additionally, based on this isomerization an anti-tumor natural product can successfully be synthesized as has been demonstrated.[65] To ensure that there is no disturbance arising from the nanoparticles, **127** was added to a reaction mixture which was set up as described in the literature without any impact in the reaction outcome (entry 2). Moreover, to exclude any background reactions originating from the graphene-like coating or the silica shell of the nanoparticles, respectively, the reaction was performed with only silica-coated MNP **127** resulting in hardly any conversion (entry 3). To our delight, employing the immobilized catalyst **147** in this reaction gave the same *Z/E*-ratio as the homogeneous *fac*-Ir(ppy)$_3$ (**5**, entry 1 and 5). Noteworthy, the catalyst could be reused in seven successive runs without any loss in reactivity and hardly any leaching of iridium into the reaction mixture (2.5% combined leaching over 7 runs, entry 5). Only from run 8, the *Z/E*-ratio decreased continuously from 93:7 to 59:41 in the tenth run (entry 6 – 8).

Table 14: Photochemical *E/Z*-isomerization of **148**.

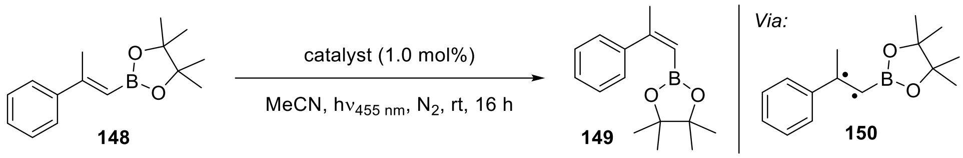

Entry	Catalyst	Run	*Z/E* ratio[a]	Leaching [Ir]/%[b]
1	*fac*-Ir(ppy)$_3$ (**5**)	-	93:7	-
2	*fac*-Ir(ppy)$_3$ (**5**) + MNP **127** (3 mg)		92:8	
3	MNP **127** (3 mg)		19:81	
4	no catalyst		20:80	
5	MNP-Ir(ppy)$_3$ (**147**)	1-7	93:7	2.5 (combined)
6		8	82:18	1.5 (combined)
7		9	65:35	
8		10	59:41	

The reactions were performed on a 0.10 mmol scale in MeCN (1.5 mL) at room temperature under a nitrogen atmosphere. Irradiation took place for 16 h by a blue LED (λ = 455 nm). [a]Ratio determined by ^{1}H-NMR integration of the crude reaction mixture. [b]Leaching determined by ICP-OES.

Besides, we performed a [2+2] cycloaddition of **151** invented by Weaver *et al.* (Table 15).[66] The reaction is based on isomerization of the double bond, which increases the ring strain of the alkene (**153**) and, therefore, drives the cycloaddition. The products obtained may act as a building block for biologically relevant molecules.[67] Also, for this reaction the immobilized catalyst **147** performed well, however, the yield deteriorated in the course of the recyclability test from 80 to 54% within five runs (entries 5-9). Having only a little iridium leaching – approximately 4.8% combined leaching within 5 runs – into the reaction mixture, the decline was rather addressed to the deactivation of the catalyst.[68] This is especially noticeable in this example due to the generally very low catalyst loading of 0.125 mol%.

Table 15: Photochemical [2+2] cycloaddition of **151**.

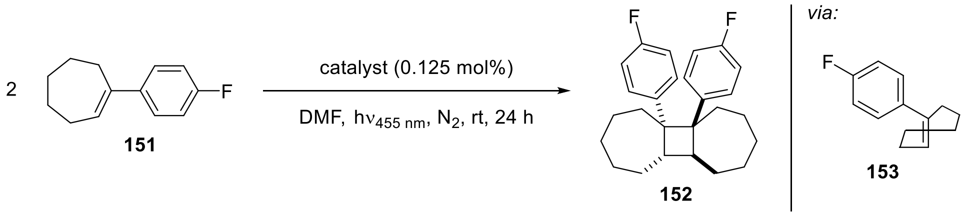
2
151
catalyst (0.125 mol%)
DMF, hν455 nm, N2, rt, 24 h
F
F
152
via:
F
153

Entry	Catalyst	Run	Yield / %[a]	Leaching [Ir]/%[b]
1	*fac*-Ir(ppy)$_3$ (**5**)	-	80[c]	-
2	*fac*-Ir(ppy)$_3$ (**5**) + MNP **127** (3 mg)		80[c]	-
3	MNP **127** (3 mg)		n.r.	-
4	no catalyst		n.r.	-
5	MNP-Ir(ppy)$_3$ (**147**)	1	80	3.0
6		2	77	1.8
7		3	75	<0.1
8		4	70	<0.1
9		5	54	<0.1

The reaction was performed on a 0.6 mmol scale in DMF (3 mL). Irradiation was ensured by a blue LED (λ = 455 nm) for 24 h at room temperature under a nitrogen atmosphere. [a]Yield determined by ^{1}H-NMR using 4-nitro benzaldehyde as internal standard. [b]Leaching determined by ICP-OES.

3.4. Conclusion

It has been demonstrated that carbon-coated Co/C nanoparticles **124** represent a competitive solid support for various transition metal-based photocatalysts, convincing through their easy recovery. Whereas attaching $[Ru(bpy)_3]Cl_2$ (**1**) *via* electrostatic interactions led to high catalyst loadings and show overall good reactivity in the photochemical isomerization of *trans*-stilbene (**24**) and an aza-Henry reaction, the leaching or ruthenium was almost twice as high as this was the case for Nafion-$Ru(bpy)_3Cl$ (**107**). Since various attempts to anchor the catalyst covalently to the nanoparticles remained fruitless, the issues were addressed to the ionic nature of the ruthenium catalyst. Therefore, we switched to an iridium-based photosensitizer, i.e. modified *fac*-$Ir(ppy)_3$. With this, the covalent attaching *via* click chemistry worked well, and the catalyst **147** exhibited excellent catalytic performance and recyclability in an isomerization reaction as well as a [2+2] cycloaddition. Notably, the leaching of the reactive species could be reduced to a minimum, which is especially important for drug synthesis.

4. Graphitic carbon nitrides as novel photoredox catalysts

4.1. Introduction

Due to their chemical stability and versatility, iridium- and ruthenium-based photocatalysts dominate the field of photoredox chemistry. However, they are very expensive and despite great efforts towards immobilizing them have been made, one is still looking for potent alternatives. One cost-efficient and capable replacement would be for example using copper-based photocatalysts like $[Cu(dap)_2]Cl$,[69] $Cu(dap)Cl_2$,[70] or $[Cu(dmp)_2Cl]Cl$,[71] of which the latter is particularly appealing due to its readily available and inexpensive ligand. Other attractive substitutes depict organic dyes or semiconductors, which find their application more and more in photoredox chemistry.[72] Inorganic semiconductors, such as TiO_2, ZnO, or organic, metal-free semiconductors like graphitic carbon nitrides (g-CNs), are in general heterogeneously operating catalysts. This makes them easily recoverable from reaction mixtures *via* centrifugation or filtration.[73] Due to their thermal and chemical stability, g-CNs in particular represent an especially valuable alternative to transition metal-based catalysts.[74] Graphitic carbon nitrides are easily prepared in gram scale *via* thermolysis of nitrogen-rich precursors such as urea,[75] melamine,[76] amitrole[77] or guanidine[46] at ~550 °C. The accompanying self-polymerization affords structures in a 2D fashion, the most stable allotrope of which, g-C_3N_4 (**154**), is shown in Figure 11. Due to this special arrangement, which is driven by van der Waals forces, the layers are stacked in a graphene-like fashion, giving the particles their name.

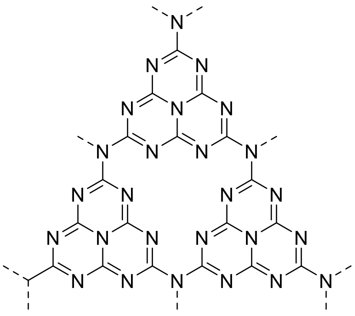

g-C_3N_4, **154**

Figure 11: Graphitic carbon nitride unit g-C_3N_4 (**154**).

Concerning its structure, one has to distinguish between bulky graphitic carbon nitride (g-C_3N_4) and mesoporous graphitic carbon nitrides (mpg-C_3N_4). Whereas g-C_3N_4 exhibits only small surface areas about 10 m^2/g, by introducing controlled porosity, mpg-C_3N_4 can attain surface areas in the range of 400 m^2/g, which is required to enhance its catalytic performance.[74,78]

Another important aspect to be suitable as a catalyst for photochemically driven reactions, is an appropriate band gap and band position. In case of mpg-C_3N_4, the band gap is 2.7 eV, which shifts its absorption maxima to 420 nm.[74] Moreover, the particles are well comparable in terms of their redox potentials to conventional transition metal-based catalysts such as $[Ru(bpy)_3]^{2+}$ (**1**), *fac*-$Ir(ppy)_3$ (**5**) and $[Cu(dap)_2]^+$ (**7**), as can be seen in Figure 12. Through visible light irradiation, an electron is shifted from the valence band (VB) to the conductivity band (CB), forming an electron-hole pair. Whereas the free electron can be used for photoreduction processes, photooxidation can take place at the valence band.[74]

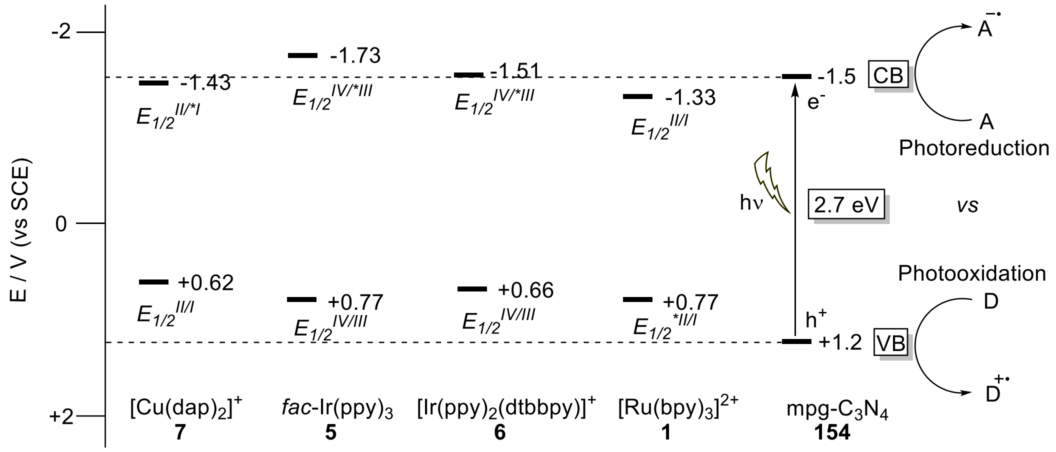

Figure 12: Comparison between well-established transition metal-based photocatalysts and mpg-C_3N_4. All measurements were performed in acetonitrile at room temperature unless otherwise noted. **154** was determined in aqueous solution. A = acceptor, D = donor. References: $[Cu(dap)_2]^+$: [69e]; *fac*-$Ir(ppy)_3$: [79]; $[Ir(ppy)_2(dtbbpy)]^+$: [80]; $[Ru(bpy)_3]^{2+}$: [41,81]; mpg-C_3N_4: [74].

Graphitic carbon nitrides have found broad application, for instance as catalyst for water splitting,[82] degradation of pollutants,[83] or for biomedical purposes,[84] however, were only lately considered as potential photoredox catalyst.[85] The group of Blechert presented an early example for exploiting the photoreduction cycle of mpg-C_3N_4 to promote radical cyclizations. Their model reaction and the corresponding reaction mechanism are depicted in Scheme 34.[86] The activation of the bromomalonate **155** and the subsequent transformation towards the product **156** is already known to proceed when exploiting the reductive quenching cycle of $[Ru(bpy)_3]Cl_2$ (**1**), using NEt_3 as sacrificial electron donor and DMF as solvent.[80a] When these conditions were applied using mpg-C_3N_4 as photocatalyst, full conversion was obtained even in the absence of NEt_3, however, the brominated side product **157** was also formed in a ratio of almost 1:1. This suggests that for mpg-C_3N_4 on the one hand no sacrificial electron donor is needed, and that the reaction mechanism disagrees with the one postulated, on the other. Moreover, they found that THF is crucial for the reaction to proceed in high yields, to give almost selectively the desired product **156**, and to accelerate the reaction. Therefore, a mechanism was proposed in which upon visible light irradiation of mpg-C_3N_4, an electron is transferred from the valence band to the conductivity band. This electron, in turn, is used to trigger a mesolysis of the C-Br bond of **155**, forming the carbon-centered radical **158**, which rapidly undergoes cyclization towards **159**. Subsequent hydrogen abstraction from THF (**160**) affords the desired product **156** and the THF radical **161** which is oxidized by mpg-C_3N_4 to the cation **162**. Traces of MeOH or EtOH act as nucleophile forming the ether scaffold **163**. The process was further improved by the development of a flow reactor, in which the substrates are flushed through an irradiated FEP tube, charged with mpg-C_3N_4 (2.5 wt%), silica gel and glass beads. This way, various bromomalonates were transferred to their cyclization products in moderate to excellent yields (58 – 89%) in 0.04 mmol scales. Moreover, the authors claim to only have a marginal loss in reactivity after 60-70 reaction cycles.

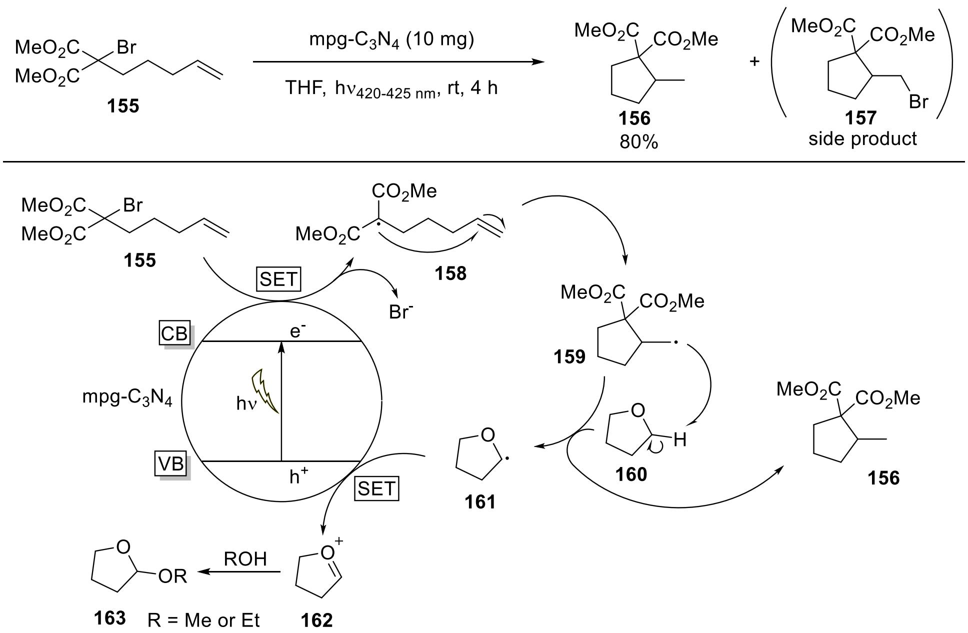
MeO2C Br
MeO2C
155
mpg-C3N4 (10 mg)
THF, hν420-425 nm, rt, 4 h
MeO2C CO2Me
156
80%
+
MeO2C CO2Me
Br
157
side product
MeO2C Br
MeO2C
155
SET
CO2Me
MeO2C
158
Br-
CB
e-
mpg-C3N4
hν
VB
h+
SET
MeO2C CO2Me
159
O
H
160
O
161
MeO2C CO2Me
156
O
OR
163
R = Me or Et
ROH
O+
162

Scheme 34: Graphitic carbon nitride photocatalyzed radical cyclization of bromomalonate **155**.

Only recently, Niu *et al.* established a protocol for graphitic carbon nitride catalyzed Meerwein hydration reactions (Scheme 35).[87] Again, the reaction makes use of the high reduction potential of mpg-C_3N_4, transferring an electron to the aryldiazonium salt **164**, and causes, therefore, the release of nitrogen and BF_4^-. The formed radical **167** adds to alkene **165**, leading to the corresponding intermediate **168**, which is subsequently oxidized by the valence band of mpg-C_3N_4 to the carbocation **169**. A final nucleophilic attack from water affords the desired product **166**. Notably, instead of using potentially toxic solvents such as DMF or

DMSO, in this reaction water acts as both solvent and reagent. Although all transformations were performed employing a 250 W xenon lamp, the authors have shown that the reaction also proceeds with sunlight as the sole energy source within the same time. Moreover, by increasing the reaction time from 4 h to 7 h, they were even able to scale the reaction to 10 mmol without any impact in yield. A recyclability test proved to be successful and has shown that the catalytic performance decreases only slightly within five consecutive runs, i.e. the yield dropped from 76% in the first run to 66% in the last one.

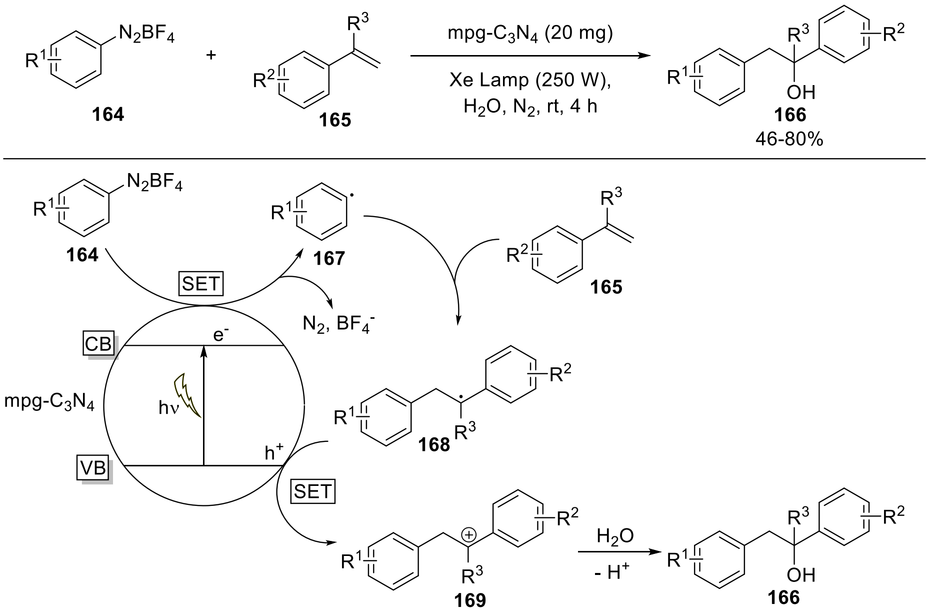

Scheme 35: Visible light-induced Meerwein hydration reaction catalyzed by mpg-C_3N_4.

Based on a similar reaction mechanism, Blechert *et al.* demonstrated trifluoromethylations of (hetero)arenes **170** *via* the reductive activation of triflyl chloride **171** through visible light irradiated mpg-C_3N_4 (Scheme 36).[88] The so caused release of SO_2 and cleavage of Cl^- generates a CF_3-radical. This radical attacks to different (hetero)arenes **170**, forming upon SET to the valence band of mpg-C_3N_4 and subsequent hydrogen abstraction the desired products. These are for example trifluoromethylated benzene **172a**, caffeine **172c** or tryptophane **172d**. Similarly, König *et al.* recently also performed trifluoromethylations and even installed two different functionalities *via* two- and three-component reactions on hetereo(arenes).[89]

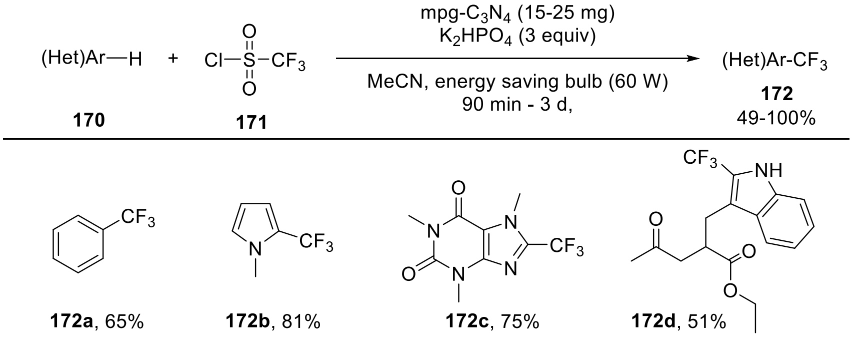

Scheme 36: Trifluoromethylations of arenes **170** catalyzed by mpg-C_3N_4 and selected examples with their respective yields. (Het)Ar-H = heteroaryl.

Lotsch and König *et al*. impressively demonstrated on the photocatalytic synthesis of vinyl sulfones that the functionalization of graphitic carbon nitrides can have a huge impact on the reaction outcome.[90] Based on previous literature examples,[91] where Eosin Y was used as a visible light catalyst for sulfonylations, the organic dye was replaced by various graphitic carbon nitrides to perform reactions as depicted in Scheme 37. They found that compared to pristine mpg-C_3N_4, cyanamide-functionalized carbon nitride (NCN-CN_x) gives twice as high yields and, therefore, as much as eosin Y does. Moreover, as shown by Zhao *et al*. through the introduction of cyano groups in mpg-C_3N_4, the band gap could be drastically narrowed (2.29 eV), thus shifting the absorbance maximum to 590 nm.[92] Therefore, irradiation with green light (520 nm) was sufficient to generate the same results, rendering the reaction even more valuable. It is assumed that also the mechanism is well comparable to that of the homogeneously operating catalyst. More precisely, the reaction proceeds *via* reductive quenching, initiated by the oxidation of the sulfinate salt **173** through visible light-excited NCN-CN_x. The short-living radical **176** adds to the alkene **174** whereas NCN-CN_x is oxidized to its ground state by nitrobenzene (**178**) which itself is reduced to **179**. A subsequent electron transfer to **177** affords the desired product **175**. A final recyclability test exhibited that the catalytic activity only decreased slightly within four cycles, affording 75% yield in the first and 67% in the fourth run.

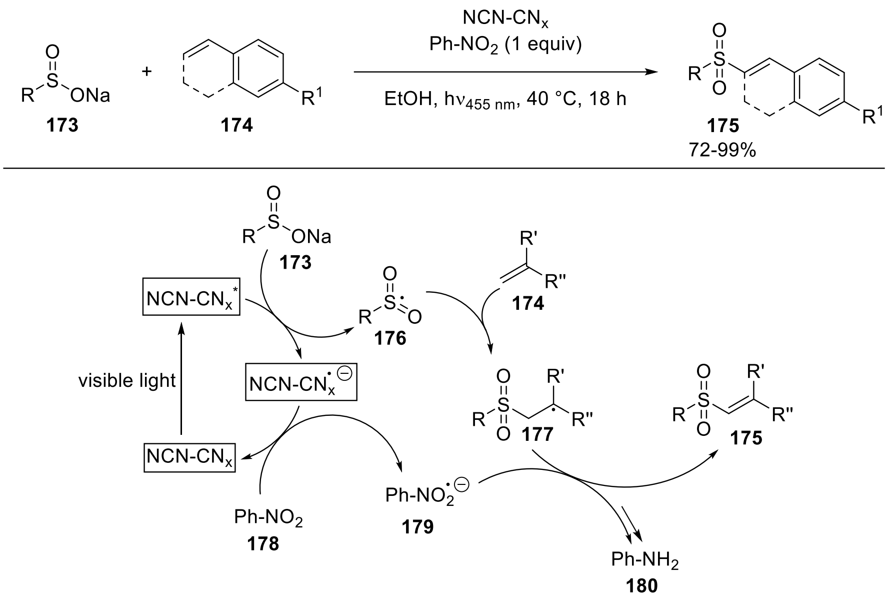
NCN-CN$_x$
Ph-NO$_2$ (1 equiv)
EtOH, hν$_{455\ nm}$, 40 °C, 18 h
173
174
175
72-99%
176
177
178
179
180
visible light
NCN-CN$_x^*$
NCN-CN$_x^{\bullet\ominus}$
NCN-CN$_x$
Ph-NO$_2$
Ph-NO$_2^{\bullet\ominus}$
Ph-NH$_2$

Scheme 37: NCN-CN$_x$ catalyzed sulfonylation reactions.

In this chapter, the potential of mesoporous graphitic carbon nitrides was further explored. Therefore, the semiconductors were contrasted to well-established transition metal-based photocatalysts, such as [Ru(bpy)$_3$]Cl$_2$ (**1**) or [Cu(dap)$_2$]Cl (**7**) in various photochemically driven reactions. Moreover, different modified graphitic carbon nitrides were compared to each other by examination of their photocatalytic performance as well as recyclability. More precisely, mpg-C$_3$N$_5$, possessing a higher nitrogen content than the common mpg-C$_3$N$_4$ (**154**), mesoporous graphitic C$_3$N$_5$ particles doped with silver (mpg-C$_3$N$_5$/Ag) and mesoporous graphitic C$_3$N$_4$ particles doped with silver (mpg-C$_3$N$_4$/Ag) were employed.[ii] Introducing more nitrogen to graphitic carbon nitrides leads to smaller band gaps (~2.20 eV for mpg-C$_3$N$_5$)[93] and therefore enhances the visible-light absorption.[94] Doping the carbon nitrides with silver, on the other hand, improves the photocatalytic activity since the charge separation efficiency is improved and the recombination of electron-hole pairs is impeded.[95]

[ii] The particles were provided by Dr. Manoj Gawande from the Regional Centre of Advanced Technologies and Materials in the Czech Republic.

4.2. Application of graphitic carbon nitrides in photochemical reactions

Whereas mainly mpg-C_3N_4 (**154**) has been employed as photoredox catalyst (see previous chapter), the other aforementioned mesoporous graphitic carbon nitrides are largely unexplored and have so far only found application for water splitting[96] or degradation of organic pollutants.[97] To investigate their photocatalytic activity, the reaction between TMS protected methylaniline **181** and cyclohexenol **182** originally developed by Nishibayashi and coworkers, employing an iridium-based photocatalyst, was conducted.[98] Rueping and his group slightly modified this reaction by adding CsF and using MeOH instead of DCM as solvent so that it performs well with mpg-C_3N_4 as catalyst (Table 16).[46] To our delight, not only mpg-C_3N_4 provided high yields for this transformation (85%, entry 1), but also all other carbon nitrides exhibited a sufficiently strong oxidation potential as well as activity to promote this reaction (entry 2 – 4). Whereas mpg-C_3N_4/Ag afforded the same yield as the non-silver doped parent carbon nitride (entry 2), the mpg-C_3N_5 and mpg-C_3N_5/Ag gave slightly diminished yields of 79% and 75%, respectively (entry 3 – 4).

Table 16: Carbon nitride catalyzed desilylative addition towards **183**.

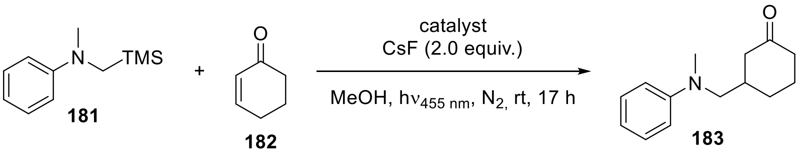

Entry	Catalyst	Yield [%][a]
1	mpg-C_3N_4	85 (80)[b]
2	mpg-C_3N_4/Ag	85
3	mpg-C_3N_5	79
4	mpg-C_3N_5/Ag	75

The reactions were performed using **181** (0.13 mmol, 1.30 equiv), **182** (0.10 mmol, 1.00 equiv), CsF (0.20 mmol, 2.00 equiv), carbon nitride (10 mg) and MeOH (1 mL). Irradiation with blue LED (λ = 455 nm) for 17 h at room temperature under nitrogen atmosphere. [a]Yield determined by ^{1}H-NMR using 1,3,5-trimethoxybenzene as internal standard. [b]Isolated yield.

Since all presented carbon nitrides proved to be photochemically active, we proceeded with an ATRA reaction between hexenol **109** and perfluoroiodooctane **115** that has already been shown before to operate satisfactorily with immobilized versions of $[Ru(bpy)_3]Cl_2$ (Table 17).[40b] Contrary to the photocatalytic desilylative addition, the reaction exploits the reductive quenching cycle of the catalyst using sodium ascorbate as sacrificial electron donor. To our delight, mpg-C_3N_4, as well as mpg-C_3N_4/Ag, performed well providing almost the same yields as the transition metal-based catalyst **1** (entry 3 and 5). It should be noted that the heterogeneous nature of the particles is likely the reason for prolonged reaction time, i.e. 3 h instead of 30 min. Furthermore, the addition of sodium ascorbate accelerates the transformation (entry 3-4) which indicates that carbon nitrides behave similarly to [Ru(bpy)$_3$]Cl$_2$ (**1**). Only mpg-C_3N_5 and mpg-C_3N_5/Ag could not compete. Whereas mpg-C_3N_5 has hardly shown any product formation (5%, entry 6), its relative endowed with silver still attained 63% yield (entry 7), impressively demonstrating that altering the surface can have a drastic effect.

Table 17: Photochemical ATRA reaction between hexenol **109** and perfluoroiodooctane **115** employing carbon nitrides as catalytic species.

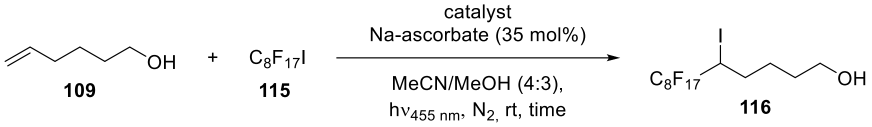

Entry	Catalyst	Time [h]	Yield [%][a]
1	[Ru(bpy)$_3$]Cl$_2$ (**1**, 1.0 mol%)	0.5	99 (95)[b]
2	-	0.5	n.r.
3	mpg-C_3N_4 (5 mg)	3	92
4[c]	mpg-C_3N_4 (5 mg)	3	54
5	mpg-C_3N_4/Ag (5 mg)	3	97
6	mpg-C_3N_5 (5 mg)	3	5
7	mpg-C_3N_5/Ag (5 mg)	3	63

Standard reaction conditions: hexenol **109** (0.25 mmol, 1.00 equiv), perfluoroiodooctane **115** (0.325 mmol, 1.30 equiv), MeCN (2.0 mL), MeOH (1.5 mL), sodium ascorbate (88 µmol, 0.35 equiv) and catalyst were irradiated with a blue LED (λ = 455 nm) at room temperature under nitrogen atmosphere for the indicated time. [a]Yield determined by ^{1}H-NMR using 1,3,5-trimethoxybenzene as internal standard. [b]Isolated yield. [c]Reaction was performed without sodium ascorbate.

For a valuable recyclable catalyst, it is essential to not only have a convincing recovery, which is inherently given for heterogeneous operating catalysts, but also a persuasive activity in successive runs. Driven by the auspicious result obtained in the former ATRA reaction, the next logical step was to test the recyclability of both mpg-C_3N_4 and mpg-C_3N_4/Ag for this transformation. The results for 10 consecutive runs are depicted in Figure 13. As can be seen, mpg-C_3N_4 afforded throughout very high yields ranging from 82 – 95%. Although mpg-C_3N_4/Ag attained slightly higher conversions in the first five cycles, its reactivity continuously dropped from the sixth run to 43% in the tenth which suggests that these particles are not as stable as the undoped parent carbon nitrides. Also, the fluctuations in the reaction outcomes, most likely due to the heterogeneous nature, are very conspicuous as the yield of a run is hardly the same as the previous one and partially deviates as much as 20%. Nevertheless, these findings are very pleasant particularly in comparison with the immobilized Nafion-Ru(bpy)$_3$Cl (**107**) which turned out to be completely inactive for this reaction already in the fifth run (see chapter 2.3).

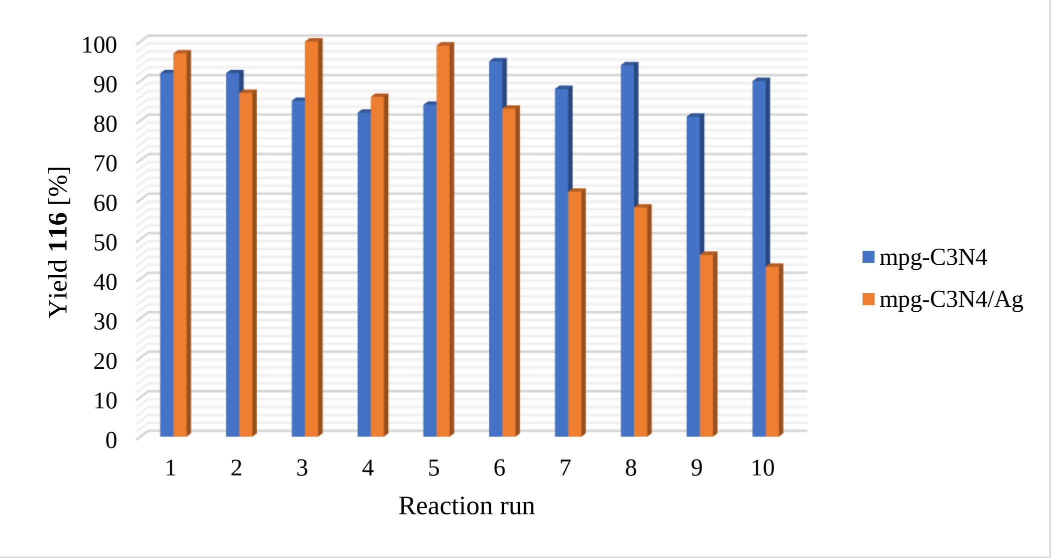

Figure 13: Recyclability test of mpg-C$_3$N$_4$ and mpg-C$_3$N$_4$/Ag. The reaction parameters for a single run are as follows: hexenol **109** (0.25 mmol, 1.00 equiv), perfluoroiodooctane **115** (0.325 mmol, 1.30 equiv), MeCN (2.0 mL), MeOH (1.5 mL), sodium ascorbate (88 µmol, 0.35 equiv) and carbon nitride (5 mg) were irradiated with a blue LED (λ = 455 nm) at room temperature under nitrogen atmosphere for 3 h.

Furthermore, the associated ATRA reaction originally making use of the oxidative quenching cycle of [Ru(bpy)$_3$]Cl$_2$ (**1**), i. e. the reaction between diethyl bromomalonate (**110**) and hexenol **109**, was conducted employing mpg-C$_3$N$_4$ as catalyst (Table 18).[40b] Although it is known that the semiconductor is capable of reducing bromomalonates,[86] we were very grateful to see that the particles also performed exceptionally well in this case and gave the same yield as [Ru(bpy)$_3$]Cl$_2$ (**1**) only by increasing the reaction time from 8 to 24 h (entry 2). Moreover, the particles were recovered and reused twice without any loss in reactivity (entry 3 – 4). In contrast to Nafion-Ru(bpy)$_3$Cl (**107**), which remained inactive after a single run, these particles proved to be much more durable and are not limited to a non-polar environment but can also be employed in solvents such as DMSO without negative effects.

Table 18: Carbon nitride catalyzed ATRA reaction between hexenol **109** and diethyl bromomalonate (**110**).

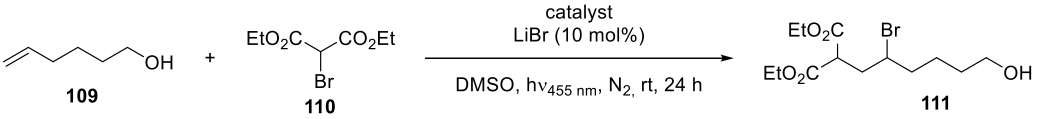

Entry	Catalyst	Run	Yield [%][a]
1[b]	[Ru(bpy)$_3$]Cl$_2$ (**1**, 1.0 mol%)	-	98[c]
2	mpg-C$_3$N$_4$ (10 mg)	1	95
3		2	94
4		3	95

Standard reaction conditions: hex-5-en-1-ol (**109**, 0.25 mmol, 1.00 equiv), diethyl bromomalonate (**110**, 0.30 mmol, 1.20 equiv), LiBr (25 µmol, 10 mol%), catalyst and DMSO (1.0 mL) were irradiated for 24 h under nitrogen atmosphere at room temperature. [a]Yields determined by ^{1}H-NMR using 4-nitrobenzaldehyde as internal standard. [b]8 h reaction time. [c]Literature reported yield.[40b]

To examine further possible advantages of these graphitic carbon nitrides a more challenging ATRA reaction between styrene (**184**) and perfluoroiodooctane **115** established within our group was conducted (Table 19).[70c] What makes this transformation special is that it solely proceeds with [Cu(dap)$_2$]Cl (**7**) as catalytically active species due to its unique characteristic to undergo an inner sphere catalytic cycle, other prominent catalysts such as [Ru(bpy)$_3$]Cl$_2$ (**1**) or *fac*-Ir(ppy)$_3$ (**5**) are not capable of. It was therefore not surprising that a first test reaction using mpg-C$_3$N$_4$ as catalyst resulted in no reaction (entry 2). Also, when the solvent was changed to MeCN/MeOH (entry 3) or when sodium ascorbate was added (entry 4), as this proved to be advantageous in the former transformation, only traces of product could be obtained. The addition of CuCl$_2$ also led to no conversion of the starting material (entry 5). Therefore, the reaction was not further investigated, and it can be stated that graphitic carbon nitrides have no beneficial properties to promote this reaction.

Table 19:Photochemical ATRA reaction between styrene (**184**) and perfluoroiodooctane **115**.

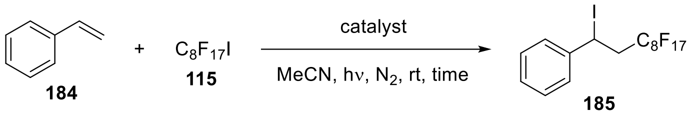

Entry	Catalyst	Deviation from standard conditions[a]	Yield [%][b]
1	[Cu(dap)$_2$]Cl (**7**)	green LED (λ = 530 nm) used, 16 h	82 (78)[c]
2	mpg-C_3N_4 (5 mg)	-	n.r.
3	mpg-C_3N_4 (5 mg)	MeCN/MeOH (4:3) used as solvent, 24 h	n.r.
4	mpg-C_3N_4 (5 mg)	MeCN/MeOH (4:3), Na-asc (0.35 equiv), 24 h	traces
5	mpg-C_3N_4 (5 mg)	addition of $CuCl_2$ (1.0 equiv), 24 h	n.r.

[a]Standard reaction conditions: styrene (**184**, 0.25 mmol, 1.00 equiv), perfluoroiodooctane (**115**, 0.50 mmol, 2.00 equiv), catalyst (1.0 mol%) and dry MeCN (1.5 mL) were irradiated by a blue LED (λ = 455 nm) at room temperature under nitrogen atmosphere. [b]Yield determined by ^{1}H-NMR using 4-nitrobenzaldehyde as internal standard. [c]Isolated yield.

For this reason, another similar ATRA reaction between styrene (**184**) and *p*-toluenesulfonyl chloride (**186**) was performed, which was established by Stephenson *et al.* (Table 20).[40b] It is not limited to being catalyzed only by [Cu(dap)$_2$]Cl (**7**), but also other complexes such as [Ru(bpy)$_3$]Cl$_2$ (**1**) are capable of. Whereas both provide very high yields between 80% and 96% (entry 1 – 2),[70b] a substitution with mpg-C_3N_4 resulted in a drastically decreased reaction outcome of 16% (entry 3). Adding a base to trap traces of HCl that may occur during the reaction, extending the reaction time from 24 h to 48 h, or increasing the catalyst loading, showed only little effect (entry 4 – 6). Besides, employing the silver doped graphitic carbonitride mpg-C_3N_4/Ag or the nitrogen-doped versions mpg-C_3N_5 and mpg-C_3N_5/Ag led to no improvement (entry 7 – 8). Since the reduction potential of the graphitic carbon nitrides should be sufficient to generate the toluolsulfonyl radical (E_{red} = -0.94 V vs SCE)[70b] *via* mesolysis of the S-Cl bond upon an electron transfer from the catalyst, this result is fairly unforeseen. Noteworthy, in no case full conversion of starting material was observed, suggesting that something could be formed in the course of the reaction, which impacts the activity of the catalyst.

Table 20:Visible light-mediated ATRA reaction between styrene (**184**) and sulfonyl chloride **186**.

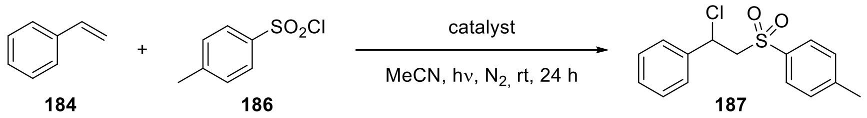

Entry	Catalyst	Deviation from standard conditions[a]	Yield [%][b]
1	[Cu(dap)$_2$]Cl (**7**)	green LED (λ = 530 nm) was used	96 (94)[c]
2	[Ru(bpy)$_3$]Cl$_2$ (**1**)		80
3	mpg-C$_3$N$_4$ (5 mg)		16
4	mpg-C$_3$N$_4$ (5 mg)	Na$_2$CO$_3$ (1.0 equiv) was added	12
5	mpg-C$_3$N$_4$ (5 mg)	48 h reaction time	21
6	mpg-C$_3$N$_4$ (10 mg)	0.25 mmol scale, 48 h reaction time	12
7	mpg-C$_3$N$_4$/Ag (5 mg)		12
8	mpg-C$_3$N$_5$ (5 mg)		17
9	mpg-C$_3$N$_5$/Ag (5 mg)		16

[a]Standard reaction conditions: styrene (**184**, 0.50 mmol, 1.00 equiv), tosyl chloride (**186**, 0.50 mmol, 1.00 equiv), catalyst (1.0 mol%) and dry MeCN (2.0 mL) were irradiated for 24 h with a blue LED (λ = 455 nm) at room temperature under nitrogen atmosphere. [b]Yield determined by ^{1}H-NMR using 4-nitrobenzaldehyde as internal standard. [c]Isolated yield.

To investigate whether these issues arise from styrene (**184**) or activated alkenes in general, we conducted the same reaction using octene **188** as trapping reagent instead (Table 21).[70b] Noteworthy, employing [Cu(dap)$_2$]Cl (**7**) as catalyst for inactivated alkenes requires the presence of stoichiometric amounts of Na$_2$CO$_2$, whereas [Ru(bpy)$_3$]Cl$_2$ (**1**) suffers from the addition of a base, as has been demonstrated in our group.[70b]. Unfortunately, mpg-C$_3$N$_4$ provided for this transformation only 36% yield, even after 3 d of irradiation (entry 5). Interestingly, a crude ^{1}H-NMR revealed a complete consumption of tosyl chloride **186**, however, without the formation of by-products. This suggests that the tosyl chloride was either transferred to an easily volatile compound or underwent a reaction with the carbon nitride. Taking into account that the particles did not increase in weight and were still active for a consecutive reaction run (entry 6), the former is considered more likely. Without the addition of Na$_2$CO$_3$, no conversion of starting material took place (entry 4).

Table 21: Visible light-mediated ATRA reaction between 1-octene (**188**) and sulfonyl chloride **186**.

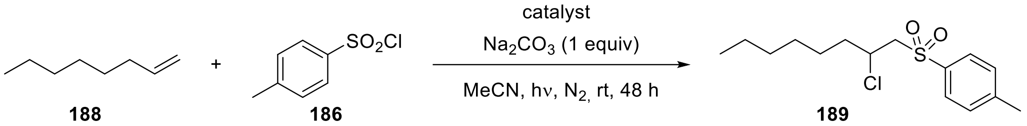

Entry	Catalyst	Deviation from standard conditions[a]	Yield [%][b]
1	[Cu(dap)$_2$]Cl (**7**)	green LED (λ = 530 nm) was used	84 (80)[c]
2	mpg-C_3N_4 (10 mg)	72 h reaction time	36
3	mpg-C_3N_4	run 2 with recovered particles from entry 2	35
4	mpg-C_3N_4 (10 mg)	without Na_2CO_3	n.r.

[a]Standard reaction conditions: octene **188** (0.50 mmol, 2.00 equiv), tosyl chloride (**186**, 0.25 mmol, 1.00 equiv), catalyst (1.0 mol%), Na_2CO_3 (0.25 mmol, 1.00 equiv) and dry MeCN (2.0 mL) were irradiated for 48 h with a blue LED (λ = 455 nm) at room temperature under nitrogen atmosphere. [b]Yield determined by ^{1}H-NMR using 4-nitrobenzaldehyde as internal standard. [c]Isolated yield.

The oxidation of *N*-aryltetrahydroisoquinolines **89** to their corresponding iminium cations (**191**) and the subsequent trapping by nucleophiles is already reported to operate well using mpg-C_3N_4 (**154**) as catalyst under an oxygen atmosphere (Scheme 38, upper pathway).[99] Therefore, we wondered whether it is also possible to generate the corresponding radical **193**, which itself acts as nucleophile (lower pathway). As reported by our group,[100] this can be achieved photochemically under oxygen-free conditions using [Ru(bpy)$_3$]Cl$_2$ (**1**) as catalyst. Moreover, the successful coupling of the generated α-amino radicals **193** to Michael acceptors **194** was demonstrated, leading to potential immunosuppressive agents. The addition of TFA and additional heating to 50 °C proved to severely accelerate the reaction as well as increase the yields.[101] Whereas Nafion-Ru(bpy)$_3$Cl (**107**) cannot be employed in this reaction due to the high leaching caused by the strong acid, graphitic carbon nitride is very durable and, therefore, may be a powerful recyclable alternative to the conventional [Ru(bpy)$_3$]Cl$_2$ (**1**).

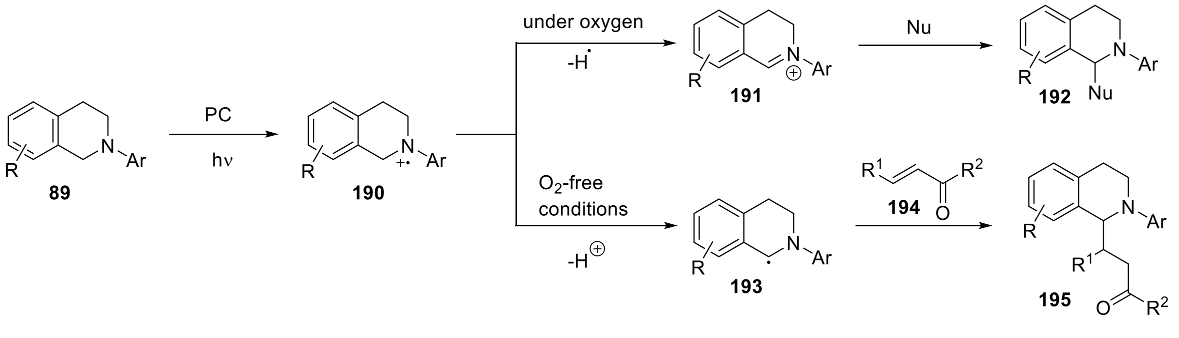

Scheme 38: Photochemical activation of *N*-aryltetrahydroisoquinolines **89** under oxygen (upper pathway) and oxygen-free (lower pathway) conditions.

With this in mind, we started our investigations using *N*-phenyltetrahydroisoquinoline (**89a**) and methyl vinyl ketone (**196**) as model substrates (Table 22). Following the literature conditions[101] afforded 79% isolated yield (entry 1). To our delight, exchanging [Ru(bpy)$_3$]Cl$_2$ (**1**) by mpg-C$_3$N$_4$ (**154**) worked fine and provided 53% yield (entry 2). Since ^{1}H-NMR revealed only 85% conversion of starting material, the reaction time was increased to 18 h, which resulted in a partial decomposition of the product and led to deteriorated yields (20%, entry 3). Increasing the catalyst loading from 10 mg to 20 mg (entry 4) or employing the originally reported conditions,[100] i.e. without TFA, prolonged reaction time and at room temperature, did not lead to any improvements (entry 5).

Table 22: Photochemically driven addition of *N*-phenyltetrahydroisoquinoline (**89a**) to methyl vinyl ketone (**196**).

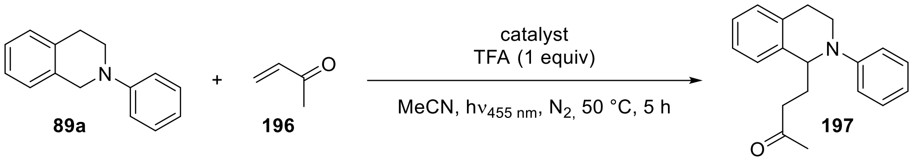

Entry	Catalyst	Deviation from standard conditions[a]	Yield [%][b]
1	[Ru(bpy)$_3$]Cl$_2$ (**1**, 2 mol%)	-	79[c]
2	mpg-C$_3$N$_4$ (10 mg)	-	53
3	mpg-C$_3$N$_4$ (10 mg)	18 h reaction time	20
4	mpg-C$_3$N$_4$ (20 mg)	-	45
5	mpg-C$_3$N$_4$ (10 mg)	no TFA, 18 h reaction time, at rt	30

[a]Standard reaction conditions: *N*-phenyltetrahydroisoquinoline (**89a**, 0.25 mmol, 1.0 equiv), methyl vinyl ketone (**196**, 0.50 mmol, 2.0 equiv), TFA (0.25 mmol, 1.0 equiv), catalyst and dry MeCN (1 mL) were irradiated with a blue LED (λ = 455 nm) for 5 h at 50 °C under nitrogen atmosphere. [b]Yield determined by ^{1}H-NMR using 4-nitrobenzaldehyde as internal standard. [c]Isolated yield.

4.3. Conclusion

To conclude, different graphitic carbon nitrides were tested for their photochemical reactivity as well as their recyclability in various reactions. Whereas for a desilylative addition all particles were found to be reactive, mpg-C_3N_5 and mpg-C_3N_5/Ag were outperformed by mpg-C_3N_4 and its silver doped relative mpg-C_3N_4/Ag in two ATRA reactions tested. Besides, they showed great recyclability and could be reused for at least 10 or 6 consecutive runs, respectively, with only negligible loss in reactivity. Although graphitic carbon nitrides have great potential and may be considered as an alternative to transition metal-based catalysts, when it comes to more challenging photochemical conversions a simple substitution of the photocatalyst proved to be difficult and might require further optimization. Amongst others, this was demonstrated by Rueping *et al.*, as for their decarboxylative and desilylative additions it was not possible to simply exchange the iridium-based catalyst, but a base was required for the reaction to proceed with mpg-C_3N_4.[46] Moreover, the extremely short fluorescence lifetime of roughly 2 ns[102] could also play a crucial role, as this might not be sufficient to promote some visible light-mediated reactions.

6. Literature

[1] J. J. Berzelius, *Jahres-Bericht* **1835**, *14*, 237–245.

[2] M. Beller, A. Renken, R. A. van Santen, *Catalysis : from principles to applications;* Wiley-VCH, Weinheim, **2012**.

[3] a) J. Wisniak, *Educ. quim.* **2010**, *21*, 60–69; b) J. A. Moulijn, P. W. N. M. van Leeuwen, R. A. van Santen in *Elsevier B.V, 1993,*pp. 3–21.

[4] M. Benaglia, *Recoverable and recyclable catalysts;* Wiley, Hoboken N.J, **2009**.

[5] G. Rothenberg, *Catalysis*: Concepts and Green Applications; Wiley-VCH, Weinheim, **2008**.

[6] D. C. Fabry, M. A. Ronge, M. Rueping, *Chem. Eur. J.* **2015**, *21*, 5350–5354.

[7] a) D. E. Bergbreiter, *ACS Macro Lett.* **2014**, *3*, 260–265; b) D. E. Bergbreiter, S. D. Sung, *Adv. Synth. Catal.* **2006**, *348*, 1352–1366.

[8] N. Priyadarshani, Y. Liang, J. Suriboot, H. S. Bazzi, D. E. Bergbreiter, *ACS Macro Lett.* **2013**, *2*, 571–574.

[9] Y. Liang, D. E. Bergbreiter, *Catal. Sci. Technol.* **2016**, *6*, 215–221.

[10] H. Sun, C. Yang, F. Gao, Z. Li, W. Xia, *Org. Lett.* **2013**, *15*, 624–627.

[11] M. A. Ischay, M. E. Anzovino, J. Du, T. P. Yoon, *J. Am. Chem. Soc.* **2008**, *130*, 12886–12887.

[12] D. Rackl, P. Kreitmeier, O. Reiser, *Green Chem.* **2016**, *18*, 214–219.

[13] X. Zhang, Y. Li, X. Hao, K. Jin, R. Zhang, C. Duan, *Tetrahedron* **2018**, *74*, 1742–1748.

[14] X. Zhang, Y. Li, X. Hao, K. Jin, R. Zhang, C. Duan, *Tetrahedron* **2018**, *74*, 7358–7363.

[15] J. Guerra, D. Cantillo, C. O. Kappe, *Catal. Sci. Technol.* **2016**, *6*, 4695–4699.

[16] a) Y.-P. Wu, M. Yan, Z.-Z. Gao, J.-L. Hou, H. Wang, D.-W. Zhang, J. Zhang, Z.-T. Li, *Chinese Chem. Lett.* **2019**, *30*, 1383–1386; b) Y.-X. Tan, S.-X. Lin, C. Liu, Y. Huang, M. Zhou, Q. Kang, D. Yuan, M. Hong, *Appl. Catal, B* **2018**, *227*, 425–432; c) C. Wang, Z. Xie, K. E. deKrafft, W. Lin, *J. Am. Chem. Soc.* **2011**, *133*, 13445–13454; d) J. Liu, K. Zhang, Z. Chen, Z.-W. Wei, L. Zhang, *Chem. Asian J.* **2020**; e) E. M. Thoresen, S. Øien-Ødegaard, G. Kaur, M. Tilset, K. P. Lillerud, M. Amedjkouh, *RSC Adv.* **2020**, *10*, 9052–9062; f) A. Santiago-Portillo, H. G. Baldoví, E. Carbonell, S. Navalón, M. Álvaro, H.

García, B. Ferrer, *J. Phys. Chem. C* **2018**, *122*, 29190–29199; g) X. Yu, S. M. Cohen, *Chem. Commun.* **2015**, *51*, 9880–9883; h) X. Deng, Y. Qin, M. Hao, Z. Li, *Inorg. Chem.* **2019**, *58*, 16574–16580; i) G. Lan, Y. Quan, M. Wang, G. T. Nash, E. You, Y. Song, S. S. Veroneau, X. Jiang, W. Lin, *J. Am. Chem. Soc.* **2019**, *141*, 15767–15772.

[17] P. Ghosh, T. G. Spiro, *J. Am. Chem. Soc.* **1980**, *102*, 5543–5549.

[18] H. He, W. Li, Z. Xie, X. Jing, Y. Huang, *Chem. Res. Chin. Univ.* **2014**, *30*, 310–314.

[19] H. Takeda, M. Ohashi, Y. Goto, T. Ohsuna, T. Tani, S. Inagaki, *Chem. Eur. J.* **2014**, *20*, 9130–9136.

[20] G. J. Barbante, T. D. Ashton, E. H. Doeven, F. M. Pfeffer, D. J. D. Wilson, L. C. Henderson, P. S. Francis, *ChemCatChem* **2015**, *7*, 1655–1658.

[21] A. Jana, J. Mondal, P. Borah, S. Mondal, A. Bhaumik, Y. Zhao, *Chem. Commun.* **2015**, *51*, 10746–10749.

[22] P. Kohls, Thesis, University of Regensburg, **2015**.

[23] Z. Hao, S. Li, J. Sun, S. Li, F. Zhang, *Appl. Catal, B* **2018**, *237*, 366–372.

[24] P. Kumar, S. Varma, S. L. Jain, *J. Mater. Chem. A* **2014**, *2*, 4514–4519.

[25] F. Peng, P. Zhi, H. Ji, H. Zhao, F.-Y. Kong, X.-Z. Liang, Y.-M. Shen, *RSC Adv.* **2017**, *7*, 19948–19953.

[26] X. Ju, D. Li, W. Li, W. Yu, F. Bian, *Adv. Synth. Catal.* **2012**, *354*, 3561–3567.

[27] P. Zhi, Z.-W. Xi, D.-Y. Wang, W. Wang, X.-Z. Liang, F.-F. Tao, R.-P. Shen, Y.-M. Shen, *New J. Chem.* **2018**, *43*, 709–717.

[28] S. Kramer, N. R. Bennedsen, S. Kegnæs, *ACS Catal.* **2018**, *8*, 6961–6982.

[29] a) C.-A. Wang, Y.-F. Han, K. Nie, Y.-W. Li, *Mater. Chem. Front.* **2019**, *3*, 1909–1917; b) Z.-Y. Xu, Y. Luo, D.-W. Zhang, H. Wang, X.-W. Sun, Z.-T. Li, *Green Chem.* **2019**, *22*, 136–143.

[30] Z. Xie, C. Wang, K. E. deKrafft, W. Lin, *J. Am. Chem. Soc.* **2011**, *133*, 2056–2059.

[31] J.-L. Wang, C. Wang, K. E. deKrafft, W. Lin, *ACS Catal.* **2012**, *2*, 417–424.

[32] C. Wang, Z. Xie, K. E. deKrafft, W. Lin, *ACS Appl. Mater. Interfaces* **2012**, *4*, 2288–2294.

[33] W.-J. Yoo, S. Kobayashi, *Green Chem.* **2014**, *16*, 2438–2442.

[34] H.-P. Liang, Q. Chen, B.-H. Han, *ACS Catal.* **2018**, *8*, 5313–5322.

[35] G. Zhang, I. Y. Song, T. Park, W. Choi, *Green Chem.* **2012**, *14*, 618–621.

[36] B. Tambosco, K. Segura, C. Seyrig, D. Cabrera, M. Port, C. Ferroud, Z. Amara, *ACS Catal.* **2018**, *8*, 4383–4389.

[37] X. Li, Z. Hao, F. Zhang, H. Li, *ACS Appl. Mater. Interfaces* **2016**, *8*, 12141–12148.

[38] C. Eichinger, Master Thesis, University of Regensburg, **2016**.

[39] J. M. Fraile, J. I. García, M. A. Harmer, C. I. Herrerías, J. A. Mayoral, O. Reiser, H. Werner, *J. Mater. Chem.* **2002**, *12*, 3290–3295.

[40] a) J. D. Nguyen, J. W. Tucker, M. D. Konieczynska, C. R. J. Stephenson, *J. Am. Chem. Soc.* **2011**, *133*, 4160–4163; b) C.-J. Wallentin, J. D. Nguyen, P. Finkbeiner, C. R. J. Stephenson, *J. Am. Chem. Soc.* **2012**, *134*, 8875–8884.

[41] K. Kalyanasundaram, *Coord. Chem. Rev.* **1982**, *46*, 159–244.

[42] A. G. Condie, J. C. González-Gómez, C. R. J. Stephenson, *J. Am. Chem. Soc* **2010**, *132*, 1464–1465.

[43] H. Bartling, A. Eisenhofer, B. König, R. M. Gschwind, *J. Am. Chem. Soc.* **2016**, *138*, 11860–11871.

[44] C. Eichinger, S. Budde, O. Reiser, *Manuscript in preparation* **2020**.

[45] D. Cambié, C. Bottecchia, N. J. W. Straathof, V. Hessel, T. Noël, *Chem. Rev.* **2016**, *116*, 10276–10341.

[46] Y. Cai, Y. Tang, L. Fan, Q. Lefebvre, H. Hou, M. Rueping, *ACS Catal.* **2018**, *8*, 9471–9476.

[47] V. Blanchard, Z. Asbai, K. Cottet, G. Boissonnat, M. Port, Z. Amara, *Org. Process Res. Dev.* **2020**, *24*, 822–826.

[48] A. Schätz, O. Reiser, W. J. Stark, *Chem. Eur. J.* **2010**, *16*, 8950–8967.

[49] A. Akbarzadeh, M. Samiei, S. Davaran, *Nanoscale Res. Lett.* **2012**, *7*, 1–13.

[50] a) S. Laurent, D. Forge, M. Port, A. Roch, C. Robic, L. Vander Elst, R. N. Muller, *Chem. Rev.* **2008**, *108*, 2064–2110; b) Q. M. Kainz, O. Reiser, *Acc. Chem. Res.* **2014**, *47*, 667–677.

[51] a) D. Ma, J. Guan, S. Dénommée, G. Enright, T. Veres, B. Simard, *Chem. Mater.* **2006**, *18*, 1920–1927; b) D. Ma, Z. J. Jakubek, B. Simard, *J. Nanosci. Nanotechnol.* **2006**, *6*, 3677–3684.

[52] R. N. Grass, E. K. Athanassiou, W. J. Stark, *Angew. Chem. Int. Ed.* **2007**, *46*, 4909–4912.

[53] a) L. Stadler, M. Homafar, A. Hartl, S. Najafishirtari, M. Colombo, R. Zboril, P. Martin, M. B. Gawande, J. Zhi, O. Reiser, *ACS Sustainable Chem. Eng.* **2019**, *7*, 2388–2399; b) G. Purohit, D. S. Rawat, O. Reiser, *ChemCatChem* **2020**, *12*, 569–575; c) Q. M. Kainz, R. Linhardt, R. N. Grass, G. Vilé, J. Pérez-Ramírez, W. J. Stark, O. Reiser, *Adv. Funct. Mater.* **2014**, *24*, 2020–2027.

[54] C. M. Eichenseer, B. Kastl, M. A. Pericàs, P. R. Hanson, O. Reiser, *ACS Sustainable Chem. Eng.* **2016**, *4*, 2698–2705.

[55] S. Fernandes, Thesis, University of Regensburg, **2016**.

[56] R. K. Singh, T.-H. Kim, K. D. Patel, J. C. Knowles, H.-W. Kim, *J. Biomed. Mater. Res. A* **2012**, 1734–1742.

[57] C. Liu, Y. Li, Q. Duan, *Appl. Surf. Sci.* **2020**, *503*, 144111.

[58] Y. Lu, L. Xu, C. Liu, *Appl Organometal Chem.* **2020**, 1–15.

[59] a) M. J. Lima, M. J. Sampaio, C. G. Silva, A. M.T. Silva, J. L. Faria, *Catal. Today* **2019**, *328*, 293–299; b) Z. Wu, X. Chen, X. Liu, X. Yang, Y. Yang, *Nanoscale Res. Lett.* **2019**, *14*, 147; c) X. Zhou, B. Jin, R. Chen, F. Peng, Y. Fang, *Mater. Res. Bull.* **2013**, *48*, 1447–1452.

[60] P. Li, G.-W. Wang, X. Zhu, L. Wang, *Tetrahedron* **2019**, *75*, 3448–3455.

[61] C. S. Gill, B. A. Price, C. W. Jones, *J. Catal.* **2007**, *251*, 145–152.

[62] M. Walker, W. E. Rudzinski, *Microchem. J.* **1993**, *47*, 178–181.

[63] J. V. Nguyen, C. W. Jones, *Macromolecules* **2004**, *37*, 1190–1203.

[64] a) Q. M. Kainz, S. Fernandes, C. M. Eichenseer, F. Besostri, H. Körner, R. Müller, O. Reiser, *Faraday Discuss.* **2014**, *175*, 27–40; b) C.-J. Yoo, D. Rackl, W. Liu, C. B. Hoyt, B. Pimentel, R. P. Lively, H. M. L. Davies, C. W. Jones, *Angew. Chem. Int. Ed.* **2018**, *57*, 10923–10927.

[65] J. J. Molloy, J. B. Metternich, C. G. Daniliuc, A. J. B. Watson, R. Gilmour, *Angew. Chem. Int. Ed.* **2018**, *57*, 3168–3172.

[66] K. Singh, W. Trinh, R. Latifi, J. D. Weaver, *Org. Biomol. Chem.* **2019**, *17*, 1854–1861.

[67] a) V. M. Dembitsky, *J. Nat. Med.* **2008**, *62*, 1–33; b) V. M. Dembitsky, *Phytomedicine* **2014**, *21*, 1559–1581.

[68] a) J. J. Devery Iii, J. J. Douglas, J. D. Nguyen, K. P. Cole, R. A. Flowers Ii, C. R. J. Stephenson, *Chem. Sci.* **2015**, *6*, 537–541; b) S. Schmidbauer, A. Hohenleutner, B. König, *Beilstein J. Org. Chem.* **2013**, *9*, 2088–2096.

[69] a) M. Pirtsch, S. Paria, T. Matsuno, H. Isobe, O. Reiser, *Chem. Eur. J.* **2012**, *18*, 7336–7340; b) S. Paria, O. Reiser, *ChemCatChem* **2014**, *6*, 2477–2483; c) O. Reiser, *Acc. Chem. Res.* **2016**, *49*, 1990–1996; d) T. Rawner, M. Knorn, E. Lutsker, A. Hossain, O. Reiser, *J. Org. Chem.* **2016**, *81*, 7139–7147; e) J.-M. Kern, J.-P. Sauvage, *J. Chem. Soc, Chem. Commun.* **1987**, 546–548; f) A. Hossain, A. Vidyasagar, C. Eichinger, C. Lankes, J. Phan, J. Rehbein, O. Reiser, *Angew. Chem. Int. Ed.* **2018**, *57*, 8288–8292.

[70] a) A. Hossain, A. Bhattacharyya, O. Reiser, *Science* **2019**, *364*; b) A. Hossain, S. Engl, E. Lutsker, O. Reiser, *ACS Catal.* **2019**, *9*, 1103–1109; c) T. Rawner, E. Lutsker, C. A. Kaiser, O. Reiser, *ACS Catal.* **2018**, *8*, 3950–3956.

[71] S. Engl, O. Reiser, *Eur. J. Org. Chem.* **2020**, 1523–1533.

[72] a) D. Friedmann, A. Hakki, H. Kim, W. Choi, D. Bahnemann, *Green Chem.* **2016**, *18*, 5391–5411; b) X. Lang, X. Chen, J. Zhao, *Chem. Soc. Rev.* **2014**, *43*, 473–486; c) J. Chen, J. Cen, X. Xu, X. Li, *Catal. Sci. Technol.* **2016**, *6*, 349–362.

[73] S. Gisbertz, B. Pieber, *ChemPhotoChem* **2020**, *4*, 1–21.

[74] Y. Wang, X. Wang, M. Antonietti, *Angew. Chem. Int. Ed.* **2012**, *51*, 68–89.

[75] J. Liu, T. Zhang, Z. Wang, G. Dawson, W. Chen, *J. Mater. Chem.* **2011**, *21*, 14398.

[76] X. Li, J. Zhang, L. Shen, Y. Ma, W. Lei, Q. Cui, G. Zou, *Appl. Phys. A* **2009**, *94*, 387–392.

[77] A. Savateev, S. Pronkin, J. D. Epping, M. G. Willinger, M. Antonietti, D. Dontsova, *J. Mater. Chem. A* **2017**, *5*, 8394–8401.

[78] X. Wang, K. Maeda, X. Chen, K. Takanabe, K. Domen, Y. Hou, X. Fu, M. Antonietti, *J. Am. Chem. Soc.* **2009**, *131*, 1680–1681.

[79] L. Flamigni, A. Barbieri, C. Sabatini, B. Ventura, F. Barigelletti, *Top. Curr. Chem.* **2007**, *281*, 143–203.

[80] a) J. W. Tucker, J. D. Nguyen, J. M. R. Narayanam, S. W. Krabbe, C. R. J. Stephenson, *Chem. Commun.* **2010**, *46*, 4985–4987; b) M. S. Lowry, J. I. Goldsmith, J. D. Slinker, R. Rohl, R. A. Pascal, G. G. Malliaras, S. Bernhard, *Chem. Mater.* **2005**, *17*, 5712–5719.

[81] A. Juris, V. Balzani, P. Belser, A. von Zelewsky, *Helv. Chim. Acta* **1981**, *64*, 2175–2182.

[82] X. Wang, K. Maeda, A. Thomas, K. Takanabe, G. Xin, J. M. Carlsson, K. Domen, M. Antonietti, *Nat. Mater.* **2009**, *8,* 76–80.

[83] J. Wen, J. Xie, X. Chen, X. Li, *Appl. Surf. Sci.* **2017**, *391*, 72–123.

[84] J. Liu, H. Wang, M. Antonietti, *Chem. Soc. Rev.* **2016**, *45*, 2308–2326.

[85] A. Savateev, I. Ghosh, B. König, M. Antonietti, *Angew. Chem. Int. Ed.* **2018**, *57*, 15936–15947.

[86] M. Woźnica, N. Chaoui, S. Taabache, S. Blechert, *Chem. Eur. J.* **2014**, *20*, 14624–14628.

[87] J. Wang, L. Xue, M. Hong, B. Ni, T. Niu, *Green Chem.* **2020**, *22*, 411–416.

[88] M. Baar, S. Blechert, *Chem. Eur. J.* **2015**, *21*, 526–530.

[89] I. Ghosh, J. Khamrai, A. Savateev, N. Shlapakov, M. Antonietti, B. König, *Science* **2019**, *365*, 360–366.

[90] A. U. Meyer, V. W.-h. Lau, B. König, B. V. Lotsch, *Eur. J. Org. Chem.* **2017**, *2017*, 2179–2185.

[91] a) A. U. Meyer, S. Jäger, Hari, Durga, Prasad, B. König, *Adv. Synth. Catal.* **2015**, *357*, 2050–2054; b) A. U. Meyer, K. Straková, T. Slanina, B. König, *Chem. Eur. J.* **2016**, *22*, 8694–8699.

[92] L. Li, D. Cruz, A. Savateev, G. Zhang, M. Antonietti, Y. Zhao, *Appl. Catal, B* **2018**, *229*, 249–253.

[93] G. P. Mane, S. N. Talapaneni, K. S. Lakhi, H. Ilbeygi, U. Ravon, K. Al-Bahily, T. Mori, D.-H. Park, A. Vinu, *Angew. Chem. Int. Ed.* **2017**, *56*, 8481–8485.

[94] L. Huang, Z. Liu, W. Chen, D. Cao, A. Zheng, *J. Mater. Chem. A* **2018**, *6*, 7168–7174.

[95] a) L. Ge, C. Han, J. Liu, Y. Li, *Appl. Catal, A* **2011**, *409-410*, 215–222; b) L. Zi-ya, Z. Man-ying, W. Jing-ling, *ChemistrySelect* **2018**, *3*, 10630–10636; c) Y. Bu, Z. Chen, W. Li, *Appl. Catal, B* **2014**, *144*, 622–630.

[96] S. Qi, Y. Fan, J. Wang, X. Song, W. Li, M. Zhao, *Nanoscale* **2020**, *12*, 306–315.

[97] a) H. Wang, M. Li, Q. Lu, Y. Cen, Y. Zhang, S. Yao, *ACS Sustainable Chem. Eng.* **2019**, *7*, 625–631; b) S. Vadivel, S. Hariganesh, B. Paul, S. Rajendran, A. Habibi-Yangjeh, D. Maruthamani, M. Kumaravel, *Chem. Phys. Lett.* **2020**, *738*, 136862.

[98] Y. Miyake, Y. Ashida, K. Nakajima, Y. Nishibayashi, *Chem. Commun.* **2012**, *48*, 6966–6968.

[99] a) L. Möhlmann, M. Baar, J. Rieß, M. Antonietti, X. Wang, S. Blechert, *Adv. Synth. Catal.* **2012**, *354*, 1909–1913; b) L. Möhlmann, S. Blechert, *Adv. Synth. Catal.* **2014**, *356*, 2825–2829.

[100] P. Kohls, D. Jadhav, G. Pandey, O. Reiser, *Org. Lett.* **2012**, *14*, 672–675.

[101] L. Ruiz Espelt, E. M. Wiensch, T. P. Yoon, *J. Org. Chem.* **2013**, *78*, 4107–4114.

[102] A. Savateev, S. Pronik, J. D. Epping, M. G. Willinger, C. Wolff, D. Nehler, M. Antonietti, D. Dontsova, *ChemCatChem* **2017**, *9*, 167–174.

C. Photochemical Decarboxylations

1. Introduction

Carboxylic acids are widespread in nature. Ranging from simple compounds such as formic acid or fatty acids and amino acids, to more complex structures such as pipecolic acid (**198**), which is present in plants and animals, abietic acid (**199**), occurring in trees, or biotin (vitamin H, **200**), playing a crucial role in metabolic processes (Figure 14).

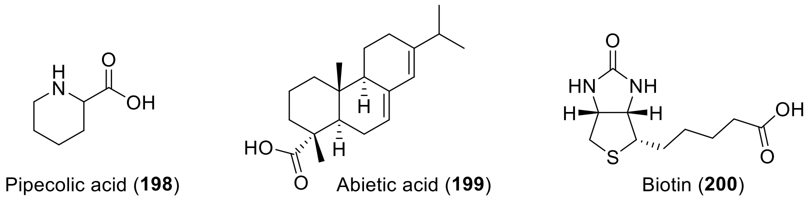

Figure 14: Various carboxylic acids occurring in nature.

Due to their easy accessibility and low price, carboxylic acids became a target for organic chemists to perform decarboxylations with a long time ago.[1] As early as 1848, Kolbe presented the first electrolytic decarboxylation using valeric acid and butyric acid.[2] This strategy, the so-called Kolbe electrolysis, gives rise to the corresponding homocoupling products or – in case multiple carboxylic acids are present – hetero coupling products and carbon dioxide as the sole byproduct. Other prominent examples include the Hundsdiecker reaction, i.e. to decarboxylate the silver or mercury salt of a carboxylic acid by treatment with elemental bromine, which results in the formation of a C-Br bond.[3] In 1983 the Barton decarboxylation was invented, opening up the way to UV light-driven decarboxylations. In presence of DCC and DMAP, the carboxylic acid **201** is coupled with the hydroxypyridinethione **202** to give the corresponding thioxypyridinyl **203** (Scheme 39).[4] The latter is then treated with tributyltin hydride and AIBN as radical initiator, which is triggered by heat or UV light irradiation to give the decarboxylated alkene **204**.

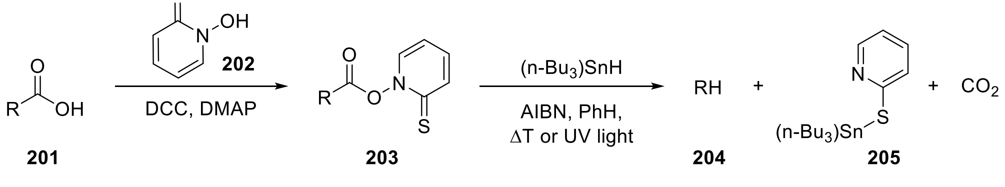

Scheme 39: Schematic representation of the Barton decarboxylation.

Next to the decarboxylation *via* benzophenone oxime esters through UV light irradiation, invented by Tsuchiya *et al.*,[5] in 1988 Okada presented the first photosensitized decarboxylation with visible light *via N*-(acyloxy)phthalimides.[6] For this, stoichiometric amounts of both *tert*-butylthiol as hydrogen source and 1,6-bis(dimethyl-amino)pyrene (BDMAP) as photosensitizer were needed to generate the corresponding alkene, carbon dioxide, and phthalimide. Due to the unpleasant atom economy, further improvements were made in the same group until they developed a protocol in which catalytic amounts of $[Ru(bpy)_3]Cl_2$ (**1**) could be employed as photosensitizer along with BNAH as sacrificial electron donor.[7] Moreover, following the same procedure, decarboxylative Michael additions were established by exchanging the hydrogen source *tert*-butylthiol for a coupling partner such as methyl vinyl ketone (**196**, Scheme 40).[8] As can be seen, the excited ruthenium catalyst is reduced by BNAH (**206**), and has, therefore, a sufficiently high reduction potential to transfer an electron to the *N*-(acyloxy)phthalimide **205**. Upon the so caused extrusion of carbon dioxide and phthalimide (**209**), the radical **213** is formed, which undergoes a subsequent Michael-like addition with methyl vinyl ketone (**196**). Hence, the desired product **207** could be isolated in 68%, however, also the unwanted reduced product **208** was obtained in 18%. This was successfully suppressed by increasing the amount of the alkene **196** from 1.0 equiv to 1.9 equiv.

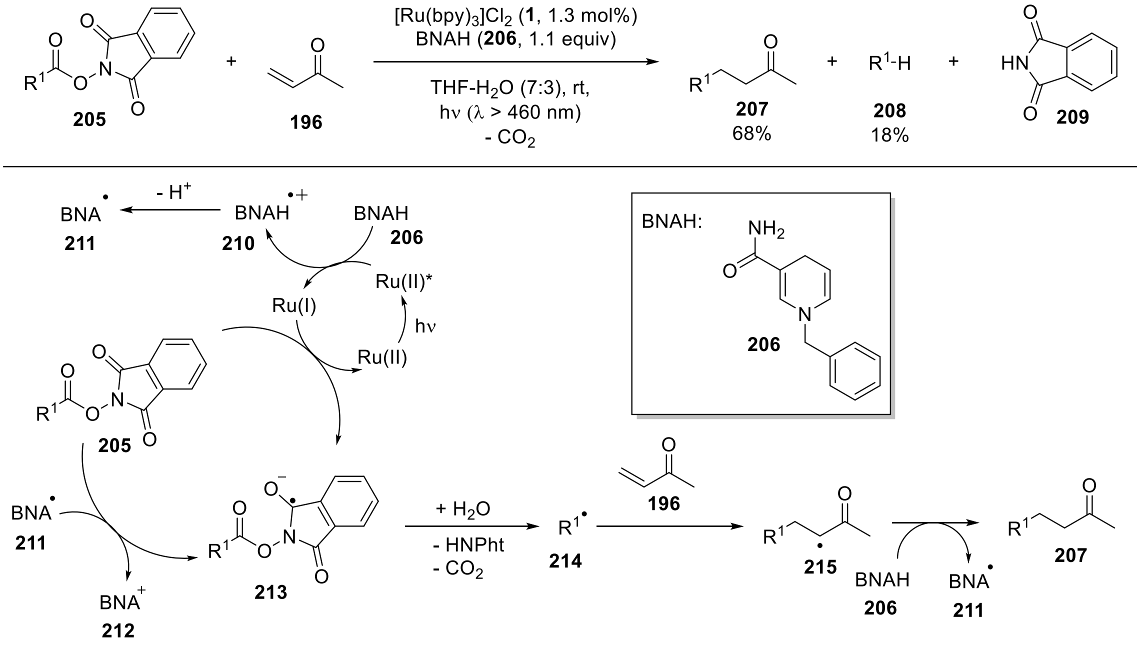

205
196
[Ru(bpy)3]Cl2 (1, 1.3 mol%)
BNAH (206, 1.1 equiv)
THF-H2O (7:3), rt,
hν (λ > 460 nm)
- CO2
207
68%
R1-H
208
18%
209
BNA• 211
- H+
BNAH•+ 210
BNAH 206
Ru(I)
Ru(II)*
hν
Ru(II)
BNAH:
206
205
BNA• 211
BNA+ 212
213
+ H2O
- HNPht
- CO2
R1• 214
196
215
BNAH 206
BNA• 211
207

Scheme 40: First visible light-mediated decarboxylative Michael addition.

Based on these research results, many studies on photocatalytic decarboxylations followed. Among others the group of Overman was a pioneer in this field, establishing the synthesis of (-)aplyviolene, where decarboxylation plays a crucial role.[9] However, due to the high reduction potentials of the starting materials, the reductive quenching cycle of [Ru(bpy)$_3$]Cl$_2$ (**1**) had to be exploited in basically every example in which the decarboxylation takes place *via* *N*-(acyloxy)phthalimides.[10] Only in 2013, our group was the first reporting the synthesis of (spiro)anellated furans by exploiting the oxidative quenching cycle of [Ir(ppy)$_2$(dtbbpy)]PF$_6$ (**6**) and thus improving the atom economy by overcoming the need for a sacrificial electron donor (Scheme 41).[11]

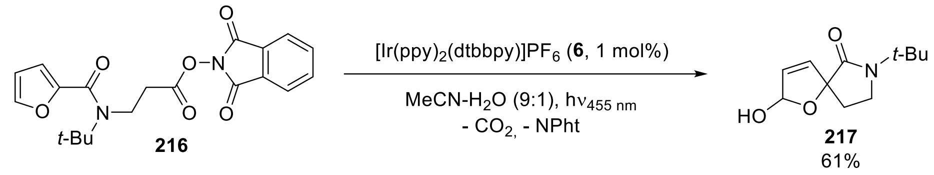

Scheme 41: First decarboxylative cyclization exploiting the oxidative quenching cycle of a photocatalyst.

Taking advantage of the fact that the electron-acceptor strength of *N*-(acyloxy)phthalimides can be increased *via* hydrogen bonding,[12] Glorius and coworkers demonstrated the decarboxylative alkylation of various styrenes exploiting the oxidative quenching cycle of a photocatalyst in the presence of water or alcohols (Scheme 42).[13] A SET from the excited catalyst to the *N*-(acyloxy)pthalimide **218** causes the cleavage of CO$_2$ and phthalimide (**209**). The generated radical **222** rapidly undergoes a reaction with styrene **219** to form **223**, which is subsequently oxidized from the catalyst to the carbocation **224**. Noteworthy, closing the catalytic cycle requires the formed alcoholate or hydroxy anion to act as nucleophile, generating an alcohol or ether scaffold to afford the product **220**.

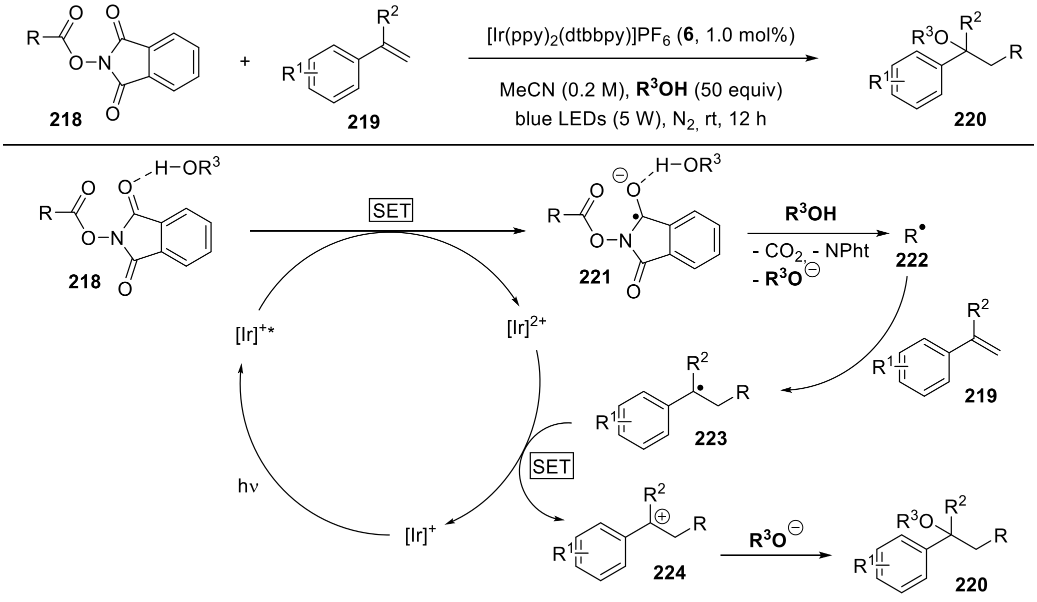

Scheme 42: Visible light-mediated decarboxylative alkylation of styrenes.

Similar to this research, Song and his group established the decarboxylative alkylation of silyl enol ethers **218** (Scheme 43).[14] Taking into account that the reaction proceeds *via* the same mechanism as presented before, and because TMS is a good leaving group, this bears the advantage that the cation which is formed during the reaction (**224**) would not have to be trapped by a nucleophile, but the catalytic cycle is closed by TMS cleavage, furnishing various ketones **226**.

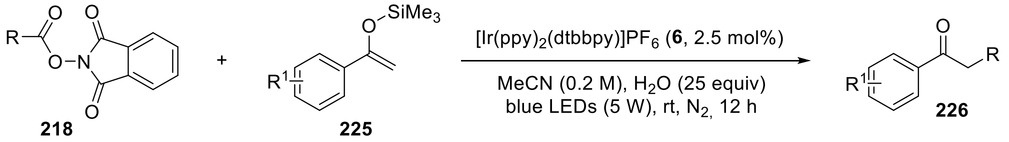

Scheme 43: Visible light-mediated decarboxylative alkylation of silyl enol ethers.

Only recently Fu *et al.* further developed this protocol by omitting the iridium-based catalyst and using a combination of PPh_3 and NaI as catalytic active species instead.[15] Remarkably, not only additions to silyl enol ethers were presented, but also Minisci-type alkylations, even in an enantioselective fashion by employing chiral phosphoric acids as auxiliary.

Building on these techniques, starting from readily available L-glutamic acid (**227**) we established the photochemical synthesis of various unnatural amino acids and their subsequent transformation to pipecolic acid derivatives. The complete sequence is shown in Scheme 44. Protecting the α-carboxylic acid of **227** by derivatization to an oxazolidinone or hydantoin, and activating the γ-carboxylic acid by forming an active ester with phthalimide made L-glutamic acid an ideal, yet affordable starting material (**228**). Exploiting different quenching cycles of [Ru(bpy)$_3$]Cl$_2$ (**1**) and *fac*-Ir(ppy)$_3$ (**5**) for photochemical decarboxylation a variety of intermolecular coupling partners (upper pathway), as well as intramolecular reactions (lower pathway), were tested with moderate to excellent yields. Moreover, the chiral information is retained in all products and a successful upscaling to 4.0 mmol was demonstrated.[iii]

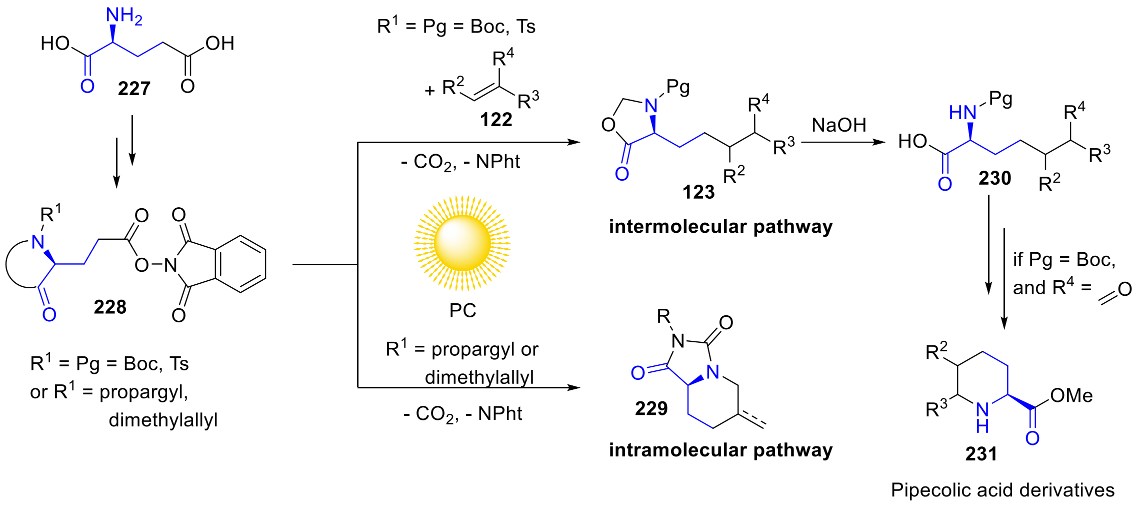
NH2
HO
OH
O
227
O
R1 = Pg = Boc, Ts
+ R2
R4
R3
122
- CO2, - NPht
PC
R1 = propargyl or dimethylallyl
- CO2, - NPht
R1
N
O
O
O-N
O
228
O
R1 = Pg = Boc, Ts
or R1 = propargyl,
dimethylallyl
Pg
N
O
O
R4
R3
R2
123
intermolecular pathway
NaOH
HN
Pg
HO
O
230
R4
R3
R2
if Pg = Boc,
and R4 = O
R
N
O
O
N
229
intramolecular pathway
R2
R3
N
H
OMe
O
231
Pipecolic acid derivatives

Scheme 44: Photochemical decarboxylation of L-glutamic acid derivatives followed by intermolecular reactions towards pipecolic acid derivatives (upper) and intramolecular reactions (lower).

[iii] The project was developed in collaboration with S. Budde. The individual contributions are indicated.

2. Synthesis of starting materials

As already mentioned, for both intermolecular and intramolecular reactions, readily available L-glutamic acid (**227**) served as basis. Starting with the synthesis of *N*-(acyloxy)phthalimides **121a** and **121b**, respectively, suitable for intermolecular reactions, overall three reaction steps had to be conducted (Scheme 45). Upon amine protection as *tert*-butoxycarbonyl (Boc) or toluenesulfonyl (Ts), the α-carboxylic acid was converted to an oxazolidinone derivative through treatment with paraformaldehyde in presence of catalytic amounts of acid. The oxazolidinone functionalization bears the advantage that it protects the carboxylic acid during the following reaction steps. At the same time the group can easily be removed again under mild reaction conditions to obtain the corresponding amino acid. The final reaction to the active esters with *N*-hydroxyphthalimide led to the desired starting materials TsGluOxNPhth **121a** and BocGluOxNPhth **121b**.

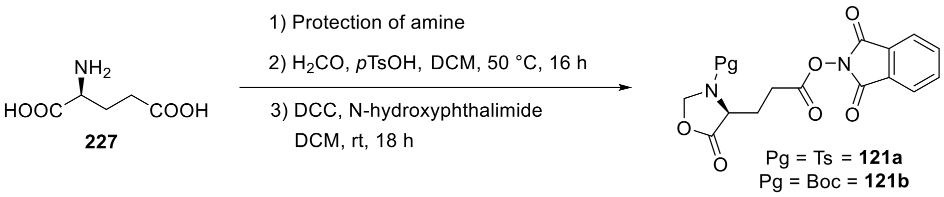

Scheme 45: Synthesis of *N*-(acyloxy)phthalimides **121a** and **121b** suitable for intermolecular reactions.

The synthetic steps towards the *N*-(acyloxy)phthalimides for intramolecular reactions are depicted in Scheme 46.[iv] For this, two different routes were explored. In case the final compound should be functionalized with a benzyl group (pathway A), at first, the hydantoin **232** is formed, followed by esterification with methanol and subsequent benzylation (**233**). After coupling with propargyl derivative **234** or 3,3-dimethylallylbromid (**238**), respectively, an ensuing hydrolysis of the methyl ether and activation with *N*-hydroxyphthalimide provided the starting materials **237a** and **239**. Reacting L-glutamic acid (**227**) with phenyl isocyanate, on the other hand, gave directly rise to phenyl substituted hydantoin **236** (pathway B). Esterification with methanol and alkylation with propargyl **234** led to intermediate **235**, which was hydrolyzed to the free carboxylic acid and finally activated with *N*-hydroxyphthalimide to give the desired *N*-(acyloxy)phthalimide **237b**. Overall, the yields were in a very high range between 60% and 93%.

[iv] Starting materials for intramolecular reactions were synthesized by S. Budde.

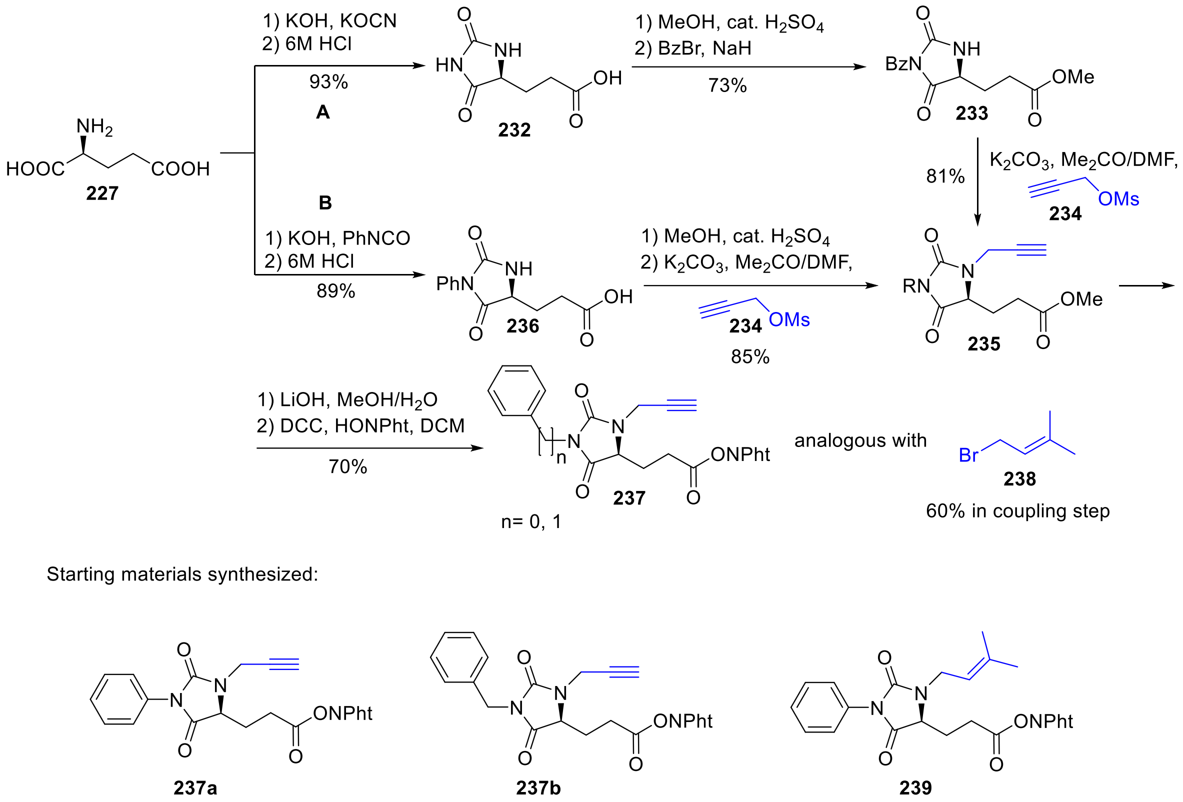
1) KOH, KOCN
2) 6M HCl
93%
A
232
1) MeOH, cat. H2SO4
2) BzBr, NaH
73%
233
227
B
1) KOH, PhNCO
2) 6M HCl
89%
236
1) MeOH, cat. H2SO4
2) K2CO3, Me2CO/DMF,
234
85%
81%
K2CO3, Me2CO/DMF,
234
235
1) LiOH, MeOH/H2O
2) DCC, HONPht, DCM
70%
237
n= 0, 1
analogous with
238
60% in coupling step
Starting materials synthesized:
237a
237b
239

Scheme 46: Synthesis of different *N*-(acyloxy)phthalimides suitable for intramolecular reactions.

3. Photochemical reactions

3.1. Intermolecular reactions exploiting the reductive quenching cycle of catalyst

With these substances in hand, we started our investigations towards the best reaction conditions for the intermolecular pathway exploiting the reductive quenching cycle of $[Ru(bpy)_3]Cl_2$ (**1**).[v] Therefore, fluorinated crotonate ester **122a** served as model reaction partner for activated L-glutamic acid **121a**, forming the coupling product **123aa** (Table 23).

Table 23: Investigation of the best reaction conditions for exploiting the reductive quenching cycle of catalyst.

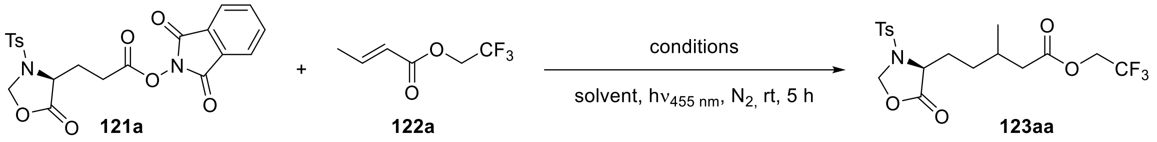

Entry	Solvent	Deviation from standard reaction conditions[a]	Yield [%][b]
1	THF/H_2O (3:1)	15 mol% Hantzsch ester, 1.0 equiv DIPEA	15
2	Acetone/H_2O (6:1)	-	43
3	Acetone/H_2O (3:1)	-	51
4	THF/H_2O (3:1)	10 equiv **122a**	35
5	Acetone/H_2O (3:1)	10 equiv **122a**	71 (68)[c]
6	MeCN (dry)	no	45
7	Acetone/H_2O (3:1)	2.0 equiv Hantzsch ester	68
8	Acetone/H_2O (3:1)	1.2 equiv **122a**	20
9	Acetone/H_2O (3:1)	2.0 equiv Hantzsch ester, 10 equiv **122a**	30
10	DMF	no	17
11	Acetone/H_2O (3:1)	2 mol% $[Ir(dtbbpy)(ppy)_2]PF_6$ (**6**)	37
12	Acetone/H_2O (3:1)	0.5 mol% $[Ru(bpy)_3]Cl_2$ (**1**)	4
13	Acetone/H_2O (3:1)	0.5 mol% $[Ru(bpy)_3]Cl_2$ (**1**), 16 h irradiation	42
14	Acetone/H_2O (3:1)	1 equiv LiBr	23
15	MeCN (dry)	2 mol% *fac*-$Ir(ppy)_3$ (**5**), no Hantzsch ester	n.r.

[a]Standard reaction conditions: **121a** (0.20 mmol, 1.0 equiv), **122a** (1.0 mmol, 5.0 equiv), Hantzsch ester (0.20 mmol, 1.0 equiv), $[Ru(bpy)_3]Cl_2$ (**1**, 2.0 mol%), solvent (2 mL), N_2 atmosphere, irradiation with blue LED (λ = 455 nm) for 5. [b]Yields determined by ^{19}F-NMR using 1,4-di(trifluoro)methylbenzene as internal standard. [c]Isolated yield.

---

[v] Optimization reactions for the reductive quenching cycle were performed by S. Budde.

Employing 2.0 mol% [Ru(bpy)$_3$]Cl$_2$ (**1**) as photocatalyst, 1.0 equiv Hantzsch ester as sacrificial electron donor, acetone/water (3:1) as solvent and 10 equiv alkene gave the best results for the test substrate **123aa** (71%, Table 23, entry 5). Lower catalyst loadings (entry 12 and 13), lower substrate concentration (entry 3 and 8) and other solvent systems (entry 4, 6 and 10) proved to impair the reaction. It should be noted that using *fac*-Ir(ppy)$_3$ (**5**) as catalyst, exploiting its oxidative quenching cycle, did not lead to any conversion of the starting material (entry 15).

Next, we explored the capability of this reaction by testing various alkenes (Table 24).[vi] As already stated, fluorinated crotonate **122a** gave 68% isolated yield (entry 1). When employing the corresponding acrylate **122b** and Boc-protected *N*-(acyloxy)phthalimide **121b** the yield dropped to 60%. As shown below, the variation of the protecting group from Boc to Ts does not affect the reaction outcome (entry 6 – 7). Thus, it can be concluded that primary alkenes are slightly less reactive than secondary ones. Whereas the Boc-protection of hydroxycyclopentenone **122d** turned out to be a good leaving group, forming product **123ad** in good yields (50%, entry 4), TBDMS (**122e)** is not, and only the addition product **123ae** was obtained (entry 5). Besides, the yield dropped to 36% which is due to the more sterically demanding protecting group compared to Boc. Furthermore, enol acetate **122f** proved to be a good coupling partner and gave the same yield for both Boc- and Ts-protected starting material (entry 6 – 7). Interestingly, enol acetate **122f** behaved like silyl enol ethers,[14] forming upon acetate cleavage the ketone **123af** and **123bf**, respectively.

[vi] Entries 1-3 were performed by S. Budde.

Table 24: Substrate scope exploiting the reductive quenching cycle of $[Ru(bpy)_3]Cl_2$ (**1**).

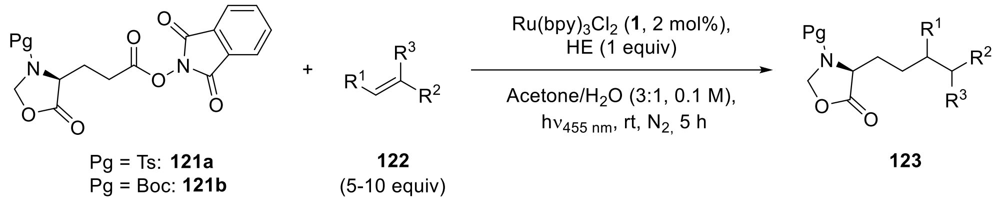
Pg
Ru(bpy)3Cl2 (1, 2 mol%), HE (1 equiv)
Acetone/H2O (3:1, 0.1 M), hν455 nm, rt, N2, 5 h
R1
R2
R3
Pg = Ts: 121a
Pg = Boc: 121b
122
(5-10 equiv)
123

Entry	Substrate		Product		Yield [%][a]
1	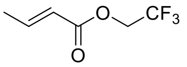	**122a**	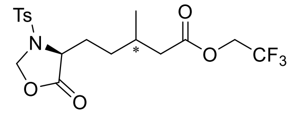	**123aa**	68
2	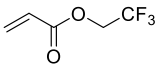	**122b**	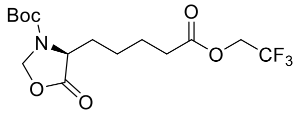	**123bb**	60
3	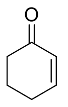	**122c**	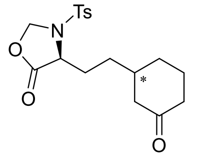	**123ac**	46
4	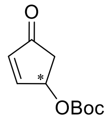	**122d**	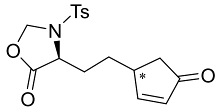	**123ad**	50
5	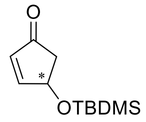	**122e**	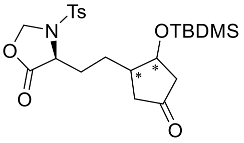	**123ae**	36
6	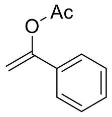	**122f**	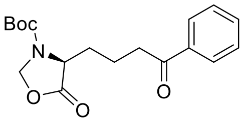	**123bf**	45
7	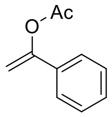	**122f**	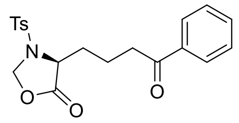	**123af**	45

Unless otherwise noted, the reaction conditions are as follows: *N*-(acyloxy)phthalimide **121a** or **121b** (0.20 mmol, 1.0 equiv), alkene **122** (2.0 mmol, 10 equiv), Hantzsch ester (0.20 mmol, 1.0 equiv) and $[Ru(bpy)_3]Cl_2$ (**1**, 2.0 mol%) were dissolved in acetone/water (3:1, 2 mL) and irradiated with a blue LED (λ = 455 nm) for 5 h at room temperature under N_2 atmosphere. [a]Isolated yields are given. [b]The amount of alkene **122** was reduced to 5.0 equiv (1.0 mmol).

Although these reaction conditions allow for a reasonable variety of coupling partners and unique reaction products, only moderate yields were obtained on average. As a result of the numerous components contained, it is difficult to adopt the conditions for the individual substrates. In other words, one has to fight against the bad solubility of Hantzsch ester and most alkenes other than crotonate **122a** or acrylate **122b**. This is why only half the amount of the alkene was utilized, i.e. 5 equiv. In addition, the need for Hantzsch ester as a sacrificial electron donor renders the reaction workup tedious due to multiple overlapping spots on TLC. However, attempts towards finding an appropriate substitute as electron donor were not successful and resulted in lower yields.

The proposed reaction mechanism is depicted in Scheme 47. First, Ru^{II} is transferred to its excited singlet state *via* visible light irradiation to abstract an electron from Hantzsch ester **240**. Having a sufficiently high reduction potential ($E_{1/2}^{II/I}$ = -1.33 V vs. SCE),[16] an electron is transferred to the *N*-(acyloxy)phthalimide **121** causing the extrusion of phthalimide and CO_2. This gives rise to a carbon-centered radical **244** which is trapped by an alkene **122**. The resulting radical intermediate **245**, in turn, abstracts a hydrogen atom from the Hantzsch ester radical **242** to form the desired product **123**.

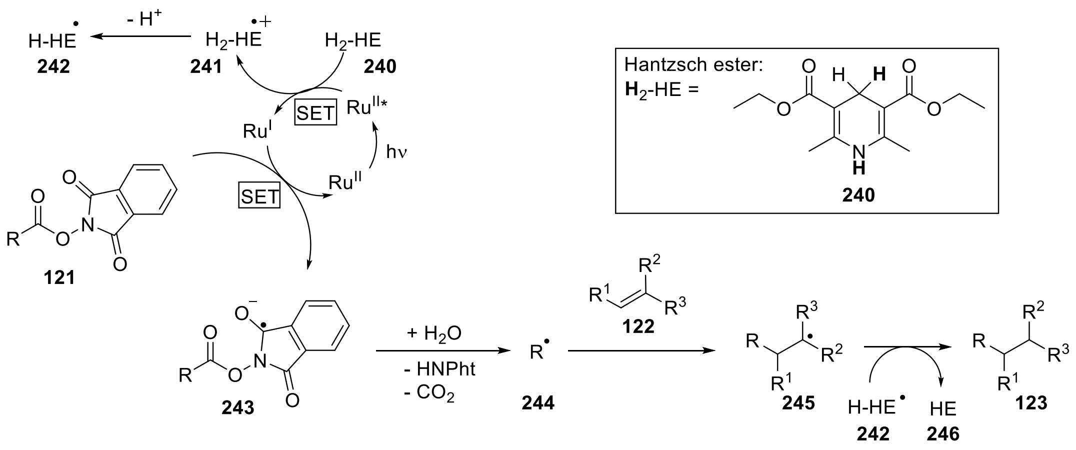

Scheme 47: Proposed reaction mechanism exploiting the reductive quenching cycle of $[Ru(bpy)_3]Cl_2$.

3.2. Intermolecular reactions exploiting the oxidative quenching cycle of catalyst

Driven by the work of F. Glorius,[13] Q. Song,[14] and our group,[11] we envisioned to perform this decarboxylative alkylation by exploiting the oxidative quenching cycle of the photocatalyst. This would make an additional sacrificial electron donor redundant and therefore not only make the reaction more environmentally benign, but also lead to more easily tunable reaction conditions. However, in the literature precedent, closing the catalytic cycle inevitably introduces a hydroxy or alcoholate anion, forming an alcohol or ether scaffold, respectively (see above, Scheme 42). Additionally, exploiting the oxidative quenching cycle using crotonate **122a** as a substrate led to no product formation. Therefore, we decided to trap the radical generated by decarboxylation with enol acetates or silyl enol ethers, as shown by Q. Song.[14] Doing so, the catalytic cycle is closed by cleaving the acetate or silane, respectively, forming a ketone. Therefore, various reactions based on *N*-(acyloxy)phthalimide **121b** and 1-phenylvinyl acetate (**122f**) or the corresponding silyl enol ether **122g** were screened to establish the best parameters (Table 25). When the same conditions were applied as in the research of Q. Song, employing [Ir(ppy)$_2$(dtbbpy)](PF$_6$) (**6**) as catalyst,[14] the same yield as with the reductive quenching cycle was obtained (47%, entry 1). Only when the *N*-(acyloxy)phthalimide **121b** was set as limiting factor and the silyl compound **122g** was used as trapping reagent, the yield could be increased to 70% (entry 4). Using PPh$_3$ and NaI as the photoredox active species[15a] did not lead to any improvement (entry 5). Screening of different transition metal-based photocatalysts revealed that *fac*-Ir(ppy)$_3$ (**5**) provided the best results for both Ac and TMS leaving group (entry 9 – 10). Noteworthy, solely for the enol acetate **122f** the catalyst loading could be reduced to 1 mol% without any negative impact (entry 14). The reaction did not proceed neither without photocatalyst or light, nor in the presence of oxygen (entry 16 – 18).

Table 25: Investigation of best reaction conditions for exploiting the oxidative quenching cycle of various photocatalysts.

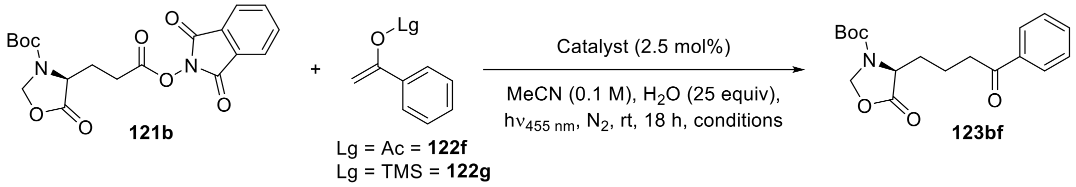
Boc
121b
Lg = Ac = 122f
Lg = TMS = 122g
Catalyst (2.5 mol%)
MeCN (0.1 M), H2O (25 equiv),
hν455 nm, N2, rt, 18 h, conditions
Boc
123bf

Entry	Photocatalyst	Lg	equiv **121b**	equiv **122**	Yield [%][a]
1	$[Ir(ppy)_2(dtbbpy)](PF_6)$ (**6**)	Ac	1.5	1.0	47
2	$[Ir(ppy)_2(dtbbpy)](PF_6)$ (**6**)	Ac	1.0	5.0	47
3	$[Ir(ppy)_2(dtbbpy)](PF_6)$ (**6**)	TMS	1.5	1.0	61
4	$[Ir(ppy)_2(dtbbpy)](PF_6)$ (**6**)	TMS	1.0	5.0	70
5[b]	PPh_3 and NaI	TMS	1.0	2.0	37
6	$[Ru(bpy)_3]Cl_2$ (**1**)	Ac	1.0	5.0	-
7	$[Cu(dap)_2]Cl$ (**7**)	Ac	1.0	5.0	-
8	$[Cu(dap)Cl_2]$	Ac	1.0	5.0	-
9	*fac*-$Ir(ppy)_3$ (**5**)	Ac	1.0	5.0	80
10	*fac*-$Ir(ppy)_3$ (**5**)	TMS	1.0	5.0	79
11	*fac*-$Ir(ppy)_3$ (**5**)	TMS	1.0	2.0	67
12	*fac*-$Ir(ppy)_3$ (**5**)	TMS	1.5	1.0	25
13[c]	*fac*-$Ir(ppy)_3$ (**5**)	TMS	1.0	5.0	57
14[c]	*fac*-$Ir(ppy)_3$ (**5**)	Ac	1.0	5.0	80 (76)[d]
15[c]	*fac*-$Ir(ppy)_3$ (**5**)	Ac	1.0	3.0	73
16	-	Ac	1.0	5.0	n.r.
17[e]	*fac*-$Ir(ppy)_3$ (**5**)	Ac	1.0	5.0	n.r.
18[f]	*fac*-$Ir(ppy)_3$ (**5**)	Ac	1.0	5.0	n.r.

Standard reaction conditions: 0.20 mmol scale, photocatalyst (2.5 mol%), H_2O (5.0 mmol, 25 equiv), dry MeCN (2 mL), N_2 atmosphere, rt, 18 h, blue LED (λ = 455 nm). [a]Yield determined by ^1H-NMR using 1,3,5-trimethoxybenzene as internal standard. [b]PPh_3 (20 mol%) and NaI (1.5 equiv) were used as catalytic active species; no water was added.[15a] [c]1.0 mol% catalyst was used. [d]Isolated yield. [e]Without light. [f]Without degassing, under air.

Having established a protocol for the oxidative quenching cycle, different enol acetates and silyl enol ethers were investigated (Table 26). In case silyl enol ethers were employed, the catalyst loading was increased from 1.0 to 2.5 mol%. We found that electron-rich enol acetates **122h** – **122k** (entry 2 – 5) and electron-rich silyl enol ether **122o** (entry 9) were well tolerated. Excellent yields were obtained with moderately electron-deficient enol acetates **122l** and **122m** (entry 6 – 7). To our delight, sterically more demanding enol acetate **122n** (entry 8) and various heterocycles, which were unreactive in the literature paragon,[14] proved to be very good coupling partners and gave moderate to excellent yields (entry 10 – 12). Solely very electron-deficient silyl enol ethers (entry 13 – 14) and alkyl substitution in the enol acetates (entry 15 – 17) were not tolerated and no product formation was observed, indicating that an adjacent aromatic system is crucial for stabilizing the resulting radical.

Table 26: Investigation of different enol acetates and silyl enol ethers for decarboxylative alkylation exploiting the oxidative quenching cycle of *fac*-Ir(ppy)3 (**5**).[vii]

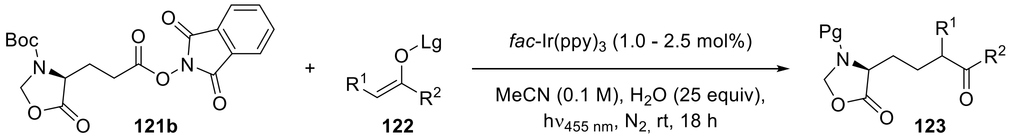
Boc
121b
+
Lg
R^1
R^2
122
fac-Ir(ppy)$_3$ (1.0 - 2.5 mol%)
MeCN (0.1 M), H_2O (25 equiv),
hν$_{455\ nm}$, N_2, rt, 18 h
Pg
R^1
R^2
123

Entry	Substrate		Product		Yield [%][a]
1	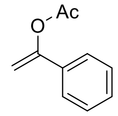	**122f**	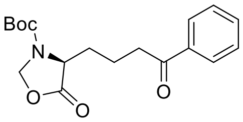	**123bf**	76
2	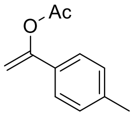	**122h**	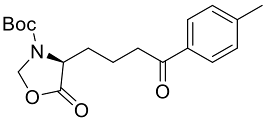	**123bh**	71
3	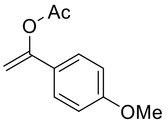	**122i**	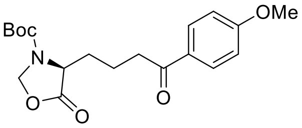	**123bi**	74
4	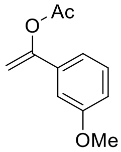	**122j**	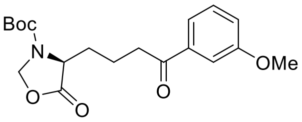	**123bj**	66
5	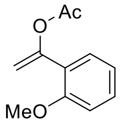	**122k**	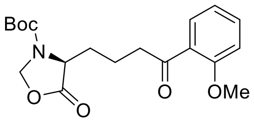	**123bk**	65
6	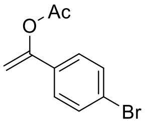	**122l**	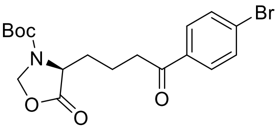	**123bl**	83
7	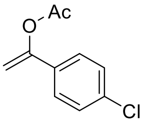	**122m**	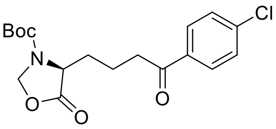	**123bm**	80

[vii] Enol acetates from entries 2 – 8 and 15 – 16 were kindly provided by T. Föll.

8	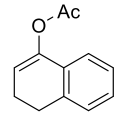	**122n**	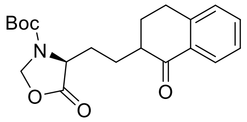	**123bn**	61
9[b]	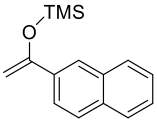	**122o**	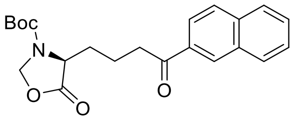	**123bo**	73
10[b]	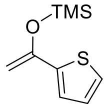	**122p**	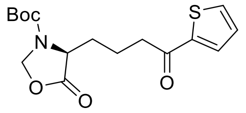	**123bp**	83
11[b]	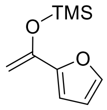	**122q**	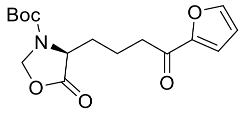	**123bq**	40
12[b]	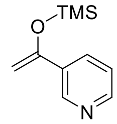	**122r**	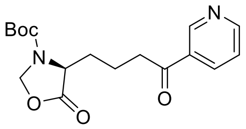	**123br**	74
13	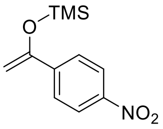	**122s**	-		n.r.
14	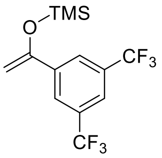	**122t**	-		n.r.
15	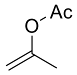	**122u**	-		n.r.
16	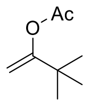	**122v**	-		n.r.
17	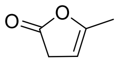	**122w**	-		n.r.

Standard reaction conditions: **121b** (0.20 mmol, 1.0 equiv), **122** (1.0 mmol, 5 equiv), *fac*-Ir(ppy)$_3$ (**5**, 1.0 mol%), H_2O (5.0 mmol, 25 equiv), dry MeCN (2 mL, c = 0.1 M), N_2 atmosphere, rt, 18 h, blue LED (λ = 455 nm). [a]Isolated yields are given. [b]Silyl enol ether (1.0 mmol, 5.0 equiv) and *fac*-Ir(ppy)$_3$ (2.5 mol%) were used.

The proposed reaction mechanism depicted in Scheme 48 is an adapted version of the proposal from F. Glorius *et al.*[13] and Q. Song *et al.*[14] Through visible light irradiation, the Ir^{III} complex is transferred to its excited state and is, therefore, able to directly trigger a single-electron transfer to *N*-(acyloxy)phthalimide **121** - it should be noted that the presence of water is crucial for the reaction to proceed by decreasing the reduction potential of the active ester through hydrogen bonding.[12] Upon N-O mesolysis of phthalimide (**209**) and subsequent decarboxylation, the carbon-centered radical **248** is furnished, which is trapped by a silyl enol ether or enol acetate **122**, respectively. In comparison to the reductive quenching cycle, the formed radical intermediate **249** is not trapped by hydrogen, but rather a single electron transfer towards the oxidized photocatalyst takes place forming the oxidized species **250**. The latter is transferred to the final product **123** by hydrolysis and the concurrent cleavage of the leaving group.

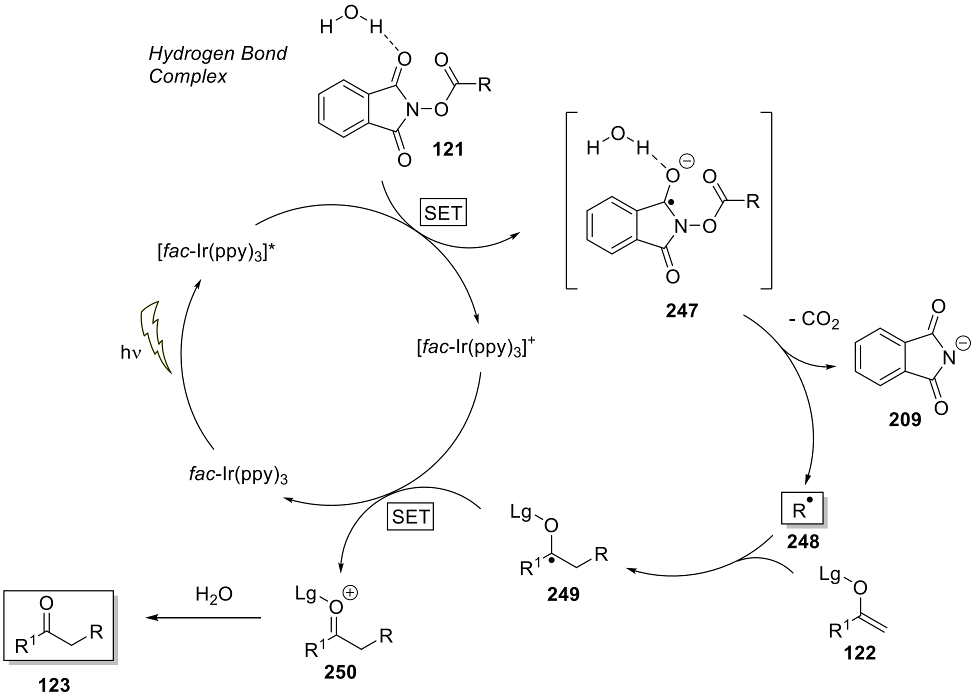
Hydrogen Bond Complex
121
SET
247
- CO2
209
[fac-Ir(ppy)3]*
hν
[fac-Ir(ppy)3]+
fac-Ir(ppy)3
SET
248
249
122
H2O
250
123

Scheme 48: Proposed mechanism for the photochemical decarboxylative alkylation following the oxidative quenching cycle of *fac*-Ir(ppy)$_3$ (**5**).

3.3. Reaction upscaling

Prompted by these excellent results, our next aim was to increase the scale for the reaction between BocGluOxNPhth **121b** and 1-phenylvinyl acetate (**122f**) to synthetically useful amounts (Table 27). As reported by Q. Song *et al.*,[14] for their system the yield drastically dropped from 90% to 44% when the reaction was scaled from 0.20 mmol to 1.5 mmol. This was explained by the formation of a side product, i.e. the decarboxylative protonation of the *N*-(acyloxy)phthalimide. The same was true for our reaction system when the scale was increased to 1.0 mmol in a batch setup and even after 5 days of irradiation merely a yield of 55% was obtained (entry 1). Only when a flow-system was applied, the formation of the byproduct was suppressed and after some optimization, regarding concentration and flowrate, the same yield as in the batch setup was attained (80%, entry 5). To our delight, we were able to transform 4.0 mmol (1.62 g) in excellent yield (78% NMR yield, 73% (971 mg) isolated yield, entry 6). As transition metal-based catalysts in large quantities are quite expensive and unsustainable even at a loading of 1.0 mol%, we switched to recyclable *fac*-Ir(PIB-ppy)(ppy)$_2$ (**40**), originally established by our group.[17] Therefore, half the amount of acetonitrile was replaced with heptane as an additional solvent, generating a two-phase system. Since the catalyst is only soluble in non-polar solvents it is easily recovered after a reaction by separation of the two phases. Despite the very high yield in the first run (85%, entry 7), the reaction outcome decreased continuously to 50% within three runs (entry 8 – 9). ICP-OES revealed an overall leaching of only 12% iridium into the reaction mixture, which is why the decline was rather attributed to the catalyst getting poisoned by acetic acid, formed as a result of the acetate cleavage, and the additional deactivation during the reaction.[18] Moreover, in previous studies a similar complex, i.e. [Ir(PIB-dtb-bpy)(ppy)$_2$]BArF, was employed as a homogeneously operating recyclable photocatalyst for visible light-mediated decarboxylation reactions.[19] In this case, the reaction time had to be increased from 16 h to 96 h within five cycles to ensure a constant yield, which also suggests the deactivation of the iridium catalyst.

Table 27: Optimization of reaction up-scaling.

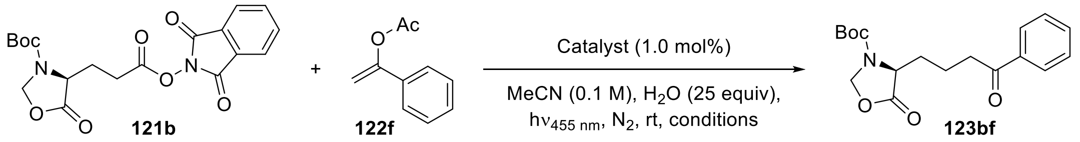

Entry	Photocatalyst	Scale [mmol]	Conditions[a]	Yield [%][b]
1	*fac*-Ir(ppy)$_3$ (**5**)	1.0	batch, 5 d reaction time	55
2[c]	*fac*-Ir(ppy)$_3$ (**5**)	0.20	c = 0.1 M, 1 mL/h	30
3[c]	*fac*-Ir(ppy)$_3$ (**5**)	0.20	c = 0.05 M, 1 mL/h	42
4[c]	*fac*-Ir(ppy)$_3$ (**5**)	0.20	c = 0.05 M, 0.5 mL/h flowrate	71
5[d]	*fac*-Ir(ppy)$_3$ (**5**)	0.20	c = 0.05 M, 0.5 mL/h flowrate	80
6[d]	*fac*-Ir(ppy)$_3$ (**5**)	4.0	c = 0.05 M, 0.5 mL/h flowrate	78(73)[e]
7[f]	*fac*-Ir(PIB-ppy)(ppy)$_2$ (**40**)	0.20	batch, run 1, 18 h	85
8[f]		0.20	batch, run 2, 18 h	70
9[f]		0.20	batch, run 3, 18 h	50

[a] Standard reaction conditions: **121b** (1.0 equiv), **122f** (5.0 equiv), photocatalyst (1.0 mol%), H_2O (25 equiv), dry MeCN (0.1 M), N_2 atmosphere, rt, 18 h, blue LED (λ = 455 nm). [b] Yield determined by ^{1}H-NMR using 4-nitrobenzaldehyde as internal standard. [c] Micro reactor was used. [d] 2 micro reactors in series were used. [e] Isolated yield. [f] Two-phase system was used, MeCN/heptane = 1:1 (2 mL, c = 0.1 M).

In summary, we developed a protocol to scale the reaction successfully to synthetically useful amounts with the aid of a micro-reactor, having no forfeits in yields compared to a batch setup. This up-scaling is particularly important when it comes to possible applications, such as the processing of pipecolic acid derivatives which is discussed later on.

3.4. Intramolecular reactions

Besides the auspicious results obtained, another part of this research was to investigate intramolecular reactions starting with submitting the compounds **237a** and **237b** to photoreactions (Scheme 49).[viii] Since exploiting the oxidative quenching cycle of *fac*-Ir(ppy)$_3$ (**5**) led to no product formation, we focused on the reductive quenching cycle of [Ru(bpy)$_3$]Cl$_2$ (**1**), using DIPEA as sacrificial electron donor. To our delight, both starting materials provided the six-exo dig (**251**) and seven-endo dig (**252**) cyclization products as two inseparable isomers in a ratio of 2:1 in excellent yields.

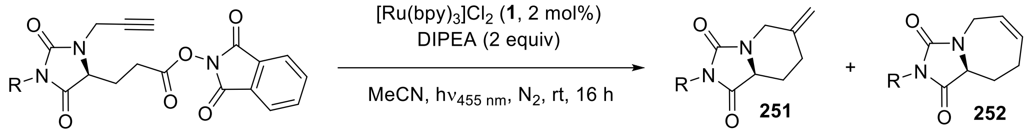
[Ru(bpy)$_3$]Cl$_2$ (**1**, 2 mol%)
DIPEA (2 equiv)
MeCN, hν$_{455\ nm}$, N$_2$, rt, 16 h
251
252

R = Ph, **237a**
R = Bz, **237b**

R = Ph: 91%, ratio **251a**:**252a** = 2:1
Bz: 84%, ratio **251b**:**252b** = 2:1

Scheme 49: Intramolecular decarboxylative cyclization reactions.

Furthermore, the starting material **239** was tested for its reactivity (Scheme 50). Exploiting the oxidative quenching cycle of *fac*-Ir(ppy)$_3$ (**5**, upper pathway) provided the inseparable cyclization products **253** and **254** in a ratio of 1:1 and an overall yield of 75%. *Via* a dehydration reaction of the former, only the unsaturated product can be obtained, which would therefore allow for further functionalization. Moreover, by opening the hydantoin *via* hydration, pipecolic acid derivatives could be furnished. Applying the reductive quenching cycle of [Ru(bpy)$_3$]Cl$_2$ (**1**) instead (lower pathway), utilizing DIPEA as sacrificial electron donor, the products **255** and **254** were formed in a ratio of 1:1 in almost the same yield as before (73%). In this case, the latter was successfully reduced *via* hydrogenation to the saturated isomer **255**, and thus only one product was furnished.

[viii] Reactions towards **251** and **252** and towards **253** were performed by S. Budde.

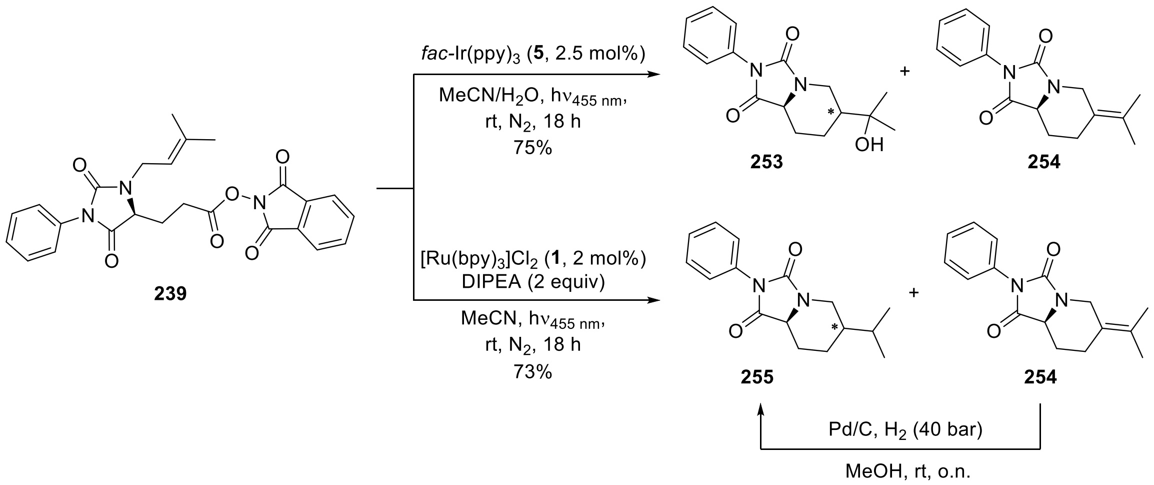
239
fac-Ir(ppy)$_3$ (**5**, 2.5 mol%)
MeCN/H_2O, hν$_{455\ nm}$,
rt, N_2, 18 h
75%
253
254
[Ru(bpy)$_3$]Cl_2 (**1**, 2 mol%)
DIPEA (2 equiv)
MeCN, hν$_{455\ nm}$,
rt, N_2, 18 h
73%
255
254
Pd/C, H_2 (40 bar)
MeOH, rt, o.n.

Scheme 50: Intramolecular reactions starting from **239**, exploiting both oxidative (upper) and reductive (lower) quenching cycle of photocatalysts.

4. Synthesis of pipecolic acid derivatives

To prove the importance of our application we established the synthesis of C-6 substituted pipecolic acid derivatives, which are particularly interesting due to their potential bioactivity.[20] The full synthesis was demonstrated on the basis of two examples, i.e. the phenyl-substituted photoreaction product **123bf** from the up-scaling process and the thiophen-substituted photoreaction product **123bp** (Scheme 51). In the first step, the oxazolidinone protection group was removed by treating the starting materials with 1 M aqueous NaOH to form the free acids **230a** and **230b**. Since the direct conversion to the imine **256** was unsuccessful due to multiple side reactions, we decided to go *via* the esterification products **257a** and **257b**. Doing so, the imine formation was achieved by treatment with TFA and could be in situ reduced to the desired products **231a** and **231b**, respectively, in overall reasonable yields. Benefitting from the chiral center, which is preserved from the initial L-glutamic acid, high diastereomeric ratios of 6:1 were obtained. Whereas only the synthesis of the phenyl-substituted pipecolic acid is known so far,[21] we were able to successfully establish a pipecolic acid derivative comprising an additional heterocycle. Moreover, these reaction steps can be extended to various photoreaction products, providing different novel C-6-substituted pipecolic acid derivatives, which could be tested for their biological activity.

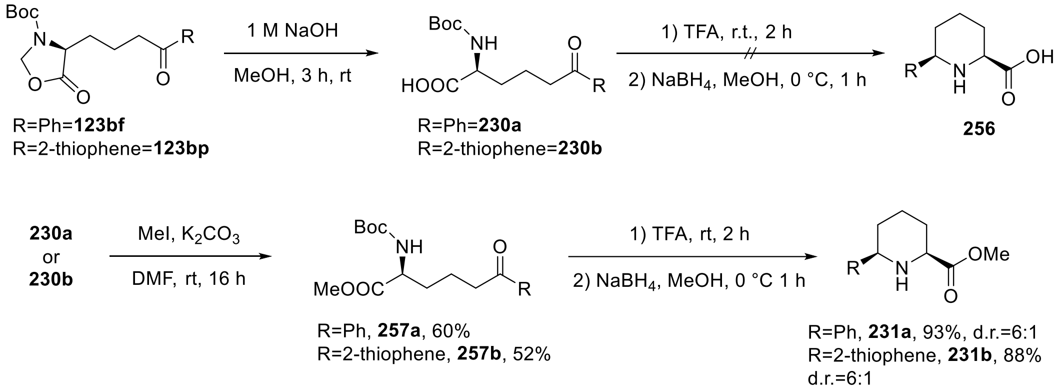
Boc
N
R
O
O
O
R=Ph=**123bf**
R=2-thiophene=**123bp**
1 M NaOH
MeOH, 3 h, rt
Boc
NH
O
HOOC
R
R=Ph=**230a**
R=2-thiophene=**230b**
1) TFA, r.t., 2 h
2) NaBH4, MeOH, 0 °C, 1 h
R
N
H
OH
O
256
230a
or
230b
MeI, K2CO3
DMF, rt, 16 h
Boc
NH
O
MeOOC
R
R=Ph, **257a**, 60%
R=2-thiophene, **257b**, 52%
1) TFA, rt, 2 h
2) NaBH4, MeOH, 0 °C 1 h
R
N
H
OMe
O
R=Ph, **231a**, 93%, d.r.=6:1
R=2-thiophene, **231b**, 88%
d.r.=6:1

Scheme 51: Synthesis of pipecolic acid derivatives from photoreaction products **123bf** and **123bp**.

5. Conclusion

In summary, a protocol for the visible light-mediated synthesis of novel amino acid derivatives from cheap and readily available L-glutamic acid was developed. Whereas exploiting the reductive quenching cycle of $[Ru(bpy)_3]Cl_2$ (**1**) only led to moderate yields, but provided a reasonable variety of coupling partners, more success has been achieved with the oxidative quenching cycle of *fac*-$Ir(ppy)_3$ (**5**). For this, various enol acetates and silyl enol ethers served as radical trapping reagents, forming ketones as photoreaction products. Furthermore, its successful upscaling and transformation to pipecolic acid derivatives containing a phenyl or thiophene moiety, respectively, was demonstrated, which makes the reaction especially valuable.

6. Literature

[1] a) J. Schwarz, B. König, *Green Chem.* **2018**, *20*, 323–361; b) S. Murarka, *Adv. Synth. Catal.* **2018**, *360*, 1735–1753.

[2] a) H. Kolbe, *Liebigs Ann. Chem.* **1848**, *64*, 339–341; b) H. Kolbe, *Liebigs Ann. Chem.* **1849**, *69*, 257–294.

[3] H. Hunsdiecker, C. Hunsdiecker, *Ber. Dtsch. Chem. Ges.* **1942**, *75*, 291–297.

[4] D. H. R. Barton, D. Crich, W. B. Motherwell, *J. Chem. Soc, Chem. Commun.* **1983**, *17*, 939–941.

[5] M. Hasebe, T. Tsuchiya, *Tetrahedron Lett.* **1987**, *28*, 6207–6210.

[6] K. Okada, K. Okamoto, M. Oda, *J. Am. Chem. Soc.* **1988**, *110*, 8736–8738.

[7] K. Okada, K. Okubo, N. Morita, M. Oda, *Tetrahedron Lett.* **1992**, *33*, 7377–7380.

[8] K. Okada, K. Okamoto, N. Morita, K. Okubo, M. Oda, *J. Am. Chem. Soc.* **1991**, *113*, 9401–9402.

[9] M. L. Schnermann, L. E. Overman, *Angew. Chem. Int. Ed.* **2012**, *51*, 9576–9580.

[10] a) G. Pratsch, G. L. Lackner, L. E. Overman, *J. Org. Chem.* **2015**, *80*, 6025–6036; b) J. Schwarz, B. König, *Green Chem.* **2016**, *18*, 4743–4749; c) Y. Jin, M. Jiang, H. Wang, H. Fu, *Sci. Rep.* **2016**, *6*, 1–8.

[11] G. Kachkovskyi, C. Faderl, O. Reiser, *Adv. Synth. Catal.* **2013**, *355*, 2240–2248.

[12] M. Oelgemöller, A. G. Griesbeck, J. Lex, A. Haeuseler, M. Schmittel, M. Niki, D. Hesek, Y. Inoue, *Org. Lett.* **2001**, *3*, 1593–1596.

[13] A. Tlahuext-Aca, R. A. Garza-Sanchez, F. Glorius, *Angew. Chem. Int. Ed.* **2017**, *56*, 3708–3711.

[14] W. Kong, C. Yu, H. An, Q. Song, *Org. Lett.* **2018**, *20*, 349–352.

[15] a) M.-C. Fu, R. Shang, B. Zhao, B. Wang, Y. Fu, *Science* **2019**, *363*, 1429–1434; b) Y.-T. Wang, M.-C. Fu, B. Zhao, R. Shang, Y. Fu, *Chem. Commun.* **2020**, *56*, 2495–2498.

[16] a) A. Juris, V. Balzani, P. Belser, A. von Zelewsky, *Helv. Chim. Acta* **1981**, *64*, 2175–2182; b) K. Kalyanasundaram, *Coord. Chem. Rev.* **1982**, *46*, 159–244.

[17] D. Rackl, P. Kreitmeier, O. Reiser, *Green Chem.* **2016**, *18*, 214–219.

[18] a) J. J. Devery Iii, J. J. Douglas, J. D. Nguyen, K. P. Cole, R. A. Flowers Ii, C. R. J. Stephenson, *Chem. Sci.* **2015**, *6*, 537–541; b) S. Schmidbauer, A. Hohenleutner, B. König, *Beilstein J. Org. Chem.* **2013**, *9*, 2088–2096.

[19] a) C. Faderl, S. Budde, G. Kachkovskyi, D. Rackl, O. Reiser, *J. Org. Chem.* **2018**, *83*, 12192–12206; b) D. Rackl, Thesis, University of Regensburg, **2015**;

[20] C. Kadouri-Puchot, S. Comesse, *Amino acids* **2005**, *29*, 101–130.

[21] M. E. Swarbrick, F. Gosselin, W. D. Lubell, *J. Org. Chem.* **1999**, *64*, 1993–2002.

D. Summary / Zusammenfassung

1. Summary

The present work opens with a short overview of photochemical processes and the underlying photophysical aspects of transition metal-based photocatalysts. Furthermore, recent advancements in photocatalytic flow chemistry are covered, using pertinent examples.

The chapter “Recyclable Photocatalysts” deals with the heterogenization of ruthenium- and iridium-based photocatalysts, their application, and recycling. Initially, Nafion, a perfluoronic resin with terminal sulfonic acid groups, which is commonly used as an ionic exchanger, served as solid support to electrostatically attach $[Ru(bpy)_3]^{2+}$. The easy to prepare immobilized catalyst was successfully employed in a batch process for various photochemical transformations, such as *E/Z*-isomerization of stilbene, or ATRA reactions. Its heterogeneous nature allowed on the one hand for recovery *via* centrifugation and, depending on the reaction, subsequent reuse for at least five times without greater loss in activity. On the other hand, a solid-phase flow system was realized, greatly improving the yield and reaction times for the *E/Z*-isomerization. To circumvent the time-consuming centrifugation step in batch reactions and, therefore, improve this system even further, carbon-coated magnetic cobalt (Co/C) nanoparticles were conceived as non-covalent solid support for the ruthenium(II) complex. Even though the recovery of the catalyst was facilitated, as applying an external magnet was sufficient to separate the particles from the reaction mixture, they exhibited high leaching of ruthenium. Therefore, the immobilization strategy was streamlined by covalently attach derivatives of $[Ru(bpy)_3]^{2+}$ and *fac*-$Ir(ppy)_3$. Whereas an immobilized version of the former proved to be inactive, the heterogenized iridium(III) complex was effectively employed for the *E/Z*-isomerization of a pinacol ester as well as a [2+2] cycloaddition. The catalyst revealed high activity as well as recyclability, inasmuch 5 – 10 consecutive runs were feasible without any greater losses in activity. Noteworthy, the leaching of iridium was decreased to a minimum. In the following section, novel graphitic carbon nitrides were tested for their photochemical performance in various transformations, mainly ATRA reactions. The particles were compared to other well-established transition metal-based photocatalysts, such as $[Cu(dap)_2]^{+}$.

The chapter “Photochemical Decarboxylations” details results on the visible light-mediated decarboxylation of modified, cheap, and readily available L-glutamic acid. After optimization of the reaction parameters, various intermolecular - employing alkenes as coupling partners - as well as intramolecular reactions were conducted. Therefore, the reductive and oxidative quenching cycles of $[Ru(bpy)_3]^{2+}$ and *fac*-Ir(ppy)$_3$ were exploited. A reaction upscaling to synthetically useful amounts, i.e. 4.0 mmol, was achieved *via* a flow process. The ensuing synthesis of unnatural amino acids and their transformation to potentially bioactive pipecolic acid derivatives was demonstrated in two examples. Noteworthy, the chiral information of the L-glutamic acid is conserved throughout all steps, providing products with high diastereomeric ratios.

2. Zusammenfassung

Die vorliegende Arbeit beginnt mit einem kurzen Überblick über photochemische Prozesse und die zugrunde liegenden photophysikalischen Aspekte von Photokatalysatoren auf Übergangsmetallbasis. Des Weiteren werden die jüngsten Fortschritte in der photokatalytischen Durchflusschemie anhand einschlägiger Beispiele behandelt.

Das Kapitel „Recyclable Photocatalysts“ befasst sich mit der Heterogenisierung von Photokatalysatoren auf Ruthenium- und Iridiumbasis, sowie deren Anwendung und Recycling. Zu Beginn diente Nafion, ein perfluoronisches Harz mit endständigen Sulfonsäuregruppen, welches normalerweise als Ionenaustauscher Verwendung findet, als fester Träger zur elektrostatischen Anbringung von $[Ru(bpy)_3]^{2+}$. Der leicht herzustellende, immobilisierte Katalysator wurde erfolgreich im Batchprozess für verschiedenste Transformationen, wie der *E/Z*-Isomerisierung von Stilben oder ATRA Reaktionen eingesetzt. Seine heterogene Natur ermöglichte einerseits die Rückgewinnung mittels Zentrifugation, und, je nach Reaktion, eine anschließende mindestens fünfmalige Wiederverwendung ohne größeren Aktivitätsverlust. Andererseits konnte ein Festphasen-Durchflusssystem realisiert werden, welches sowohl die Ausbeute als auch die Reaktionszeiten der *E/Z*-Isomerisierung stark verbesserte. Um den zeitintensiven Zentrifugationsschritt in Batchprozessen zu umgehen und damit das System noch weiter zu verbessern, wurden kohlenstoffbeschichtete magnetische Kobaltnanopartikel (Co/C) als nichtkovalenter, fester Träger für den Ruthenium(II)-Komplex konzipiert. Obwohl so zwar die Rückgewinnung des Katalysators erleichtert wurde, da das Aufbringen eines externen Magneten ausreichte, um die Partikel von der Reaktionsmischung zu trennen, wiesen sie jedoch ein hohes Rutheniumleaching auf. Daher wurde die Immobilisierungsstrategie optimiert, indem Derivate von $[Ru(bpy)_3]^{2+}$ und *fac*-$Ir(ppy)_3$ kovalent angebracht wurden. Während sich eine immobilisierte Variante des ersteren als inaktiv erwies, wurde der heterogenisierte Iridium(III)-Komplex erfolgreich zur *E/Z*-Isomerisierung eines Pinakolesters sowie einer [2+2] Cycloaddition angewendet. Dabei wies der Katalysator eine sehr hohe Aktivität sowie Recyclingfähigkeit auf, da 5 – 10 aufeinanderfolgende Reaktionen ohne größere Aktivitätsverluste möglich waren. Bemerkenswerterweise wurde das Iridiumleaching auf ein Minimum reduziert. Im darauf folgenden Abschnitt wurden neue graphitische Kohlenstoffnitride auf ihre photochemische Leistungsfähigkeit in verschiedenen Transformationen, hauptsächlich ATRA Reaktionen, getestet. Dabei wurden die Partikel mit anderen etablierten Photokatalysatoren auf Übergangsmetallbasis, wie z. B. $[Cu(dap)_2]^{+}$, verglichen.

Das Kapitel „Photochemical Decarboxylations“ beschreibt die Ergebnisse der durch sichtbares Licht vermittelten Decarboxylierung von modifizierter, kostengünstiger und leicht verfügbarer L-Glutaminsäure. Nach Optimierung der Reaktionsparameter, wurden verschiedene intermolekulare Reaktionen mit Alkenen als Kopplungspartner, sowie intramolekulare Reaktionen durchgeführt. Dazu wurden der reduktive sowie oxidative Quenching-Zyklus von $[Ru(bpy)_3]^{2+}$ und *fac*-$Ir(ppy)_3$ genutzt. Eine Hochskalierung der Reaktion auf synthetisch nützliche Mengen, sprich 4.0 mmol, wurde durch einen Flussprozess erreicht. Die anschließende Synthese unnatürlicher Aminosäuren und deren Umwandlung zu potenziell bioaktiven Derivaten der Pipecolinsäure wurde anhand zweier Beispiele demonstriert. Bemerkenswerterweise bleibt die chirale Information der L-Glutaminsäure in allen Schritten erhalten und liefert so Produkte mit hohen Diastereomerenverhältnissen.

E. Experimental Part

1. General information

Nafion® SAC-13 was purchased from Sigma Aldrich. Carbon coated cobalt nanoparticles (Co/C) were obtained from Prof. W. J. Stark from the ETH Zurich, Switzerland. Prior to use, they were washed according to the general procedure (see below). They were dispersed by the aid of an ultrasound bath (Sonorex RK 255 H-R, Bandelin) and recovered with the help of a commercially available neodymium-based magnet (15 x 30 mm). Graphitic carbon nitrides (mpg-C_3N_4, mpg-C_3N_5, g-C_3N_4/Ag and g-C_3N_5/Ag) were obtained from Dr. Manoj Gawande from the Regional Centre of Advanced Technologies and Materials in the Czech Republic. All other chemicals were used as received or purified according to the 'purification of common laboratory chemicals' if necessary.[1] Elemental microanalysis (EA) was performed by the Micro Analytical Laboratory of the University of Regensburg using a Vario MICRO cube or Titrino plus 848. Samples for the inductively coupled plasma optical emission spectrometry (ICP-OES) were measured on Spectroblue FMX36. IR spectroscopy measurements were performed on an Agilent Cary 630 FTIR spectrometer equipped with a Diamond Single Reflection Accessory. Analytical thin-layer chromatography was performed on Merck TLC aluminum sheets silica gel 60 F 254. Reactions were monitored by TLC and visualized by a short-wave UV lamp and stained with a solution of potassium permanganate or vanillin. Flash column chromatography was performed using Merck flash silica gel 60 (0.040-0.063 mm). The blue light irradiation in batch processes was performed using a CREE XP-E LED (3 W, λ_{max} = 450 – 465 nm) or, in case the LED plate was used (see below), OSRAM Oslon SSl 80 LDCQ7P-1U3U (1.12 W, λ_{max} = 455 nm). In flow processes, 8 OSRAM OSLON Black Series LD H9GP LEDs (λ = 455±10 nm) were employed. Green light irradiation was ensured by CREE XP-E LED (3 W, λ_{max} = 520 – 535 nm). NMR spectra were recorded on Bruker Avance 300 and Bruker Avance 400 spectrometers. All spectra were recorded in $CDCl_3$ or commercially available deuterated solvents. Chemical shifts are reported as δ, parts per million, relative to the signal of the solvent. Coupling constants *J* are given in Hertz (Hz). The following notations indicate the multiplicity of the signals: s = singlet, brs = broad singlet, d = doublet, t = triplet, q = quartet, quint = quintet, sept = septet, and m = multiplet. Chiral gas chromatography was performed on a Fisons GC 8000. CP-Chirasil-Dex CB (25 m x 0.25 mm, 0.25 m film, injection temperature 140 °C, detector temperature 140 °C, P = 100 kPa He gas) was used as chiral stationary phase. Mass spectra were recorded at the Central Analytical Laboratory at the Department of

Chemistry of the University of Regensburg on a Varian MAT 311A, Finnigan MAT 95, Thermoquest Finnigan TSQ 7000 or Agilent Technologies 6540 UHD Accurate-Mass Q-TOF LC/MS. The yields reported are referred to the isolated compounds unless otherwise stated.

General procedure for washing Co/C nanoparticles 124

Prior to use, the carbon-coated cobalt nanoparticles (Co/C) **124** were washed five times for 24 h in a $HCl_{conc}/H_2O_{millipore}$ mixture (1:1). To remove any residual acid the particles were magnetically collected and washed with Millipore water until the pH of the decanted solution was neutral. Subsequently, the particles were washed with acetone (3x) and diethyl ether (2x) and dried at 50 °C under vacuum. **Elemental microanalysis** [%]: C, 4.50; H, traces; N, 0.

General sample preparation for ICP-OES for ruthenium

To determine the leaching of ruthenium the samples were prepared by evaporating the solvent of the reaction mixture and boiling the residue for 10 min in 2.4 mL HCl_{conc} and 0.8 mL HNO_3. Subsequently, the mixture was filtered through a 0.2 µm syringe filter, diluted to 10 mL with Millipore water, giving a 32% solution of aqua regia, which was measured in the ICP apparatus.

To determine the loading of MNP-Ru(bpy)$_3$Cl, 5 mg of the particles were boiled for 10 min in 2.4 mL HCl_{conc} and 0.8 mL HNO_3. The particles were magnetically collected, the supernatant was decanted, and the procedure was repeated. The combined supernatants were diluted with Millipore water to a total of 10 mL leading to a 64% solution of aqua regia. 5 mL of this solution were filtered through a 0.2 µm and diluted to 10 mL to give a 32% aqua regia solution which was measured in the ICP apparatus.

General sample preparation for ICP-OES for iridium

For the ICP-OES analysis, the procedure from Reiser *et al.* was adopted.[2] After evaporation of the reaction solvent, the residue was dissolved in concentrated HNO_3 and boiled for about 3 min until the evolution of nitrous gases stopped. Subsequently, 2 mL concentrated H_2SO_4 was added and the mixture was again boiled for about 2 min, followed by the addition of another 2 mL of concentrated HNO_3 and boiling for about 2 min. After cooling to room temperature, the sample was diluted to a total volume of 10 mL, filtered through a 0.2 µm syringe filter, and measured in the ICP apparatus.

Catalyst synthesis

The photocatalysts *fac*-Ir(ppy)$_3$ (**5**)[3] and [Cu(dap)$_2$]Cl (**7**)[4] were synthesized following the literature procedures. The spectra are in agreement with the literature.

Setup for photochemical reactions

All photochemical reactions in batch were conducted using either

- *Irradiation system invented by Dr. Peter Kreitmeier:*

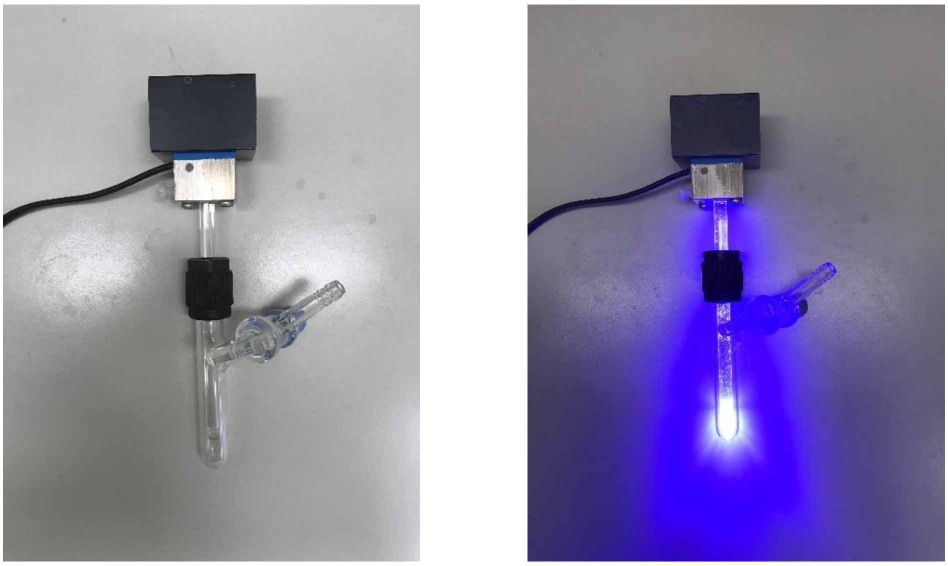

or

- *LED plate with water-cooled aluminum block:*

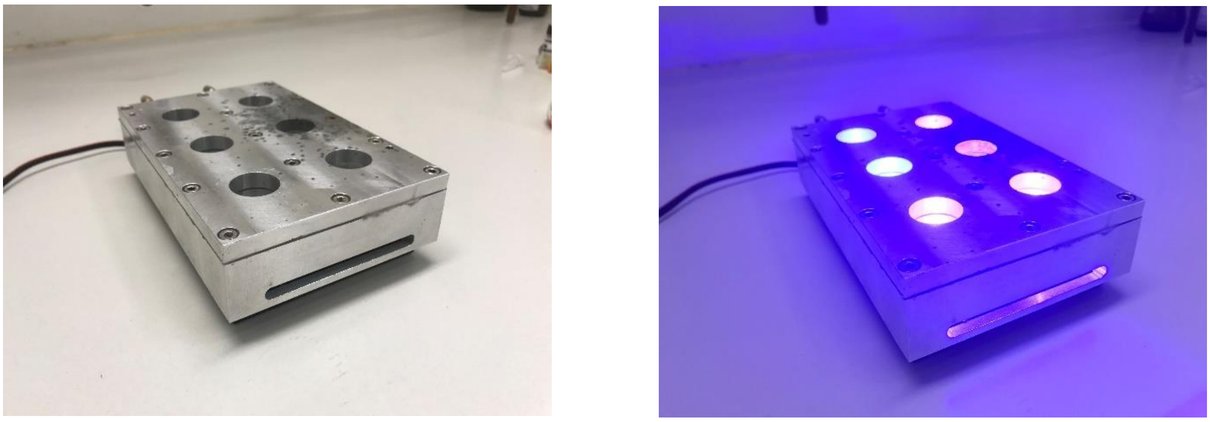

The equipment used for the single reactions is indicated.

2. Chapter B: Recyclable Photocatalysts

2.1. Immobilization of photocatalysts on Nafion

Nafion-Ru(bpy)$_3$Cl (107)

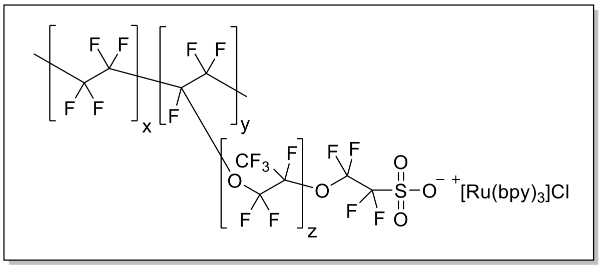

Following a literature procedure,[5] Nafion® SAC-13 (**105**) firstly had to be transferred to its corresponding sodium salt **106**. This was achieved by charging a glass filter frit with Nafion® SAC-13 (**105**) and passing a 2 M aqueous solution of NaCl through until the pH remained neutral. Subsequently, the particles were washed with water followed by drying *in vacuo* at 150 °C for 5 h. For immobilization, Nafion **106** (115 mg, 17.2 µmol (based on -SO_3Na), 1.00 equiv) and [Ru(bpy)$_3$]Cl_2 (**1**, 26 mg, 34.4 µmol, 2.00 equiv) were dissolved in MeCN (1 mL) and stirred for 24 h at room temperature. Afterwards, the particles were filtered and washed with MeCN until the washing solution remained colorless. Drying *in vacuo* afforded the product as orange solid (120 mg).

ICP-OES: loading [Ru]: 0.102 mmol/g; corresponds to 68% of maximal possible loading.

The reaction was also performed using various conditions:

(*1*) Nafion **106** (115 mg, 17.2 µmol (-SO_3Na), 1.00 equiv) and [Ru(bpy)$_3$]Cl_2 (**1**, 13 mg, 17.2 µmol, 1.00 equiv) were dissolved in MeCN (1 mL).

ICP-OES: loading [Ru]: 0.101 mmol/g; corresponds to 67% of maximal possible loading.

(*2*) Nafion **106** (115 mg, 17.2 µmol (-SO_3Na), 1.00 equiv) and [Ru(bpy)$_3$]Cl_2 (**1**, 8.8 mg, 11.7 µmol, 0.68 equiv) were dissolved in MeCN (1 mL).

ICP-OES: loading [Ru]: 0.087 mmol/g; corresponds to 58% of maximal possible loading.

(*3*) Nafion **106** (115 mg, 17.2 µmol (-SO_3Na), 1.00 equiv) and [Ru(bpy)$_3$](BF_4)$_2$ (32.5 mg, 34.4 µmol, 2.00 equiv) were dissolved in DCM (1 mL).

ICP-OES: loading [Ru]: 0.096 mmol/g; corresponds to 64% of maximal possible loading.

(*4*) Nafion **106** (115 mg, 17.2 µmol (-SO_3Na), 1.00 equiv) and [Ru(bpy)$_3$]Cl_2 (**1**, 26 mg, 34.4 µmol, 2.00 equiv) were dissolved in MeOH (1 mL).

ICP-OES: loading [Ru]: 0.074 mmol/g; corresponds to 49% of maximal possible loading.

(*5*) Nafion **106** (115 mg, 17.2 µmol (-SO_3Na), 1.00 equiv) and [Ru(bpy)$_3$]Cl_2 (**1**, 26 mg, 34.4 µmol, 2.00 equiv) were dissolved in H_2O (1 mL).

ICP-OES: loading [Ru]: 0.036 mmol/g; corresponds to 24% of maximal possible loading.

2.2. Photochemical reactions employing photocatalyst on Nafion

(*Z*)-1,2-diphenylethene (25) [6]

Literature conditions

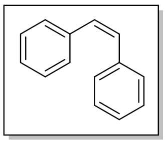

A 10 mL Schlenk tube was charged with (*E*)-1,2-diphenylethene (**24**, 36 mg, 0.20 mmol, 1.00 equiv), $[Ru(bpy)_3]Cl_2$ (**1**, 3.8 mg, 6.0 µmol, 3.0 mol%) and MeCN (2 mL). The reaction mixture was irradiated with a blue LED (λ = 455 nm) under an oxygen-atmosphere for 8 h at room temperature. The crude *Z/E*-ratio was determined by GC-FID to be 93:7. Subsequent purification was achieved by flash silica column chromatography (hexanes / EtOAc, 19:1) to give the product as colorless oil (29 mg, 0.160 mmol, 80%). Spectral data are in agreement with those reported in literature.[6]

^{1}H-NMR (400 MHz, $CDCl_3$): δ 7.29 – 7.16 (m, 10H), 6.61 (s, 2H); **^{13}C-NMR**: (101 MHz, $CDCl_3$): δ 137.28, 130.29, 128.91, 128.24, 127.12.

Recycling conditions

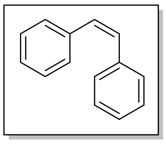

A 10 mL Schlenk tube was charged with (*E*)-1,2-diphenylethene (**24**, 36 mg, 0.20 mmol, 1.00 equiv), Nafion-$Ru(bpy)_3Cl$ (**107**, 59 mg, 6.0 µmol, 3.0 mol%) and DCM (2 mL). The reaction mixture was irradiated with a blue LED (λ = 455 nm) under an oxygen atmosphere for 8 h at room temperature. Subsequently, the reaction mixture was transferred to a test tube with the aid of DCM (1 mL) and centrifuged for 3 min. The supernatant was decanted and DCM (4 mL) was added to the residue. Again, the mixture was centrifuged, and the supernatant was decanted. This step was repeated one more time and the DCM layers were combined. The *Z/E*-ratio was determined by GC-FID and the leaching of ruthenium into the solvent by ICP-OES. The catalyst, on the other hand, was transferred to a Schlenk tube with the help of DCM (2 mL) and reused in a subsequent run.

All following runs were set up equally to the first run without changing any reaction parameters. The result for each reaction run is given in the main part.

Diethyl 2-(2-bromo-6-hydroxyhexyl)malonate (111) [7]

Literature conditions

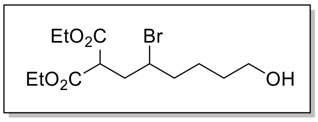

A Schlenk tube was charged with 5-hexen-1-ol (**109**, 30 µL, 0.25 mmol, 1.00 equiv), diethyl 2-bromomalonate (**110**, 85 µL, 0.50 mmol, 2.00 equiv), LiBr (43 mg, 0.50 mmol, 2.00 equiv), [Ru(bpy)$_3$]Cl$_2$ (**1**, 1.9 mg, 2.5 µmol, 1.0 mol%) and MeCN (1.0 mL). The tube was sealed with a screw-cap and degassed by three freeze-pump-thaw cycles. The screw-cap was replaced with a Teflon sealed inlet for a glass rod, through which irradiation with a blue LED (λ = 455 nm) took place from above while allowing for magnetic stirring from below. After 24 h the reaction mixture was transferred to a separation funnel with the aid of EtOAc (5 mL) and H$_2$O (5 mL). The phases were separated, and the aqueous layer was extracted with EtOAc (2 x 5 mL). The combined organic layers were dried over Na$_2$SO$_4$ and the solvent was evaporated. After purification with flash silica column chromatography (hexanes / EtOAc, 4:1), the pure product was obtained as colorless oil (70.6 mg, 0.208 mmol, 83%). The spectra are in accordance with those reported in literature.[7a]

^{1}H-NMR (300 MHz, CDCl$_3$): δ 4.34 – 4.12 (m, 4H), 4.08 – 3.94 (m, 1H), 3.78 (dd, J = 10.2, 4.2 Hz, 1H), 3.65 (t, J = 6.1 Hz, 2H), 2.46 (ddd, J = 14.9, 10.2, 3.1 Hz, 1H), 2.24 (ddd, J = 14.9, 10.6, 4.3 Hz, 1H), 2.00 – 1.82 (m, 2H), 1.68 – 1.45 (m, 5H), 1.38 – 1.18 (m, 7H); **^{13}C-NMR**: (75 MHz, CDCl$_3$): δ 168.95, 168.77, 62.53, 61.71, 61.64, 54.65, 50.52, 39.09, 37.79, 31.89, 23.72, 14.04, 14.00.

Recycling conditions

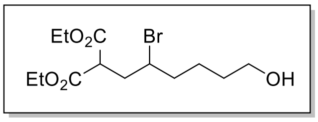

A Schlenk tube was charged with 5-hexen-1-ol (**109**, 30 µL, 0.25 mmol, 1.00 equiv), diethyl 2-bromomalonate (**110**, 85 µL, 0.50 mmol, 2.00 equiv), LiBr (43 mg, 0.50 mmol, 2.00 equiv), Nafion-Ru(bpy)$_3$Cl (**107**, 25 mg, 2.5 µmol, 1.0 mol%) and MeCN (1.0 mL). The tube was sealed with a screw-cap and degassed by three freeze-pump-thaw cycles. The screw-cap was replaced with a Teflon sealed inlet for a glass rod, through which irradiation with a blue LED (λ = 455 nm) took place from above while allowing for magnetic stirring from below. After 24 h the reaction mixture was transferred to a test tube with the aid of MeCN (2 mL) and centrifuged for 3 min. The catalyst settled whereas the LiBr remained on top of the catalyst. Therefore, the Lewis acid could be decanted and MeCN (4 mL) was added to the remaining solid.

After centrifuging again, the supernatant was decanted. This step was repeated once again, the organic layers were combined and the solvent evaporated. 1,3,5-trimethoxybenzene was added as internal standard and the crude mixture was submitted to ^{1}H-NMR to determine the yield (68%). The leaching of ruthenium was determined by ICP-OES to be 2.4%.

The catalyst was dried *in vacuo* and re-used in a second reaction run, however, remained inactive.

5-iodo-6-perfluorooctylhexanol (116) [7b]

Literature conditions

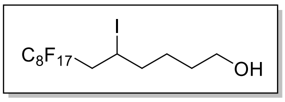

A 5 mL vial equipped with a magnetic stirring bar was charged with 5-hexen-1-ol (**109**, 30 µL, 0.25 mmol, 1.00 equiv), heptadecafluoro-1-iodooctane (**115**, 86 µL, 0.33 mmol, 1.30 equiv), sodium ascorbate (17 mg, 88 µmol, 0.35 equiv), $[Ru(bpy)_3]Cl_2$ (**1**, 1.9 mg, 2.5 µmol, 1.0 mol%), MeOH (1.5 mL) and MeCN (2.0 mL). The vial was capped with a rubber septum and the mixture was degassed by nitrogen sparging for 10 min. After irradiation for 0.5 h with a blue LED (λ = 455 nm) at room temperature, the solvent was evaporated and purification was achieved with flash silica column chromatography (hexanes / EtOAc, 4:1) to give the pure product as a white solid (154 mg, 0.238 mmol, 95%). The analytical spectra are in accordance with literature.[7b]

^{1}H-NMR (300 MHz, $CDCl_3$): δ 4.39 – 4.24 (m, 1H), 3.65 (t, J = 6.0 Hz, 2H), 3.03 – 2.62 (m, 2H), 1.91 – 1.71 (m, 2H), 1.68 – 1.47 (m, 5H).**^{13}C-NMR**: (75 MHz, $CDCl_3$): δ 62.48, 41.64 (t, J = 20.6 Hz), 40.04, 31.51, 26.02, 20.48.

Recycling conditions

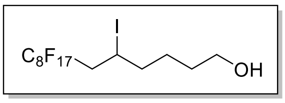

A 5 mL vial equipped with a magnetic stirring bar was charged with 5-hexen-1-ol (**109**, 30 µL, 0.25 mmol, 1.00 equiv), heptadecafluoro-1-iodooctane (**115**, 86 µL, 0.33 mmol, 1.30 equiv), sodium ascorbate (17 mg, 88 µmol, 0.35 equiv), Nafion-$Ru(bpy)_3Cl$ (**107**, 25 mg, 2.5 µmol, 1.0 mol%), MeOH (1.5 mL) and MeCN (2.0 mL). The vial was capped with a rubber septum and the mixture was degassed by nitrogen sparging for 10 min. After irradiation for 0.5 h with a blue LED (λ = 455 nm) at room temperature, the reaction mixture was transferred to a test tube with the aid of MeCN (2 mL) and centrifuged. The supernatant was decanted and the remaining solid was dispersed in MeCN

(2 mL) and centrifuged again. After decantation of the supernatant, this step was repeated one more time and the organic phases were combined. The solvents were evaporated and 4-nitrobenzaldehyde was added as internal standard for ^{1}H-NMR.

The recovered catalyst was dried and re-used in a second reaction run, setting all parameters as before. The yields of the single runs are given in the main part.

1-(nitromethyl)-2-phenyl-1,2,3,4-tetrahydroisoquinoline (90a)[8]

Literature conditions

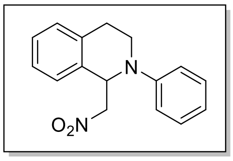

A Schlenk tube was charged with 2-phenyl-1,2,3,4-tetrahydroisoquinoline[9] (**89a**, 52 mg, 0.25 mmol, 1.00 equiv), [Ru(bpy)$_3$]Cl$_2$ (**1**, 1.9 mg, 2.5 µmol, 1.0 mol%) and nitromethane (**120**, 1.0 mL). The tube was sealed with a Teflon sealed inlet for a glass rod to ensure irradiation with a blue LED (λ = 455 nm) from above while allowing for magnetic stirring from below. Without degassing and opened to air the mixture was irradiated for 4 h at room temperature after which full consumption of starting material was obtained. Purification by flash silica column chromatography (hexanes / EtOAc, 9:1) afforded the pure product as yellow solid (55.8 mg, 0,208 mmol, 83%). The analytical data is in accordance with literature.[10]

^{1}H-NMR (300 MHz, CDCl$_3$): δ 7.17 – 6.96 (m, 6H), 6.90 – 6.77 (m, 2H), 6.75 – 6.63 (m, 1H), 5.40 (t, J = 7.2 Hz, 1H), 4.71 (dd, J = 11.8, 7.8 Hz, 1H), 4.41 (dd, J = 11.8, 6.6 Hz, 1H), 3.60 – 3.37 (m, 2H), 2.93 (ddd, J = 16.4, 8.4, 5.9 Hz, 1H), 2.63 (dt, J = 16.3, 5.0 Hz, 1H).

Recycling conditions

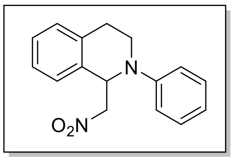

A Schlenk tube was charged with 2-phenyl-1,2,3,4-tetrahydroisoquinoline[9] (**89a**, 52 mg, 0.25 mmol, 1.00 equiv), Nafion-Ru(bpy)$_3$Cl (**107**, 25 mg, 2.5 µmol, 1.0 mol%) and nitromethane (1.0 mL). The tube was sealed with a Teflon sealed inlet for a glass rod to ensure irradiation with a blue LED (λ = 455 nm) from above while allowing for magnetic stirring from below. Without degassing and opened to air the mixture was irradiated for 4 h at room temperature. Subsequently, the reaction mixture was transferred to a test tube with the aid of MeNO$_2$ (3 mL) and centrifuged. The supernatant was decanted and the remaining solid was dispersed in MeNO$_2$ (4 mL) and again centrifuged. After decanting the supernatant this step was repeated one more time and the organic phases were combined and evaporated. 1,3,5-trimethoxybenzene was added as internal standard for ^{1}H-NMR and crude NMR was submitted to determine the yield.

The catalyst was dried and reused in a second run without changing any reaction parameters. The yields of the single reaction runs are given in the main part.

2,2,2-trifluoroethyl 3-methyl-5-((*S*)-5-oxo-3-tosyloxazolidin-4-yl)pentanoate (123aa)

Literature conditions

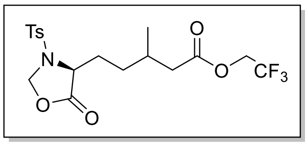

A Schlenk tube was charged with 1,3-dioxoisoindolin-2-yl (*S*)-3-(5-oxo-3-tosyloxazolidin-4-yl)propanoate[***] (**121a**, 91.7 mg, 200 µmol, 1.00 equiv), 2,2,2-trifluoroethyl E-but-2-enolate (**122a**, 336 mg, 2.00 mmol, 10.0 equiv), diethyl 2,6-dimethyl-1,4-dihydropyridine-3,5-dicarboxylate (Hantzsch ester, **240**, 50.6 mg, 200 µmol, 1.00 equiv), [Ru(bpy)$_3$]Cl$_2$ (**1**, 3.00 mg, 4.00 µmol, 2.0 mol%) and MeOH and water (3:1, 2.00 mL, 0.1 M). The Schlenk tube was sealed with a plastic screw-cap and the mixture was degassed by three freeze-pump-thaw cycles. The screw-cap was replaced by a Teflon sealed inlet for a glass rod through which irradiation by a blue LED (λ = 455 nm) was ensured from above while the reaction was magnetically stirred from below. After 5 h of irradiation, the LED was switched off and the reaction mixture was transferred to a separation funnel. EtOAc (5 mL) and water (5 mL) were added. The phases were separated, and the aqueous layer was extracted with EtOAc (3x 5 mL). The combined organic phases were washed with 10 mL brine and dried over Na$_2$SO$_4$. After evaporation of the solvent, 1,4-bis(trifluoromethyl)benzene was added as internal standard and the yield was determined by crude ^{19}F-NMR (51% yield). The pure product was isolated by S. Budde during his optimization studies (see chapter C).

Recycling conditions

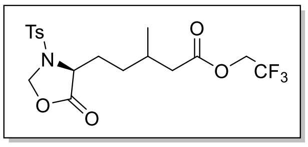

A Schlenk tube was charged with 1,3-dioxoisoindolin-2-yl (*S*)-3-(5-oxo-3-tosyloxazolidin-4-yl)propanoate (**121a**, 91.7 mg, 200 µmol, 1.00 equiv), 2,2,2-trifluoroethyl E-but-2-enolate (**122a**, 336 mg, 2.00 mmol, 10.0 equiv), diethyl 2,6-dimethyl-1,4-dihydropyridine-3,5-dicarboxylate (Hantzsch ester, **240**, 50.6 mg, 200 µmol, 1.00 equiv), Nafion-Ru(bpy)$_3$Cl (**107**, 40 mg,

---

[***] For starting material synthesis and further details see chapter C – photochemical decarboxylations.

4.00 µmol, 2.0 mol%) and MeOH and water (3:1, 2.00 mL, 0.1 M). The Schlenk tube was sealed with a plastic screw-cap and the mixture was degassed by three freeze-pump-thaw cycles. The screw-cap was replaced by a Teflon sealed inlet for a glass rod through which irradiation by a blue LED (λ = 455 nm) was ensured from above while the reaction was magnetically stirred from below. After 5 h of irradiation the LED was switched off and the reaction mixture was transferred to a test tube with the aid of MeOH (2 mL). The mixture was centrifuged, the supernatant was decanted and the remaining solid was dispersed in MeOH (4 mL). After centrifuging and decanting the supernatant again, this step was repeated one more time and the organic phases were combined. The solvents were evaporated and 1,4-bis(trifluoromethyl)benzene was added as internal standard. The yields were determined by crude ^{19}F-NMR.

The catalyst was dried and reused in a second run without changing the reaction parameters. The yields of the single runs are given in the main part.

2.3. Reaction upscaling employing photocatalyst on Nafion

(*Z*)-1,2-diphenylethene (25) [6]

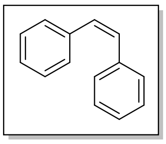

Setup

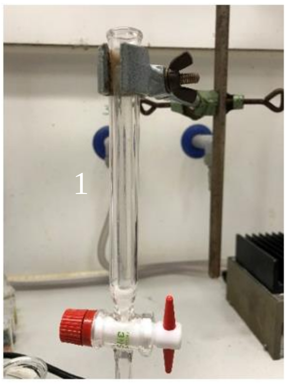

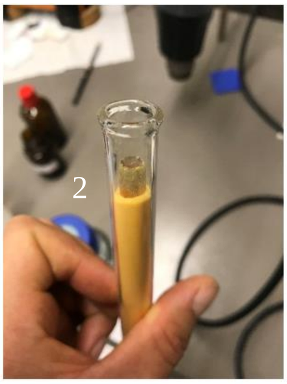

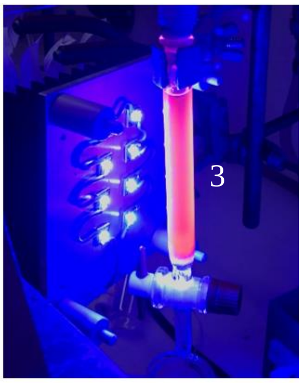

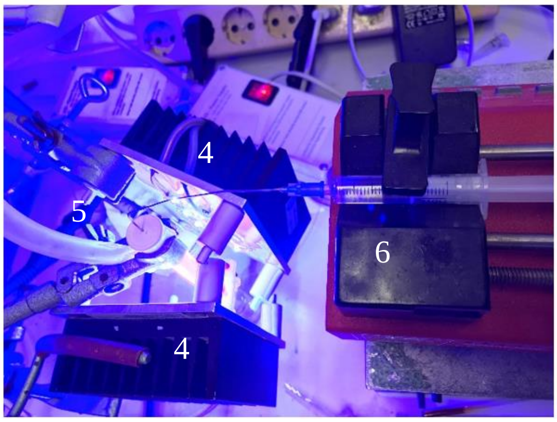

A column (1) with a glass filter frit was charged with a mixture of Nafion-Ru(bpy)$_3$Cl (**107**, 60 mg, 6.0 µmol) and silica (2.5 g) which was ground before. In the middle was placed a glass rod (2) to enlarge the surface area and to ensure the light penetration by reducing the depth of the silica-catalyst layer. The column was flushed with oxygen saturated DCM (dead volume of column = 2.0 mL). The irradiation was realized by 2 x 8 high power blue (λ = 455 nm) LEDs (4) and cooling was guaranteed by a stream of nitrogen (5). The substrate(s) were flushed through the column with the aid of a syringe pump (6) and collected in a vial.

This setup was used for both investigation of the best reaction conditions and up-scaling.

Investigation of best reaction conditions

To evaluate the best reaction conditions for the photochemical *Z/E*-isomerization, the reaction was conducted several times on a 0.20 mmol scale. Therefore, a 10 mL Schlenk tube was charged with (*E*)-1,2-diphenylethene (**24**, 36 mg, 0.20 mmol, 1.00 equiv) and DCM (2 mL). The mixture was saturated with oxygen by sparging oxygen through it for 3 min. Subsequently, the reaction mixture was transferred to a 2.0 mL syringe and flushed through the column with the aid of a syringe pump while being irradiated from the outside. To rinse the column the syringe was charged with DCM (2.5 mL), which was flushed through. The fractions were collected, the solvent was evaporated, and the *Z/E*-ratio was determined by integrating the crude ^{1}H-NMR peaks.

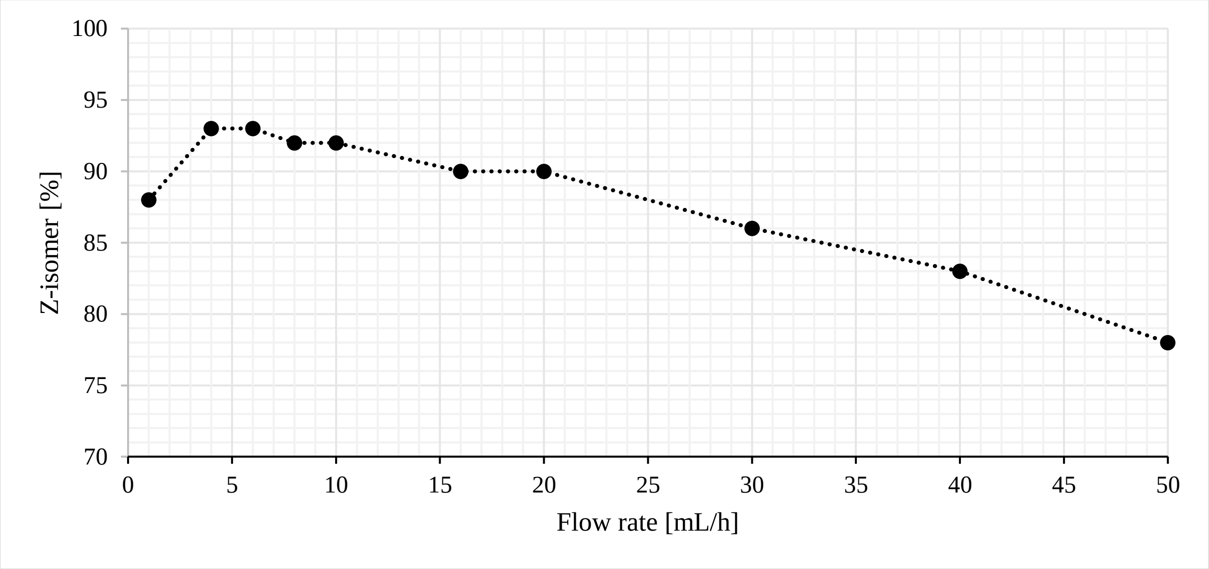

Upscaling of reaction

For upscaling, the same reaction setup as before was used. A 100 mL Schlenk flask was charged with (*E*)-1,2-diphenylethene (**24**, 1.082 g, 6.00 mmol, 1.00 equiv) and DCM (60 mL). The reaction mixture was saturated with oxygen by sparging oxygen through it for 10 min. Subsequently, a 20 mL syringe was charged with a third of the reaction solution and flushed through the column (flow rate: 20 mL/h) while being irradiated from the outside. The syringe was recharged two times with the reaction mixture and the column was finally rinsed with additional DCM (4 mL). The product was collected in 1.0 mmol or 10 mL fractions, respectively. The solvent was evaporated, and the *Z/E*-ratio was determined by integration of crude ^{1}H-NMR integrals. The leaching of ruthenium was determined by ICP-OES. The results are given in the main part.

5-iodo-6-perfluorooctylhexanol (116) [7b]

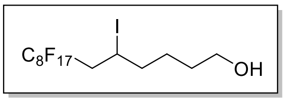

Setup

The same setup as for the *Z/E*-isomerization was used, except that the column was purged with a stream of nitrogen for 10 min before flushing the reaction mixture through. Moreover, less immobilized catalyst was used for both following reactions, i.e. Nafion-Ru(bpy)$_3$Cl (**107**, 25 mg, 2.5 µmol).

Reaction upscaling

1.0 mmol: A 25 mL Schlenk flask was charged with 5-hexen-1-ol (**109**, 120 µL, 1.00 mmol, 1.00 equiv), heptadecafluoro-1-iodooctane (**115**, 343 µL, 1.30 mmol, 1.30 equiv), sodium ascorbate (69 mg, 0.35 mmol, 0.35 equiv), MeOH (6.0 mL) and MeCN (12 mL). The reaction mixture was degassed by nitrogen sparging for 10 min and transferred to a 20 mL syringe. The mixture was flushed through the column (flow rate: 40 mL/h) while being irradiated from the outside. Subsequently, the column was rinsed with MeCN (4 mL) and the fractions were combined. The solvents were evaporated, 4-nitrobenzaldehyde was added as internal standard and the yield was determined by ^{1}H-NMR (87%).

1.5 mmol: A 25 mL Schlenk flask was charged with 5-hexen-1-ol (**109**, 180 µL, 1.50 mmol, 1.00 equiv), heptadecafluoro-1-iodooctane (**115**, 515 µL, 1.95 mmol, 1.30 equiv), L-ascorbate (104 mg, 0.53 mmol, 0.35 equiv), MeOH (9.0 mL) and MeCN (18 mL). The reaction mixture was degassed by nitrogen sparging for 10 min and transferred to a 20 mL syringe. The mixture was flushed through the column (flow rate: 40 mL/h) while irradiated from the outside. Subsequently, the column was rinsed with MeCN (4 mL) and the fractions were combined. The solvents were evaporated, 4-nitrobenzaldehyde was added as internal standard and the yield was determined by ^{1}H-NMR (78%).

2.4. Non-covalent immobilization of photocatalysts on magnetic nanoparticles

4-(2-Aminoethyl)phenyl functionalized Co/C nanoparticles (126) [11]

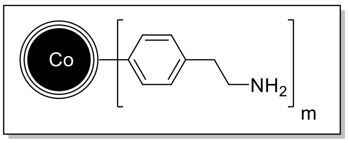

A 50 mL round bottom flask was charged with Co/C nanobeads (**124**, 500 mg), HCl_{conc} (0.5 mL), 4-(2-aminoethyl)aniline (**125**, 66 µL, 500 µmol) and H_2O (15 mL). After sonication for 15 min, the mixture was cooled to 0 °C and a solution of $NaNO_2$ (52 mg, 750 µmol) in H_2O (15 mL) was dropwise added. After stirring for 30 min at 0 °C, the mixture was sonicated for another 30 min at room temperature. Subsequently, the particles were magnetically collected, the solution decantated, followed by washing with 1 M NaOH (3 x 5 mL), H_2O (3 x 5 mL), acetone (2 x 5 mL) and diethyl ether (2 x 5 mL). The particles were dried *in vacuo* to yield 505 mg of **126**.
IR (neat): 3421, 2920, 2819, 1622, 1548, 1369, 1073, 812 cm^{-1}; **elemental microanalysis** [%]: C, 4.95; H, 0.12; N, 0.13.

Silica-coated Co/C nanoparticles (127) [12]

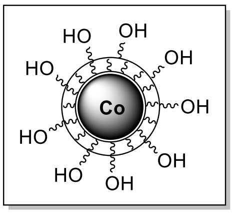

In a 250 mL round bottom flask, 4-(2-aminoethyl)phenyl functionalized Co/C nanoparticles **126** (100 mg) and ammonia solution (25%, 20 mL) were sonicated in EtOH (200 mL) for 30 min at room temperature. Tetraethyl orthosilicate (400 µL, 376 mg, 1.80 mmol) was added and the mixture was sonicated for another 2 h at room temperature. Afterwards, the particles were magnetically collected and the supernatant decanted. The particles were washed with EtOH (5 x 15 mL) and dried *in vacuo* yielding 233 mg of silica-coated Co/C nanoparticles **127**.
IR (neat): 3230, 2117, 1636, 1062, 947, 734 cm^{-1}; **elemental microanalysis** [%]: C, 2.97; H, 1.03; N, 1.05.

Thiol-functionalized Co/C nanoparticles (129)

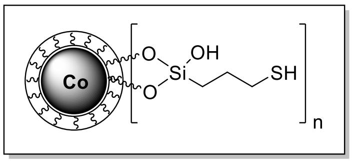

Following a modified literature procedure,[13] a 10 mL pressure tube was charged with silica-coated Co/C nanoparticles **127** (50 mg), (3-mercaptopropyl)trimethoxysilane (**128**, 200 µL, 1.1 mmol), H_2O (2.0 mL) and ethanol (2.0 mL). The reaction mixture was sonicated for 15 min at room temperature followed by stirring at 80 °C for 16 h. Subsequently, the particles were magnetically collected, and the supernatant was decanted. Washing with H_2O (3 x 3 mL) and acetone (3 x 3 mL) and drying *in vacuo* gave the thiol-functionalized Co/C nanoparticles **129** (150 mg).

IR (neat): 2926, 1438, 1342, 1305, 1025, 794, 686 cm^{-1}

Sulfonic acid-functionalized Co/C nanoparticles (130)

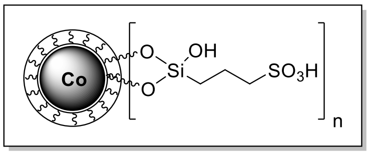

Modifying a literature procedure,[13] in a 10 mL Schlenk flask thiol-functionalized Co/C nanoparticles **129** (120 mg) were stirred in H_2O_2 (30%, 4 mL) for 5 h at room temperature. After collecting the particles magnetically, the supernatant was decanted and they were washed with H_2O (2 x 3 mL), H_2SO_4 (1 M, 2 x 3 mL) followed by H_2O (5 x 3 mL). Drying *in vacuo* gave the sulfonic acid-functionalized Co/C nanoparticles **130** as slightly grey solid (123 mg).

IR (neat): 3220, 2933, 2110, 1640, 1457, 1412, 1297, 1077, 1025, 738, 690 cm^{-1}; **elemental microanalysis** [%]: C, 15.06; H, 3.37; S, 12.25; corresponds to: loading (S): 3.8 mmol/g; titration with 1 M NaOH revealed: loading of (-SO_3H): 1.80 mmol/g.

MNP-Ru(bpy)$_3$Cl (131)

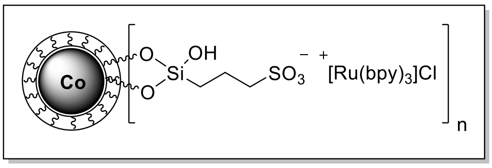

For deprotonation, the sulfonic acid-functionalized Co/C nanoparticles **130** (20 mg, 36 µmol (-SO_3H), 1.00 equiv) were placed in a pressure tube and treated with brine (6 x 2 mL). The particles were washed with water (3 x 2 mL) and dried *in vacuo* to give the corresponding sodium salt. Subsequently, these nanoparticles and $[Ru(bpy)_3]Cl_2$ (**1**, 45 mg, 60 µmol, 1.67 equiv) were dispersed in water (2.25 mL) by sonication in an ultrasonic bath for 30 min and subsequently stirred for 24 h at room temperature. The particles were magnetically collected, the supernatant was decanted, and they were washed with water until the supernatant remained colorless. Drying *in vacuo* gave the product as slightly brownish solid (23 mg).

IR (neat): 3258, 2937, 2117, 1737, 1651, 1446, 1413, 1349, 1301, 1092, 1029, 913, 731, 686; **ICP-OES**: loading [Ru]: 0.463 mmol/g.

The reaction was also performed with (1) heating to 85 °C (loading [Ru]: 0.406 mmol/g) and (2) using MeOH as solvent (loading [Ru]: 0.076 mmol/g).

2.5. Photochemical reactions employing electrostatically bound catalyst

Literature conditions

(*Z*)-1,2-diphenylethene (25) [6]

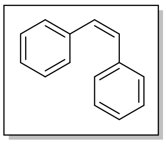

A Schlenk tube was charged with (*E*)-1,2-diphenylethene (**24**, 36 mg, 0.20 mmol, 1.00 equiv), [Ru(bpy)$_3$]Cl$_2$ (**1**, 3.8 mg, 6.0 µmol, 3.0 mol%) and MeCN (2 mL). The tube was sealed with a Teflon inlet for a glass rod to ensure irradiation from above with a blue LED (λ = 455 nm) while allowing for magnetic stirring from below. A balloon filled with oxygen was attached and the reaction mixture was irradiated with a blue LED (λ = 455 nm) under an oxygen-atmosphere for 8 h at room temperature. The *Z/E*-ratio was determined by GC-FID to be 93:7.

The reaction was performed under the same conditions and (1) adding silica-coated magnetic nanoparticles **127** (5.0 mg); (2) without [Ru(bpy)$_3$]Cl$_2$ (**1**) but with silica-coated MNP **127** (5.0 mg) and (3) without any catalyst. The results for the single experiments are given in the main part.

1-(1-nitroethyl)-2-phenyl-1,2,3,4-tetrahydroisoquinoline (90b)[8]

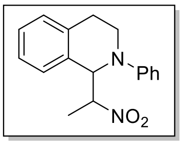

A Schlenk tube was charged with 2-phenyl-1,2,3,4-tetrahydroisoquinoline[9] (**89a**, 52 mg, 0.25 mmol, 1.00 equiv), [Ru(bpy)$_3$]Cl$_2$ (**1**, 1.9 mg, 2.5 µmol, 1.0 mol%) and nitroethane (**132**, 1.0 mL). The tube was sealed with a Teflon sealed inlet for a glass rod to ensure irradiation with a blue LED (λ = 455 nm) from above while allowing for magnetic stirring from below. Without degassing and opened to air the mixture was irradiated for 5.5 h at room temperature after which full consumption of starting material was obtained (as judged by TLC). Purification by flash silica column chromatography (hexanes / EtOAc, 9:1) afforded the pure product as yellow solid (51 mg, 0.181 mmol, 72%). The analytical data is in accordance with literature.[8] The ratio of diastereomers is 2:1.

^{1}H-NMR (300 MHz, CDCl$_3$): major diastereomer: δ 5.14 – 4.99 (m, 1H), 3.65 – 3.51 (m, 2H), 1.55 (d, J = 6.7 Hz, 3H); minor diastereomer: δ 4.95 – 4.85 (m), 3.89 – 3.78 (m), 1.71 (d, J = 6.8 Hz); overlap signals: δ 7.32 – 7.10 (m), 7.03 – 6.99 (m), 6.86 – 6.80 (m), 5.30 – 5.23 (m), 3.12 – 3.02 (m), 2.97 – 2.84 (m); **^{13}C-NMR**: (75 MHz, CDCl$_3$): major diastereomer: δ 147.82, 134.57, 130.96, 128.27, 127.31, 127.16,125.08, 118.26, 114.35, 84.39, 61.69, 41.59, 25.32, 15.35; minor diastereomer: δ 148.10, 133.74, 132.76, 128.39, 128.07, 127.68, 126.20, 125.55, 117.72, 113.41, 87.91, 60.10, 42.49, 25.69, 16.38.

The reaction was also performed (1) adding silica-coated magnetic nanoparticles **127** (5.0 mg); (2) without $[Ru(bpy)_3]Cl_2$ (**1**) but with silica-coated MNP **127** (5.0 mg) and (3) without any catalyst.

Recycling conditions

(*Z*)-1,2-diphenylethene (25) [6]

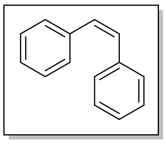

A Schlenk tube was charged with (*E*)-1,2-diphenylethene (**24**, 36 mg, 0.20 mmol, 1.00 equiv), MNP-$[Ru(bpy)_3]Cl$ (**131**, 13.5 mg, 6.0 µmol, 3.0 mol%, **or** 4.5 mg, 2.0 µmol, 1.0 mol%) and MeCN (2 mL). The tube was sealed with a Teflon sealed inlet for a glass rod to ensure irradiation from above with a blue LED (λ = 455 nm) while allowing for magnetic stirring from below. A balloon filled with oxygen was attached and the mixture was irradiated for 8 h (with 3.0 mol% catalyst loading) **or** 16 h (with 1.0 mol% catalyst loading), respectively. Subsequently, the catalyst was magnetically collected, the supernatant was decanted, and the particles were dispersed in MeCN (2 mL) again, magnetically collected and the supernatant decanted. These steps were repeated one more time. The organic phases were combined, and the solvent evaporated. The *Z/E*-ratio was determined by integrating the signals of the crude ^{1}H-NMR.

The catalyst was directly reused in a second reaction run applying the same reaction parameters as before. The *Z/E*-ratios of the single runs employing 3.0 or 1.0 mol% catalyst loading, respectively, are given in the main part.

1-(1-nitroethyl)-2-phenyl-1,2,3,4-tetrahydroisoquinoline (90b)[8]

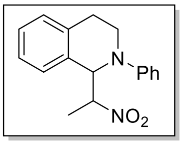

A Schlenk tube was charged with 2-phenyl-1,2,3,4-tetrahydroisoquinoline[9] (**89a**, 52 mg, 0.25 mmol, 1.00 equiv), Nafion-$Ru(bpy)_3Cl$ (**131**, 5.4 mg, 2.5 µmol, 1.0 mol%) and nitroethane (**132**, 1.0 mL). The tube was sealed with a Teflon sealed inlet for a glass rod to ensure irradiation with a blue LED (λ = 455 nm) from above while allowing for magnetic stirring from below. Without degassing and opened to air the mixture was irradiated for 5.5 h at room temperature after which the catalyst was magnetically collected and the supernatant decanted. The particles were dispersed in DCM, magnetically collected and the supernatant decanted. These steps were repeated one more time and the organic phases were combined. The solvents were evaporated and 1,3,5-trimethoxy benzene was added as internal standard for ^{1}H-NMR.

The catalyst was dried and reused in a second reaction run without changing the reaction parameters. The yields of the single runs are given in the main part.

2.6. Covalent immobilization of photocatalysts on magnetic nanoparticles

4-(but-3-en-1-yl)-4'-methyl-2,2'-bipyridine (136)

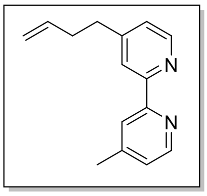

The reaction was performed modifying a literature known procedure.[14] 4,4’-dimethyl-2,2’-bipyridine (550 mg, 2.99 mmol, 1.00 equiv) was dissolved in dry THF (30 mL) and cooled to 0 °C. LDA, freshly prepared by adding ^{n}BuLi (1.6 M in heptane, 1.87 mL, 2.99 mmol, 1.00 equiv) to a solution of diisopropylamine (453 µL, 326 mg, 3.22 mmol, 1.08 equiv) in dry THF (8 mL) was added. The mixture turned immediately dark red/brownish. After stirring for 1 h at 0 °C, allyl bromine (258 µL, 361 mg, 2.99 mmol, 1.00 equiv) dissolved in THF (3 mL) was slowly added, whereupon the mixture turned yellowish. The mixture was allowed to warm to room temperature overnight. Afterwards, water (2 mL) was added and THF was evaporated. The product was extracted with Et_2O (3 x 5 mL) and the combined organic layers were dried over $MgSO_4$. Purification was achieved by flash silica column chromatography (hexanes / EtOAc, 5:1) to give the pure compound as colorless oil (640 mg, 186 mmol, 95%). The spectra are in accordance with those reported in literature.[15]

^{1}H-NMR (400 MHz, $CDCl_3$): δ 8.54 (dd, J = 9.8, 5.0 Hz, 2H), 8.23 (dd, J = 4.6, 1.5 Hz, 2H), 7.12 (td, J = 4.4, 3.8, 1.6 Hz, 2H), 5.91 – 5.76 (m, 1H), 5.10 – 4.94 (m, 2H), 2.79 (dd, J = 8.8, 6.8 Hz, 2H), 2.48 – 2.43 (m, 2H), 2.42 (s, 3H); **^{13}C-NMR** (101 MHz, $CDCl_3$): δ 156.20, 156.04, 151.80, 149.02, 148.94, 148.13, 137.17, 124.66, 123.93, 122.02, 121.30, 115.61, 34.85, 34.32, 21.18.

Bis-(2,2’-bipyridine)(4-(but-3-en-1-yl)-4'-methyl-2,2'-bipyridine) ruthenium(II) bishexafluorophosphate (137) [15]

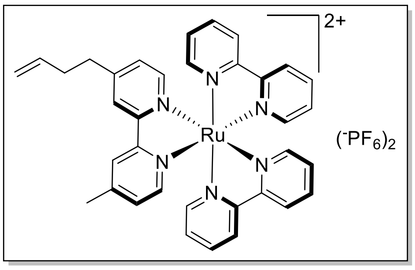

Modifying a literature known procedure,[15] $[Ru(bpy)_2]Cl_2$[16] (100 mg, 192 µmol, 1.00 equiv) and ligand **136** (43.1 mg, 192 µmol, 1.00 equiv) were dissolved in H_2O (6.70 mL) and MeOH (13.3 mL) and heated to 85 °C for 24 h. The solvents were evaporated to give a bright red solid, which was dissolved in less DMF (1 mL). The pure catalyst was precipitated with a saturated aqueous solution of KPF_6, filtrated and washed with H_2O. After drying over high vacuo, the product was obtained as bright red solid (170 mg, 183 µmol, 95%). The analytical data is in accordance with the literature.[15]

^{1}H-NMR (300 MHz, CD_2Cl_2): δ 8.49 – 8.38 (m, 4H), 8.27 – 8.24 (m, 2H), 8.11 – 7.99 (m, 4H), 7.76 – 7.64 (m, 4H), 7.55 – 7.38 (m, 6H), 7.28 – 7.22 (m, 2H), 5.96 – 5.75 (m, 1H), 5.12 – 4.99 (m, 2H), 2.82 (d, J = 0.6 Hz, 1H), 2.58 (s, 3H), 2.53 – 2.38 (m, 3H); **^{13}C-NMR** (75 MHz, CD_2Cl_2): δ 157.29, 157.20, 156.79, 156.63, 154.65, 151.66, 151.56, 151.39, 150.88, 150.67, 138.32, 136.94, 129.34, 128.58, 128.37, 125.48, 124.76, 124.59, 116.47, 34.89, 34.07, 21.52.

(3-azidopropyl)trimethoxysilane (139) [17]

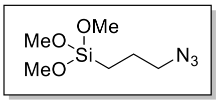

A flame dried 100 mL Schlenk flask was charged with NaN_3 (910 mg, 14.0 mmol, 1.40 equiv), tetrabutylammonium bromide (644 mg, 2.00 mmol, 0.20 equiv) and dry MeCN (40 mL). 3-chloropropyltrimethoxysilane (1.82 mL, 1.99 g, 1.00 equiv) was added and the mixture was refluxed for 24 h under nitrogen atmosphere. Afterwards, the solvent was evaporated under reduced pressure, diethyl ether (10 mL) was added and the suspension was filtered and washed with additional diethyl ether (2 x 10 mL). The solvent was removed under reduced pressure yielding the pure product **139** as colorless oil. The spectra are in accordance with those reported in literature.[18]

^{1}H-NMR (400 MHz, $CDCl_3$): δ 3.57 (s, 9H), 3.26 (t, J = 6.9 Hz, 2H), 1.77 – 1.65 (m, 2H), 0.75 – 0.62 (m, 2H); **^{13}C-NMR** (101 MHz, $CDCl_3$): δ 53.74, 50.58, 22.45, 6.33.

Azide-functionalized Co/C nanoparticles (140)

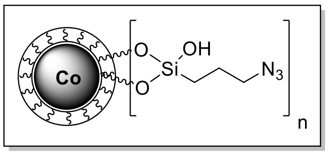

In a 10 mL Schlenk tube silica-coated Co/C nanoparticles **127** (20 mg) were dispersed in H_2O (1 mL) and EtOH (0.5 mL). Ammonia solution (25%, 25 µL) was added and the mixture was ultrasonicated for 5 min. A solution of (3-azidopropyl)trimethoxysilane (**139**, 100 mg, 487 µmol) in EtOH (0.5 mL) was added within 1 h with the aid of a syringe pump under vigorous stirring. During this time the solution became cloudy. The mixture was allowed to stir for 18 h at room temperature. The particles were magnetically collected, the supernatant decantated and subsequently washed with acetone (5 x 3 mL). After drying *in vacuo* 100 mg of slightly gray azide-functionalized Co/C nanoparticles **140** were obtained.

IR (neat): 2937, 2874, 2087, 1450, 1346, 1275, 1237, 1185, 1085, 1006, 775, 693 cm^{-1}; **elemental microanalysis** [%]: C, 18.69; H, 3.26; N, 20.58 – **loading** (N): 14.7 mmol/g.

6-(trimethylsilyl)hex-5-yn-1-ol [19]

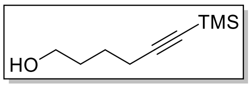

Under a nitrogen-atmosphere, hex-7-yn-ol (1.50 mL, 1.50 g, 15.28 mmol, 1.00 equiv) was dissolved in dry and degassed THF (45 mL) and cooled to -78 °C. ^{n}BuLi (1.6 M in hexanes, 21.0 mL, 33.62 mmol, 2.20 equiv) and DMAP (396 mg, 3.24 mmol, 0.21 equiv) were added and the mixture was stirred for 1 h at - 78 °C. Afterwards, TMSCl (7.18 mL, 6.14 g, 56.55 mmol, 3.70 equiv) was added and the cooling bath was removed. After stirring for 2 h at room temperature the mixture was quenched with HCl (1 M, 15 mL). Subsequently, EtOAc (50 mL) was added, the phases were separated, and the aqueous phase was extracted with EtOAc (3 x 25 mL). The combined organic phases were washed with sat. $NaOCO_3$ (50 mL), brine (50 mL) and dried over Na_2SO_4. Purification was achieved by flash silica column chromatography (hexanes / EtOAc, 4:1). The pure product was obtained as colorless oil (2.26 g, 13.27 mmol, 87%). The spectra are in accordance with those reported in literature.[20]

^{1}H-NMR (300 MHz, $CDCl_3$): δ 3.67 (td, J = 6.3, 0.7 Hz, 1H), 2.26 (t, J = 6.7 Hz, 1H), 1.72 – 1.53 (m, 1H), 0.14 (s, 2H); **^{13}C-NMR** (75 MHz, $CDCl_3$): δ 107.01, 84.64, 62.23, 31.64, 24.73, 19.47, 0.00.

(6-iodohex-1-yn-1-yl)trimethylsilane

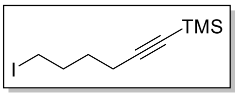

The reaction was performed following an adopted literature procedure.[21] A 50 mL round bottom flask was charged with 6-(trimethylsilyl)hex-5-yn-1-ol (1.00 g, 5.87 mmol, 1.00 equiv), imidazole (759 mg, 11.2 mmol, 2.40 equiv), triphenylphosphine (2.77 g, 10.6 mmol, 1.80 equiv), Et_2O (15 mL) and MeCN (10.5 mL). The mixture was cooled to 0 °C and iodine (3.54 g, 14.0 mmol, 2.40 equiv) was added. After stirring for 2 h at 0 °C the mixture was transferred to a separation funnel with the aid of Et_2O (100 mL) and washed with sat. aq. $Na_2S_2O_3$ until the organic phase was colorless. The organic phase was dried over Na_2SO_4. Purification was achieved by flash silica column chromatography (pure hexanes). The product was obtained as colorless oil (1.12 g, 4.00 mmol, 68%).The ^{1}H-NMR spectra is in accordance with literature.[22]

^{1}H-NMR (400 MHz, $CDCl_3$): δ 3.22 (t, J = 6.9 Hz, 2H), 2.26 (t, J = 7.0 Hz, 2H), 2.00 – 1.88 (m, 2H), 1.69 – 1.59 (m, 2H), 0.15 (s, 9H); **^{13}C-NMR** (101 MHz, $CDCl_3$): δ 106.41, 85.23, 32.42, 29.21, 18.84, 6.20, 0.15.

4-methyl-4'-(7-(trimethylsilyl)hept-6-yn-1-yl)-2,2'-bipyridine (141)

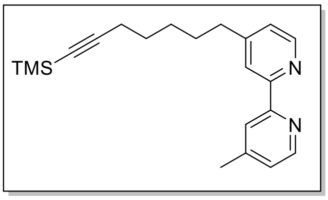

A 25 mL Schlenk flask was charged with 4,4’-dimethyl-2,2’-bipyridine (250 mg, 1.36 mmol, 1.00 equiv) and dry and degassed THF (10 mL). The mixture was cooled to 0 °C and freshly prepared LDA (from diisopropylamine (206 µL, 148 mg, 1.47 mmol, 1.08 equiv) and ^{n}BuLi (1.6 M, 848 µL, 1.36 mmol, 1.00 equiv) in THF (4 mL)) was added after which the mixture turned immediately black. After stirring for 1 h at 0 °C, (6-iodohex-1-yn-1-yl)trimethylsilane (380 mg, 1.36 mmol, 1.00 equiv) dissolved in THF (1.5 mL) was slowly added and the mixture was allowed to warm to room temperature overnight. Water (5 mL) was added and THF was evaporated. DCM (10 mL) was added and the organic phase was washed with water (2 x 5 mL) followed by brine (1 x 5 mL). The organic phase was dried over Na_2SO_4, filtrated and the solvent was evaporated. Purification by flash silica column chromatography (hexanes / EtOAc, 5:1) gave the pure compound as colorless oil (431 mg, 1.28 mmol, 94%). **^{1}H-NMR** (300 MHz, $CDCl_3$): δ 8.55 (t, J = 4.9 Hz, 2H), 8.22 (s, 2H), 7.21 – 7.05 (m, 2H), 2.70 (t, J = 7.7 Hz, 2H), 2.44 (s, 3H), 2.22 (t, J = 6.8 Hz, 2H), 1.76 – 1.66 (m, 2H), 1.51 (s, 4H), 0.13 (s, 9H); **^{13}C-NMR** (75 MHz, $CDCl_3$): δ 155.96, 152.43, 148.84, 148.76, 147.97, 124.47, 123.74, 121.85, 121.10, 107.14, 84.41, 35.21, 29.75, 28.26, 28.22, 21.04, 19.59, 0.00; **R_f** (hexanes / EtOAc, 4:1) = 0.5; **IR** (neat): 3053, 3008, 2937, 2863, 2177, 1595, 1554, 1461, 1420, 1379, 1245, 1107, 1055, 842, 760, 701 cm^{-1}; **HRMS** (EI-MS) m/z calculated for $C_{21}H_{27}N_2Si$ ($[M-H]^-$) 335.19380, found 335.19362.

Bis-(2,2’-bipyridine)(4-methyl-4'-(7-(trimethylsilyl)hept-6-yn-1-yl)-2,2'-bipyridine) ruthenium(II) bishexafluorophosphate

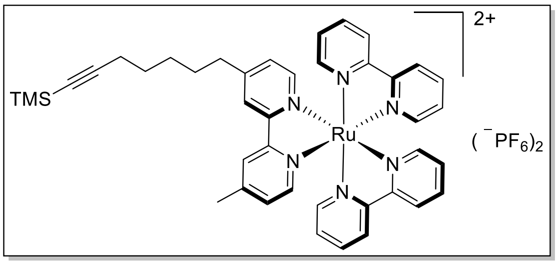

A 50 mL round bottom flask was charged with $[Ru(bpy)_2]Cl_2$[16] (100 mg, 192 µmol, 1.0 equiv), 4-methyl-4'-(7-(trimethylsilyl)-hept-6-yn-1-yl)-2,2'-bipyridine (**141**, 67.9 mg, 202 mmol, 1.05 equiv), MeOH (13.3 mL) and H_2O (6.7 mL) and the mixture was stirred for 4.5 h at 85 °C. Subsequently, the solvents were evaporated, and the residue was re-dissolved in DMF (1 mL). The catalyst was precipitated with a saturated aqueous KPF_6 solution, filtrated and washed with water. Drying over high vacuo gave the pure product as bright red solid (253 mg, 147 µmol, 77%).

^{1}H-NMR (300 MHz, CD_3OD): δ 8.51 – 8.40 (m, 4H), 8.32 – 8.22 (m, 2H), 8.12 – 7.98 (m, 4H), 7.77 – 7.65 (m, 4H), 7.55 – 7.38 (m, 6H), 7.29 – 7.18 (m, 2H), 2.90 – 2.78 (m, 2H), 2.57 (s, 3H), 2.24 – 2.12 (m, 2H), 1.95 (t, J = 2.6 Hz, 1H), 1.80 – 1.65 (m, 2H), 1.64 – 1.42 (m, 4H); **^{13}C-NMR** (101 MHz, CD_3OD): δ 158.37, 158.29, 157.91, 157.75, 156.08, 152.41, 152.36, 152.29, 151.86, 151.60, 151.37, 138.72, 129.52, 128.71, 128.65, 128.61, 126.16, 125.38, 125.25, 108.27, 84.74, 35.86, 30.46, 29.32, 29.16, 20.94, 20.01, 0.00; **IR** (neat): 2930, 2169, 2117, 1618, 1446, 1312, 1245, 831, 760 cm^{-1}; **HRMS** (ESI-MS) m/z calculated for $C_{41}H_{44}N_6RuSi$ ($[M-2(PF_6)]^{2+}$) 372.1231, found 372.1234.

Bis-(2,2’-bipyridine)(4-(hept-6-yn-1-yl)-4’-methyl-2,2’-bipyridine) ruthenium(II) bishexafluorophosphate (142)

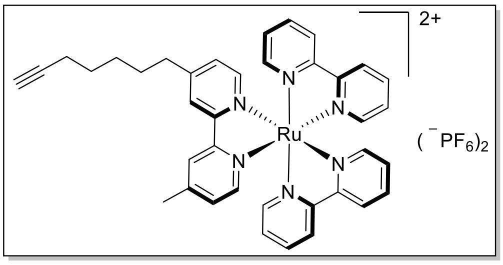

Bis-(2,2’-bipyridine)(4-methyl-4'-(7-(trimethylsilyl)-hept-6-yn-1-yl)-2,2'-bipyridine) ruthenium(II) bishexafluorophosphate (100 mg, 96 µmol, 1.00 equiv) and K_2CO_3 were dissolved in MeOH (4 mL) and stirred for 16 h at room temperature. MeOH was evaporated and the residue was re-dissolved in DCM (10 mL) and extracted with H_2O (3 x 5 mL). Evaporation of the solvent gave the pure product as bright red solid (93 mg, 96 µmol, 100%).

^{1}H-NMR (400 MHz, CD_2Cl_2): δ 8.66 (d, J = 8.2 Hz, 4H), 8.56 (d, J = 10.3 Hz, 2H), 8.09 (t, J = 7.9 Hz, 4H), 7.86 – 7.77 (m, 4H), 7.60 (dd, J = 11.6, 5.8 Hz, 2H), 7.47 (q, J = 7.0 Hz, 4H), 7.36 – 7.27 (m, 2H), 2.88 – 2.80 (m, 2H), 2.57 (s, 3H), 2.22 (t, J = 6.6 Hz, 2H), 1.74 (q, J = 7.5 Hz, 2H), 1.64 – 1.45 (m, 4H), 0.07 (s, 9H); **^{13}C-NMR** (75 MHz, CD_2Cl_2): δ 156.12, 156.03, 155.62, 155.46, 154.29, 150.43, 150.34, 150.17, 149.65, 149.45, 137.13, 128.12, 127.26, 127.16, 124.30, 123.44, 83.59, 67.48, 34.36, 28.64, 27.52, 27.30, 20.29, 17.34; **IR** (neat): 3288, 2926, 2113, 1618, 1446, 1312, 1264, 1025, 831, 760 cm^{-1}; **HRMS** (ESI-MS) m/z calculated for $C_{38}H_{36}N_6Ru$ ([M-2(PF_6)]$^{2+}$) 336.1033, found 336.1037.

MNP-Ru(bpy)$_2$(hexyne-bpy)(PF_6)$_2$ (143)

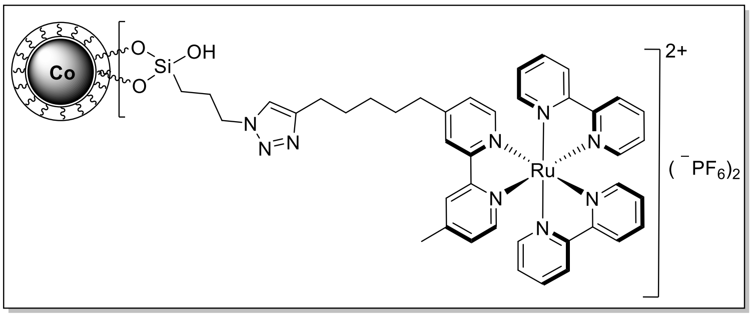

A Schlenk tube was charged with azide-functionalized nanoparticles **140** (22 mg), CuI (2.0 mg, 11 µmol, 60 mol%) and Ru^{II} complex **142** (21 mg, 18 µmol, 1.00 equiv). The tube was evacuated and backfilled with nitrogen three times. Subsequently, dry and degassed DCM (1 mL) and DIPEA (4.5 mg, 5.9 µL, 35 µmol, 2.00 equiv) were added and the mixture was allowed to stir for 3 d at room temperature, after which it lost its characteristic red color and turned slightly orange instead. The particles were magnetically collected, the supernatant decanted and they were washed with DCM (3 x 3 mL) until the supernatant remained colorless. The MNP were dried over high vacuo to give the product as slightly brownish solid (39 mg).

The loading of catalyst, based on recovered non-immobilized Ru^{II} complex **142**, was determined to be 0.45 mmol/g.

IR (neat): 2933, 2870, 2091, 1748, 1446, 1409, 1346, 1088, 1010, 779, 693 cm^{-1}.

2-phenyl-4-(7-(trimethylsilyl)hept-6-yn-1-yl)pyridine (145)

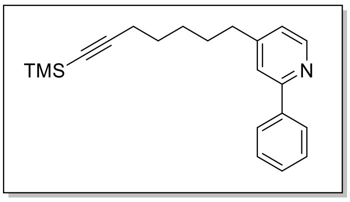

In a 50 mL Schlenk flask 4-methyl-2-phenylpyridine[22] (250 mg, 1.48 mmol, 1.00 equiv) was dissolved in dry and degassed THF (8 mL). Freshly prepared LDA solution (diisopropylamine (270 µL, 1.92 mmol, 1.30 equiv) and ^{n}BuLi (1.6 M in hexanes, 1.10 mL, 1.77 mmol, 1.20 equiv) dissolved in THF (3 mL)) was added at -78 °C. The mixture turned immediately red. After stirring for 30 min at -78 °C, (6-iodohex-1-yn-1-yl)trimethylsilane (414 mg, 1.48 mmol, 1.00 equiv), dissolved in THF (4 mL) was dropwise added and the mixture was allowed to warm to room temperature over night, after which it turned colorless. H_2O (10 mL) was added and THF was evaporated on the rotary evaporator. The product was extracted with EtOAc (3 x 10 mL) and the combined organic phases were washed with brine (1 x 10 mL) and dried over Na_2SO_4. Purification was achieved by flash silica column chromatography (hexanes / EtOAc, 5:1). The product **145** was obtained as colorless oil (398 mg, 1.24 mmol, 84%).

^{1}H-NMR (400 MHz, $CDCl_3$): δ 8.59 (d, J = 5.0 Hz, 1H), 8.08 – 7.92 (m, 2H), 7.56 (s, 1H), 7.53 – 7.46 (m, 2H), 7.46 – 7.39 (m, 1H), 7.09 (dd, J = 5.0, 1.4 Hz, 1H), 2.76 – 2.65 (m, 2H), 2.25 (t, J = 7.0 Hz, 2H), 1.77 – 1.68 (m, 2H), 1.63 – 1.55 (m, 2H), 1.53 – 1.45 (m, 2H), 0.15 (s, 9H); **^{13}C-NMR** (75 MHz, $CDCl_3$): δ 157.25, 152.16, 149.28, 139.33, 128.69, 128.54, 126.81, 122.25, 120.71, 107.07, 84.47, 35.20, 29.73, 28.19, 19.59, 0.00; **R_f** (hexanes / EtOAc, 4:1) = 0.5; **IR** (neat): 3056, 2937, 2859, 2173, 1603, 1554, 1476, 1405, 1249, 1074, 1029, 992, 835, 760, 693 cm^{-1}; **HRMS** (EI-MS) m/z calculated for $C_{21}H_{26}NSi$ ($[M-H]^-$) 320.18290, found 320.18311.

Bis(2-phenylpyridine-C^2,N)((2-phenyl-4-(7-(trimethylsilyl)hept-6-yn-1-yl)pyridine))iridium

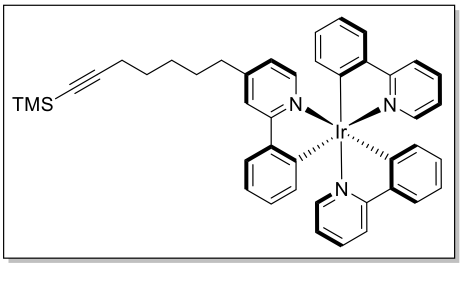

The catalyst was prepared by modifying a literature known procedure.[23] In a 50 mL round bottom flask $[Ir(ppy)_2Cl]_2$[3a] (200 mg, 186 µmol, 1.00 equiv) was dissolved in DCM (18.5 mL). AgOTf (101 mg, 391 µmol, 2.10 equiv) dissolved in MeOH (9 mL) was dropwise added and the mixture was stirred for 18 h in the dark. After filtering through a short plug of Celite® with the aid of DCM (20 mL) the solvent was evaporated to give $[Ir(ppy)_2(MeOH)_2](OTf)$ (**144**, 265 mg, 372 µmol, 100%) as a green solid which was used without further purification.

A 20 mL Schlenk flask was charged with $[Ir(ppy)_2(MeOH)_2](OTf)$ (**144**, 265 mg, 372 µmol, 1.00 equiv), 2-phenyl-4-(7-(trimethylsilyl)hept-6-yn-1-yl)pyridine (**145**, 359 mg, 1.12 mmol, 3.00 equiv), MeOH (7.5 mL) and EtOH (7.5 mL). Subsequently, the mixture was degassed by N_2 sparging for 5 min and heated to reflux for 24 h. Celite® (1.5 g) was added and the mixture was stirred for another 5 min. The mixture was filtration through a short plug of Celite® and washed with MeOH (25 mL), followed by hexanes (25 mL). The product was eluted with the aid of DCM (20 mL). Evaporation of the solvent gave the pure product (140 mg, 171 µmol, 46%) as bright yellow solid.

^{1}H-NMR (300 MHz, $CDCl_3$): δ 7.89 – 7.76 (m, 2H), 7.72 – 7.59 (m, 4H), 7.56 – 7.44 (m, 4H), 7.39 (d, J = 5.7 Hz, 1H), 6.98 – 6.76 (m, 11H), 6.70 (dd, J = 5.8, 1.8 Hz, 1H), 2.64 (t, J = 7.8 Hz, 2H), 2.24 (t, J = 6.9 Hz, 2H), 1.76 – 1.38 (m, 6H), 0.16 (s, 9H); **^{13}C-NMR** (75 MHz, $CDCl_3$): δ 166.42, 165.97, 161.29, 160.92, 151.37, 146.80, 146.40, 143.57, 143.52, 143.48, 136.89, 136.82, 135.63, 129.57, 129.44, 123.64, 123.42, 122.10, 121.66, 119.42, 118.46, 107.06, 84.41, 35.15, 29.51, 28.33, 28.14, 19.56, 0.00; **IR** (neat): 3034, 2930, 2855, 2169, 2110, 1737, 1580, 1469, 1409, 1301, 1245, 1156, 1059, 1029, 839, 753 cm^{-1}; **HRMS** (EI-MS) m/z calculated for $C_{43}H_{42}{}^{191}IrN_3Si$ ([M]$^+$) 819.27484, found 819.27569.

Bis(2-phenylpyridine-C^2,N)(4-(hept-6-yn-1-yl)-2-phenylpyridine)iridium (146)

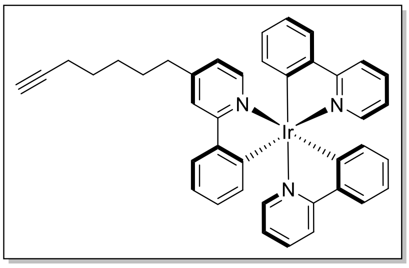

A Schlenk tube was charged with bis(2-phenylpyridine-C^2,N)((2-phenyl-4-(7-(trimethylsilyl)hept-6-yn-1-yl)pyridine))iridium (100 mg, 122 µmol, 1.00 equiv) and THF (1 mL). The mixture was cooled to 0 °C and TBAF (1 M in THF, 159 µL, 159 µmol, 1.30 equiv) was added. After stirring for 1 h at room temperature, DCM (10 mL) was added and the organic phase was extracted with H_2O (1 x 10 mL). To get rid of the excess TBAF, DCM was evaporated, the crude mixture was dispersed in MeOH (5 mL) and filtered over a short plug of Celite® which was then washed with MeOH (20 mL) followed by hexanes (20 mL) The product was eluted with DCM (50 mL). Evaporation of the solvent gave the pure product **146** as bright yellow solid (84 mg, 112 µmol, 92%).

^{1}H-NMR (300 MHz, $CDCl_3$): δ 7.87 – 7.76 (m, 2H), 7.72 – 7.58 (m, 4H), 7.58 – 7.45 (m, 4H), 7.39 (d, J = 5.7 Hz, 1H), 6.96 – 6.75 (m, 11H), 6.70 (dd, J = 5.7, 1.8 Hz, 1H), 2.72 – 2.57 (m, 2H), 2.20 (td, J = 6.8, 2.6 Hz, 2H), 1.91 (t, J = 2.6 Hz, 1H), 1.71 – 1.43 (m, 6H); **^{13}C-NMR** (75 MHz, $CDCl_3$): δ 166.69, 166.23, 161.57, 161.52, 161.17, 151.54, 147.07, 146.65, 143.81, 143.75, 143.72, 137.14, 137.07, 135.87, 129.83, 129.70, 123.88, 123.67, 122.38, 121.90, 119.68, 119.65, 118.73, 84.33, 68.51, 35.38, 29.71, 28.32, 28.14, 18.31; **IR** (neat): 3288, 3084, 2930, 2855, 2113, 1707, 1599, 1469, 1409, 1297, 1260, 1156, 1103, 1059, 1029, 880, 820, 753 cm^{-1}; **HRMS** (EI-MS) m/z calculated for $C_{40}H_{34}{}^{191}IrN_3$ ([M]$^+$) 747.23532, found 747.23742.

Bis(2-phenylpyridine-C²,N)(4-(hept-6-yn-1-yl)-2-phenylpyridine)iridium @ azide-functionalized Co/C nanoparticles (147)

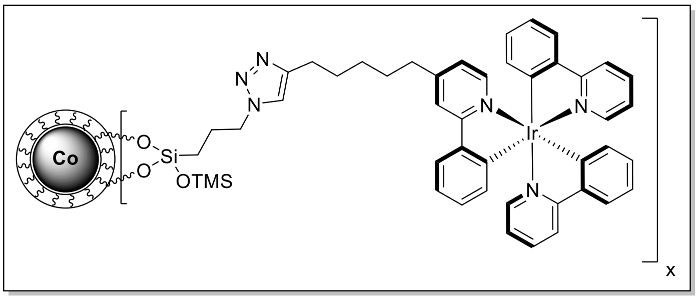

A Schlenk tube was charged with azide-functionalized Co/C nanoparticles (**140**, 100 mg, 363 µmol (N_3), 9.08 equiv), bis(2-phenylpyridine-C^2,N)(4-(hept-6-yn-1-yl)-2-phenylpyridine)iridium (**146**, 30 mg, 40 µmol, 1.00 equiv) and CuI (5.7 mg, 30 µmol, 0.75 equiv). The tube was evacuated and backfilled with nitrogen three times. Dry and degassed MeCN (2 mL) and DIPEA (10.3 mg, 13.6 µL, 80 µmol, 2.00 equiv) were added. The mixture was allowed to stir for 48 h at room temperature. Subsequently, the particles were magnetically collected, the supernatant decanted and washed with MeCN (5 x 3 mL). Drying *in vacuo* afforded the greenish immobilized catalyst (120 mg). Since these particles are not stable against moisture, the free hydroxy groups were end-capped with TMS. Therefore, a Schlenk flask was charged with the particles and dried for 8 h at 75 C under high vacuo. Subsequently, the flask was cooled with a liquid nitrogen bath and HMDS (1 mL) was added under vacuo. The mixture was slowly warmed to room temperature followed by heating to 75 °C for 18 h. Afterwards, the excess HMDS was evaporated to give the end-capped immobilized catalyst **147** (125 mg).

ICP-OES measurement revealed a loading of 0.236 mmol/g [Ir], which corresponds to an incorporation of 86% of the [Ir]. **IR** (neat): 2937, 2095, 1580, 1472, 1413, 1346, 1260, 1185, 1092, 1014, 798, 753, 693 cm^{-1}.

2.7. Photochemical reactions employing covalently bound catalyst

Literature conditions

(*Z*)-4,4,5,5-tetramethyl-2-(2-phenylprop-1-en-1-yl)-1,3,2-dioxaborolane (149)[24]

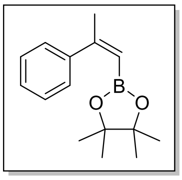

A 5 mL vial was charged with (*E*)-4,4,5,5-tetramethyl-2-(2-phenylprop-1-en-1-yl)-1,3,2-dioxaborolane[24] (**148**, 24 mg, 0.10 mmol, 1.00 equiv), *fac*-Ir(ppy)$_3$ (**5**, 0.7 mg, 1.0 µmol, 1.0 mol%) and MeCN (1.5 mL). The vial was sealed with a rubber septum and degassed by sparging N_2 for 15 min. The mixture was placed on a blue LED plate (λ = 455 nm) and irradiated for 16 h. Afterwards, the catalyst was removed by filtration over a short silica plug with the aid of Et_2O (5 mL). Evaporation of the solvent furnished the product **149** as slightly yellow oil (24 mg, 0.10 mmol, 100%; *Z:E*, 94:6). The analytical spectra are in agreement with the literature.[25]

^{1}H-NMR (300 MHz, $CDCl_3$): δ 7.33 – 7.27 (m, 5H), 5.48 (q, J = 1.4 Hz, 1H), 2.22 (d, J = 1.4 Hz, 3H), 1.15 (s, 12H); **^{13}C-NMR** (75 MHz, $CDCl_3$): δ 157.68, 143.14, 127.59, 127.45, 82.99, 27.75, 24.63.

The reaction was also performed (1) without catalyst, (2) with *fac*-Ir(ppy)$_3$ (**5**, 0.7 mg, 1.0 µmol, 1.0 mol%) and silica-coated MNP **127** (3 mg), and (3) with only silica-coated MNP **127** (3 mg). The results for the single experiments are given in the main part.

(5a*R*,5b*R*,10a*S*,10b*S*)-5a,5b-bis(4-fluorophenyl)tetradecahydrocyclobuta[1,2:3,4]di[7]-annulene (152)[26]

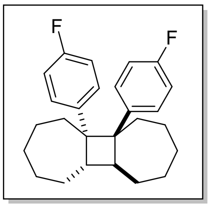

A 5 mL vial was charged with 1-(4-fluorophenyl)cyclohept-1-ene[26] (**151**, 114.2 mg, 600 µmol, 1.00 equiv), *fac*-Ir(ppy)$_3$ (**5**, 0.5 mg, 0.75 µmol, 0.125 mol%) and MeCN (1.2 mL). The vial was sealed with a rubber septum and the mixture was degassed by N_2 sparging for 10 min. The mixture was placed on a blue LED plate (λ = 455 nm) to ensure irradiation and magnetic stirring from below. After 24 h of irradiation, the product precipitated as white solid which was filtered and washed with additional MeCN (5 mL) to give the pure compound **152** (91 mg, 240 µmol, 80%) after drying *in vacuo*. The analytical spectra are in agreement with the literature.[26]

^{1}H-NMR (400 MHz, $CDCl_3$): δ 7.80 – 7.63 (m, 2H), 7.22 – 7.09 (m, 2H), 7.11 – 6.93 (m, 4H), 2.95 – 2.73 (m, 2H), 2.10 – 1.94 (m, 2H), 1.92 – 1.80 (m, 2H), 1.79 – 1.62 (m, 4H), 1.57 – 1.41 (m, 4H), 1.31 – 1.13 (m, 4H), 0.90 – 0.75 (m, 2H), 0.42 (dt, J = 13.4, 3.8 Hz, 2H); **^{13}C-NMR** (101 MHz, $CDCl_3$): δ 160.70 (d, J = 244.1 Hz), 140.25 (d, J = 3.5 Hz), 129.83 (d, J = 7.3 Hz), 129.18 (d, J = 7.2 Hz), 115.07 (d, J = 20.8 Hz), 114.16 (d, J = 20.4 Hz), 55.72 , 47.53 , 41.88 , 28.02 , 27.75 , 26.83 , 26.58; **^{19}F-NMR** (377 MHz, $CDCl_3$): δ -118.63.

Since an additional solid may disturb the heterogeneous catalyst, the reaction was also performed using DMF as solvent. In this case, the product did not precipitate, which is why the solvent had to be evaporated after the reaction. To get rid of the photocatalyst, the solid residue was suspended in MeCN and filtered, yielding the pure product **152** in the same amount as with MeCN as solvent (90 mg, 237 µmol, 79%).

The reaction was also performed (1) without catalyst, (2) with *fac*-Ir(ppy)$_3$ (**5**, 0.5 mg, 0.75 µmol, 0.125 mol%) and silica-coated MNP **127** (3 mg), and (3) with only silica-coated MNP **127** (3 mg). The results of the single experiments are given in the main part.

Recycling conditions

(*Z*)-4,4,5,5-tetramethyl-2-(2-phenylprop-1-en-1-yl)-1,3,2-dioxaborolane (149)[24]

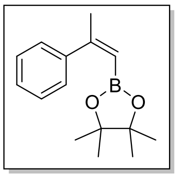

A 5 mL vial was charged with (*E*)-4,4,5,5-tetramethyl-2-(2-phenylprop-1-en-1-yl)-1,3,2-dioxaborolane[24] (**148**, 24 mg, 0.10 mmol, 1.00 equiv), immobilized catalyst **147** (4.2 mg, 1.0 µmol, 1.0 mol%) and MeCN (1.5 mL). The vial was sealed with a rubber septum and degassed by sparging N_2 for 15 min. The mixture was placed on a blue LED plate (λ = 455 nm) to ensure irradiation and magnetic stirring from below. After 16 h, the catalyst **147** was magnetically collected and the reaction mixture was decanted. The particles were washed with additional MeCN (2 mL). The organic layers were combined, and the solvent was evaporated. 4-nitrobenzaldehyde was added as an internal standard and the yield was determined by ^{1}H-NMR. The catalyst **147**, on the other hand, was directly used in the next run. All following catalyst runs were set up equally to the first run, all reaction parameters were kept constant.

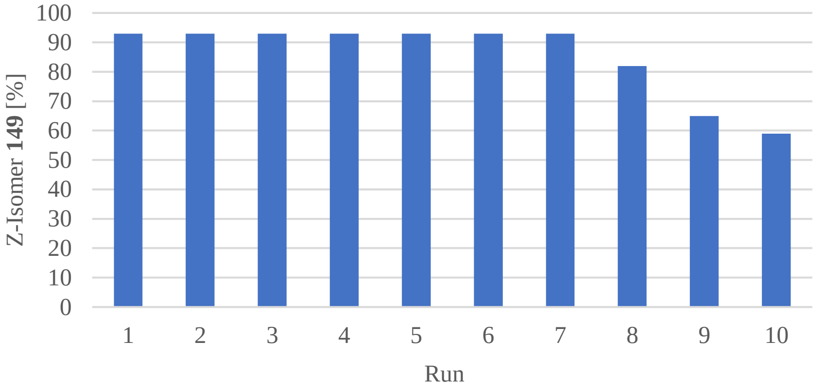

(5a*R*,5b*R*,10a*S*,10b*S*)-5a,5b-bis(4-fluorophenyl)tetradecahydrocyclobuta[1,2:3,4]di[7]annulene (152)[26]

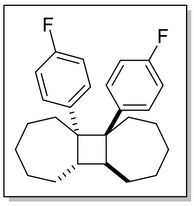

A 5 mL vial was charged with 1-(4-fluorophenyl)cyclohept-1-ene[26] (**151**, 114.2 mg, 600 µmol, 1.00 equiv), immobilized catalyst **147** (3.2 mg, 0.75 µmol, 0.125 mol%) and DMF (1.2 mL). The vial was sealed with a rubber septum and the mixture was degassed by N_2 sparging for 10 min. The mixture was placed on a blue LED (λ = 455 nm) plate to ensure irradiation and magnetic stirring from below. After 24 h, the catalyst **147** was collected with an external magnet and the reaction mixture was decanted. The particles were washed with additional DMF (2 mL). The organic layers were combined, and the solvent was evaporated. 4-nitrobenzaldehyde was added as an internal standard and the yield was determined by ^{1}H-NMR. The catalyst, on the other hand, was directly used in the next run. All following catalyst runs were set up equally to the first run; all reaction parameters were kept constant.

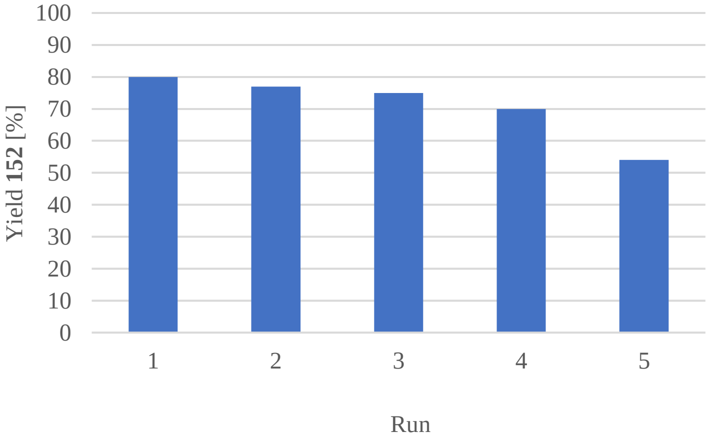

2.8. Photochemical reactions employing graphitic carbon nitrides as catalyst

3-((methyl(phenyl)amino)methyl)cyclohexan-1-one (183)[27]

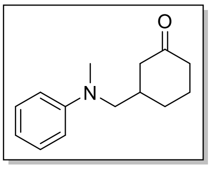

A 5 mL vial was charged with *N*-methyl-*N*-((trimethylsilyl)-methyl)aniline[28] (**181**, 25.1 mg, 130 µmol, 1.30 equiv), cyclohex-2-en-1-one (**182**, 9.6 mg, 9.7 µL, 100 µmol, 1.00 equiv), CsF (30.4 mg, 200 µmol, 2.00 equiv), the respective mesoporous graphitic carbon nitride (10 mg) and MeOH (1.0 mL). The vial was sealed with a rubber septum and the mixture was degassed by nitrogen sparging for 10 min. Afterwards, the vial was placed on a blue LED plate (λ = 455 nm) to ensure irradiation as well as magnetic stirring from below. After irradiation for 17 h at room temperature, the reaction mixture was filtered, and the solvent was evaporated. 1,3,5-trimethoxybenzene was added as internal standard and the yield was determined *via* ^{1}H-NMR. Subsequent purification was achieved by flash silica column chromatography (hexanes / EtOAc, 9:1) to obtain the product as colorless oil (17.4 mg, 80 µmol, 80%; mpg-C_3N_4 was employed as catalyst). The analytical spectrum is in accordance with the literature.[27,29]

^{1}H-NMR (300 MHz, $CDCl_3$): δ 7.27 – 7.19 (m, 2H), 6.78 – 6.61 (m, 3H), 3.31 – 3.23 (m, 2H), 2.97 (s, 3H), 2.53 – 2.18 (m, 4H), 2.15 – 2.03 (m, 2H), 2.02 – 1.91 (m, 1H), 1.74 – 1.56 (m, 1H), 1.49 – 1.34 (m, 1H).

5-iodo-6-perfluorooctylhexanol (116) [7b]

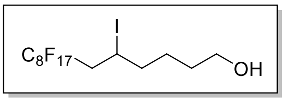

A 5 mL vial equipped with a magnetic stirring bar was charged with 5-hexen-1-ol (**109**, 30 µL, 0.25 mmol, 1.00 equiv), heptadecafluoro-1-iodooctane (**115**, 86 µL, 0.325 mmol, 1.30 equiv), sodium ascorbate (17 mg, 88 µmol, 0.35 equiv), the respective carbon nitride (5 mg), MeOH (1.5 mL) and MeCN (2.0 mL). The vial was capped with a rubber septum and the mixture was degassed by nitrogen sparging for 10 min. After irradiation for 3 h with a blue LED (λ = 455 nm) at room temperature, the reaction mixture was transferred to a test tube with the aid of MeCN (2 mL) and centrifuged. The supernatant was decanted and the remaining solid was dispersed in MeCN (2 mL) and centrifuged again. After decantation of the supernatant, this step was repeated one more time and the organic phases were combined. The solvents were evaporated and 1,3,5-trimethoxybenzene was added as internal standard for ^{1}H-NMR.

The recovered catalyst was used in a second reaction run and all parameters were set as before. The yields of the single reaction runs are given in the main part.

Diethyl 2-(2-bromo-6-hydroxyhexyl)malonate (111) [7]

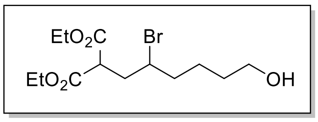

A 5 mL vial was charged with 5-hexen-1-ol (**109**, 30 µL, 0.25 mmol, 1.00 equiv), diethyl 2-bromomalonate (**110**, 51 µL, 0.30 mmol, 1.20 equiv), LiBr (2.2 mg, 25 µmol, 10 mol%), mpg-C_3N_4 (**154**, 10 mg) and DMSO (1.0 mL). The vial was sealed with a rubber septum and the reaction mixture was degassed by nitrogen sparging for 10 min. The reaction was placed on a blue LED plate (λ = 455 nm) and irradiated for 24 h at room temperature while magnetically stirred from below. Subsequently, the reaction mixture was transferred to a test tube with the aid of H_2O (2 mL) and centrifuged. The supernatant was decanted and the remaining solid was dispersed in H_2O (3 mL), centrifuged and the supernatant was decanted again. These steps were repeated one more time and the aqueous phases were combined and extracted with EtOAc (3 x 5 mL). The organic phases were combined and extracted with brine (1 x 5 mL), dried over Na_2SO_4 and the solvent was evaporated. 4-nitrobenzaldehyde was added as internal standard and the yield was determined by ^{1}H-NMR.

The catalyst was dried and reused in a consecutive reaction run. The yields of the single runs are given in the main part.

(3,3,4,4,5,5,6,6,7,7,8,8,9,9,10,10,10-Heptadecafluoro-1-iododecyl)benzene (185)[30]

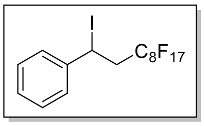

A 5 mL vial equipped with a magnetic stirring bar was charged with heptadecafluoro-1-iodooctane (**115**, 273 mg, 132 µmol, 0.50 mmol, 2.00 equiv), $[Cu(dap)_2]Cl$ (**7**, 2.2 mg, 2.5 µmol, 1.0 mol%) and dry MeCN (1.0 mL). The vial was sealed with a rubber septum and the reaction mixture was degassed by nitrogen sparging for 10 min. Styrene (**184**, 26 mg, 29 µL, 0.25 mmol, 1.00 equiv) was added and the mixture was irradiated for 16 h with a green LED (λ = 530 nm) at room temperature. Afterwards, the solvent was evaporated, and the residue was purified by flash silica column chromatography (hexanes) to give the pure compound as white solid (126 mg, 0.194 mmol, 78%). The analytical data is in accordance with literature.[30]

^{1}H-NMR (300 MHz, $CDCl_3$): δ 7.46 – 7.41 (m, 2H), 7.37 – 7.25 (m, 3H), 5.46 (dd, J = 9.6, 5.2 Hz, 1H), 3.44 – 3.04 (m, 2H).

The reaction was also performed by irradiating with a blue LED (λ = 455 nm) using mpg-C_3N_4 (**154**, 5 mg) instead of [Cu(dap)$_2$]Cl in (**1**) MeCN (1.0 mL), (**2**) in MeOH (1.5 mL) and MeCN (2.0 mL), (**3**) in MeOH (1.5 mL) and MeCN (2.0 mL) with the addition of sodium ascorbate (17.3 mg, 88 µmol, 0.35 equiv) and (**4**) in MeCN (1.0 mL) with the addition of $CuCl_2$ (33.6 mg, 0.25 mmol, 1.00 equiv). In all cases, no reaction or only traces of product were obtained.

1-((2-chloro-2-phenylethyl)sulfonyl)-4-methylbenzene (187)[31]

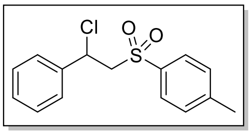

A 5 mL vial equipped with a magnetic stirring bar was charged with 4-methylbenzenesulfonyl chloride (**186**, 95.3 mg, 0.50 mmol, 1.00 equiv), [Cu(dap)$_2$]Cl (**7**, 4.4 mg, 5 µmol, 1.0 mol%) and dry MeCN (2.0 mL). The vial was sealed with a rubber septum and the mixture was degassed by nitrogen sparging for 10 min. Styrene (**184**, 52.1 mg, 57.2 µL, 0.50 mmol, 1.00 equiv) was added and the mixture was irradiated with a green LED (λ = 530 nm) for 24 h at room temperature while magnetically stirred from below. Subsequently, the solvent was evaporated, and the crude residue was purified by flash silica column chromatography (hexanes / EtOAc, 5:1) to afford the pure product as white solid (139 mg, 0.472 mmol, 94%). The analytical data is in accordance with literature.[32]

^{1}H-NMR (300 MHz, $CDCl_3$): δ 7.63 (d, J = 8.3 Hz, 2H), 7.32 – 7.19 (m, 7H), 5.33 (t, J = 6.9 Hz, 1H), 4.02 – 3.77 (m, 2H), 2.41 (s, 3H); **^{13}C-NMR** (75 MHz, $CDCl_3$): δ 144.94, 138.61, 136.21, 129.81, 129.11, 128.93, 128.20, 127.17, 64.15, 55.15, 21.67.

The reaction was also performed using various mesoporous graphitic carbon nitrides (5 – 10 mg). Except for irradiating with a blue LED (λ = 455 nm) the reaction parameters were kept the same. After evaporation of the solvent, 4-nitrobenzaldehyde was added as internal standard to determine the yield by ^{1}H-NMR. The yields for the single reactions are given in the main part.

1-((2-chlorooctyl)sulfonyl)-4-methylbenzene (189)[31]

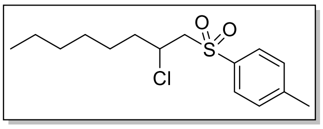

A Schlenk tube was charged with 4-methylbenzenesulfonyl-chloride (**186**, 47.7 mg, 0.25 mmol, 1.00 equiv), Na_2CO_3 (26.5 mg, 0.25 mmol, 1.00 equiv), [Cu(dap)$_2$]Cl (**7**, 2.2 mg, 2.5 µmol, 1.0 mol%) and dry MeCN (1.0 mL). The Schlenk tube was sealed with a screw-cap and degassed by three freeze-pump-thaw cycles. Oct-1-ene (**188**, 56.1 mg, 78.5 µL, 2.00 equiv) was added and the screw-cap was replaced by a Teflon-sealed inlet for a glass rod to ensure irradiation with a green LED (λ = 530 nm) from above while being magnetically stirred from below. After irradiation for 48 h at room temperature, the mixture was transferred to a separation funnel and was saturated with brine (10 mL). The aqueous phase was extracted with EtOAc (3 x 10 mL) and the combined organic phases were dried over Na_2SO_4. The solvent was evaporated, and the crude residue was purified by flash silica column chromatography (hexanes / EtOAc, 4:1) to afford the pure product as colorless oil (60.6 mg, 0.20 mmol, 80%). The analytical data is in accordance with literature.[31]

^{1}H-NMR (300 MHz, $CDCl_3$): δ 7.86 – 7.75 (m, 2H), 7.41 – 7.34 (m, 2H), 4.37 – 4.23 (m, 1H), 3.56 (dd, J = 14.6, 6.2 Hz, 1H), 3.45 (dd, J = 14.6, 6.5 Hz, 1H), 2.46 (s, 3H), 2.04 – 1.90 (m, 1H), 1.83 – 1.68 (m, 1H), 1.54 – 1.22 (m, 8H), 0.91 – 0.84 (m, 3H).

The reaction was also performed using mpg-C_3N_4 (10 mg) as catalyst, irradiating with a blue LED (λ = 455 nm) for 72 h.

4-(2-phenyl-1,2,3,4-tetrahydroisoquinolin-1-yl)butan-2-one (197)[33]

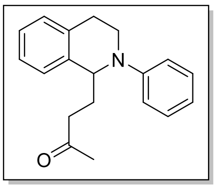

A Schlenk tube was charged with 2-phenyl-1,2,3,4-tetrahydroisoquinoline (**89a**, 52.3 mg, 250 µmol, 1.00 equiv), but-3-en-2-one (**196**, 35.1 mg, 42 µL, 500 µmol, 2.00 equiv), trifluoroacetic acid (29 mg, 19 µL, 250 µmol, 1.00 equiv) and [Ru(bpy)$_3$]Cl$_2$ (**1**, 3.7 mg, 5.0 µmol, 2.0 mol%). Dry MeCN (1.0 mL) was added, the tube was closed with a screw-cap and the mixture was degassed by three freeze-pump-thaw cycles. The screw-cap was replaced by a Teflon-sealed inlet for a glass rod to ensure irradiation from above with a blue LED (λ = 455 nm) while being magnetically stirred from below. After irradiation for 5 h at 50 °C the mixture was allowed to cool to room temperature and was neutralized with K_2CO_3 (69 mg, 500 µmol, 2.00 equiv). Purification was achieved by flash silica column chromatography (hexanes / EtOAc, 9:1) to obtain the pure product as colorless oil (55 mg, 197 µmol, 79%). The analytical data is in agreement with the one reported in literature.[33a]

^{1}H-NMR (300 MHz, $CDCl_3$): δ 7.30 – 7.21 (m, 2H), 7.21 – 7.15 (m, 3H), 7.15 – 7.09 (m, 1H), 6.96 – 6.88 (m, 2H), 6.77 (tt, J = 7.2, 1.1 Hz, 1H), 4.76 (dd, J = 9.2, 5.7 Hz, 1H), 3.70 – 3.51 (m, 2H), 3.02 (ddd, J = 15.3, 9.2, 5.8 Hz, 1H), 2.77 (dt, J = 16.2, 4.6 Hz, 1H), 2.60 (t, J = 6.9 Hz, 2H), 2.34 – 2.18 (m, 1H), 2.15 – 2.01 (m, 4H); **^{13}C-NMR** (101 MHz, $CDCl_3$): δ 208.65, 149.90, 138.42, 134.95, 129.38, 128.83, 127.32, 126.60, 125.99, 117.78, 114.64, 57.99, 41.54, 40.42, 30.43, 30.30, 26.42.

The reaction was also performed (**1**) using mpg-C_3N_4 (10 mg) under the same conditions as above, (**2**) using mpg-C_3N_4 (10 mg) at 18 h reaction time, (**3**) using mpg-C_3N_4 (20 mg), and (**4**) using mpg-C_3N_4 (10 mg), without TFA and without heating, 18 h reaction time. The yields of the single reactions are given in the main part.

3. Chapter C: Photochemical Decarboxylations

3.1. Synthesis of *N*-(acyloxy)phthalimides for intermolecular reactions

(*S*)-3-(5-oxo-3-tosyloxazolidin-4-yl)propanoic acid

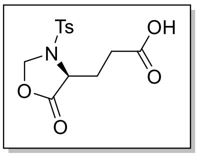

Tosyl-L-glutamic acid[34] (2.70 g, 8.96 mmol, 1.00 equiv) was dissolved in 20 mL DCM, followed by the addition of paraformaldehyde (538 mg, 17.9 mmol, 2.00 equiv) and *p*-TsOH (30.9 mg, 0.179 mmol, 2.0 mol%). The reaction mixture was heated to 50 °C for 18 h using a reverse Dean-Stark trap. Subsequently, the mixture was allowed to cool to room temperature and extracted with 1 M HCl (4 x 5 mL) and the organic layer was dried over Na_2SO_4. Evaporation of the solvent gave the pure product (2.34 g, 7.47 mmol, 83%) as colorless, viscous oil. The compound is literature known,[35] however, not sufficiently characterized.

^{1}H-NMR (400 MHz, CD_3OD): δ 8.64 (d, J = 8.0 Hz, 2H), 8.24 (d, J = 8.0 Hz, 2H), 6.02 (brs, 3H), 4.83 (dd, J = 9.1, 4.9 Hz, 1H), 4.27 (s, 3H), 3.28 (d, J = 7.5 Hz, 2H), 3.05 – 2.87 (m, 1H), 2.81 – 2.63 (m, 1H); **^{13}C-NMR** (101 MHz, CD_3OD): δ 176.15, 174.33, 144.67, 138.97, 130.55, 128.11, 56.23, 49.85, 30.57, 29.15, 21.45; **IR** (neat): 3290, 3049, 2945, 1730, 1703, 1599, 1498, 1431, 1308, 1215, 1141, 1088, 984, 902, 816, 693, 671 cm^{-1}; **HRMS** (ESI-MS) m/z calculated for $C_{11}H_{17}NO_6$ ($[M-H]^-$) , found .

1,3-dioxoisoindolin-2-yl (*S*)-3-(5-oxo-3-tosyloxazolidin-4-yl)propanoate (121a)

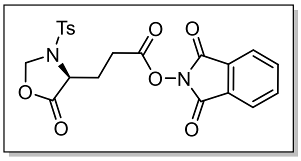

(*S*)-3-(5-oxo-3-tosyloxazolidin-4-yl)propanoic acid (2.00 g, 6.38 mmol, 1.00 equiv) and DCC (1.45 g, 7.02 mmol, 1.10 equiv) were dissolved in 20 mL dry DCM. The mixture was cooled to 0 °C and *N*-hydroxyphthalimide (1.15 g, 7.02 mmol, 1.10 equiv) was added. After stirring for 18 h at room temperature, the precipitate was filtered, and the solvent was evaporated. The residue was re-dissolved in EtOAc and extracted with 1 M HCl (3 x 5 mL). The organic phase was dried over Na_2SO_4 and the solvent was evaporated. Purification was achieved by flash silica column chromatography (hexanes / EtOAc, 2:1) to give the pure product as white solid (2.43 g, 5.30 mmol, 82%).

^{1}H-NMR (300 MHz, $CDCl_3$): δ 7.94 – 7.86 (m, 2H), 7.85 – 7.78 (m, 2H), 7.78 – 7.72 (m, 2H), 7.43 – 7.35 (m, 2H), 5.53 (d, J = 7.2 Hz, 1H), 5.28 (d, J = 7.2 Hz, 1H), 4.12 (dd, J = 8.8, 5.4 Hz, 1H), 3.08 – 2.95 (m, 2H), 2.45 (s, 3H), 2.43 – 2.31 (m, 1H), 2.30 – 2.16 (m, 1H); **^{13}C-NMR**

(75 MHz, $CDCl_3$): δ 170.94, 168.53, 161.70, 145.86, 134.86, 132.25, 130.68, 128.86, 127.85, 124.08, 79.06, 55.97, 26.88, 25.02, 21.73; **R_f** (hexanes / EtOAc, 2:1) = 0.4; **mp**: 58 – 62 °C; **IR** (neat): 2930, 2113, 1789, 1737, 1595, 1495, 1357, 1163, 1081, 969, 880, 816, 697, 664 cm^{-1}; **HRMS** (ESI-MS) m/z calculated for $C_{21}H_{19}N_2O_8S$ ($[M+H]^+$) 459.0857, found 459,0864.

(*S*)-3-(3-(*tert*-butoxycarbonyl)-5-oxooxazolidin-4-yl)propanoic acid

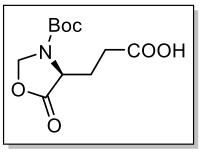

(*tert*-butoxycarbonyl)-L-glutamic acid[36] (45.0 g, 182 mmol, 1.00 equiv) was dissolved in 250 mL DCM followed by the addition of paraformaldehyde (10.93 g, 364 mmol, 2.00 equiv) and *p*-TsOH (627 mg, 3.64 mmol, 2.0 mol%). The mixture was heated to 50 °C for 19 h using a reverse Dean-Stark trap. Subsequently, the mixture was allowed to cool to room temperature und was extracted with 0.5 M HCl (4 x 50 mL). The organic layer was dried over Na_2SO_4. Evaporation of the solvent gave the pure product (42.5 g, 164 mmol, 90%) as colorless, viscous oil.

^{1}H-NMR (400 MHz, $CDCl_3$): δ 10.38 (brs, 1H), 5.49 (s, 1H), 5.34 – 5.03 (m, 1H), 4.33 (t, J = 6.2 Hz, 1H), 2.51 (t, J = 7.3 Hz, 2H), 2.35 – 2.23 (m, 1H), 2.22 – 2.12 (m, 1H), 1.48 (s, 9H); **^{13}C-NMR** (101 MHz, $CDCl_3$): δ 178.02, 172.23, 152.42, 82.62, 77.96, 53.96, 29.22, 28.19, 25.76; **IR** (neat): 3168, 2982, 2937, 1804, 1744, 1684, 1402, 1371, 1252, 1141, 1070, 1033, 989, 768, 700 cm^{-1}; **HRMS** (ESI-MS) m/z calculated for $C_{11}H_{16}NO_6$ ($[M-H]^-$) 258.0983, found 258.0988.

tert-butyl(*S*)-4-(3-((1,3-dioxoisoindolin-2-yl)oxy)-3-oxopropyl)-5-oxooxazolidine-3-carboxylate (121b)

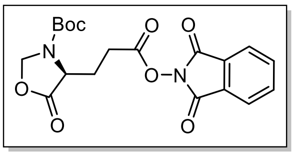

(*S*)-3-(3-(*tert*-butoxycarbonyl)-5-oxooxazolidin-4-yl)propanoic acid (18.95 g, 73.1 mmol, 1.00 equiv) and DCC (16.59 g, 80.4 mmol, 1.10 equiv) were dissolved in 250 mL dry DCM and cooled to 0 °C. *N*-hydroxyphthalimide (13.12 g, 80.4 mmol, 1.10 equiv) was added and the mixture was allowed to stir for 18 h at room temperature. After filtration of the precipitate, the solvent was evaporated, and the yellow residue was dissolved in ethyl acetate and extracted with 0.5 M HCl (3 x 50 mL). The organic layer was dried over Na_2SO_4 and the solvent was evaporated. The yellowish solid was recrystallized from EtOH to give the pure product (23.36 g, 57.8 mmol, 79%) as white solid.

^{1}H-NMR (300 MHz, $CDCl_3$): δ 7.91 ‑ 7.86 (m, 2H), 7.82 ‑ 7.76 (m, 2H), 5.51 (s, 1H), 5.34 ‑ 5.20 (m, 1H), 4.37 (t, J = 6.1 Hz, 1H), 2.93 ‑ 2.80 (m, 2H), 2.50 ‑ 2.26 (m, 2H), 1.49 (s, 9H); **^{13}C-NMR** (101 MHz, $CDCl_3$): δ 171.93, 168.53, 161.74, 152.40, 134.86, 128.84, 124.03, 82.71, 78.10, 53.84, 28.21, 26.54, 25.73; **R_f** (hexanes / EtOAc, 2:1) = 0.2; **mp**: 98 – 100 °C; **IR** (neat): 3131, 2978, 2937, 1819, 1793, 1744, 1700, 1461, 1368, 1320, 1249, 1163, 1133, 1066, 965, 880, 783, 693 cm^{-1}; **HRMS** (ESI-MS) m/z calculated for $C_{19}H_{21}NO_8$ ($[M+H]^+$) 405.1292, found 405.1292.

3.2. Synthesis of trapping reagents

Boc-hydroxycyclopentenone **122d** was prepared following a literature procedure, the spectra are in accordance with those reported.[37] TBDMS-hydroxycyclopentenone **122e** was synthesized following a literature procedure, the spectra are in accordance with those reported.[38]

The enol acetates **122h – 122n** and **122u** – **122v** were kindly provided by Thomas Föll from our group, who synthesized these for his project on visible-light-mediated reactions of α-chloro cinnamates.[39]

General procedure for the synthesis of silyl enol ethers (**GP-A**)

The silyl enol ethers were prepared following a literature procedure.[40] NaI (840 mg, 5.6 mmol, 1.4 equiv) was placed in a Schlenk tube which was subsequently flame dried with a heat gun. After cooling down to room temperature, the respective ketone (4.0 mmol, 1.0 equiv) and NEt_3 (836 µL, 607 mg, 1.5 equiv) were added and dissolved in dry MeCN (4.0 mL). The mixture was cooled to 0 °C and Me_3SiCl (660 µL, 565 mg, 5.2 mmol, 1.3 equiv) was added. The mixture was allowed to stir for 16 h at room temperature. The solvent was evaporated under reduced pressure and the solid residue was washed with pentane (3 x 20 mL). The combined organic layers were concentrated under reduced pressure to give the silyl enol ether which was used without further purification.

The analytical spectra of silyl enol ethers **122o**,[41] **122p**,[41] **122q**,[41] **122r**,[42] and **122s**[43] are in agreement with the reported spectra.

((1-(3,5-bis(trifluoromethyl)phenyl)vinyl)oxy)trimethylsilane (122t)

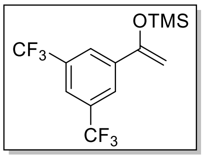

Following **GP-A** using 1-(3,5-bis(trifluoromethyl)phenyl)ethan-1-one (1.02 g, 4.0 mmol, 1.0 equiv) furnished the product as colorless oil (1.18 g, 3.60 mmol, 90%).

^{1}H-NMR (400 MHz, $CDCl_3$): δ 8.03 – 7.98 (m, 2H), 7.81 – 7.77 (m, 1H), 5.05 (d, J = 2.5 Hz, 1H), 4.60 (d, J = 2.5 Hz, 1H), 0.31 (s, 9H); **^{13}C-NMR** (75 MHz, $CDCl_3$): δ 152.96, 139.66, 131.77, 131.33, 125.18, 121.72, 93.30, 0.00; **^{19}F-NMR** (377 MHz, $CDCl_3$) δ -63.54; **IR** (neat): 2967, 1707, 1629, 1464, 1387, 1275, 1147, 1126, 1014, 876, 842, 757, 708 cm^{-1}; **HRMS** (EI-MS) m/z calculated for $C_{13}H_{14}F_6OSi$ ($[M]^+$) 328.07126, found 328.07107.

3.3. Photochemical reactions exploiting the reductive quenching cycle

General procedure for the photochemical functionalization of L-glutamic acid derivatives exploiting the reductive quenching cycle of [Ru(bpy)$_3$]Cl$_2$ (**GP-B**).

A flame dried Schlenk tube equipped with a magnetic stirring bar was charged with 1,3-dioxoisoindolin-2-yl (*S*)-3-(5-oxo-3-tosyloxazolidin-4-yl)propanoate (TsGluOxNPhth **121a**, 91.7 mg, 200 µmol, 1.00 equiv) or *tert*-butyl(*S*)-4-(3-((1,3-dioxoisoindolin-2-yl)oxy)-3-oxopropyl)-5-oxooxazolidine-3-carboxylate (BocGluOxNPhth, **121b**, 80.9 mg, 200 µmol, 1.00 equiv), alkene **122** (1.00 – 2.00 mmol, 5.00 – 10.0 equiv), diethyl 2,6-dimethyl-1,4-dihydropyridine-3,5-dicarboxylate (Hantzsch ester, **240**, 50.6 mg, 200 µmol, 1.00 equiv) and [Ru(bpy)$_3$]Cl$_2$ (**1**, 3.00 mg, 4.00 µmol, 2.0 mol%), acetone and water (3:1, 2.00 mL, 0.1 M). The Schlenk tube was sealed with a plastic screw-cap and the mixture was degassed by three freeze-pump-thaw cycles. The screw-cap was replaced by a Teflon sealed inlet for a glass rod. A blue LED (λ = 455 nm) was attached on the top of the glass rod to ensure irradiation from above while the reaction was magnetically stirred from below. After 5 h of irradiation the LED was switched off and the reaction mixture was transferred to a separation funnel. EtOAc (5 mL) and water (5 mL) were added. The phases were separated, and the aqueous phase was extracted with EtOAc (3x 5 mL). The combined organic phases were washed with 10 mL brine and dried over Na$_2$SO$_4$. After evaporation of the solvent the residue was purified by column chromatography on SiO$_2$ (hexanes / EtOAc, 7:1 to 2:1).

(4*S*)-4-(2-(4-oxocyclopent-2-en-1-yl)ethyl)-3-tosyloxazolidin-5-one (123ad)

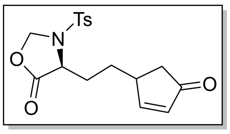

Following general procedure **GP-B** using 1,3-dioxoisoindolin-2-yl (*S*)-3-(5-oxo-3-tosyloxazolidin-4-yl)propanoate (**121a**, 91.7 mg, 200 µmol, 1.00 equiv) and *tert*-butyl (4-oxocyclopent-2-en-1-yl) carbonate (**122d**, 198 mg, 1.00 mmol, 5.00 equiv) gave the pure product as yellow oil (35.0 mg, 100 µmol, 50%) after purification by silica gel chromatography (hexanes / EtOAc, 2:1).

^{1}H-NMR (300 MHz, CDCl$_3$): two inseparable diastereomers: δ 7.76 – 7.66 (m, 2H), 7.62 – 7.59 (m, 1H), 7.39 – 7.36 (m, 2H), 6.18 (dd, *J* = 5.6, 2.0 Hz, 1H), 5.44 (d, *J* = 6.8 Hz, 1H), 5.22 (d, *J* = 6.7 Hz, 1H), 3.96 (dd, *J* = 7.0, 5.4 Hz, 1H), 2.99 (ddt, *J* = 6.4, 4.5, 2.1 Hz, 1H), 2.55 (ddd, *J* = 18.8, 6.4, 2.6 Hz, 1H), 2.44 (s, 3H), 2.04 – 1.47 (m, 5H); **^{13}C-NMR** (75 MHz, CDCl$_3$): two inseparable diastereomers: δ 209.10, 171.47, 167.17, 167.04, 145.86, 134.39, 134.34, 132.35, 132.29, 130.64, 130.58, 127.70, 79.00, 57.11, 56.99, 40.64, 40.54, 40.49, 29.75, 28.30, 28.25, 21.70; **R$_f$** (hexanes / EtOAc, 2:1) = 0.2; **IR** (neat): 3258, 3034, 2926, 2870, 2102, 1789, 1707, 1666, 1595, 1495, 1450, 1389, 1353, 1185, 1092, 958, 924, 812, 783, 753, 705, 664 cm^{-1}; **HRMS** (ESI-MS) m/z calculated for $C_{17}H_{20}NO_5S$ ([M+H]$^+$) 350.1057, found 350.1063.

(4S)-4-(2-(2-((*tert*-butyldimethylsilyl)oxy)-4-oxocyclopentyl)ethyl)-3-tosyloxazolidin-5-one (123ae)

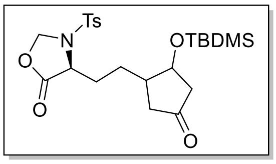

Following general procedure **GP-B** using 1,3-dioxoisoindolin-2-yl (*S*)-3-(5-oxo-3-tosyloxazolidin-4-yl)propanoate (**121a**, 91.7 mg, 200 µmol, 1.00 equiv) and 4-((*tert*-butyldimethylsilyl)oxy)cyclopent-2-en-1-one (**122e**, 531 mg, 1.00 mmol, 5.00 equiv) gave the pure product as a white solid (86.3 mg, 179 µmol, 36%) after purification by silica gel chromatography (hexanes / EtOAc, 4:1).

^{1}H-NMR (400 MHz, CDCl$_3$): mixture of inseparable diastereomers: δ 7.70 (d, *J* = 8.3 Hz, 2H), 7.37 (d, *J* = 7.8 Hz, 2H), 5.47 (dd, *J* = 6.9, 2.9 Hz, 1H), 5.21 (dd, *J* = 6.9, 3.5 Hz, 1H), 4.07 (t, *J* = 6.3 Hz, 1H), 3.97 (td, *J* = 4.8, 2.4 Hz, 1H), 2.54 (ddt, *J* = 17.0, 10.6, 3.9 Hz, 2H), 2.45 (s, 3H), 2.26 – 2.07 (m, 2H), 2.02 – 1.78 (m, 4H), 0.89 (s, 9H), 0.06 (s, 6H); **^{13}C-NMR** (101 MHz, CDCl$_3$): mixture of inseparable diastereomers: δ 214.95, 171.54, 145.66, 132.54, 130.54, 127.63, 77.32, 77.00, 76.68, 74.54, 57.36, 57.23, 47.53, 47.44, 44.84, 44.82, 42.68, 42.55, 28.87, 28.81, 28.39, 28.34, 25.71, 21.64, 17.92, 0.99, -4.57, -4.82, -4.84; **R$_f$** (hexanes / EtOAc, 2:1) = 0.5; **mp**: 94 – 97 °C; **IR**: 3257, 2956, 2855, 1789, 1733, 1595, 1495, 1450, 1387, 1357, 1260, 1158, 1163, 1092, 1029, 980, 910, 813, 779, 705, 664 cm^{-1}; **HRMS** (ESI-MS) m/z calculated for $C_{23}H_{36}NO_6SSi$ ([M+H]$^+$) 482.2027, found 482.2033.

tert-butyl (*S*)-5-oxo-4-(4-oxo-4-phenylbutyl)oxazolidine-3-carboxylate (123bf)

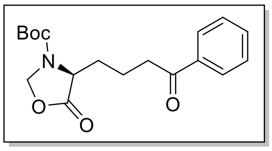

Following general procedure **GP-B** using *tert*-butyl(*S*)-4-(3-((1,3-dioxoisoindolin-2-yl)oxy)-3-oxopropyl)-5-oxooxazolidine-3-carboxylate (**121b**, 80.9 mg, 200 µmol, 1.00 equiv) and 1-phenylvinyl acetate (**122f**, 162 mg, 1.00 mmol, 5.00 equiv) gave the pure product as a white solid (30.0 mg, 90.0 µmol, 45%). Purification was achieved by column chromatography on SiO$_2$ (hexanes / EtOAc, 5:1).

^{1}H-NMR (300 MHz, CDCl$_3$): δ 7.97 – 7.87 (m, 2H), 7.58 – 7.49 (m, 1H), 7.48 – 7.38 (m, 2H), 5.46 (s, 1H), 5.18 (dd, J = 4.7, 1.0 Hz, 1H), 4.28 (s, 1H), 3.01 (t, J = 7.0 Hz, 2H), 2.17 – 2.00 (m, 1H), 1.99 – 1.82 (m, 2H), 1.82 – 1.62 (m, 1H), 1.47 (s, 9H); **^{13}C-NMR** (75 MHz, CDCl$_3$): δ 199.11, 172.82, 152.25, 136.74, 133.13, 128.63, 127.97, 82.15, 78.09, 54.83, 37.80, 30.27, 28.24, 19.08; **R$_f$** (hexanes / EtOAc, 2:1) = 0.66; **mp**: 65 – 68 °C; **IR** (neat): 2978, 1797, 1700, 1678, 1595, 1506, 1450, 1405, 1380, 1308, 1252, 1200, 1170, 1137, 1036, 977, 850, 760 cm^{-1}; **HRMS** (ESI-MS) m/z calculated for $C_{18}H_{24}NO_5$ ([M+H]$^+$) 334.1649, found 334.1651.

(S)-4-(4-oxo-4-phenylbutyl)-3-tosyloxazolidin-5-one (123af)

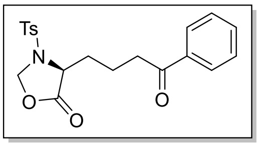

Following general procedure **GP-B** using 1,3-dioxoisoindolin-2-yl (*S*)-3-(5-oxo-3-tosyloxazolidin-4-yl)propanoate (**121a**, 91.7 mg, 200 µmol, 1.00 equiv) and 1-phenylvinyl acetate (**122f**, 162 mg, 1.00 mmol, 5.00 equiv) gave the pure product as a white solid (35.0 mg, 90.3 µmol, 45%) after purification by column chromatography on SiO$_2$ (hexanes / EtOAc, 5:1).

^{1}H-NMR (400 MHz, CDCl$_3$): δ 7.98 – 7.90 (m, 2H), 7.78 – 7.66 (m, 2H), 7.59 – 7.52 (m, 1H), 7.50 – 7.40 (m, 2H), 7.38 – 7.30 (m, 2H), 5.50 (d, J = 7.2 Hz, 1H), 5.23 (d, J = 7.1 Hz, 1H), 4.08 – 4.01 (m, 1H), 3.13 – 2.95 (m, 2H), 2.40 (s, 3H), 2.05 – 1.84 (m, 4H); **^{13}C-NMR** (101 MHz, CDCl$_3$): δ 199.12, 171.85, 145.64, 136.76, 133.20, 132.73, 130.56, 128.68, 128.04, 127.75, 79.02, 57.36, 37.39, 29.64, 21.67, 19.74; **R$_f$** (hexanes / EtOAc, 2:1) = 0.4; **mp**: 89 – 92 °C; **IR** (neat): 3060, 2967, 2930, 2080, 1793, 1718, 1681, 1595, 1491, 1446, 1409, 1361, 1286, 1245, 1189, 1096, 1029, 984, 887, 820, 760, 734, 697, 664 cm^{-1}; **HRMS** (ESI-MS) m/z calculated for $C_{20}H_{22}NO_5S$ ([M+H]$^+$) 388.1213, found 388.1216.

3.4. Photochemical reactions exploiting the oxidative quenching cycle

General procedure for the photochemical functionalization of L-glutamic acid derivatives exploiting the oxidative quenching cycle of fac-Ir(ppy)$_3$ (**GP-C**)

A flame dried Schlenk tube equipped with a magnetic stirring bar was charged with *tert*-butyl(*S*)-4-(3-((1,3-dioxoisoindolin-2-yl)oxy)-3-oxopropyl)-5-oxooxazolidine-3-carboxylate (BocGluOxNPhth, **121b**, 80.9 mg, 200 µmol, 1.00 equiv), alkene **122** (1.00 mmol, 5.00 equiv), and *fac*-Ir(ppy)$_3$[3b,44] (**5**, 1.0 – 2.5 mol%). Water (90 µL, 5.00 mmol, 25.0 equiv) and dry MeCN (2.00 mL) were added and the flask was sealed with a plastic screw-cap. The mixture was degassed by three freeze-pump-thaw cycles after which the screw-cap was replaced by a Teflon sealed inlet for a glass rod. A blue LED (λ = 455 nm) was attached on the top of the glass rod to ensure irradiation from above while the reaction was magnetically stirred from below. After 18 h the LED was switched off and the solvent was evaporated. The crude mixture was purified by flash silica gel chromatography (hexanes / EtOAc, 7:1 to 1:1).

tert-butyl (_S_)-5-oxo-4-(4-oxo-4-phenylbutyl)oxazolidine-3-carboxylate (123bf)

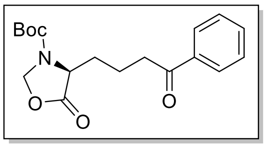

Following general procedure **GP-C** using 1-phenylvinyl acetate (**122f**, 162 mg, 1.00 mmol, 5.00 equiv) and *fac*-Ir(ppy)$_3$ (**5**, 1.3 mg, 2.00 µmol, 1.00 mol%) gave the pure product as a white solid (53.3 mg, 160 µmol, 80%). Purification was achieved by column chromatography on SiO$_2$ (hexanes / EtOAc, 5:1). **^{1}H-NMR** (300 MHz, CDCl$_3$): δ 7.97 – 7.87 (m, 2H), 7.58 – 7.49 (m, 1H), 7.48 – 7.38 (m, 2H), 5.46 (s, 1H), 5.18 (dd, J = 4.7, 1.0 Hz, 1H), 4.28 (s, 1H), 3.01 (t, J = 7.0 Hz, 2H), 2.17 – 2.00 (m, 1H), 1.99 – 1.82 (m, 2H), 1.82 – 1.62 (m, 1H), 1.47 (s, 9H); **^{13}C-NMR** (75 MHz, CDCl$_3$): δ 199.11, 172.82, 152.25, 136.74, 133.13, 128.63, 127.97, 82.15, 78.09, 54.83, 37.80, 30.27, 28.24, 19.08; **R$_f$** (hexanes / EtOAc, 2:1) = 0.66; **mp**: 65 – 68 °C; **IR** (neat): 2978, 1797, 1700, 1678, 1595, 1506, 1450, 1405, 1380, 1308, 1252, 1200, 1170, 1137, 1036, 977, 850, 760 cm^{-1}; **HRMS** (ESI-MS) m/z calculated for $C_{18}H_{24}NO_5$ ([M+H]$^+$) 334.1649, found 334.1651.

***tert*-butyl (*S*)-5-oxo-4-(4-oxo-4-(p-tolyl)butyl)oxazolidine-3-carboxylate (123bh)**

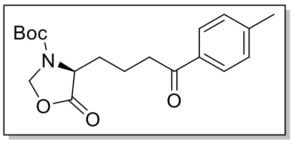

Following general procedure **GP-C** using 1-(*p*-tolyl)vinyl acetate (**122h**, 176 mg, 1.00 mmol, 5.00 equiv) and *fac*-Ir(ppy)$_3$ (**5**, 1.3 mg, 2.00 µmol, 1.00 mol%) gave the pure product as colorless oil (49.3 mg, 142 µmol, 71%) after purification by flash silica gel chromatography (hexanes / EtOAc, 7:1).

^{1}H-NMR (400 MHz, $CDCl_3$): δ 7.89 – 7.78 (m, 2H), 7.31 – 7.17 (m, 2H), 5.49 (s, 1H), 5.20 (d, J = 5.0 Hz, 1H), 4.30 (s, 1H), 3.00 (td, J = 7.3, 2.1 Hz, 2H), 2.40 (s, 3H), 2.21 – 2.02 (m, 1H), 2.00 – 1.84 (m, 2H), 1.82 – 1.69 (m, 1H), 1.49 (s, 9H); **^{13}C-NMR** (101 MHz, $CDCl_3$): δ 198.76, 172.81, 152.26, 143.91, 134.32, 129.31, 128.11, 82.16, 77.24, 54.86, 37.71, 30.32, 28.26, 21.63, 19.21; **R_f** (hexanes / EtOAc, 4:1) = 0.33; **IR** (neat): 2974, 2926, 1797, 1703, 1692, 1606, 1513, 1390, 1319, 1256, 1167, 1047, 902, 850, 809, 752 cm^{-1}; **HRMS** (ESI-MS) m/z calculated for $C_{19}H_{26}NO_5$ ($[M+H]^+$) 348.1805, found 348.1811.

***tert*-butyl (*S*)-4-(4-(4-methoxyphenyl)-4-oxobutyl)-5-oxooxazolidine-3-carboxylate (123bi)**

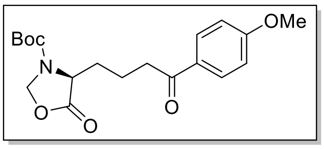

Following general procedure **GP-C** using 1-(4-methoxyphenyl)vinyl acetate (**122i**, 192 mg, 1.00 mmol, 5.00 equiv) and *fac*-Ir(ppy)$_3$ (**5**, 1.3 mg, 2.00 µmol, 1.00 mol%) gave the pure product as colorless oil (53.7 mg, 148 µmol, 74%) after purification by flash silica gel chromatography (hexanes / EtOAc, 4:1).

^{1}H-NMR (400 MHz, $CDCl_3$): δ 7.97 – 7.85 (m, 2H), 6.99 – 6.86 (m, 2H), 5.49 (s, 1H), 5.19 (d, J = 4.6 Hz, 1H), 4.29 (s, 1H), 3.86 (s, 3H), 2.97 (dq, J = 7.6, 2.5 Hz, 2H), 2.18 – 2.02 (m, 1H), 2.00 – 1.83 (m, 2H), 1.82 – 1.66 (m, 1H), 1.48 (s, 9H); **^{13}C-NMR** (101 MHz, $CDCl_3$): δ 197.69, 172.83, 163.50, 152.23, 130.26, 129.89, 113.76, 82.16, 78.09, 55.48, 54.86, 37.47, 30.31, 28.26, 19.32; **R_f** (hexanes / EtOAc, 2:1) = 0.5; **IR** (neat): 2978, 2933, 1797, 1703, 1683, 1599, 1510, 1457, 1390, 1312, 1252, 1167, 1029, 839, 753, 667 cm^{-1}; **HRMS** (ESI-MS) m/z calculated for $C_{19}H_{26}NO_6$ ($[M+H]^+$) 364.1755, found 364.1759.

tert-butyl (*S*)-4-(4-(3-methoxyphenyl)-4-oxobutyl)-5-oxooxazolidine-3-carboxylate (123bj)

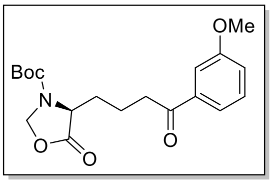

Following general procedure **GP-C** using 1-(3-methoxyphenyl)vinyl acetate (**122j**, 192 mg, 1.00 mmol, 5.00 equiv) and *fac*-Ir(ppy)$_3$ (**5**, 1.3 mg, 2.00 µmol, 1.00 mol%) gave the pure product as colorless oil (48.0 mg, 132 µmol, 66%) after purification by flash silica gel chromatography (hexanes / EtOAc, 4:1).

^{1}H-NMR (400 MHz, $CDCl_3$): δ 7.54 – 7.49 (m, 1H), 7.48 – 7.44 (m, 1H), 7.40 – 7.33 (m, 1H), 7.17 – 7.05 (m, 1H), 5.50 (s, 1H), 5.20 (d, J = 4.7 Hz, 1H), 4.30 (s, 1H), 3.85 (s, 3H), 3.01 (t, J = 6.9 Hz, 2H), 2.21 – 2.00 (m, 1H), 1.99 – 1.83 (m, 2H), 1.82 – 1.69 (m, 1H), 1.49 (s, 9H); **^{13}C-NMR** (101 MHz, $CDCl_3$): δ 198.91, 172.78, 159.86, 138.14, 134.30, 129.62, 123.59, 120.61, 119.56, 112.27, 82.19, 78.09, 55.45, 37.93, 30.26, 28.26, 19.19; **R_f** (hexanes / EtOAc, 2:1) = 0.5; **IR** (neat): 2937, 2912, 1796, 1685, 1584, 1487, 1454, 1394, 1368, 1327, 1256, 1159, 1044, 857, 768, 686 cm^{-1}; **HRMS** (ESI-MS) m/z calculated for $C_{19}H_{26}NO_6$ ($[M+H]^+$) 364.1755, found 364.1757.

tert-butyl (*S*)-4-(4-(2-methoxyphenyl)-4-oxobutyl)-5-oxooxazolidine-3-carboxylate (123bk)

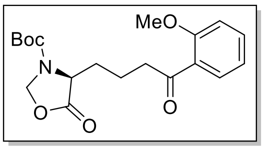

Following general procedure **GP-C** using 1-(2-methoxyphenyl)vinyl acetate (**122k**, 192 mg, 1.00 mmol, 5.00 equiv) and *fac*-Ir(ppy)$_3$ (**5**, 1.3 mg, 2.00 µmol, 1.00 mol%) gave the pure product as colorless oil (47.2 mg, 130 µmol, 65%) after purification by flash silica gel chromatography (hexanes / EtOAc, 4:1).

^{1}H-NMR (400 MHz, $CDCl_3$): δ 7.70 – 7.65 (m, 1H), 7.49 – 7.41 (m, 1H), 7.03 – 6.93 (m, 2H), 5.50 (s, 1H), 5.19 (d, J = 4.6 Hz, 1H), 4.29 (s, 1H), 3.90 (s, 3H), 3.12 – 2.92 (m, 2H), 2.18 – 1.99 (m, 1H), 1.98 – 1.79 (m, 2H), 1.75 – 1.64 (m, 1H), 1.49 (s, 9H); **^{13}C-NMR** (101 MHz, $CDCl_3$): δ 201.53, 172.93, 158.55, 134.32, 133.50, 130.27, 128.18, 123.60, 120.70, 111.56, 82.11, 78.11, 55.51, 43.11, 30.49, 28.29, 19.34; **R_f** (hexanes / EtOAc, 2:1) = 0.5; **IR** (neat): 2974, 2933, 1797, 1703, 1683, 1595, 1484, 1390, 1282, 1245, 1159, 1047, 893, 857, 813, 757 cm^{-1}; **HRMS** (ESI-MS) m/z calculated for $C_{19}H_{26}NO_6$ ($[M+H]^+$) 364.1755, found 364.1756.

***tert*-butyl (S)-4-(4-(4-bromophenyl)-4-oxobutyl)-5-oxooxazolidine-3-carboxylate (123bl)**

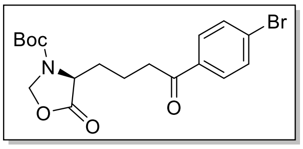

Following general procedure **GP-C** using 1-(4-bromophenyl)vinyl acetate (**122l**, 241 mg, 1.00 mmol, 5.00 equiv) and *fac*-Ir(ppy)$_3$ (**5**, 1.3 mg, 2.00 µmol, 1.00 mol%) gave the pure product as pale yellow oil (68.6 mg, 166 µmol, 83%) after purification by flash silica gel chromatography (hexanes / EtOAc, 4:1).

^{1}H-NMR (400 MHz, CDCl$_3$): δ 7.88 – 7.73 (m, 2H), 7.69 – 7.49 (m, 2H), 5.48 (s, 1H), 5.19 (d, J = 4.8 Hz, 1H), 4.29 (s, 1H), 2.99 (t, J = 7.0 Hz, 2H), 2.17 – 2.01 (m, 1H), 1.98 – 1.84 (m, 2H), 1.82 – 1.67 (m, 1H), 1.48 (s, 9H); **^{13}C-NMR** (101 MHz, CDCl$_3$): δ 198.03, 172.75, 152.24, 135.48, 131.97, 129.53, 128.31, 82.23, 78.10, 54.81, 37.77, 30.19, 28.27, 19.01; **R$_f$** (hexanes / EtOAc, 2:1) = 0.6; **IR** (neat): 2974, 2930, 1797, 1759, 1703, 1640, 1588, 1487, 1394, 1382, 1256, 1200, 1088, 1047, 1006, 887, 828, 788, 727 cm^{-1}; **HRMS** (ESI-MS) m/z calculated for $C_{18}H_{23}BrNO_5$ ([M+H]$^+$) 412.0749, found 412.0753.

***tert*-butyl (S)-4-(4-(4-chlorophenyl)-4-oxobutyl)-5-oxooxazolidine-3-carboxylate (123bm)**

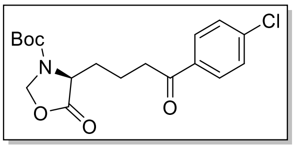

Following general procedure **GP-C** using 1-(4-chlorophenyl)vinyl acetate (**122m**, 197 mg, 1.00 mmol, 5.00 equiv) and *fac*-Ir(ppy)$_3$ (**5**, 1.3 mg, 2.00 µmol, 1.00 mol%) gave the pure product as colorless oil (59.0 mg, 160 µmol, 80%) after purification by flash silica gel chromatography (hexanes / EtOAc, 5:1).

^{1}H-NMR (400 MHz, CDCl$_3$): δ 7.88 (d, J = 8.4 Hz, 2H), 7.42 (d, J = 8.3 Hz, 2H), 5.49 (s, 1H), 5.20 (d, J = 4.6 Hz, 1H), 4.29 (s, 1H), 2.99 (t, J = 6.9 Hz, 2H), 2.16 – 2.01 (m, 1H), 1.97 – 1.85 (m, 2H), 1.79 – 1.70 (m, 1H), 1.48 (s, 9H); **^{13}C-NMR** (101 MHz, CDCl$_3$): δ 197.82, 172.73, 152.24, 139.56, 135.05, 129.40, 128.95, 82.22, 78.09, 54.77, 37.77, 30.19, 28.25, 19.01; **R$_f$** (hexanes / EtOAc, 2:1) = 0.7; **IR** (neat): 2978, 2933, 1797, 1685, 1588, 1476, 1394, 1320, 1230, 1159, 1092, 1047, 1014, 902, 816, 768, 719 cm^{-1}; **HRMS** (ESI-MS) m/z calculated for $C_{18}H_{23}ClNO_5$ ([M+H]$^+$) 368.1259, found 368.1261.

tert-butyl (4*S*)-5-oxo-4-(2-(1-oxo-1,2,3,4-tetrahydronaphthalen-2-yl)ethyl)oxazolidine-3-carboxylate (123bn)

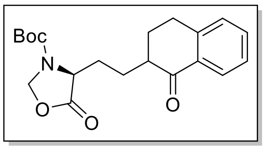

Following general procedure **GP-C** using 1-(1-oxo-1,2,3,4-tetrahydronaphthalen-2-yl)vinyl acetate (**122n**, 188 mg, 1.00 mmol, 5.00 equiv) and *fac*-Ir(ppy)$_3$ (**5**, 1.3 mg, 2.00 µmol, 1.00 mol%) gave the product as two inseparable diastereomers as colorless oil (43.8 mg, 122 µmol, 61%) after purification by flash silica gel chromatography (hexanes / EtOAc, 4:1).

^{1}H-NMR (400 MHz, CDCl$_3$): mixture of two inseparable diastereomers: δ 8.06 – 7.97 (m, 1H), 7.49 – 7.43 (m, 1H), 7.32 – 7.27 (m, 1H), 7.25 – 7.20 (m, 1H), 5.49 (s, 1H), 5.21 (d, J = 4.6 Hz, 1H), 4.31 (s, 1H), 3.05 – 2.96 (m, 2H), 2.55 – 2.45 (m, 1H), 2.28 – 2.12 (m, 2H), 2.11 – 1.83 (m, 3H), 1.67 – 1.57 (m, 1H), 1.50 (s, 9H); **^{13}C-NMR** (101 MHz, CDCl$_3$): mixture of two inseparable diastereomers: δ 199.33, 172.83, 143.79, 133.32, 133.29, 132.40, 132.33, 128.75, 128.71, 127.47, 126.67, 82.20, 78.18, 78.10, 47.12, 47.05, 28.65, 28.51, 28.43, 28.29; **R$_f$** (hexanes / EtOAc, 2:1) = 0.6; **IR** (neat): 2974, 2930, 2863, 1797, 1704, 1603, 1476, 1390, 1312, 1256, 1226, 1159, 1047, 917, 880, 813, 742, 671 cm^{-1}; **HRMS** (ESI-MS) m/z calculated for $C_{20}H_{26}NO_5$ ([M+H]$^+$) 360.1805, found 360.1809.

tert-butyl (*S*)-4-(4-(naphthalen-2-yl)-4-oxobutyl)-5-oxooxazolidine-3-carboxylate (123bo)

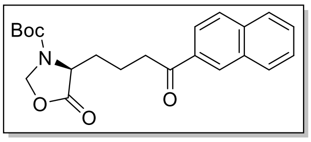

Following general procedure **GP-C** using trimethyl((1-(naphthalen-2-yl)vinyl)oxy)silane (**122o**, 242 mg, 1.00 mmol, 5.00 equiv) and *fac*-Ir(ppy)$_3$ (**5**, 3.3 mg, 5.00 µmol, 2.50 mol%) gave the pure product as white solid (56.0 mg, 146 µmol, 73%) after purification by flash silica gel chromatography (hexanes / EtOAc, 5:1).

^{1}H-NMR (300 MHz, CDCl$_3$): δ 8.44 – 8.39 (m, 1H), 8.00 – 7.95 (m, 1H), 7.95 – 7.89 (m, 1H), 7.88 – 7.80 (m, 2H), 7.60 – 7.47 (m, 2H), 5.47 (s, 1H), 5.18 (d, J = 3.6 Hz, 1H), 4.29 (s, 1H), 3.21 – 3.05 (m, 2H), 2.19 – 2.04 (m, 1H), 2.02 – 1.87 (m, 2H), 1.86 – 1.70 (m, 1H), 1.45 (s, 9H); **^{13}C-NMR** (75 MHz, CDCl$_3$): δ 199.06, 172.84, 152.27, 135.61, 134.09, 132.52, 129.66, 129.58, 128.50, 127.79, 126.82, 123.77, 123.60, 82.22, 78.13, 37.90, 30.37, 28.28, 19.28; **R$_f$** (hexanes / EtOAc, 2:1) = 0.6; **mp**: 73 – 75 °C; **IR** (neat): 3202, 3060, 2978, 2933, 1782, 1744, 1681, 1409, 1368, 1252, 1219, 1170, 1044, 939, 890, 857, 828, 768, 667 cm^{-1}; **HRMS** (ESI-MS) m/z calculated for $C_{22}H_{26}NO_5$ ([M+H]$^+$) 384.1805, found 384.1813.

tert-butyl (*S*)-5-oxo-4-(4-oxo-4-(thiophen-2-yl)butyl)oxazolidine-3-carboxylate (123bp)

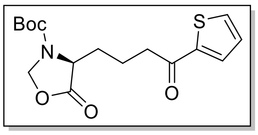

Following general procedure **GP-C** using trimethyl((1-(thiophen-2-yl)vinyl)oxy)silane (**122p**, 198 mg, 1.00 mmol, 5.00 equiv) and *fac*-Ir(ppy)$_3$ (**5**, 3.3 mg, 5.00 µmol, 2.50 mol%) gave the pure product as white solid (56.1 mg, 166 µmol, 83%) after purification by flash silica gel chromatography (hexanes / EtOAc, 5:1).

^{1}H-NMR (400 MHz, CDCl$_3$): δ 7.84 (dd, J = 3.8, 1.1 Hz, 1H), 7.77 (dd, J = 5.0, 1.1 Hz, 1H), 7.26 (dd, J = 4.9, 3.8 Hz, 1H), 5.63 (s, 1H), 5.33 (d, J = 4.7 Hz, 1H), 4.43 (s, 1H), 3.10 (t, J = 7.2 Hz, 2H), 2.32 – 2.14 (m, 1H), 2.05 (ddt, J = 11.1, 7.7, 4.0 Hz, 2H), 1.97 – 1.83 (m, 1H), 1.62 (s, 9H); **^{13}C-NMR** (101 MHz, CDCl$_3$): δ 192.07, 172.73, 152.25, 144.06, 133.63, 131.85, 128.14, 82.21, 78.07, 54.77, 38.52, 30.27, 28.24, 19.50.; **R_f** (hexanes / EtOAc, 2:1) = 0.55; **mp**: 84 – 86 °C; **IR** (neat): 3116, 2982, 2933, 1797, 1752, 1696, 1651, 1476, 1405, 1304, 1256, 1170, 1133, 1036, 988, 932, 846, 775, 730 cm^{-1}; **HRMS** (ESI-MS) m/z calculated for $C_{16}H_{22}NO_5S$ ([M+H]$^+$) 340.1213, found 340.1219.

tert-butyl (*S*)-4-(4-(furan-2-yl)-4-oxobutyl)-5-oxooxazolidine-3-carboxylate (123bq)

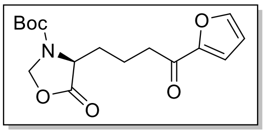

Following general procedure **GP-C** using ((1-(furan-2-yl)vinyl)oxy)trimethylsilane (**122q**, 182 mg, 1.00 mmol, 5.00 equiv) and *fac*-Ir(ppy)$_3$ (**5**, 3.3 mg, 5.00 µmol, 2.50 mol%) gave the pure product as colorless oil (25.9 mg, 80.0 µmol, 40%) after purification by flash silica gel chromatography (hexanes / EtOAc, 3:1).

^{1}H-NMR (300 MHz, CDCl$_3$): δ 7.57 (dd, *J* = 1.7, 0.8 Hz, 1H), 7.18 (dd, *J* = 3.6, 0.8 Hz, 1H), 6.53 (dd, *J* = 3.6, 1.7 Hz, 1H), 5.49 (s, 1H), 5.19 (d, *J* = 3.7 Hz, 1H), 4.29 (s, 1H), 2.88 (td, *J* = 7.3, 1.5 Hz, 2H), 2.08 – 2.00 (m, 1H), 1.99 – 1.81 (m, 2H), 1.82 – 1.66 (m, 1H), 1.49 (s, 9H); **^{13}C-NMR** (101 MHz, CDCl$_3$): δ 188.36, 172.72, 152.58, 152.23, 146.32, 116.98, 112.24, 82.21, 78.07, 37.65, 31.89, 54.78, 28.24, 19.07; **R_f** (hexanes / EtOAc, 2:1) = 0.4; **IR** (neat): 3131, 2978, 2930, 1797, 1700, 1674, 1569, 1469, 1390, 1320, 1245, 1156, 1044, 883, 764, 705 cm^{-1}; **HRMS** (ESI-MS) m/z calculated for $C_{16}H_{22}NO_6$ ([M+H]$^+$) 324.1442, found 324.1446.

tert-butyl (*S*)-5-oxo-4-(4-oxo-4-(pyridin-3-yl)butyl)oxazolidine-3-carboxylate (123br)

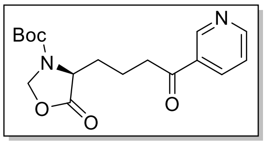

Following general procedure **GP-C** using 3-(1-((trimethylsilyl)oxy)-vinyl)pyridine (**122r**, 193 mg, 1.00 mmol, 5.00 equiv) and *fac*-Ir(ppy)$_3$ (**5**, 3.3 mg, 5.00 µmol, 2.50 mol%) gave the pure product as yellow oil (49.3 mg, 147 µmol, 74%) after purification by flash silica gel chromatography (hexanes / EtOAc, 1:1).

^{1}H-NMR (300 MHz, $CDCl_3$): δ 9.23 - 9.07 (m, 1H), 8.77 (dd, J = 4.8, 1.7 Hz, 1H), 8.22 (dt, J = 8.0, 1.9 Hz, 1H), 7.42 (ddd, J = 8.1, 4.8, 0.9 Hz, 1H), 5.49 (s, 1H), 5.20 (dd, J = 4.6, 1.1 Hz, 1H), 4.30 (s, 1H), 3.07 – 3.03 (m, 2H), 2.16 - 2.02 (m, 1H), 2.01 - 1.86 (m, 2H), 1.83 - 1.70 (m, 1H), 1.48 (s, 9H); **^{13}C-NMR** (75 MHz, $CDCl_3$): δ 197.80, 172.71, 153.43, 152.28, 149.40, 135.42, 132.00, 123.76, 82.27, 78.10, 54.76, 38.09, 30.16, 28.26, 18.72; **R_f** (hexanes / EtOAc, 2:1) = 0.1; **IR** (neat): 2974, 2933, 1797, 1689, 1588, 1510, 1394, 1238, 1159, 1044, 857, 768, 700 cm^{-1}; **HRMS** (ESI-MS) m/z calculated for $C_{17}H_{23}N_2O_5$ ($[M+H]^+$) 335.1601, found 335.1607.

3.5. Upscaling of photoreaction

tert-butyl (*S*)-5-oxo-4-(4-oxo-4-phenylbutyl)oxazolidine-3-carboxylate (123bf)

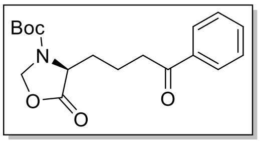

One-phase batch conditions

The photoreaction was performed on a 1.0 mmol scale. A 20 mL flame dried Schlenk tube equipped with a magnetic stirring bar was charged with *tert*-butyl 4-(3-((1,3-dioxoisoindolin-2-yl)oxy)-3-oxopropyl)-5-oxooxazolidine-3-carboxylate (**121b**, 404 mg, 1.00 mmol, 1.00 equiv), 1-phenylvinyl acetate (**122f**, 811 mg, 5.00 mmol, 5.00 equiv), and *fac*-Ir(ppy)$_3$ (**5**, 6.5 mg, 10 µmol, 1.00 mol%). Water (450 µL, 25.0 mmol, 25.0 equiv) and dry MeCN (10.0 mL) were added and the tube was sealed with a screw-cap. The mixture was degassed by three freeze-pump-thaw cycles. Subsequently, the screw-cap was replaced by a Teflon sealed inlet for a glass rod, through which irradiation with a 455 nm LED took place from above while the reaction was magnetically stirred from below. After 5 d the LED was switched off and the solvent was evaporated. The yield was determined by ^{1}H-NMR using 4-nitrobenzaldehyde as internal standard (55% yield).

Two-phase batch conditions

The reactions were performed on a 0.20 mmol scale using polyisobutylene tagged *fac*-Ir(ppy)$_2$(PIB-ppy) (**40**) as catalyst, which was established by Reiser *et al.*[2] A flame dried Schlenk tube equipped with a magnetic stirring bar was charged with *tert*-butyl 4-(3-((1,3-dioxoisoindolin-2-yl)oxy)-3-oxopropyl)-5-oxooxazolidine-3-carboxylate (**121b**, 80.9 mg, 200 µmol, 1.00 equiv) and 1-phenylvinyl acetate (**122f**, 162 mg, 1.00 mmol, 5.00 equiv). Water (90 µmol, 5.00 mmol, 25.0 equiv) and dry MeCN (1.00 mL) were added. In a second Schlenk tube *fac*-Ir(ppy)$_2$(PIB-ppy) (**40**, 3.4 mg, 2.0 µmol, 1.00 mol%) was dissolved in heptane (1.00 mL) and added to the reaction mixture and the tube was sealed with a plastic screw-cap. The combined phases were degassed by three freeze-pump-thaw cycles. Subsequently, the screw-cap was replaced by a Teflon sealed inlet for a glass rod, through which irradiation with a 455 nm LED took place from above while the reaction was magnetically stirred from below at room temperature. After 18 h the LED was switched off and the reaction mixture was transferred to a separation funnel with the aid of 5 mL MeCN and 5 mL heptane. The phases were separated. The MeCN phase was evaporated and the yield was determined by ^{1}H-NMR using 4-nitrobenzaldehyde as internal standard (85% yield).

The heptane phase was evaporated, and the catalyst was re-dissolved in heptane (1.00 mL) to be reused in a second run. The yields of the consecutive runs are given in the main part.

Flow conditions

The reaction was performed several times, varying the concentration, flowrate and scale of the reaction. Additionally, in some cases two micro reactors were connected in series to lower the reaction time.

Flow conditions for a 0.20 mmol scale – general procedure

A flame dried Schlenk tube was charged with *tert*-butyl 4-(3-((1,3-dioxoisoindolin-2-yl)oxy)-3-oxopropyl)-5-oxooxazolidine-3-carboxylate (**121b**, 80.9 mg, 200 µmol, 1.00 equiv), 1-phenylvinyl acetate (**122f**, 162 mg, 1.00 mmol, 5.00 equiv), and *fac*-Ir(ppy)$_3$ (**5**, 1.3 mg, 2.0 µmol, 1.0 mol%). Water (90 µL, 5.00 mmol, 25.0 equiv) and dry MeCN (2.0 mL (0.1 M) or 4.0 mL (0.05 M)) were added and the mixture was degassed by three freeze-pump-thaw cycles. The mixture was transferred to a 5 mL syringe and connected to one (or two) micro reactor(s), which was (were) purged with nitrogen for 10 min before. The flowrate was set to 1.0 or 0.5 mL/h with the aid of a syringe pump. The solvent was evaporated, and the yield was determined by ^{1}H-NMR using 4-nitrobenzaldehyde as internal standard. The results for the different experiments are given in the main part.

Flow conditions – 4.0 mmol scale

A flame dried Schlenk flask was charged with *tert*-butyl 4-(3-((1,3-dioxoisoindolin-2-yl)oxy)-3-oxopropyl)-5-oxooxazolidine-3-carboxylate (**121b**, 1.62 g, 4.00 mmol, 1.00 equiv), 1-phenylvinyl acetate (**122f**, 3.24 g, 20.0 mmol, 5.00 equiv), and *fac*-Ir(ppy)$_3$ (**5**, 26.2 mg, 40.0 µmol, 1.0 mol%). Water (1.80 mL, 100 mmol, 25.0 equiv) and dry MeCN (80.0 mL (0.05 M)) were added and the mixture was degassed by N_2 sparging for 15 min. The mixture was transferred to a 20 mL syringe and connected to two micro reactors, which were connected in series and purged with nitrogen for 10 min before. The flowrate was set to 0.5 mL/h with the aid of a syringe pump. The syringe was refilled four times under nitrogen atmosphere. The solvent was evaporated, and the yield was determined by ^{1}H-NMR using 4-nitrobenzaldehyde as internal standard (78% yield). Afterwards, the crude mixture was submitted to column chromatography (hexanes / EtOAc, 5:1) to give the pure compound **123bf** as a white solid (971 mg, 2.91 mmol, 73%).

3.6. Intramolecular reactions

(8a*S*)-6-isopropyl-2-phenyltetrahydroimidazo[1,5-a]pyridine-1,3(2H,5H)-dione (255)

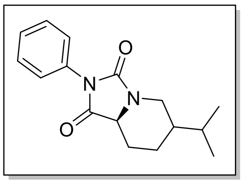

A Schlenk tube was charged with 1,3-dioxoisoindolin-2-yl (*S*)-3-(3-(3-methylbut-2-en-1-yl)-2,5-dioxo-1-phenylimidazolidin-4-yl)propanoate (**239**, 92.3 mg, 200 µmol, 1.00 equiv), [Ru(bpy)$_3$]Cl$_2$ (**1**, 3.0 mg, 4.0 µmol, 2.0 mol%), DIPEA (70 µL, 400 µmol, 2.00 equiv) and MeCN (2.0 mL). The tube was sealed with a screw-cap and degassed by three freeze-pump-thaw cycles. Subsequently, the screw-cap was replaced by a Teflon sealed inlet for a glass rod to ensure irradiation from above with a blue LED (λ = 455 nm) while being magnetically stirred from below. After 18 h, the irradiation was stopped, and the solvent was evaporated. The crude residue was purified by flash silica column chromatography (hexanes / EtOAc, 4:1) to give the product as an inseparable 1:1 mixture of (8a*S*)-6-isopropyl-2-phenyltetrahydroimidazo[1,5-a]pyridine-1,3(2H,5H)-dione (**255**) and (*S*)-2-phenyl-6-(propan-2-ylidene)tetrahydroimidazo[1,5-a]pyridine-1,3(2H,5H)-dione (**254**). *Via* hydrogenation of the mixture using Pd/C (2.0 µmol, 1.0 mol%) in MeOH (1.0 mL) at 40 bar H$_2$ pressure, solely product **255** was obtained in two diastereomers as a white solid (39 mg, 143 µmol, 72%).

^{1}H-NMR (400 MHz, CDCl$_3$): δ 7.48 – 7.32 (m, 5H), 4.34 – 4.25 (m, 1H), 3.87 (dd, J = 12.0, 4.3 Hz, 1H), 2.61 (dd, J = 13.2, 11.0 Hz, 1H), 2.40 – 2.31 (m, 1H), 2.12 – 2.03 (m, 1H), 1.56 – 1.41 (m, 2H), 1.35 – 1.21 (m, 2H), 0.97 (dd, J = 6.8, 2.0 Hz, 6H); **^{13}C-NMR** (101 MHz, CDCl$_3$): δ 171.94, 153.50, 131.87, 129.00, 127.96, 126.08, 57.25, 42.86, 42.37, 30.83, 27.97, 26.73, 19.86, 19.85; **R$_f$** (hexanes / EtOAc, 2:1) = 0.6; **mp**: 103 – 106 °C; **IR** (neat): 2974, 2933, 1797, 1689, 1588, 1510, 1394, 1238, 1159, 1044, 857, 768, 700 cm^{-1}; **HRMS** (ESI-MS) m/z calculated for $C_{16}H_{21}N_2O$ ([M+H]$^+$) 273.1598, found 273.1599.

3.7. Synthesis of pipecolic acid derivatives

(*S*)-2-((tert-butoxycarbonyl)amino)-6-oxo-6-phenylhexanoic acid (230a)

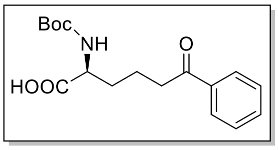

The oxazolidinone ring opening towards **230a** was performed following a literature procedure.[45] A 10 mL round-bottom flask was charged with *tert*-butyl (*S*)-5-oxo-4-(4-oxo-4-phenylbutyl)oxazolidine-3-carboxylate (**123bf**, 167 mg, 500 µmol, 1.00 equiv) and MeOH (2.0 mL). Subsequently, aqueous NaOH (1.0 mL, 1.0 M) was added, whereby the mixture turned yellowish. After stirring for 2 h at room temperature, the starting material was completely gone (as judged by TLC). MeOH was evaporated and the residual aqueous phase was transferred to a separation funnel with the aid of water (5 mL) and was extracted with ethyl acetate (2 x 5 mL), after which the aqueous phase was acidified with HCl (2.0 mL, 1.0 M). A white precipitate occurred. EtOAc (10 mL) was added and the phases were separated. The aqueous phase was extracted with EtOAc (3 x 10 mL). The combined organic phases were washed with brine (10 mL) and dried over Na_2SO_4. Evaporation of the solvent yielded a colorless oil (161 mg, 500 µmol, 100%). The crude mixture was submitted to the next step without further purification.

(*S*)-2-((*tert*-butoxycarbonyl)amino)-6-oxo-6-(thiophen-2-yl)hexanoic acid (230b)

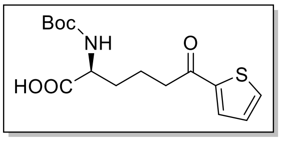

The oxazolidinone ring opening towards **230b** was performed following a literature procedure.[45] A 10 mL round bottom flask was charged with *tert*-butyl 5-oxo-4-(4-oxo-4-(thiophen-2-yl)butyl)oxazolidine-3-carboxylate (**123bp**, 102 mg, 301 µmol, 1.00 equiv) which was dissolved in MeOH (1.5 mL). Subsequently, aqueous NaOH (0.5 mL, 1.0 M) was added, whereby the mixture turned yellow. After stirring for 2 h at room temperature, the starting material was completely gone (as judged by TLC). MeOH was evaporated and the residual aqueous phase was transferred to a separation funnel with the aid of water (5 mL) and was extracted with ethyl acetate (2 x 5 mL), after which the aqueous phase was acidified with HCl (2 mL, 1.0 M). A white precipitate occurred. EtOAc (10 mL) was added and the phases were separated. The aqueous phase was extracted with EtOAc (3 x 10 mL). The combined organic phases were washed with brine (10 mL) and dried over Na_2SO_4. Evaporation of the solvent gave a yellow oil (98.3 mg, 300 µmol, 100%). The crude mixture was submitted to the next step without further purification.

methyl (*S*)-2-((*tert*-butoxycarbonyl)amino)-6-oxo-6-phenylhexanoate (257a)

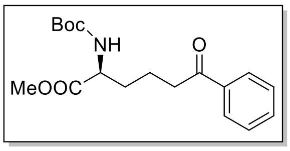

The substrate **257a** was synthesized following a modified literature procedure.[46] A flame dried 10 mL Schlenk flask was charged with crude (*S*)-2-((tert-butoxycarbonyl)amino)-6-oxo-6-phenylhexanoic acid (**230a**, 161 mg, 500 µmol, 1.00 equiv), methyl iodide (124 µL, 283 mg, 2.00 mmol, 4.00 equiv), Na_2CO_3 (106 mg, 1.00 mmol, 2.00 equiv), and dry DMF (5 mL). The mixture was allowed to stir for 16 h at room temperature after which the solution turned yellowish and a white precipitate occurred. EtOAc (10 mL) was added and the mixture was extracted with H_2O (2 x 10 mL) and brine (2 x 10 mL). The organic phase was dried over Na_2SO_4 and the solvent was evaporated. Purification was achieved by flash silica chromatography (hexanes / EtOAc, 3:1) to give the pure product as colorless oil (100 mg, 298 µmol, 60% over two steps)

^{1}H-NMR (300 MHz, $CDCl_3$): δ 7.98 – 7.91 (m, 2H), 7.60 – 7.52 (m, 1H), 7.50 – 7.42 (m, 2H), 5.16 (dd, J = 30.4, 6.6 Hz, 1H), 4.36 (s, 0H), 3.74 (s, 3H), 3.08 – 2.95 (m, 2H), 1.91 – 1.69 (m, 4H), 1.44 (s, 9H); **^{13}C-NMR** (101 MHz, $CDCl_3$): δ 199.52, 173.17, 155.43, 136.84, 133.09, 128.62, 128.01, 79.92, 53.19, 52.31, 37.66, 32.15, 28.32, 19.84; **R_f** (hexanes / EtOAc, 2:1) = 0.4; **IR** (neat): 3358, 2974, 1800, 1658, 1599, 1510, 1450, 1364, 1249, 1208, 1159, 1051, 1029, 913, 865, 731, 693 cm^{-1}; **HRMS** (ESI-MS) m/z calculated for $C_{18}H_{26}NO_5$ ($[M+H]^+$) 336.1805, found 336.1802.

methyl (*S*)-2-((*tert*-butoxycarbonyl)amino)-6-oxo-6-(thiophen-2-yl)hexanoate 257b

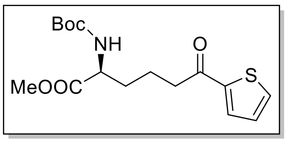

The substrate **257b** was synthesized following a modified literature procedure.[46] A flame dried 10 mL Schlenk flask was charged with crude (*S*)-2-((*tert*-butoxycarbonyl)amino)-6-oxo-6-(thiophen-2-yl)hexanoic acid (**230b**, 98.3 mg, 300 µmol, 1.00 equiv), methyl iodide (75 µL, 170 mg, 1.20 mmol, 4.00 equiv), Na_2CO_3 (63.5 mg, 599 µmol, 2.00 equiv), and dry DMF (5 mL). The mixture was allowed to stir for 16 h at room temperature after which a white precipitate occurred. EtOAc (10 mL) was added and the mixture was extracted with H_2O (2 x 10 mL) and brine (2 x 10 mL). The organic phase was dried over Na_2SO_4 and the solvent was evaporated. Purification was achieved by flash silica chromatography (hexanes / EtOAc, 2:1) to give the pure product as colorless oil (53.0 mg, 155 µmol, 52%, over two steps)

^{1}H-NMR (400 MHz, $CDCl_3$): δ 7.71 (dd, J = 3.8, 1.1 Hz, 1H), 7.63 (dd, J = 5.0, 1.1 Hz, 1H), 7.12 (dd, J = 5.0, 3.8 Hz, 1H), 5.20 – 4.95 (m, 1H), 4.44 – 4.24 (m, 1H), 3.73 (s, 3H), 3.04 –

2.85 (m, 2H), 1.93 – 1.70 (m, 4H), 1.44 (s, 9H); **^{13}C-NMR** (101 MHz, $CDCl_3$): δ 192.46, 173.10, 155.41, 144.18, 133.59, 131.87, 128.10, 79.95, 53.11, 52.33, 38.38, 32.16, 28.32, 20.23; **R_f** (hexanes / EtOAc, 2:1) = 0.3; **IR** (neat): 3362, 2974, 1744, 1707, 1659, 1513, 1454, 1364, 1208, 1163, 1055, 857, 727 cm^{-1}; **HRMS** (ESI-MS) m/z calculated for $C_{16}H_{24}NO_5S$ ($[M+H]^+$) 343.1370, found 343.1370.

methyl (2*S*,6*R*)-6-phenylpiperidine-2-carboxylate (231a)

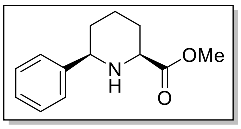

Following a modified literature procedure,[47] methyl (*S*)-2-((*tert*-butoxycarbonyl)amino)-6-oxo-6-phenylhexanoate (**257a**, 20.0 mg, 60 µmol, 1.00 equiv) was placed in a 5 mL round-bottom flask. Trifluoroacetic acid (1.00 mL) was added in access and the mixture was allowed to stir at room temperature until full conversion of starting material (as judged by TLC, $R_{f,\ intermediate}$ (DCM / MeOH, 9:1) = 0.5, UV active), 2 h). During this time, it turned yellowish. Trifluoroacetic acid was evaporated under reduced pressure. Subsequently, the residue was dissolved in 1 mL MeOH, cooled to 0 °C, and $NaBH_4$ (2.7 mg, 72 µmol, 1.20 equiv) was added and the mixture was allowed to stir for 1 h at 0 °C. After full conversion of starting material ($R_{f,\ product}$ (DCM / MeOH, 9:1) = 0.7, not UV active, stains with $KMnO_4$), MeOH was evaporated and H_2O (10 mL) and EtOAc (10 mL) were added. The phases were separated, and the aqueous phase was extracted with EtOAc (5 x 5 mL). The combined organic phases were dried over Na_2SO_4. Evaporation of the solvent yielded the pure product as brownish oil (12.3 mg, 56 µmol, 94%) in a diastereomeric ratio of 6:1.

^{1}H-NMR (400 MHz, $CDCl_3$): δ for major diastereomer 7.43 – 7.36 (m, 2H), 7.37 – 7.28 (m, 2H), 7.30 – 7.23 (m, 1H), 3.72 (s, 3H), 3.71 – 3.64 (m, 1H), 3.52 (dd, J = 10.5, 2.5 Hz, 1H), 2.48 (brs, 1H), 2.14 – 2.04 (m, 1H), 2.05 – 1.92 (m, 1H), 1.83 – 1.74 (m, 1H), 1.61 – 1.44 (m, 3H); **^{13}C-NMR** (101 MHz, $CDCl_3$): δ major diastereomer 173.28, 144.31, 128.44, 127.34, 126.77, 61.80, 59.73, 51.99, 33.93, 28.39, 24.99; **R_f** (DCM / MeOH, 9:1) = 0.7; **IR**: 2922, 2855, 2796, 2684, 2363, 2113, 1737, 1498, 1431, 1305, 1200, 1025, 910, 883, 857, 760, 697 cm^{-1}; **HRMS** (EI-MS) m/z calculated for $C_{13}H_{17}NO_2$ ($[M]^+$) 219.12538, found 219.12495.

methyl (2*S*,6*R*)-6-(thiophen-2-yl)piperidine-2-carboxylate (231b)

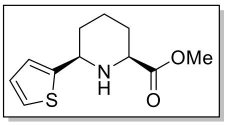

Following a modified literature procedure,[47] methyl(*S*)-2-((*tert*-butoxycarbonyl)amino)-6-oxo-6-(thiophen-2-yl)hexanoate (**257b**, 20 mg, 59 µmol, 1.00 equiv) was placed in a 5 mL round bottom flask. Trifluoroacetic acid (1.00 mL) was added in access and the mixture was allowed to stir at room temperature until full conversion of starting material (as judged by TLC, $R_{f,\ intermediate}$ (hexanes / EtOAc, 2:1) = 0.50, UV active), 2 h). During this time, it turned reddish. Trifluoroacetic acid was evaporated under reduced pressure. Subsequently, the residue was dissolved in 1 mL MeOH, cooled to 0 °C, and $NaBH_4$ (2.7 mg, 70 µmol, 1.20 equiv) was added and the mixture was allowed to stir for 1 h at 0 °C. After full conversion of starting material ($R_{f,\ product}$ (hexanes / EtOAc, 2:1) = 0.45, not UV active, stains with $KMnO_4$), MeOH was evaporated and H_2O (10 mL) and EtOAc (10 mL) were added. The phases were separated, and the aqueous phase was extracted with EtOAc (5 x 5 mL). The combined organic phases were dried over Na_2SO_4. Evaporation of the solvent yielded the pure product as brownish oil (11.6 mg, 51 µmol, 88%) in a diastereomeric ratio of 6:1.

^{1}H-NMR (300 MHz, $CDCl_3$): δ major diastereomer 7.20 (dd, J = 5.0, 1.3 Hz, 1H), 6.99 (ddd, J = 3.5, 1.4, 0.7 Hz, 1H), 6.95 (dd, J = 5.0, 3.5 Hz, 1H), 4.05 – 3.95 (m, 1H), 3.72 (s, 3H), 3.57 – 3.48 (m, 1H), 2.61 (brs, 1H), 2.13 – 1.91 (m, 3H), 1.65 – 1.47 (m, 3H); **^{13}C-NMR** (101 MHz, $CDCl_3$): δ for major diastereomer 173.02, 148.13, 126.39, 123.84, 123.21, 59.51, 56.80, 52.03, 34.79, 28.42, 24.70; **R_f** (hexanes / EtOAc, 2:1) = 0.6; **IR**: 3325, 2937, 2855, 2792, 2091, 1733, 1435, 1375, 1290, 1204, 1133, 1055, 1018, 924, 828, 798, 753, 697 cm^{-1}; **HRMS** (EI-MS) m/z calculated for $C_{11}H_{16}NO_2S$ ($[M+H]^+$) 228.0896, found 228.0900.

4. Literature

[1] W. L. F. Armarego, C. L. L. Chai, *Purification of laboratory chemicals;* Elsevier/Butterworth-Heinemann, Amsterdam, Boston, **2009**.

[2] D. Rackl, P. Kreitmeier, O. Reiser, *Green Chem.* **2016**, *18*, 214–219.

[3] a) S. Sprouse, K. A. King, P. J. Spellane, R. J. Watts, *J. Am. Chem. Soc.* **1984**, *106*, 6647–6653; b) J. Sun, W. Wu, J. Zhao, *Chem. Eur. J.* **2012**, *18*, 8100–8112.

[4] a) J. Frey, T. Kraus, V. Heitz, J.-P. Sauvage, *Chem. Eur. J.* **2007**, *13*, 7584–7594; b) T. Rawner, Thesis, University of Regensburg, **2016**.

[5] J. M. Fraile, J. I. García, M. A. Harmer, C. I. Herrerías, J. A. Mayoral, O. Reiser, H. Werner, *J. Mater. Chem.* **2002**, *12*, 3290–3295.

[6] D. C. Fabry, M. A. Ronge, M. Rueping, *Chem. Eur. J.* **2015**, *21*, 5350–5354.

[7] a) J. D. Nguyen, J. W. Tucker, M. D. Konieczynska, C. R. J. Stephenson, *J. Am. Chem. Soc.* **2011**, *133*, 4160–4163; b) C.-J. Wallentin, J. D. Nguyen, P. Finkbeiner, C. R. J. Stephenson, *J. Am. Chem. Soc.* **2012**, *134*, 8875–8884.

[8] A. G. Condie, J. C. González-Gómez, C. R. J. Stephenson, *J. Am. Chem. Soc* **2010**, *132*, 1464–1465.

[9] Z. Li, C.-J. Li, *J. Am. Chem. Soc.* **2005**, *127*, 6968–6969.

[10] Z. Li, C.-J. Li, *J. Am. Chem. Soc.* **2005**, *127*, 3672–3673.

[11] Q. M. Kainz, S. Fernandes, C. M. Eichenseer, F. Besostri, H. Körner, R. Müller, O. Reiser, *Faraday Discuss.* **2014**, *175*, 27–40.

[12] S. Fernandes, Thesis, University of Regensburg, **2016**.

[13] Gill, C, S, Price, B, A, Jones, C, W, *J. Catal.* **2007**, *251*, 145–152.

[14] J. V. Nguyen, C. W. Jones, *Macromolecules* **2004**, *37*, 1190–1203.

[15] R. Martín, L. Jiménez, M. Alvaro, J. C. Scaiano, H. Garcia, *Chem. Eur. J.* **2010**, *16*, 7282–7292.

[16] B. P. Sullivan, D. J. Salmon, T. J. Meyer, *Inorg. Chem.* **1978**, *17*, 3334–3341.

[17] G. Zhang, Y. Wang, X. Wen, C. Ding, Y. Li, *Chem. Commun.* **2012**, *48*, 2979–2981.

[18] J. Lim, S. Seong Lee, J. Y. Ying, *Chem. Commun.* **2010**, *46*, 806–808.

[19] P. A. Peixoto, J.-A. Richard, R. Severin, D. Y.-K. Chen, *Org. Lett.* **2011**, *13*, 5724–5727.

[20] B. Witulski, U. Bergsträßer, M. Gößmann, *Tetrahedron* **2000**, *56*, 4747–4752.

[21] a) S. Bräse, H. Wertal, D. Frank, D. Vidović, A. de Meijere, *Eur. J. Org. Chem.* **2005**, 4167–4178; b) P. Kohls, Thesis, University of Regensburg, **2015**.

[22] Y. Kita, R. Okunaka, T. Honda, M. Shindo, M. Taniguchi, M. Kondo, M. Sasho, *J. Org. Chem.* **1991**, *56*, 119–125.

[23] a) N. Ansari, Z. Elshenawy, A. Deangelis, C. Xia. Heteroleptic iridium complexes as dopants - European Patent Office - EP 2551933 A1(EP 2551933 A1); b) D. Rackl, P. Kreitmeier, O. Reiser, *Green Chem.* **2016**, *18*, 214–219.

[24] J. J. Molloy, J. B. Metternich, C. G. Daniliuc, A. J. B. Watson, R. Gilmour, *Angew. Chem. Int. Ed.* **2018**, *57*, 3168–3172.

[25] C. Wang, T. Tobrman, Z. Xu, E.-i. Negishi, *Org. Lett.* **2009**, *11*, 4092–4095.

[26] K. Singh, W. Trinh, R. Latifi, J. D. Weaver, *Org. Biomol. Chem.* **2019**, *17*, 1854–1861.

[27] Y. Cai, Y. Tang, L. Fan, Q. Lefebvre, H. Hou, M. Rueping, *ACS Catal.* **2018**, *8*, 9471–9476.

[28] S. H. Lim, J. Yi, G. M. Moon, C. S. Ra, K. Nahm, D. W. Cho, K. Kim, T. G. Hyung, U. C. Yoon, G. Y. Lee, S. Kim, J. Kim, P. S. Mariano, *J. Org. Chem.* **2014**, *79*, 6946–6958.

[29] Y. Miyake, Y. Ashida, K. Nakajima, Y. Nishibayashi, *Chem. Commun.* **2012**, *48*, 6966–6968.

[30] T. Rawner, E. Lutsker, C. A. Kaiser, O. Reiser, *ACS Catal.* **2018**, *8*, 3950–3956.

[31] A. Hossain, S. Engl, E. Lutsker, O. Reiser, *ACS Catal.* **2019**, *9*, 1103–1109.

[32] Y. Oe, Y. Uozumi, *Adv. Synth. Catal.* **2008**, *350*, 1771–1775.

[33] a) P. Kohls, D. Jadhav, G. Pandey, O. Reiser, *Org. Lett.* **2012**, *14*, 672–675; b) L. Ruiz Espelt, E. M. Wiensch, T. P. Yoon, *J. Org. Chem.* **2013**, *78*, 4107–4114.

[34] N. R. Paz, D. Rodríguez-Sosa, H. Valdés, R. Marticorena, D. Melián, M. B. Copano, C. C. González, A. J. Herrera, *Org. Lett.* **2015**, *17*, 2370–2373.

[35] F. Micheel, H. Haneke, *Peptidsynthesen nach dem Oxazolidinonverfahren* **1959**, *92*, 309–312.

[36] A. G. Zhdanko, A. V. Gulevich, V. G. Nenajdenko, *Tetrahedron* **2009**, *65*, 4692–4702.

[37] K. Ulbrich, Thesis, University of Regensburg, **2014**.

[38] N. Becker, E. M. Carreira, *Org. Lett.* **2007**, *9*, 3857–3858.

[39] T. Föll, J. Rehbein, O. Reiser, *Org. Lett.* **2018**, *20*, 5794–5798.

[40] O. V. Fedorov, M. D. Kosobokov, V. V. Levin, M. I. Struchkova, A. D. Dilman, *J. Org. Chem.* **2015**, *80*, 5870–5876.

[41] S. Wei, H. Du, *J. Am. Chem. Soc.* **2014**, *136*, 12261–12264.

[42] S. Mahboobi, W. Wiegrebe, *Arch. Pharm.* **1988**, *321*, 175–177.

[43] J. Strehl, G. Hilt, *Org. Lett.* **2019**, *21*, 5259–5263.

[44] S. Sprouse, K. A. King, P. J. Spellane, R. J. Watts, *J. Am. Chem. Soc.* **1984**, *106*, 6647–6653.

[45] R. K. Olsen, K. Ramasamy, *J. Org. Chem.* **1985**, *50*, 2264–2271.

[46] a) S. C. Welch, C. Chou, J. M. Gruber, J. M. Assercq, *J. Org. Chem.* **1985**, *50*, 2668–2676; b) Z. Xu, J. C. DiCesare, P. W. Baures, *J. Comb. Chem.* **2010**, *12*, 248–254;

[47] S. Hussain, F. Leipold, H. Man, E. Wells, S. P. France, K. R. Mulholland, G. Grogan, N. J. Turner, *ChemCatChem* **2015**, *7*, 579–583.

F. Appendix

1. GC-FID analysis

An example GC-FID spectrum of the reaction mixture of the photochemical *E/Z*-isomerization of *trans*-stilbene (**24**) is depicted below, using the following temperature program:

Starting temperature:	140 °C
Hold:	3 min
Heating rate:	16 °C/min
End temperature:	300 °C

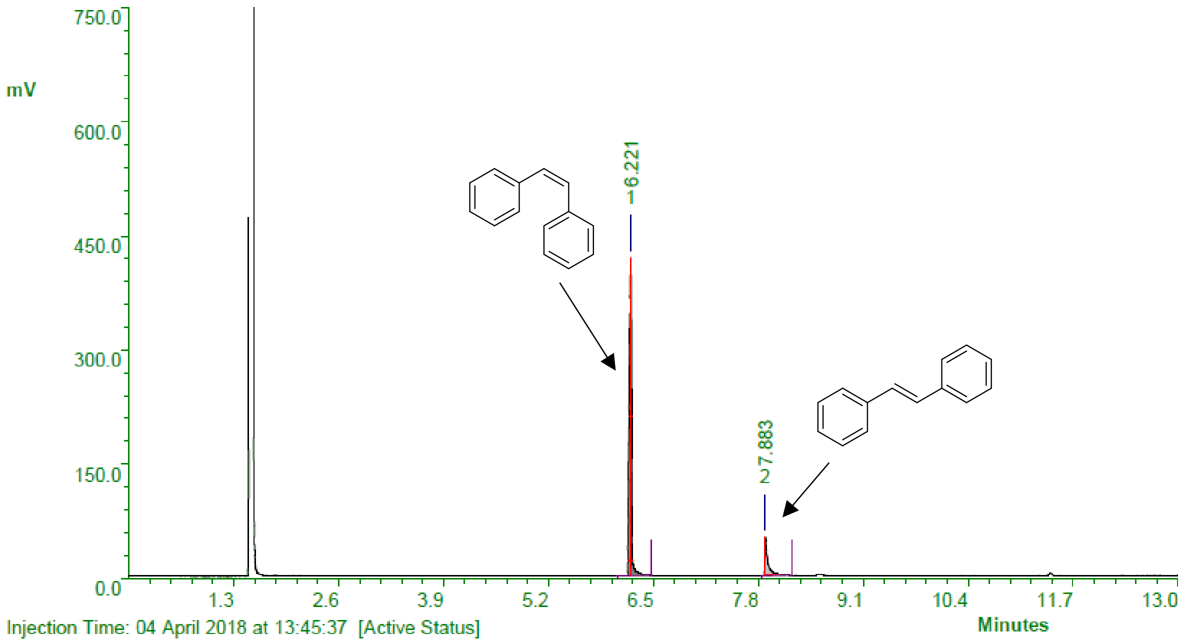

```
Injection Time: 04 April 2018 at 13:45:37  [Active Status]
Type: AUTOINJ   Injection Number: 53   Channel: Channel A   Acquisition Rate: 8Hz
Method File: C:\PW4\eic29485\0001_eic29485.mth   Baseline noise: (not calculated)
Standard File: (none)   Sequence File: C:\PW4\eic29485\eic29485.seq
```

```
Peak     RT         Area     %Ar   Conc.(Ar)        Height   M      Units   Name
   1  6.221      828.346   85.73 Not Calculated    418.372   1
   2  7.883      137.842   14.27 Not Calculated     50.571   1
```

2. NMR spectra

The upper images show the ^{1}H-NMR spectra whereas the lower images describe the ^{13}C-NMR spectra.

All compounds were dissolved in $CDCl_3$ unless otherwise stated.

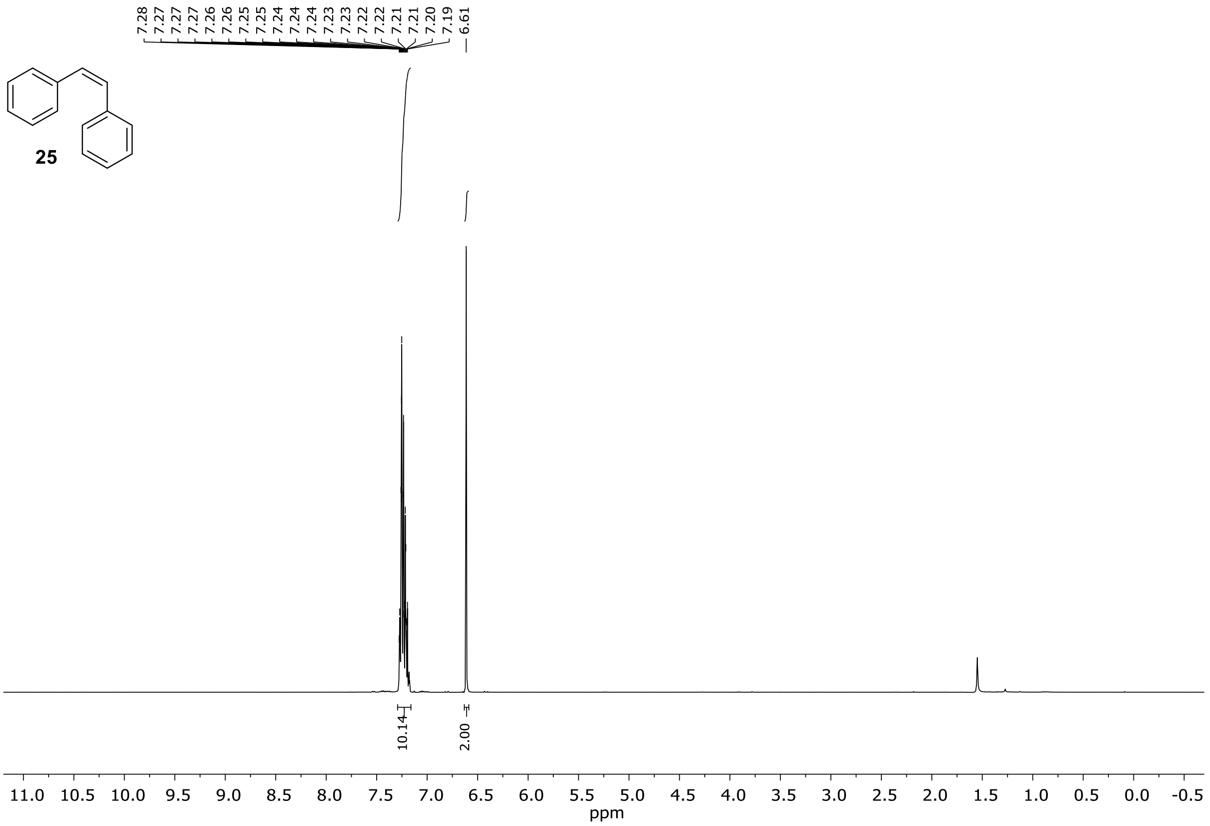
25

7.28
7.27
7.27
7.27
7.26
7.26
7.25
7.25
7.24
7.24
7.24
7.23
7.23
7.22
7.22
7.21
7.21
7.20
7.19
6.61
10.14
2.00
11.0 10.5 10.0 9.5 9.0 8.5 8.0 7.5 7.0 6.5 6.0 5.5 5.0 4.5 4.0 3.5 3.0 2.5 2.0 1.5 1.0 0.5 0.0 -0.5
ppm

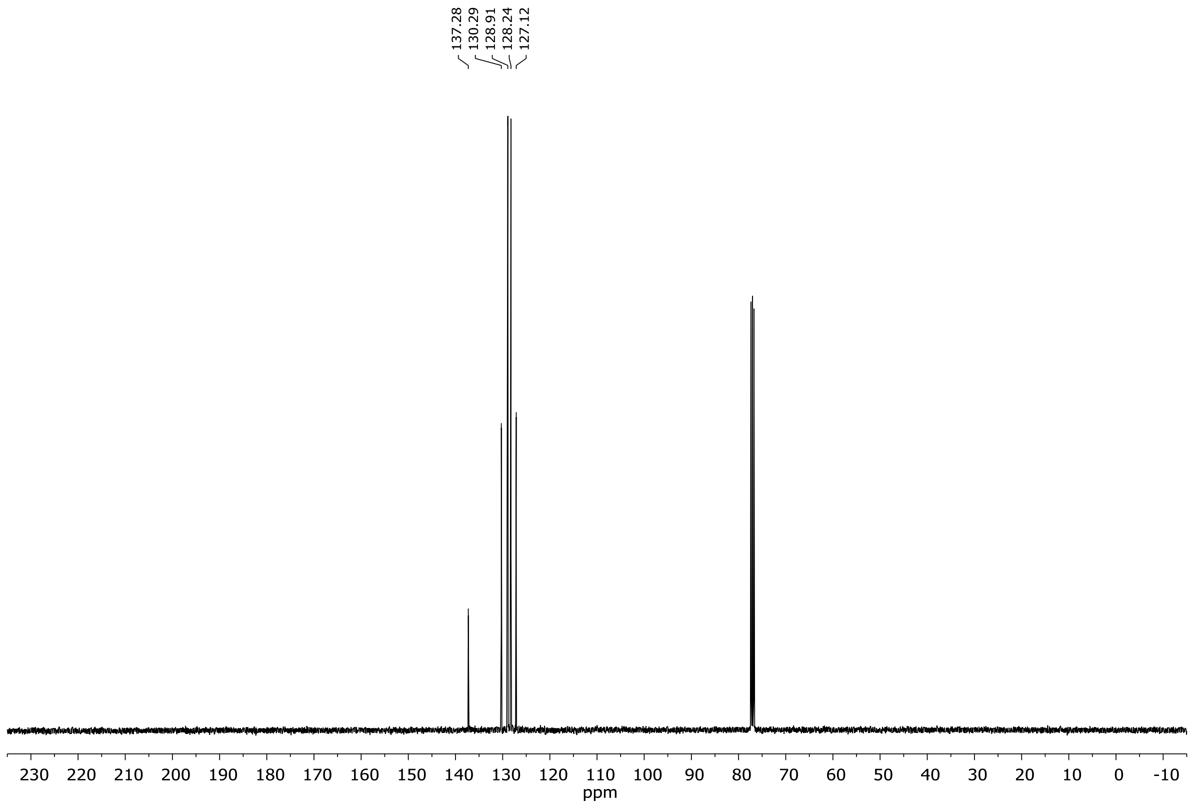
137.28
130.29
128.91
128.24
127.12
230 220 210 200 190 180 170 160 150 140 130 120 110 100 90 80 70 60 50 40 30 20 10 0 -10
ppm

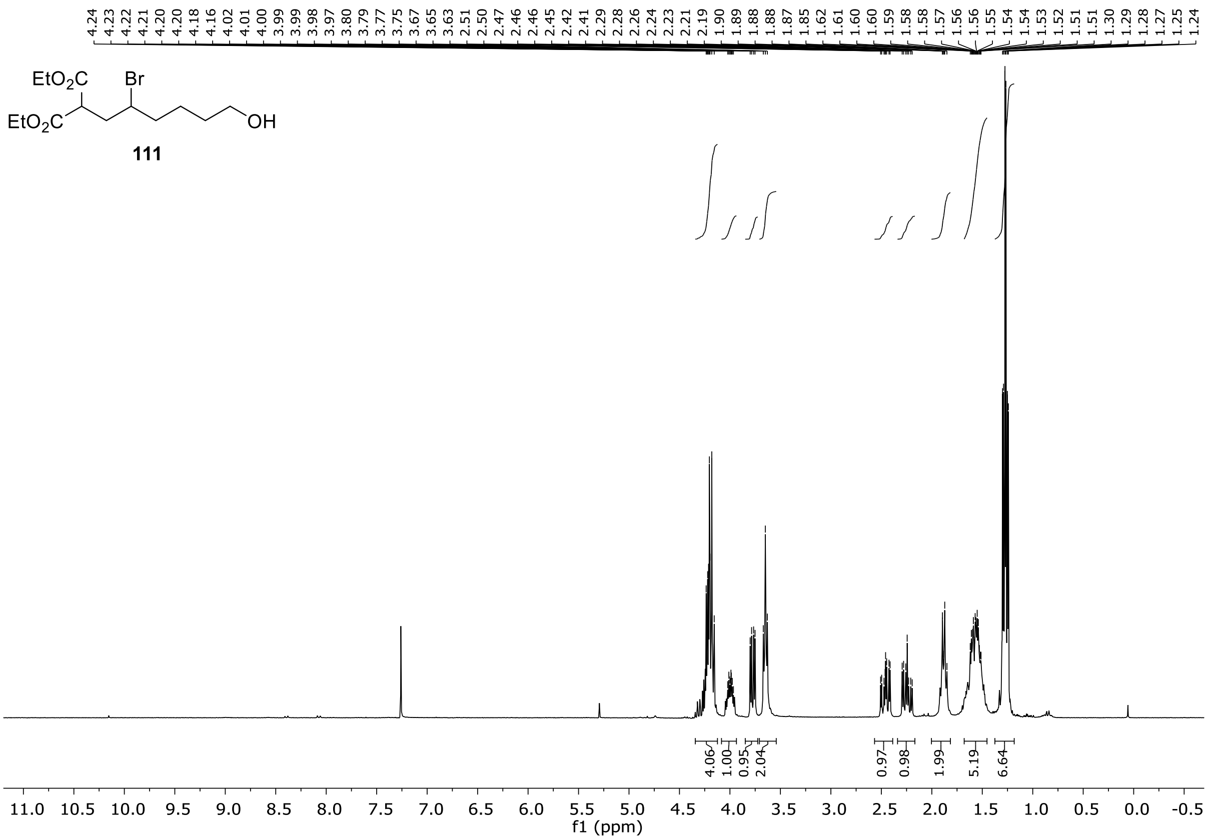
EtO2C
Br
EtO2C
OH
111
4.24 4.23 4.22 4.21 4.20 4.20 4.18 4.16 4.02 4.01 4.00 3.99 3.99 3.98 3.97 3.80 3.79 3.77 3.75 3.67 3.65 3.63 2.51 2.50 2.47 2.46 2.46 2.45 2.42 2.41 2.29 2.28 2.26 2.24 2.23 2.21 2.19 1.90 1.89 1.88 1.88 1.87 1.85 1.62 1.61 1.60 1.60 1.59 1.58 1.58 1.57 1.56 1.56 1.55 1.54 1.54 1.53 1.52 1.51 1.51 1.30 1.29 1.28 1.27 1.25 1.24
4.06
1.00
0.95
2.04
0.97
0.98
1.99
5.19
6.64
11.0 10.5 10.0 9.5 9.0 8.5 8.0 7.5 7.0 6.5 6.0 5.5 5.0 4.5 4.0 3.5 3.0 2.5 2.0 1.5 1.0 0.5 0.0 -0.5
f1 (ppm)

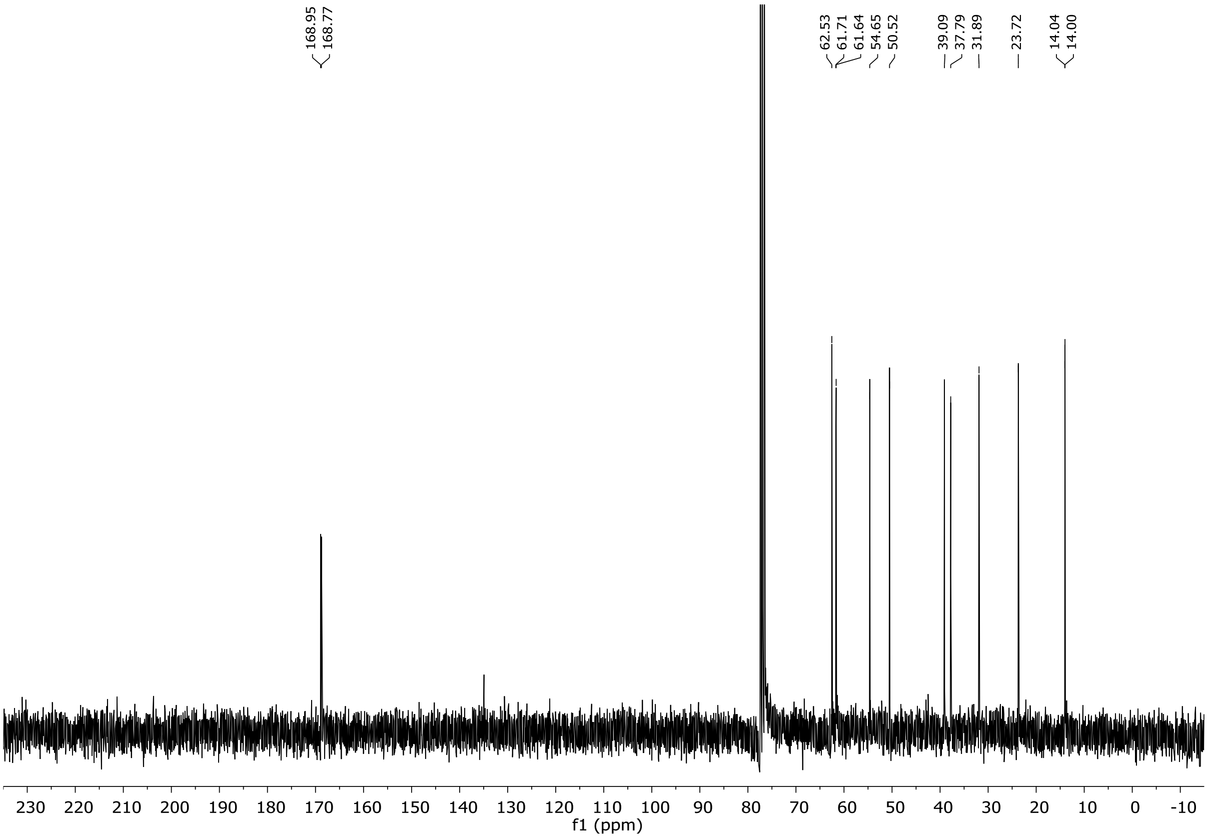
168.95
168.77
62.53
61.71
61.64
54.65
50.52
39.09
37.79
31.89
23.72
14.04
14.00
230 220 210 200 190 180 170 160 150 140 130 120 110 100 90 80 70 60 50 40 30 20 10 0 -10
f1 (ppm)

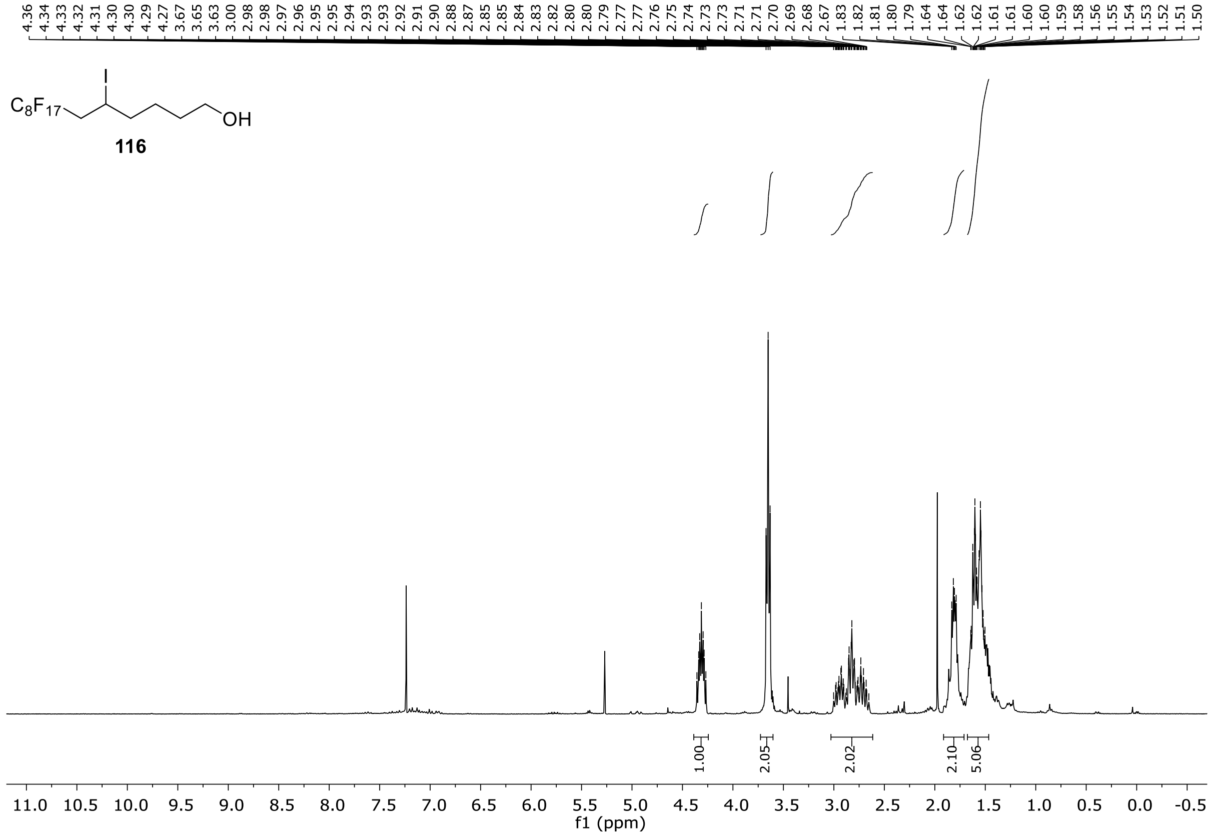
116
4.36
4.34
4.33
4.32
4.31
4.30
4.30
4.29
4.27
3.67
3.65
3.63
3.00
2.98
2.98
2.97
2.96
2.95
2.95
2.94
2.93
2.93
2.92
2.91
2.90
2.88
2.87
2.85
2.85
2.84
2.83
2.82
2.80
2.80
2.79
2.77
2.77
2.76
2.75
2.74
2.73
2.73
2.71
2.71
2.70
2.69
2.68
2.67
1.83
1.82
1.81
1.80
1.79
1.64
1.64
1.62
1.62
1.61
1.61
1.60
1.60
1.59
1.58
1.56
1.55
1.54
1.53
1.52
1.51
1.50
I
C8F17
OH
1.00
2.05
2.02
2.10
5.06
11.0 10.5 10.0 9.5 9.0 8.5 8.0 7.5 7.0 6.5 6.0 5.5 5.0 4.5 4.0 3.5 3.0 2.5 2.0 1.5 1.0 0.5 0.0 -0.5
f1 (ppm)

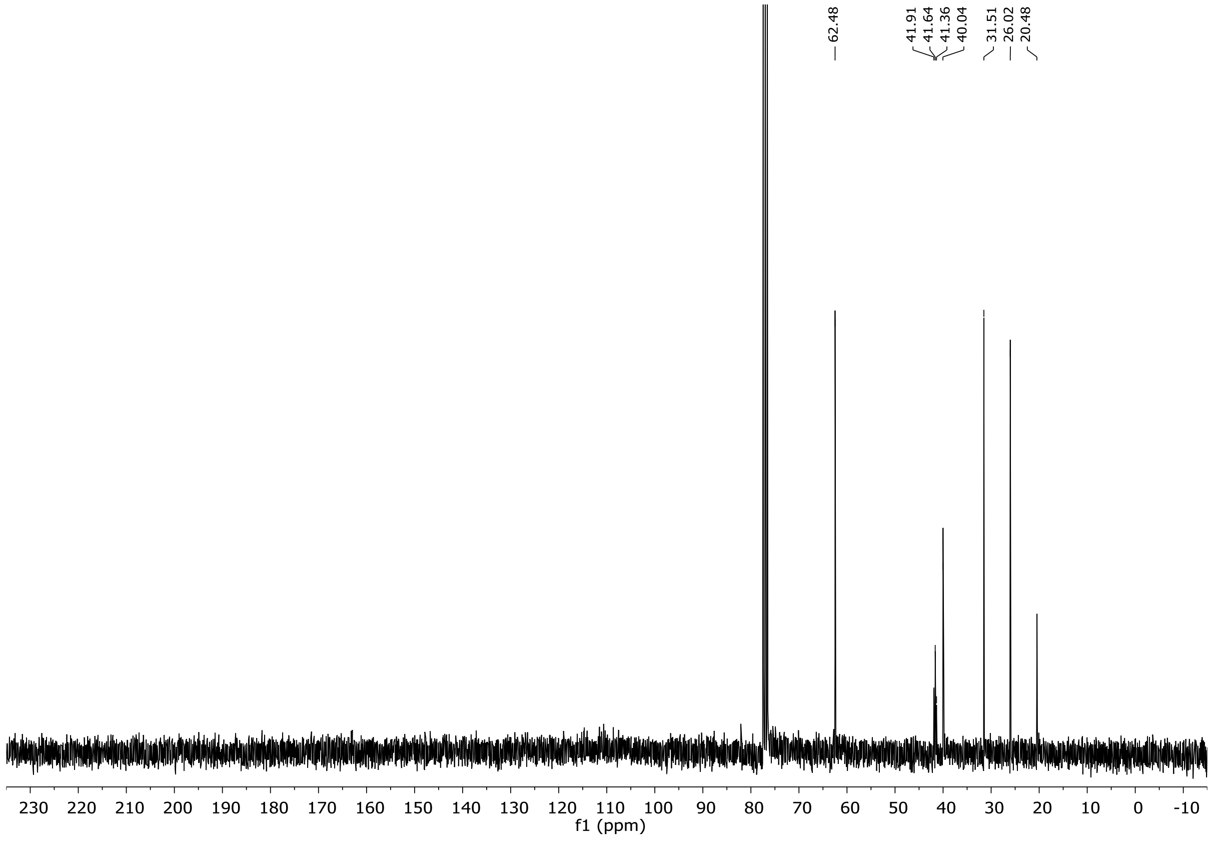
62.48
41.91
41.64
41.36
40.04
31.51
26.02
20.48
230 220 210 200 190 180 170 160 150 140 130 120 110 100 90 80 70 60 50 40 30 20 10 0 -10
f1 (ppm)

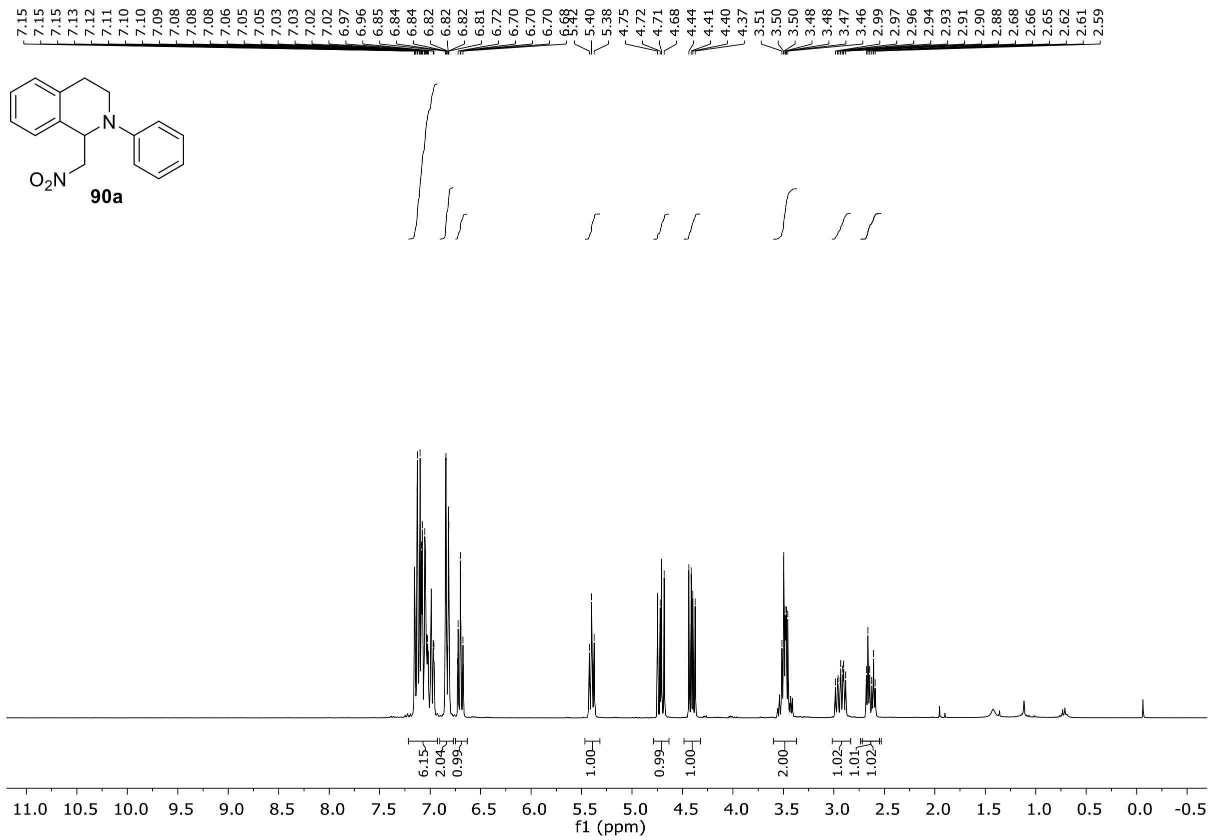
7.15
7.15
7.15
7.13
7.12
7.11
7.10
7.10
7.09
7.08
7.08
7.08
7.06
7.05
7.05
7.03
7.03
7.02
7.02
6.97
6.96
6.85
6.84
6.82
6.82
6.82
6.81
6.72
6.70
6.70
6.70
6.68
5.42
5.40
5.38
4.75
4.72
4.71
4.68
4.44
4.41
4.40
4.37
3.51
3.50
3.50
3.48
3.48
3.47
3.46
2.99
2.97
2.96
2.94
2.93
2.91
2.90
2.88
2.68
2.66
2.65
2.62
2.61
2.59
N
O_2N
90a
6.15
2.04
0.99
1.00
0.99
1.00
2.00
1.02
1.01
1.02
11.0
10.5
10.0
9.5
9.0
8.5
8.0
7.5
7.0
6.5
6.0
5.5
5.0
4.5
4.0
3.5
3.0
2.5
2.0
1.5
1.0
0.5
0.0
-0.5
f1 (ppm)

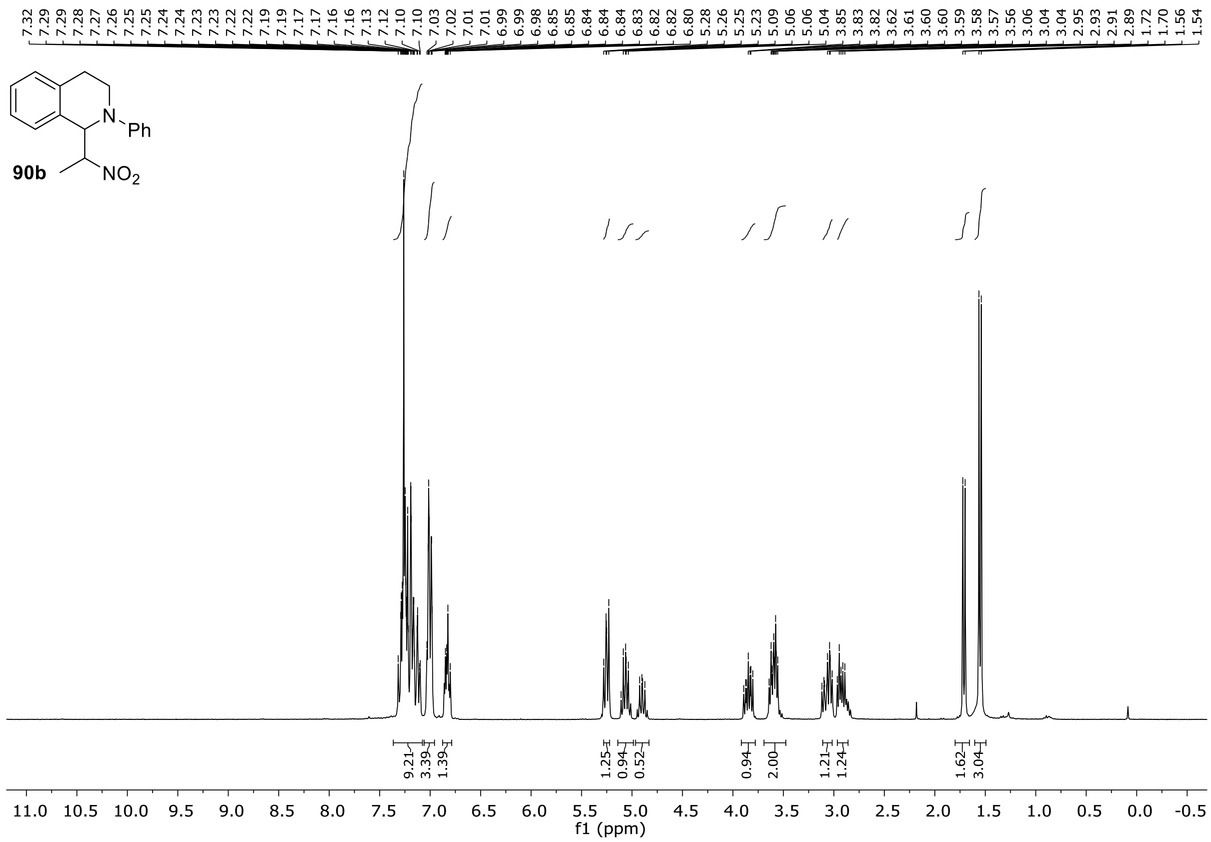

90b

N
Ph
NO2
7.32 7.29 7.29 7.28 7.27 7.26 7.25 7.25 7.24 7.24 7.23 7.23 7.22 7.22 7.19 7.19 7.17 7.17 7.16 7.16 7.13 7.12 7.10 7.10 7.03 7.02 7.01 7.01 6.99 6.99 6.98 6.85 6.85 6.84 6.84 6.84 6.83 6.82 6.82 6.80 5.28 5.26 5.25 5.23 5.09 5.06 5.06 5.04 3.85 3.83 3.82 3.62 3.61 3.60 3.60 3.59 3.58 3.57 3.56 3.06 3.04 3.04 2.95 2.93 2.91 2.89 1.72 1.70 1.56 1.54
9.21
3.39
1.39
1.25
0.94
0.52
0.94
2.00
1.21
1.24
1.62
3.04
11.0 10.5 10.0 9.5 9.0 8.5 8.0 7.5 7.0 6.5 6.0 5.5 5.0 4.5 4.0 3.5 3.0 2.5 2.0 1.5 1.0 0.5 0.0 -0.5
f1 (ppm)

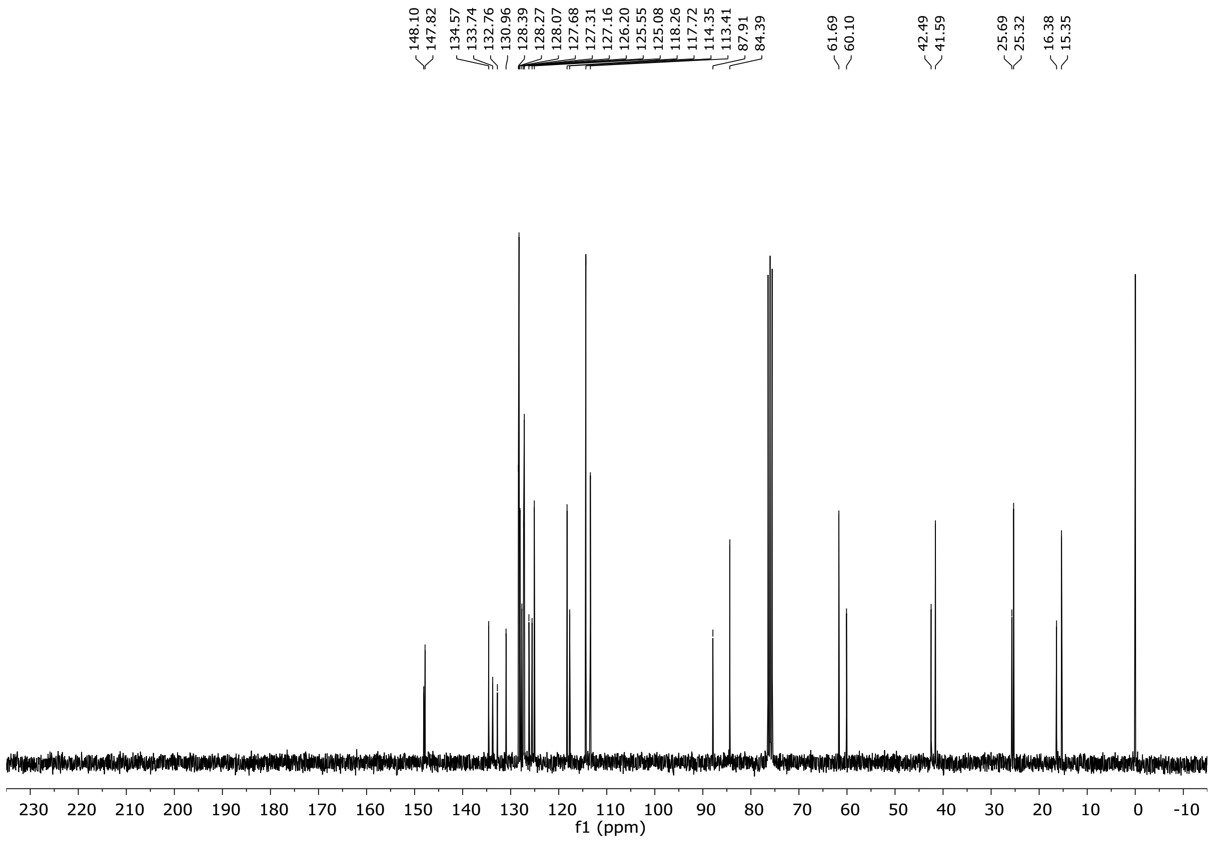

148.10 147.82 134.57 133.74 132.76 130.96 128.39 128.27 128.07 127.68 127.31 127.16 126.20 125.55 125.08 118.26 117.72 114.35 113.41 87.91 84.39 61.69 60.10 42.49 41.59 25.69 25.32 16.38 15.35
230 220 210 200 190 180 170 160 150 140 130 120 110 100 90 80 70 60 50 40 30 20 10 0 -10
f1 (ppm)

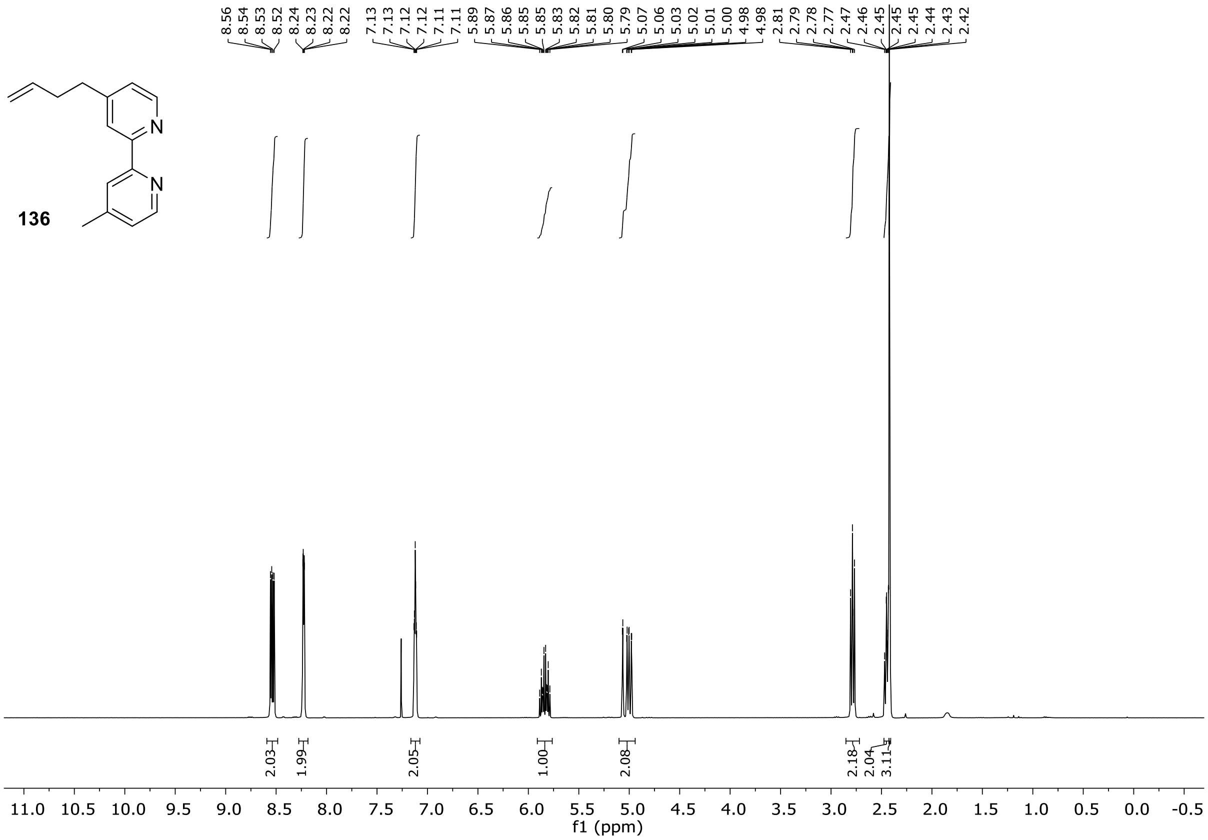
136
8.56
8.54
8.53
8.52
8.24
8.23
8.22
8.22
7.13
7.13
7.12
7.12
7.11
7.11
5.89
5.87
5.86
5.85
5.85
5.83
5.82
5.81
5.80
5.79
5.07
5.06
5.03
5.02
5.01
5.00
4.98
4.98
2.81
2.79
2.78
2.77
2.47
2.46
2.45
2.45
2.45
2.44
2.43
2.42
N
N
2.03
1.99
2.05
1.00
2.08
2.18
2.04
3.11
11.0
10.5
10.0
9.5
9.0
8.5
8.0
7.5
7.0
6.5
6.0
5.5
5.0
4.5
4.0
3.5
3.0
2.5
2.0
1.5
1.0
0.5
0.0
-0.5
f1 (ppm)

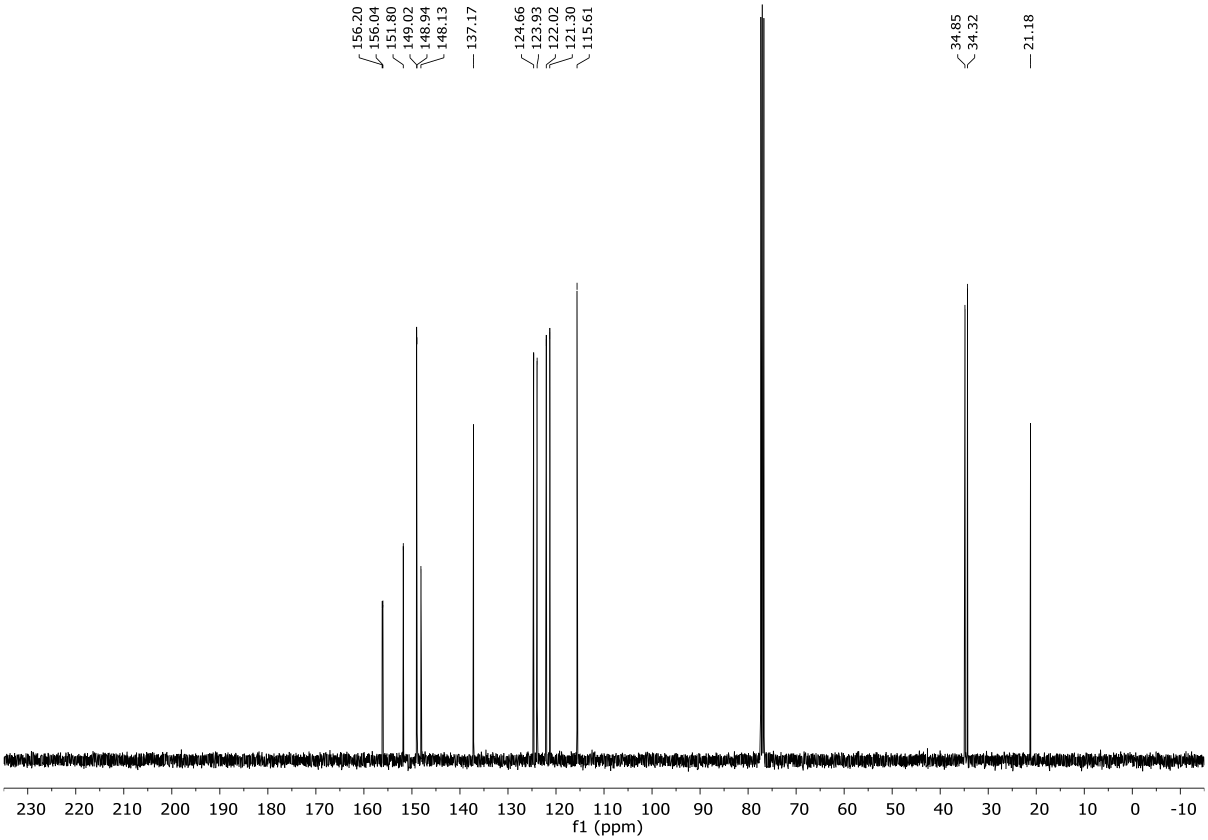
156.20
156.04
151.80
149.02
148.94
148.13
137.17
124.66
123.93
122.02
121.30
115.61
34.85
34.32
21.18
230
220
210
200
190
180
170
160
150
140
130
120
110
100
90
80
70
60
50
40
30
20
10
0
-10
f1 (ppm)

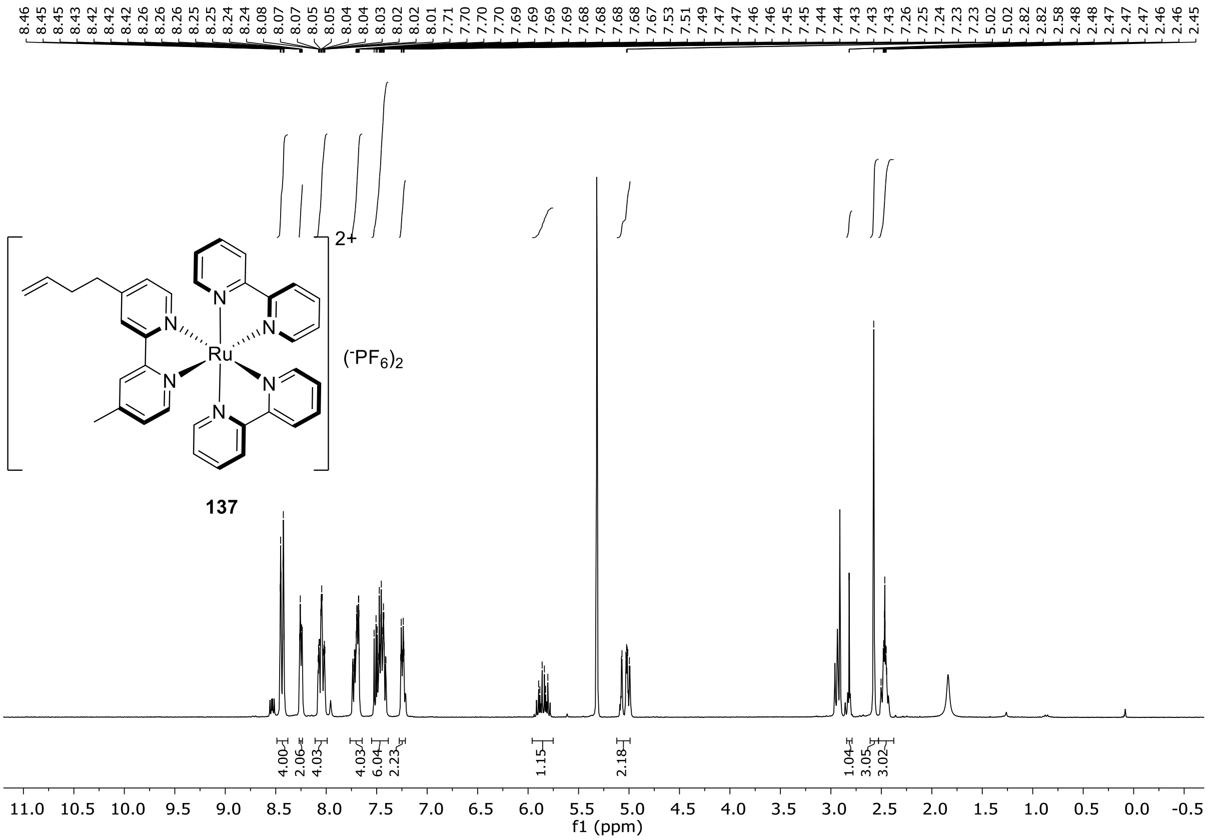
8.46
8.45
8.45
8.43
8.42
8.42
8.42
8.26
8.26
8.26
8.25
8.25
8.24
8.24
8.08
8.07
8.07
8.05
8.05
8.04
8.04
8.03
8.02
8.02
8.01
7.71
7.70
7.70
7.70
7.69
7.69
7.69
7.69
7.68
7.68
7.68
7.68
7.67
7.53
7.51
7.49
7.47
7.47
7.46
7.46
7.45
7.45
7.44
7.44
7.43
7.43
7.43
7.26
7.25
7.24
7.23
7.23
5.02
5.02
2.82
2.82
2.58
2.48
2.48
2.47
2.47
2.47
2.46
2.46
2.45
2+
N
N
Ru
N
N
N
N
($^-$PF$_6$)$_2$
4.00
2.06
4.03
4.03
6.04
2.23
1.15
2.18
1.04
3.05
3.02
11.0
10.5
10.0
9.5
9.0
8.5
8.0
7.5
7.0
6.5
6.0
5.5
5.0
4.5
4.0
3.5
3.0
2.5
2.0
1.5
1.0
0.5
0.0
-0.5
f1 (ppm)

137

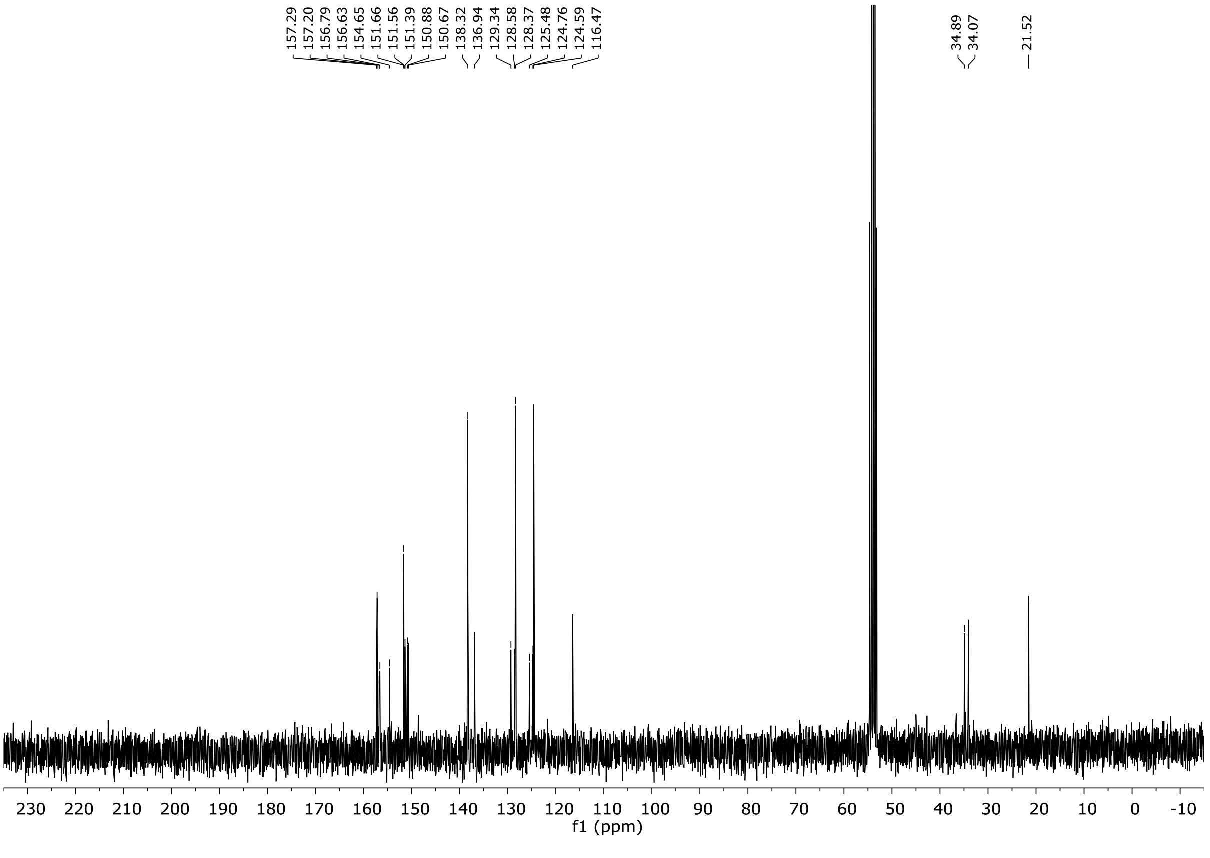
157.29
157.20
156.79
156.63
154.65
151.66
151.56
151.39
150.88
150.67
138.32
136.94
129.34
128.58
128.37
125.48
124.76
124.59
116.47
34.89
34.07
21.52
230
220
210
200
190
180
170
160
150
140
130
120
110
100
90
80
70
60
50
40
30
20
10
0
-10
f1 (ppm)

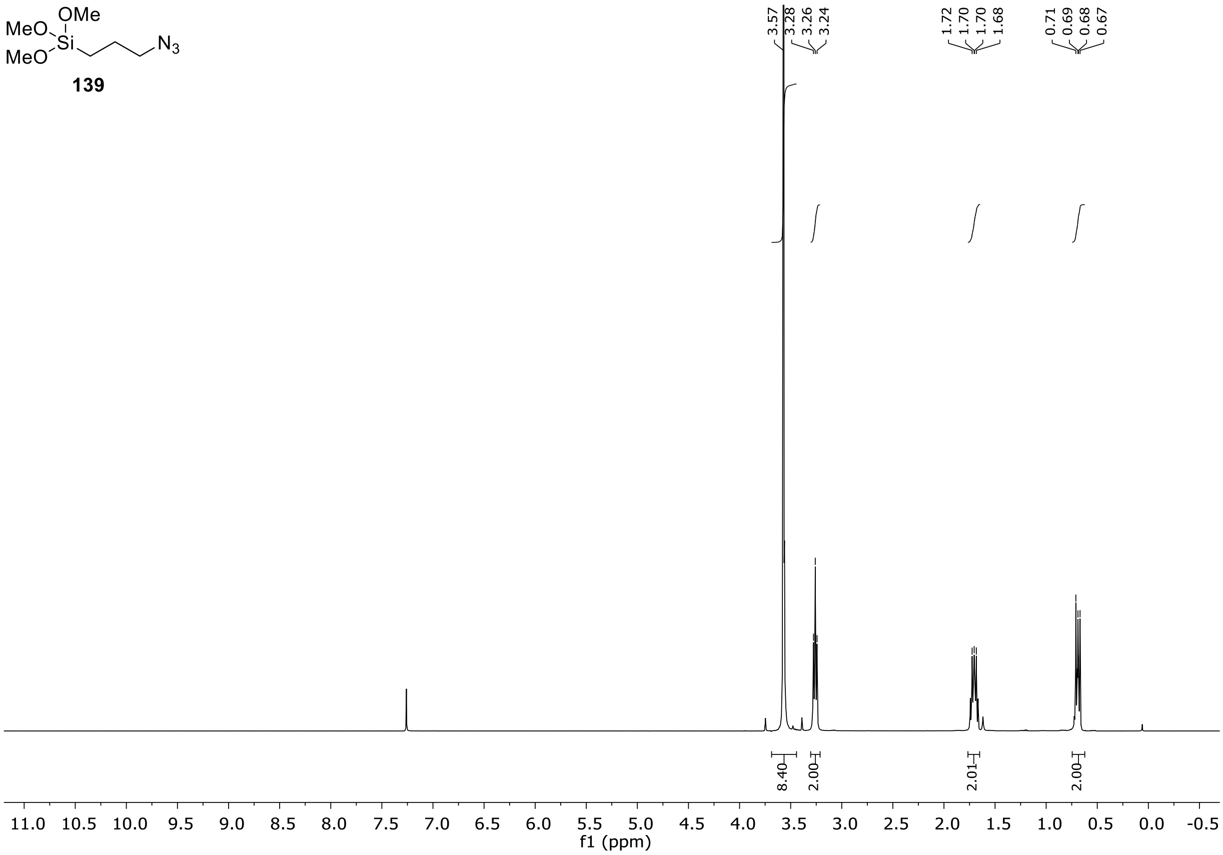

139

MeO
OMe
MeO
Si
N3
3.57
3.28
3.26
3.24
1.72
1.70
1.70
1.68
0.71
0.69
0.68
0.67
8.40
2.00
2.01
2.00
11.0 10.5 10.0 9.5 9.0 8.5 8.0 7.5 7.0 6.5 6.0 5.5 5.0 4.5 4.0 3.5 3.0 2.5 2.0 1.5 1.0 0.5 0.0 -0.5
f1 (ppm)

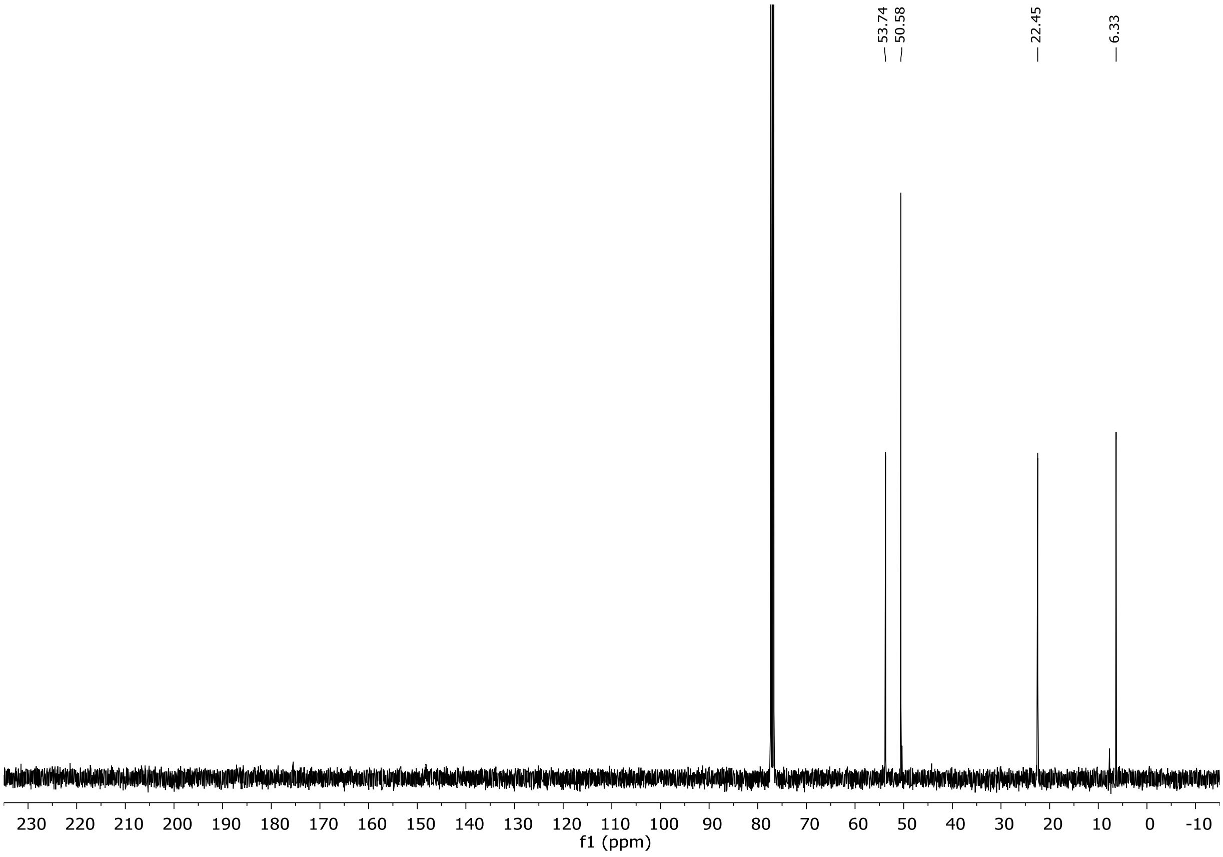

53.74
50.58
22.45
6.33
230 220 210 200 190 180 170 160 150 140 130 120 110 100 90 80 70 60 50 40 30 20 10 0 -10
f1 (ppm)

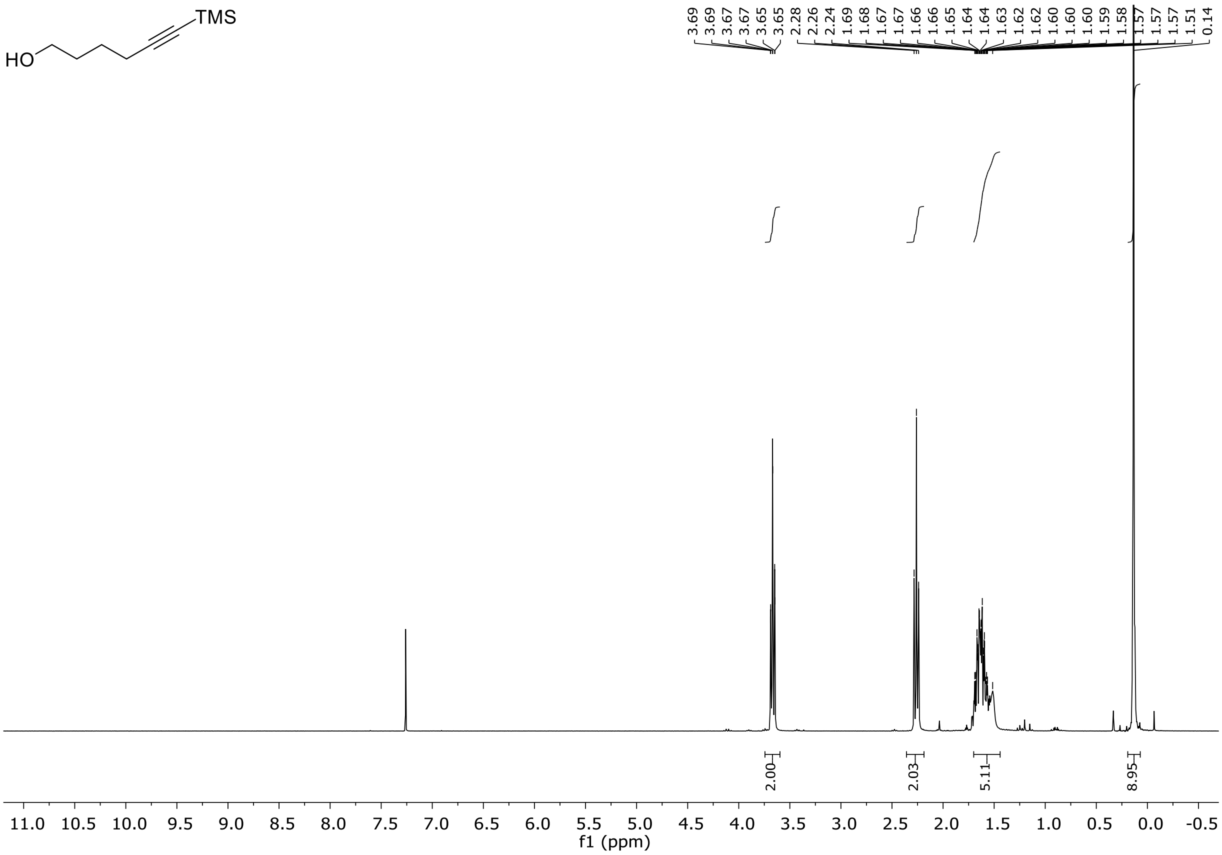
TMS
HO
3.69
3.69
3.67
3.67
3.65
3.65
2.28
2.26
2.24
1.69
1.68
1.67
1.67
1.66
1.66
1.65
1.64
1.64
1.63
1.62
1.62
1.60
1.60
1.60
1.59
1.58
1.57
1.57
1.57
1.51
0.14
2.00
2.03
5.11
8.95
11.0 10.5 10.0 9.5 9.0 8.5 8.0 7.5 7.0 6.5 6.0 5.5 5.0 4.5 4.0 3.5 3.0 2.5 2.0 1.5 1.0 0.5 0.0 -0.5
f1 (ppm)

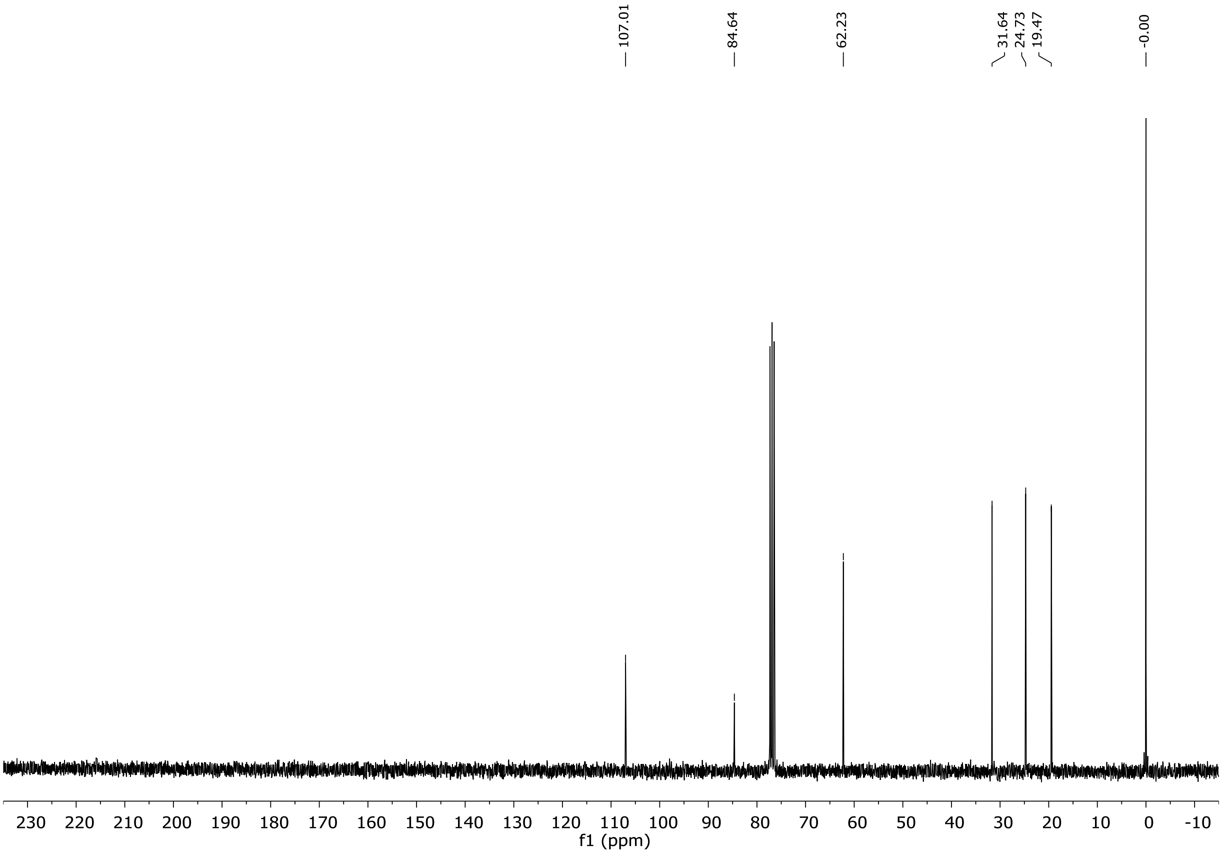
107.01
84.64
62.23
31.64
24.73
19.47
-0.00
230 220 210 200 190 180 170 160 150 140 130 120 110 100 90 80 70 60 50 40 30 20 10 0 -10
f1 (ppm)

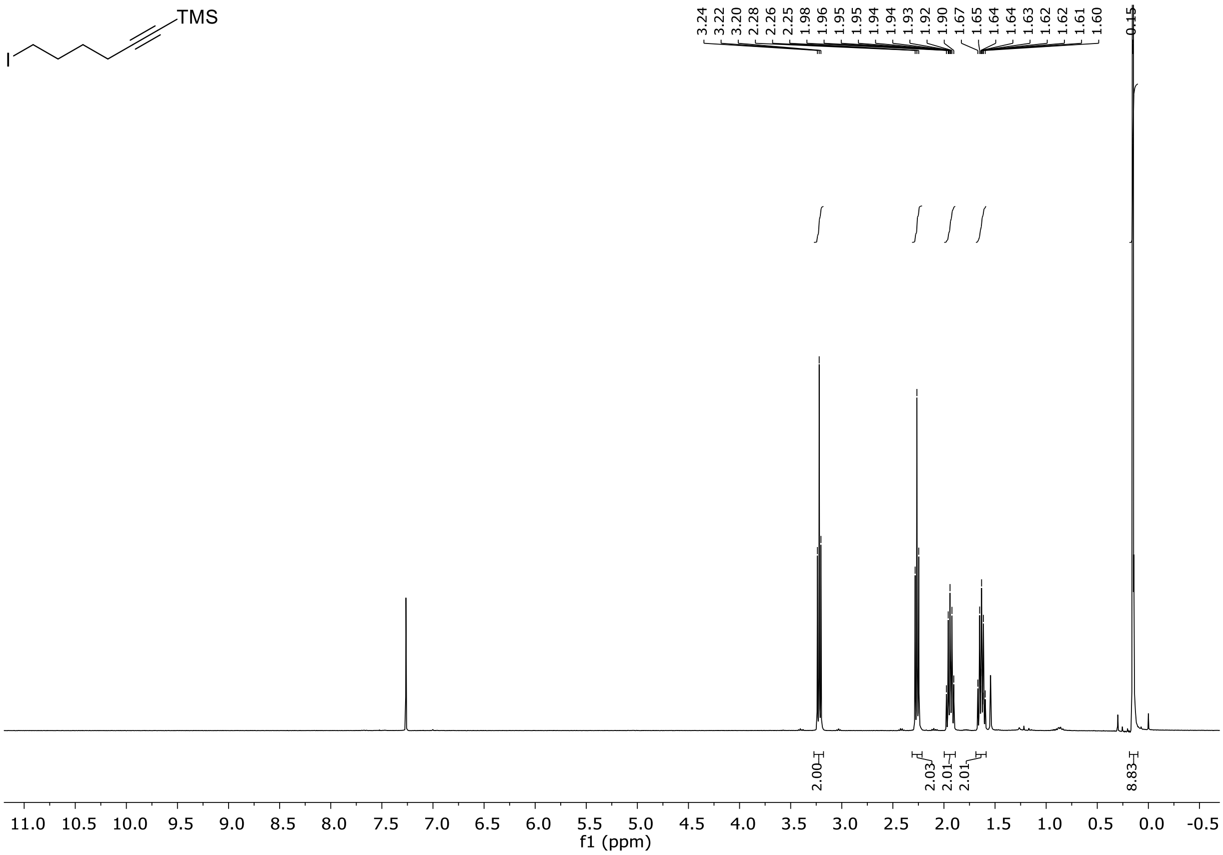
TMS
I
3.24
3.22
3.20
2.28
2.26
2.25
1.98
1.96
1.95
1.95
1.94
1.94
1.93
1.92
1.90
1.67
1.65
1.64
1.64
1.63
1.62
1.62
1.61
1.60
0.15
2.00
2.03
2.01
2.01
8.83
11.0 10.5 10.0 9.5 9.0 8.5 8.0 7.5 7.0 6.5 6.0 5.5 5.0 4.5 4.0 3.5 3.0 2.5 2.0 1.5 1.0 0.5 0.0 -0.5
f1 (ppm)

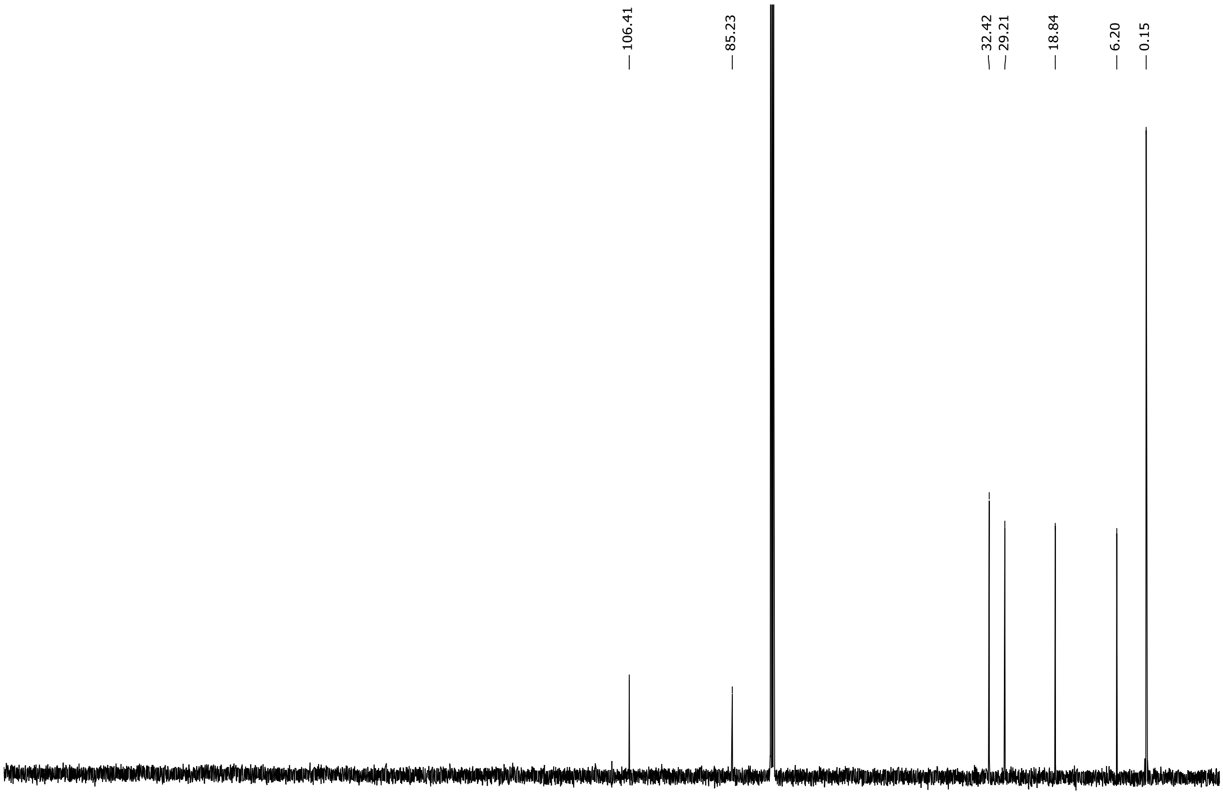
106.41
85.23
32.42
29.21
18.84
6.20
0.15
230 220 210 200 190 180 170 160 150 140 130 120 110 100 90 80 70 60 50 40 30 20 10 0 -10
f1 (ppm)

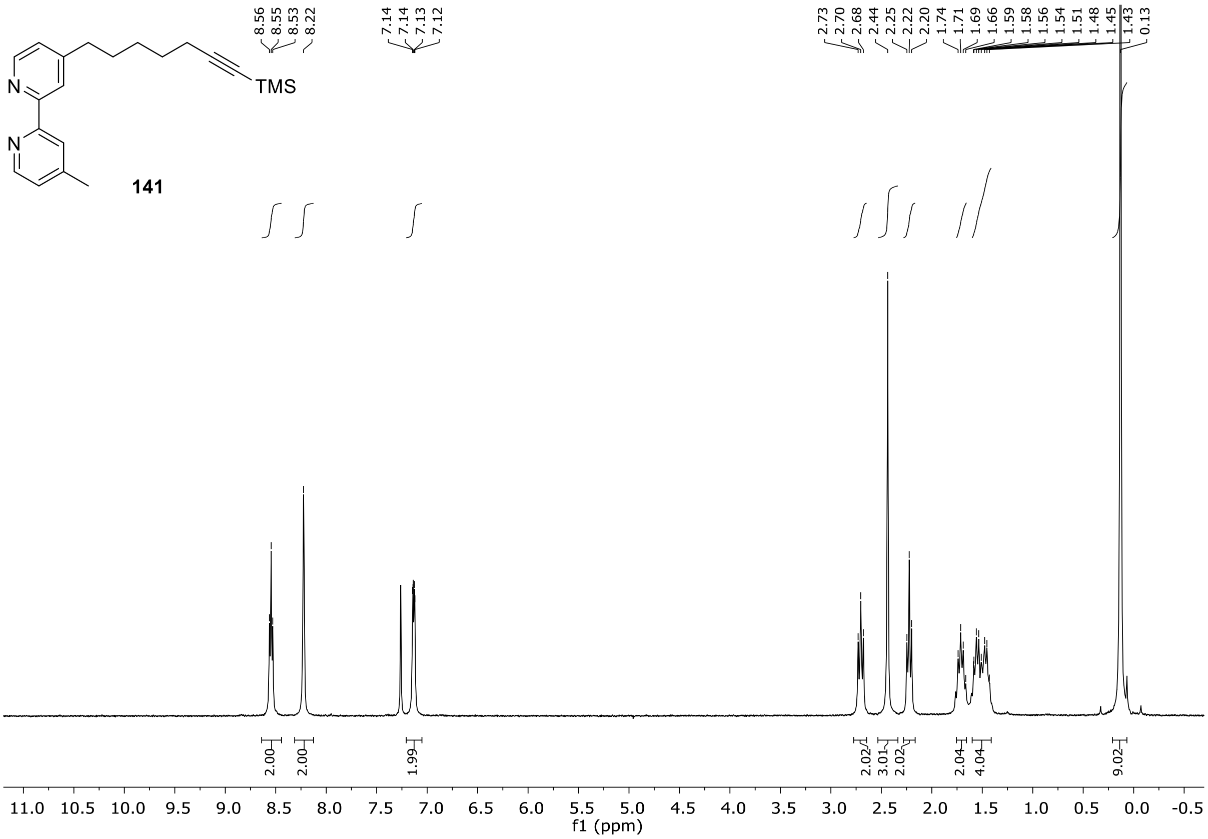
N
N
TMS
141
8.56
8.55
8.53
8.22
7.14
7.14
7.13
7.12
2.73
2.70
2.68
2.44
2.25
2.22
2.20
1.74
1.71
1.69
1.66
1.59
1.58
1.56
1.54
1.51
1.48
1.45
1.43
0.13
2.00
2.00
1.99
2.02
3.01
2.02
2.04
4.04
9.02
11.0 10.5 10.0 9.5 9.0 8.5 8.0 7.5 7.0 6.5 6.0 5.5 5.0 4.5 4.0 3.5 3.0 2.5 2.0 1.5 1.0 0.5 0.0 -0.5
f1 (ppm)

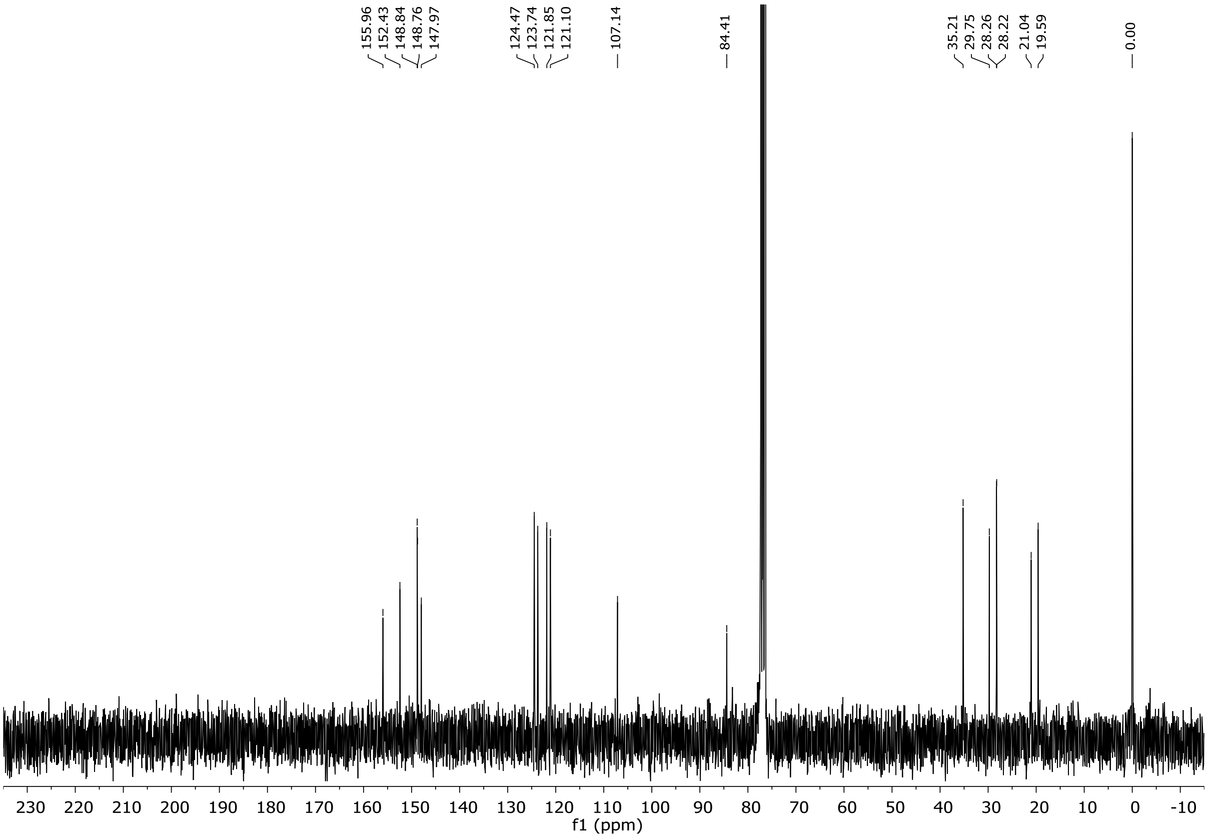
155.96
152.43
148.84
148.76
147.97
124.47
123.74
121.85
121.10
107.14
84.41
35.21
29.75
28.26
28.22
21.04
19.59
0.00
230 220 210 200 190 180 170 160 150 140 130 120 110 100 90 80 70 60 50 40 30 20 10 0 -10
f1 (ppm)

^{1}H-NMR (400 MHz, CD$_3$OD):

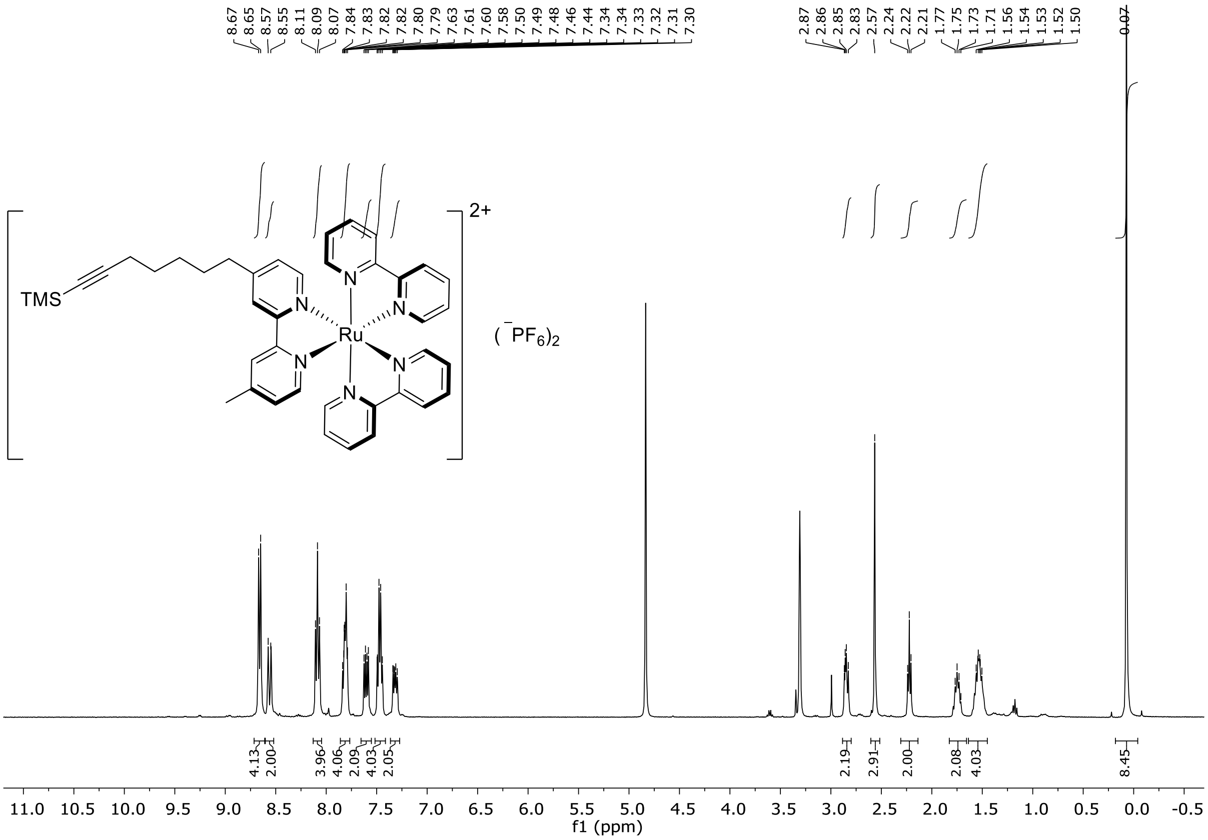

^{13}C-NMR (101 MHz, CD$_3$OD):

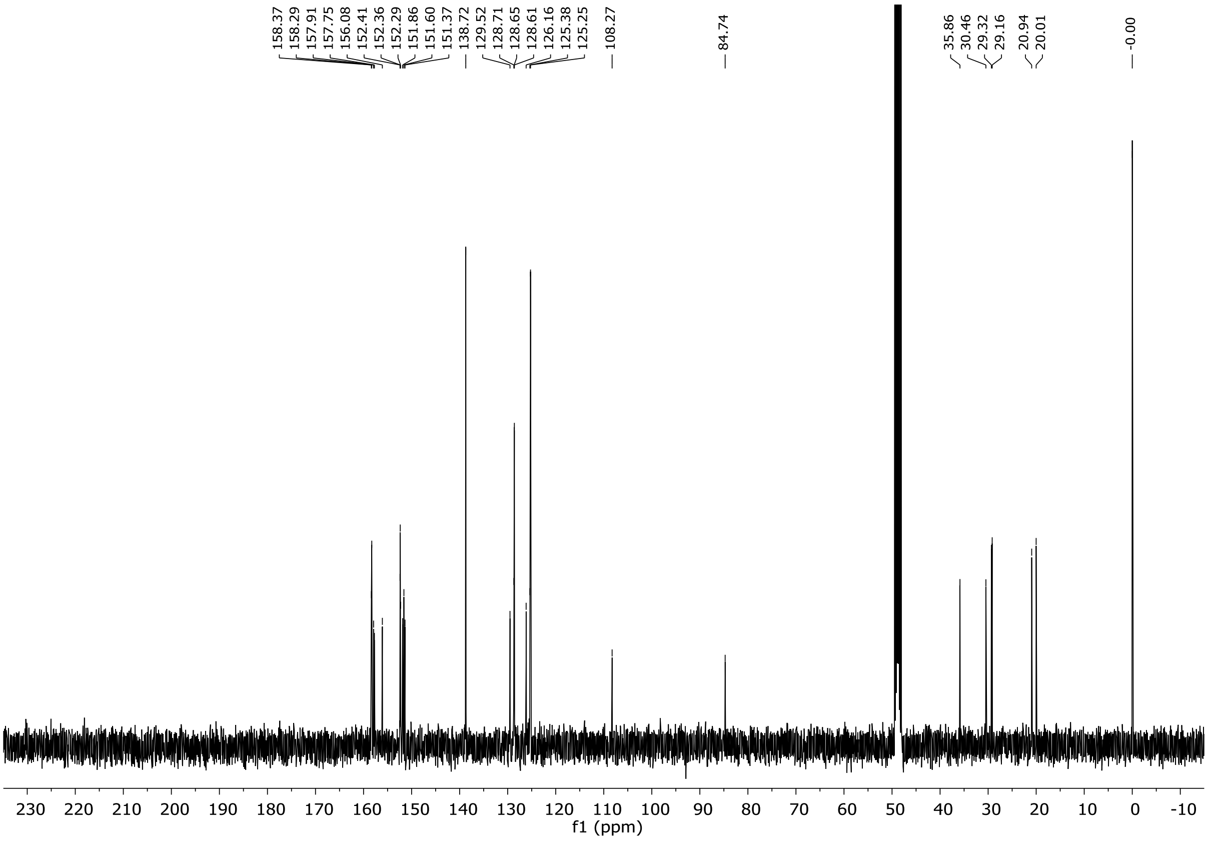

^{1}H-NMR (300 MHz, CD_2Cl_2):

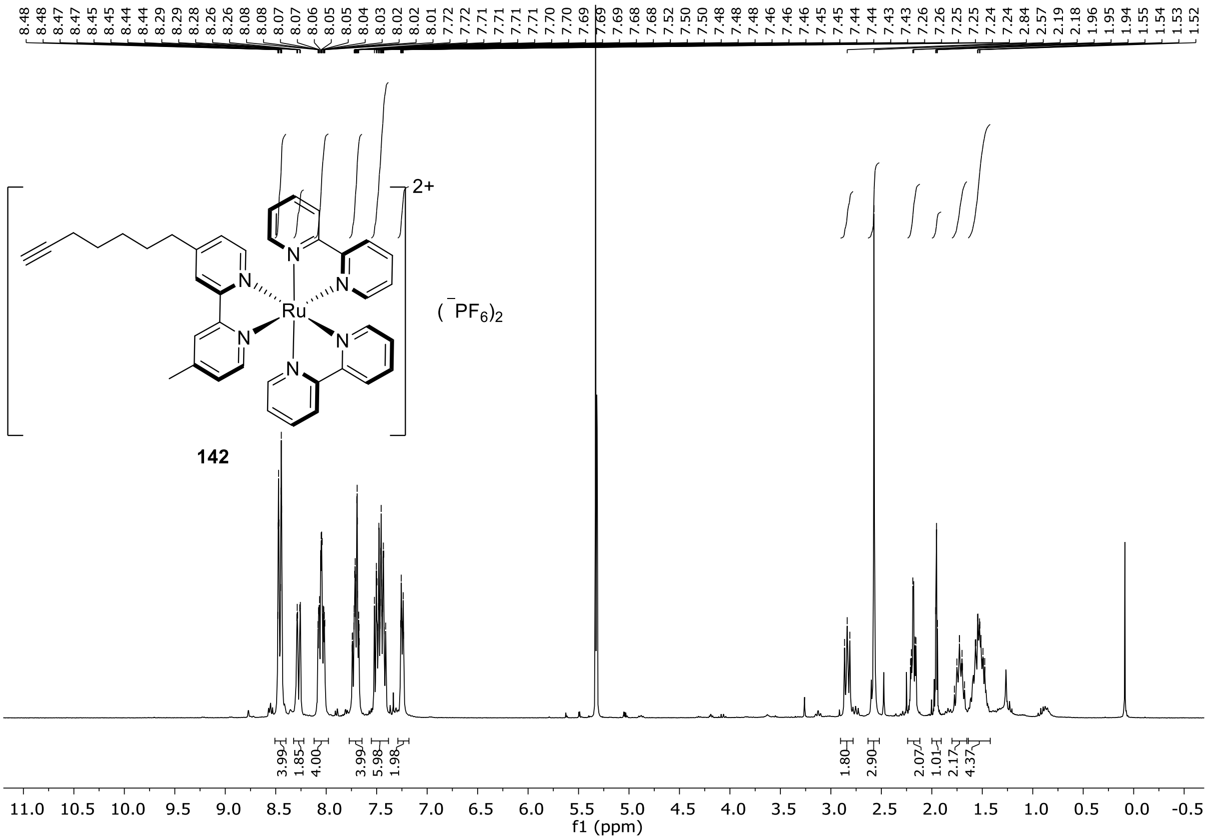
142

^{13}C-NMR (75 MHz, CD_2Cl_2):

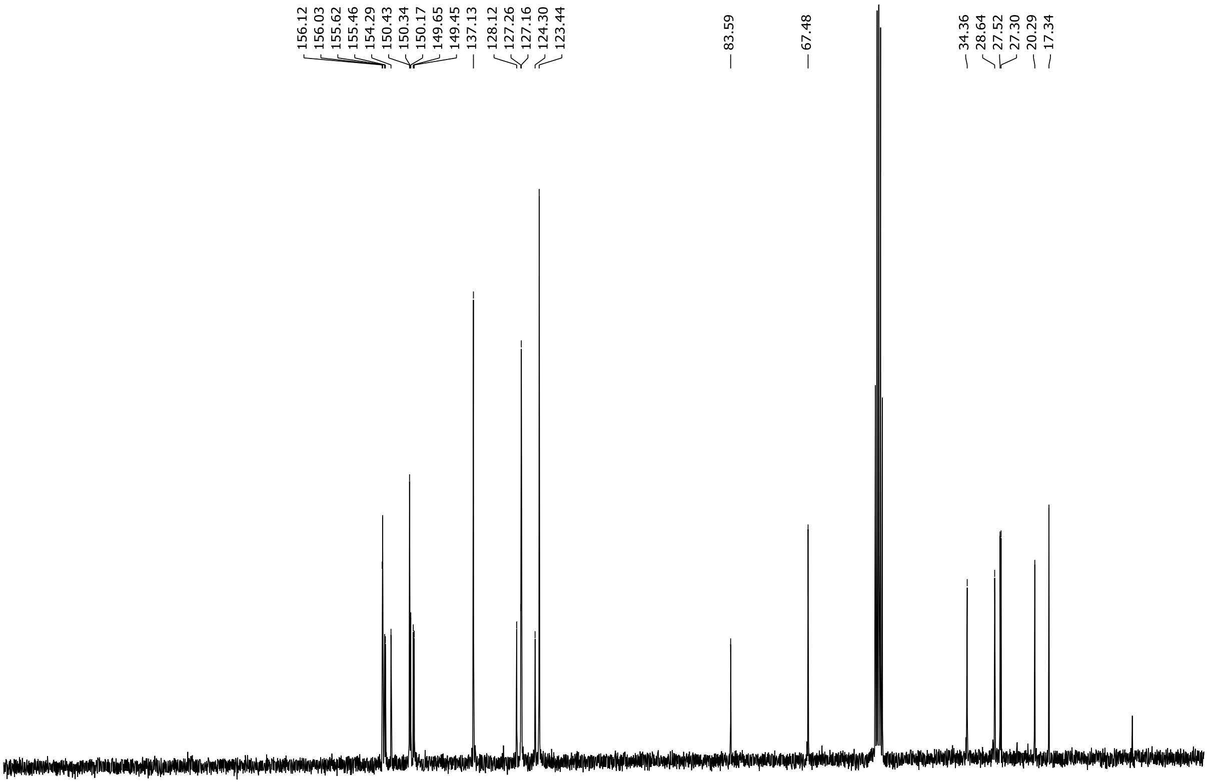

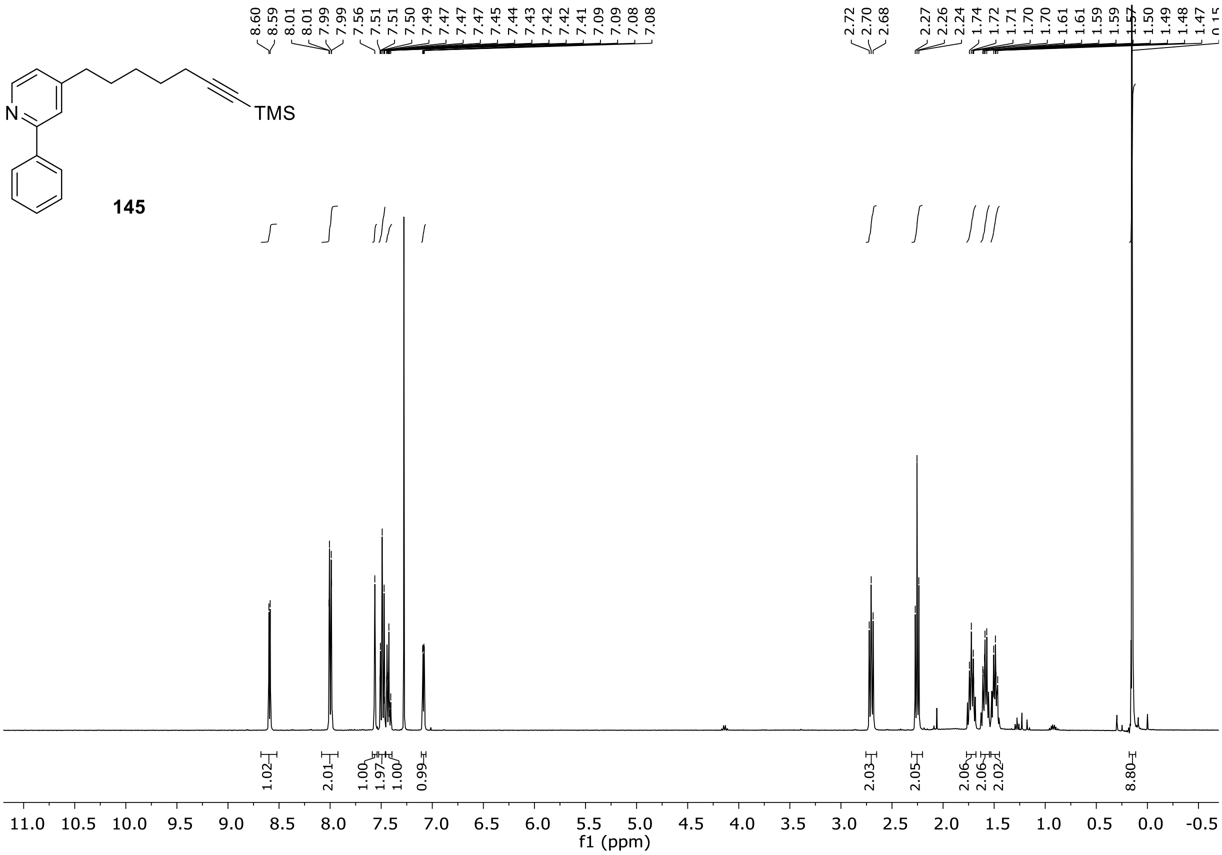
8.60
8.59
8.01
8.01
7.99
7.99
7.56
7.51
7.51
7.50
7.49
7.47
7.47
7.47
7.45
7.44
7.43
7.42
7.42
7.41
7.09
7.09
7.08
7.08
2.72
2.70
2.68
2.27
2.26
2.24
1.74
1.72
1.71
1.70
1.70
1.61
1.61
1.59
1.59
1.57
1.50
1.49
1.48
1.47
N
TMS
145
1.02
2.01
1.00
1.97
1.00
0.99
2.03
2.05
2.06
2.06
2.02
8.80
11.0 10.5 10.0 9.5 9.0 8.5 8.0 7.5 7.0 6.5 6.0 5.5 5.0 4.5 4.0 3.5 3.0 2.5 2.0 1.5 1.0 0.5 0.0 -0.5
f1 (ppm)

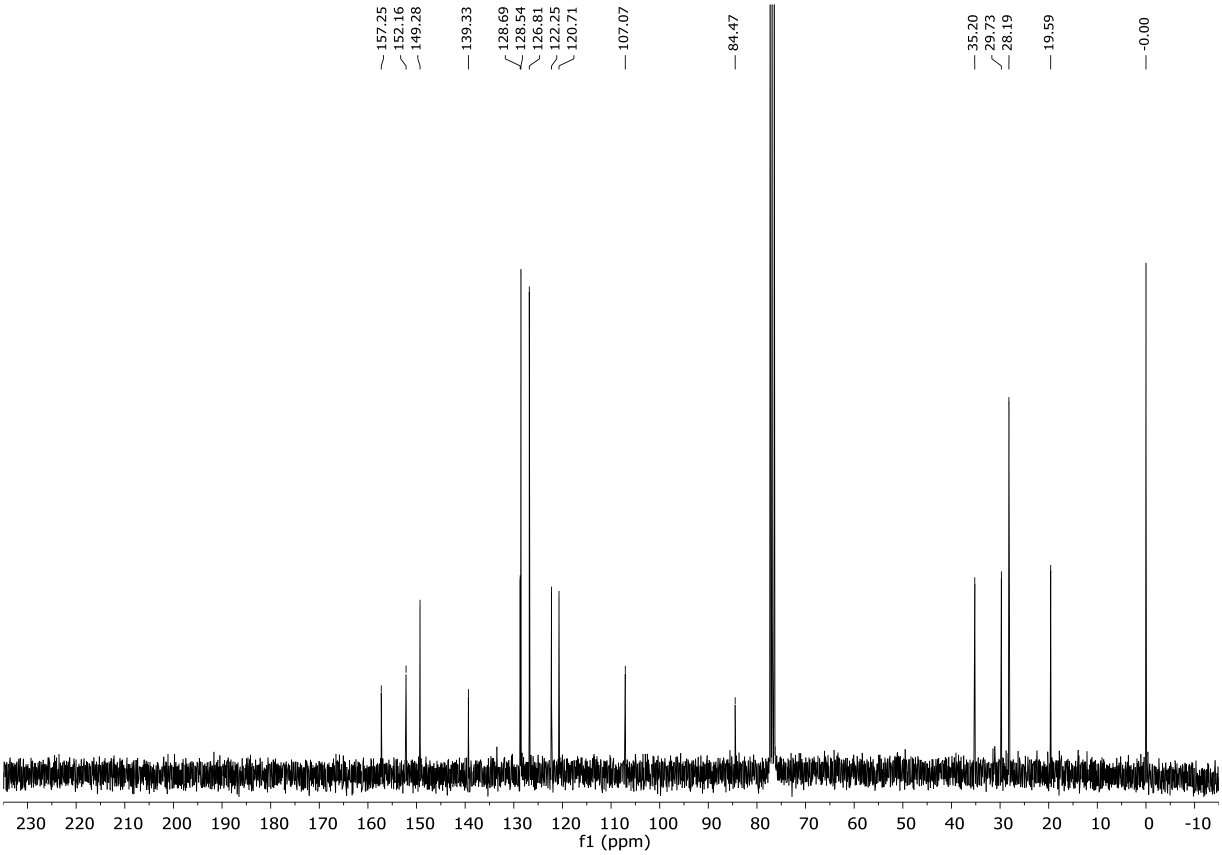
157.25
152.16
149.28
139.33
128.69
128.54
126.81
122.25
120.71
107.07
84.47
35.20
29.73
28.19
19.59
-0.00
230 220 210 200 190 180 170 160 150 140 130 120 110 100 90 80 70 60 50 40 30 20 10 0 -10
f1 (ppm)

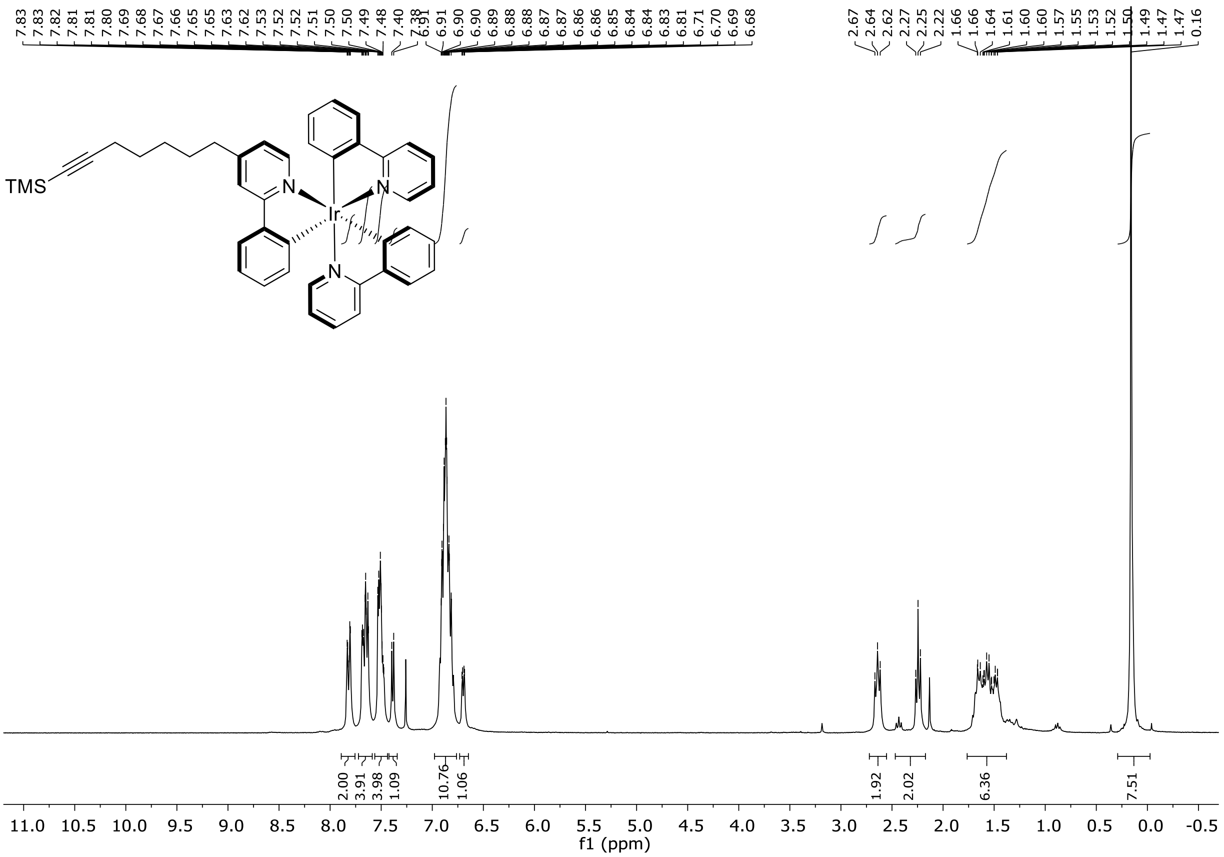
7.83
7.83
7.82
7.81
7.81
7.80
7.69
7.68
7.67
7.66
7.65
7.63
7.62
7.53
7.52
7.52
7.51
7.50
7.50
7.49
7.48
7.40
7.38
6.91
6.91
6.90
6.90
6.89
6.88
6.88
6.87
6.86
6.86
6.85
6.84
6.84
6.83
6.81
6.71
6.70
6.69
6.68
2.67
2.64
2.62
2.27
2.25
2.22
1.66
1.66
1.64
1.61
1.60
1.60
1.57
1.55
1.53
1.52
1.50
1.49
1.47
1.47
0.16
TMS
N
Ir
N
N
2.00
3.91
3.98
1.09
10.76
1.06
1.92
2.02
6.36
7.51
11.0
10.5
10.0
9.5
9.0
8.5
8.0
7.5
7.0
6.5
6.0
5.5
5.0
4.5
4.0
3.5
3.0
2.5
2.0
1.5
1.0
0.5
0.0
-0.5
f1 (ppm)

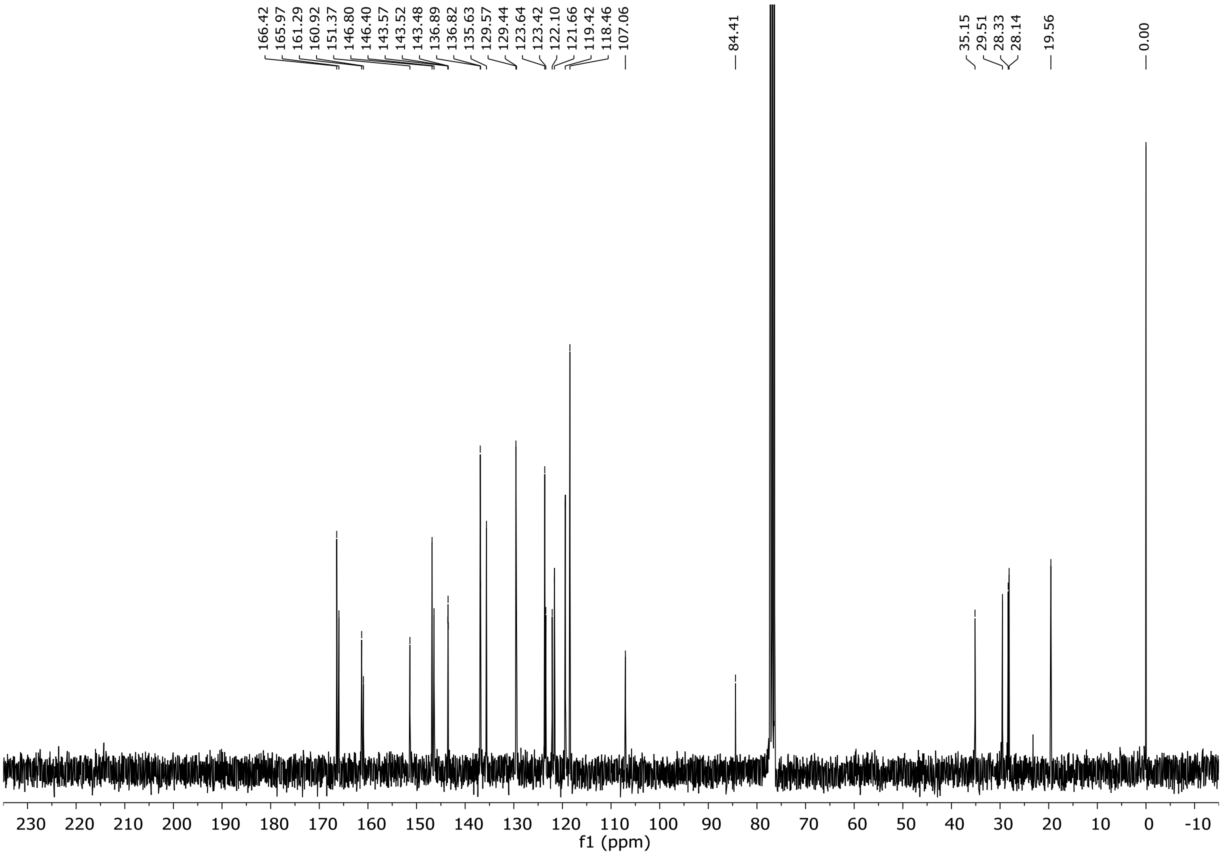
166.42
165.97
161.29
160.92
151.37
146.80
146.40
143.57
143.52
143.48
136.89
136.82
135.63
129.57
129.44
123.64
123.42
122.10
121.66
119.42
118.46
107.06
84.41
35.15
29.51
28.33
28.14
19.56
0.00
230
220
210
200
190
180
170
160
150
140
130
120
110
100
90
80
70
60
50
40
30
20
10
0
-10
f1 (ppm)

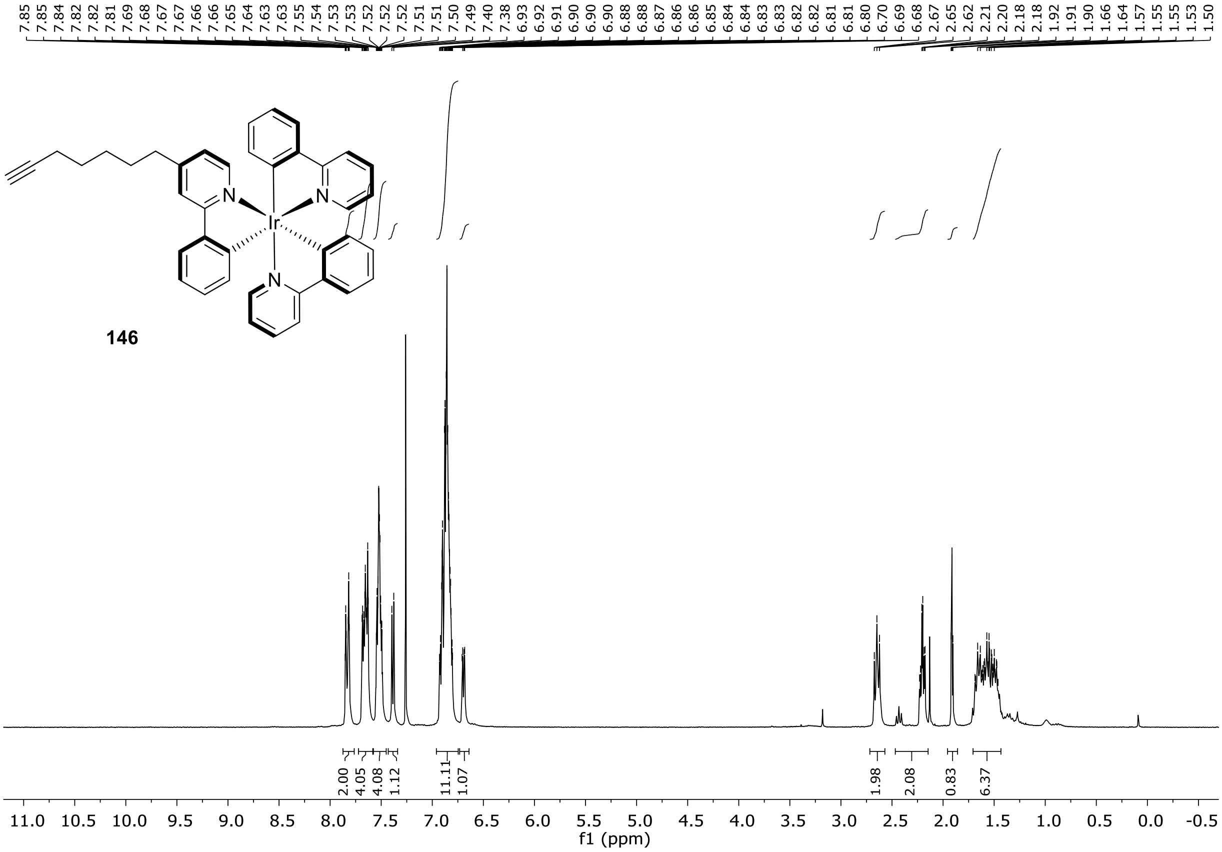
146

7.85
7.85
7.84
7.82
7.82
7.81
7.69
7.68
7.67
7.67
7.66
7.66
7.65
7.64
7.63
7.63
7.55
7.54
7.53
7.53
7.52
7.52
7.52
7.51
7.51
7.50
7.49
7.40
7.38
6.93
6.92
6.91
6.91
6.90
6.90
6.90
6.88
6.88
6.87
6.86
6.86
6.85
6.84
6.84
6.83
6.83
6.82
6.82
6.81
6.81
6.80
6.70
6.69
6.68
2.67
2.65
2.62
2.21
2.20
2.18
1.92
1.91
1.90
1.66
1.64
1.57
1.55
1.53
1.50
N
Ir
N
N
2.00
4.05
4.08
1.12
11.11
1.07
1.98
2.08
0.83
6.37
11.0 10.5 10.0 9.5 9.0 8.5 8.0 7.5 7.0 6.5 6.0 5.5 5.0 4.5 4.0 3.5 3.0 2.5 2.0 1.5 1.0 0.5 0.0 -0.5
f1 (ppm)

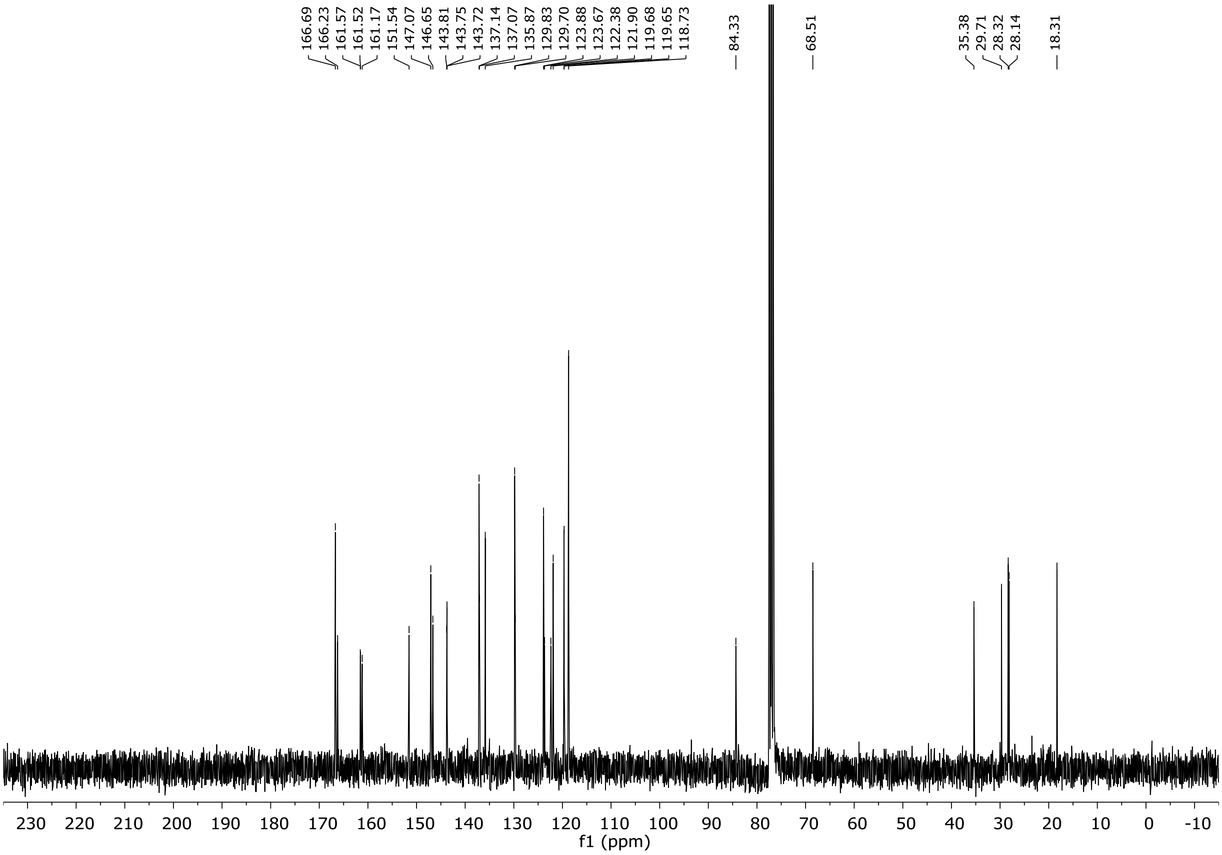
166.69
166.23
161.57
161.52
161.17
151.54
147.07
146.65
143.81
143.75
143.72
137.14
137.07
135.87
129.83
129.70
123.88
123.67
122.38
121.90
119.68
119.65
118.73
84.33
68.51
35.38
29.71
28.32
28.14
18.31
230 220 210 200 190 180 170 160 150 140 130 120 110 100 90 80 70 60 50 40 30 20 10 0 -10
f1 (ppm)

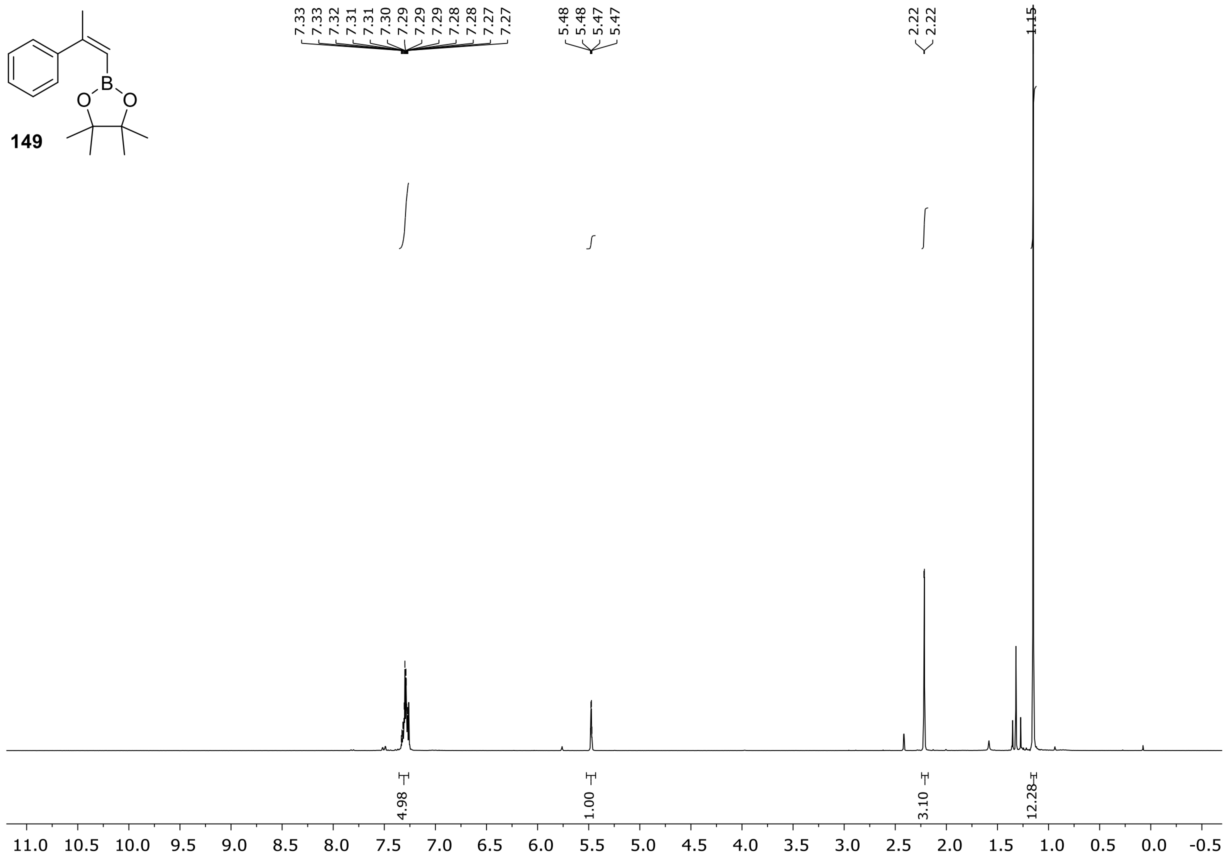
B
O
O
149
7.33
7.33
7.32
7.31
7.31
7.30
7.29
7.29
7.29
7.28
7.28
7.27
7.27
5.48
5.48
5.47
5.47
2.22
2.22
1.15
4.98
1.00
3.10
12.28
11.0 10.5 10.0 9.5 9.0 8.5 8.0 7.5 7.0 6.5 6.0 5.5 5.0 4.5 4.0 3.5 3.0 2.5 2.0 1.5 1.0 0.5 0.0 -0.5

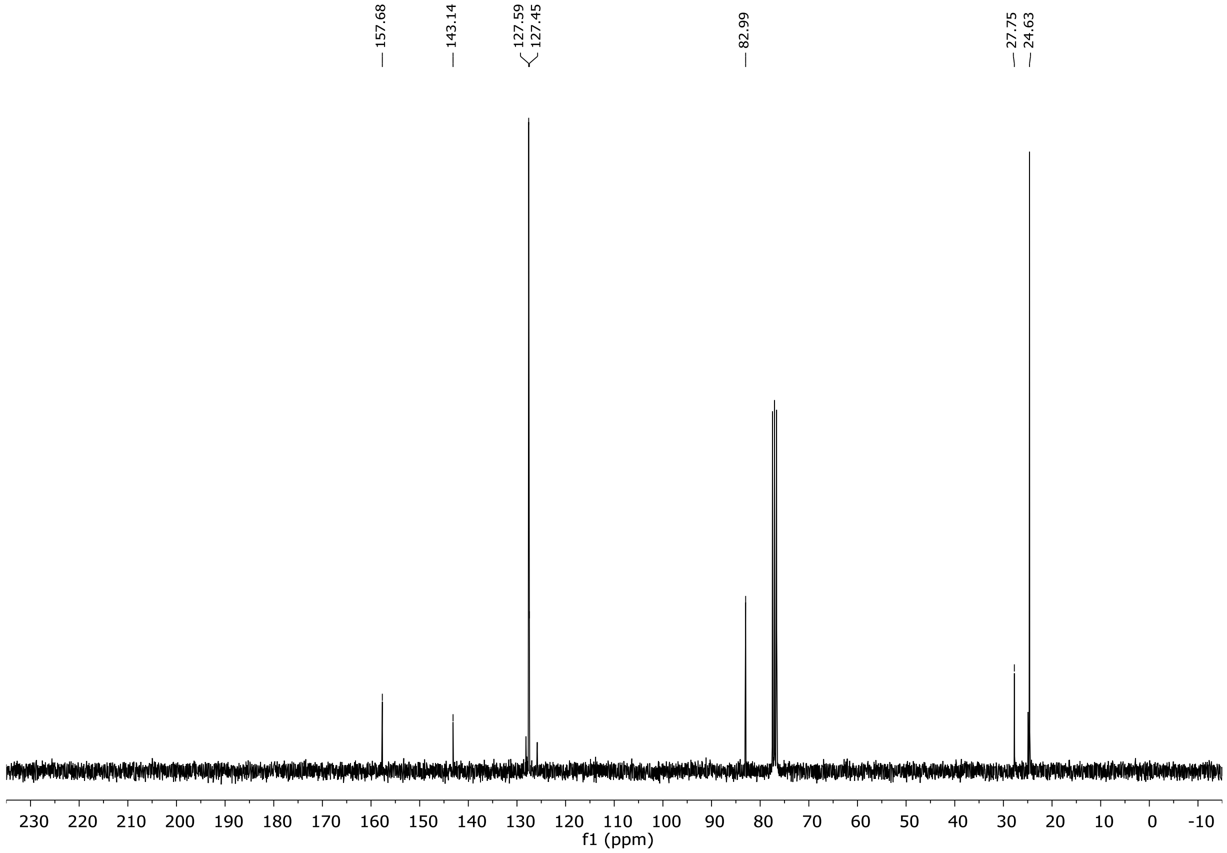
157.68
143.14
127.59
127.45
82.99
27.75
24.63
230 220 210 200 190 180 170 160 150 140 130 120 110 100 90 80 70 60 50 40 30 20 10 0 -10
f1 (ppm)

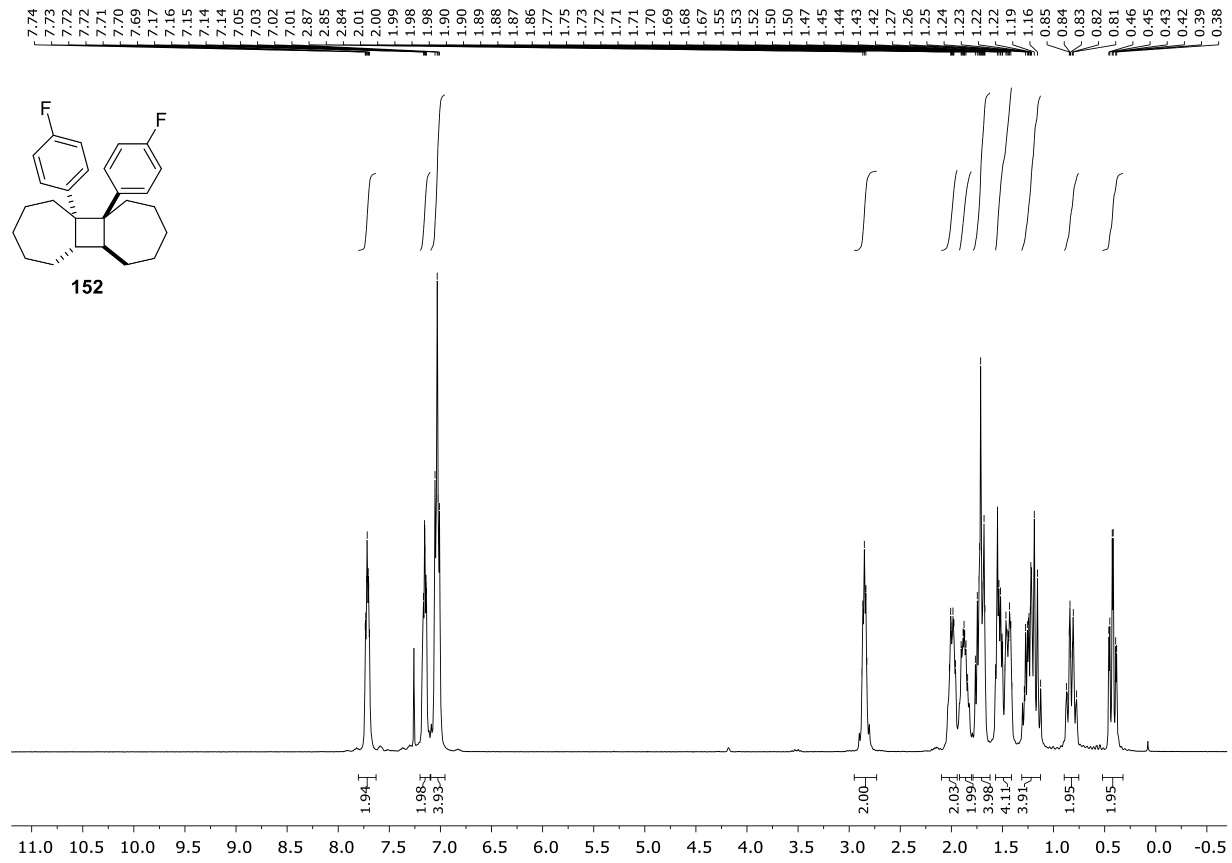
7.74
7.73
7.72
7.72
7.71
7.70
7.69
7.17
7.16
7.15
7.14
7.14
7.05
7.03
7.02
7.01
2.87
2.85
2.84
2.01
2.00
1.99
1.98
1.98
1.90
1.90
1.89
1.88
1.87
1.86
1.77
1.75
1.73
1.72
1.71
1.71
1.70
1.69
1.68
1.67
1.55
1.53
1.52
1.50
1.50
1.47
1.45
1.44
1.43
1.42
1.27
1.26
1.25
1.24
1.23
1.22
1.22
1.19
1.16
0.85
0.84
0.83
0.82
0.81
0.46
0.45
0.43
0.42
0.39
0.38
F
F
152
1.94
1.98
3.93
2.00
2.03
1.99
3.98
4.11
3.91
1.95
1.95
11.0
10.5
10.0
9.5
9.0
8.5
8.0
7.5
7.0
6.5
6.0
5.5
5.0
4.5
4.0
3.5
3.0
2.5
2.0
1.5
1.0
0.5
0.0
-0.5

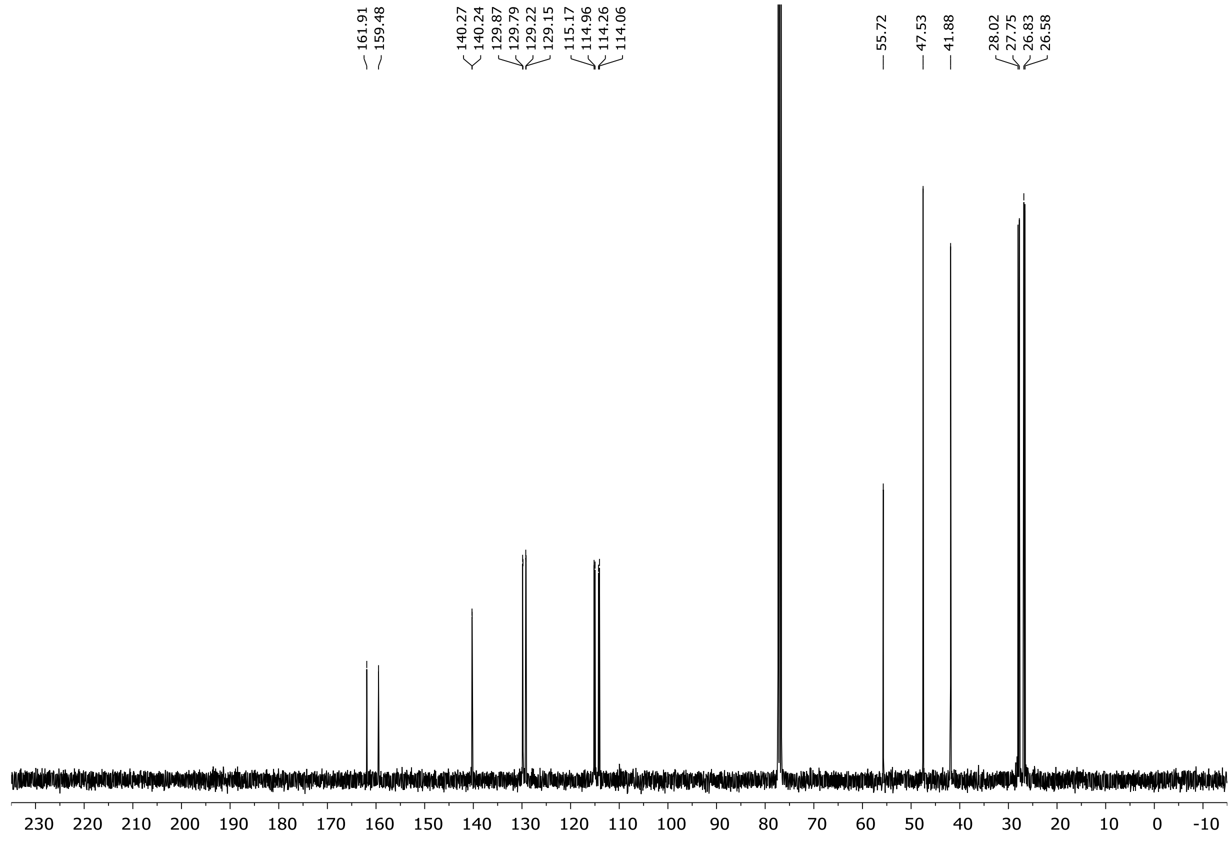
161.91
159.48
140.27
140.24
129.87
129.79
129.22
129.15
115.17
114.96
114.26
114.06
55.72
47.53
41.88
28.02
27.75
26.83
26.58
230
220
210
200
190
180
170
160
150
140
130
120
110
100
90
80
70
60
50
40
30
20
10
0
-10

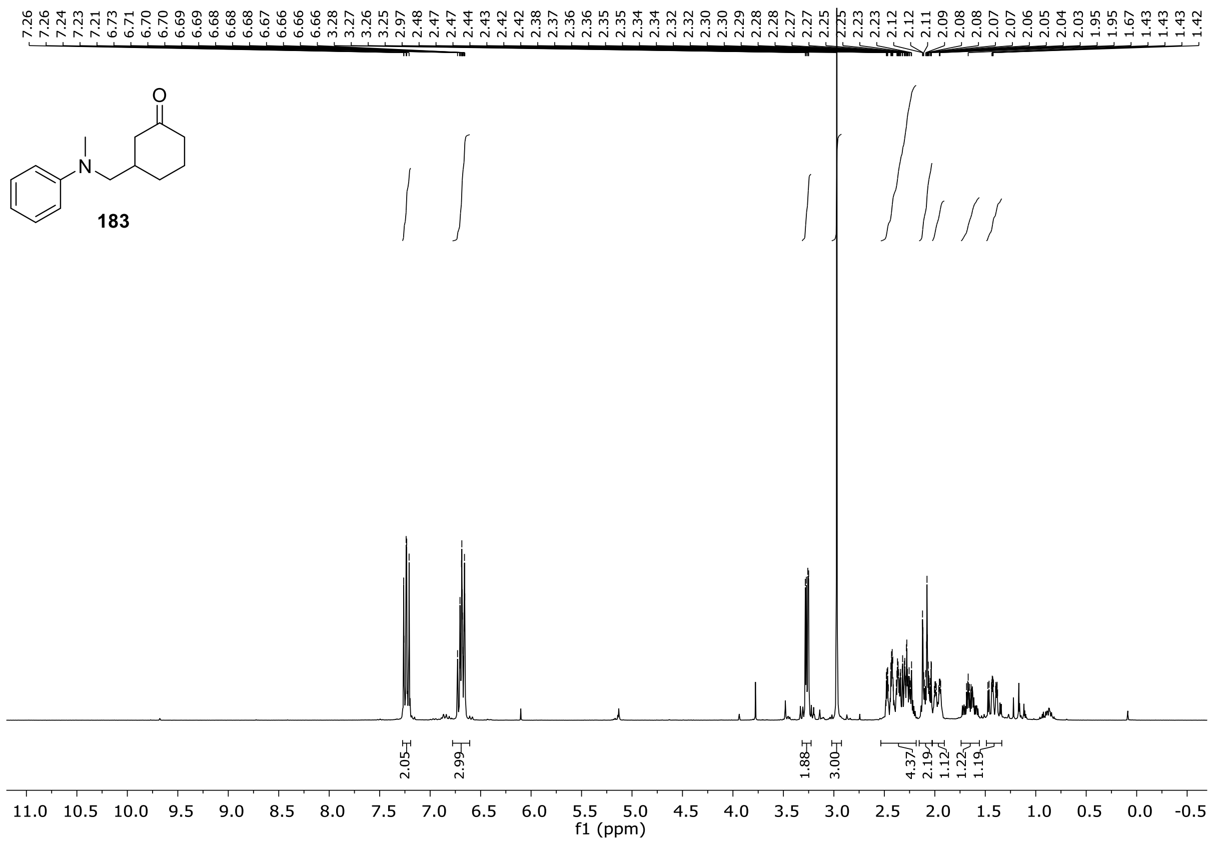
7.26
7.26
7.24
7.23
7.21
6.73
6.71
6.70
6.69
6.69
6.68
6.68
6.67
6.66
6.66
6.66
3.28
3.27
3.26
3.25
2.97
2.48
2.47
2.47
2.44
2.43
2.42
2.42
2.38
2.37
2.36
2.36
2.35
2.34
2.34
2.32
2.32
2.30
2.30
2.29
2.28
2.28
2.27
2.27
2.25
2.25
2.23
2.23
2.12
2.12
2.11
2.09
2.08
2.08
2.07
2.07
2.06
2.05
2.04
2.03
1.95
1.95
1.67
1.43
1.43
1.42
O
N
183
2.05
2.99
1.88
3.00
4.37
2.19
1.12
1.22
1.19
11.0
10.5
10.0
9.5
9.0
8.5
8.0
7.5
7.0
6.5
6.0
5.5
5.0
4.5
4.0
3.5
3.0
2.5
2.0
1.5
1.0
0.5
0.0
-0.5
f1 (ppm)

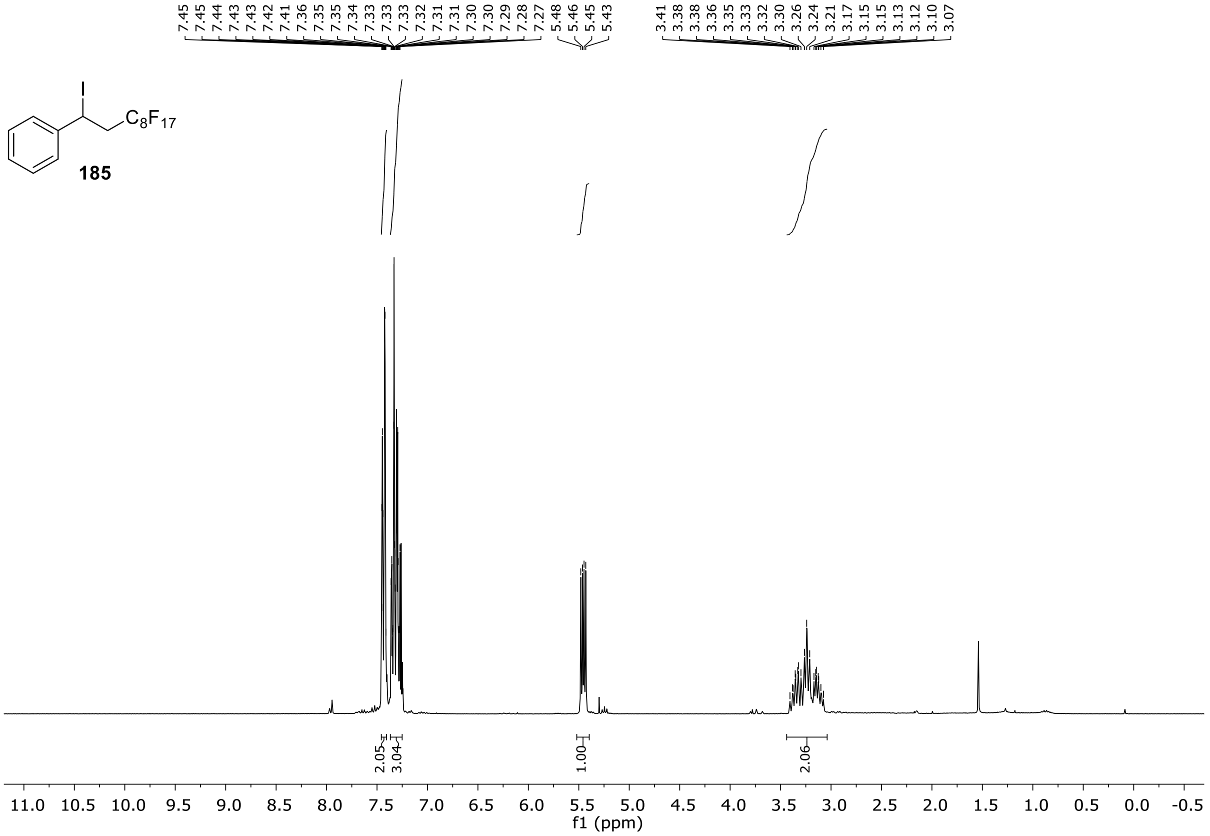
7.45
7.45
7.44
7.43
7.43
7.42
7.41
7.36
7.35
7.35
7.34
7.33
7.33
7.33
7.32
7.31
7.31
7.30
7.30
7.29
7.28
7.27
5.48
5.46
5.45
5.43
3.41
3.38
3.38
3.36
3.35
3.33
3.32
3.30
3.26
3.24
3.21
3.17
3.15
3.15
3.13
3.12
3.10
3.07
I
C_8F_{17}
185
2.05
3.04
1.00
2.06
11.0
10.5
10.0
9.5
9.0
8.5
8.0
7.5
7.0
6.5
6.0
5.5
5.0
4.5
4.0
3.5
3.0
2.5
2.0
1.5
1.0
0.5
0.0
-0.5
f1 (ppm)

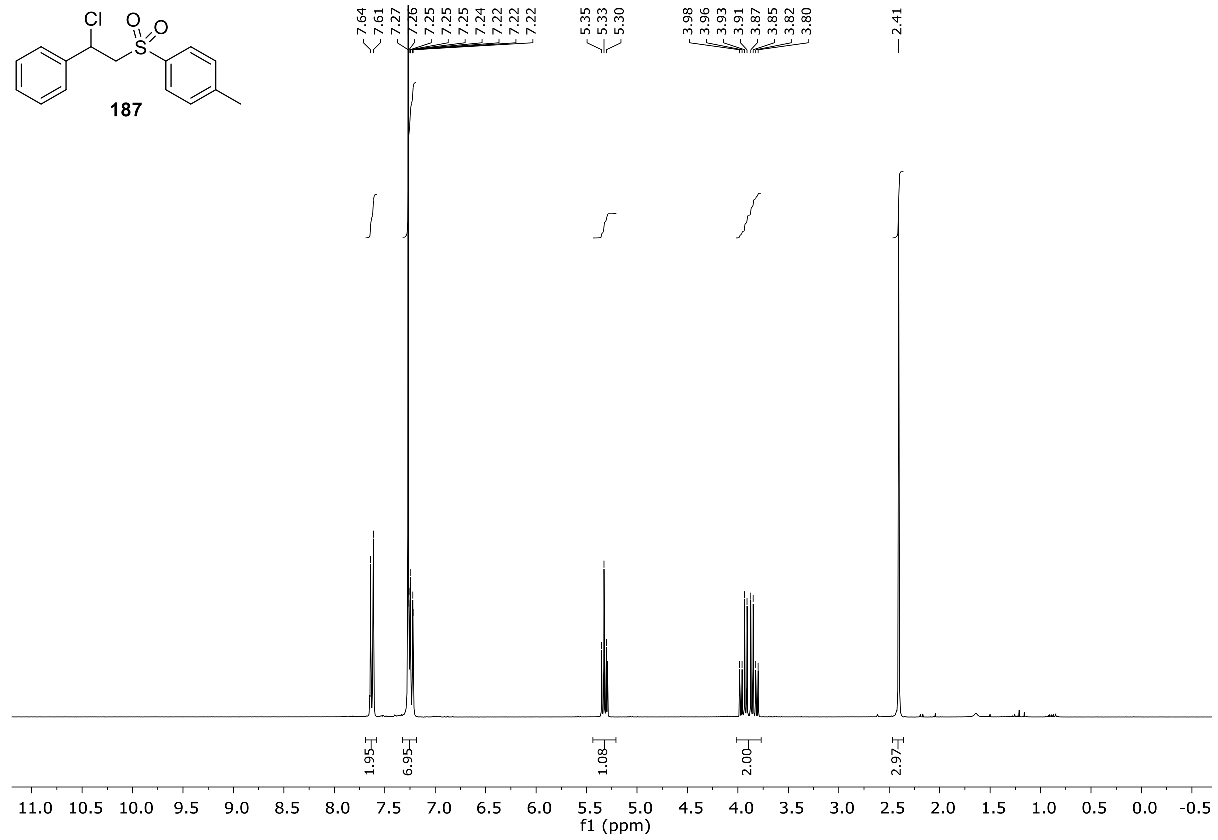
Cl
O
O
S
187
7.64
7.61
7.27
7.26
7.25
7.25
7.25
7.24
7.22
7.22
7.22
5.35
5.33
5.30
3.98
3.96
3.93
3.91
3.87
3.85
3.82
3.80
2.41
1.95
6.95
1.08
2.00
2.97
11.0 10.5 10.0 9.5 9.0 8.5 8.0 7.5 7.0 6.5 6.0 5.5 5.0 4.5 4.0 3.5 3.0 2.5 2.0 1.5 1.0 0.5 0.0 -0.5
f1 (ppm)

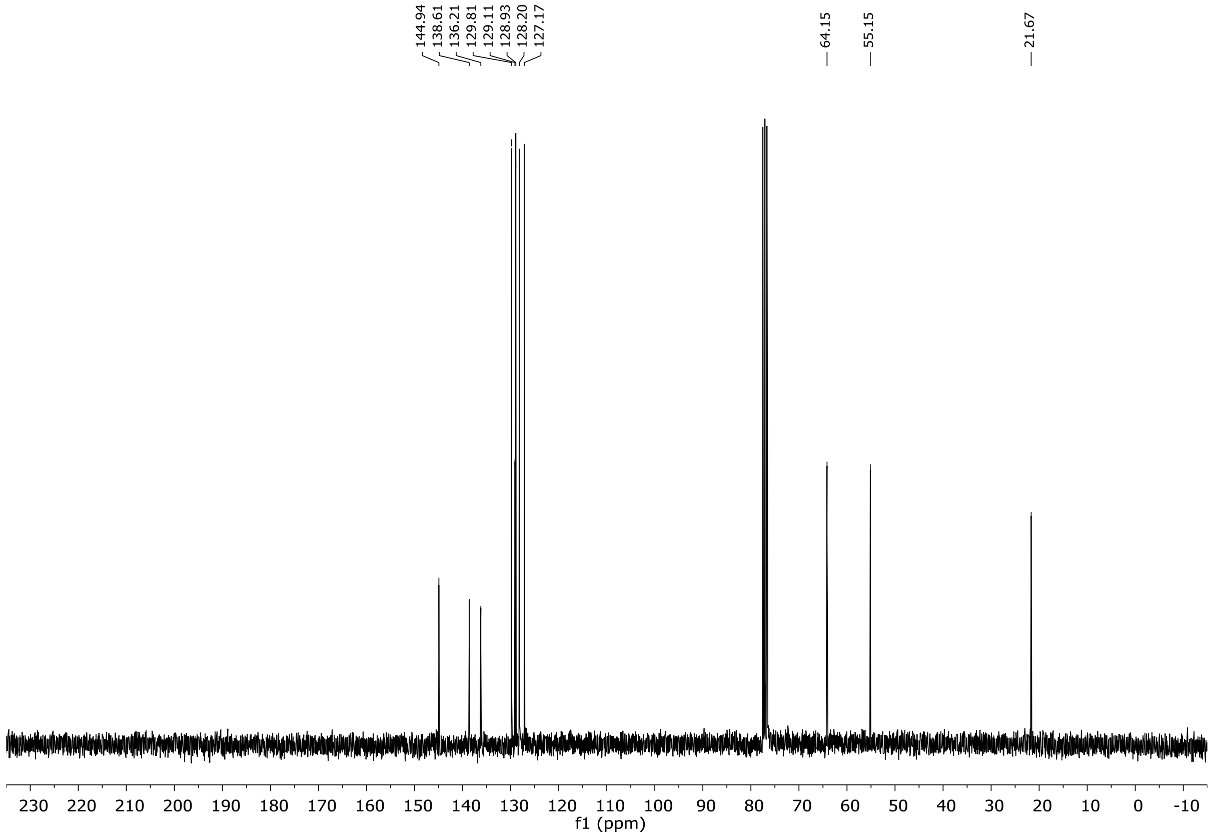
144.94
138.61
136.21
129.81
129.11
128.93
128.20
127.17
64.15
55.15
21.67
230 220 210 200 190 180 170 160 150 140 130 120 110 100 90 80 70 60 50 40 30 20 10 0 -10
f1 (ppm)

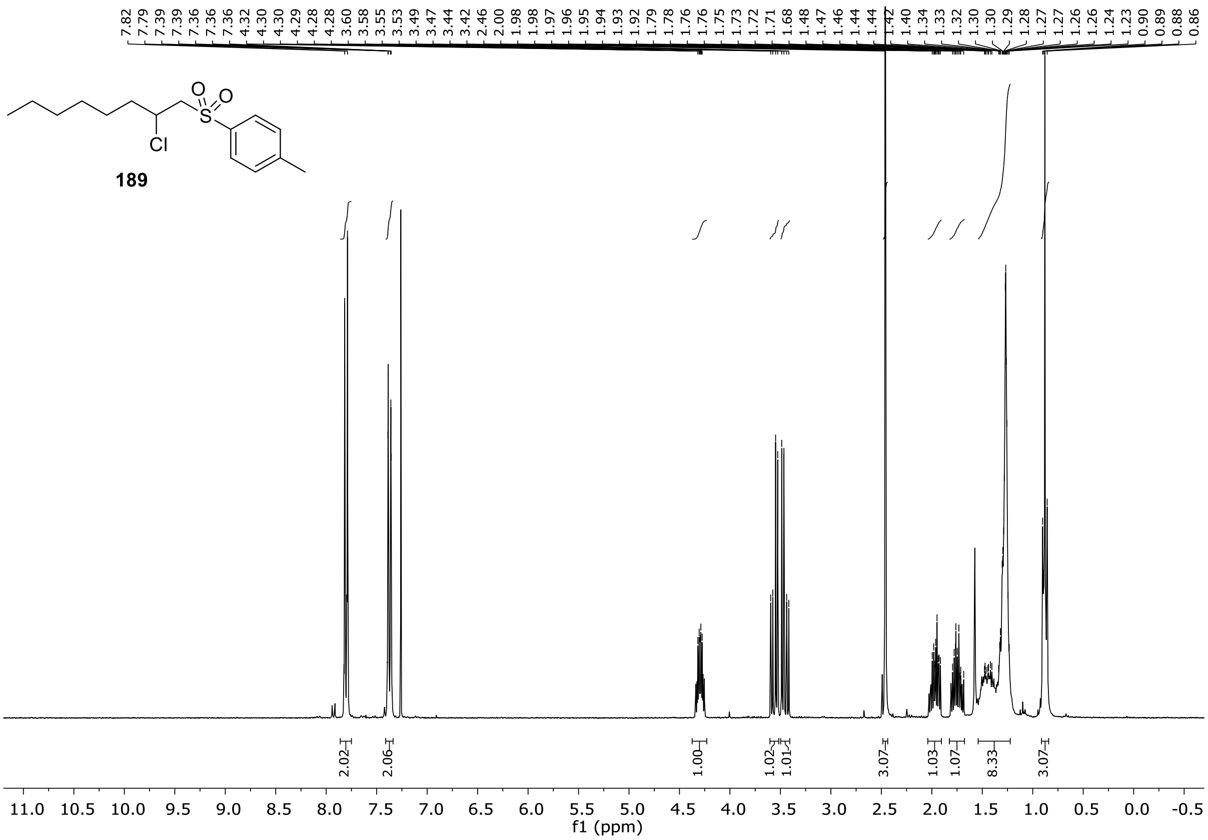
7.82
7.79
7.39
7.39
7.36
7.36
4.32
4.30
4.29
4.28
4.28
3.60
3.58
3.55
3.53
3.49
3.47
3.44
3.42
2.46
2.00
1.98
1.98
1.97
1.96
1.95
1.94
1.93
1.92
1.79
1.78
1.76
1.75
1.73
1.72
1.71
1.68
1.48
1.47
1.46
1.44
1.44
1.42
1.40
1.34
1.33
1.32
1.30
1.30
1.29
1.28
1.27
1.27
1.26
1.24
1.23
0.90
0.89
0.88
0.86
O
O
S
Cl
2.02
2.06
1.00
1.02
1.01
3.07
1.03
1.07
8.33
3.07
11.0
10.5
10.0
9.5
9.0
8.5
8.0
7.5
7.0
6.5
6.0
5.5
5.0
4.5
4.0
3.5
3.0
2.5
2.0
1.5
1.0
0.5
0.0
-0.5
f1 (ppm)

189

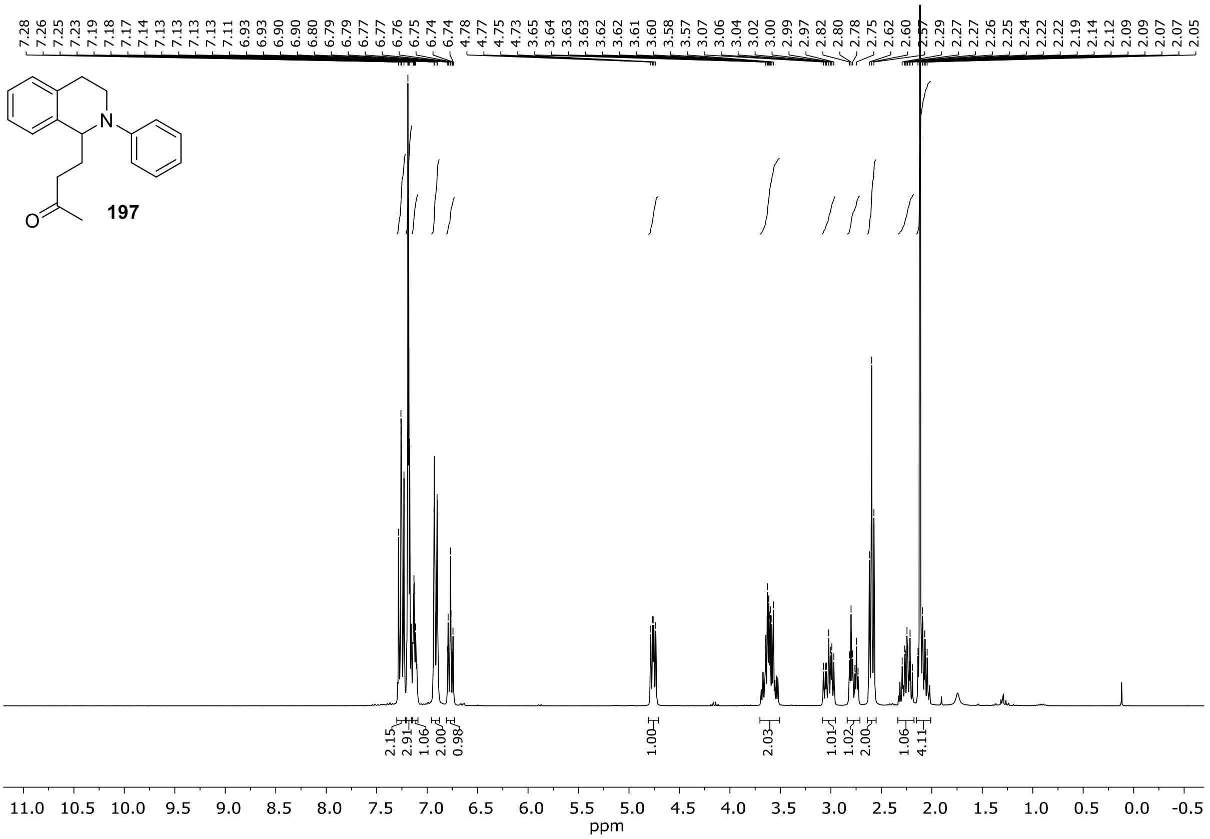
7.28
7.26
7.25
7.23
7.19
7.18
7.17
7.14
7.13
7.13
7.13
7.13
7.11
6.93
6.93
6.90
6.90
6.80
6.79
6.79
6.77
6.77
6.76
6.75
6.74
6.74
4.78
4.77
4.75
4.73
3.65
3.64
3.63
3.63
3.62
3.62
3.61
3.60
3.58
3.57
3.07
3.06
3.04
3.02
3.00
2.99
2.97
2.82
2.80
2.78
2.75
2.62
2.60
2.57
2.29
2.27
2.27
2.26
2.25
2.24
2.22
2.22
2.19
2.14
2.12
2.09
2.09
2.07
2.07
2.05
N
O
2.15
2.91
1.06
2.00
0.98
1.00
2.03
1.01
1.02
2.00
1.06
4.11
11.0
10.5
10.0
9.5
9.0
8.5
8.0
7.5
7.0
6.5
6.0
5.5
5.0
4.5
4.0
3.5
3.0
2.5
2.0
1.5
1.0
0.5
0.0
-0.5
ppm

197

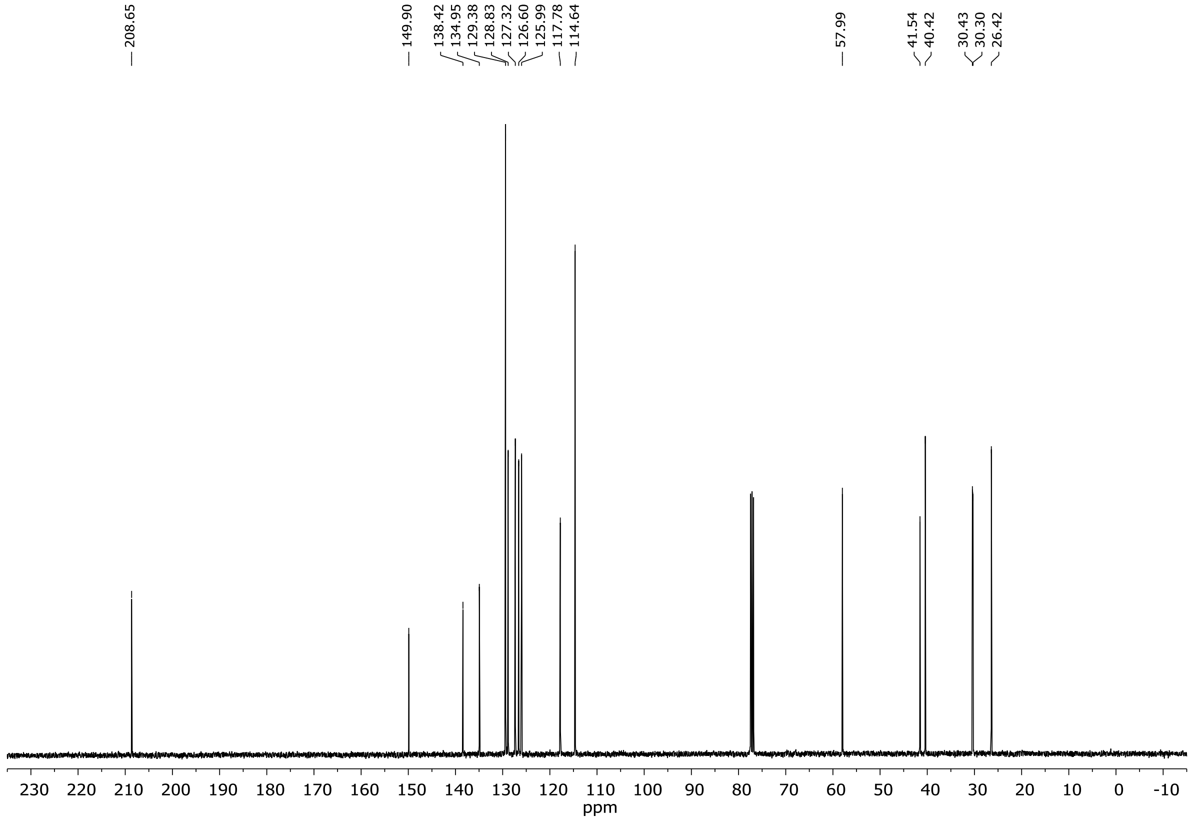
208.65
149.90
138.42
134.95
129.38
128.83
127.32
126.60
125.99
117.78
114.64
57.99
41.54
40.42
30.43
30.30
26.42
230
220
210
200
190
180
170
160
150
140
130
120
110
100
90
80
70
60
50
40
30
20
10
0
-10
ppm

^{1}H-NMR (400 MHz, CD_3OD):

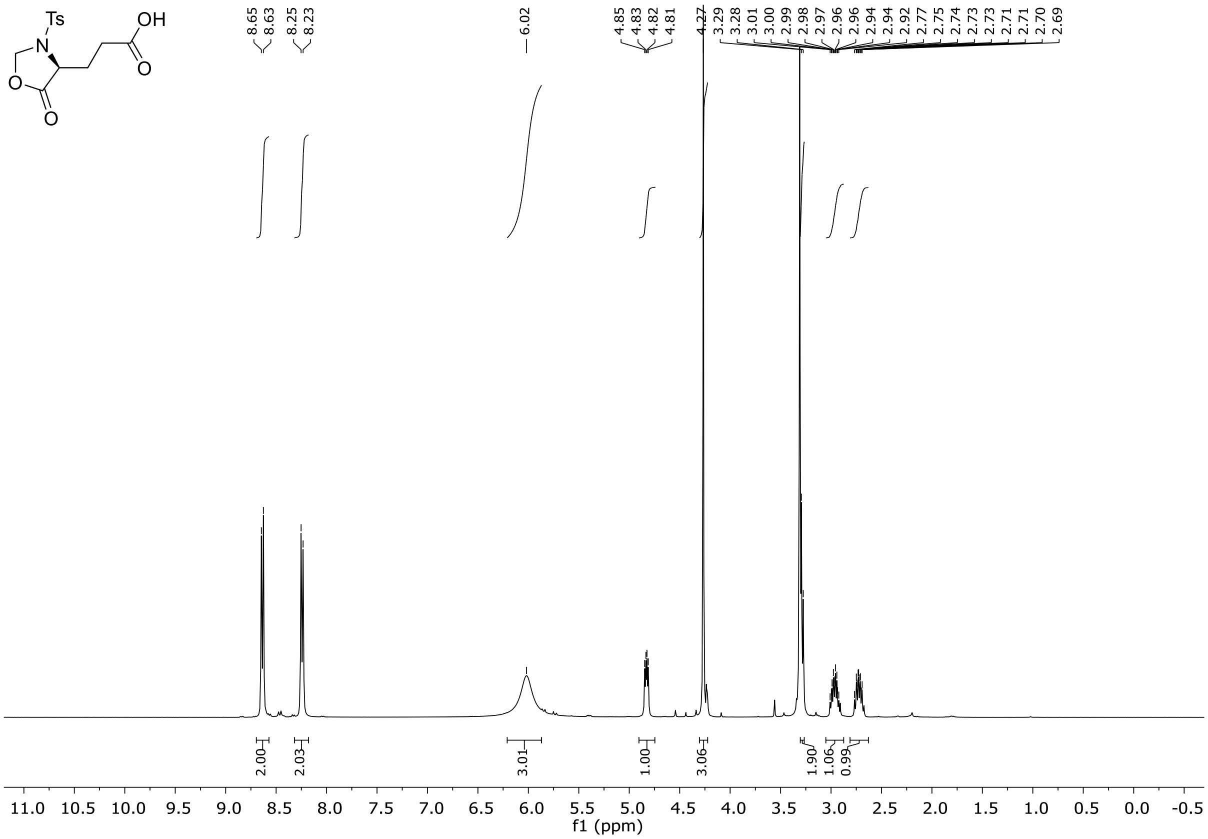

^{13}C-NMR (101 MHz, CD_3OD):

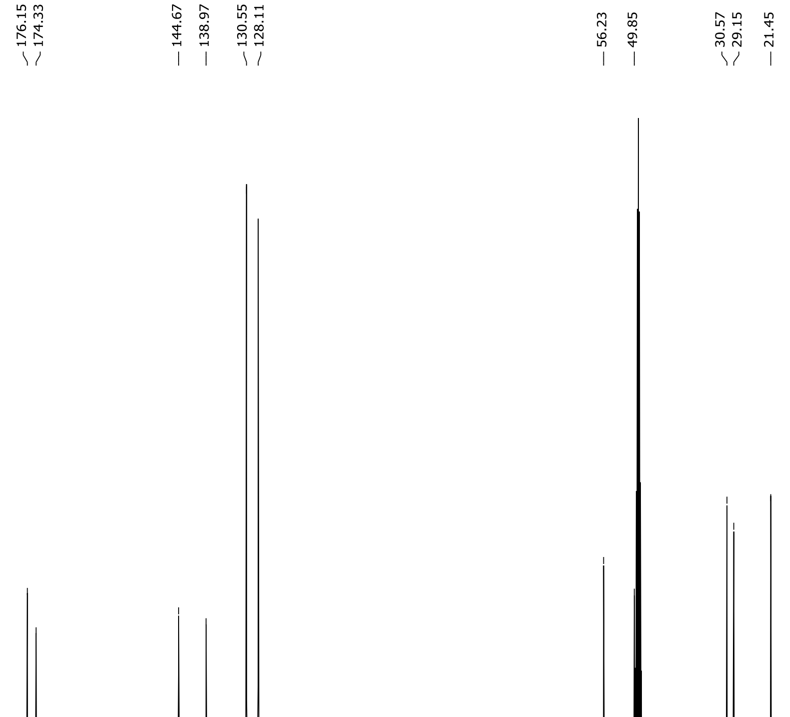

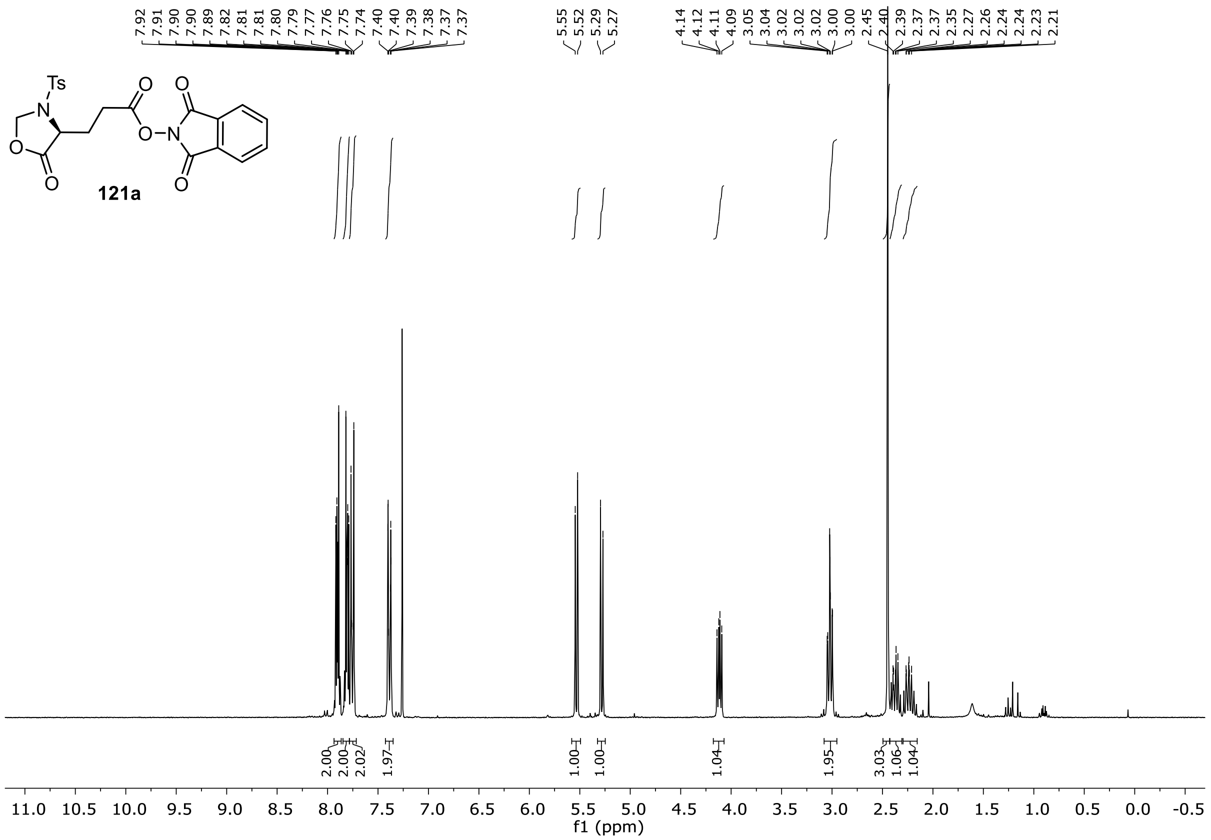
7.92
7.91
7.90
7.90
7.89
7.82
7.81
7.81
7.80
7.79
7.77
7.76
7.75
7.74
7.40
7.40
7.39
7.38
7.37
7.37
5.55
5.52
5.29
5.27
4.14
4.12
4.11
4.09
3.05
3.04
3.02
3.02
3.02
3.00
3.00
2.45
2.40
2.39
2.37
2.37
2.35
2.27
2.26
2.24
2.24
2.23
2.21
Ts
N
O
O
O
O
N
O
O
121a
2.00
2.00
2.02
1.97
1.00
1.00
1.04
1.95
3.03
1.06
1.04
11.0 10.5 10.0 9.5 9.0 8.5 8.0 7.5 7.0 6.5 6.0 5.5 5.0 4.5 4.0 3.5 3.0 2.5 2.0 1.5 1.0 0.5 0.0 -0.5
f1 (ppm)

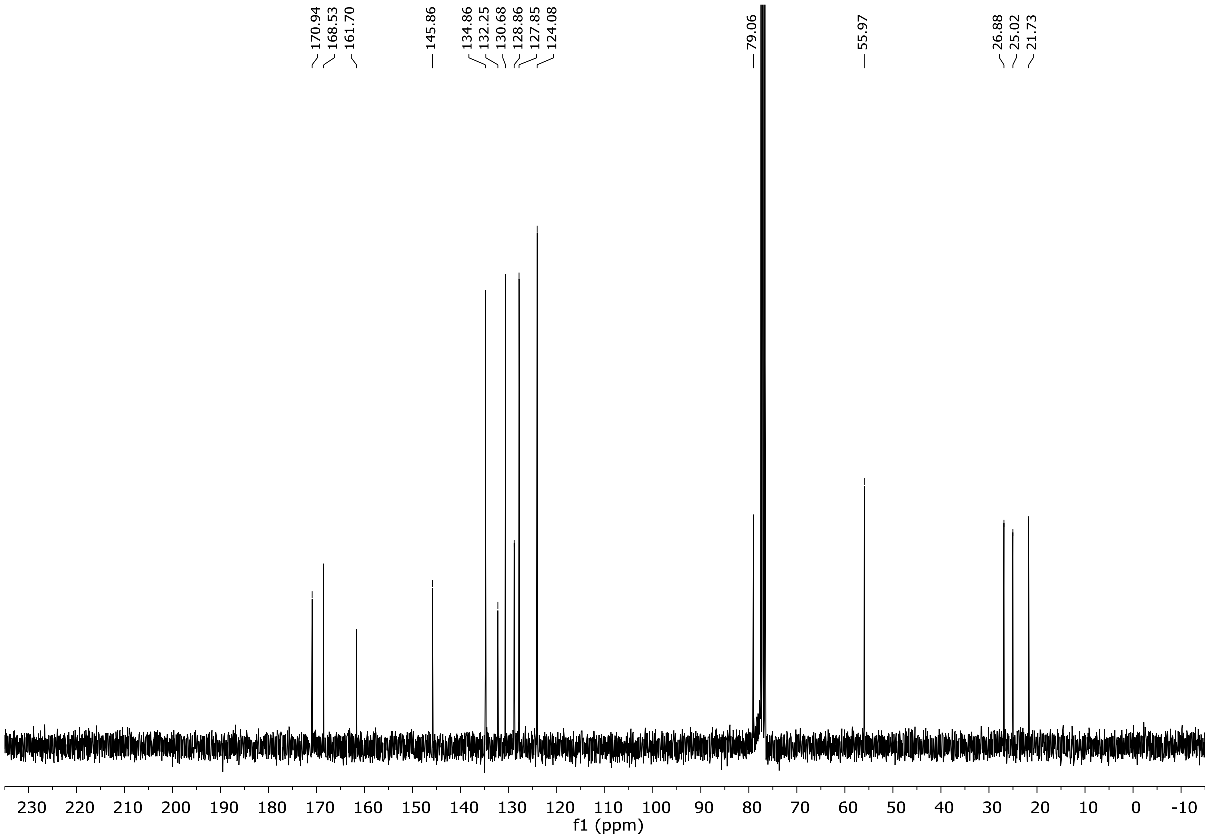
170.94
168.53
161.70
145.86
134.86
132.25
130.68
128.86
127.85
124.08
79.06
55.97
26.88
25.02
21.73
230 220 210 200 190 180 170 160 150 140 130 120 110 100 90 80 70 60 50 40 30 20 10 0 -10
f1 (ppm)

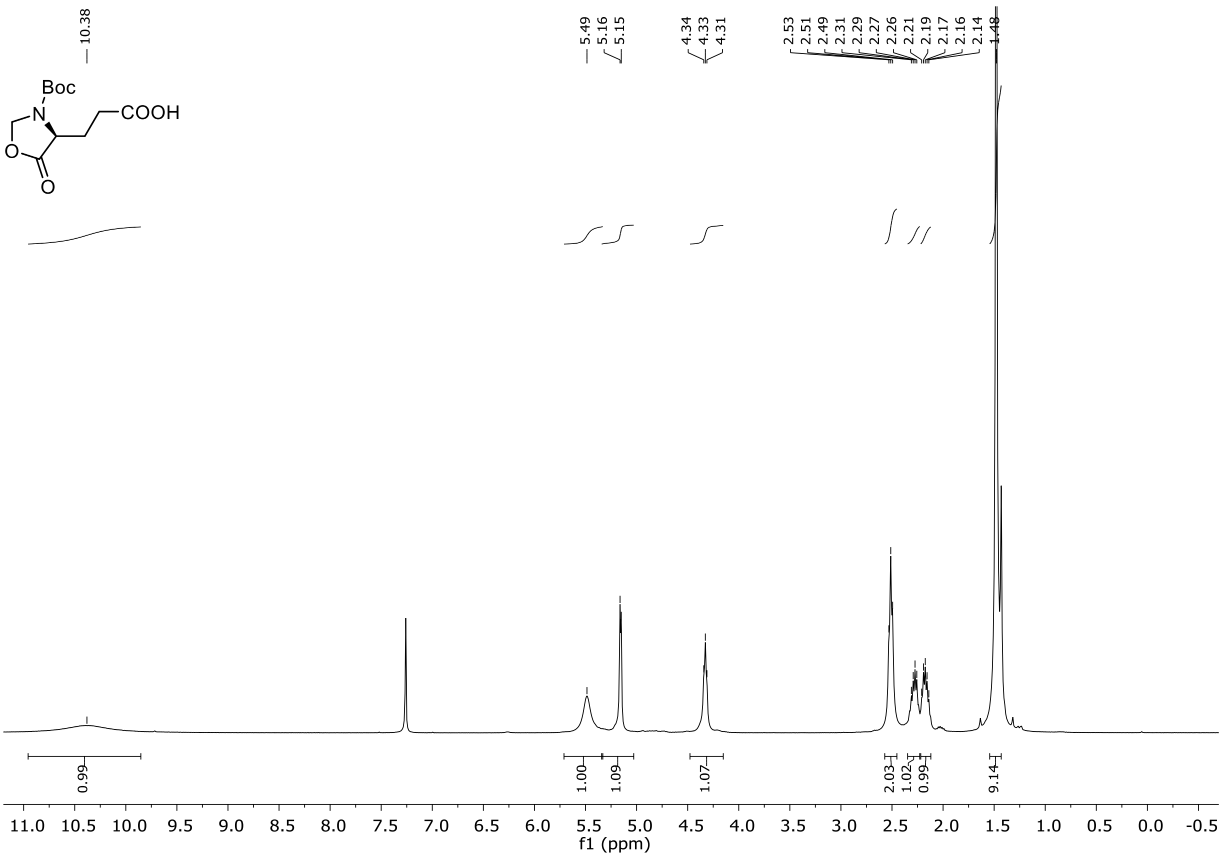
10.38
5.49
5.16
5.15
4.34
4.33
4.31
2.53
2.51
2.49
2.31
2.29
2.27
2.26
2.21
2.19
2.17
2.16
2.14
1.48
Boc
N
COOH
O
O
0.99
1.00
1.09
1.07
2.03
1.02
0.99
9.14
11.0 10.5 10.0 9.5 9.0 8.5 8.0 7.5 7.0 6.5 6.0 5.5 5.0 4.5 4.0 3.5 3.0 2.5 2.0 1.5 1.0 0.5 0.0 -0.5
f1 (ppm)

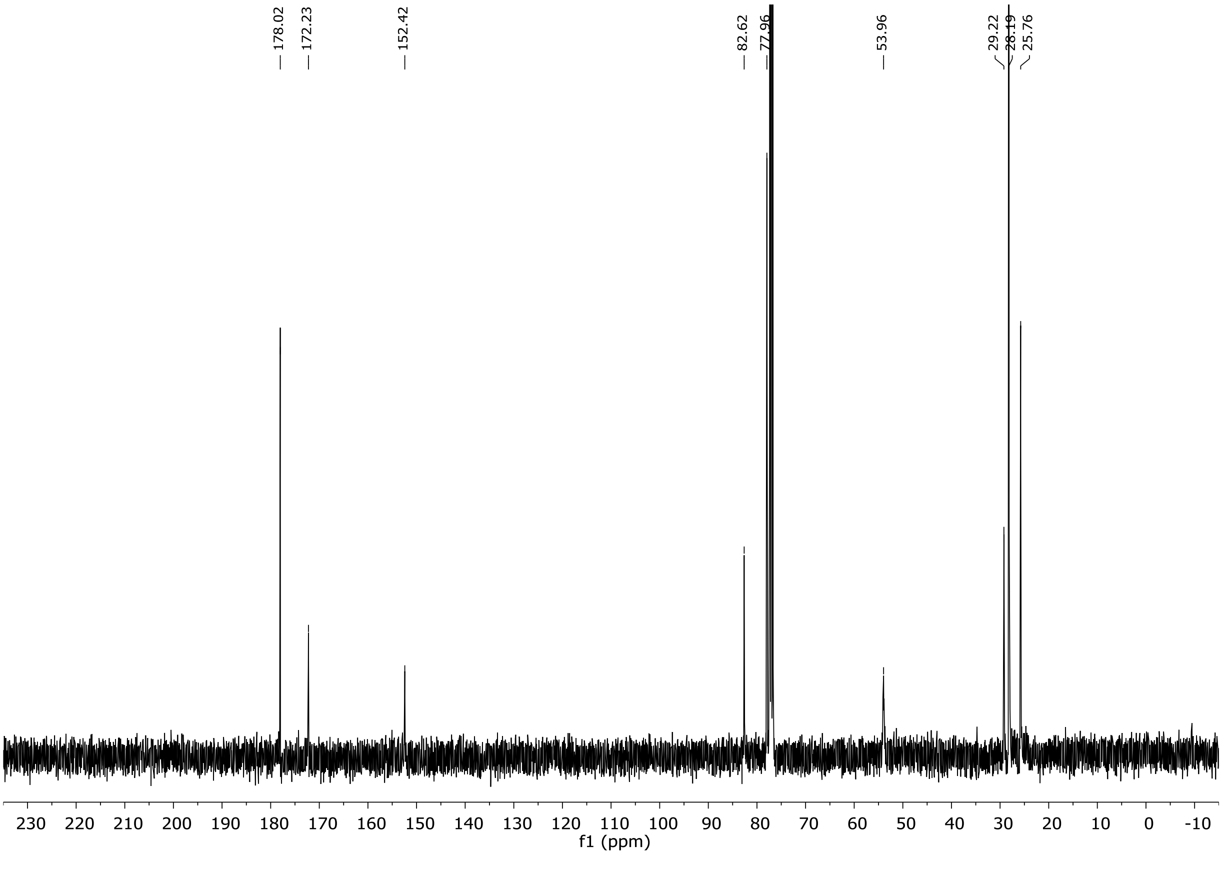
178.02
172.23
152.42
82.62
77.96
53.96
29.22
28.19
25.76
230 220 210 200 190 180 170 160 150 140 130 120 110 100 90 80 70 60 50 40 30 20 10 0 -10
f1 (ppm)

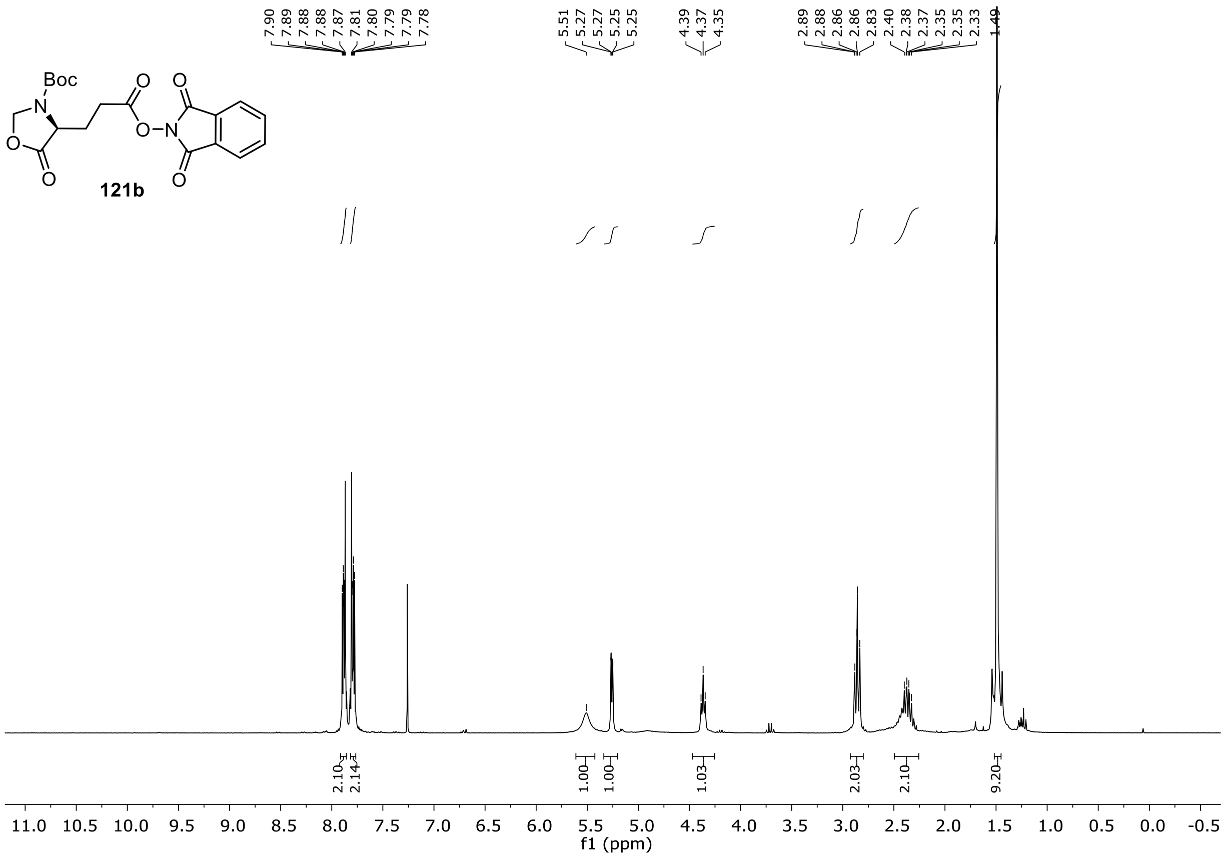
7.90
7.89
7.88
7.88
7.87
7.81
7.80
7.79
7.79
7.78
5.51
5.27
5.27
5.25
5.25
4.39
4.37
4.35
2.89
2.88
2.86
2.86
2.83
2.40
2.38
2.37
2.35
2.35
2.33
1.49
Boc
N
O
O
O
O-N
O
O
121b
2.10
2.14
1.00
1.00
1.03
2.03
2.10
9.20
11.0 10.5 10.0 9.5 9.0 8.5 8.0 7.5 7.0 6.5 6.0 5.5 5.0 4.5 4.0 3.5 3.0 2.5 2.0 1.5 1.0 0.5 0.0 -0.5
f1 (ppm)

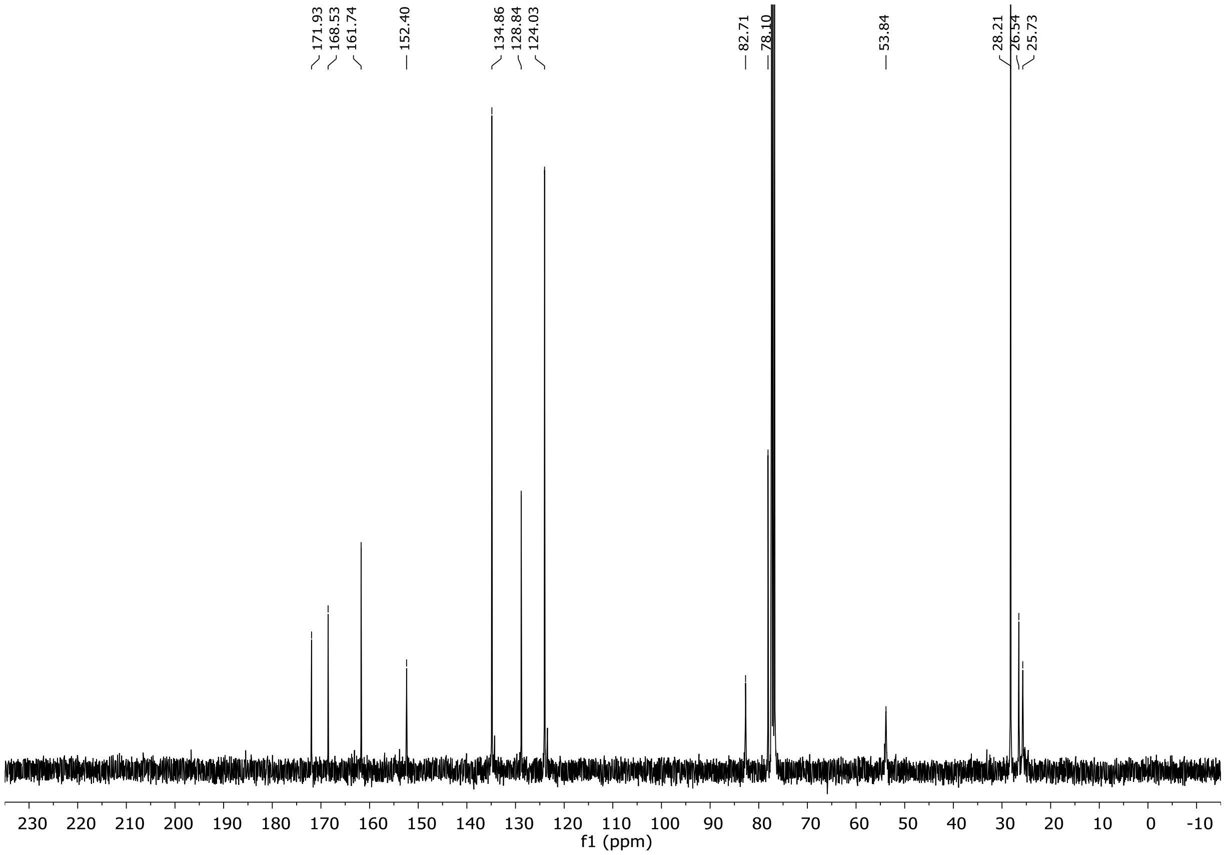
171.93
168.53
161.74
152.40
134.86
128.84
124.03
82.71
78.10
53.84
28.21
26.54
25.73
230 220 210 200 190 180 170 160 150 140 130 120 110 100 90 80 70 60 50 40 30 20 10 0 -10
f1 (ppm)

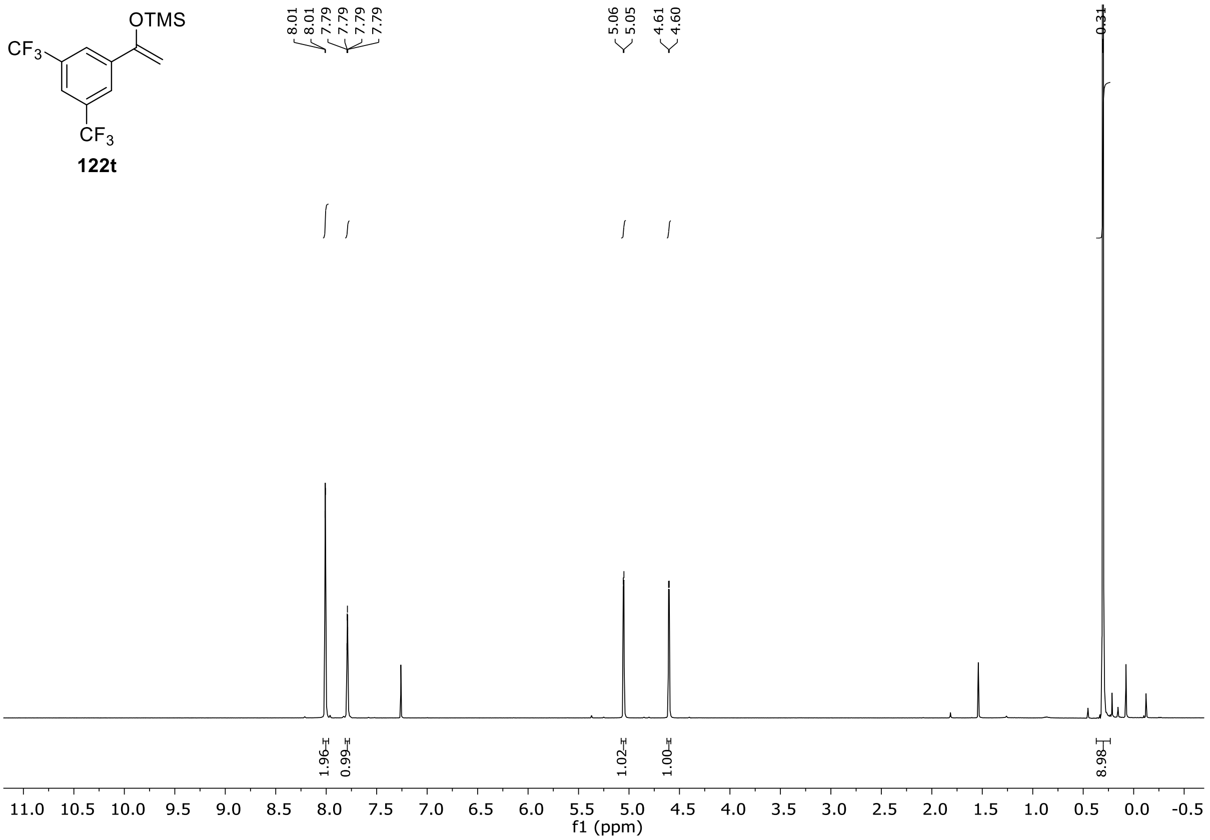
OTMS
CF3
CF3
122t
8.01
8.01
7.79
7.79
7.79
7.79
5.06
5.05
4.61
4.60
0.31
1.96
0.99
1.02
1.00
8.98
11.0 10.5 10.0 9.5 9.0 8.5 8.0 7.5 7.0 6.5 6.0 5.5 5.0 4.5 4.0 3.5 3.0 2.5 2.0 1.5 1.0 0.5 0.0 -0.5
f1 (ppm)

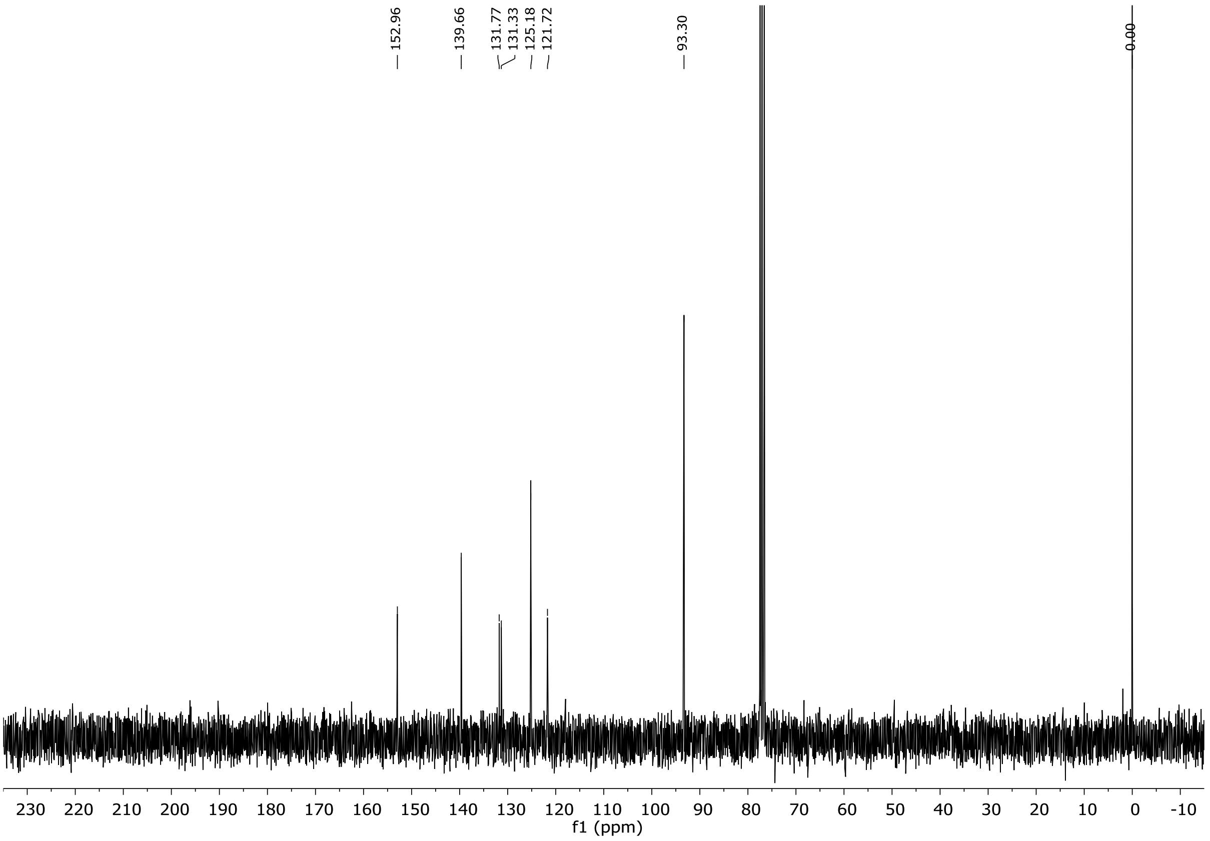
152.96
139.66
131.77
131.33
125.18
121.72
93.30
0.00
230 220 210 200 190 180 170 160 150 140 130 120 110 100 90 80 70 60 50 40 30 20 10 0 -10
f1 (ppm)

122t ^{19}F-NMR (377 MHz, CDCl$_3$):

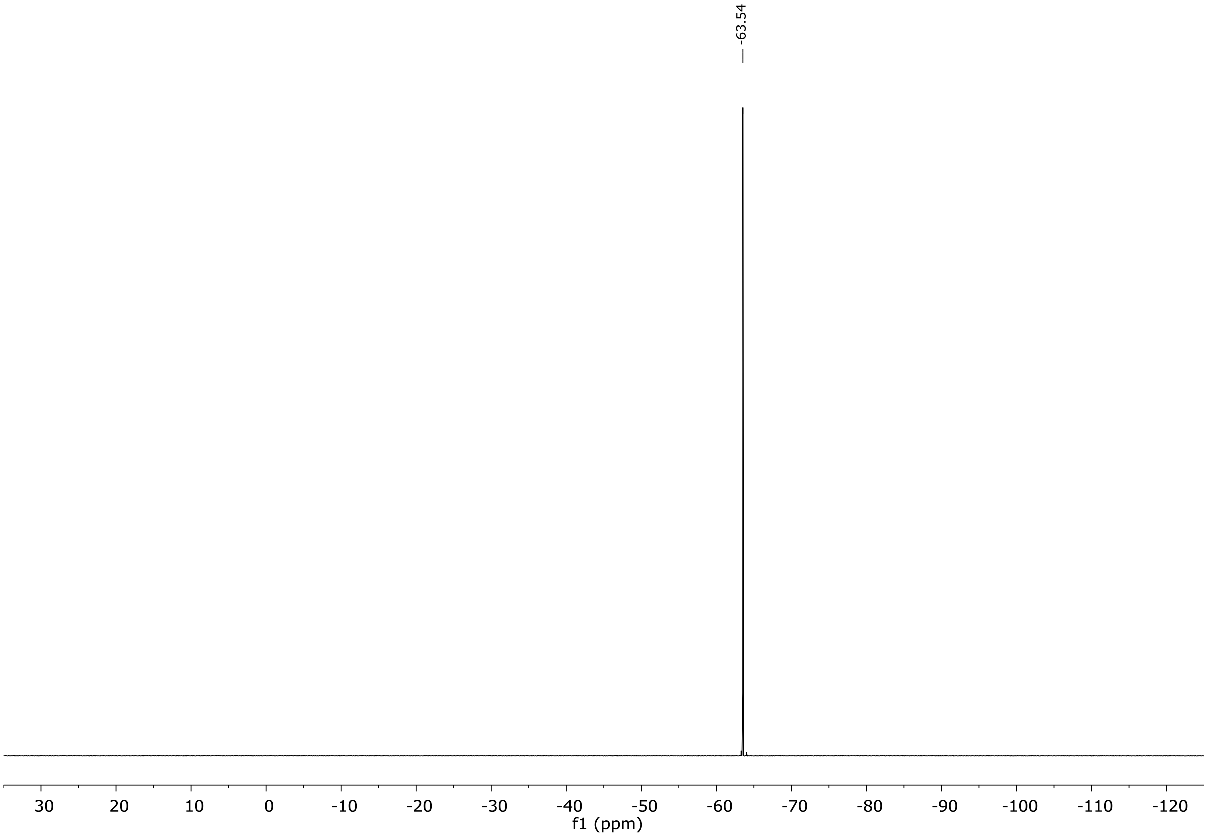

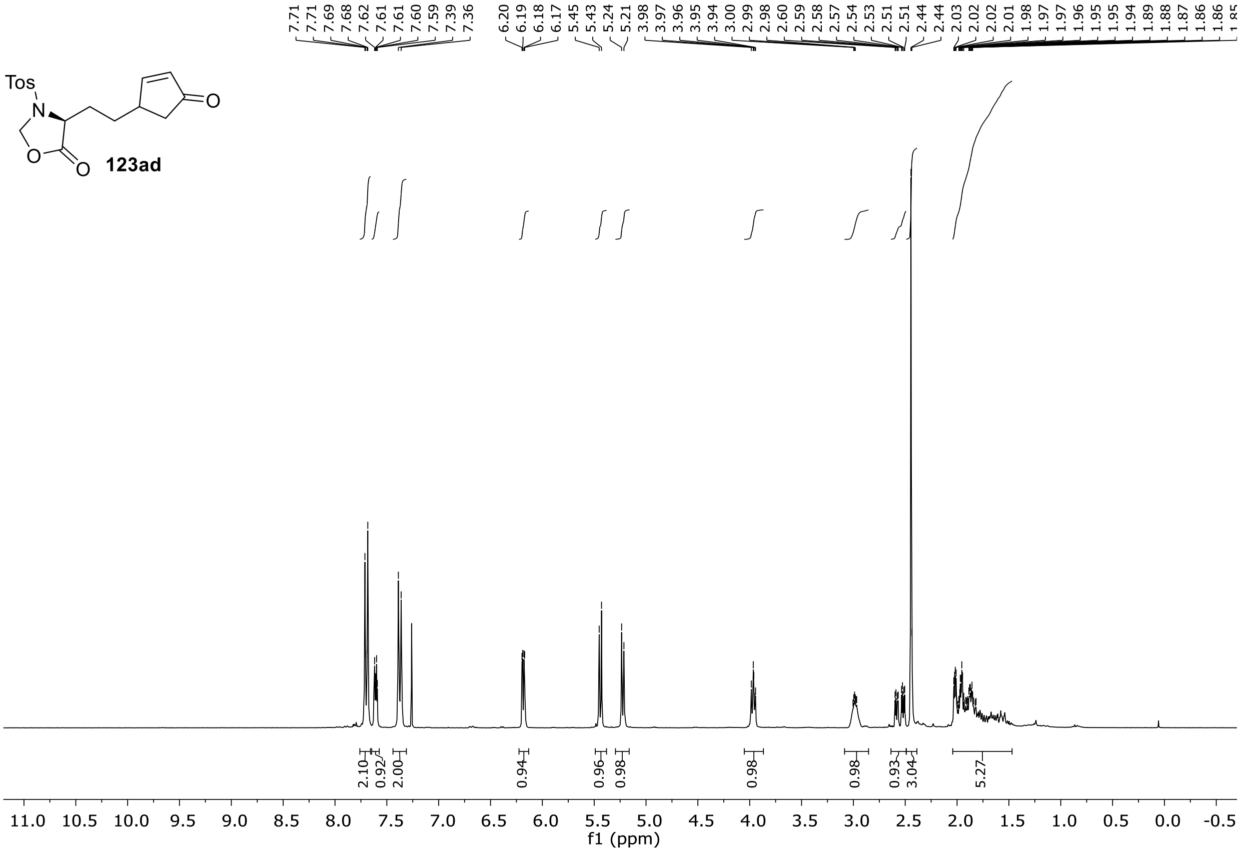
Tos
N
O
O
O
123ad
7.71
7.71
7.69
7.68
7.62
7.61
7.61
7.60
7.59
7.39
7.36
6.20
6.19
6.18
6.17
5.45
5.43
5.24
5.21
3.98
3.97
3.96
3.95
3.94
3.00
2.99
2.98
2.60
2.59
2.58
2.57
2.54
2.53
2.51
2.51
2.44
2.44
2.03
2.02
2.02
2.01
1.98
1.97
1.96
1.95
1.95
1.94
1.89
1.88
1.87
1.86
1.86
2.10
0.92
2.00
0.94
0.96
0.98
0.98
0.98
0.93
3.04
5.27
11.0
10.5
10.0
9.5
9.0
8.5
8.0
7.5
7.0
6.5
6.0
5.5
5.0
4.5
4.0
3.5
3.0
2.5
2.0
1.5
1.0
0.5
0.0
-0.5
f1 (ppm)

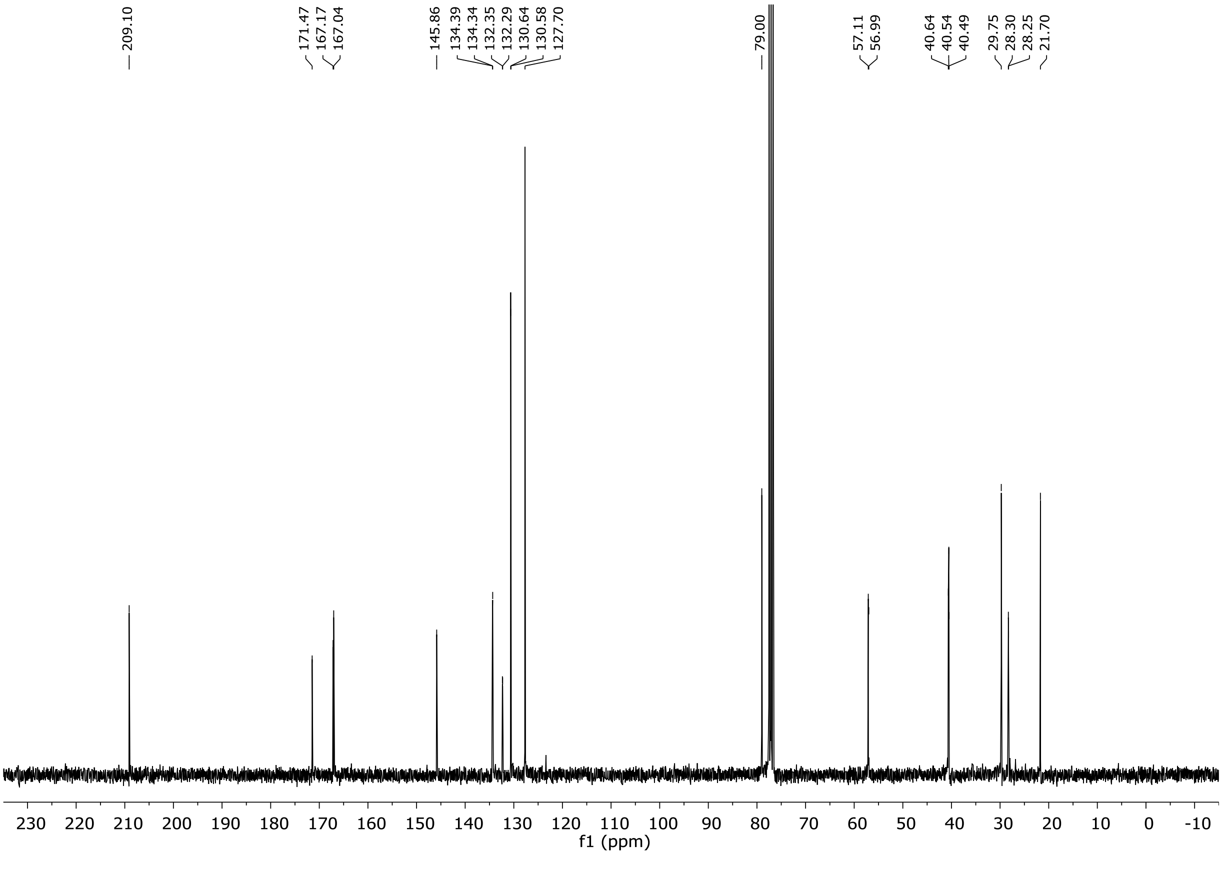
209.10
171.47
167.17
167.04
145.86
134.39
134.34
132.35
132.29
130.64
130.58
127.70
79.00
57.11
56.99
40.64
40.54
40.49
29.75
28.30
28.25
21.70
230
220
210
200
190
180
170
160
150
140
130
120
110
100
90
80
70
60
50
40
30
20
10
0
-10
f1 (ppm)

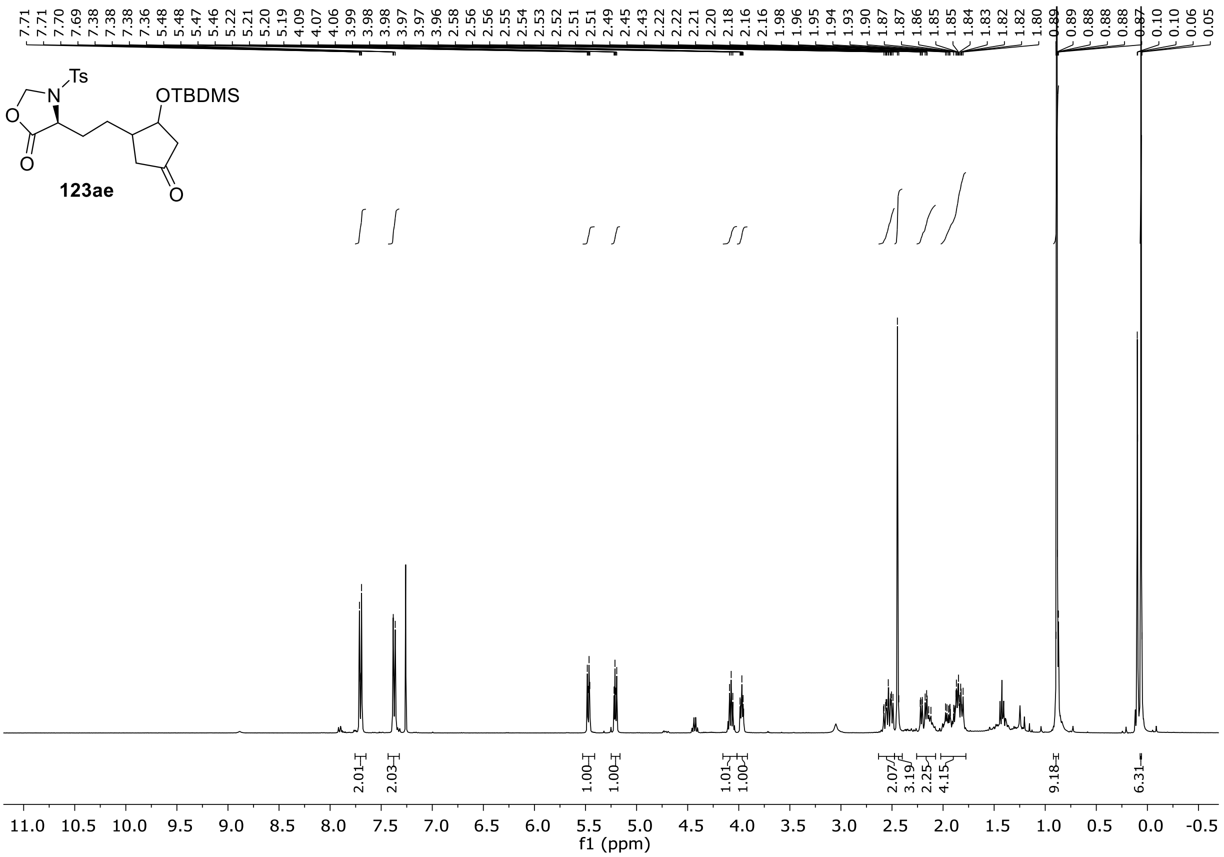
7.71
7.71
7.70
7.69
7.38
7.38
7.38
7.36
5.48
5.48
5.47
5.46
5.22
5.21
5.20
5.19
4.09
4.07
4.06
3.99
3.98
3.98
3.97
3.97
3.96
2.58
2.56
2.56
2.55
2.54
2.53
2.52
2.51
2.51
2.49
2.45
2.43
2.22
2.22
2.21
2.20
2.18
2.16
2.16
1.98
1.96
1.95
1.94
1.93
1.90
1.87
1.87
1.86
1.85
1.85
1.84
1.83
1.82
1.82
1.80
0.89
0.89
0.88
0.88
0.88
0.87
0.10
0.10
0.06
0.05
Ts
N
O
O
OTBDMS
O
2.01
2.03
1.00
1.00
1.01
1.00
2.07
3.19
2.25
4.15
9.18
6.31
11.0 10.5 10.0 9.5 9.0 8.5 8.0 7.5 7.0 6.5 6.0 5.5 5.0 4.5 4.0 3.5 3.0 2.5 2.0 1.5 1.0 0.5 0.0 -0.5
f1 (ppm)

123ae

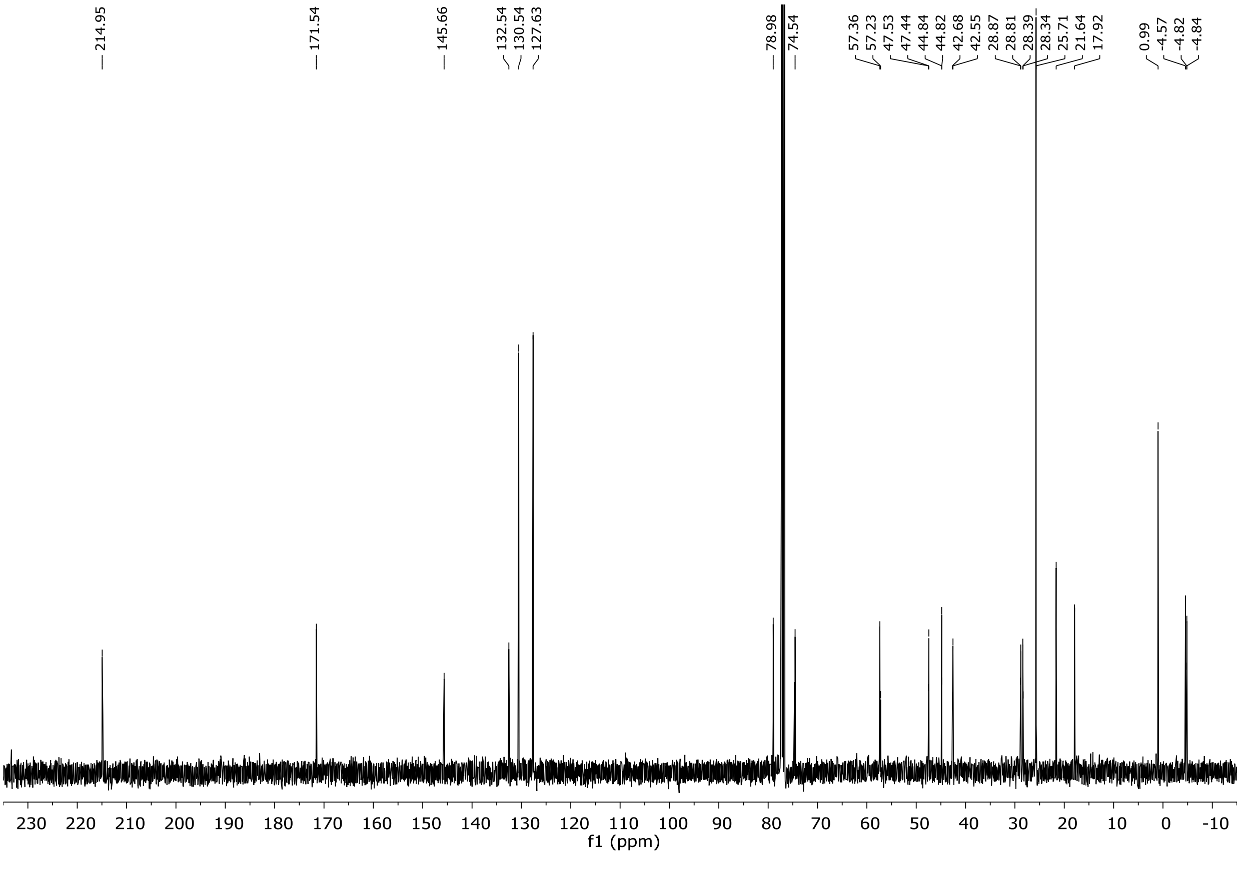
214.95
171.54
145.66
132.54
130.54
127.63
78.98
74.54
57.36
57.23
47.53
47.44
44.84
44.82
42.68
42.55
28.87
28.81
28.39
28.34
25.71
21.64
17.92
0.99
-4.57
-4.82
-4.84
230 220 210 200 190 180 170 160 150 140 130 120 110 100 90 80 70 60 50 40 30 20 10 0 -10
f1 (ppm)

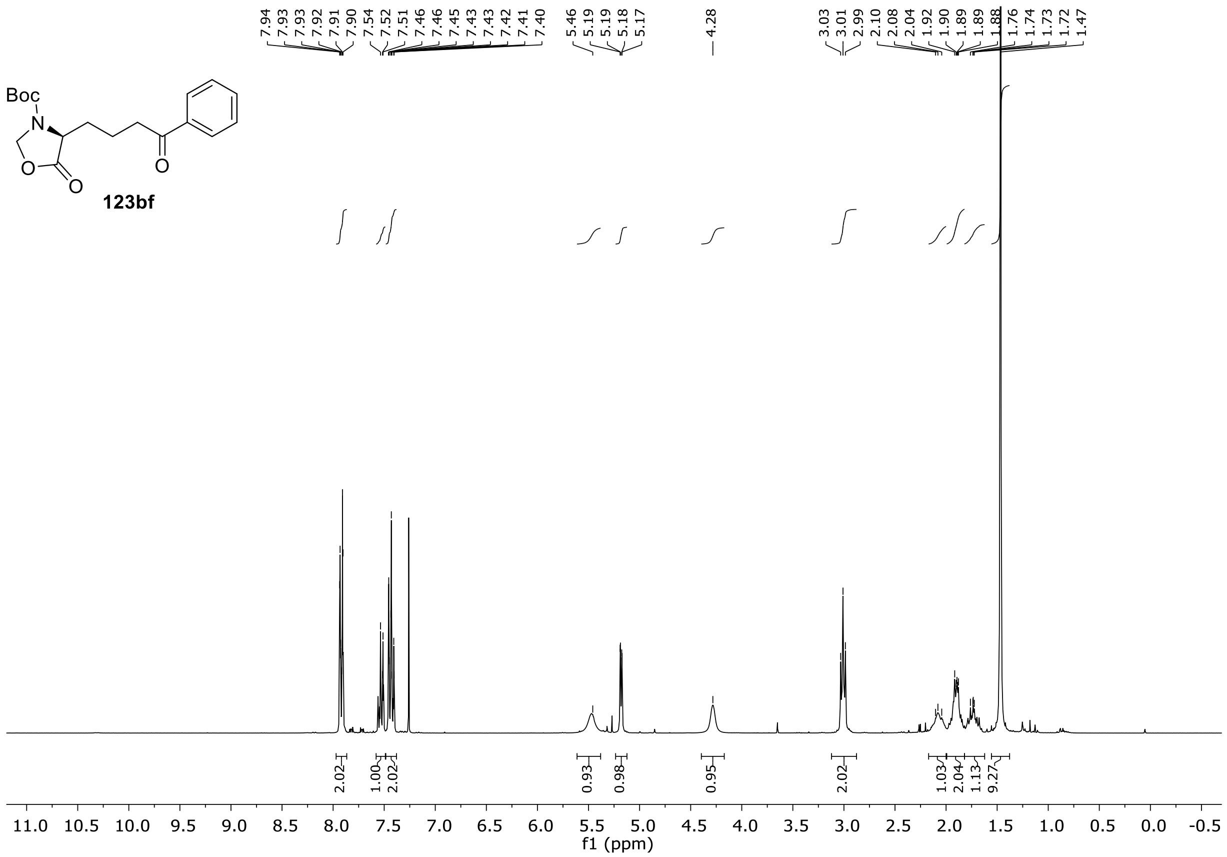
Boc
N
O
O
O
7.94
7.93
7.93
7.92
7.91
7.90
7.54
7.52
7.51
7.46
7.46
7.45
7.43
7.43
7.43
7.42
7.41
7.40
5.46
5.19
5.19
5.18
5.17
4.28
3.03
3.01
2.99
2.10
2.08
2.04
1.92
1.90
1.89
1.89
1.88
1.76
1.74
1.73
1.72
1.47
2.02
1.00
2.02
0.93
0.98
0.95
2.02
1.03
2.04
1.13
9.27
11.0
10.5
10.0
9.5
9.0
8.5
8.0
7.5
7.0
6.5
6.0
5.5
5.0
4.5
4.0
3.5
3.0
2.5
2.0
1.5
1.0
0.5
0.0
-0.5
f1 (ppm)

123bf

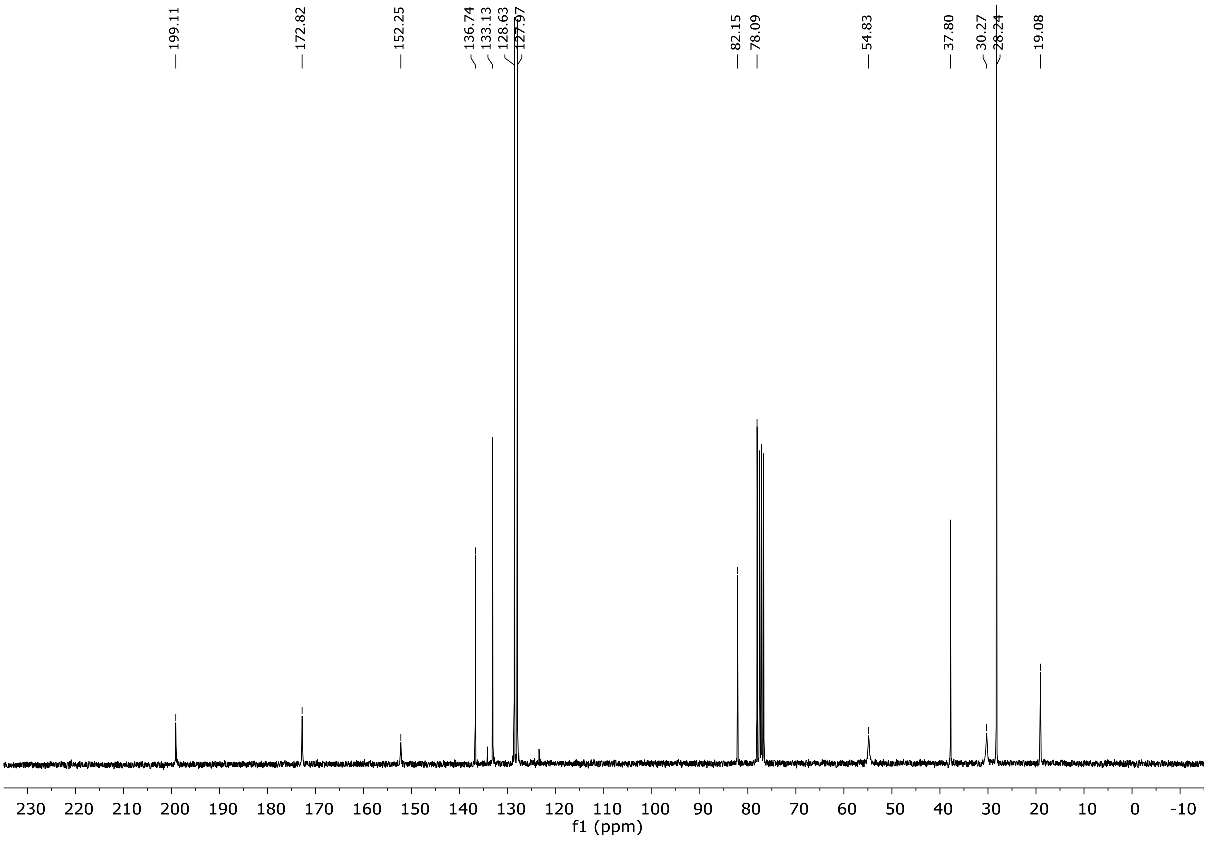
199.11
172.82
152.25
136.74
133.13
128.63
127.97
82.15
78.09
54.83
37.80
30.27
28.24
19.08
230
220
210
200
190
180
170
160
150
140
130
120
110
100
90
80
70
60
50
40
30
20
10
0
-10
f1 (ppm)

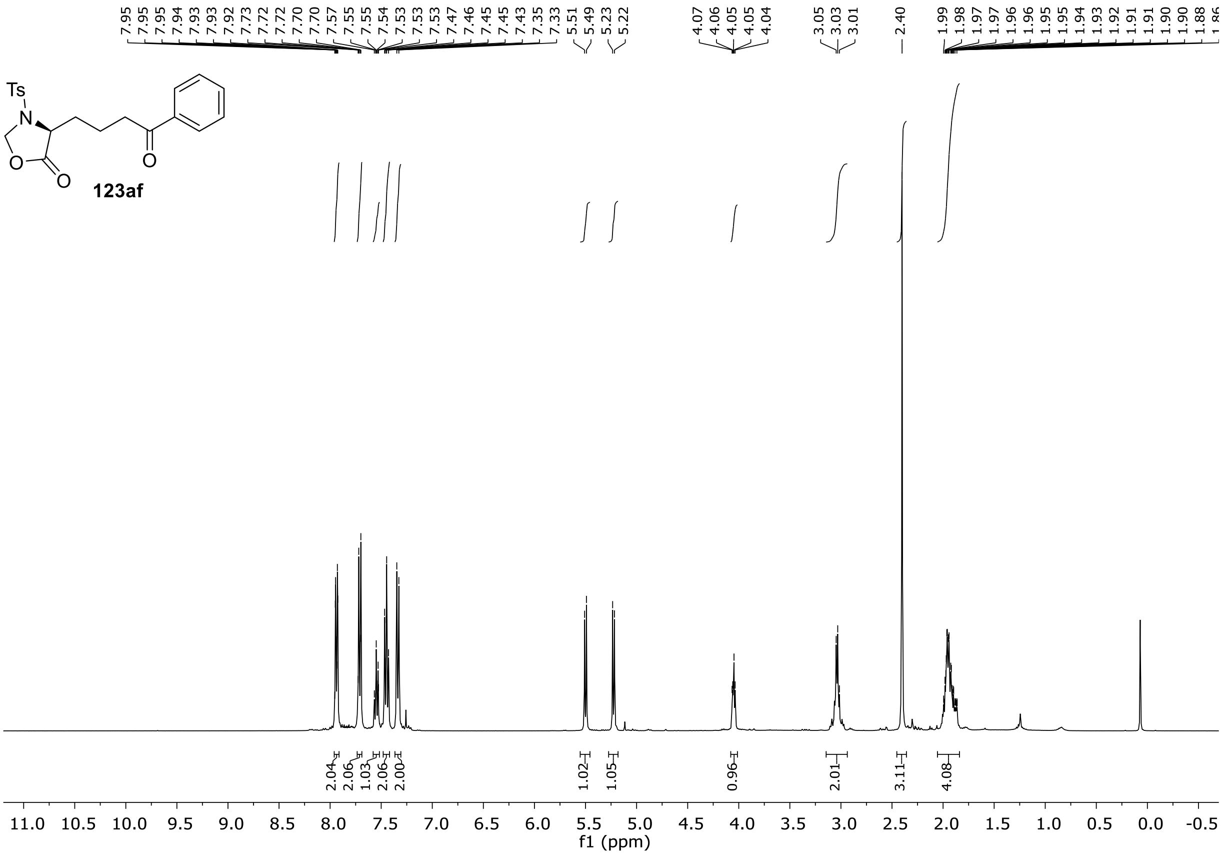
123af
7.95
7.95
7.95
7.94
7.93
7.93
7.92
7.73
7.72
7.72
7.70
7.70
7.57
7.55
7.55
7.54
7.53
7.53
7.53
7.47
7.46
7.45
7.45
7.43
7.35
7.33
5.51
5.49
5.23
5.22
4.07
4.06
4.05
4.05
4.04
3.05
3.03
3.01
2.40
1.99
1.98
1.97
1.97
1.96
1.96
1.95
1.95
1.94
1.93
1.92
1.91
1.91
1.90
1.90
1.88
Ts
N
O
O
O
2.04
2.06
1.03
2.06
2.00
1.02
1.05
0.96
2.01
3.11
4.08
11.0
10.5
10.0
9.5
9.0
8.5
8.0
7.5
7.0
6.5
6.0
5.5
5.0
4.5
4.0
3.5
3.0
2.5
2.0
1.5
1.0
0.5
0.0
-0.5
f1 (ppm)

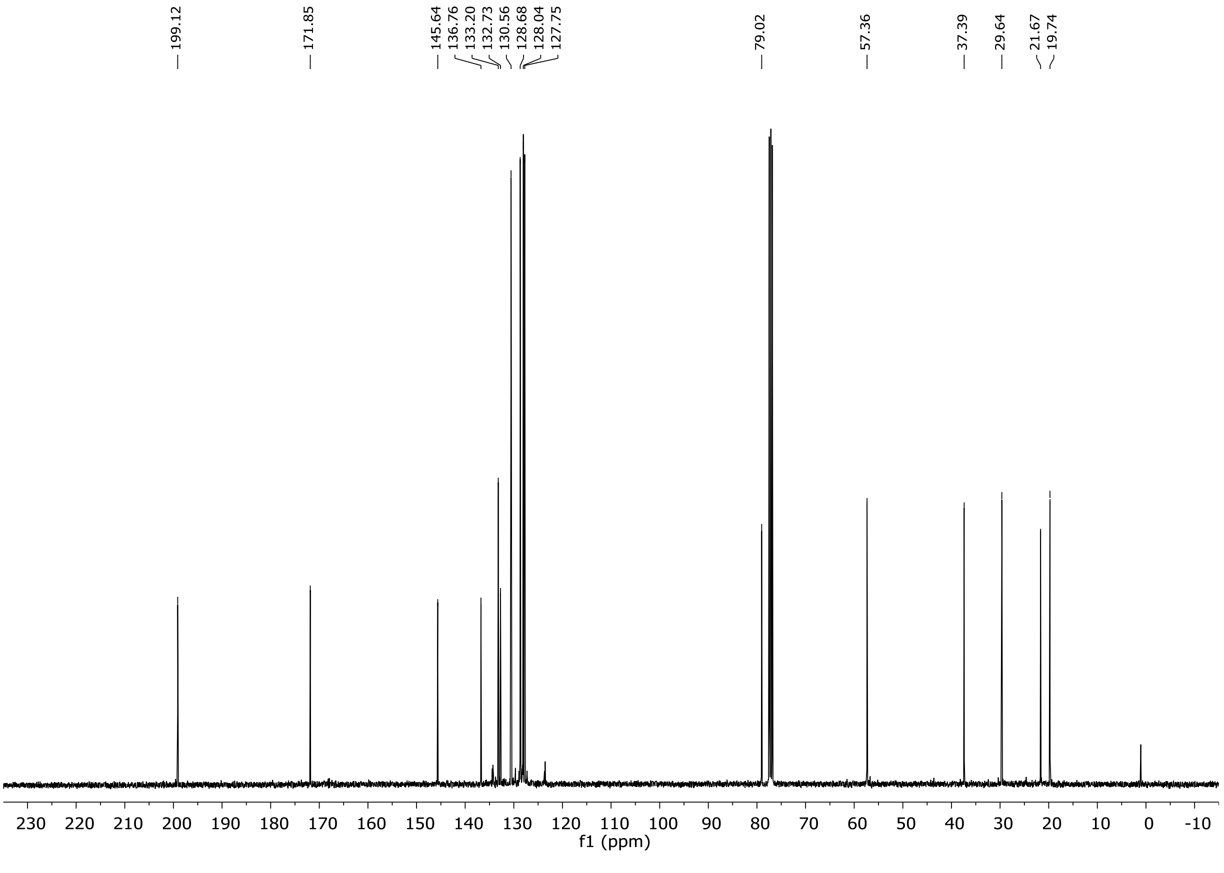
199.12
171.85
145.64
136.76
133.20
132.73
130.56
128.68
128.04
127.75
79.02
57.36
37.39
29.64
21.67
19.74
230
220
210
200
190
180
170
160
150
140
130
120
110
100
90
80
70
60
50
40
30
20
10
0
-10
f1 (ppm)

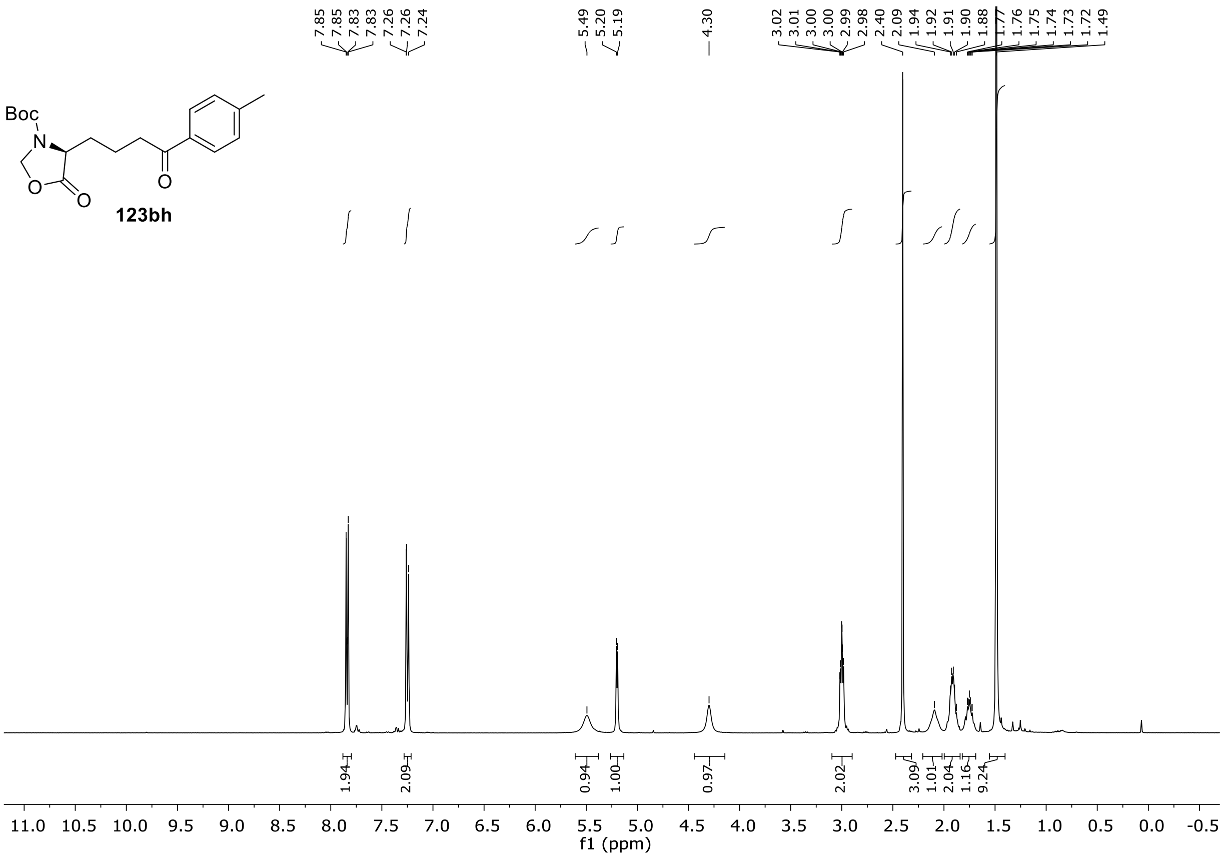
Boc
N
O
O
O
123bh
7.85
7.85
7.83
7.83
7.26
7.26
7.24
5.49
5.20
5.19
4.30
3.02
3.01
3.00
3.00
2.99
2.98
2.40
2.09
1.94
1.92
1.91
1.90
1.88
1.77
1.76
1.75
1.74
1.73
1.72
1.49
1.94
2.09
0.94
1.00
0.97
2.02
3.09
1.01
2.04
1.16
9.24
11.0 10.5 10.0 9.5 9.0 8.5 8.0 7.5 7.0 6.5 6.0 5.5 5.0 4.5 4.0 3.5 3.0 2.5 2.0 1.5 1.0 0.5 0.0 -0.5
f1 (ppm)

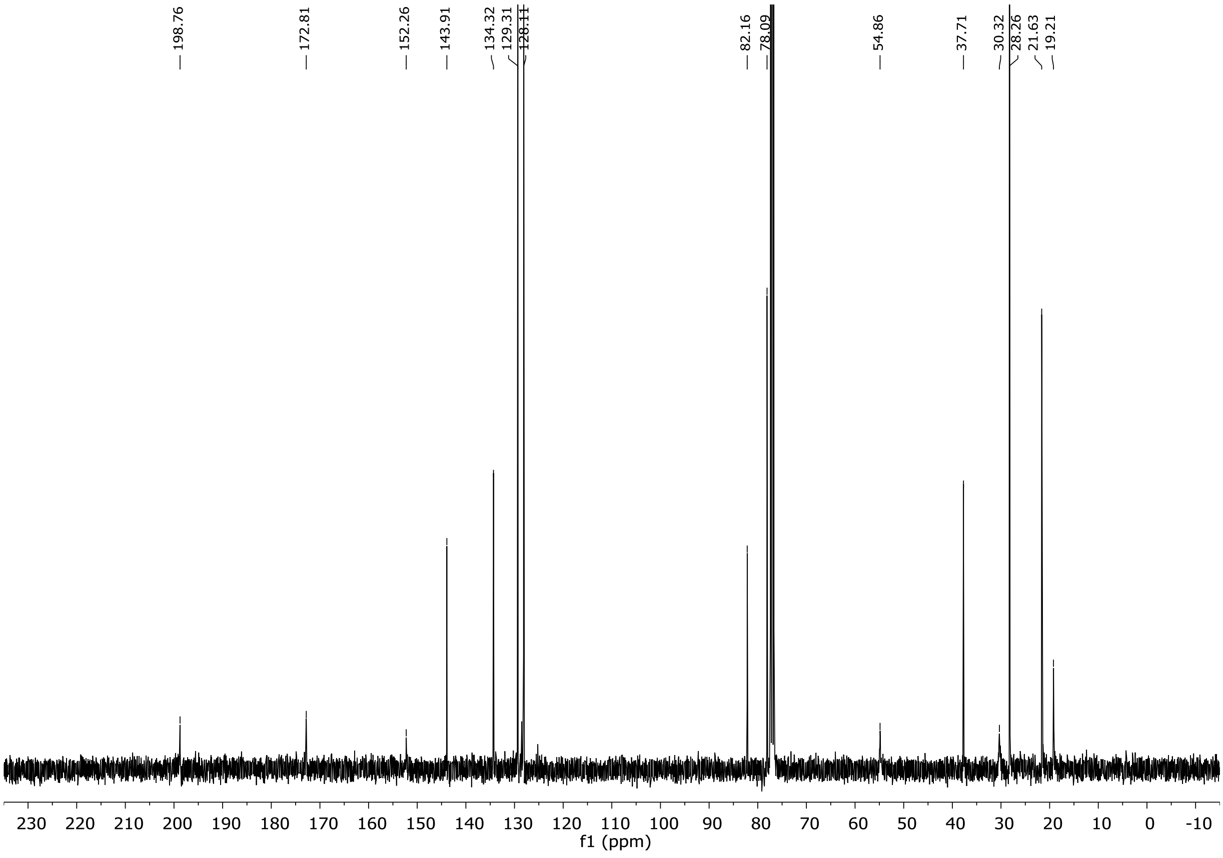
198.76
172.81
152.26
143.91
134.32
129.31
128.11
82.16
78.09
54.86
37.71
30.32
28.26
21.63
19.21
230 220 210 200 190 180 170 160 150 140 130 120 110 100 90 80 70 60 50 40 30 20 10 0 -10
f1 (ppm)

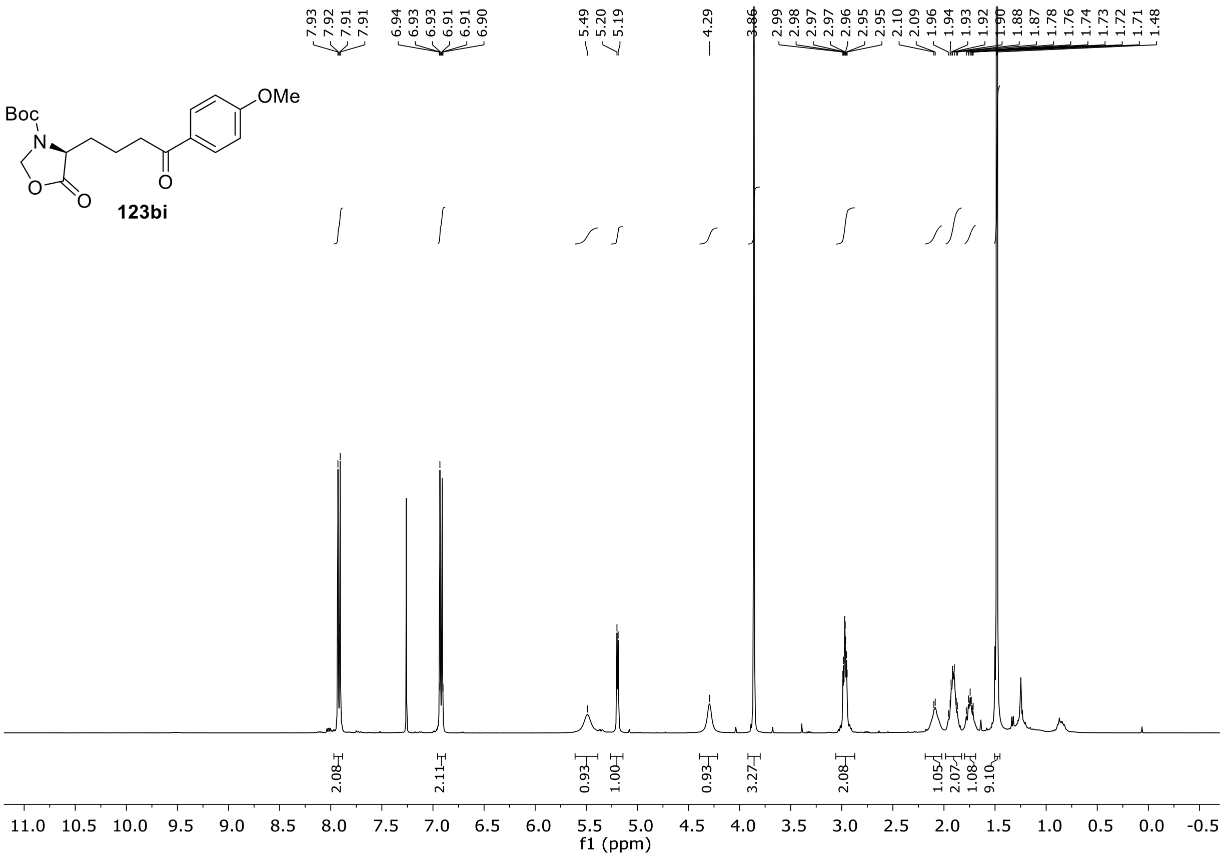
Boc
N
O
O
OMe
O
123bi
7.93
7.92
7.91
7.91
6.94
6.93
6.93
6.91
6.91
6.90
5.49
5.20
5.19
4.29
3.86
2.99
2.98
2.97
2.97
2.96
2.95
2.95
2.10
2.09
1.96
1.94
1.93
1.92
1.90
1.88
1.87
1.78
1.76
1.74
1.73
1.72
1.71
1.48
2.08
2.11
0.93
1.00
0.93
3.27
2.08
1.05
2.07
1.08
9.10
11.0 10.5 10.0 9.5 9.0 8.5 8.0 7.5 7.0 6.5 6.0 5.5 5.0 4.5 4.0 3.5 3.0 2.5 2.0 1.5 1.0 0.5 0.0 -0.5
f1 (ppm)

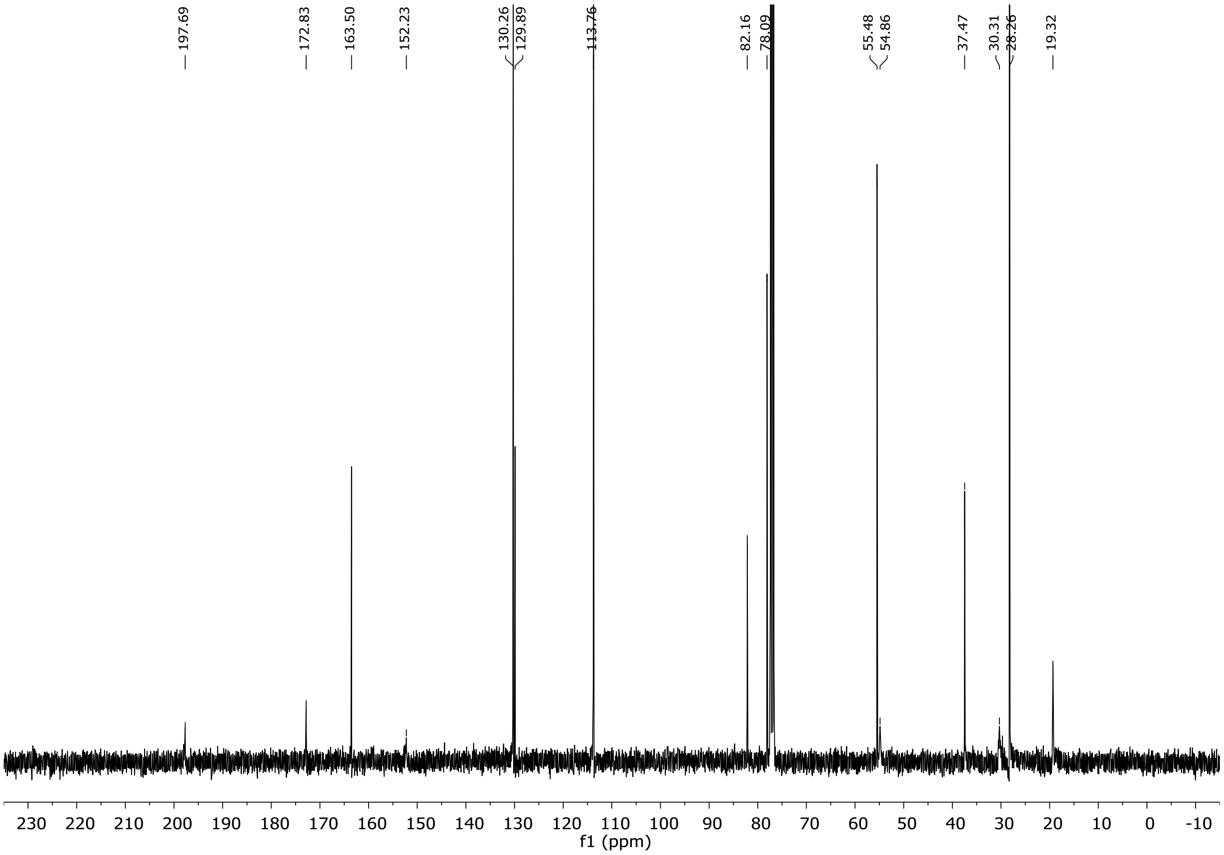
197.69
172.83
163.50
152.23
130.26
129.89
113.76
82.16
78.09
55.48
54.86
37.47
30.31
28.26
19.32
230 220 210 200 190 180 170 160 150 140 130 120 110 100 90 80 70 60 50 40 30 20 10 0 -10
f1 (ppm)

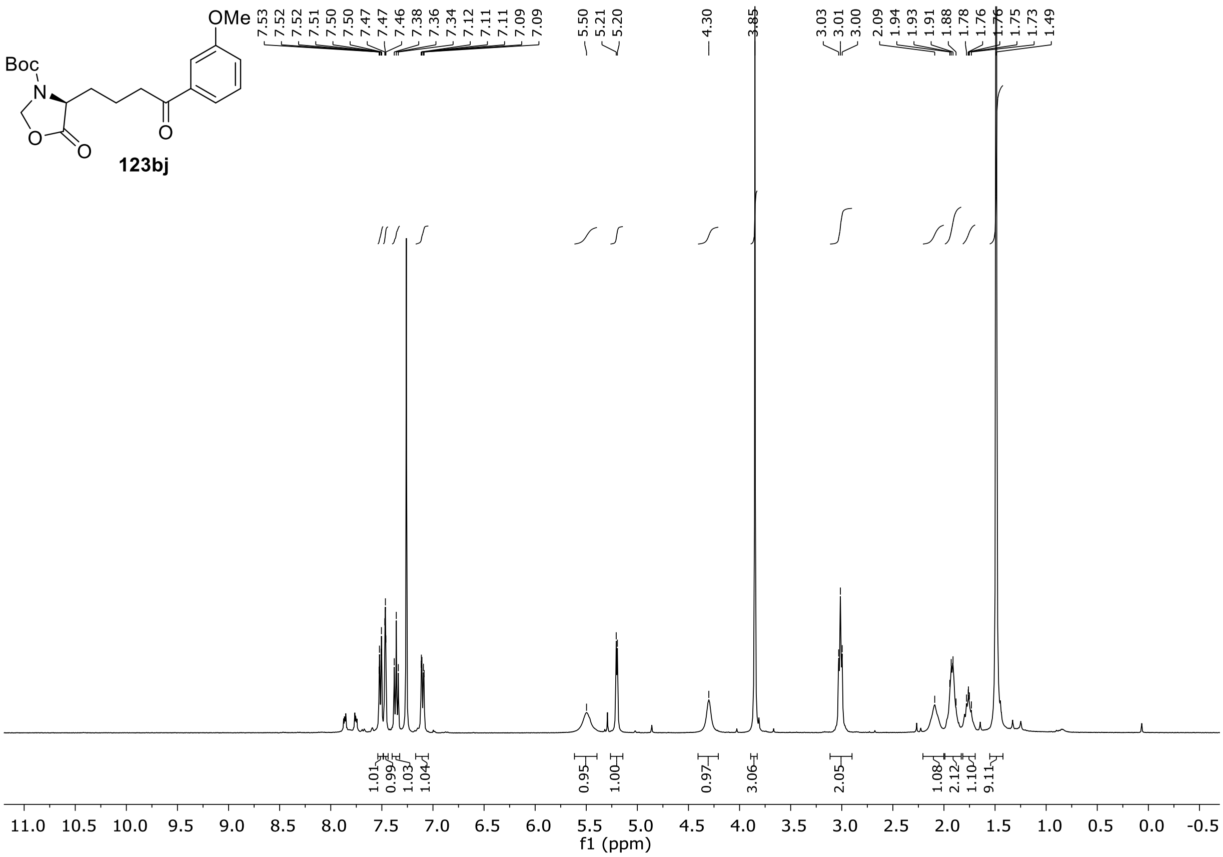
OMe
Boc
N
O
O
O
7.53
7.52
7.52
7.51
7.50
7.50
7.47
7.46
7.38
7.36
7.34
7.12
7.11
7.11
7.09
7.09
5.50
5.21
5.20
4.30
3.85
3.03
3.01
3.00
2.09
1.94
1.93
1.91
1.88
1.78
1.76
1.76
1.75
1.73
1.49
1.01
0.99
1.03
1.04
0.95
1.00
0.97
3.06
2.05
1.08
2.12
1.10
9.11
11.0
10.5
10.0
9.5
9.0
8.5
8.0
7.5
7.0
6.5
6.0
5.5
5.0
4.5
4.0
3.5
3.0
2.5
2.0
1.5
1.0
0.5
0.0
-0.5
f1 (ppm)

123bj

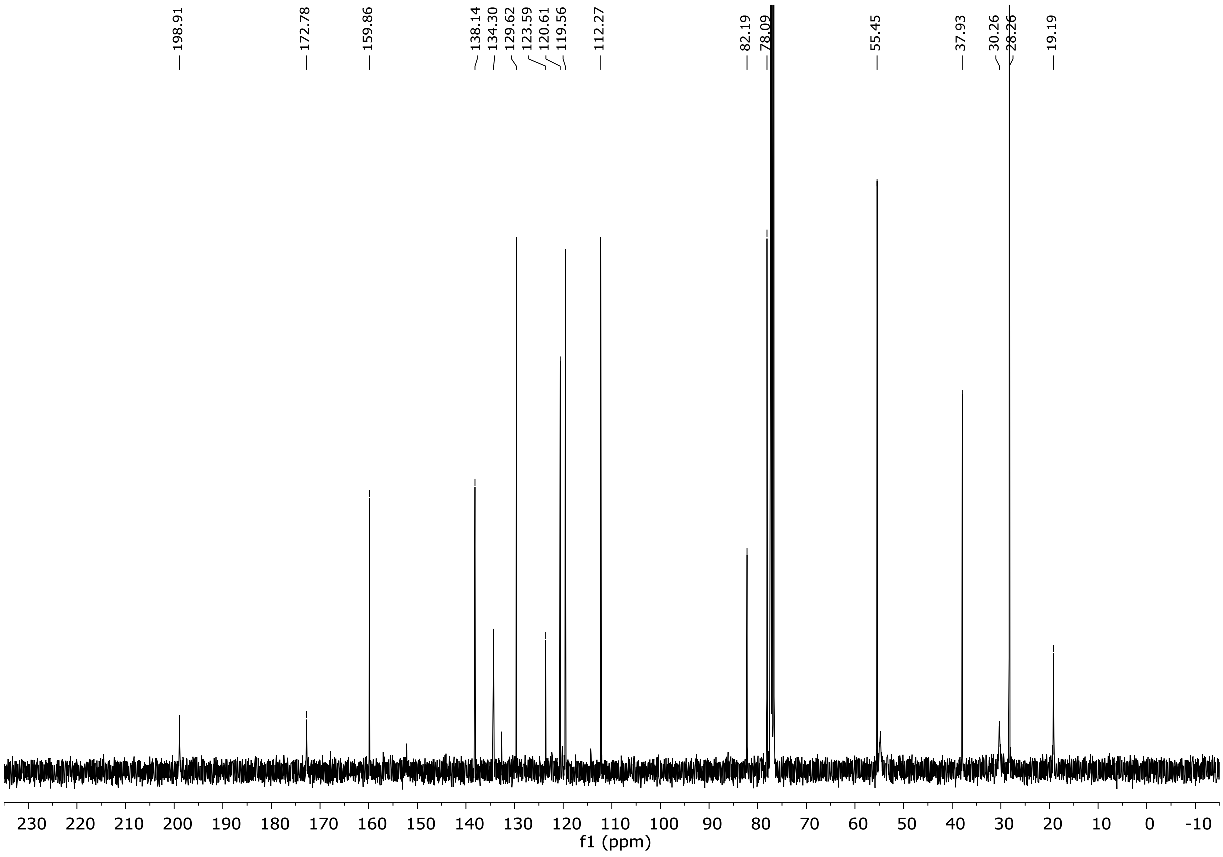
198.91
172.78
159.86
138.14
134.30
129.62
123.59
120.61
119.56
112.27
82.19
78.09
55.45
37.93
30.26
28.26
19.19
230
220
210
200
190
180
170
160
150
140
130
120
110
100
90
80
70
60
50
40
30
20
10
0
-10
f1 (ppm)

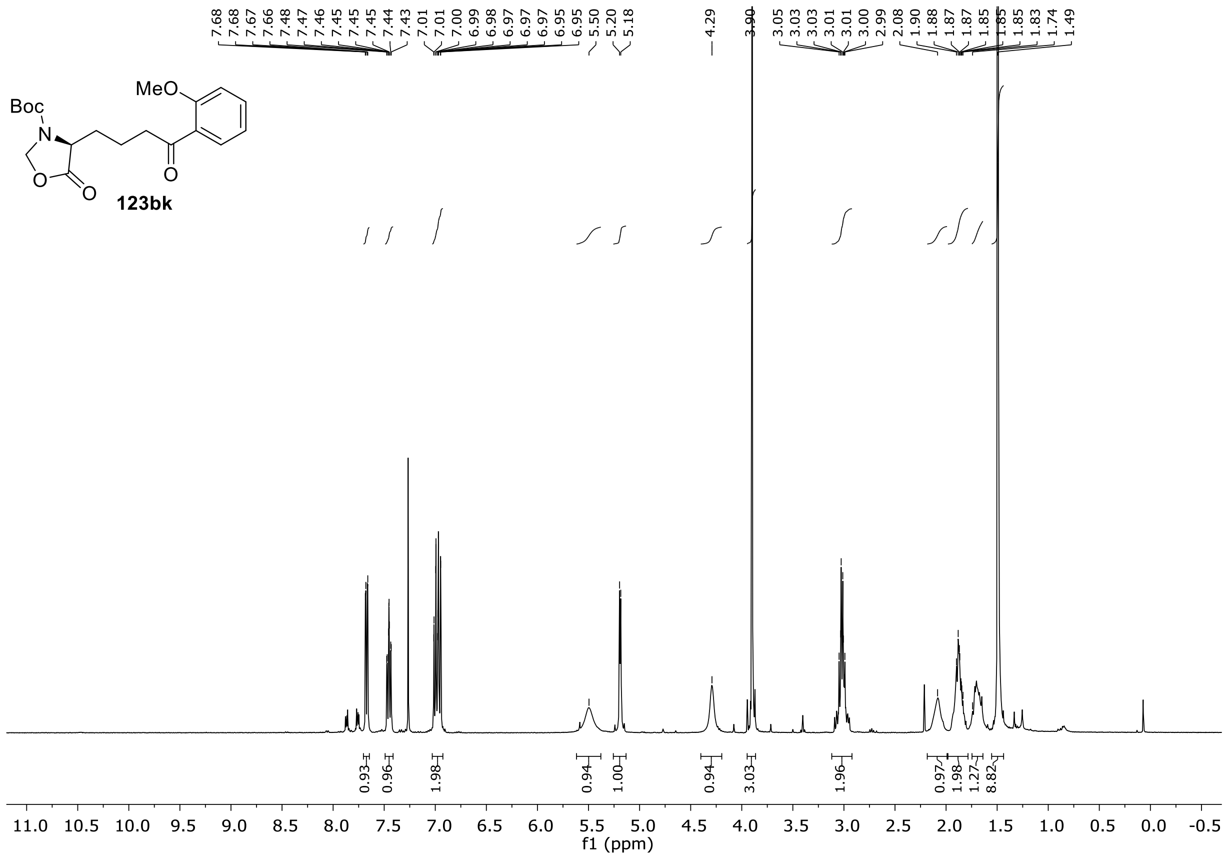
MeO
Boc
N
O
O
O
7.68
7.68
7.67
7.66
7.48
7.47
7.46
7.45
7.45
7.45
7.44
7.43
7.01
7.01
7.00
6.99
6.98
6.97
6.97
6.97
6.95
6.95
5.50
5.20
5.18
4.29
3.90
3.05
3.03
3.03
3.01
3.01
3.00
2.99
2.08
1.90
1.88
1.87
1.87
1.85
1.85
1.85
1.83
1.74
1.49
0.93
0.96
1.98
0.94
1.00
0.94
3.03
1.96
0.97
1.98
1.27
8.82
11.0 10.5 10.0 9.5 9.0 8.5 8.0 7.5 7.0 6.5 6.0 5.5 5.0 4.5 4.0 3.5 3.0 2.5 2.0 1.5 1.0 0.5 0.0 -0.5
f1 (ppm)

123bk

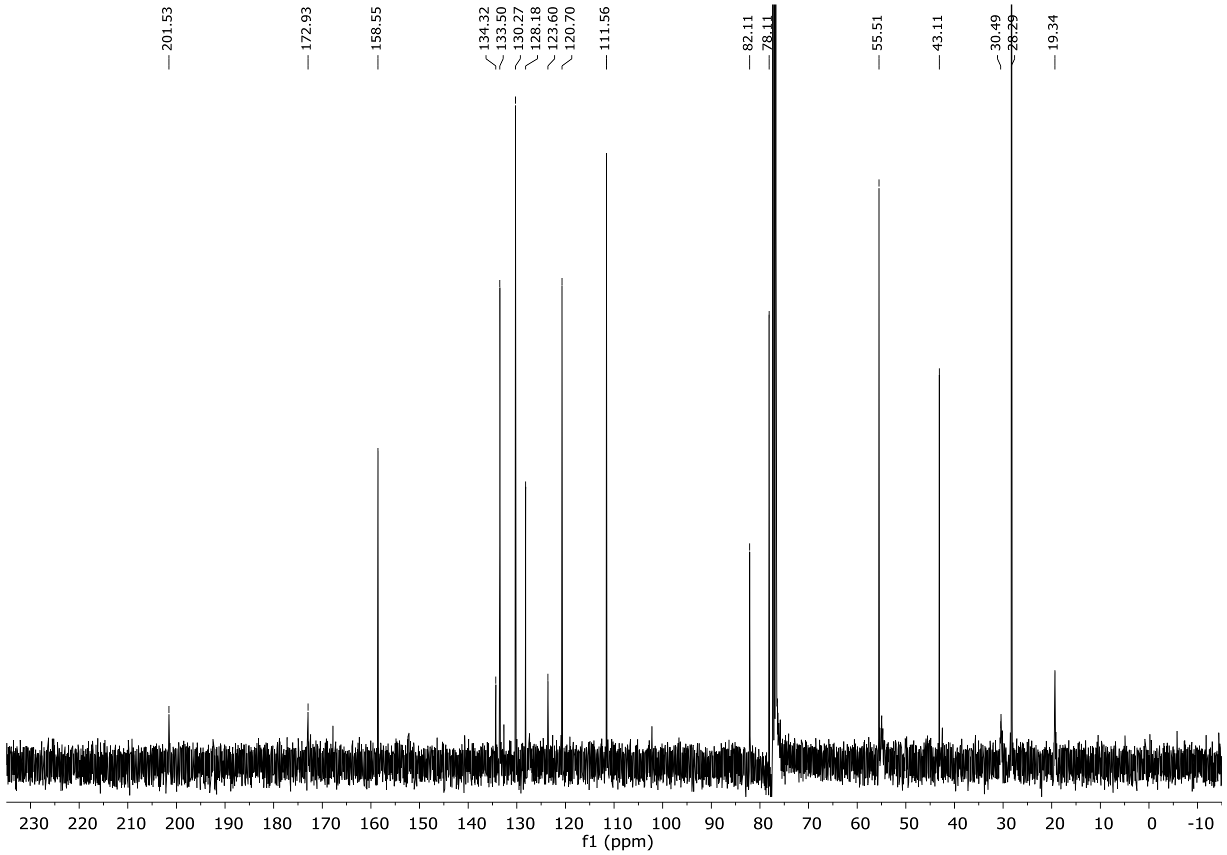
201.53
172.93
158.55
134.32
133.50
130.27
128.18
123.60
120.70
111.56
82.11
78.11
55.51
43.11
30.49
28.29
19.34
230 220 210 200 190 180 170 160 150 140 130 120 110 100 90 80 70 60 50 40 30 20 10 0 -10
f1 (ppm)

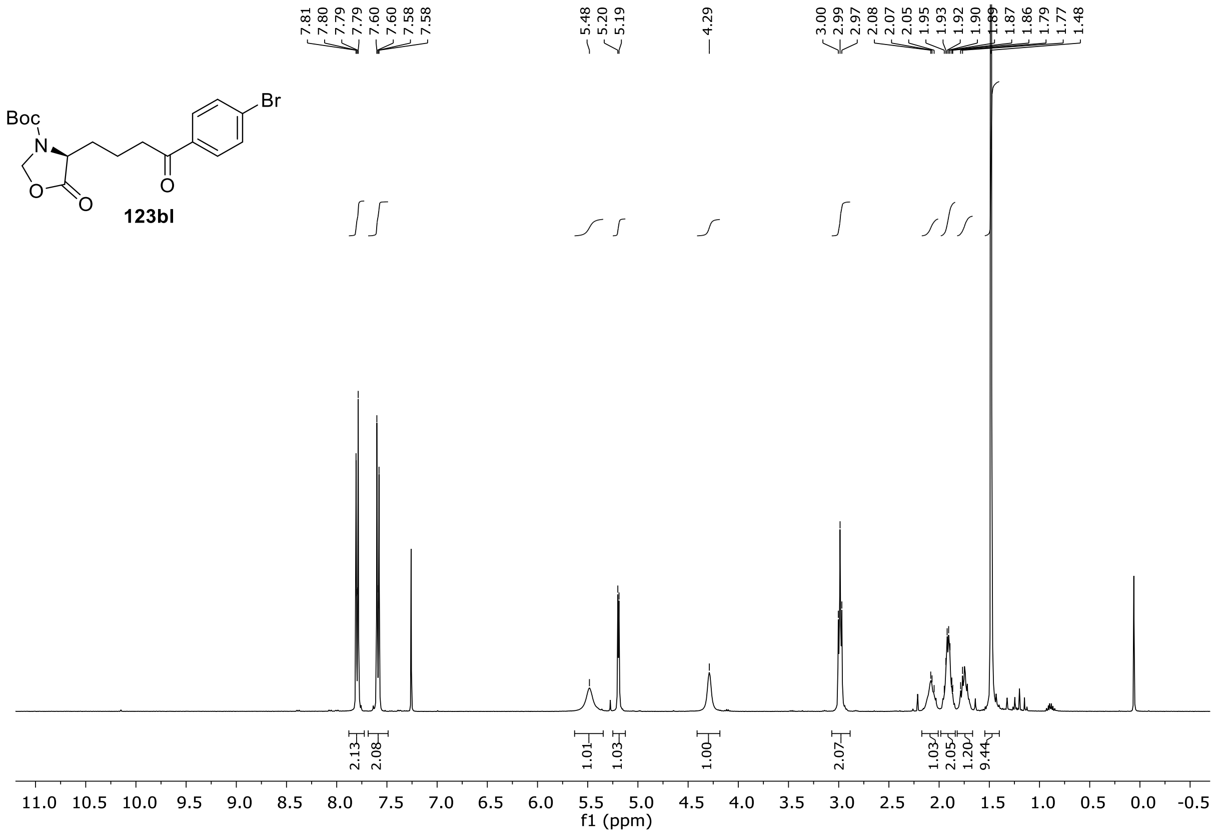
7.81
7.80
7.79
7.79
7.60
7.60
7.58
7.58
5.48
5.20
5.19
4.29
3.00
2.99
2.97
2.08
2.07
2.05
1.95
1.93
1.92
1.90
1.89
1.87
1.86
1.79
1.77
1.48
Boc
N
O
O
O
Br
123bl
2.13
2.08
1.01
1.03
1.00
2.07
1.03
2.05
1.20
9.44
11.0 10.5 10.0 9.5 9.0 8.5 8.0 7.5 7.0 6.5 6.0 5.5 5.0 4.5 4.0 3.5 3.0 2.5 2.0 1.5 1.0 0.5 0.0 -0.5
f1 (ppm)

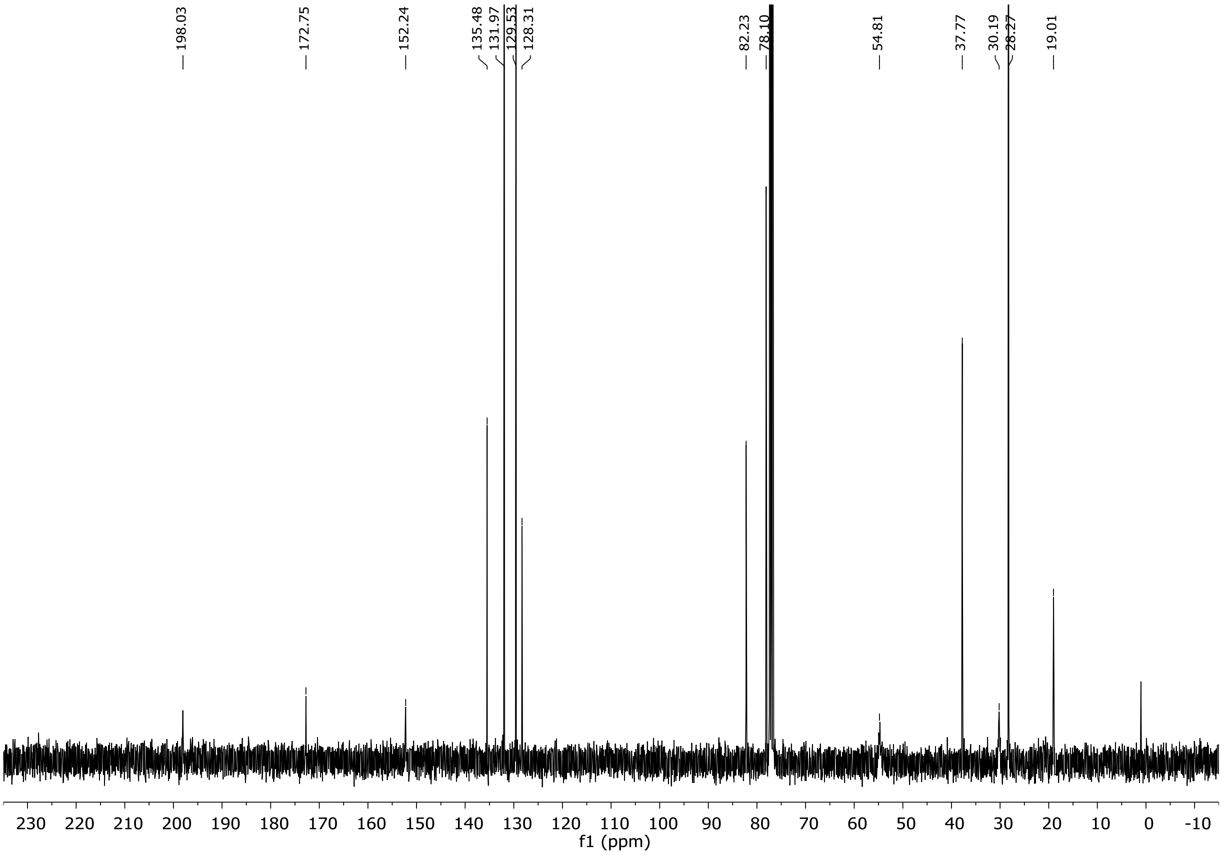
198.03
172.75
152.24
135.48
131.97
129.53
128.31
82.23
78.10
54.81
37.77
30.19
28.27
19.01
230 220 210 200 190 180 170 160 150 140 130 120 110 100 90 80 70 60 50 40 30 20 10 0 -10
f1 (ppm)

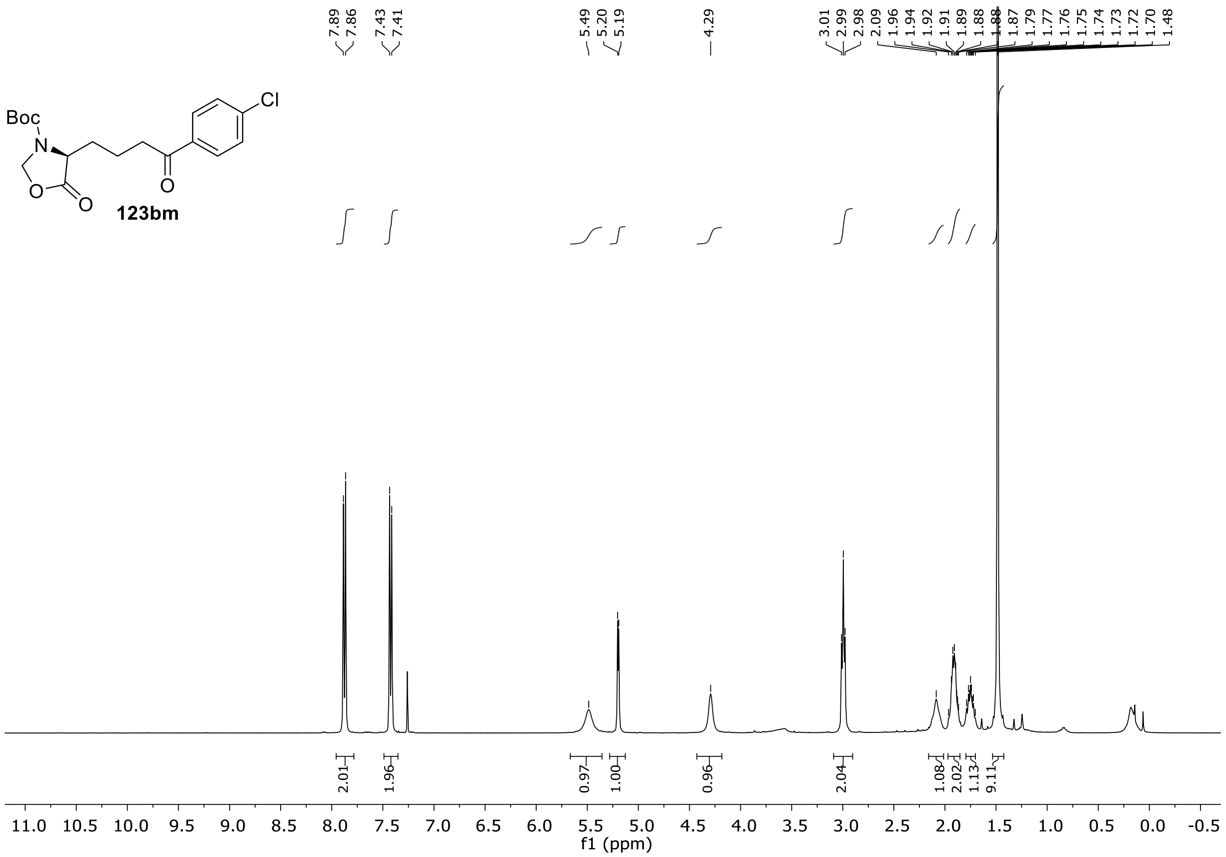
Boc
N
O
O
O
Cl
7.89
7.86
7.43
7.41
5.49
5.20
5.19
4.29
3.01
2.99
2.98
2.09
1.96
1.94
1.92
1.91
1.89
1.88
1.88
1.87
1.79
1.77
1.76
1.75
1.74
1.73
1.72
1.70
1.48
2.01
1.96
0.97
1.00
0.96
2.04
1.08
2.02
1.13
9.11
11.0 10.5 10.0 9.5 9.0 8.5 8.0 7.5 7.0 6.5 6.0 5.5 5.0 4.5 4.0 3.5 3.0 2.5 2.0 1.5 1.0 0.5 0.0 -0.5
f1 (ppm)

123bm

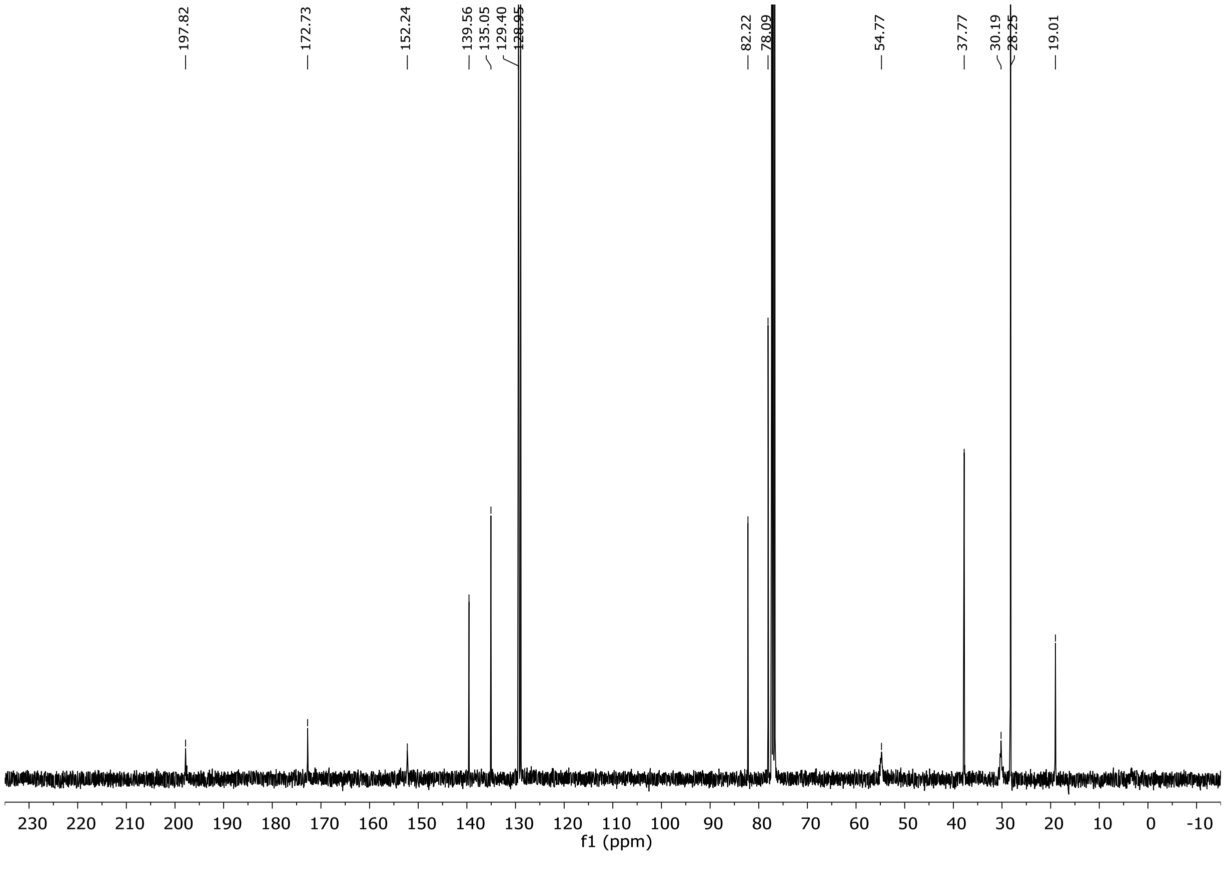
197.82
172.73
152.24
139.56
135.05
129.40
128.95
82.22
78.09
54.77
37.77
30.19
28.25
19.01
230 220 210 200 190 180 170 160 150 140 130 120 110 100 90 80 70 60 50 40 30 20 10 0 -10
f1 (ppm)

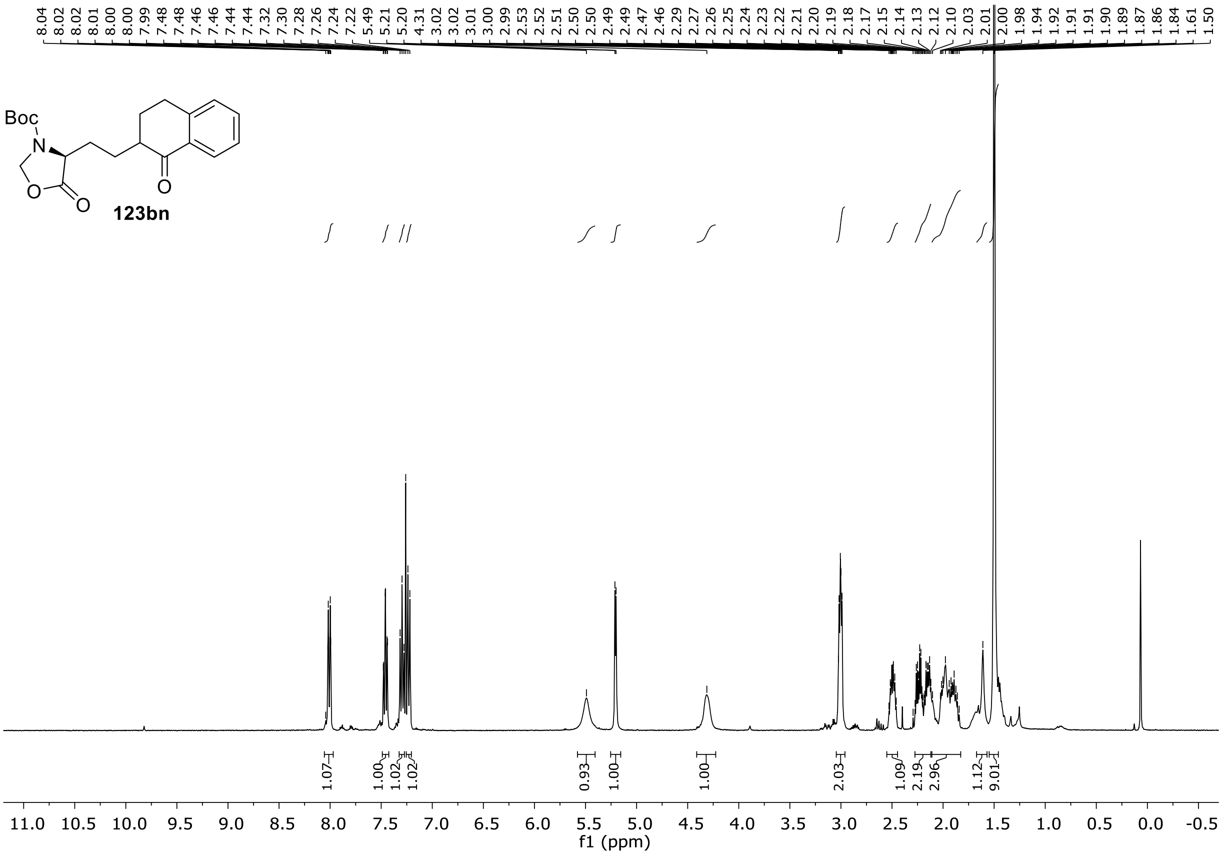
8.04
8.02
8.02
8.01
8.00
8.00
7.99
7.48
7.48
7.46
7.46
7.44
7.44
7.32
7.30
7.28
7.26
7.24
7.22
5.49
5.21
5.20
4.31
3.02
3.02
3.01
3.00
2.99
2.53
2.52
2.51
2.50
2.50
2.49
2.49
2.47
2.46
2.29
2.27
2.26
2.25
2.24
2.23
2.22
2.21
2.20
2.19
2.18
2.17
2.15
2.14
2.13
2.12
2.10
2.03
2.01
2.00
1.98
1.94
1.92
1.91
1.91
1.90
1.89
1.87
1.86
1.84
1.61
1.50
Boc
N
O
O
O
123bn
1.07
1.00
1.02
1.02
0.93
1.00
1.00
2.03
1.09
2.19
2.96
1.12
9.01
11.0 10.5 10.0 9.5 9.0 8.5 8.0 7.5 7.0 6.5 6.0 5.5 5.0 4.5 4.0 3.5 3.0 2.5 2.0 1.5 1.0 0.5 0.0 -0.5
f1 (ppm)

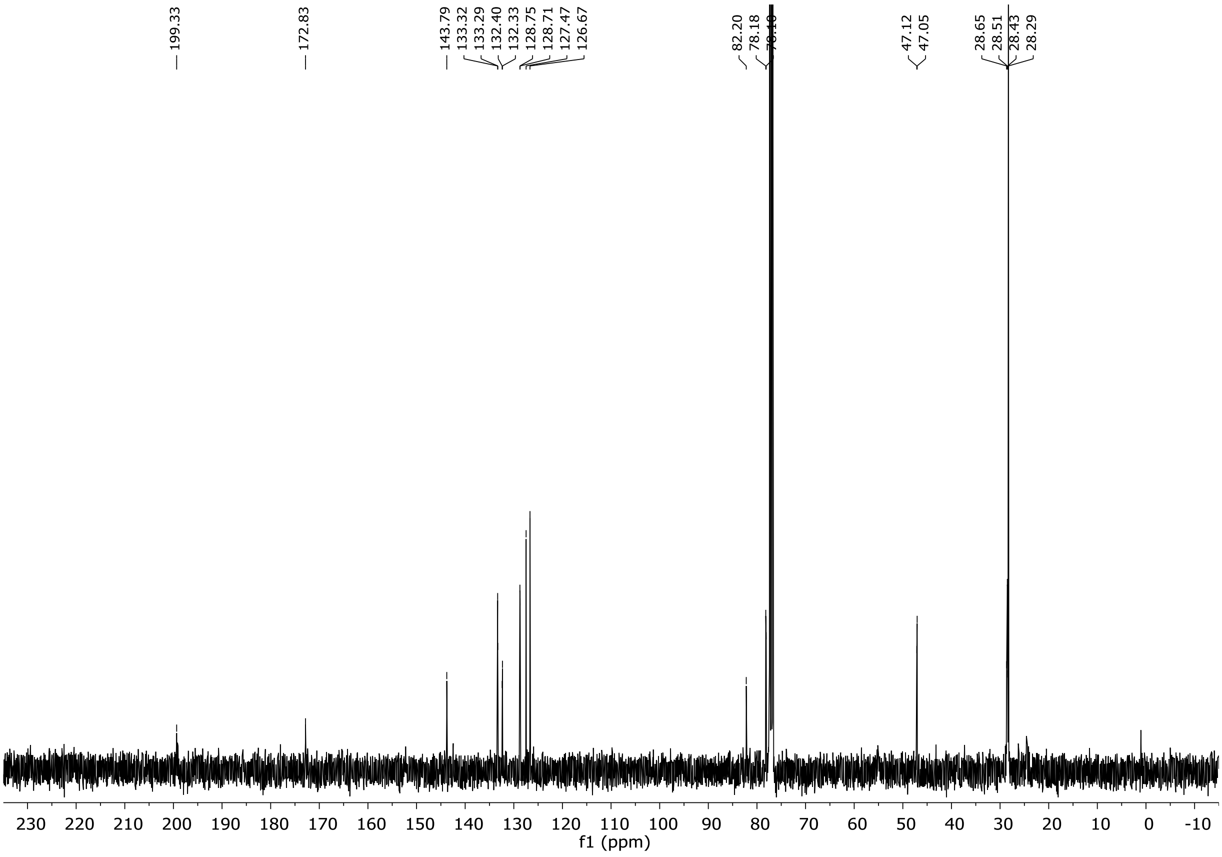
199.33
172.83
143.79
133.32
133.29
132.40
132.33
128.75
128.71
127.47
126.67
82.20
78.18
47.12
47.05
28.65
28.51
28.43
28.29
230 220 210 200 190 180 170 160 150 140 130 120 110 100 90 80 70 60 50 40 30 20 10 0 -10
f1 (ppm)

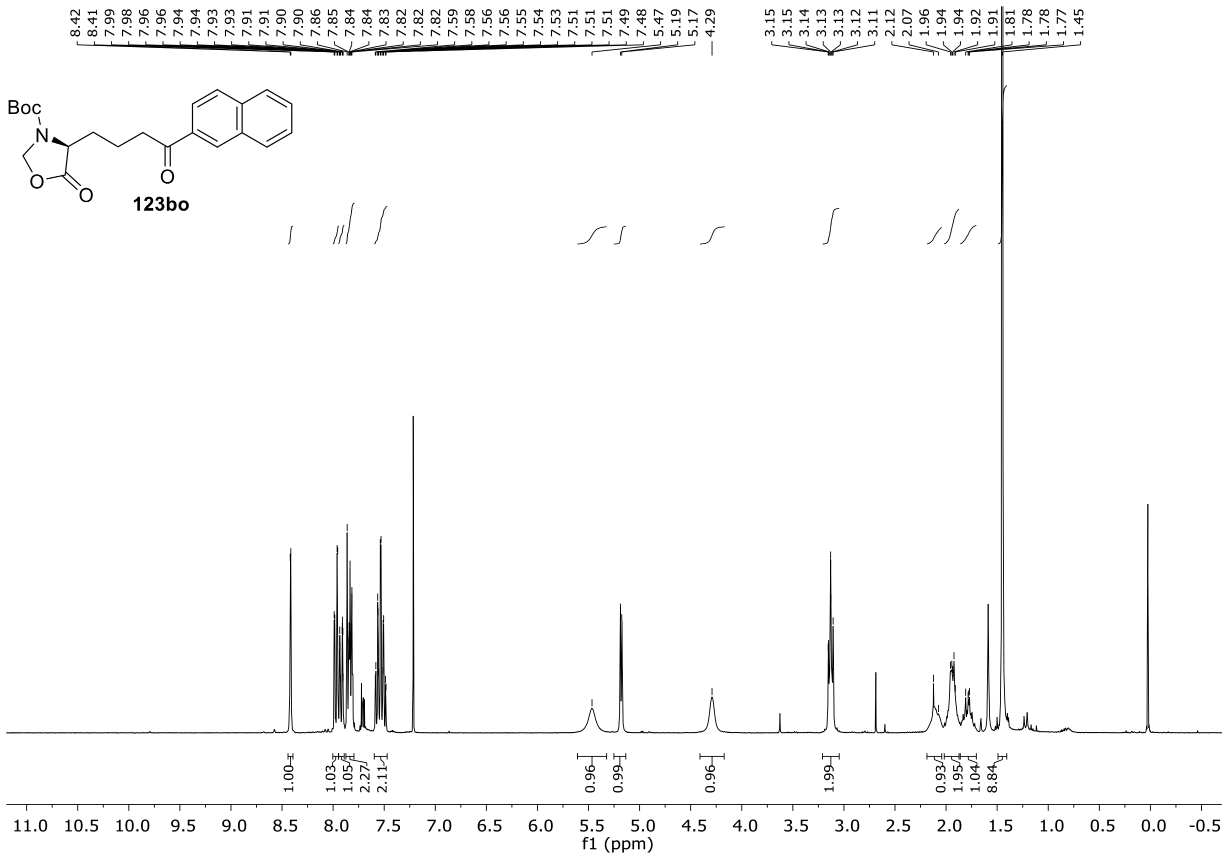
8.42
8.41
7.99
7.98
7.96
7.96
7.94
7.94
7.93
7.93
7.91
7.91
7.90
7.90
7.86
7.85
7.84
7.84
7.83
7.82
7.82
7.82
7.59
7.58
7.56
7.56
7.55
7.54
7.53
7.51
7.51
7.49
7.48
5.47
5.19
5.17
4.29
3.15
3.15
3.14
3.13
3.13
3.12
3.11
2.12
2.07
1.96
1.94
1.94
1.92
1.91
1.81
1.78
1.77
1.45
Boc
N
O
O
O
123bo
1.00
1.03
1.05
2.27
2.11
0.96
0.99
0.96
1.99
0.93
1.95
1.04
8.84
11.0
10.5
10.0
9.5
9.0
8.5
8.0
7.5
7.0
6.5
6.0
5.5
5.0
4.5
4.0
3.5
3.0
2.5
2.0
1.5
1.0
0.5
0.0
-0.5
f1 (ppm)

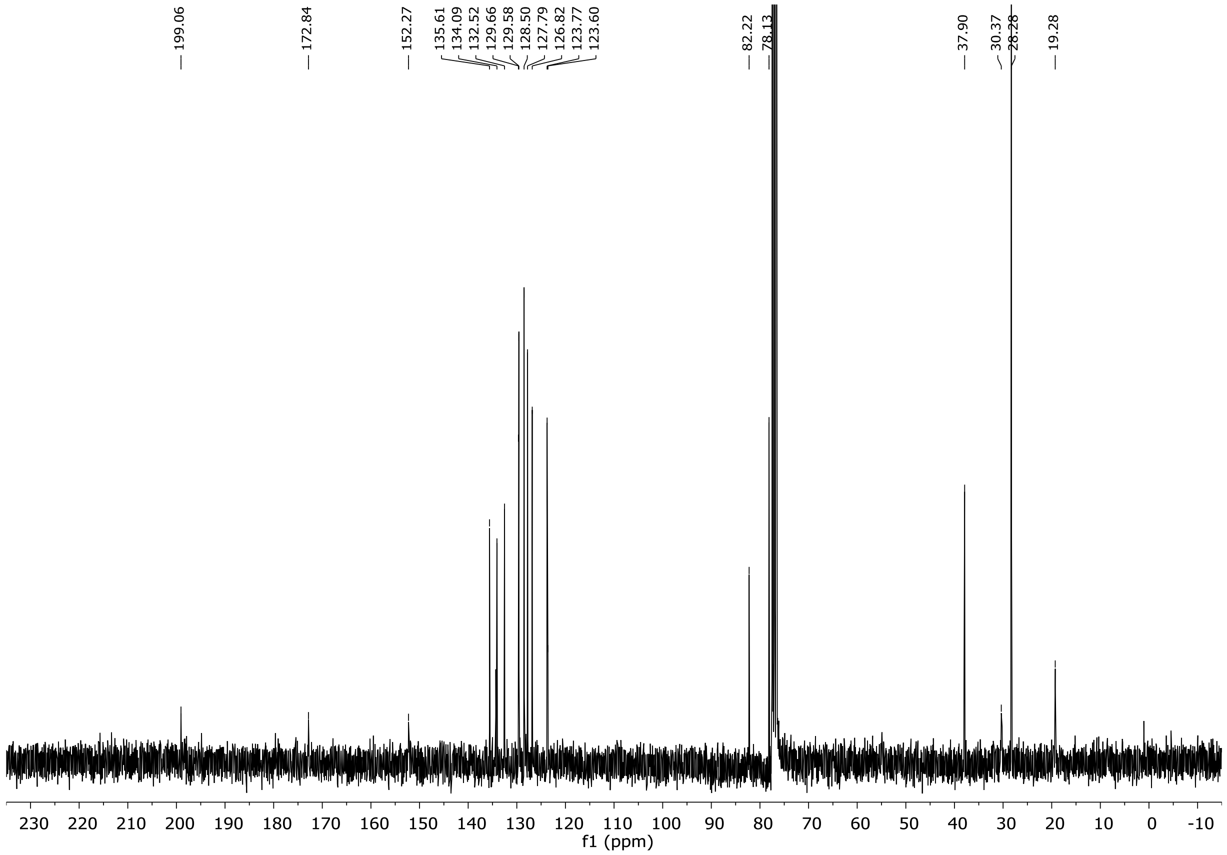
199.06
172.84
152.27
135.61
134.09
132.52
129.66
129.58
128.50
127.79
126.82
123.77
123.60
82.22
78.13
37.90
30.37
28.28
19.28
230
220
210
200
190
180
170
160
150
140
130
120
110
100
90
80
70
60
50
40
30
20
10
0
-10
f1 (ppm)

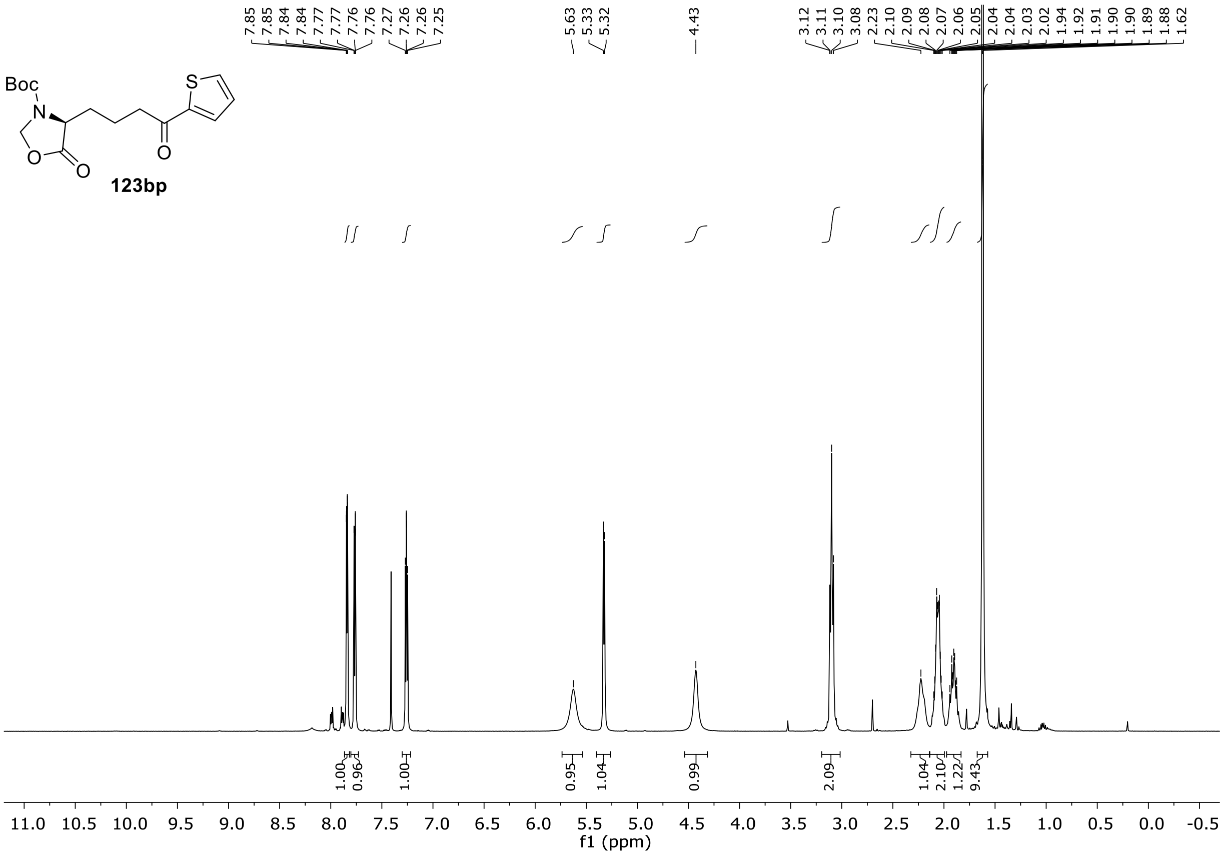
Boc
N
S
O
O
O
7.85
7.85
7.84
7.84
7.77
7.77
7.76
7.76
7.27
7.26
7.26
7.25
5.63
5.33
5.32
4.43
3.12
3.11
3.10
3.08
2.23
2.10
2.09
2.08
2.07
2.06
2.05
2.04
2.04
2.03
2.02
1.94
1.92
1.91
1.90
1.90
1.89
1.88
1.62
1.00
0.96
1.00
0.95
1.04
0.99
2.09
1.04
2.10
1.22
9.43
11.0
10.5
10.0
9.5
9.0
8.5
8.0
7.5
7.0
6.5
6.0
5.5
5.0
4.5
4.0
3.5
3.0
2.5
2.0
1.5
1.0
0.5
0.0
-0.5
f1 (ppm)

123bp

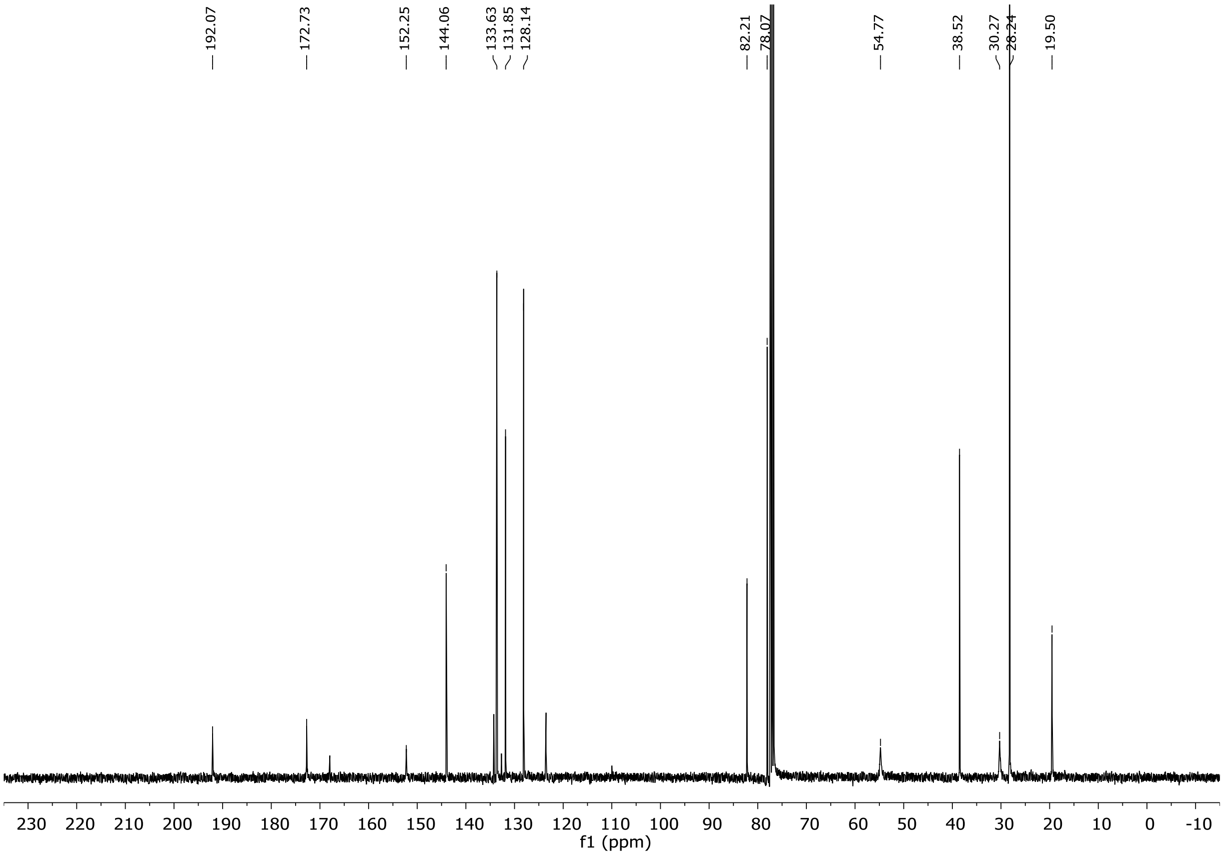
192.07
172.73
152.25
144.06
133.63
131.85
128.14
82.21
78.07
54.77
38.52
30.27
28.24
19.50
230
220
210
200
190
180
170
160
150
140
130
120
110
100
90
80
70
60
50
40
30
20
10
0
-10
f1 (ppm)

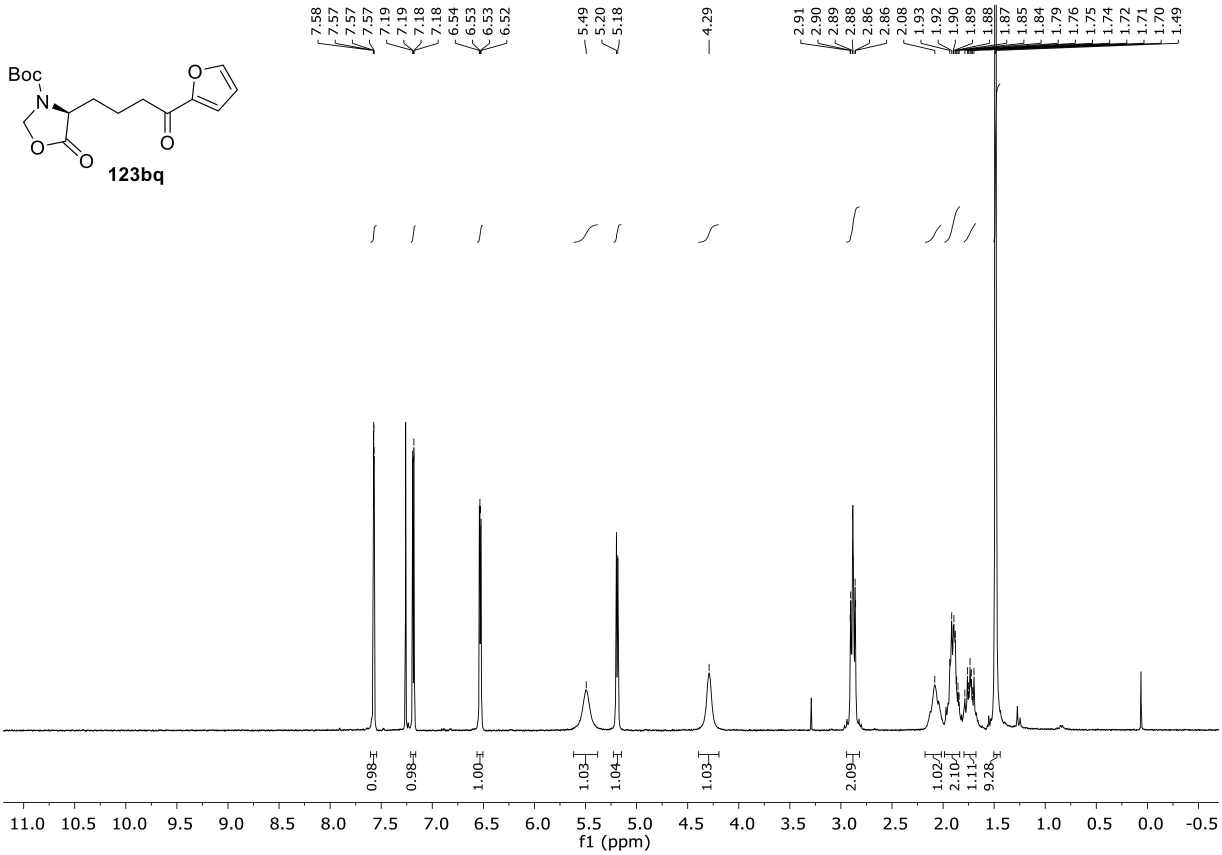
Boc
N
O
O
O
O
7.58
7.57
7.57
7.57
7.19
7.19
7.18
7.18
6.54
6.53
6.53
6.52
5.49
5.20
5.18
4.29
2.91
2.90
2.89
2.88
2.86
2.86
2.08
1.93
1.92
1.90
1.89
1.88
1.87
1.85
1.84
1.79
1.76
1.75
1.74
1.72
1.71
1.70
1.49
0.98
0.98
1.00
1.03
1.04
1.03
2.09
1.02
2.10
1.11
9.28
11.0 10.5 10.0 9.5 9.0 8.5 8.0 7.5 7.0 6.5 6.0 5.5 5.0 4.5 4.0 3.5 3.0 2.5 2.0 1.5 1.0 0.5 0.0 -0.5
f1 (ppm)

123bq

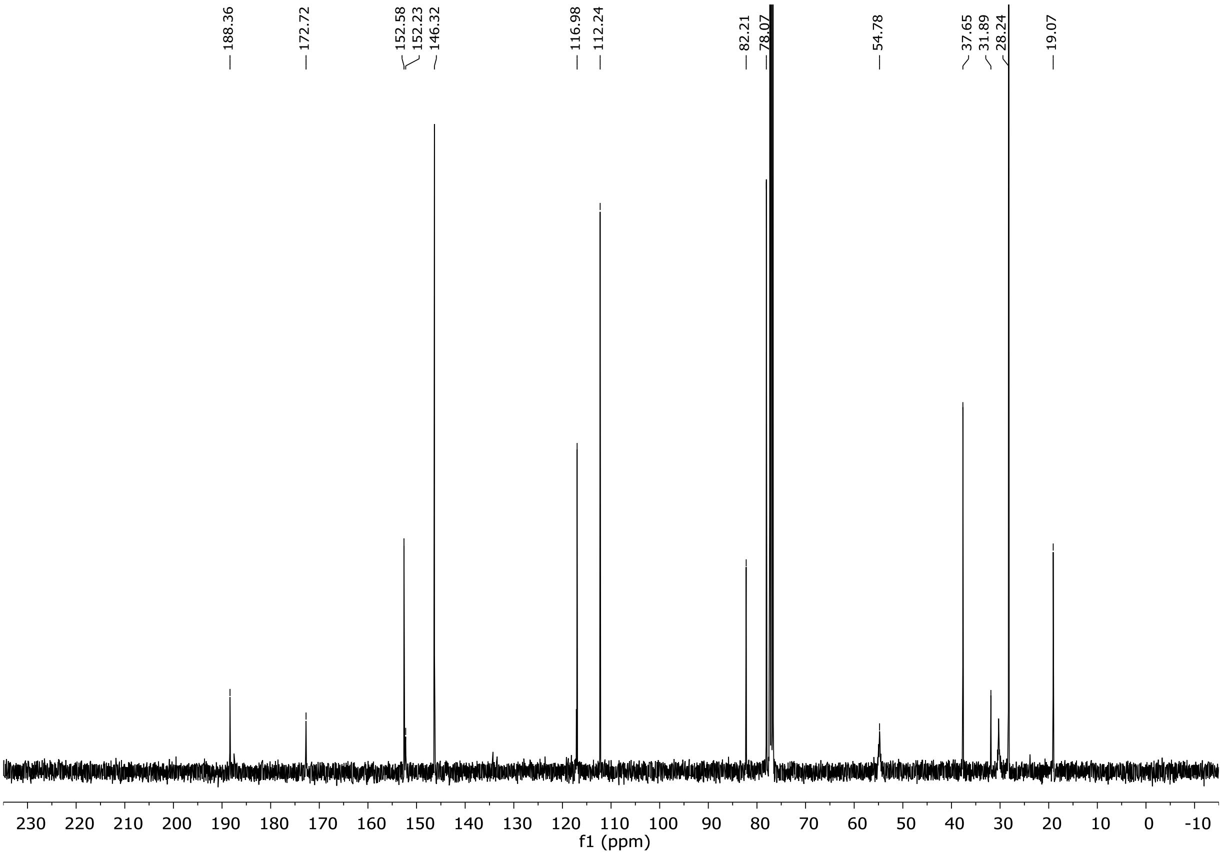
188.36
172.72
152.58
152.23
146.32
116.98
112.24
82.21
78.07
54.78
37.65
31.89
28.24
19.07
230 220 210 200 190 180 170 160 150 140 130 120 110 100 90 80 70 60 50 40 30 20 10 0 -10
f1 (ppm)

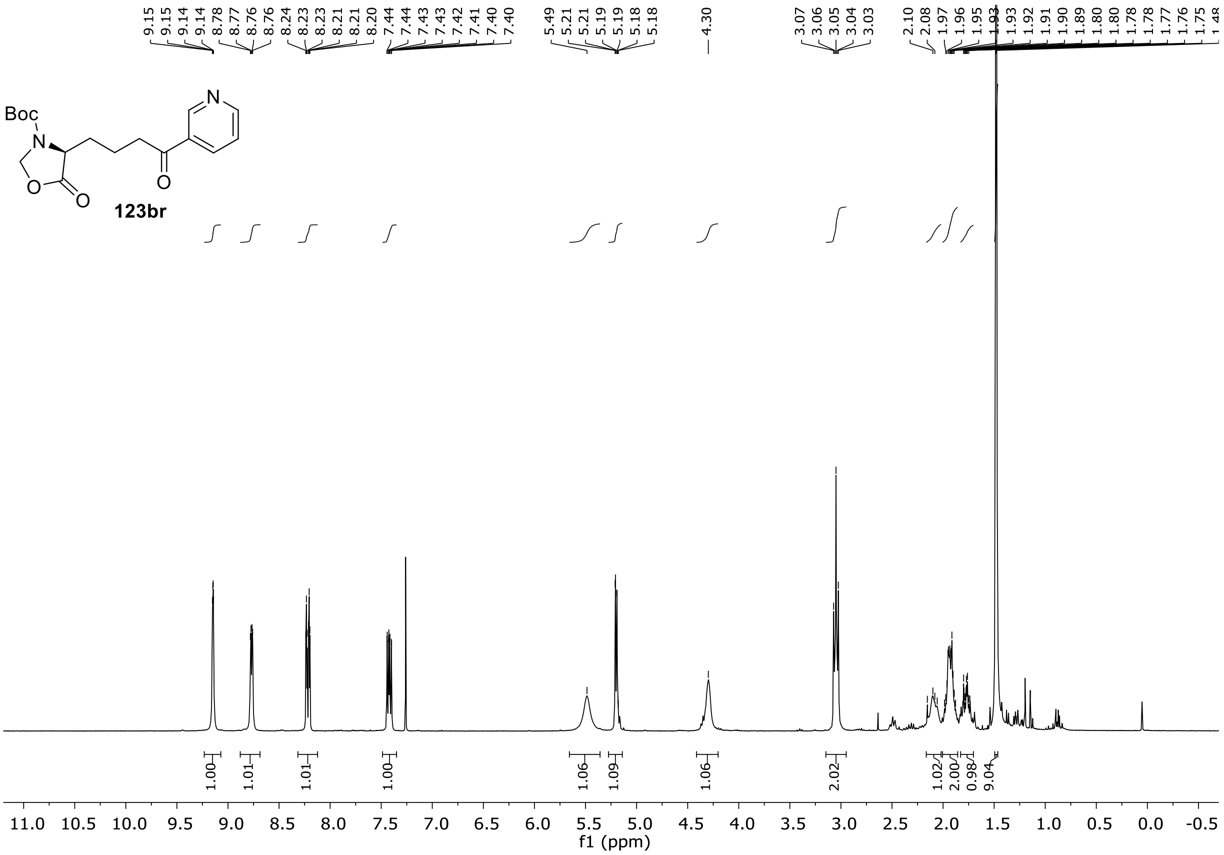
123br

Boc
N
O
O
O
N
9.15 9.15 9.14 9.14 8.78 8.77 8.76 8.76 8.24 8.23 8.23 8.21 8.21 8.20 7.44 7.44 7.43 7.43 7.42 7.41 7.40 7.40
5.49 5.21 5.21 5.19 5.19 5.18 5.18
4.30
3.07 3.06 3.05 3.04 3.03
2.10 2.08 1.97 1.96 1.95 1.93 1.93 1.92 1.91 1.90 1.89 1.80 1.80 1.78 1.78 1.77 1.76 1.75 1.48
1.00 1.01 1.01 1.00 1.06 1.09 1.06 2.02 1.02 2.00 0.98 9.04
11.0 10.5 10.0 9.5 9.0 8.5 8.0 7.5 7.0 6.5 6.0 5.5 5.0 4.5 4.0 3.5 3.0 2.5 2.0 1.5 1.0 0.5 0.0 -0.5
f1 (ppm)

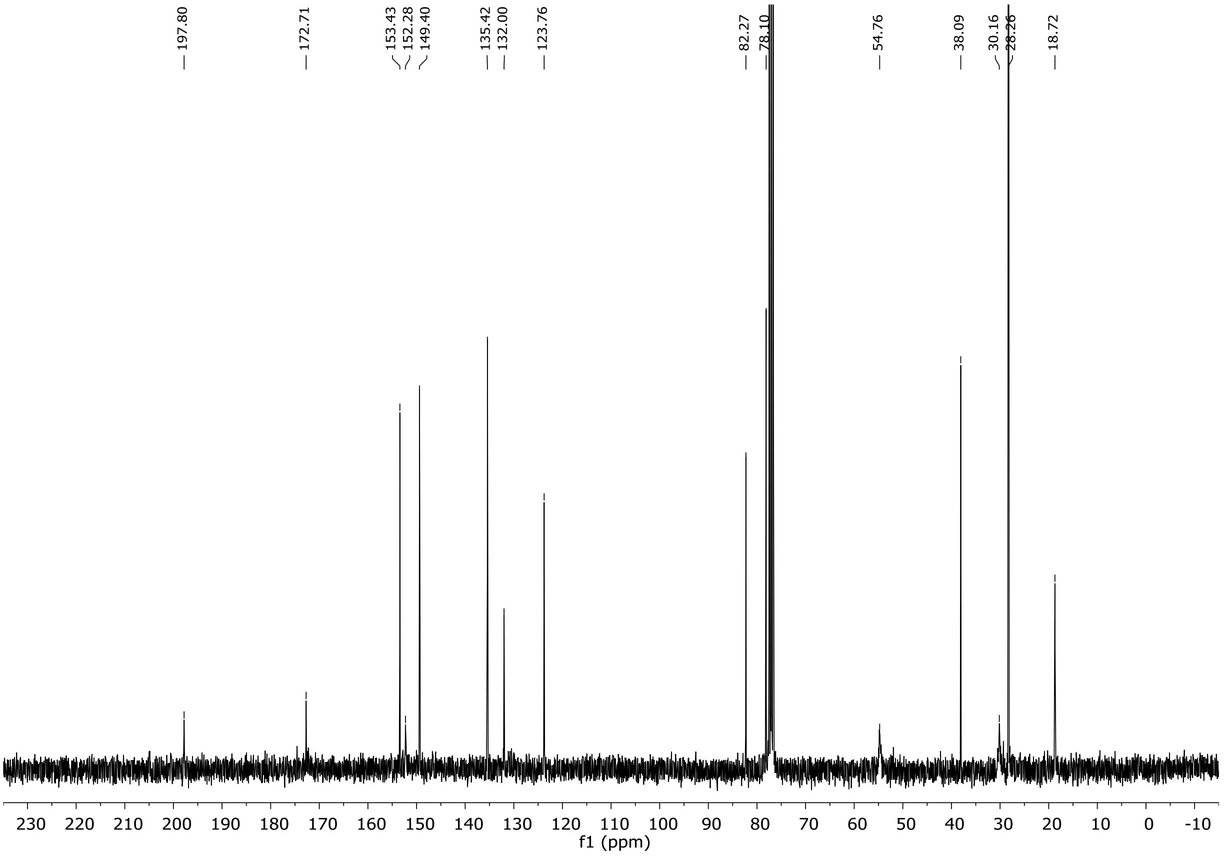
197.80
172.71
153.43 152.28 149.40
135.42 132.00
123.76
82.27 78.10
54.76
38.09
30.16 28.26
18.72
230 220 210 200 190 180 170 160 150 140 130 120 110 100 90 80 70 60 50 40 30 20 10 0 -10
f1 (ppm)

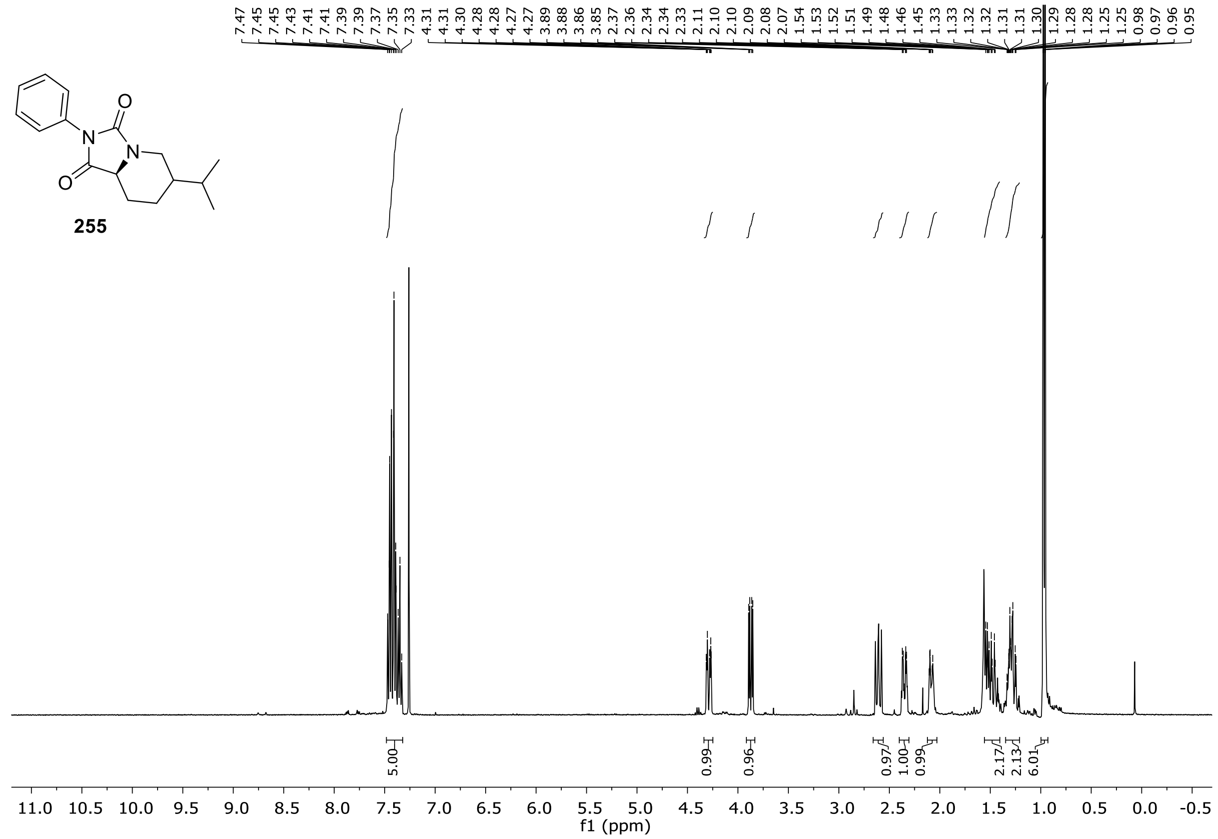
O
N
N
O
255
7.47
7.45
7.45
7.43
7.41
7.41
7.39
7.39
7.37
7.35
7.33
4.31
4.31
4.30
4.28
4.28
4.27
4.27
3.89
3.88
3.86
3.85
2.37
2.36
2.34
2.34
2.33
2.11
2.10
2.10
2.09
2.08
2.07
1.54
1.53
1.52
1.51
1.49
1.48
1.46
1.45
1.33
1.33
1.32
1.32
1.31
1.31
1.30
1.29
1.28
1.28
1.25
0.98
0.97
0.96
0.95
5.00
0.99
0.96
0.97
1.00
0.99
2.17
2.13
6.01
11.0
10.5
10.0
9.5
9.0
8.5
8.0
7.5
7.0
6.5
6.0
5.5
5.0
4.5
4.0
3.5
3.0
2.5
2.0
1.5
1.0
0.5
0.0
-0.5
f1 (ppm)

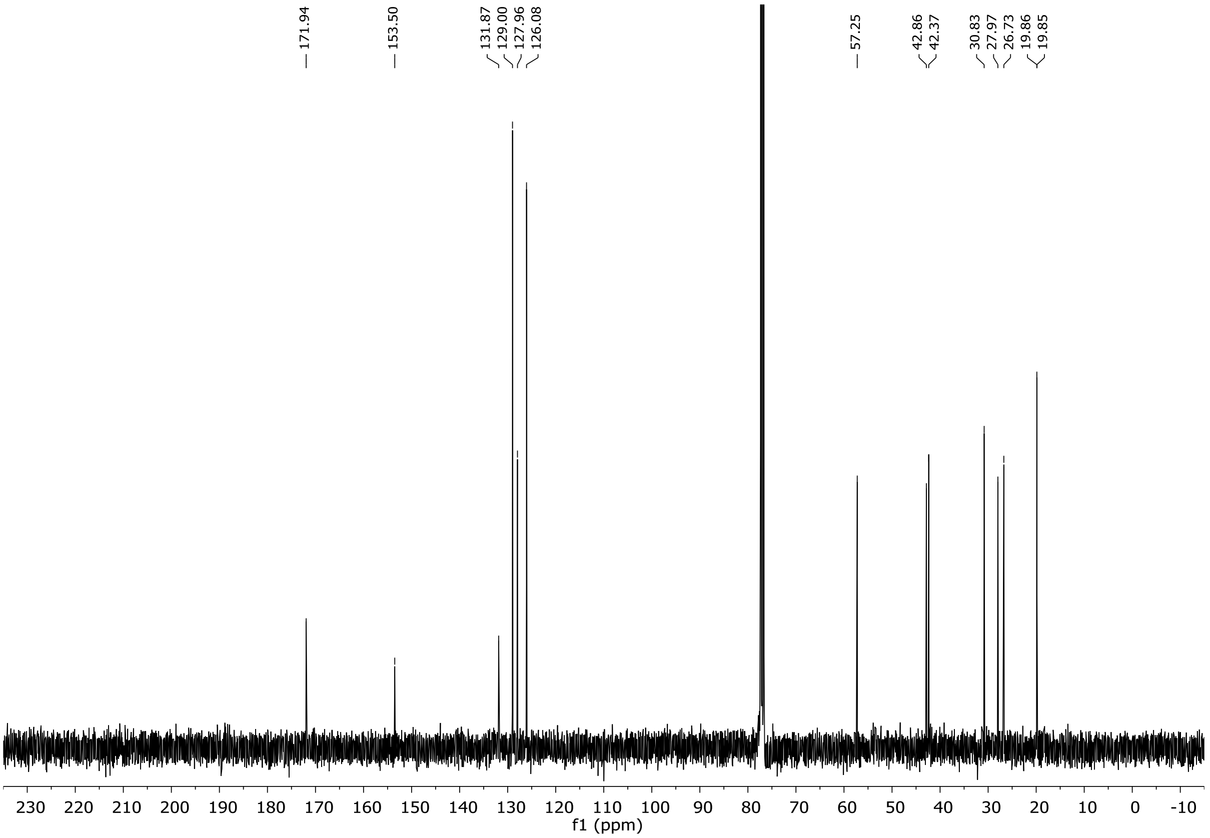
171.94
153.50
131.87
129.00
127.96
126.08
57.25
42.86
42.37
30.83
27.97
26.73
19.86
19.85
230
220
210
200
190
180
170
160
150
140
130
120
110
100
90
80
70
60
50
40
30
20
10
0
-10
f1 (ppm)

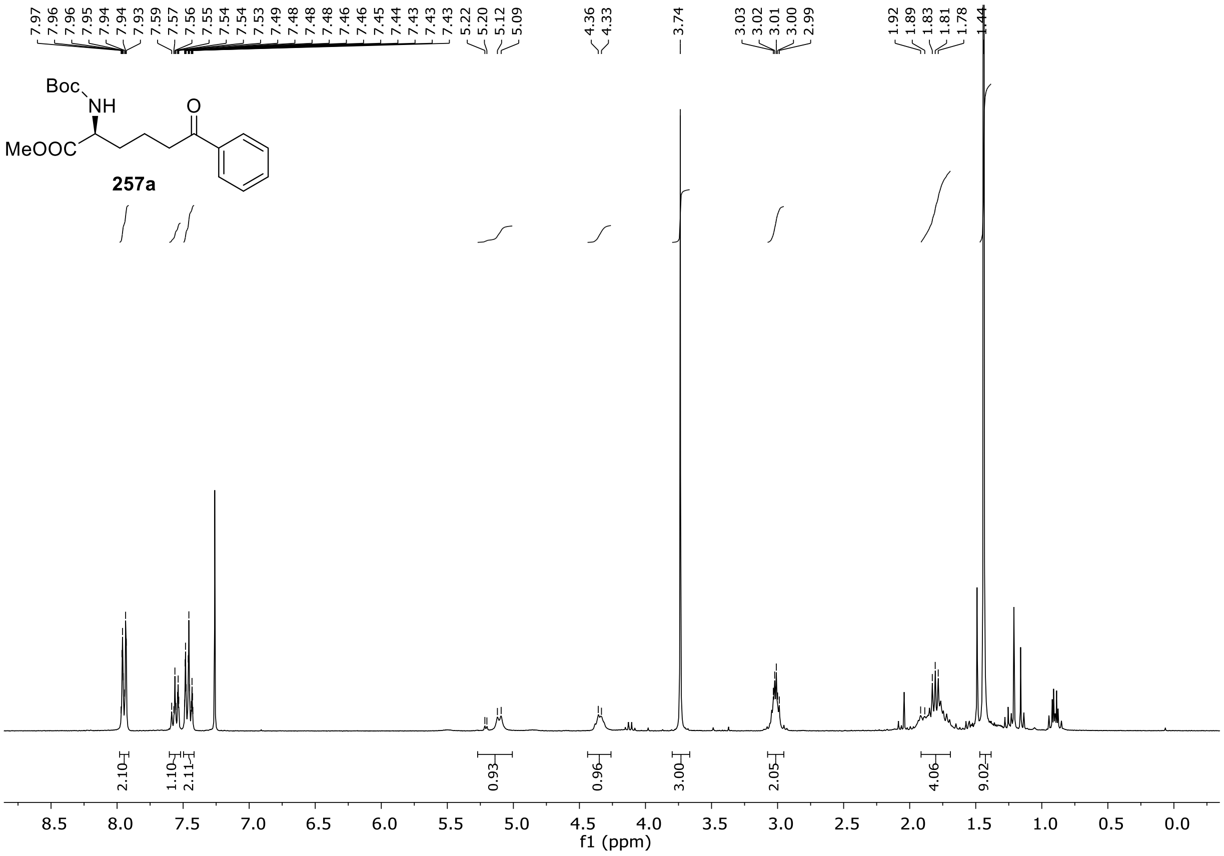
7.97
7.96
7.96
7.95
7.94
7.94
7.93
7.59
7.57
7.56
7.55
7.54
7.54
7.53
7.49
7.48
7.48
7.48
7.46
7.46
7.45
7.44
7.43
7.43
7.43
5.22
5.20
5.12
5.09
4.36
4.33
3.74
3.03
3.02
3.01
3.00
2.99
1.92
1.89
1.83
1.81
1.78
1.44
Boc
NH
O
MeOOC
257a
2.10
1.10
2.11
0.93
0.96
3.00
2.05
4.06
9.02
8.5
8.0
7.5
7.0
6.5
6.0
5.5
5.0
4.5
4.0
3.5
3.0
2.5
2.0
1.5
1.0
0.5
0.0
f1 (ppm)

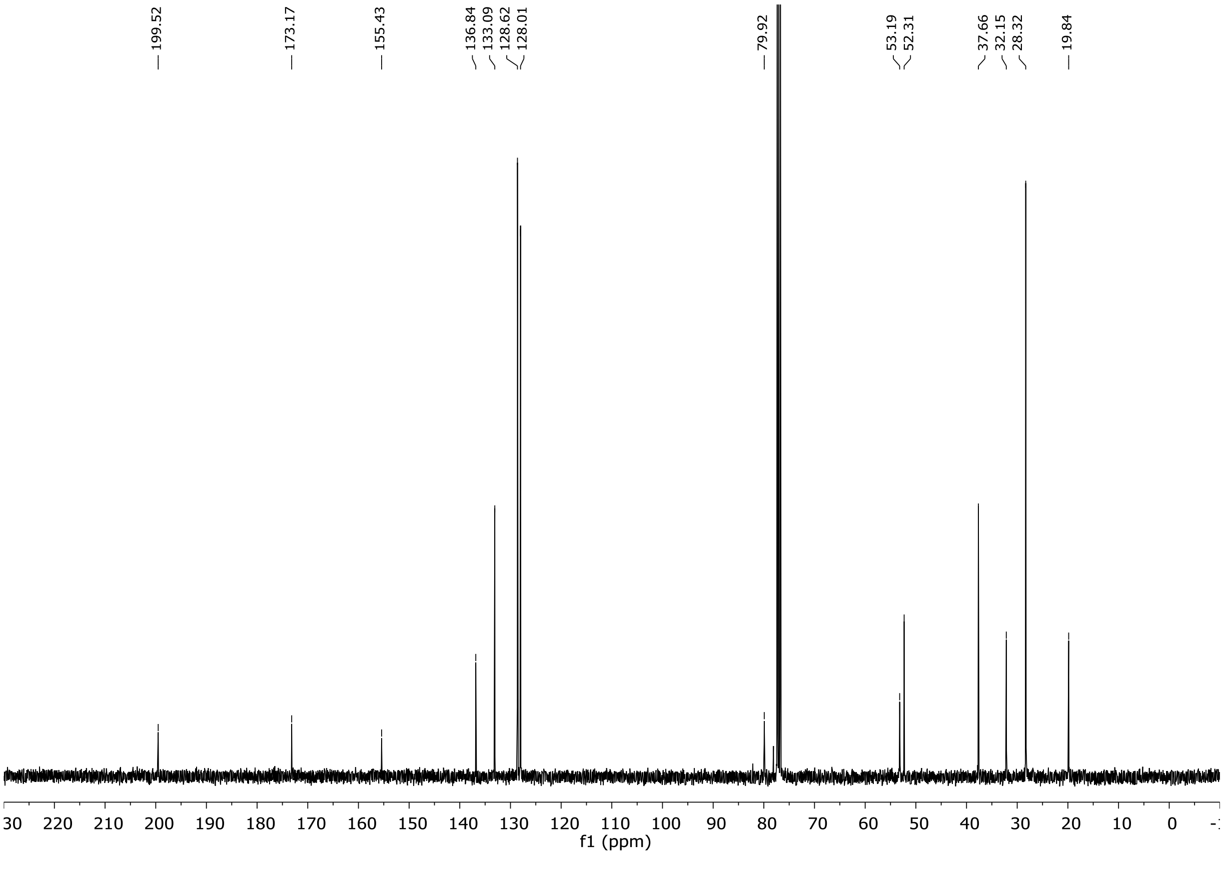
199.52
173.17
155.43
136.84
133.09
128.62
128.01
79.92
53.19
52.31
37.66
32.15
28.32
19.84
30
220
210
200
190
180
170
160
150
140
130
120
110
100
90
80
70
60
50
40
30
20
10
0
f1 (ppm)

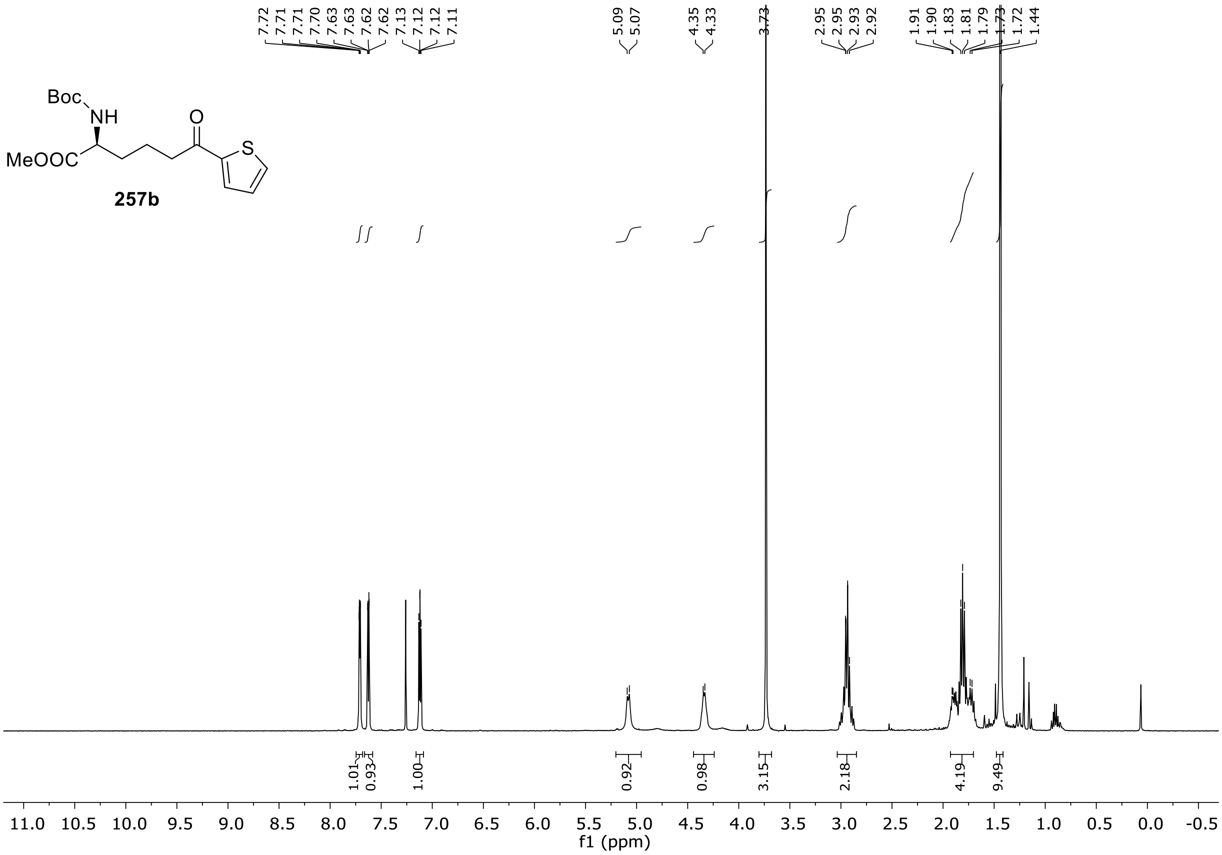
Boc
NH
O
S
MeOOC
7.72
7.71
7.71
7.70
7.63
7.63
7.62
7.62
7.13
7.12
7.12
7.11
5.09
5.07
4.35
4.33
3.73
2.95
2.95
2.93
2.92
1.91
1.90
1.83
1.81
1.79
1.73
1.72
1.44
1.01
0.93
1.00
0.92
0.98
3.15
2.18
4.19
9.49
11.0 10.5 10.0 9.5 9.0 8.5 8.0 7.5 7.0 6.5 6.0 5.5 5.0 4.5 4.0 3.5 3.0 2.5 2.0 1.5 1.0 0.5 0.0 -0.5
f1 (ppm)

257b

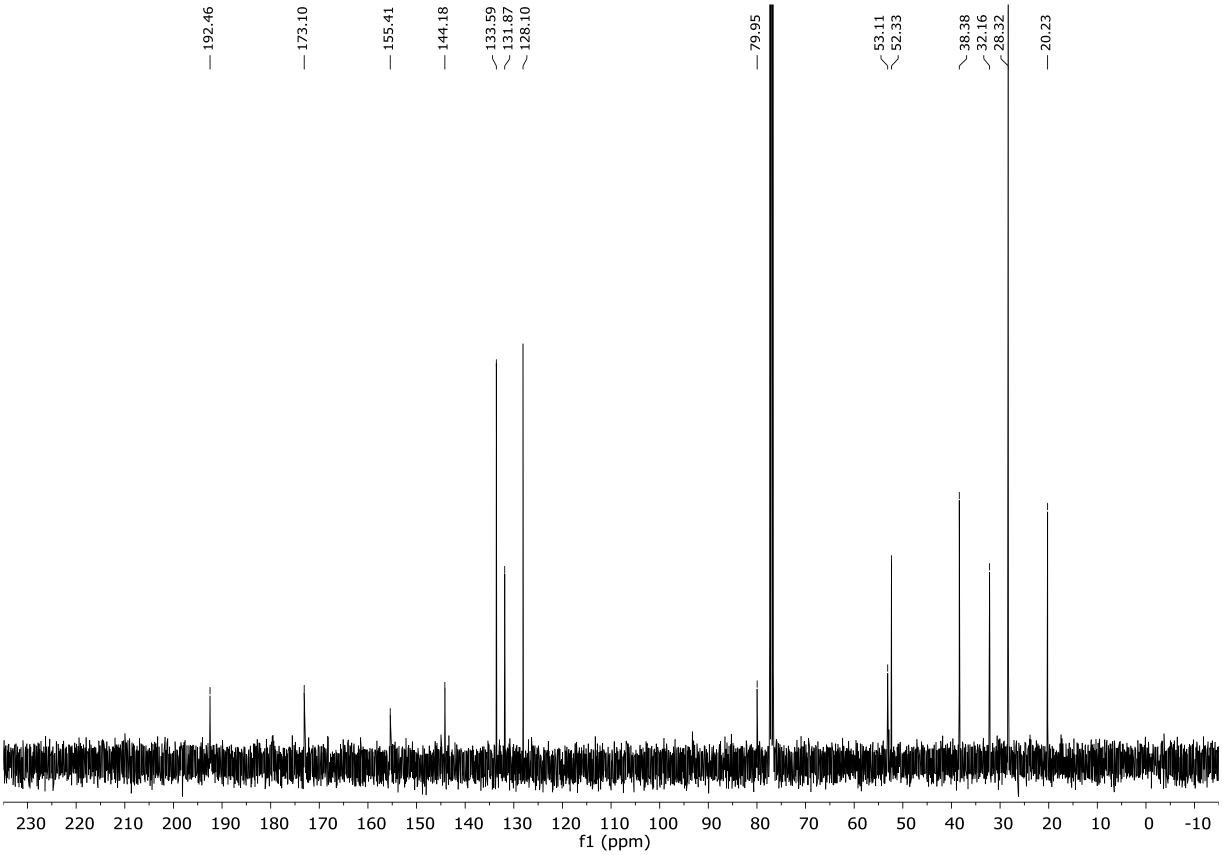
192.46
173.10
155.41
144.18
133.59
131.87
128.10
79.95
53.11
52.33
38.38
32.16
28.32
20.23
230 220 210 200 190 180 170 160 150 140 130 120 110 100 90 80 70 60 50 40 30 20 10 0 -10
f1 (ppm)

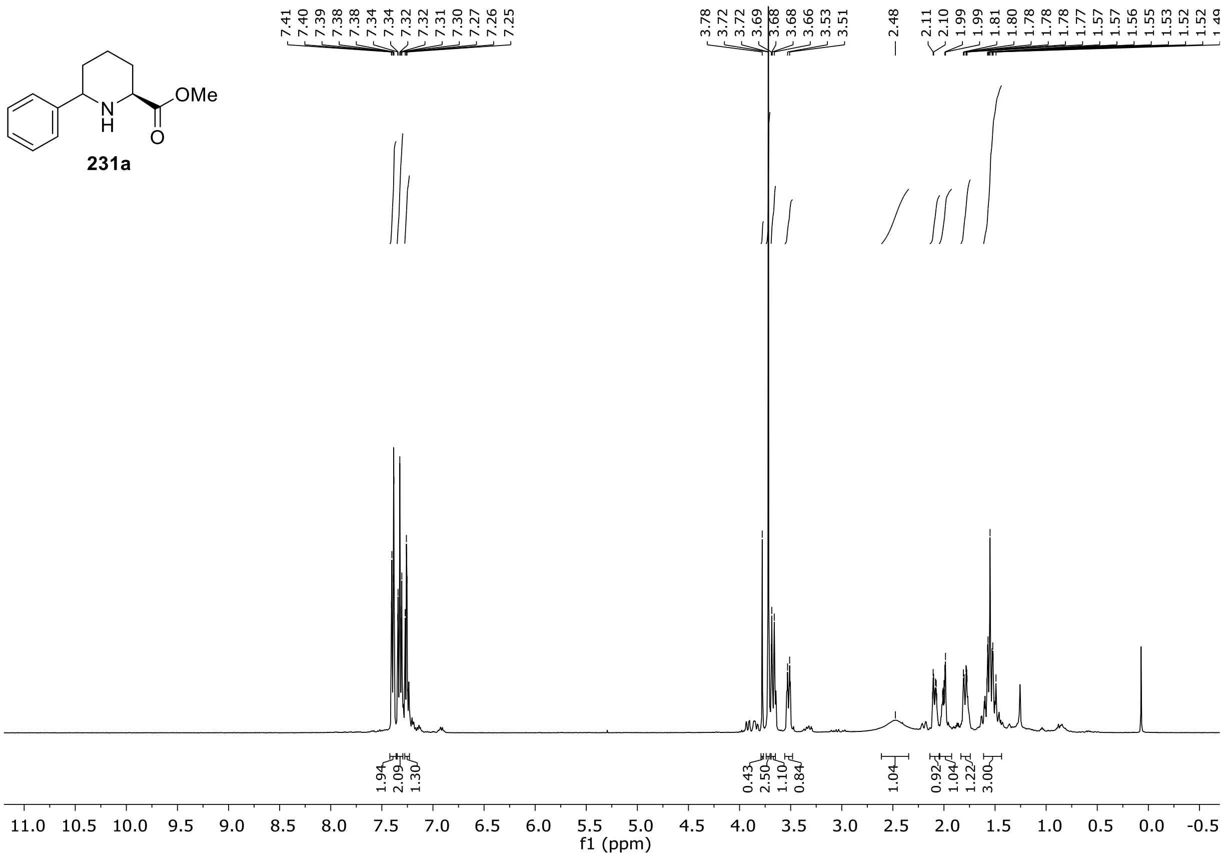
OMe
N
H
O
231a
7.41
7.40
7.39
7.38
7.38
7.34
7.34
7.32
7.32
7.31
7.30
7.27
7.26
7.25
3.78
3.72
3.72
3.69
3.68
3.68
3.66
3.53
3.51
2.48
2.11
2.10
1.99
1.99
1.81
1.80
1.78
1.78
1.77
1.57
1.57
1.56
1.55
1.53
1.52
1.52
1.94
2.09
1.30
0.43
2.50
1.10
0.84
1.04
0.92
1.04
1.22
3.00
11.0
10.5
10.0
9.5
9.0
8.5
8.0
7.5
7.0
6.5
6.0
5.5
5.0
4.5
4.0
3.5
3.0
2.5
2.0
1.5
1.0
0.5
0.0
-0.5
f1 (ppm)

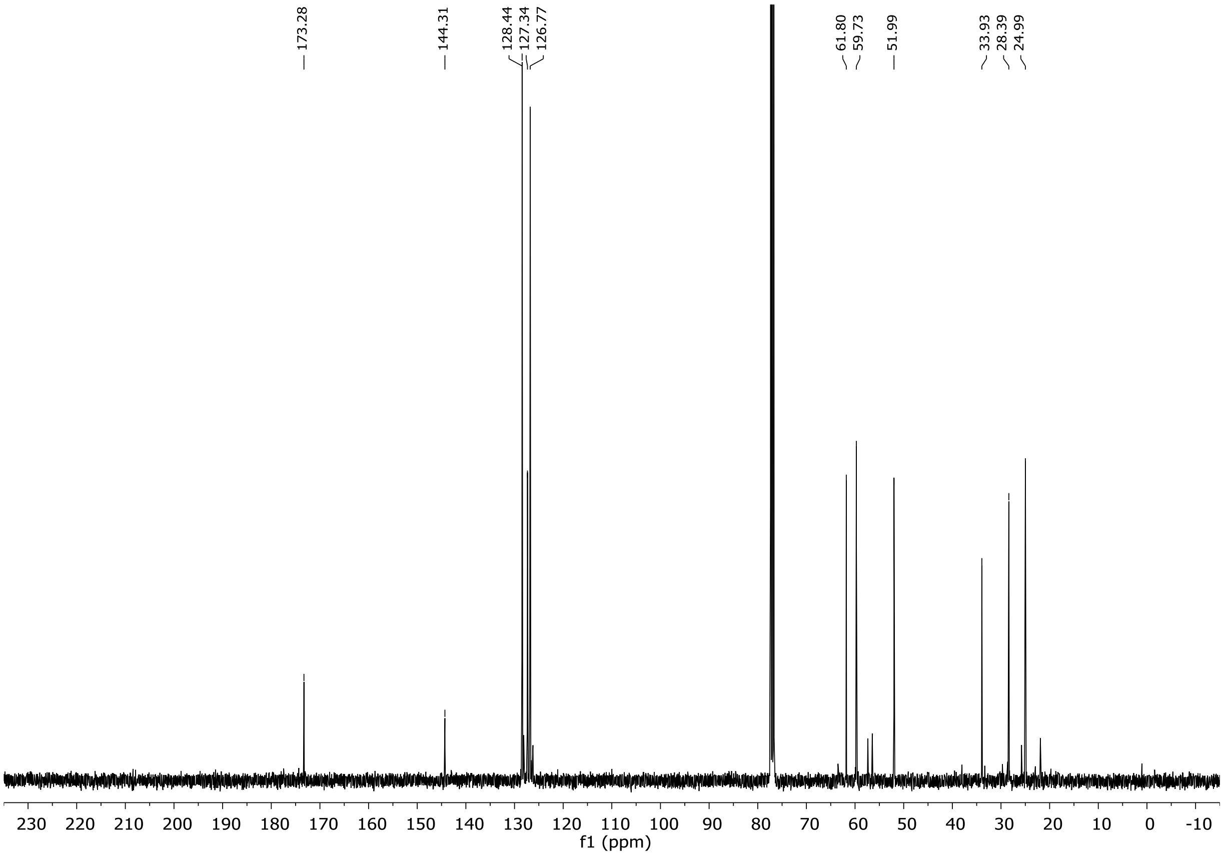
173.28
144.31
128.44
127.34
126.77
61.80
59.73
51.99
33.93
28.39
24.99
230
220
210
200
190
180
170
160
150
140
130
120
110
100
90
80
70
60
50
40
30
20
10
0
-10
f1 (ppm)

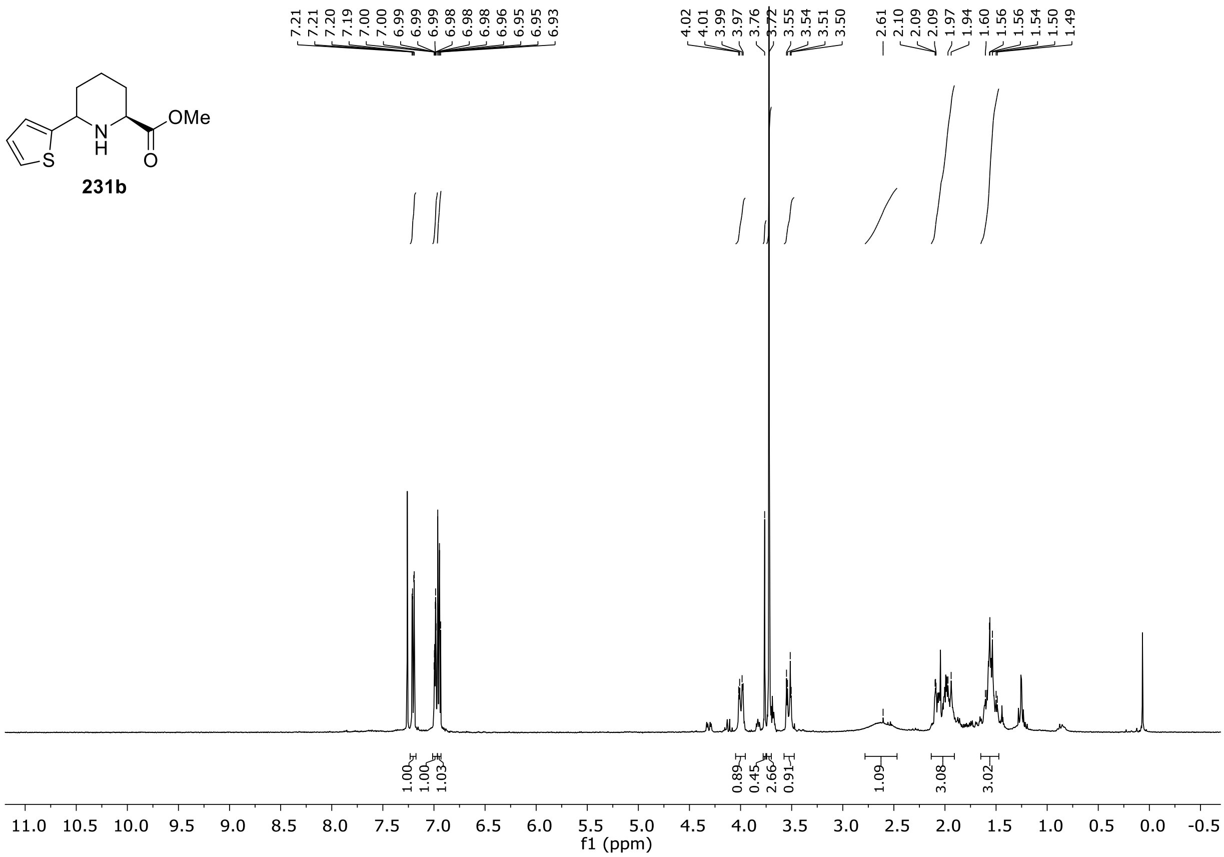
OMe
N
H
S
O
231b
7.21
7.21
7.20
7.19
7.00
6.99
6.99
6.99
6.98
6.98
6.98
6.96
6.95
6.95
6.93
4.02
4.01
3.99
3.97
3.76
3.72
3.55
3.54
3.51
3.50
2.61
2.10
2.09
2.09
1.97
1.94
1.60
1.56
1.56
1.54
1.50
1.49
1.00
1.00
1.03
0.89
0.45
2.66
0.91
1.09
3.08
3.02
11.0 10.5 10.0 9.5 9.0 8.5 8.0 7.5 7.0 6.5 6.0 5.5 5.0 4.5 4.0 3.5 3.0 2.5 2.0 1.5 1.0 0.5 0.0 -0.5
f1 (ppm)

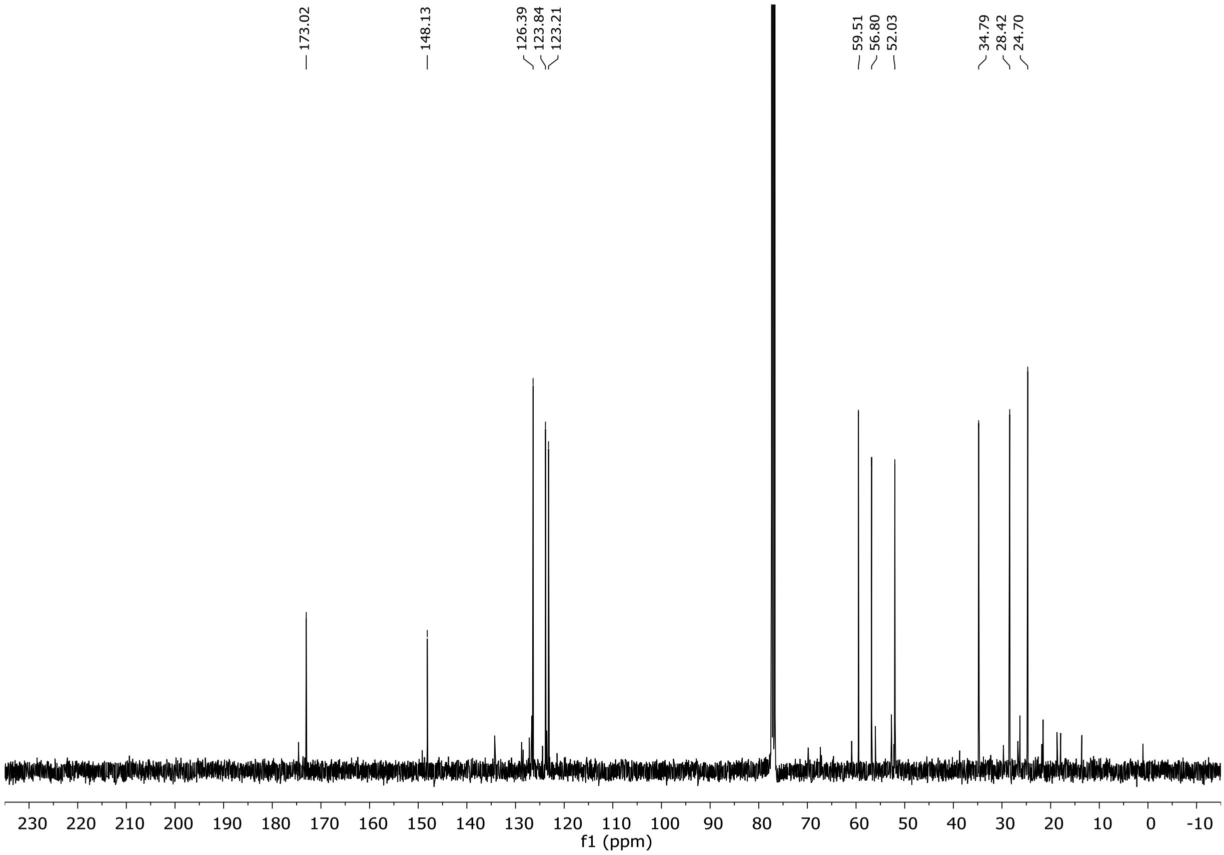
173.02
148.13
126.39
123.84
123.21
59.51
56.80
52.03
34.79
28.42
24.70
230 220 210 200 190 180 170 160 150 140 130 120 110 100 90 80 70 60 50 40 30 20 10 0 -10
f1 (ppm)

3. X-Ray

tert-butyl (*S*)-5-oxo-4-(4-oxo-4-phenylbutyl)oxazolidine-3-carboxylate (123bf)

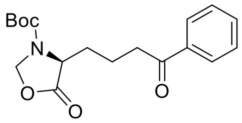

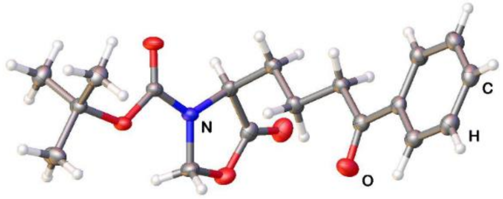

Formula	$C_{18}H_{23}NO_5$
$D_{calc.}$/ g cm^{-3}	1.277
μ/mm^{-1}	0.767
Formula Weight	333.37
Colour	clear colourless
Shape	prism
Size/mm^3	0.19×0.17×0.05
T/K	123.01(10)
Crystal System	orthorhombic
Flack Parameter	-0.01(7)
Hooft Parameter	0.00(7)
Space Group	$P2_12_12_1$
a/Å	5.93630(10)
b/Å	14.4526(3)
c/Å	20.2083(4)
α/°	90
β/°	90
γ/°	90
V/Å^3	1733.77(6)
Z	4
Z'	1
Wavelength/Å	1.54184
Radiation type	CuK$_\alpha$
Θ_{min}/°	3.760
Θ_{max}/°	76.221
Measured Refl.	20011
Independent Refl.	3608
Reflections with I > 2(I)	3461
R_{int}	0.0399
Parameters	309
Restraints	0
Largest Peak	0.129
Deepest Hole	-0.153
GooF	1.044
wR_2 (all data)	0.0669
wR_2	0.0658
R_1 (all data)	0.0281
R_1	0.0265

4. List of abbreviation

A	acceptor
Å	angstrom
abs	absolute
Ac	acetyl
AIBN	azobis*iso*butyronitrile
aq	aqueous
Ar	aryl
Asc	ascorbate
ATRA	atom transfer radical addition
bpy	2,2'-bipyridine, 2,2'bipyridyl
BDMAP	1,6-bis(dimethylamino)-pyrene
bmim	1-butyl-3-methylimidazolium
Bn	benzyl (PhCH$_2$)
Boc	*tert*-butoxycarbonyl
BNAH	1-benzyl-1,4-dihydronicotinamide
br	broad (spectral peak)
Bu	butyl
^{t}Bu	*tert*-butyl
BuLi	butyl lithium
Bz	benzoyl (PhCO)
°C	degrees Celsius
^{13}C-NMR	carbon NMR
CB	conduction band
CDC	cross dehydrogenative coupling
CFL	compact fluorescent lamp
cm	centimeter
cm^{-1}	wavenumber(s)
Co/C	carbon-coated cobalt nanoparticles
conc.	concentrated
CTAB	cetrimonium bromide
CuAAC	copper(I)-catalyzed azide-alkyne cycloaddition
d	day(s); doublet (spectral)
D	donor
DABCO	1,4-diazabicyclo[2.2.2]octane
dap	dianisol phenanthrolin
DBU	1,8-diazabicyclo[5.4.0]undec-7-ene
DCC	*N*,*N*'-dicyclohexylcarbodiImide
DCM	dichloromethane
dF(CF$_3$)ppy	2-(2,4-difluorophenyl)-5-(trifluoromethyl)pyridine
DHAA	dihydroartemisinic acid
DIPA	diisopropylamine
DIPEA	*N*,*N*-diisopropylethylamine
DMA	dimethylacetamide
DMAP	4-(*N*,*N*-dimethylamino)-pyridine
DMF	dimethylformamide
DMSO	dimethylsulfoxide
DNM	dinonylmethyl
dr	diastereomeric ratio
dtb-bpy	4,4'-di-*tert*-butyl-2,2'-bipyridine
$E_{1/2}$	standard reduction potential
EA	electron acceptor; elemental analysis
ED	electron donor
eq	equation
e.g.	for example
equiv	equivalents
ET	energy transfer
Et	ethyl
et al.	and others (co-authors)
etc.	and so forth
EtOAc	ethyl acetate
ESI	electrospray ionization

eV	electron volt
fac	facial
FEP	fluorinated ethylene propylene
FRET	Förster resonance energy transfer
g	gram(s); gaseous
g-C_3N_4	graphenic carbon nitride
GC-FID	gas chromatography with a Flame ionization detector
h	hours
hdppy	heptadecanyl-2-phenylpyridine
HE	Hantzsch ester, diethyl 1,4-dihydro-2,6-dimethyl-3,5-yridinedicarboxylate
HMDS	hexamethyldisilazane
^{1}H-NMR	proton NMR
hν	light
HOMO	highest occupied molecular orbital
HPLC	high-performance liquid chromatography
HRMS	high-resolution mass spectrometry
Hz	Hertz
i.e.	that is
ICP-OES	inductively coupled plasma optical emission spectrometry
IR	infrared
ISC	intersystem crossing
J	coupling constant (in NMR analysis)
k	kilo
K	Kelvin
L	liter
LDA	lithium diisopropylamide
LED	light emitting diode
Lg	leaving group
λ_{max}	max. UV-vis wavelength
LUMO	lowest unoccupied molecular orbital
m	meter; milli; multiplet (spectral)
M	molar (moles per liter)
M^+	parent molecular ion (in MS)
µ	micro
max	maximum
MCFs	mesocellular silica foams
Me	methyl
MeCN	acetonitrile
MHz	megahertz
min	minute(s); minimum
mL	milliliter
MLCT	metal to ligand charge transfer
mM	millimolar
mmol	millimole(s)
MNP	magnetic nanoparticle
MOF	metal organic framework
mol	mole(s)
mp	melting point
mpg-C_3N_4	mesoporous graphitic carbon nitride
MS	mass spectrometry
m/z	mass to charge ratio (in MS)
NEt_3	triethyl amine
^{n}Bu	normal butyl (primary)
NCN-CN_x	cyanamide-functionalized carbon nitride
nm	nanometer
NMP	*N*-methyl-2-pyrrolidone
NMR	nuclear magnetic resonance
Nu	nucleophile
n.r.	no reaction
ns	nanoseconds
on	over night
PAMAM	polyamidoamine

PC	photocatalyst
PCP	porous crosslinked polymers
Pd/C	palladium on activated charcoal
PDVB	polydivinylbenzene
PET	photoinduced electron transfer
Pg	protective group
Ph	phenyl
Phth	phthaloyl
PIB	poly*iso*butylene
pp	pages
ppm	part per million
ppy	2-phenylpyridine
^{i}Pr	*iso*-propyl
PWh	peta watt hour(s)
q	quartet (spectral)
R	arbitrary residue
red	reduction
redox	reduction-oxidation
Ref	reference
R_f	retention factor
rt	room temperature
rxn	reaction
s	seconds; singlet (spectral)
sat.	saturated
SCE	saturated calomel electrode
SET	single electron transfer
t	triplet (spectral)
T	temperature in Kelvin
TBAB	tetra-*n*-butylammonium bromide
TBAF	tetra-*n*-butylammonium fluoride
TBDMS	*tert*-butyldimethylsilyl
Tf	trifluoromethansulfonyl (triflyl)
TFA	trifluoroacetic acid
TFAA	trifluoroacetic acid anhydride
THF	tetrahydrofuran
TLC	thin-layer chromatography
TMS	trimethylsilyl; tetramethylsilane; thermomorphic solvent system
tosyl	*p*-toluenesulfonyl
t_R	retention time (in chromatography)
Ts	*p*-toluenesulfonyl (tosyl)
UV	ultraviolet (light)
UV-Vis	ultraviolet-visible absorption Spectroscopy
VB	valence band
vis	visible
vs	versus
w/o	without
wt%	weight percent

5. Curriculum vitae

Personal Data

Name	Christian Eichinger
Date and place of birth	October, 18th 1992 in Schwandorf
Nationality	German
Email	Christian1.Eichinger@chemie.uni-regensburg.de

Professional Record

11/2016 – current	Research Assistant, Institute of Organic Chemistry, University of Regensburg

Education

11/2016 – current	Doctoral Student, University of Regensburg Thesis: *“Immobilization of Photocatalysts on Solid Support and Photochemical Decarboxylations”* Supervisor: Prof. Dr. Oliver Reiser
10/2014 – 09/2016	Master studies, Chemistry, University of Regensburg Subjects: organic chemistry, bioanalytical chemistry and physical chemistry Thesis: *“Immobilization of fac-Ir(ppy)$_3$ and [Ru(bpy)$_3$]Cl$_2$ and application in photocatalysis”* Supervisor: Prof. Dr. Oliver Reiser
10/2011 – 07/2014	Bachelor Studies, Chemistry, University of Regensburg Thesis: *“Preparation and characterization of functionalized vesicles”* Supervisor: Prof. Dr. Burkhardt König
09/2003 – 06/2011	Abitur (*A-levels*), Regental-Gymnasium, Nittenau

Publications

[1] A. Hossain, A. Vidyasagar, C. Eichinger, C. Lankes, J. Phan, J. Rehbein, O. Reiser, *Angew. Chem. Int. Ed.* **2018**, *57*, 8288-8292.
„Visible-Light Accelerated Copper(II)-Catalyzed Regio- and Chemoselective Oxo-Azidation of Vinyl Arenes"

[2] C. Eichinger, O. Reiser, *Manuscript in preparation*
„Magnetic Nanoparticles as Solid Support for fac-Ir(ppy)$_3$ and its Application as Recyclable Photocatalyst"

[3] C. Eichinger, S. Budde, O. Reiser, *Manuscript in preparation*
„Photochemical Decarboxylation of Glutamic Acid Derivatives towards unnatural Amino Acids and their Transformation to Pipecolic Acid Derivatives"

Congresses and Scientific Meetings

GRK 1626 – 28th Seminar Days, Plankstetten Monastery (Germany), March 2017
"Immobilization of [Ru(bpy)$_3$]Cl$_2$ onto Nafion and Photocatalyzed Enantioselective Dehydrogenative Cross-Coupling Reactions" (Oral)

26th ISHC Congress, Regensburg (Germany), September 2017
"Study on the Photochemical Decarboxylation of Asp and Glu Derivatives: Optimized Conditions and Substrate Scope" (Poster)

GRK 1626 – 32nd Seminar Days, Regensburg (Germany), March 2018
"Immobilization of [Ru(bpy)$_3$]$^{2+}$ on Solid Support via Electrostatic Interaction and its Application as Easily Recyclable Visible-Light Photocatalyst" (Poster)

EuCheMS Conference on Organic Free Radicals (ECOFR), Marseille (France), June 2018
"Immobilization of [Ru(bpy)$_3$]$^{2+}$ on Solid Support via Electrostatic Interaction and its Application as Easily Recyclable Visible-Light Photocatalyst" (Poster)

GRK 1626 – 33rd Seminar Days, Kostenz Monastery (Germany), June 2018
"Immobilization of [Ru(bpy)$_3$]Cl$_2$ on Solid Supports" (Oral)

Professional References

Prof. Dr. Oliver Reiser
Institut für Organische Chemie
Universität Regensburg
Universitätsstr. 31
93053 Regensburg, Germany
Phone: 0049 941 943 4631
Email: Oliver.Reiser@chemie.uni-regensburg.de

G. Acknowledgement

I am grateful to my research supervisor Prof. Dr. Oliver Reiser for giving me the opportunity to work in his research group, the challenging and interesting topic, the accompanying discussions on chemical problems and his constant support during my work.

I thank Dr. Peter Kreitmeier for the help and expertise he provided me on chemical and technical problems. Thanks to Brigitte Eichenseher, Roxane Harteis, Johannes Floß, Klaus Döring and Helena Konkel for synthesizing starting materials, your constant support, and for all your help on everyday problems. The same is true for our secretaries Antje Weigert and especially Michaela Schüle. Thank you for solving all bureaucratic matters!

Thanks to all co-workers in the central analytical department, especially the NMR department (Fritz Kastner, Veronica Scheidler, Annette Schramm and Georgine Stühler) and the mass spectroscopy (Josef Kiermaier and Wolfgang Söllner) for the numerous samples they have measured. Moreover, I would like to thank Joachim Rewitzer and Vanessa Tomanek for measuring all the ICP samples.

A special thanks goes to my lab mates Simon Budde, Andreas Hartl, Anurag Chinchole and Anna Rustler for the fantastic lab atmosphere, the help and discussions on chemical and practical problems. Most of all, however, I would like to thank you for all the talks about non-chemical stuff, the versatile music we listened to and the great time we spent outside the university. You made life a lot easier!

I would also like to thank Dr. Asik Hossain for all the discussions and help on chemical problems. I really enjoyed the time and all the conversations with you in the office. All the best for your future in America!

Thanks to Tobias Babl, Simon Budde, Anurag Chinchole, Robert Eckl, Peter Ehrnsberger, Sebastian Engl, Sebastian Fischer, Andreas Hartl, Tomislav Krolo, Michael Leitner, Natalija Moor, Eva Plut, Alexander Reichle, Carina Sonnleitner, Lisa Stadler, Lukas Traub, Thomas Weinbender, Dr. Thomas Föll, Dr. Matthias Gnahn, Dr. Asik Hossain, Dr. Benjamin Kastl, and all other former and current members of the Reiser group for the home-like atmosphere.

Thanks to Dr. Thomas Föll for providing enol acetates, to Alex Abramov for helpful discussions on recyclable photocatalysts and to Dr. Indrajit Ghosh for helpful discussions on graphitic carbon nitrides.

I would also like to thank my bachelor and research students Lisa Uhlstein, Caroline Hiefinger, Julia Erl and Delphine Benay for their work in the lab and their fruitful input.

For proof reading of this thesis I thank Anna Rustler, Simon Budde, and Anurag Chinchole for their spent time and helpful remarks.

A special thank you also goes to my friends outside the university, especially Michael Plank, Sebastian Humbs and Matthias Zach. Thank you for your continuous support, your motivation and for always being there for me since almost 20 years. You are the best friends one can wish for!

Finally, I would like to thank my parents Albert and Andrea, my sister Julia and my girlfriend Silvia. I am very grateful to all of you for your love, believe and support that you gave me. I would like to especially thank Silvia for all her patience and encouragement. You are the one who always kept me grounded!

H. Declaration

Herewith I declare that this present thesis is a presentation of my original work prepared single-handed. Wherever contributions from others are involved, all of them are marked clearly, with reference to the literature, license and acknowledgement of collaborative research.

Regensburg, 09.06.2020

Christian Eichinger